Journal of Applied Mechanics

(Contributions of the ASME Applied Mechanics Division)

[illegible] Stresses and Strains in Work-Hardening Plastic Solids . . William Prager 499
[illegible] Testing Tests . . . . . S. S. [illegible] 497
[illegible] on Multiple Plastic Supports . . . . . R. A. Di Taranto 503
[illegible] Bending of Beams . . . . . D. C. Drucker 509
[illegible] Plastic Beams . . . J. A. Sollo, R. A. Cotter, and P. S. [illegible] 515
[illegible] of Rear Circles of Any Shape . . . . . M. M. Abbott 522
[illegible] Bearing Plate . . . . . Brahmadeo Dhawan 527
[illegible] of Rectangular Elastic Plates . . . Kuo-Hsiao Chu and George Herrmann 532
[illegible] Load upon Elastic Body . . . G. L. Neidhardt and Eli Sternberg 541
[illegible] Two Elastic Bodies . . . . . A. Signorini 555
[illegible] of Axially Symmetric Bending . . . George Herrmann and I. Nikiel 563
[illegible] Under Normal Pressure . . . . . L. E. Dupuit 569
[illegible] of Cylindrical Shells . . . . . Walter Freiberger 576
[illegible] Bending . . . . . C. F. Kossiakoff 581
[illegible] . . . . . C. F. Kossiakoff 584
[illegible] Conical Surface Due to Point . . . . . H. E. Weber 587
[illegible] in Tangential and Equatorial Flow . . . . . H. E. Weber 593
[illegible] of Solid Spheres in Viscous Fluid . . . G. E. Currier and R. C. Di Prima 601
[illegible] by Oblique Impact of Rigid Spheres . . . . . D. R. Cunningham and Warner Goldsmith 606
[illegible] of a Sphere on a Beam . . . Warner Goldsmith and D. M. Cunningham 612
[illegible] Characteristics for Deformation of Shells . . . . . P. G. Hodge, Jr. 617
[illegible] Buckling of Circular Cones Under Axial Compression . . . . . Paul Seide 625
[illegible] Stresses of Two Degrees of Freedom . . . . . C. F. Zorowski 629
[illegible] of a Nonlinear System . . . . . E. I. Rivin 635
[illegible]
[illegible] Shells . . . . . R. A. Brooks 649
[illegible] Readings for Cylindrical Shells . . . . . E. H. Kennard 648
[illegible] Buckling Experiments . . . W. H. Hoppmann II and W. G. Speer 646
[illegible] Polyacrylamide Cylinders . . . Herbert Becker and George Gerard 647
[illegible] Stress in Spherical and Ellipsoidal Shells . . . . . Sanmiguel Sobrepena 648
[illegible] Wake of Streamlined Cylinders . . . . . R. F. Stoddard, Jr. 649
[illegible] published papers by Zvi Hetényi and Lloyd Rumbold; Chieh-Chien Chang and W. Seeley and E. G. Thomas 658
[illegible] 659

DECEMBER, 1956

VOL. 23, NO. 4

Transactions of The American Society of Mechanical Engineers

Journal of Applied Mechanics

Transactions of the ASME Applied Mechanics Division

E. Reissner, Secretary

John M. Lessells, Technical Editor

Published Quarterly by

The American Society of Mechanical Engineers

Publication Office, 20th and Northampton Streets, Easton, Pa.
Editorial Department of the Society, 29 West Thirty-Ninth Street, New York 18, N. Y.

OFFICERS OF THE SOCIETY
F. W. Hoyns, *President*
C. E. Davies, *Secretary*

PUBLICATIONS COMMITTEE
J. J. Jakosky, Jr., *Acting Editor*
R. E. Wenzel, *Asst. Managing Editor*

... responsible only for statements or opinions advanced in papers or ... printed in its publications (B13, Par. 4)

... Publication Office, 20th and Northampton Streets, Easton, Pa. The editorial ... Department of the Society, 29 West Thirty-Ninth Street, New York 18, N. Y. ... Subscription ... Canada, $8.00; other countries, $9.00. ... Entered as second-class matter ... at the Post Office at Easton, Pa., under the act of August 24, 1912. ... Acceptance for mailing at the special rate of postage prescribed by section ... Act of ... authorized ...

A New Method of Analyzing Stresses and Strains in Work-Hardening Plastic Solids[1]

By WILLIAM PRAGER,[2] PROVIDENCE, R. I.

For work-hardening plastic solids, segmentwise linear yield conditions and the associated flow rules constitute a reasonable compromise between the mathematically convenient but physically unsound total stress-strain laws and the physically sound but mathematically inconvenient incremental laws. They allow total stress-strain laws to be used in the small, but retain the characteristic features of incremental laws in the large. The use of a segmentwise linear yield condition and the associated flow rule is illustrated by the analysis of the bending moments and deflections of a simply supported circular plate that is made of a work-hardening material and subjected to a uniformly distributed transverse load.

1 Introduction

As far as perfectly plastic solids are concerned, recent years have brought significant advances in both the general theory and its applications to specific practical problems. Advances in the field of work-hardening solids have been less spectacular and have affected primarily the general theory. Foremost among these is the achievement of a better understanding of the general structure of stress-strain laws in the work-hardening range. As a consequence of this, theoretical work in this field is now based exclusively on incremental stress-strain laws; except for the case of proportional loading, where they can be shown to be integrated forms of incremental laws, total stress-strain laws have been discarded by the theoreticians. However, because the total laws are mathematically more convenient than the incremental laws, many solutions of specific problems offered in the contemporary literature are still based on the total laws. In a typical paper of this kind, the author begins by stating that, in principle, these laws are physically unsound; he then proceeds to argue that, in the particular case treated in his paper, they may all the same be expected to yield approximately correct results, even though the conditions for proportional loading are not completely fulfilled.

The present paper indicates a compromise designed to avoid this paradoxical situation. It is shown that segmentwise linear yield conditions used in conjunction with the appropriate flow rules assure the mathematical advantages of the total stress-strain laws without sacrificing the essential features of the incremental laws.

The following section is devoted to some models of the mechanical behavior of plastic solids, and the advantages of segmentwise linear yield conditions and the associated flow rules are discussed with the aid of these models. In section 3 the bending of a simply supported circular plate by a uniformly distributed transverse load is treated as an example. The rigid, work-hardening plate material is supposed to obey Tresca's yield condition and the associated flow rule.

2 Models of the Mechanical Behavior of Plastic Solids

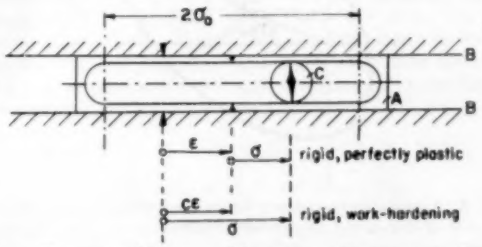

Fig. 1 Kinematic Model of Mechanical Behavior of Rigid, Plastic Solids in Uniaxial Stress

Fig. 1 shows the simple model which the author used in his James Clayton Lecture (1)[3] to represent the mechanical behavior of plastic solids under uniaxial stress. The slotted plate A slides freely between horizontal frictionless guides B. The pin C slides without friction in the slot and imparts a motion of the plate only when it engages with one or the other end of the slot. Each of the plate A, the guides B, and the pin C carries a vertical index and these indexes are originally aligned. For the rigid, perfectly plastic solid with the stress-strain diagram of Fig. 2(*a*), the displacement of the pin index with respect to the plate index represents the stress σ, and the displacement of the plate index with respect to the guide index represents the strain ϵ, the total free displacement of the pin in the slot corresponding to twice the yield stress σ_0.

The same device can be used for the rigid, work-hardening solid with the stress-strain diagram of Fig. 2(*b*). The manner in which stress and strain are represented in this case is indicated in Fig. 1, where c denotes the constant slope of the work-hardening branch of the stress-strain diagram.

Fig. 3 shows a similar model which represents the mechanical behavior of plastic solids in plane stress with fixed principal axes. The principal stresses are denoted by σ_1 and σ_2, and the corresponding strains by ϵ_1 and ϵ_2. The elliptical frame is mounted so that it can perform any translation in its plane. The perfectly smooth pin P is free to move inside the frame and imparts a motion to the frame only when it pushes against it.

---

[1] The results presented in this paper were obtained in the course of research sponsored by the Office of Naval Research, under Contract Nonr-562(10), with Brown University.

[2] Chairman, Physical Sciences Council, Brown University. Mem. ASME.

Presented at the National Applied Mechanics Division Conference, Urbana, Ill., June 14–16, 1956, of The American Society of Mechanical Engineers.

Discussion of this paper should be addressed to the Secretary, ASME, 29 West 39th Street, New York, N. Y., and will be accepted until January 10, 1957, for publication at a later date. Discussion received after the closing date will be returned.

Note: Statements and opinions advanced in papers are to be understood as individual expressions of their authors and not those of the Society. Manuscript received by ASME Applied Mechanics Division, March 12, 1956. Paper No. 56—APM-34.

[3] Numbers in parentheses refer to the Bibliography at the end of the paper.

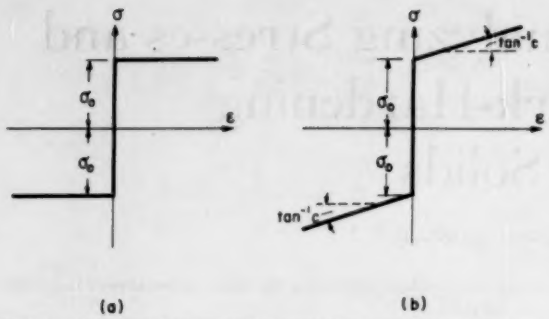

FIG. 2 (a) RIGID, PERFECTLY PLASTIC SOLID IN UNIAXIAL STRESS; (b) RIGID, WORK-HARDENING SOLID IN UNIAXIAL STRESS

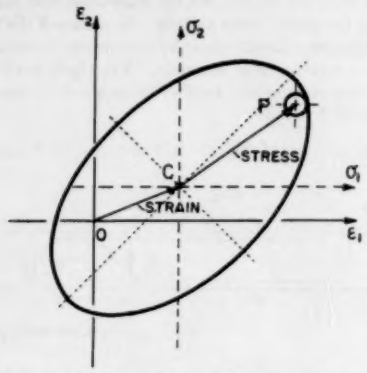

FIG. 3 KINEMATIC MODEL FOR RIGID, PERFECTLY PLASTIC SOLID IN PLANE STRESS

Consider first a rigid, perfectly plastic solid. Originally frame and pin are centered at the origin O of the ϵ_1, ϵ_2-plane. As the frame is displaced by the moving pin, the vector from the origin O to the center C of the frame has the components ϵ_1 and ϵ_2, and the vector from C to the center P of the pin has the components σ_1 and σ_2. The reader will readily verify that this model corresponds to the yield condition and flow rule of von Mises. Indeed, the shape of the frame is dictated by von Mises' yield condition (2); for plane stress this has the form

$$\sigma_1^2 + \sigma_2^2 - \sigma_1\sigma_2 = \sigma_0^2 \ldots\ldots\ldots\ldots\ldots [1]$$

where σ_0 is the yield stress in simple tension. Furthermore, in the absence of friction between frame and pin, the instantaneous translation of the frame is always directed along the exterior normal of the frame at the instantaneous point of contact between pin and frame. This relation between the position of the point of contact (stress) and the instantaneous direction of motion of the frame (strain rate) corresponds to the flow rule which the theory of the plastic potential (3) associates with the Yield Condition [1].

The manner in which the model of Fig. 1 can be used for both the rigid, perfectly plastic and the rigid, work-hardening solids suggests that a reasonable stress-strain law for a rigid, work-hardening solid in plane stress can be obtained from the model of Fig. 3 by interpreting the components of the vector OC as $c\epsilon_1$ and $c\epsilon_2$, and the components of the vector OP as σ_1 and σ_2, Fig. 4. This is obviously an incremental law. Given the states of stress and strain (positions of pin and frame) and an infinitesimal stress increment (displacement of pin), the model predicts a uniquely determined strain increment (displacement of frame), but various manners of stressing leading to the same final state of stress (various paths of the pin leading to the same final position) will result in different final states of strain (final positions of the frame).

It is precisely this dependence of the strain on the history of stressing that makes the incremental laws mathematically inconvenient, because the final state can be determined only by following the loading process step by step. This cumbersome procedure is avoided when total laws are used, which establish a direct relation between the final states of stress and strain. Total laws, however, are physically unsound (4).

The mechanical behavior indicated by the model of Fig. 4 will not change radically if the elliptical frame is replaced by an inscribed polygonal frame provided that the polygon has a sufficiently large number of vertexes which are reasonably spaced along the ellipse, Fig. 5. From the mathematical point of view there is, however, an important difference between the stress-strain laws corresponding to the two types of frame. As long as the pin presses against one and the same side of the polygonal frame, the rectilinear translation of the frame is directed along the exterior normal of this side. The instantaneous position of the frame then depends only on (a) its position when the pin began to push against the considered side, and (b) the instantaneous position of the pin. Similarly, as long as the pin remains engaged with a corner of the frame, the curvilinear translation of the frame is identical with that of the pin. In this case the instan-

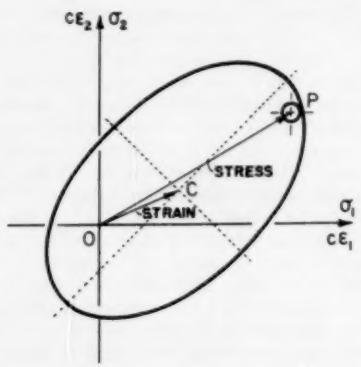

FIG. 4 KINEMATIC MODEL FOR RIGID, WORK-HARDENING SOLID IN PLANE STRESS

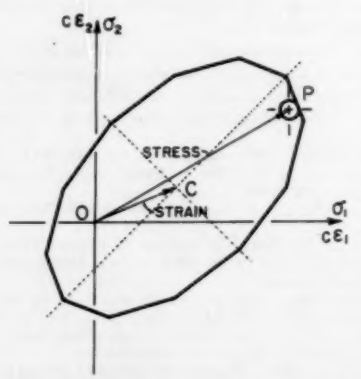

FIG. 5 POLYGONAL APPROXIMATION TO ELLIPTIC FRAME OF MODEL IN FIG. 4

taneous position of the frame depends only on (*a*) its position when the pin first engaged with the corner, and (*b*) the instantaneous position of the pin.

The use of a polygonal frame, i.e., the use of a segmentwise linear yield condition, thus results in a limited independence of the strain from the history of stressing. While this independence allows total stress-strain laws to be used "in the small," the fact that the pin will as a rule come in contact with several sides and corners of the frame requires the successive use of different types of total laws. "In the large," segmentwise linear yield conditions and the associated flow rules therefore lack the physically unsound features of total stress-strain laws.

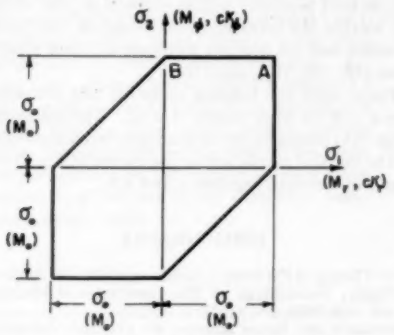

FIG. 6 TRESCA YIELD CONDITION

Rather than being merely a mathematically convenient approximation, a segmentwise linear yield condition may represent the actual yield limit of a plastic material. For plane stress with fixed principal axes, for instance, Tresca's yield condition (5) is represented by the hexagon in Fig. 6.

3 EXAMPLE

As an example illustrating the use of a segmentwise linear yield condition and the associated flow rule for a rigid, work-hardening material, consider a simply supported circular plate of the radius R and the uniform thickness h that is subjected to a uniformly distributed transverse load of the intensity p per unit area of the horizontal middle plane of the plate.

In the spirit of the technical theory of the bending of plates, the states of stress and strain at a generic point of the middle surface of the plate are specified by the radial and circumferential bending moments M_r and M_φ, and the radial and circumferential curvatures κ_r and κ_φ. The bending moments must satisfy the equation of equilibrium

$$(rM_r')' - M_\varphi = -pr^2/2 \quad \ldots\ldots [2]$$

where the prime denotes differentiation with respect to r. In terms of the deflection $w = w(r)$ of the middle surface, the curvatures are given by

$$\kappa_r = -w'', \quad \kappa_\varphi = -w'/r \quad \ldots\ldots [3]$$

So that earlier results regarding the incipient plastic flow can be used, it will be assumed that for the rigid, work-hardening plate the relation between the bending moments and curvatures is represented by a pin-frame model with the hexagonal frame in Fig. 6, where the labels in parentheses should be used and $M_0 = \sigma_0 h^2/4$. According to Hopkins and Prager (6), plastic flow then begins when the load reaches the intensity

$$p_0 = 6M_0/R^2 \quad \ldots\ldots [4]$$

and the bending moments at this instant are distributed along the radius according to

$$M_r = M_0\left(1 - \frac{r^2}{R^2}\right), \quad M_\varphi = M_0 \quad \ldots\ldots [5]$$

At the onset of plastic flow, the pin of the model corresponding to a generic value of r between 0 and R thus is in contact with the side AB of the frame in Fig. 6; for the models corresponding to $r = 0$ and $r = R$, the pins are at A and B, respectively. This situation may be briefly described by the statement that, at the onset of plastic flow, the plate center is in regime A, the plate edge in regime B, and the rest of the plate in regime AB.

A plate element that enters into the plastic state in regime AB will have

$$\kappa_r = 0, \quad M_\varphi = M_0 + c\kappa_\varphi \quad \ldots\ldots [6]$$

as long as it remains in this regime; it will change to regime A when M_r reaches the value M_0; thereafter

$$M_r = M_0 + c\kappa_r, \quad M_\varphi = M_0 + c\kappa_\varphi \quad \ldots\ldots [7]$$

as long as the element remains in regime A.

Assume first that the neighborhood of the plate center remains in regime AB as the load intensity increases beyond p_0. According to the first Equation [6], the deformed middle surface of the plate would then have a conical vertex at $r = 0$. The deflection of a work-hardening plate cannot have this singularity; a central region of gradually increasing radius ρ must therefore enter into regime A as the load p grows beyond p_0. According to Equations [6], [7], and [3], we therefore have

$$M_r = M_0 - cw'', \quad M_\varphi = M_0 - cw'/r \text{ for } r \le \rho \quad \ldots\ldots [8]$$

$$\kappa_r = 0, \quad M_\varphi = M_0 - cw'/r \text{ for } r \ge \rho \quad \ldots\ldots [9]$$

When Equations [8] are substituted into the equation of equilibrium, Equation [2], the following differential equation for w is obtained

$$rw''' + w'' - \frac{w'}{r} = \frac{pr^2}{2c} \quad \text{for} \quad r \le \rho \quad \ldots\ldots [10]$$

The first Equations [9] and [3], on the other hand, yield

$$w'' = 0 \quad \text{for} \quad r \ge \rho \quad \ldots\ldots [11]$$

The differential Equations [10] and [11] must be integrated under the following boundary and transition conditions: $w' = 0$ at $r = 0$, $w = 0$ at $r = R$, and w, w', and w'' must all be continuous at $r = \rho$. Thus

$$w = \begin{cases} \dfrac{p}{64c}(8\rho^2 R - 3\rho^4 - 6\rho^2 r^2 + r^4) & \text{for} \quad r \le \rho \\ \dfrac{p\rho^2}{8c}(R - r) & \text{for} \quad r \ge \rho \end{cases} \quad \ldots\ldots [12]$$

Substitution of the second Equation [12] into the second Equation [9] now furnishes

$$M_\varphi = M_0 + \frac{p\rho^2}{8r} \quad \text{for} \quad r \ge \rho \quad \ldots\ldots [13]$$

When this is in turn substituted into the equation of equilibrium, Equation [2], there results the following differential equation for M_r

$$(rM_r)' = M_0 + \frac{p\rho^2}{8r} - \frac{pr^2}{2} \quad \text{for} \quad r \ge \rho \quad \ldots\ldots [14]$$

which must be integrated under the condition that $M_r = 0$ for $r = R$. Thus

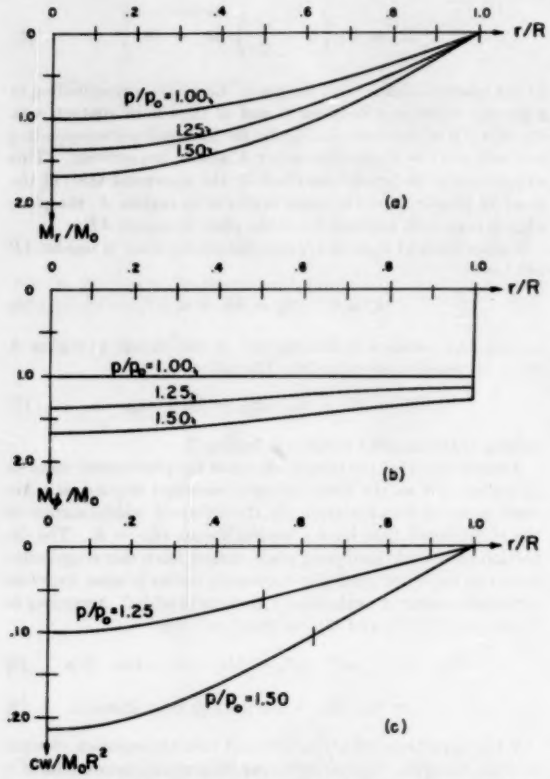

FIG. 7 SIMPLY SUPPORTED CIRCULAR PLATE OF RIGID, WORK-HARDENING MATERIAL UNDER UNIFORMLY DISTRIBUTED LOAD p [(a) Radial bending moments M_r; (b) circumferential bending moments M_φ; (c) deflections w; (M_0 = fully plastic moment; $p_0 = 6M_0/R^2$).]

$$M_r = M_0\left(1 - \frac{R}{r}\right) + \frac{p\rho^2}{8r}\log\frac{r}{R} + \frac{pR^2}{6}\left(\frac{R}{r} - \frac{r^2}{R^2}\right) \quad \text{for} \quad r \geq \rho \ldots\ldots [15]$$

Since $r = \rho$ is the boundary between regimes A and AB, the radial bending moment must have the value M_0 for $r = \rho$. In conjunction with Equation [15] this condition furnishes the following relation between ρ and p

$$p = \frac{24M_0}{R^2}\left\{3\frac{\rho^2}{R^2}\ln\frac{\rho}{R} + 4\left(1 - \frac{\rho^2}{R^2}\right)\right\}^{-1} \ldots\ldots [16]$$

For a given load intensity p that exceeds p_0, the value of ρ is found by solving the transcendental Equation [16] numerically. The deflection and the bending moments are then obtained from Equations [12], [8], [13], and [15].

Figs. 7(a–c) show the bending moments and the deflection as functions of r/R for some values of p/p_0. The nonuniformity of M_φ in Fig. 7(b) indicates the nonuniform work-hardening of the plate. The vertical marks across the curves of Fig. 7(c) indicate the boundaries between regimes A and AB.

BIBLIOGRAPHY

1 "The Theory of Plasticity: A Survey of Recent Achievements," by W. Prager, Proceedings of The Institution of Mechanical Engineers, vol. 169, 1955, pp. 41–57.

2 "Mechanik der festen Koerper im plastisch deformablen Zûstand," by R. von Mises, Gesellschaft der Wissenschaften zu Göttingen, Mathematisch-Physikalische Klasse, Nachrichten, 1913, pp. 582–592.

3 "Mechanik der plastischen Formaenderung von Kristallen," by R. von Mises, *Zeitschrift für angewandte Mathematik und Mechanik*, vol. 8, 1928, pp. 161–185.

4 "Theory of Plastic Flow Versus Theory of Plastic Deformation," by W. Prager, *Journal of Applied Physics*, vol. 19, 1948, pp. 540–543.

5 "Mémoire sur l'écoulement des corps solides," by H. Tresca, Mémoires présentés par divers savants a l'Académie des Sciences, vol. 18, 1868, pp. 733–799.

6 "The Load Carrying Capacities of Circular Plates," by H. G. Hopkins and W. Prager, *Journal of the Mechanics and Physics of Solids*, vol. 2, 1953, pp. 1–13.

Three "Neutral" Loading Tests

By S. S. GILL,[1] MANCHESTER, ENGLAND

Three tests have been carried out using hollow tubes of alpha brass subjected to combined torsion and internal pressure. An initial torque was applied sufficient to cause plastic deformation, and then the torque was decreased and the internal pressure increased to keep the octahedral shear stress constant in two tests and the maximum shear stress constant in the third test. These loading paths were chosen because they would be neutral loading if the material obeyed the von Mises-Hencky or Guest yield criterion, respectively. Shear strain, axial, and circumferential strain were measured. All three tests gave some plastic strain during the "neutral" loading, but the constant maximum shear-stress loading gave much larger plastic strains than the constant octahedral stress loading. The plastic-strain increment vectors have been plotted to illustrate their direction relative to the loading path.

Nomenclature

The following nomenclature is used in the paper:

$\sigma_1, \sigma_2, \sigma_3$ = principal stresses
σ_s = longitudinal stress
σ_t = circumferential stress
τ = shear stress
ϵ_s = longitudinal strain
ϵ_t = circumferential strain
γ = shear strain
p = internal pressure, psi
W = load on torque arm, lb
T = torque = $24W$ lb-in.
d_i = internal diameter of tube
d_m = mean diameter of tube
t = tube-wall thickness
τ_0 = octahedral shear stress

$$= \frac{1}{3}\sqrt{(\sigma_1 - \sigma_2)^2 + (\sigma_2 - \sigma_3)^2 + (\sigma_3 - \sigma_1)^2}$$

τ_G = maximum shear stress

$$= \frac{1}{2}(\sigma_1 - \sigma_3) \qquad \sigma_1 > \sigma_2 > \sigma_3$$

G = shear modulus
ν = Poisson's ratio

Other symbols are defined when they appear in the text.

Introduction

Neutral loading tests have often been discussed in the investigation of plastic stress-strain relationships. In order to satisfy the condition of "continuity" (Handelman, Lin, Prager, 1947),[2] an increment of stress which lies in the yield surface must produce no plastic strain. Hence, by carrying out a neutral loading test in which the state of stress lies on the yield surface, the change in strain should be entirely elastic. This is, of course, the prediction of an incremental stress-strain law.

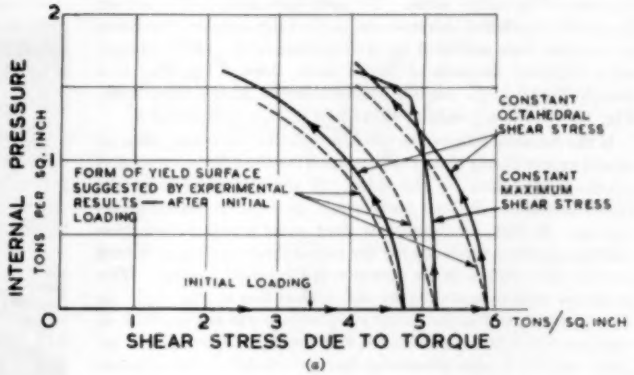

(a)

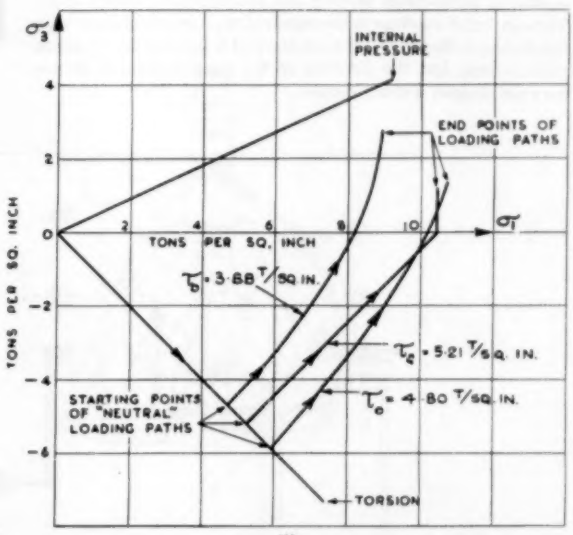

(b)

Fig. 1 Loading Paths for the Three Tests

Another problem to be investigated in the derivation of plastic stress-strain relationships is the dependence of the yield criterion on the history of loading and the possible existence of corners or

---

[1] Lecturer in Mechanical Engineering, College of Technology, University of Manchester.

Presented at the National Applied Mechanics Division Conference, Urbana, Ill., June 14–16, 1956, of The American Society of Mechanical Engineers.

Discussion of this paper should be addressed to the Secretary, ASME, 29 West 39th Street, New York, N. Y., and will be accepted until January 10, 1957, for publication at a later date. Discussion received after the closing date will be returned.

Note: Statements and opinions advanced in papers are to be understood as individual expressions of their authors and not those of the Society. Manuscript received by ASME Applied Mechanics Division, October 7, 1955. Paper No. 56—APM-18.

[2] "On Mechanical Behavior of Metals in Strain-Hardening Range," by G. H. Handelman, C. C. Lin, and W. Prager, *Quarterly of Applied Mathematics*, vol. 4, 1947, pp. 397–407.

pointed vertexes in the yield surface produced by the previous loading. Simple isotropic work-hardening theories assume that the yield surface increases in size but remains constant in shape during loading.

The experiments described here were carried out to compare the von Mises-Hencky and Guest (maximum shear stress) yield criterion for the material used. The tubes were initially loaded in torsion to cause plastic deformation, and then the torsion was decreased and the internal pressure increased to keep either the octahedral shear stress constant in two tests or the maximum shear stress constant in the third test. In one constant octahedral shear-stress test, the torque was reduced to less than half its initial value, but in the other two tests the torque was only reduced to about three quarters of its initial value. No tests have been carried out on the yield criterion of this material in the fully annealed condition so that the tests represent an investigation of the yield criterion after different amounts of initial shear stress. Fig. 1(*a*) is a sketch showing the loading paths followed in the three tests. Fig. 1(*b*) shows a principal stress plot of the loading paths.

If the material follows the von Mises-Hencky criterion, then we would expect purely elastic deformation for the first two tests and plastic deformation for the third. If the material follows the Guest criterion, all three tests would give purely elastic deformation. In fact, all three tests show some plastic deformation which suggests a tendency for the initial shear loading to stretch out the yield surface in the direction of the initial loading. This is shown diagrammatically by the dashed line in Fig. 1(*a*). In view of the fact that the initial yield surface was not established, this suggestion is not conclusive, but the path dependence of the yield surface is also illustrated by the results of the constant maximum shear-stress loading (see comments on results later). The number of readings in the region of the initial loading point is insufficient to investigate the existence of a pointed vertex on the yield surface, but the direction of the strain-increment vectors does not suggest a sharp corner.

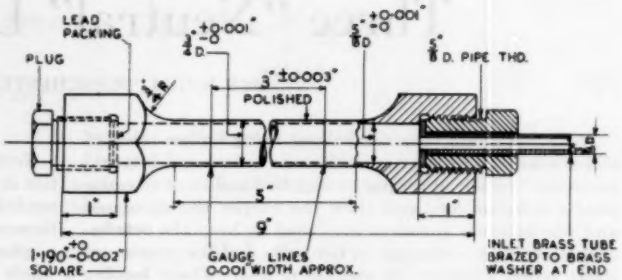

FIG. 2 SPECIMEN

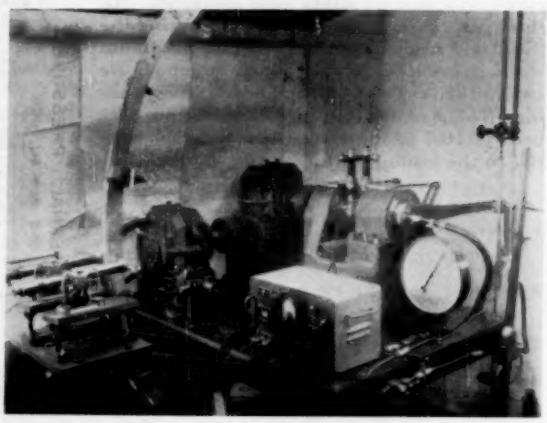

FIG. 4 TEST APPARATUS

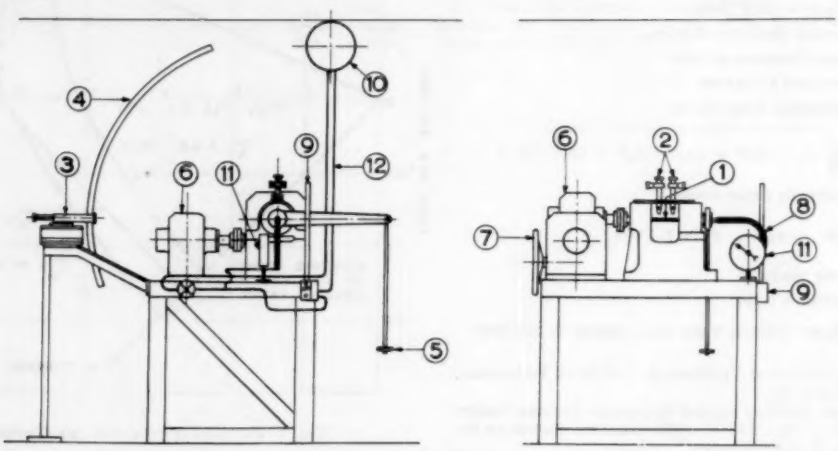

FIG. 3 TEST APPARATUS

Experimental Details

Materials and Specimens. The material used was a nominally pure 70-30 alpha brass. The composition was as follows: Cu 71.78 per cent, Zn 28.07 per cent, Sn 0.08 per cent, Fe 0.07 per cent. It was annealed in a sealed box at 400 C for 1½ hr and allowed to cool in the furnace.

The test specimen for combined torsion and internal-pressure tests is shown in Fig. 2. The ratio of wall thickness to radius is relatively high but this had to be accepted in view of the difficulty of machining the long ⅛-in-diam bore and obtaining good concentricity.

Apparatus. A diagrammatic sketch of the apparatus is shown in Fig. 3 and a photograph in Fig. 4. Two roller bearings were provided in the housing for the torque arm so that there was no endwise restraint on the change of length of the specimen.

The specimen was held in square sockets 0.062 in. larger than the square on the end of the specimen. Ground pads 0.031 in. thick were inserted on each side to hold the specimen tightly in place.

Strain-Measuring Apparatus

Longitudinal Strain. The movement of each of two gage lines marked on the specimen was measured by a microscope with a micrometer eyepiece. The squareness of the gage lines to the axis of the specimen was checked before each test. The sensitivity was approximately 1×10^{-5} strain on a 3-in. gage length.

Diametral Strain. The change of diameter was measured by an electrical capacitance extensometer especially designed for the purpose, Fig. 5. A change in diameter changed the air gap between two sets of condenser plates connected in parallel. The change of capacitance was measured by means of a Fielden ca-

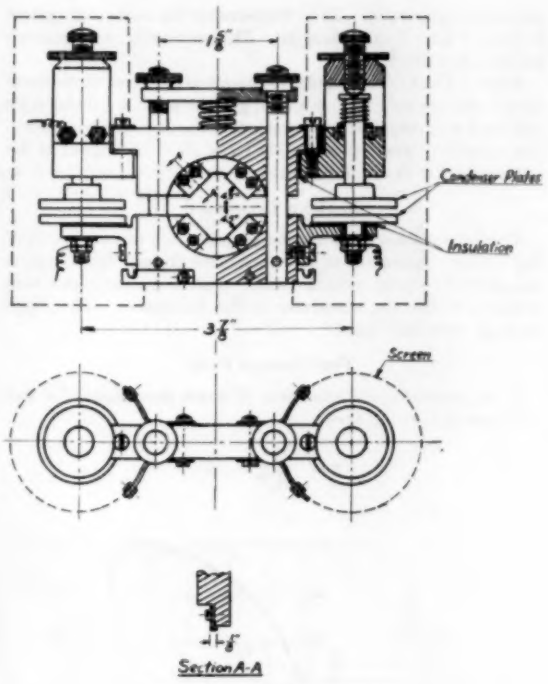

Fig. 5 Lateral Extensometer

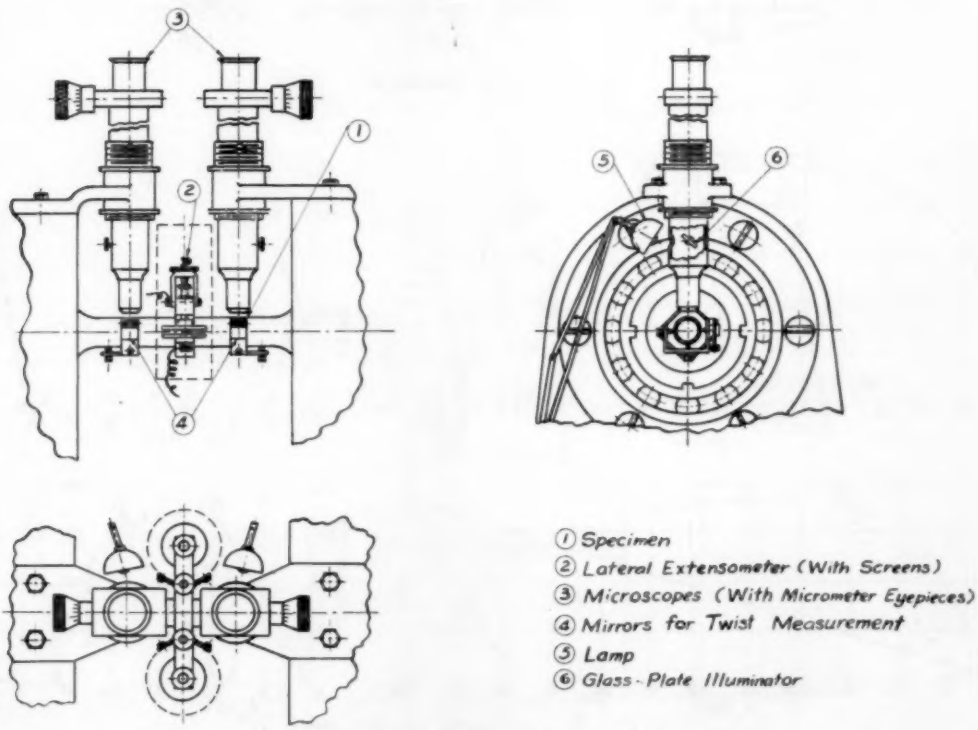

Fig. 6 Arrangement of Strain-Measuring Instruments

pacitance comparator. This extensometer was calibrated against a Lamb's lateral extensometer. The sensitivity was approximately 1.6×10^{-4}.

Angle of Twist. The angular rotation was measured by means of torsion mirrors attached on a 3-in. gage length. A circular scale was used with its center of curvature on the axis of the specimen. The sensitivity was approximately 1.7×10^{-4}. A diagram of the arrangement is shown in Fig. 6.

Loading Technique

Throughout these tests a standard procedure was used in loading. After application of any increment of load the specimen was allowed to creep until the strain-measuring instruments were constant within the sensitivity of the instrument. The strain readings were then taken.

The Loading Path

If we assume a uniform state of stress throughout the wall thickness of the tube, then

$$\tau = \frac{2T}{\pi d_m^2 t} = aT$$

$$\sigma_t = \frac{pd_i}{2t} = bp$$

$$\sigma_z = \frac{pd_i^2}{4d_m t} = cp$$

where $a = 21.54$, $b = 5$, and $c = 2.273$ for the specimen dimensions.

The radial stress is taken as zero since it is zero at the outer surface of the tube where the strain measurements are made.

For $\tau_\theta = \text{const} = K_\theta$, say the relation between p and T is given by

$$2(b^2 + c^2 - bc)p^2 + 6a^2T^2 = 9K_\theta^2$$

For $\tau_G = \text{const} = K_G$, say the relation between p and T is given by

$$(b - c)^2p^2 + 4a^2T^2 = 4K_G^2 \quad \text{for} \quad p \leqslant \frac{aT}{\sqrt{bc}}$$

and

$$a^2T^2 - bcp^2 + 2(b + c)K_Gp = 4K_G^2 \text{ for } p \geqslant \frac{aT}{\sqrt{bc}}$$

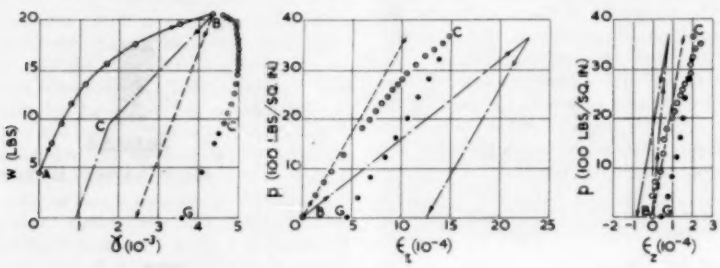

Fig. 7 $\tau_\theta = 3.88$ Tons/Sq In.

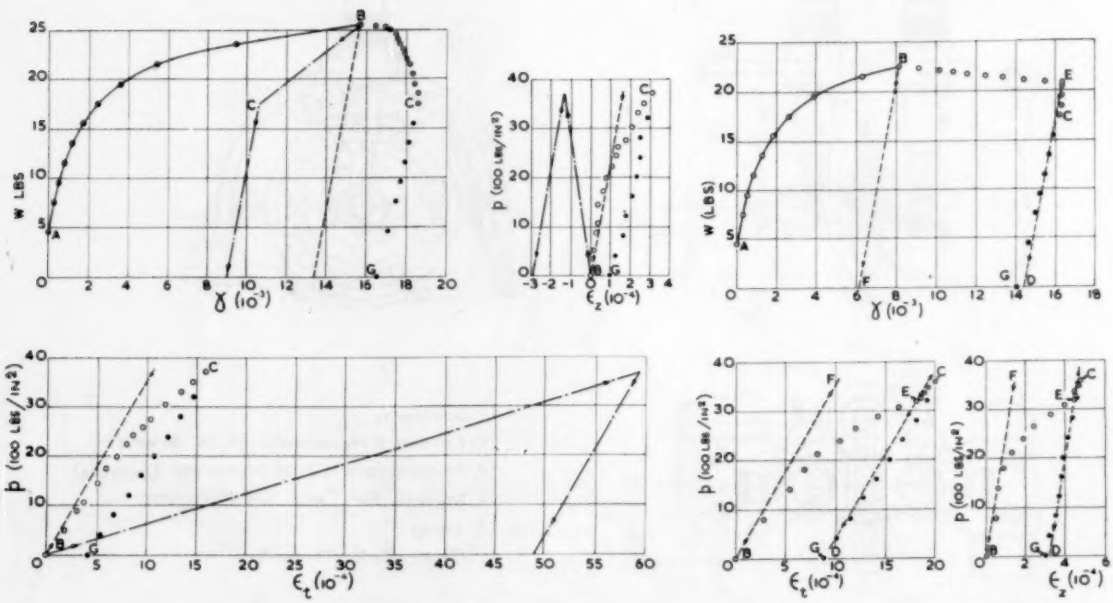

Fig. 8 $\tau_\theta = 4.80$ Tons/Sq In.

Fig. 9 $\tau_G = 5.21$ Tons/Sq In.

Results

Figs. 7, 8, 9 show the curves of the load and strain variables for the three tests. These diagrams also show the strains predicted by a finite and incremental stress-strain law for the loading path:

Fig. 7 $\tau_0 = 3.88$ tons per sq in.

Fig. 8 $\tau_0 = 4.80$ tons per sq in.

A–B is initial loading

B–C is constant τ_0 loading

C–G is unloading

The dashed line gives the prediction of an incremental law, which for this loading path reduces to Hooke's law.

The chain line gives the predictions of the following finite law

$$\epsilon_t = \frac{1}{E}(\sigma_t - \nu\sigma_s) + H\left(\sigma_t - \frac{\sigma_s}{2}\right)$$

$$\epsilon_s = \frac{1}{E}(\sigma_s - \nu\sigma_t) + H\left(\sigma_s - \frac{\sigma_t}{2}\right)$$

$$\gamma = \frac{\tau}{G} + 3H\tau$$

where

$$H = \frac{\gamma^{(B)} - \frac{\tau^{(B)}}{G}}{3\tau^{(B)}}$$

and is constant for the neutral loading. (B) refers to the values of γ and τ at the point B.

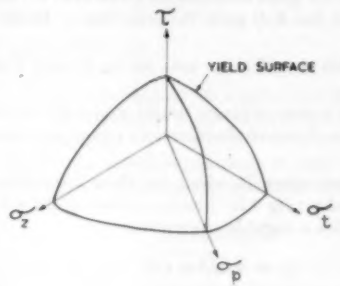

Fig. 10

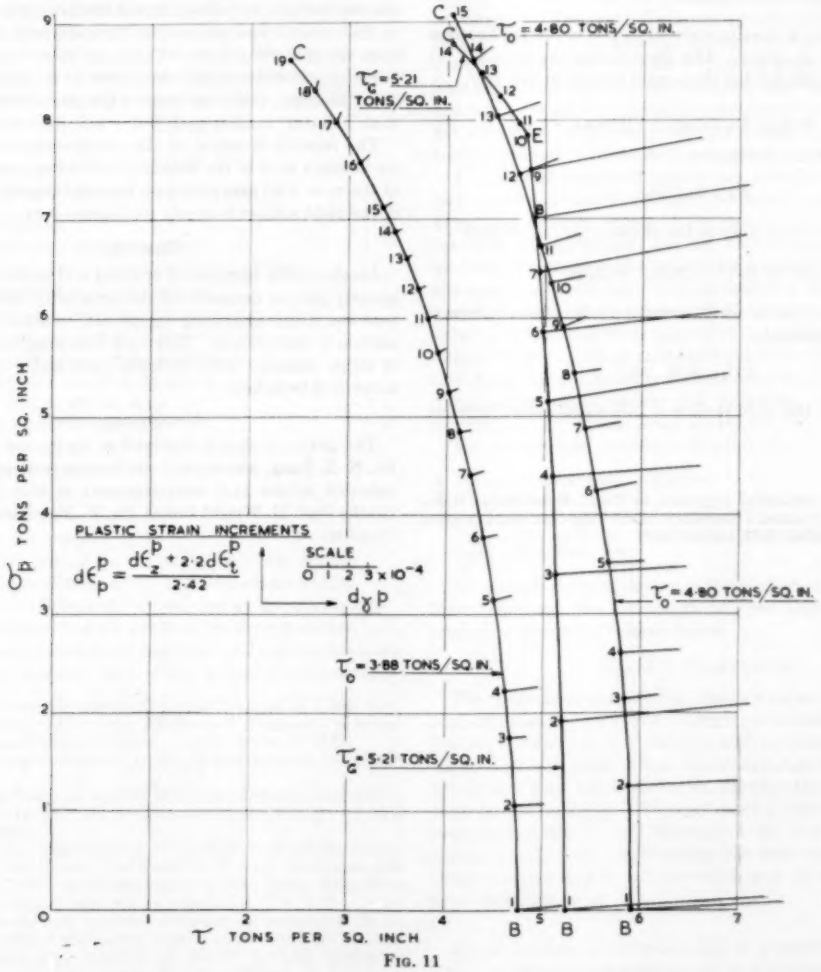
τ = 4·80 TONS/SQ. IN.
τc = 5·21 TONS/SQ. IN.
PLASTIC STRAIN INCREMENTS
SCALE
τ = 4·80 TONS/SQ. IN.
τ = 3·88 TONS/SQ. IN.
τc = 5·21 TONS/SQ. IN.
τ TONS PER SQ. INCH
TONS PER SQ. INCH

Fig. 11

Fig. 9 $\tau_G = 5.21$ tons per sq in.
A–B is initial loading
B–C constant τ_G loading
C–G unloading

At E, $p = \dfrac{aT}{\sqrt{bc}}$

The dashed line B-F gives the prediction of Hooke's law through B, and the dashed line E-D gives the prediction of Hooke's law through E.

Young's modulus = 6.67×10^3 tons per sq in. and Poisson's ratio = 0.33.

Since Figs. 7, 8, 9 all show plastic strains, it is useful to consider the direction of the plastic-strain-increment vectors relative to the yield surface.

Consider a stress space in which the three co-ordinate axes represent τ, σ_l, and σ_s (Fig. 10). Since σ_l/σ_s is constant = 5/2.273 = 2.2, we can define a variable σ_p such that

$$\sigma_p = \sqrt{\sigma_l^2 + \sigma_s^2}$$

$$= 2.42\sigma_s = 5.5\ p$$

We may consider a two-dimensional section of the yield surface with co-ordinates σ_p and τ. The three curves shown in Fig. 11 are the loading paths for the three tests plotted in this way.

Strain-Increment Vectors

If the plastic-strain increments

$$d\gamma^p,\ d\epsilon_l^p,\ d\epsilon_s^p$$

are plotted on the same axes as the stresses τ, σ_l, σ_s so that

$$dW = \tau d\gamma^p + \sigma_l d\epsilon_l^p + \sigma_s d\epsilon_s^p$$

is the increment of plastic work, then the plastic-strain-increment vector with components

$$d\gamma^p,\quad d\epsilon_l^p,\quad d\epsilon_s^p$$

will be normal to the yield surface in this stress space (Drucker, 1951).[8]

In this case

$$dW = \tau d\gamma^p + \sigma_s\left(d\epsilon_s^p + \frac{5}{2.273}d\epsilon_l^p\right)$$

$$= \tau d\gamma^p + \frac{\sigma_p}{2.42}(d\epsilon_s^p + 2.2 d\epsilon_l^p)$$

$$= \tau d\gamma^p + \sigma_p d\epsilon_p^p$$

Hence the plastic-strain increments to be plotted for the same axes as τ and σ_p are

$$d\gamma^p \text{ and } d\epsilon_p^p$$

where

$$d\epsilon_p^p = \frac{d\epsilon_s^p + 2.2\ d\epsilon_l^p}{2.42}$$

These are shown in Fig. 11. Note that the strain-increment vector at point 1 corresponds to the stress increment 1–2, the strain-increment vector at point 2 corresponds to the stress increment 2–3, and so on.

Comments on Results

The fact that the constant τ_0 tests give small plastic strain suggests that the yield surface is elongated slightly in the direction of the initial shear stress, as indicated in Fig. 1(a). The strain-increment vectors, in general, do not deviate much from the normal to the constant τ_0-curve so that the τ_0-curve is not very different from the true yield curve. The constant τ_G test obviously gives larger plastic strains and corresponds to loading of the material. Note, however, that from point E the plastic strains are zero, and that "neutral" loading path E-C is definitely elastic unloading.

The relative direction of the plastic-strain-increment vectors for points 4 to 9 of the constant τ_G-loading and for points 6–13 of the $\tau_0 = 4.80$ tons per sq in. loading is significant. The shape of the yield surface is clearly path-dependent.

Conclusion

Much smaller increments of stress will be required with consequently greater demands on the sensitivity and accuracy of the load and strain-measuring equipment, to investigate the loading surface in this manner. This work is in progress with a test piece of larger diameter/wall thickness ratio and with a more refined measuring technique.

Acknowledgment

The author is deeply indebted to his former research student, Dr. N. S. Yang, who carried out these experiments. For their invaluable advice and encouragement in this work the author thanks Prof. H. Wright Baker, Dr. W. Merchant, and Prof. D. C. Drucker.

[8] "A More Fundamental Approach to Plastic Stress-Strain Relations," by D. C. Drucker, Proceedings of the First National Congress of Applied Mechanics, 1951, pp. 487–491.

A Method for Determining the Flexural Effects of Statically Loaded Beams on Multiple Elastic Supports

By R. A. DI TARANTO,[1] PHILADELPHIA, PA.

Herein is presented a means for calculating the static deflections, slopes, moments, and shears of a nonuniform beam on two supports for any end conditions and on three simple supports when subjected to concentrated loads and/or concentrated moments. The method is an extension of a simple tabular procedure as used by Myklestad (1)[2] for use on a desk calculator or electronic digital computer. The procedure is such that it may be easily carried out by one who need not have any knowledge of beam theory. Influence coefficients may be easily and directly calculated for nonuniform beams on two and three elastic supports. The two-support beam is formulated for simply supported one overhang, two supports with linear and torsional springs, and fixed-fixed end conditions. Extensions of this method to any other boundary conditions are indicated.

Nomenclature

The following nomenclature is used in the paper:

n = station number
r = station number of right support
b = station number of last station to left of beam
c = station number of center support
l_n = length of beam between station n and $n+1$
EI_n = average stiffness between station n and $n+1$
y_n = deflection of mass n from equilibrium
α_n = slope of elastic curve at station n
S_n = shear to left of station n
M_n = moment to left of station n
ϕ = slope at station 1
δ = deflection at station 1
P_R = shear at right support
P_c = shear at center support
P_b = shear at left support
f_{in} = slope coefficient of the ith unknown at nth station
g_{in} = deflection coefficient of ith unknown at nth station
G_{in}' = moment coefficient of ith unknown at the nth station
G_{in} = shear coefficient of ith unknown at the nth station
γ_j = an operator which multiplies shear and moment reactions at each support. It is zero if station under consideration is to right of jth support and is 1 if station under consideration is to left of jth support
F = applied load
M_R = external restraining moment at right support
M_b = external restraining moment at last support

Introduction

Myklestad (1) presents a method for calculating deflections and influence coefficients of nonuniform cantilever beams and simply supported beams with and without overhangs. To quote Dr. Myklestad: "The method consists of using elastic coefficients to find the difference in slopes at the two ends of the beam and also the difference in the deflections when the slope at one end is zero. The entire beam is then rotated about the support or end that has zero slope, until the boundary conditions at the other support are satisfied." A tabular procedure is used to obtain the deflections and influence coefficients.

The method presented herein uses a similar tabular method, but accounts for all but the initial boundary conditions in a set of linear equations in terms of the initial deflection, slope, and reactions at each support and the known imposed concentrated loading. The coefficients of the unknowns in this set of equations are quantities which have been calculated in the tables. A solution of this set of R equations with R unknowns can be obtained in terms of the coefficients calculated in the tables and the known imposed loading. These calculated values of the initial deflection and slopes and reactions at each support can be used in a set of linear equations to obtain the deflection, slope, shear, and moment at each station along the beam.

The specific cases formulated herein are:

A Beam on three elastic supports
B Two supports
  I Simply supported—one overhang
  II Two supports—torsion and linear springs at each support
  III Fixed-fixed beam

An example showing the use of the method on a fixed-fixed uniform beam and the agreement between this method and the analytical solution are shown herein.

General Formulation

The nonuniform beam of Fig. 1 has s number of supports and is statically loaded by a load F. This beam is idealized to a weightless beam divided into N stations, with a station located at each support, at each point of load application, and any other point at which one may be interested in knowing the deflection, slope, shear, and/or moment. The method of analysis takes the section between two stations and determines the deflection coefficients defined as follows: Cantilevering the section of the beam between station n and $(n+1)$ at station $(n+1)$ we obtain the deflection coefficients as

d_{Fn} = deflection at station n due to a unit load at station n
d_{Mn} = deflection at station n due to a unit moment at station n

---

[1] Engineer, Defense Electronic Products Division of Radio Corporation of America. Formerly, Mechanical Engineer, Westinghouse Aviation Gas Turbine Division. Assoc. Mem. ASME.

[2] Numbers in parentheses refer to the Bibliography at the end of the paper.

Presented at the National Applied Mechanics Division Conference, Urbana, Ill., June 14–16, 1956, of The American Society of Mechanical Engineers.

Discussion of this paper should be addressed to the Secretary, ASME, 29 West 39th Street, New York, N. Y., and will be accepted until January 10, 1957, for publication at a later date. Discussion received after the closing date will be returned.

Note: Statements and opinions advanced in papers are to be understood as individual expressions of their authors and not those of the Society. Manuscript received by ASME Applied Mechanics Division, November 7, 1955. Paper No. 56—APM-24.

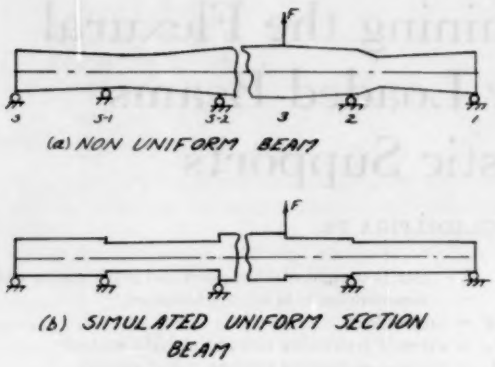

FIG. 1

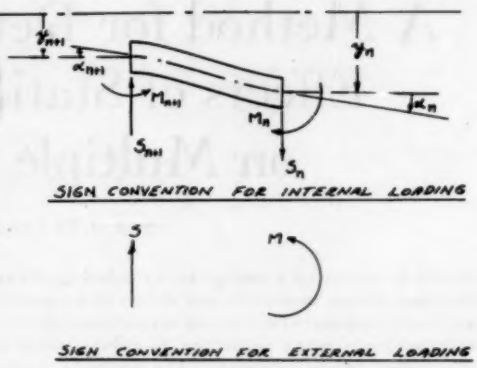

FIG. 2

v_{Mn} = slope at station n due to a unit moment at station n
v_{Pn} = slope at station n due to unit load at station n

Various methods for obtaining these deflection coefficients are available (1 to 4). One method is to take an average of the actual EI distribution thus considering each station connected by uniform stiffness beams. In this manner, the deflection coefficients become

$$d_{Pn} = \frac{l_n^3}{3(EI)_n}$$

$$d_{Mn} = v_{Pn} = \frac{l_n^2}{2(EI)_n}$$

$$v_{Mn} = \frac{l_n}{(EI)_n}$$

These may be tabulated, as in Table 1, to form a part of the data.

Taking a typical section, shown in Fig. 2, with the sign convention used herein, the relationship between deflection and slope at station $(n + 1)$ in terms of these quantities at station n may be obtained. These quantities and the shear S_n and the moment M_n are

$$\left.\begin{aligned} y_{n+1} &= y_n - l_n\alpha_{n+1} - S_n d_{Pn} - M_n d_{Mn} \\ \alpha_{n+1} &= \alpha_n - S_n v_{Pn} - M_n v_{Mn} \\ S_n &= -\gamma_j \sum_j^n S_i \\ M_n &= \sum_{i=1}^{(n-1)} l_i S_i - \gamma_j \sum_j^n M_j \end{aligned}\right\} \quad \ldots\ldots [1]$$

The deflection at station $n + 1$ is the superposition of the deflection at station n, the change in deflection from station n to $n + 1$ due to the rotation of this section considered rigid and the elastic deflection of this beam considered cantilevered at station $(n + 1)$, loaded at station n by a moment M_n and shear S_n.

The slope at station $(n + 1)$ is the superposition of the slope at station n and the change in slope between station n and $n + 1$ caused by the elastic rotation due to the shear S_n and moment M_n acting on the station n with the section considered cantilevered at station $(n + 1)$. The shear at station n is the sum of all reactions and loads at station n and to the right of station n.

The moment at station M_n is the sum of all moment contributions of reactions and loads to the right of station n plus all concentrated moments at station n and all stations to the right of station n.

TABLE 1

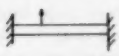

DATA SHEET

STA. n	l IN.	$EI \times 10^{-6}$ LB-IN.^{2}	$d_P \times 10^6$	$d_M = v_P \times 10^6$	$v_M \times 10^6$
1	5	20	2.08	.625	.25
2	5	20	↓	↓	↓
3	5	20	↓	↓	↓
4	5	20	↓	↓	↓
5	5	20	↓	↓	↓
6	5	20	↓	↓	↓
7					

$d_{Pn} = \frac{l_n^3}{3EI_n}$ $d_{Mn} = v_{Pn} = \frac{l_n^2}{2EI_n}$ $v_{Mn} = \frac{l_n}{EI_n}$

Assuming a linear relationship of these quantities in terms of the unknown initial deflection $\delta = y_1$, initial slope $\phi = \alpha_1$, reactions and imposed loadings P_j, we have

$$\left.\begin{aligned} y_n &= g_{\phi n}\phi + g_{\delta n}\delta + \gamma_j \sum_j^n g_{(Pj)n} P_j \\ \alpha_n &= f_{\phi n}\phi + f_{\delta n}\delta + \gamma_j \sum_j^n f_{(Pj)n} P_j \\ S_n &= G_{\phi n}\phi + G_{\delta n}\delta + \gamma_j \sum_j^n G_{(Pj)n} P_j \\ M_n &= G_{\phi n}'\phi + G_{\delta n}'\delta + \gamma_j \sum_j^n G_{(Pj)n}' P_j \end{aligned}\right\} \quad \ldots\ldots [2]$$

The symbols are similar to those used by Myklestad (1). For example, the symbol $g_{\phi n}$ is the coefficient of the unknown initial slope ϕ whose product contributes to the deflection at station n. The symbol $G_{\delta n}'$ is the coefficient of the unknown initial deflection δ whose product contributes to the moment at station n. The P_j include all reactions and external forces. These may be substituted in Equations [1] and coefficients of like terms equated to obtain the set of recurrence equations (see reference (6) for details)

Deflection Coefficients

$$\left.\begin{aligned} g_{\phi(n+1)} &= g_{\phi n} - l_n f_{\phi(n+1)} - \sum_{i=1}^{(n-1)} l_i G_{\phi i} d_{Mn} \\ g_{\delta(n+1)} &= g_{\delta n} - l_n f_{\delta(n+1)} - \sum_{i=1}^{(n-1)} l_i G_{\delta i} d_{Mn} \\ g_{(Pj)(n+1)} &= g_{(Pj)n} - l_n f_{(Pj)(n+1)} + d_{Fn} - \sum_{i=1}^{(n-1)} l_i G_{(Pj)i} d_{Mn} \\ g_{F(n+1)} &= g_{Fn} - l_n f_{F(n+1)} + d_{Fn} - \sum_{i=1}^{(n-1)} l_i G_{Fi} d_{Mn} \end{aligned}\right\} \quad \ldots [3]$$

Slope Coefficients

$$\left.\begin{aligned} f_{\phi(n+1)} &= f_{\phi n} - v_{Mn} \sum_{i=1}^{(n-1)} l_i G_{\phi i} \\ f_{\delta(n+1)} &= f_{\delta n} - v_{Mn} \sum_{i=1}^{(n-1)} l_i G_{\delta i} \\ f_{(Pj)(n+1)} &= f_{(Pj)n} + v_{Fn} - v_{Mn} \sum_{i=1}^{(n-1)} l_i G_{(Pj)i} \\ f_{F(n+1)} &= f_{Fn} + v_{Fn} - v_{Mn} \sum_{i=1}^{(n-1)} l_i G_{Fi} \end{aligned}\right\} \quad \ldots [4]$$

Moment Coefficients

$$\left.\begin{aligned} G_{\phi n}' &= \sum_{i=1}^{(n-1)} l_i G_{\phi i} \\ G_{\delta n}' &= \sum_{i=1}^{(n-1)} l_i G_{\delta i} \\ G_{(Pj)n}' &= \sum_{i=1}^{(n-1)} l_i G_{(Pj)i} \\ G_{Fn}' &= \sum_{i=1}^{(n-1)} l_i G_{Fi} \end{aligned}\right\} \quad \ldots [5]$$

Shear Coefficients

$$\left.\begin{aligned} G_{\phi n} &= 0 \\ G_{\delta n} &= 0 \\ G_{(Pj)n} &= -1 \\ G_{Fn} &= -1 \end{aligned}\right\} \quad \ldots [6]$$

These recurrence equations may be tabulated for ease of calculation in tables similar to those shown in Tables 2 and 3.

At this point, we have been able to account for the initial slope, initial deflection, and all reactions by computing their various coefficients at each station to the left of where they start, and carried these quantities along as unknowns. The imposed loading is carried along as an unknown reaction and its coefficients are computed station to station from its point of application to the left end of the beam.

To evaluate the unknown initial deflection and slope and all reactions (which constitute R unknowns) in terms of the known loading, we must set up R equations based on the remaining boundary conditions. These R equations will have as the coefficients of the unknowns, quantities previously calculated by the use of the recurrence equations. After solving for these unknowns in terms of the applied loading, the deflection, slope, moment, and shear at each station may be obtained by using Equations [2] where the coefficients at each station have been calculated in the tables and the unknown initial slope ϕ, initial deflection δ, moments at each support M_j, and shear at each support P_j have been determined. The method will be clearer as the various conditions are formulated.

TABLE 2

P TABLE

	1	2	3	4	5
n	$g_{Pn} \times 10^5$ = [1] - [2]	G_{Pn} = [2]	G'_{Pn} = [3] = [1] [2]	$f_{P(n+1)} \times 10^5$ = [4] = [3] + [2] [4]	$d_{Pn} \times 10^5$ = [5] = [4] + [2] [5]
1	0	-1.000	0	.625	1.045
2	-1.045	↓	-5	2.500	7.295
3	-8.34		-10	5.625	18.795
4	-28.135		-15	10.000	38.54
5	-66.625		-20	15.625	63.545
6	-130.22		-25	22.500	94.82
7	-225.04	↓	-30		

F TABLE

	1	2	3	4	5
n	$g_{Fn} \times 10^5$ = [1] - [2]	G_{Fn} = [2]	G'_{Fn} = [3] = [1] [2]	$f_{F(n+1)} \times 10^5$ = [4] = [3] + [2] [4]	$d_{Fn} \times 10^5$ = [5] = [4] + [2] [5]
5	0	-1.000	0	.625	1.045
6	-1.045	↓	-5	2.500	7.295
7	-8.340	↓	-10		

○—Denotes quantity in same row.
□—Denotes quantity in preceding row.

TABLE 3

M TABLE

	1	2	3	4	5
n	$g_{Mn} \times 10^5$ = [1] - [5]	G_{Mn} = [2]	G'_{Mn} = [3] = [1] [2] - [2]	$f_{M(n+1)} \times 10^5$ = [4] = [3] + [2] [4]	$d_{Mn} \times 10^5$ = [5] = [4] + [2] [5]
1	0	0	-1.000	.25	.625
2	-.625	↓	↓	.50	1.875
3	-2.500			.75	3.125
4	-5.625			1.00	4.375
5	-10.00			1.25	5.625
6	-15.625			1.50	6.875
7	-22.50				

○—Denotes quantity in same row.
□—Denotes quantity in preceding row.

THE CASE OF THREE ELASTIC SUPPORTS (FIG. 3)

As a first step to solving this problem the tables are calculated for ϕ the slope at station 1, δ the deflection at station 1, and P_R the shear at station 1, from station 1 to b; Table F, the external force, from the station of application to station b; and a P_c table from station c to station b. These tables yield the necessary quantities to set up the boundary conditions. The boundary conditions are

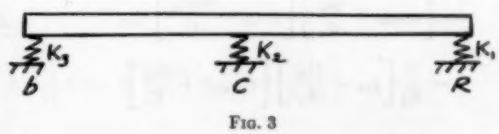

FIG. 3

$$\left.\begin{aligned} M_b &= 0 \\ K_1\delta &= P_R \\ K_2 y_c &= P_c \\ K_3 y_b &= P_b \end{aligned}\right\} \quad \ldots\ldots\ldots\ldots\ldots\ldots [7]$$

These may be written in terms of the calculated quantities

$$\left.\begin{aligned} K_3[g_{\phi c}\phi + g_{Rc}\delta + g_{(PR)bc}P_R + g_{Fc}F] &= P_c \\ K_3[g_{\phi b}\phi + g_{Rb}\delta + g_{(PR)b}P_R + g_{Fb}F] & \\ = G_{\phi b}\phi + G_{Rb}\delta + G_{(PR)b}P_R + G_{Fb}F & \\ K_1\delta &= P_R \\ M_b = 0 = G_{\phi b}'\phi + G_{Rb}'\delta & \\ + G_{(PR)b}'P_R + G_{(Pc)b}'P_c + G_{Fb}'F & \end{aligned}\right\} \ldots [8]$$

or

$$\left.\begin{aligned} g_{\phi c}\phi + \left[g_{(PR)c} + \frac{g_{Rc}}{K_1}\right]P_R - \frac{P_c}{K_2} &= -g_{Fc}F \\ \left[g_{\phi b} - \frac{G_{\phi b}}{K_3}\right]\phi & \\ + \left[g_{(PR)b} + \frac{g_{Rb}}{K_1} - \frac{G_{Rb}}{K_1K_3} - \frac{G_{(PR)b}}{K_3}\right]P_R & \\ + \left[g_{(Pc)b} - \frac{G_{(Pc)b}}{K_3}\right]P_c &= \left[\frac{G_{Fb}}{K_3} - g_{Fb}\right]F \\ G_{\phi b}'\phi + \left[\frac{G_{Rb}'}{K_1} + G_{(PR)b}'\right]P_R + G_{(Pc)b}'P_c &= -G_{Fb}'F \end{aligned}\right\} \ldots [9]$$

This may be written in matrix form as:

$$\begin{vmatrix} g_{\phi c} & \left[g_{(PR)c} + \frac{g_{Rc}}{K_1}\right] & -\frac{1}{K_2} \\ \left[g_{\phi b} - \frac{G_{\phi b}}{K_3}\right] & \left[g_{(PR)b} + \frac{g_{Rb}}{K_1} - \frac{G_{Rb}}{K_1K_3} - \frac{G_{(PR)b}}{K_3}\right] & \left[g_{(Pc)b} - \frac{G_{(Pc)b}}{K_3}\right] \\ G_{\phi b}' & \left[G_{(PR)b}' + \frac{G_{Rb}'}{K_1}\right] & G_{(Pc)b}' \end{vmatrix} \begin{vmatrix} \phi \\ P_R \\ P_c \end{vmatrix}$$

$$= \begin{vmatrix} -g_{Fc} \\ \left[\frac{G_{Fb}}{K_3} - g_{Fb}\right] \\ -G_{Fb}' \end{vmatrix} F \quad \ldots\ldots\ldots\ldots [10]$$

or letting

$$\left.\begin{aligned} \Delta = g_{\phi c}&\left[g_{(PR)b} + \frac{g_{Rb}}{K_1} - \frac{G_{Rb}}{K_1K_3} - \frac{G_{(PR)b}}{K_3}\right]G_{(Pc)b}' \\ &+ \left[g_{(PR)c} + \frac{g_{Rc}}{K_1}\right]\left[g_{(Pc)b} - \frac{G_{(Pc)b}}{K_3}\right]G_{\phi b}' \\ &- \frac{1}{K_2}\left[g_{\phi b} - \frac{G_{\phi b}}{K_3}\right]\left[G_{(PR)b}' + \frac{G_{Rb}'}{K_1}\right] \\ &+ \frac{1}{K_2}\left[g_{(PR)b} + \frac{g_{Rb}}{K_1} - \frac{G_{Rb}}{K_1K_3} - \frac{G_{(PR)b}}{K_3}\right]G_{\phi b}' \\ &- \left[g_{(PR)c} + \frac{g_{Rc}}{K_1}\right]\left[g_{\phi b} - \frac{G_{\phi b}}{K_3}\right]G_{(Pc)b}' \\ &- g_{\phi c}\left[g_{(Pc)b} - \frac{G_{(Pc)b}}{K_3}\right]\left[G_{(PR)b}' + \frac{G_{Rb}'}{K_1}\right] \end{aligned}\right\} \ldots [11]$$

$$\left.\begin{aligned} A = -g_{Fc}&\left[g_{(PR)b} + \frac{g_{Rb}}{K_1} - \frac{G_{Rb}}{K_1K_3} - \frac{G_{(PR)b}}{K_3}\right]G_{(Pc)b}' \\ &- \left[g_{(PR)c} + \frac{g_{Rc}}{K_1}\right]\left[g_{(Pc)b} - \frac{G_{(Pc)b}}{K_3}\right]G_{Fb}' \\ &- \frac{1}{K_2}\left[\frac{G_{Fb}}{K_3} - g_{Fb}\right]\left[G_{(PR)b}' + \frac{G_{Rb}'}{K_1}\right] \\ &- \frac{1}{K_2}\left[g_{(PR)b} + \frac{g_{Rb}}{K_1} - \frac{G_{Rb}}{K_1K_3} - \frac{G_{(PR)b}}{K_3}\right]G_{Fb}' \\ &- \left[g_{(PR)c} + \frac{g_{Rc}}{K_1}\right]\left[\frac{G_{Fb}}{K_3} - g_{Fb}\right]G_{(Pc)b}' \\ &+ g_{Fc}\left[G_{(PR)b}' + \frac{G_{Rb}'}{K_1}\right]\left[g_{(Pc)b} - \frac{G_{(Pc)b}}{K_3}\right] \end{aligned}\right\} \ldots [11] \text{ (cont.)}$$

$$\left.\begin{aligned} B = g_{\phi c}&\left[\frac{G_{Fb}}{K_3} - g_{Fb}\right]G_{(Pc)b}' \\ &- g_{Fc}\left[g_{(Pc)b} - \frac{G_{(Pc)b}}{K_3}\right]G_{\phi b}' + \frac{1}{K_2}\left[g_{\phi b} - \frac{G_{\phi b}}{K_3}\right]G_{Fb}' \\ &+ \frac{1}{K_2}\left[\frac{G_{Fb}}{K_3} - g_{Fb}\right]G_{\phi b}' + g_{Fc}\left[g_{\phi b} - \frac{G_{\phi b}}{K_3}\right]G_{(Pc)b}' \\ &+ g_{\phi c}\left[g_{(Pc)b} - \frac{G_{(Pc)b}}{K_3}\right]G_{Fb}' \end{aligned}\right\} \ldots [11] \text{ (cont.)}$$

$$\left.\begin{aligned} E = &\\ -g_{\phi c}&\left[g_{(PR)b} + \frac{g_{Rb}}{K_1} - \frac{G_{Rb}}{K_1K_3} - \frac{G_{(PR)b}}{K_3}\right]G_{Fb}' \\ &+ \left[g_{(PR)c} + \frac{g_{Rc}}{K_1}\right]\left[\frac{G_{Fb}}{K_3} - g_{Fb}\right]G_{\phi b}' \\ &- g_{Fc}\left[g_{\phi b} - \frac{G_{\phi b}}{K_3}\right]\left[G_{(PR)b}' + \frac{G_{Rb}'}{K_1}\right] \\ &+ g_{Fc}\left[g_{(PR)b} + \frac{g_{Rb}}{K_1} - \frac{G_{Rb}}{K_1K_3} - \frac{G_{(PR)b}}{K_3}\right]G_{\phi b}' \\ &+ \left[g_{(PR)c} + \frac{g_{Rc}}{K_1}\right]\left[g_{\phi b} - \frac{G_{\phi b}}{K_3}\right]G_{Fb}' \\ &- g_{\phi c}\left[\frac{G_{Fb}}{K_3} - g_{Fb}\right]\left[G_{(PR)b}' + \frac{G_{Rb}'}{K_1}\right] \end{aligned}\right\} \ldots [11] \text{ (cont.)}$$

We obtain a solution of

$$\left.\begin{aligned} \phi &= \frac{A}{\Delta}F \\ P_R &= \frac{B}{\Delta}F \\ P_c &= \frac{E}{\Delta}F \\ \delta &= \frac{B}{K_1\Delta}F \end{aligned}\right\} \quad \ldots\ldots\ldots\ldots [12]$$

The deflection, slope, shear, and moment may now be calculated as

$$\left.\begin{aligned} y_n &= g_{\phi n}\phi + g_{\delta n}\delta + g_{(PR)n}P_R + g_{(P_c)n}P_c + g_{Fn}F \\ \alpha_n &= f_{\phi n}\phi + f_{\delta n}\delta + f_{(PR)n}P_R + f_{(P_c)n}P_c + f_{Fn}F \\ S_n &= G_{\phi n}\phi + G_{\delta n}\delta + G_{(PR)n}P_R + G_{(P_c)n}P_c + G_{Fn}F \\ M_n &= G_{\phi n}'\phi + G_{\delta n}'\delta + G_{(PR)n}'P_R \\ &\quad + G_{(P_c)n}'P_c + G_{Fn}'F \end{aligned}\right\} \quad ..[13]$$

The case of three rigid supports means that $K_1 = K_2 = K_3 = \infty$. Inserting this value for the springs reduces the expressions for Δ, A, B, and E to readily obtained simpler forms.

The Case of Two Supports

To keep a succinct form, in the following cases, the tables to be calculated will be noted, the boundary conditions written, followed by the solution of the resulting equations.

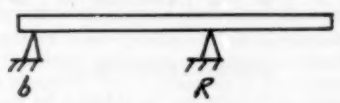

Fig. 4

1 Simple Support—One Overhang (Fig. 4). Tables ϕ and δ are calculated from station 1 to station b. Table F is calculated from station of application to station b. Table P_R is calculated from station R to station b.

Boundary Conditions

$$\left.\begin{aligned} y_R &= 0 = g_{\phi R}\phi + g_{\delta R}\delta + g_{(PR)R}P_R + g_{FR}F \\ y_b &= 0 = g_{\phi b}\phi + g_{\delta b}\delta + g_{(PR)b}P_R + g_{Fb}F \\ M_b &= 0 = G_{\phi b}'\phi + G_{\delta b}'\delta + G_{(PR)b}'P_R + G_{Fb}'F \end{aligned}\right\} \quad ..[14]$$

The solution of this yields

$$\left.\begin{aligned} \phi &= \left\{\left[g_{\delta b}\frac{g_{FR}}{g_{\delta R}} - g_{Fb}\right]G_{(PR)b}' \right. \\ &\qquad \left. - g_{(PR)b}\left[G_{\delta b}'\frac{g_{FR}}{g_{\delta R}} - G_{Fb}'\right]\right\}\frac{F}{\Delta} \\ P_R &= \left\{\left[g_{\phi b} - \frac{g_{\delta b}}{g_{\delta R}}g_{\phi R}\right]\left[G_{\delta b}'\frac{g_{FR}}{g_{\delta R}} - G_{Fb}'\right]\right. \\ &\qquad \left. - \left[g_{\delta b}\frac{g_{FR}}{g_{\delta R}} - g_{Fb}\right]\left[G_{\phi b}' - \frac{g_{\phi R}}{g_{\delta R}}G_{\delta b}'\right]\right\}\frac{F}{\Delta} \\ \delta &= -\left[\frac{g_{FR}F + g_{\phi R}\phi}{g_{\delta R}}\right] \end{aligned}\right\} \quad ..[15]$$

where

$$\Delta = \left[g_{\phi b} - \frac{g_{\delta b}}{g_{\delta R}}g_{\phi R}\right]G_{(PR)b}' - g_{(PR)b}\left[G_{\phi b}' - \frac{g_{\phi R}}{g_{\delta R}}G_{\delta b}'\right]$$

The deflection is

$$y_n = g_{\phi n}\phi + g_{\delta n}\delta + g_{(PR)n}P_R + g_{Fn}F \quad .....[16]$$

2 Two Supports—Torsion and Linear Springs at Each Support (Fig. 5). Tables ϕ and δ are calculated from station 1 to b.

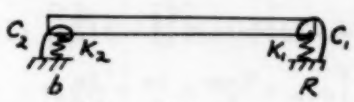

Fig. 5

Tables P_R and M_R are calculated from station R to station b. Table F is completed from the station of application to station b.

Boundary Conditions

$$\left.\begin{aligned} K_1 y_1 &= P_R \\ K_2 y_2 &= P_b \\ c_1\alpha_1 &= M_R \\ c_2\alpha_b &= M_b \end{aligned}\right\} \quad .....[17]$$

These reduce to

$$\left.\begin{aligned} &P_R\left[g_{(PR)b} + \frac{G_{(PR)b}}{K_2} + \frac{g_{\delta b}}{K_1} + \frac{G_{\delta b}}{K_1K_2}\right] \\ &\quad + M_R\left[g_{(MR)b} + \frac{G_{(MR)b}}{K_2} + \frac{g_{\phi b}}{C_1} + \frac{G_{\phi b}}{K_2C_1}\right] \\ &\qquad = -\left[g_{Fb} + \frac{G_{Fb}}{K_2}\right]F \\ &P_R\left[C_2f_{(PR)b} + G_{(PR)b}' + \frac{C_2}{K_1}f_{\delta b} + \frac{G_{\delta b}'}{K_1}\right] \\ &\quad + M_R\left[f_{(MR)b}C_2 + G_{(MR)b}' + \frac{C_2}{C_1}f_{\phi b} + \frac{G_{\phi b}'}{C_1}\right] \\ &\qquad = -[C_2f_{Fb} + G_{Fb}']F \end{aligned}\right\} \quad ..[18]$$

The solution of this yields

$$\left.\begin{aligned} P_R &= \left\{\left[g_{(MR)b} + \frac{G_{(MR)b}}{K_2} + \frac{g_{\phi b}}{C_1} + \frac{G_{\phi b}}{K_2C_1}\right]\right. \\ &\qquad [C_2f_{Fb} + G_{Fb}'] - \left[g_{Fb} + \frac{G_{Fb}}{K_2}\right] \\ &\qquad \left.\left[f_{(MR)b}C_2 + G_{(MR)b}' + \frac{C_2}{C_1}f_{\phi b} + \frac{G_{\phi b}'}{C_1}\right]\right\}\frac{F}{\Delta} \\ M_R &= \left\{\left[g_{Fb} + \frac{G_{Fb}}{K_2}\right]\right. \\ &\qquad \left[C_2f_{(PR)b} + G_{(PR)b}' + \frac{C_2}{K_1}f_{\delta b} + \frac{G_{\delta b}'}{K_1}\right] \\ &\qquad - \left[g_{(PR)b} + \frac{G_{(PR)b}}{K_2} + \frac{g_{\delta b}}{K_1} + \frac{G_{\delta b}}{K_1K_2}\right] \\ &\qquad \left.[C_2f_{Fb} + G_{Fb}']\right\}\frac{F}{\Delta} \\ \delta &= \frac{P_R}{K_1} \\ \phi &= \frac{M_R}{C_1} \end{aligned}\right\} \quad ..[19]$$

where

$$\Delta = \left[g_{(PR)b} + \frac{G_{(PR)b}}{K_2} + \frac{g_{\delta b}}{K_1} + \frac{G_{\delta b}}{K_1K_2}\right]$$

$$\left[f_{(MR)b}C_2 + G_{(MR)b}' + \frac{C_2}{C_1}f_{\phi b} + \frac{G_{\phi b}'}{C_1}\right] - \left[g_{(MR)b} + \frac{G_{(MR)b}}{K_2} + \frac{g_{\phi b}}{C_1} + \frac{G_{\phi b}}{K_2C_1}\right]\left[C_2f_{(PR)b} + G_{(PR)b}' + \frac{C_2}{C_1}f_{\delta b} + \frac{G_{\delta b}'}{K_1}\right] \quad \text{..[19] (Cont.)}$$

The deflection is

$$y_n = g_{\phi n}\phi + g_{\delta n}\delta + g_{(PR)n}P_R + g_{(MR)n}M_R + g_{Fn}F \quad \text{..[20]}$$

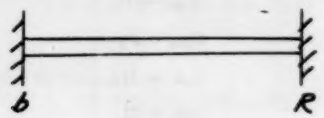

FIG. 6

3 *Fixed-Fixed Beam (Fig. 6).* Tables P_R and M_R are calculated from station 1 to station b. Table F is calculated from the station of application to station b.

Boundary Conditions

$$\left.\begin{aligned} y_b &= 0 \\ \alpha_b &= 0 \end{aligned}\right\} \quad \text{.....[21]}$$

These become

$$\left.\begin{aligned} g_{(MR)b}M_R + g_{(PR)b}P_R &= -g_{Fb}F \\ f_{(MR)b}M_R + f_{(PR)b}P_R &= -f_{Fb}F \end{aligned}\right\} \quad \text{.....[22]}$$

The solution of this yields

$$\left.\begin{aligned} M_R &= [g_{(PR)b}f_{Fb} - g_{Fb}f_{(PR)b}]\frac{F}{\Delta} \\ P_R &= [g_{Fb}f_{(MR)b} - g_{(MR)b}f_{Fb}]\frac{F}{\Delta} \end{aligned}\right\} \quad \text{.....[23]}$$

where

$$\Delta = g_{(MR)b}f_{(PR)b} - g_{(PR)b}f_{(MR)b}$$

The deflection is

$$y_n = g_{(MR)n}M_R + g_{(PR)n}P_R + g_{Fn}F \quad \text{.....[24]}$$

Example: An example of this method is given for a uniform fixed-fixed beam which has the following characteristics

$$EI = 20 \times 10^6 \text{ psi}$$

$$L = 30 \text{ in.}$$

The beam is arbitrarily divided into six sections with stations with equal lengths of 5 in. A concentrated load of F lb upward (+) is applied 10 in. from left end. The data sheet, Table 1, is shown. Calculation of Tables M_R and P_R from station 1 to station b is shown in Tables 2 and 3. The F table is calculated from station 5 to station b in Table 2.

The values of g, G, G', and f of each table at station b are used in Equation [23]. Solving for P_R and M_R, we obtain

$$P_R = 0.259F$$

$$M_R = -2.22F$$

The values of y_n, α_n, M_n, and S_n may be calculated using equations similar to Equations [13]. These resulting values are tabulated in Table 4, column A. The agreement with the analytically determined values in column B of the same table is almost exact.

TABLE 4

STA. n	$\frac{y}{F} \times 10^6$		$\frac{M}{F}$		$\frac{S}{F}$	
	A	B	A	B	A	B
1	0	0	-2.22	-2.22	.259	.259
2	-1.12	-1.12	-.925	-.925	.259	.259
3	-3.39	-3.40	.37	.37	.259	.259
4	-5.21	-5.21	1.66	1.66	.259	.259
5	-4.94	-4.94	2.97	2.97	.741	.741
6	-2.01	-2.006	-.735	-.735	.741	.741
7	0	0	-1.44	-1.44	.741	.741

INFLUENCE COEFFICIENTS

The influence coefficients may be obtained by using the same boundary-value coefficients (in general, ϕ, δ, P_i, and M_i tables) with each independently applied unit load at each station. Thus, in this case, an F table from station 2 to station b is calculated, P_R and M_R evaluated, and then y_n evaluated using Equation [24]. This is repeated for a unit load applied to each of the succeeding stations where the same P_R and M_R coefficients are used in each case. The resulting set of deflections at each station for the various unit loadings yields the required influence coefficients.

Externally Applied Moment. An extension of this procedure to include externally applied concentrated moments is directly obtained by interchanging M, the externally applied moment, for F and computing the g_m, f_m, G_m, and G_m' coefficients using the same procedure as is used for obtaining the moment-reaction coefficients. The equations expressing the boundary conditions must be suitably formulated for each case, solved for the unknowns in terms of the applied moment and then these quantities are inserted into the recurrence equations to obtain the deflection, slope, shear, and moment along the beam.

BIBLIOGRAPHY

1 "A Simple Tabular Method of Calculating Deflections and Influence Coefficients of Beams," by N. O. Myklestad, *Journal of the Aeronautical Sciences*, vol. 12, 1945, p. 23.

2 "A New Method of Calculating Natural Modes of Uncoupled Bending Vibrations of Airplane Wings, and Other Types of Beams," by N. O. Myklestad, *Journal of the Aeronautical Sciences*, vol. 11, 1944, p. 153.

3 "A General Method for Calculating Critical Speeds of Flexible Rotors," by M. A. Prohl, JOURNAL OF APPLIED MECHANICS, Trans. ASME, vol. 67, 1945, pp. A-142 to A-148.

4 "Matrix Solution for the Vibration of Nonuniform Beams," by W. T. Thomson, JOURNAL OF APPLIED MECHANICS, Trans. ASME, vol. 72, 1950, p. 337.

5 "A Systematic Method for Determining the Natural Frequencies of Nonuniform Beams on Multiple Elastic Supports," by R. A. Di Taranto, paper in preparation.

6 "Formulas for Stress and Strain," by R. J. Roark, McGraw-Hill Book Company, Inc., New York, N. Y., 1943.

The Effect of Shear on the Plastic Bending of Beams[1]

By D. C. DRUCKER,[2] PROVIDENCE, R. I.

The end-loaded cantilever beam of perfectly plastic material has been studied in considerable detail but many questions remain unanswered. As a first step in extension to plates, the concept is explored of an interaction curve relating limiting values of shearing force and bending moment for perfectly plastic beams. Simple illustrations demonstrate that, far more than in the elastic range, such interaction is not just a local matter but depends upon the geometry and loading of the entire beam. Useful interaction curves are obtained, nevertheless, with the aid of the upper and lower bound techniques of limit analysis, choosing the maximum-shearing-stress criterion of yielding for convenience. It is shown, in particular, that although a small amount of shear produces but a second-order reduction in the limit moment of beams, a small moment reduces the limiting shear value by a first-order term.

Introduction

ALL beams to be considered are assumed to be made of an idealized material which is termed perfectly plastic. Perfectly plastic material is elastic up to the yield point and then flows under constant stress. The analysis of perfectly plastic beams in the plastic range is at present in a very satisfactory state. Bending usually predominates so that the concept of simple plastic hinges is sufficient in most cases. Should there be axial force in addition, the extending or contracting hinge described by Onat and Prager (1)[3] takes care of the situation. It might be expected that shear force could be included in a similar manner. If shearing force V and bending moment M alone are considered, it would seem a simple matter to determine whether or not the beam is fully plastic at the section. In those problems where shear is important, an interaction curve relating V and M for fully plastic action would be most desirable for beams of rectangular cross section, for I-beams, and for each shape in common use. Unfortunately, such a curve does not really exist, even for any one shape, because the geometry and loading of the entire beam are important, not the properties of the section alone.

The rectangular beam only will be considered in what follows and an attempt will be made to clarify the reasons for the lack of a unique interaction curve. Studies of the cantilever beam under end load have been made by Horne (2), by Onat and Shield (3), by Green (4), and by Leth (5). Much of the information to be presented here is contained, therefore, in this previous work but the relevant parts of each have not yet been compared in principle and some of the peculiarities of the results have not previously been explained.

A start will be made by the analysis of cantilever and simple beams with constant shear force. The lower-bound technique of limit analysis (6) will be employed first to find a safe relation between V and M and to provide reference values for the subsequent work. A local criterion will then be sought to relate limit values of V and M. The impossibility of complete success with such an approach will be discussed. The upper-bound technique of limit analysis (6) will then be applied to the simple span and comparison made with the lower bound and the local criteria. The cantilever will also be studied and its peculiarities noted. The influence of the loading and the geometry away from the section should then become clearer. Finally, by comparison of all the results, a useful but by no means unique or exact interaction curve will be proposed.

Lower Bounds for Beam of Rectangular Cross Section

The lower-bound theorem of limit analysis deals with states of stress which satisfy equilibrium and which do not violate the yield condition. For convenience the maximum-shearing-stress criterion will be assumed so that the maximum shear stress may not exceed $\sigma_0/2$ where σ_0 is the yield point in tension and in compression. Any such equilibrium states of stress correspond to loads which are safe or at most at the limit load.

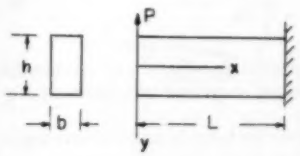

Fig. 1 Cantilever

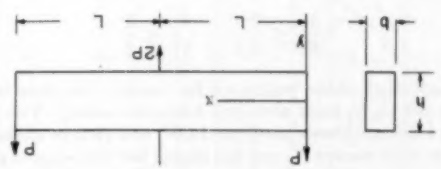

Fig. 2 Simple Span

Figs. 1 and 2 show problems which are almost but not quite equivalent, a cantilever beam under end load and a simple beam under central loading. The equations of equilibrium to be satisfied are, in the usual notation

$$\frac{\partial \sigma_x}{\partial x} + \frac{\partial \tau_{xy}}{\partial y} = 0 \quad [1]$$

$$\frac{\partial \tau_{xy}}{\partial x} + \frac{\partial \sigma_y}{\partial y} = 0 \quad [2]$$

---

[1] The results presented in this paper were obtained in the course of research sponsored by the Office of Ordnance Research, under Contract No. DA-19-020-ORD-3172, Project No. TB2-0001 (1086).

[2] Chairman, Division of Engineering, Brown University. Mem. ASME.

[3] Numbers in parentheses refer to the Bibliography at the end of the paper.

Presented at the National Applied Mechanics Division Conference, Urbana, Ill., June 14–16, 1956, of The American Society of Mechanical Engineers.

Discussion of this paper should be addressed to the Secretary, ASME, 29 West 39th Street, New York, N. Y., and will be accepted until January 10, 1957, for publication at a later date. Discussion received after the closing date will be returned.

Note: Statements and opinions advanced in papers are to be understood as individual expressions of their authors and not those of the Society. Manuscript received by ASME Applied Mechanics Division, December 13, 1955. Paper No. 56—APM-28.

If in Equation [2] σ_y is taken as identically zero, τ_{xy} is seen to be independent of x. Then from Equation [1], observing that σ_x is zero at $x = 0$

$$\sigma_x = -x \frac{d\tau_{xy}}{dy} \quad \ldots\ldots [3]$$

The usual elastic solution with linearly varying σ_x and parabolic τ_{xy}, Fig. 3(*a*), satisfies equilibrium and will not violate yield anywhere if the maximum bending stress does not exceed σ_0 and

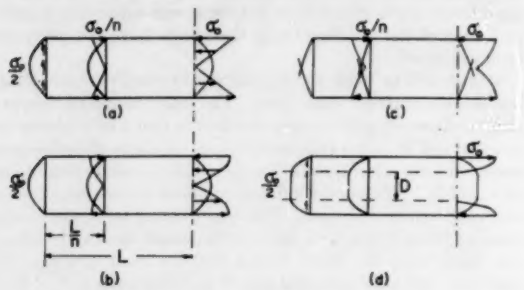

FIG. 3 EQUILIBRIUM DISTRIBUTIONS OF STRESS

the shear stress at the neutral axis is no more than $\sigma_0/2$. Calling the maximum moment $M = PL$ and the shear $V = P$, the lower-bound result is

$$\left.\begin{aligned} M &\leq \sigma_0 b h^2/6 \\ V &\leq \sigma_0 b h/3 \end{aligned}\right\} \quad \ldots\ldots [4]$$

To obtain an interaction plot, designate the known limit moment for moment alone as M_0 and the limit shear for shear alone as V_0

$$\left.\begin{aligned} M_0 &= \sigma_0 b h^2/4 \\ V_0 &= \frac{\sigma_0}{2} b h \end{aligned}\right\} \quad \ldots\ldots [5]$$

These values are obtained, respectively, by σ_0 in tension below the neutral axis and σ_0 in compression above and by a uniformly distributed shear stress $\sigma_0/2$.

The elastic solution then gives the lower-bound interaction plot shown as a square in Fig. 4

$$\frac{M}{M_0} \leq \frac{2}{3}, \qquad \frac{V}{V_0} \leq \frac{2}{3}$$

Although most of the points are far too low (too close to the origin) the $^2/_3$, $^2/_3$ point alone could be quite useful. Two other points which are known are 0,1 and 1,0. As a yield or interaction curve must be convex (7) any line joining two lower-bound points must be a lower bound. Therefore all points lying inside the two inclined dashed straight lines of Fig. 4 give permissible combinations of V and M.

The lower bound can be improved by taking a more elaborate distribution of normal and shearing stress than in Fig. 3(*a*) to satisfy the limiting maximum shear condition

$$\sigma_x^2 + 4\tau_{xy}^2 = \sigma_0^2 \quad \ldots\ldots [6]$$

over the entire critical cross section. Substituting the value of σ_x at $x = L$ from Equation [3] gives the differential equation

$$\left(-L \frac{d\tau_{xy}}{dy}\right)^2 + 4\tau_{xy}^2 = \sigma_0^2 \quad \ldots\ldots [7]$$

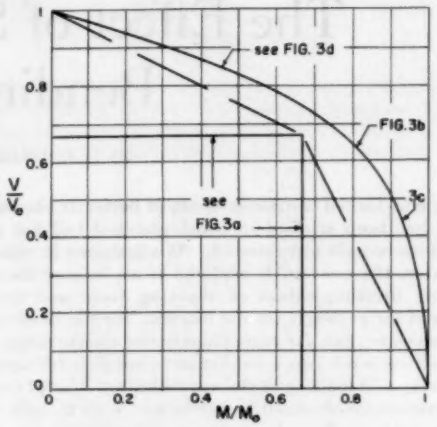

FIG. 4 LOWER-BOUND INTERACTION PLOTS

The solution for positive y is

$$\left.\begin{aligned} \frac{2\tau_{xy}}{\sigma_0} &= \sin \frac{h}{L}\left(1 - \frac{2y}{h}\right) \\ \frac{\sigma_x}{\sigma_0} &= \cos \frac{h}{L}\left(1 - \frac{2y}{h}\right) \end{aligned}\right\} \quad \ldots\ldots [8]$$

and is valid for $h/L \leq \pi/2$ as illustrated in Figs. 3(*b*, *c*). For larger values of h/L the normal stress distribution separates into two $^1/_4$-cycle loops, as shown in Fig. 3(*d*), and the shearing stress is constant at $\sigma_0/2$ in the central region D.

Integration of Equations [8] leads to

$$\left.\begin{aligned} \frac{V}{V_0} &= \frac{L}{h}\left(1 - \cos \frac{h}{L}\right) \\ \frac{M}{M_0} &= 2\left(\frac{L}{h}\right)^2\left(1 - \cos \frac{h}{L}\right) \end{aligned}\right\} \quad \ldots\ldots [9]$$

for $$\frac{h}{L} \leq \frac{\pi}{2} \quad \text{or} \quad \frac{V}{V_0} \leq \frac{2}{\pi}$$

For $$V/V_0 \geq 2/\pi$$

$$\left.\begin{aligned} \frac{V}{V_0} &= \frac{2}{\pi}\left[1 + \frac{D}{h}\left(\frac{\pi}{2} - 1\right)\right] \\ \frac{M}{M_0} &= \frac{4}{\pi}\left[1 - \frac{D}{h}\right]\frac{V}{V_0} \end{aligned}\right\} \quad \ldots\ldots [10]$$

The composite result is plotted in Fig. 4 and should be a very good lower bound indeed because equilibrium and yield are satisfied in a reasonable manner. A modification of the linear distribution of bending stress and parabolic distribution of shear along similar lines to Figs. 3(*c*) and 3(*d*) would give a fairly good lower bound.

An implicit assumption has been made, however, that the distribution of shearing stress on the cross section $x = 0$ can be whatever is called for by the lower-bound solution. In a sense, therefore, the lower bounds for Fig. 3(*a*) and for Figs. 3(*b*, *c*, *d*) do not apply to exactly the same problem. There is no simple way of resolving this difficulty. Saint Venant's principle cannot be appealed to for short beams, whether elastic or plastic, and does not generally have as much meaning in the plastic range.

A LOCAL CRITERION OF LIMIT LOADING

It is customary in the derivation of the elastic moment-curva-

ture relation for beams in bending to analyze a very short length of beam between two neighboring cross sections. Shear, if included at all, is added by supposing constancy along the length of the beam. Free-end or support conditions are satisfied in the same nominal manner as in Fig. 3. In effect, therefore, the assumption is made for general loading that each element of the beam behaves independently and exerts no restraint upon its neighbor.

The same assumption of independent action in the plastic range has much less justification, as will be seen. However, it will lead to interesting interaction relations between shear and moment. Suppose two neighboring cross sections are rotated and transversely displaced with respect to each other as in Fig. 5 or in some more complicated pattern as in Fig. 8. Transverse strain incre-

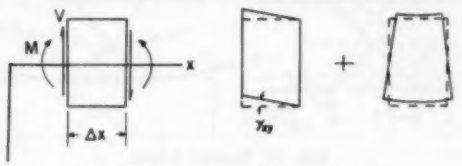

FIG. 5 SIMPLE SHEAR PLUS BENDING

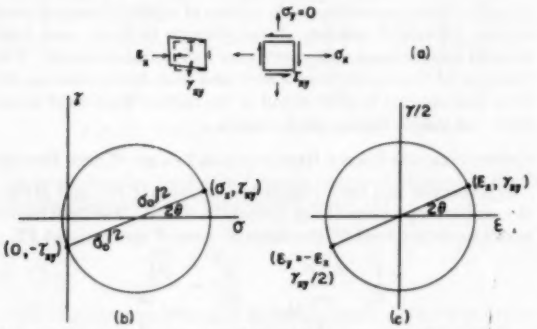

FIG. 6 STATE OF STRESS AND STRAIN INCREMENT AT EACH PLASTIC POINT IN A BENT AND SHEARED BEAM WITH $\sigma_y = 0$
(Maximum-shearing-stress criterion of yielding assumed.)

ments ϵ_y, ϵ_z accompanying the longitudinal strain increment ϵ_x are assumed unimpeded. Quite a bit of information can be deduced about the state of stress and of strain increment at each point in the plastically deforming body.

It has been established within the framework of small-displacement theory that, at the limit load, the stresses are constant and the deformation is purely plastic (6). Consider a small element of the beam which is stretched plastically with strain increment ϵ_x and sheared plastically with increment γ_{xy}, Fig. 6(*a*). As in the previous section, the normal stress σ_y will be taken as zero or negligible. The Mohr's circle for stress is as shown in Fig. 6(*b*). Assumption of the maximum-shearing-stress criterion of yielding then requires that all shearing be in the xy-plane, $\epsilon_z = 0$. As a consequence of the incompressibility in the plastic range of a material obeying the maximum shear rule the plastic and, therefore, total strain increments must satisfy

$$\epsilon_x + \epsilon_y = 0 \quad \text{or} \quad \epsilon_y = -\epsilon_x \qquad \text{.....[11]}$$

The Mohr's circle for strain increment is thus centered at the origin, Fig. 6(*c*). As the principal directions of stress and of strain increment coincide

$$\tan 2\theta = \frac{\gamma_{xy}}{2\epsilon_x} = \frac{2\tau_{xy}}{\sigma_x} \qquad \text{.....[12]}$$

Substitution in the yield criterion Equation [6] gives

$$\left.\begin{aligned} \sigma_x &= \frac{\sigma_0}{\sqrt{1 + \left(\dfrac{\gamma_{xy}}{2\epsilon_x}\right)^2}} \\ \tau_{xy} &= \frac{\sigma_0/2}{\sqrt{\left(\dfrac{2\epsilon_x}{\gamma_{xy}}\right)^2 + 1}} \end{aligned}\right\} \qquad \text{.....[13]}$$

at any point in the plastically deforming section.

The assumed deformation of Fig. 5 in analytical form is $\gamma_{xy} = \gamma$, a constant over the depth of the beam, and

$$\epsilon_x = \frac{2y}{h}\,\epsilon = \eta\epsilon$$

where ϵ is the maximum strain increment at the extreme fiber $y = h/2$ or $\eta = 1$. Integrating Expressions [13] to obtain moment and shear leads to

$$\left.\begin{aligned} M &= M_0 \int_{-1}^{+1} \frac{\eta^2 d\eta}{\sqrt{\left[\eta^2 + \left(\dfrac{\gamma}{2\epsilon}\right)^2\right]}} \\ &\text{or} \\ \frac{M}{M_0} &= \sqrt{\left[1 + \left(\frac{\gamma}{2\epsilon}\right)^2\right]} - \left(\frac{\gamma}{2\epsilon}\right)^2 \sinh^{-1}\frac{2\epsilon}{\gamma} \\ V &= V_0 \int_{-1}^{+1} \frac{d\eta/2}{\sqrt{\left[\left(\dfrac{2\epsilon}{\gamma}\right)^2 \eta^2 + 1\right]}} \\ &\text{or} \\ \frac{V}{V_0} &= \frac{\gamma}{2\epsilon} \sinh^{-1}\frac{2\epsilon}{\gamma} \end{aligned}\right\} \qquad \text{..[14]}$$

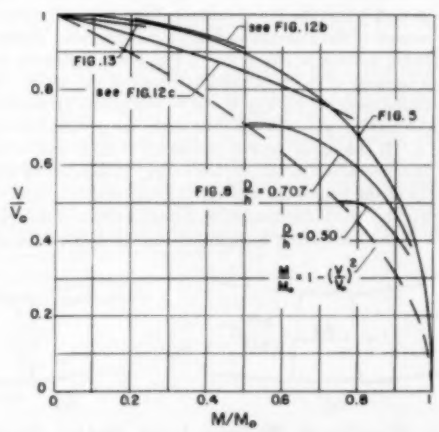

FIG. 7 INTERACTION CURVES

Fig. 7 gives the interaction curve of M/M_0 versus V/V_0.

The question which arises immediately is whether the curve represents actual limiting values, upper bounds, or lower bounds. If the length Δx of the beam were indeed free at its end cross sections to carry V and M as it liked, the result would be an upper bound. A deformation pattern was assumed and the answer is

the same as would be found by following the upper-bound procedure of equating the work done by M and V to the energy dissipation (6, 8). Stress or equilibrium conditions are not satisfied because τ_{xy} is not zero at $y = \pm h/2$, except for $\gamma = 0$.

A plastic-deformation pattern of a quite different type can be taken as in Fig. 8 in which the outer regions of the beam stretch or contract without shearing and the inner portion D shears and

FIG. 8 DISCONTINUOUS SHEAR PLUS BENDING

changes length. An interaction curve can then be obtained for each value of D/h, Fig. 7. The lowest values will be found as γ/ϵ becomes indefinitely large. At this stage the inner region D is effectively under plastic shear alone and the shear stress will be $\sigma_0/2$

$$V = \frac{\sigma_0}{2} bD$$

$$M = \sigma_0 \frac{bh^2}{4} - \sigma_0 \frac{bD^2}{4}$$

or

$$\frac{M}{M_0} = 1 - \left(\frac{V}{V_0}\right)^2 \quad \text{.....[15]}$$

which is appreciably below the local criterion corresponding to Fig. 5 (see Fig. 7).

Stresses corresponding to this deformation pattern are admissible, the surfaces $y = \pm h/2$ are free of stress. Does this mean that one of the individual interaction curves or its lower limit is the true interaction curve? The answer must be no because Equation [15] is in fact below the lower bounds, Figs. 3, 4. The confusion arises because of the attempt to find a local criterion. Neither the deformation pattern of Fig. 5 nor of Fig. 8 will ordinarily be permissible because of the remaining portions of the beam. Transverse strains required by Fig. 5 will be restrained by neighboring elastic (or rigid) regions as will even more the peculiar distortions of Fig. 8. If the upper-bound procedure of limit analysis is followed, it is necessary to include the energy dissipated by the mismatching of the length Δx and the undeforming remainder of the beam, Fig. 9. Such dissipation terms are finite and independent of Δx. They predominate, therefore, as Δx approaches zero.

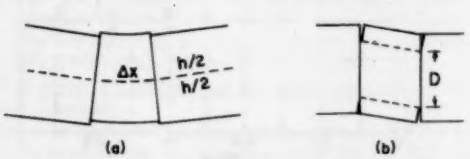

FIG. 9 MISMATCHING REQUIRES LARGE ENERGY DISSIPATION

In the elastic regime, such mismatch or its equivalent is of second order with V constant. The curvature varies linearly along the beam and there is a gradual transition from the section of maximum moment to the section of zero moment. For elastic theory to have any validity, the length of the beam must be several times the depth so that shear strains γ_{xy} resulting from the variation of ϵ_y are not significant. At the limit load, on the other hand, the deformation is entirely plastic and is strongly localized. The transition between deforming and undeforming material is abrupt. When bending predominates, a small length only is plastic. If in Fig. 9(*a*) the curvature of the plastic region is assumed instead to vary smoothly along Δx from zero to a maximum and back to zero, there will be no mismatch at the ends of the deforming portion. For Δx small compared with h, however, the γ_{xy} which is secondary in the elastic beam becomes primary and has large energy dissipation associated with it. The mismatch trouble for pure bending is avoided by the plastic hinge, Fig. 10, which spreads out over a distance equal to the depth of the beam so that the criterion is in reality no longer local.

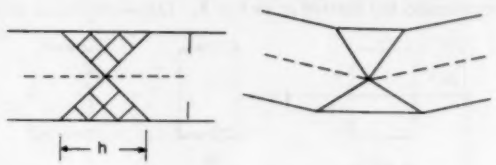

FIG. 10 PLASTIC HINGE

In general, for both elastic and plastic members it is clear that a local criterion cannot apply in regions of rapidly changing cross section. Roots of notches, abrupt changes in depth, and fixed ends all require more elaborate theory for accurate analysis. The influence of the complete geometry and load distribution on the limit load appears in more detail in the further analysis of cantilever and simple beams which follows.

CANTILEVER AND SIMPLE RECTANGULAR BEAMS—UPPER BOUNDS

If a relation had been established between V/V_0 and M/M_0, the cantilever problem of Fig. 1 would be solved. The limit load P would be determined by the value of shear P and moment PL

$$\frac{V}{V_0} = \frac{P}{\frac{\sigma_0}{2} bh}, \qquad \frac{M}{M_0} = \frac{PL}{\sigma_0 \frac{bh^2}{4}}$$

therefore

$$\frac{V}{V_0} = \frac{h}{2L} \frac{M}{M_0} \quad \text{.....[16]}$$

and the ratio $h/2L$ would give the proper point on the interaction curve. Conversely, a solution of the cantilever under end load will help to clarify the interaction relation.

Several solutions are available (2 to 5), including a fairly comprehensive treatment of upper bounds by A. P. Green (4). When the beam is very long, an ordinary plastic hinge may be assumed. Some of the confusion in the detailed analysis of results is apparent from Fig. 11(*a*). Although the hinge is of the standard type, its center is $h/2$ from the fixed end. The support is assumed capable of applying stresses which keep an elastic triangular core adjacent to the fixed end and so strengthen the beam. When the beam is very short Green (4) and Onat and Shield (3) propose the circular arc of sliding as in Fig. 11(*b*). The kinematic picture proposed by Leth (5) for an I-beam is appropriate for the short rectangular beam, Fig. 11(*c*). Again, as evidenced by the different points of view expressed in (3), (4), and (5), the length of the beam becomes questionable because of the restraint by the fixed end.

A discussion of the simple beam centrally loaded, Fig. 2, does not resolve the inherent and important problem associated with a fixed end or any abrupt change in section. It does, however, simplify the analysis of the interaction problem. In particular, if the central hinge kinematic picture is assumed, Fig. 12(*a*), equat-

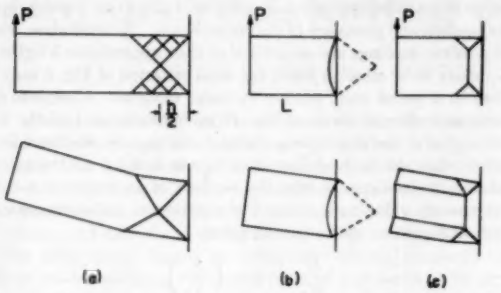

FIG. 11 CANTILEVER UNDER END LOAD—UPPER-BOUND PICTURES

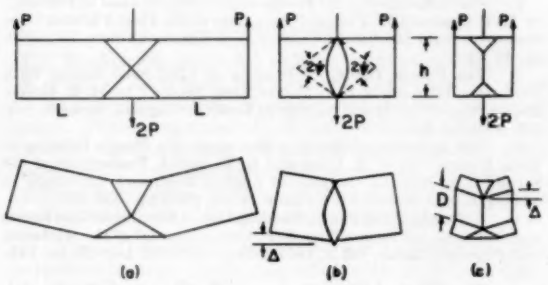

FIG. 12 SIMPLE SPAN—UPPER-BOUND PICTURES

ing work done by the forces P to the energy dissipated in plastic deformation gives the upper-bound result (6)

$$PL \leq M_0 \quad \text{or} \quad \frac{M}{M_0} \leq 1 \qquad [17]$$

This answer cannot be said to be unexpected, but it is not obtained for the cantilever, Fig. 11(*a*).

Assuming a circular slip surface for very short beams, Fig. 12(*b*), equating the work done by the external load to the internal dissipation gives as an upper bound

$$P\Delta = \frac{\sigma_0}{2} b \frac{h}{2 \sin \psi} 2\psi \frac{\Delta}{L + \frac{h}{2} \operatorname{ctn} \psi} \frac{h}{2 \sin \psi} \qquad [18]$$

The angle ψ should be chosen to minimize P because the least upper bound is desired. The result of Onat and Shield (3) is then found ($V = P$)

$$\frac{V}{V_0} = 2\psi \operatorname{ctn} \psi - 1 \qquad [19]$$

For very short beams, and consequently small M/M_0, series expansion leads to the upper bound on the interaction relation ($M = PL$) plotted in Fig. 7

$$\frac{V}{V_0} = 1 - \frac{3}{8}\left(\frac{M}{M_0}\right)^2 \qquad [20]$$

The discontinuous shear upper-bound picture, Fig.12(*c*), gives

$$P\Delta = \frac{\sigma_0}{2} \frac{\Delta}{L} bDL + \sigma_0 b \frac{(h - D)^2}{4} \frac{\Delta}{L}$$

or

$$\frac{PL}{\sigma_0 \frac{bh^2}{4}} = \frac{M}{M_0} = \frac{2L}{h} \frac{D}{h} + \left(1 - \frac{D}{h}\right)^2 \qquad [21]$$

Minimizing the upper bound by taking the derivative with respect to D/h and equating to zero

$$1 - \frac{D}{h} = \frac{L}{h} \quad \text{or} \quad D + L = h \qquad [22]$$

Substitution of Equations [22] and [16] in [21] results in the upper-bound interaction relation

$$\frac{M}{M_0} = 4 \frac{V}{V_0}\left(1 - \frac{V}{V_0}\right) \qquad [23]$$

valid for $L/h \leq 1$ or $M/M_0 \leq 2(V/V_0)$ or $V/V_0 \geq 1/2$. Note that in Equation [23] first-order changes in V/V_0 at $V/V_0 = 1$ correspond to first-order changes in M/M_0. As shown in Fig. 7, the upper bound, Equation [23], is a much better answer than Equation [20] for small M/M_0.

Extension of the simple beam to the left and to the right of the lines of action of the forces P as in Fig. 13 provides an excellent illustration of the nonlocal character of the interaction relation

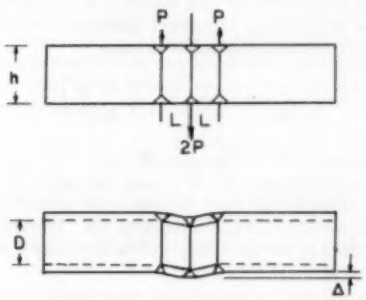

FIG. 13 FURTHER EVIDENCE OF NONLOCAL EFFECTS

calculation. There will be no change in the upper bound computed from a hinge picture like Fig. 12(*a*) or a circular arc of sliding as Fig. 12(*b*). However, comparing Fig. 12(*c*) and Fig. 13, it can be seen readily that Equation [21] does not contain a complete expression for the dissipated energy for Fig. 13. The $(1 - D/h)^2$ term must be doubled because bending occurs at the loads P as well as at the center of the beam. Here again is the mismatch trouble discussed earlier, Fig. 9(*b*), and the reason Fig. 8 leads to a result below the lower bounds of Fig. 3.

Returning then to a modified Equation [21] and minimizing the energy dissipated

$$D + \frac{L}{2} = h \qquad [24]$$

and for

$$\frac{L}{2h} \leq 1 \quad \text{or} \quad \frac{M}{M_0} \leq 4 \frac{V}{V_0}$$

$$\frac{M}{M_0} = 8 \frac{V}{V_0}\left(1 - \frac{V}{V_0}\right) \qquad [25]$$

is an upper bound on the interaction relation, Fig. 7.

COMPARISONS AND COMMENTS

Fig. 14 compares several of the results obtained. It should be

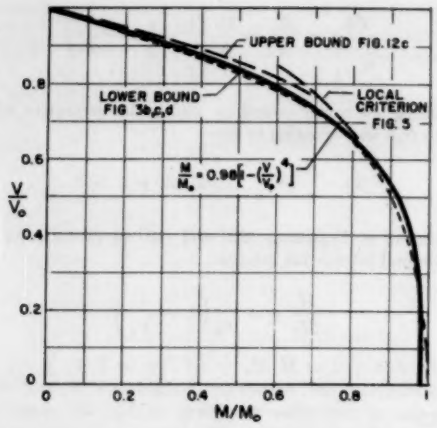

FIG. 14 PROPOSED INTERACTION CURVE AND COMPARISON OF RESULTS

kept in mind that if a unique interaction curve existed it would be convex (7). Although the local criterion is not necessarily either an upper or a lower bound and the lower bound corresponds to shear-stress distributions somewhat different from those of the upper bounds, it seems reasonable to take

$$\frac{M}{M_0} = 0.98\left[1-\left(\frac{V}{V_0}\right)^4\right] \quad \ldots\ldots\ldots\ldots [26]$$

or an expression close to Equation [26] as a working hypothesis. Such an approximation which nearly coincides with a lower bound and is not too far from possible upper bounds would seem satisfactory for practical and theoretical use. Polygonal or other approximations to the curve may well be more useful in particular problems (8, 9).

As V/V_0 will rarely exceed $^1/_2$, in most practical problems the effect of shear may be ignored completely. As the purpose of this paper is to elucidate the nature of the shear-moment interaction and not to solve problems, none will be solved. One of the main points is that the interaction is not a local affair but depends upon the loading and geometry of the entire beam. Nevertheless, when all possible loadings are considered so that appreciable lengths of beam are at or close to yield, the local criterion of Fig. 5 may be close to a useful limit loading for large moment. Complete end fixity as in the cantilever of Fig. 11 or reinforcement of the central region of the simple beam will, of course, raise the limit loads still further above those discussed here in detail. All things considered, it does appear that the concept of an interaction curve has enough value to warrant the selection of an approximation such as Equation [26] or for simplicity

$$\frac{M}{M_0} = 1-\left(\frac{V}{V_0}\right)^4 \quad \ldots\ldots\ldots\ldots [27]$$

BIBLIOGRAPHY

1 "The Influence of Axial Forces on the Collapse Load of Frames," by E. T. Onat and W. Prager, Proceedings of the First Midwest Conference on Solid Mechanics, University of Illinois, Urbana, Ill., 1953, pp. 40–42.

2 "The Plastic Theory of Bending of Mild Steel Beams With Particular Reference to the Effect of Shear Forces," by M. R. Horne, Proceedings of the Royal Society of London, England, series A, vol. 207, 1951, p. 216.

3 "The Influence of Shearing Forces on the Plastic Bending of Wide Beams," by E. T. Onat and R. T. Shield, Proceedings of the Second U. S. National Congress of Applied Mechanics, University of Michigan, Ann Arbor, Mich., June 14–18, 1954, pp. 535–537.

4 "A Theory of the Plastic Yielding Due to Bending of Cantilevers and Fixed-Ended Beams," by A. P. Green, *Journal of the Mechanics and Physics of Solids*, vol. 3, 1954, part I, pp. 1–15; part II, pp. 143–155.

5 "The Effect of Shear Stresses on the Carrying Capacity of I-Beams," by C. F. Leth, Brown University Technical Report 107 to Office of Naval Research, Contract N7onr-35801, March, 1954.

6 "Extended Limit Design Theorems for Continuous Media," by D. C. Drucker, W. Prager, and H. J. Greenberg, *Quarterly of Applied Mathematics*, vol. 9, January, 1952, pp. 381–389.

7 "A More Fundamental Approach to Stress-Strain Relations," by D. C. Drucker, Proceedings of the First U. S. National Congress for Applied Mechanics, ASME, 1951, pp. 487–491.

8 "Limit Analysis of Cylindrical Shells Under Axially Symmetric Loading," by D. C. Drucker, Proceedings of the First Midwest Conference on Solid Mechanics, University of Illinois, Urbana, Ill., 1953, pp. 158–163.

9 "The Theory of Plasticity—A Survey of Recent Achievements," by W. Prager (James Clayton Lecture), *Journal of The Institution of Mechanical Engineers*, vol. 169, no. 21, 1955, pp. 41–57.

Impulsive Loading of Elastic-Plastic Beams[1]

By J. A. SEILER,[2] B. A. COTTER,[2] and P. S. SYMONDS,[3] PROVIDENCE, R. I.

A simply supported uniform beam of ductile material, subjected to impulsive loading such that the initial velocity is a half-sine wave, is considered in this paper. The elastic and elastic-plastic motions are discussed under the assumption that plastic flow is confined to one cross section, and the final deformations are compared with those computed from an analysis which neglects all elastic deformations. The purpose of the work is to provide further information which may help in estimating the range of validity of the latter ("rigid-plastic") type of analysis.

Introduction

IT IS obviously important to have means of estimating the range of validity of the so-called "plastic-rigid" type of analysis of problems of impact and dynamic loading of beams. This assumes that the moment-curvature relation is as shown by Fig. 3, according to which the beam is rigid unless the moment is M_0; when this moment is maintained at a cross section, unlimited rotations can occur across that section, which behaves as a "plastic hinge." We also assume in this paper that:

1 The limit moment M_0 is obtained as in the elementary plastic methods for beams and frames; effects of shear and axial forces are neglected.

2 Strain-rate effects are disregarded.

3 Geometry changes are neglected in the analysis.

This plastic-rigid hypothesis allows solutions to be obtained much more simply than if elastic vibrations are taken into account. However, the solutions so obtained can be expected to be reasonably accurate only if conditions are such that the energy absorbed in plastic deformation greatly exceeds the maximum amount of energy that could be stored in the beam in the form of elastic strain energy.[4] The significant quantity is the energy ratio R, defined as

$$R = \frac{\text{energy absorbed in plastic deformation}}{\text{maximum possible elastic strain energy}} = \frac{W_p}{W_e}$$

In a beam problem W_e can be conveniently taken as $\frac{M_0^2 l}{2EI}$

where l is the beam span.

In order to find the value of R in a particular problem above which the plastic-rigid method gives results accurate to within, say, 10 per cent (in so far as neglect of elastic deformations is concerned), one must have available for comparison the results of an analysis of the same problem in which elastic deformations are included. Unfortunately, it is found that a complete solution of a beam problem in which both the elastic vibrations and the plasticity condition are taken into account is extremely difficult to obtain. No such solution has yet been found, valid in the range of variables in which the plastic-rigid solution is expected to be correct.

The particular problem discussed in this paper was selected as perhaps the simplest problem of dynamic loading of a beam. The comparisons made between the results of the rigid-plastic solution and those of an "approximate" elastic-plastic solution are presumably typical of the comparisons which can be made in problems of this type. It is found that the two solutions have ranges of validity which do not overlap, and hence no judgment can be passed as to when the rigid-plastic analysis becomes a reliable method of attack.

Aside from exemplifying the sort of comparison that can be made between rigid-plastic and elastic-plastic solutions, it is hoped that examination of a simple problem may aid in subsequent development of methods for extending the elastic-plastic analysis to the point where it can reliably be used to assess the accuracy of the rigid-plastic method of analysis.

Comparison Between Elastic-Plastic and Rigid-Plastic Solutions

The sort of comparison between elastic-plastic and rigid-plastic solutions that is wanted can be illustrated by a simple mass-spring system, as suggested by Brooks and Newmark.[5] Fig. 1 indicates

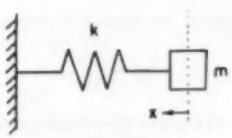

Fig. 1

the system. Fig. 2 shows the spring characteristic assumed for the elastic-plastic analysis, while Fig. 3 shows that for the rigid-plastic solution. Q_y is the "yield force" of the spring, the maximum force the spring can sustain either in tension or compression; in the elastic range the spring constant is k.

The mass m is subjected to an impulsive force such that it has an initial velocity v_0 and negligible initial displacement. Initially there is motion governed by the equation of elastic vibrations

$$m\ddot{x} + kx = 0 \quad \ldots\ldots\ldots\ldots\ldots\ldots [1]$$

with starting conditions: $t = 0$; $x = 0$, $\dot{x} = v_0$. The initial motion is therefore described by

$$x = \frac{v_0}{p} \sin pt \quad \ldots\ldots\ldots\ldots\ldots\ldots [2]$$

---

[1] The results presented in this paper were obtained in the course of research sponsored by Norfolk Naval Shipyard under Contract N189s-92558.

[2] Research Assistant, Division of Applied Mathematics, Brown University.

[3] Professor of Engineering, Brown University. Mem. ASME.

[4] "Large Plastic Deformation of Beams Under Transverse Impact," by E. H. Lee and P. S. Symonds, Journal of Applied Mechanics, Trans. ASME, vol. 74, 1952, pp. 308–314.

Presented at the National Applied Mechanics Division Conference, Urbana, Ill., June 14–16, 1956, of The American Society of Mechanical Engineers.

Discussion of this paper should be addressed to the Secretary, ASME, 29 West 39th Street, New York, N. Y., and will be accepted until January 10, 1957, for publication at a later date. Discussion received after the closing date will be returned.

Note: Statements and opinions advanced in papers are to be understood as individual expressions of their authors and not those of the Society. Manuscript received by ASME Applied Mechanics Division, July 5, 1955. Paper No. 56—APM-17.

[5] "Response of Simple Structures to Dynamic Loads," by N. B. Brooks and N. W. Newmark, Technical Report to ONR Contract N6ori-071(06) Task Order VI Project NR-064-183, University of Illinois, Urbana, Ill., 1953.

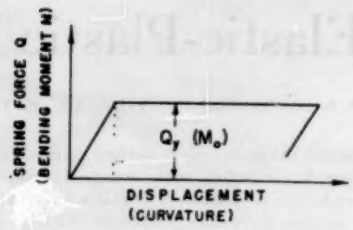

FIG. 2

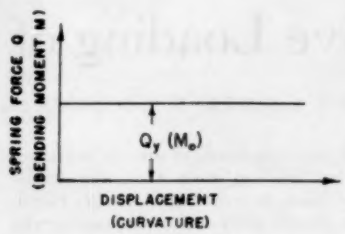

FIG. 3

where

$$p^2 = k/m$$

The elastic phase terminates at a time t_1 at which the spring force becomes equal to Q_y, so that

$$Q_y = \frac{kv_0}{p} \sin pt_1 \quad [3]$$

For later times, $t > t_1$, the spring force remains constant at Q_y and displacements are given by

$$x = -\frac{Q_y}{2m}(t - t_1)^2 + v_0(t - t_1)\cos pt_1 + \frac{Q_y}{k} \quad [4]$$

The maximum displacement x_f occurs at the time t_f when $\dot{x}(t_f) = 0$, and is easily found to be

$$x_f = \frac{mv_0^2}{2Q_y}\cos^2 pt_1 + \frac{Q_y}{k} \quad [5]$$

On the other hand, if the rigid-plastic type of spring characteristic is assumed, then the spring force is constant at Q_y during the whole motion, and the maximum displacement is found to be

$$x_f' = \frac{mv_0^2}{2Q_y} \quad [6]$$

This occurs in a time t_f' at which the velocity vanishes, where

$$t_f' = \frac{mv_0}{Q_y} \quad [7]$$

Now it is helpful to express these results in terms of the ratio R of the energy absorbed in plastic deformation to the maximum possible elastic-strain energy. We have in this problem

$$W_p = Q_y\left(x_f - \frac{Q_y}{k}\right) = \frac{mv_0^2}{2}\cos^2 pt_1 \quad [8]$$

$$W_e = \frac{Q_y^2}{2k} \quad [9]$$

Hence

$$R = \frac{W_p}{W_e} = \frac{kmv_0^2}{Q_y^2}\cos^2 pt_1$$

Using Equation [3] to express pt_1 in terms of R, we find

$$x_f = \frac{Q_y}{2k}(R + 2) \quad [10]$$

$$x_f' = \frac{Q_y}{2k}(R + 1) \quad [11]$$

The error involved in using the rigid-plastic analysis can thus be found in terms of R only. The per cent error is

$$\frac{x_f - x_f'}{x_f} \times 100 = \frac{100}{R + 2} \quad [12]$$

Thus, for example, if the error is to be less than 10 per cent, R must exceed 8.

Impulsive Motion of a Uniform Beam

We turn now to an analogous problem of impulsive motion of a uniform beam, and attempt to make the same sort of comparison between solutions based on an elastic-plastic and on a rigid-plastic characteristic relation between bending moment and curvature.

We consider a beam of length $2l$, mass per unit length m, and elastic flexural rigidity EI, subjected to an impulsive load such that the initial displacement and velocity functions are, respectively

$$y(x, 0) = 0; \quad \frac{\partial y}{\partial t}(x, 0) = V_0 \sin\frac{\pi x}{2l} \quad [13]$$

Positive directions of the displacement y, co-ordinate x, and bending moment M are shown in Fig. 4. End conditions of simple support are assumed, so that

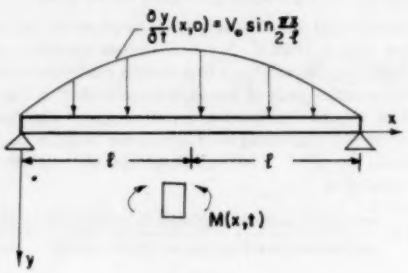

FIG. 4

$$\left.\begin{aligned} y(0, t) &= y(2l, t) = 0 \\ \frac{\partial^2 y}{\partial x^2}(0, t) &= \frac{\partial^2 y}{\partial x^2}(2l, t) = 0 \end{aligned}\right\} \quad [14]$$

The solution of this problem of initial motion will be obtained first on the basis of an elastic-plastic moment-curvature relation as illustrated in Fig. 2, and second on the assumption of rigid-plastic behavior, as in Fig. 3.

Elastic-Plastic Moment-Curvature Solution

In the elastic-plastic treatment we have first an elastic motion, in which

$$M = -EI\frac{\partial^2 y}{\partial x^2} \quad [15]$$

The equation governing this phase is taken to be

$$EI\frac{\partial^4 y}{\partial x^4} + m\frac{\partial^2 y}{\partial t^2} = 0 \quad \text{[16]}$$

The solution of this equation satisfying the initial and end conditions stipulated in Equations [13] and [14] is

$$y(x, t) = \frac{4V_0 k l^2}{\pi^2} \sin\frac{\pi x}{2l} \sin\frac{\pi^2 t}{4kl^2} \quad \text{[17]}$$

where

$$k^2 = \frac{m}{EI} \quad \text{[18]}$$

This elastic phase ends when the maximum moment in the beam reaches the limit moment magnitude M_0. This occurs at a time t_1 such that

$$M(l,t_1) = M_0 = -EI\frac{\partial^2 y}{\partial x^2}(l, t_1)$$

and hence

$$\frac{M_0}{EIkV_0} = \sin\frac{\pi^2 t_1}{4kl^2} \quad \text{[19]}$$

It is convenient to use a dimensionless "time" η defined as

$$\eta = \frac{\pi^2 t}{4kl^2} \quad \text{[20]}$$

At the instant $\eta_1 = \pi^2 t_1/4kl^2$ we have

$$y(x, t_1) = \frac{4V_0 k l^2}{\pi^2} \sin\frac{\pi x}{2l} \sin\eta_1 \quad \text{[21a]}$$

$$\frac{\partial y}{\partial t}(x, t_1) = V_0 \sin\frac{\pi x}{2l} \cos\eta_1 \quad \text{[21b]}$$

In the ensuing time interval there is an elastic-plastic phase of motion, with a plastic hinge at the beam mid-section.[6] This means that at $x = l$ the bending moment remains constant at the value M_0, while the slope angle is unrestricted in magnitude.

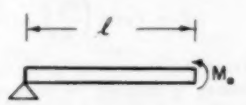

FIG. 5

Hence in this phase a solution of Equation [16] in the range $0 \leq x \leq l$ is required, satisfying the end conditions (Fig. 5)

$$y(0, t) = \frac{\partial^2 y}{\partial x^2}(0, t) = 0 \quad \text{[22a]}$$

$$-EI\frac{\partial^3 y}{\partial x^3}(l, t) = M_0; \quad \frac{\partial^2 y}{\partial x^2}(l, t) = 0 \quad \text{[22b]}$$

The solution in this phase must also satisfy Equations [21] at time t_1, as "initial" conditions.

The required general solution may be written as

$$y = \psi(x, t) + Y(x, t) \quad \text{[23]}$$

where

$$\psi(x, t) = \frac{M_0 l^2}{EI}\left[\frac{x^4}{40l^4} - \frac{x^3}{4l^3} - \frac{3x(t-t_1)^2}{2k^2l^4}\right] \quad \text{[24]}$$

$$Y(x, t) = [A_0 + B_0(t - t_1)]x + \sum_{n=1}^{\infty} X_n(x)$$

$$\left[A_n \sin\frac{\lambda_n^2(t-t_1)}{k} + B_n \cos\frac{\lambda_n^2(t-t_1)}{k}\right] \quad \text{[25]}$$

$$X_n(x) = \sin\lambda_n l \sinh\lambda_n x + \sinh\lambda_n l \sin\lambda_n x$$

and the λ_n satisfy the equation

$$\tanh\lambda_n l = \tan\lambda_n l \quad \text{[26]}$$

so that

$$\lambda_n l \doteq n\pi + \frac{\pi}{4}$$

The function $Y(x, t)$ satisfies the "homogeneous" boundary conditions; i.e., has

$$\frac{\partial^2 Y}{\partial x^2}(l, t) = 0$$

while $\psi(x, t)$ satisfies the end conditions Equation [22]. The coefficients A_0, B_0, A_n, B_n must be determined so that the conditions on displacement and velocity at $t = t_1$ are also satisfied.

By standard methods the following results are obtained

$$A_0 = \frac{M_0 l}{EI}\left(\frac{48}{\pi^4} + \frac{39}{280}\right) \quad \text{[27]}$$

$$B_0 = \frac{12M_0}{\pi^2 lkEI}\sqrt{2S-1} \quad \text{[28]}$$

$$A_n = \frac{\pi^2 M_0 l^2\sqrt{2S-1}}{\sqrt{2}\,EI} \cdot \frac{(-1)^{n+1}\cosh\lambda_n l}{\lambda_n^{5/2}\left(1 - \frac{\pi^4}{16\lambda_n^4}\right)(\sinh^2\lambda_n l - \sin^2\lambda_n l)} \quad \text{[29]}$$

$$B_n = \frac{\pi^2 M_0 l^2}{4\sqrt{2EI}} \cdot \frac{(-1)^{n+1}\cosh\lambda_n l}{\lambda_n^{7/2}\left(1 - \frac{\pi^4}{16\lambda_n^4}\right)(\sinh^2\lambda_n l - \sin^2\lambda_n l)} \quad \text{[30]}$$

where

$$S = \frac{mEIV_0^2}{2M_0^2} \quad \text{[31]}$$

The foregoing solution is correct provided both the following conditions are satisfied:

1 The bending moment $|(M(x, t)| \leq M_0$ at all points in the range $0 \leq x \leq l$.

2 The sense of the rotation across the plastic hinge must agree with that of the bending moment at the hinge. In the present problem, since $M(l, t) = +M_0$, the rate of relative rotation of the tangent lines across the plastic hinge must be such as to produce concave upward curvature. Hence if we consider the left-hand half-beam, $0 \leq x \leq l$, we must have clockwise rotation of the tangent line at $x = l$. The foregoing solution therefore holds good until a time t_f is reached when

$$\frac{\partial^2 y}{\partial t\,\partial x}(l, t_f) = 0 \quad \text{[32]}$$

[6] This is the procedure first used by Bleich and Salvadori.[7]

[7] "Impulsive Motion of Elasto-Plastic Beams," by H. H. Bleich and M. G. Salvadori, Trans. ASCE, vol. 120, 1955, p. 499.

The deformations computed at the instant t_f are the maximum plastic deformations. The quantities of practical interest are the deflection δ_f and slope θ_f at the beam mid-point. To compute these we must first obtain t_f by solving Equation [32], and then use the result in Equation [23].

Good approximations are that $a_n = \lambda_n l = n\pi + \pi/4$, $\tanh a_n = 1$, and $\sinh^2 a_n \gg 1$ for all n. Then using the notation

$$\eta_f' \equiv \frac{\pi^2}{4kl^2}(t_f - t_1) \quad \ldots\ldots\ldots\ldots\ldots\ldots [33]$$

we have

$$\eta_f' - \frac{\pi^4}{48}\sum_{n=1}^{\infty}\frac{\sin\frac{4a_n^2}{\pi^2}\eta_f'}{a_n^4\left(1-\frac{\pi^4}{16a_n^4}\right)} = \sqrt{2S-1}\left[1-\frac{\pi^4}{12}\sum_{n=1}^{\infty}\frac{\cos\frac{4a_n^2\eta_f'}{\pi^2}}{a_n^2\left(1-\frac{\pi^4}{16a_n^4}\right)}\right] \quad \ldots\ldots [34]$$

$$\frac{EI}{M_0 l}\theta_f = \frac{48}{\pi^4}+\frac{39}{280}-\frac{5}{8}+\frac{48}{\pi^4}\sqrt{2S-1}\,\eta_f' - \frac{24}{\pi^4}\eta_f'^2 - \pi^2\sqrt{2S-1}\sum_{n=1}^{\infty}\frac{\sin\frac{4a_n^2}{\pi^2}\eta_f'}{a_n^4\left(1-\frac{\pi^4}{16a_n^4}\right)} - \frac{\pi^4}{4}\sum_{n=1}^{\infty}\frac{\cos\frac{4a_n^2}{\pi^2}\eta_f'}{a_n^6\left(1-\frac{\pi^4}{16a_n^4}\right)} \quad \ldots\ldots [35]$$

$$\frac{EI}{M_0 l^2}\delta_f = \frac{48}{\pi^4}+\frac{39}{280}-\frac{9}{40}-\frac{24}{\pi^4}\eta_f'^2+\frac{48}{\pi^4}\sqrt{2S-1}\,\eta_f' - \pi^2\sqrt{2S-1}\sum_{n=1}^{\infty}\frac{\sin\frac{4a_n^2}{\pi^2}\eta_f'}{a_n^5\left(1-\frac{\pi^4}{16a_n^4}\right)} - \frac{\pi^4}{4}\sum_{n=1}^{\infty}\frac{\cos\frac{4a_n^2}{\pi^2}\eta_f'}{a_n^7\left(1-\frac{\pi^4}{16a_n^4}\right)} \quad \ldots\ldots [36]$$

The computation of the final deformations from the foregoing equations and their comparison with those obtained from the rigid-plastic solution will be discussed in the section, Comparison of Solutions.

Rigid-Plastic Analysis

The same problem is now treated according to the rigid-plastic hypothesis. The relatively simple analysis outlined previously[8] is applicable here.

From the initial conditions, Equations [13]

$$\left.\begin{aligned}\frac{\partial^2 y}{\partial x^2}(x,0) &= 0 \qquad 0 \le x \le 2l\\ \frac{\partial^2 y}{\partial l\,\partial x^2}(x,0) &= -\frac{V_0\pi^2}{4l^2}\sin\frac{\pi x}{(2l)} \qquad 0 \le x \le 2l\end{aligned}\right\} \quad \ldots\ldots [37]$$

Hence the curvature is initially zero everywhere and is decreasing. From the assumed moment-curvature relation in Fig. 3 the beam must have constant moment M_0 throughout its length at $t = 0$. Now in order to satisfy the boundary condition that the bending moment vanish at the supports and to insure continuity of the bending moment along the beam, we see that at a finite time $t > 0$ the beam must have two segments moving as rigid bodies at the ends separated by a central plastic section, as shown in Fig. 6. In the outer segments the bending moment decreases monotonically from M_0 to zero. These segments rotate

Fig. 6

about the supports with angular velocity ω. The plastic section has a constant moment M_0, zero shear force, and a velocity distribution equal to the initial one. The three segments are separated by interfaces which, we will show, travel toward the center of the beam.

Since the motion of the beam is symmetric about $x = l$ it is sufficient to study one half of the beam. If we consider the section $0 \le x \le l$, at $t > 0$ it has the configuration shown in Fig. 7. Let the angular velocity of segment A about O be ω measured positively in the clockwise direction. The interface is at $x = \xi l$ where $\xi = \xi(t)$ and $0 \le \xi \le 1$.

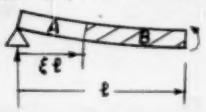

Fig. 7

$$\left.\begin{aligned}\text{For } 0 \le x \le \xi l: \quad & \frac{\partial y}{\partial t}(x,t) = \omega x\\ \text{and for } \xi l \le x \le l: \quad & \frac{\partial y}{\partial t}(x,t) = V_0 \sin\left(\frac{\pi x}{2l}\right)\end{aligned}\right\} \quad \ldots\ldots [38]$$

Since the transverse velocity is continuous

$$\omega \xi l = V_0 \sin\left(\frac{\pi\xi}{2}\right) \quad \ldots\ldots [39]$$

We next write the equation expressing the equality of angular impulse to the change of moment of momentum of the left half-beam about 0. The external moment acting on this half of the beam about 0 has magnitude M_0 at all times after $t = 0$ until plastic deformation is completed. Since the change in angular momentum of B about O during time t is zero, the equation for conservation of angular momentum becomes

$$-M_0 t = \int_0^{\xi l} m\omega x^2\,dx - \int_0^{\xi l} mV_0 \sin\left(\frac{\pi x}{2l}\right) x\,dx \quad \ldots [40]$$

Making use of Equation [39] and performing the integrations we obtain

$$\frac{3M_0 t}{mV_0 l^2} = \left(\frac{12}{\pi^2}-\xi^2\right)\sin\left(\frac{\pi\xi}{2}\right) - \frac{6}{\pi}\xi\cos\left(\frac{\pi\xi}{2}\right) \quad \ldots [41]$$

Equation [41] gives the location of the interface at any time when the configuration of Fig. 7 applies.

---

[8] "Simple Solutions of Impulsive Loading and Impact Problems of Plastic Beams and Plates," by P. S. Symonds, Report No. 3, under Contract N189s-1756A, of Brown University to Norfolk Naval Shipyard.

Differentiating Equation [41] with respect to t we obtain the expression for the velocity of the interface section

$$\frac{mV_0l^2}{M_0}\dot{\xi} = \frac{3}{\xi\left[\sin\left(\frac{\pi\xi}{2}\right) - \frac{\pi}{2}\xi\cos\left(\frac{\pi\xi}{2}\right)\right]} \quad \ldots\ldots [42]$$

Evidently for $0 < \xi < 1$, $\dot{\xi} > 0$, so that the interface is moving toward the center of the beam. To determine the time t_s when the hinge reaches the center of the beam we set $\xi = 1$ in Equation [41]. Then

$$\frac{M_0}{mV_0l^2}\,t_s = \frac{4}{\pi^2} - \frac{1}{3} \quad \ldots\ldots [43]$$

For $t > t_s$, the half-beam rotates as a rigid body about the supports, with plastic hinge at $x = l$. We again write the equation for conservation of angular momentum about O

$$> t_s\text{:}\quad -M_0l = \int_0^l m\omega x^2dx - m\int_0^l xV_0\sin\left(\frac{\pi x}{2l}\right)dx \quad \ldots\ldots [44]$$

The result is

$$t > t_s\text{:}\qquad \frac{\omega l}{V_0} = \frac{12}{\pi^2} - 3\frac{M_0t}{ml^2V_0} \quad \ldots\ldots [45]$$

The motion of the beam as described by Equation [45] continues until $t = t_f$ when ω vanishes. From Equation [45] we see that

$$\frac{M_0t_f}{ml^2V_0} = \frac{4}{\pi^2} \quad \ldots\ldots [46]$$

The deformation at the middle of the beam may be readily determined. In the interval

$$t < t_s\text{:}\qquad \frac{\partial y}{\partial t}(l, t) = V_0$$

and for $t > t_s$ from Equation [45]

$$\frac{\partial y}{\partial t}(l, t) = \omega l = \frac{12V_0}{\pi^2} - \frac{3M_0t}{ml^2}$$

Hence for $t > t_s$

$$y(l, t) = V_0t_s + \frac{12V_0}{\pi^2}(t - t_s) - \frac{3M_0}{2ml^2}(t^2 - t_s^2) \quad \ldots\ldots [47]$$

The final deflection at the middle δ_f is given by

$$\frac{M_0\delta_f}{ml^2V_0^2} = \frac{4}{\pi^2} - \frac{1}{6} = 0.2386 \quad \ldots\ldots [48]$$

To calculate the angle of deformation at the middle of the beam, observe that, for $t < t_s$

$$\frac{\partial y}{\partial x}(l, t) = 0$$

For $t > t_s$ we have

$$\frac{\partial y}{\partial x}(l, t) = \int_{t_s}^t \omega dt = \frac{12V_0}{\pi^2 l}(t - t_s) - \frac{3M_0}{2ml^2}(t^2 - t_s^2) \quad \ldots\ldots [49]$$

The final angle of the tangent line at the middle θ_f is given by

$$\frac{M_0}{mlV_0^2}\theta_f = \frac{1}{6} \quad \ldots\ldots [50]$$

The final angle of the tangent line at the support θ_{1f} may also be readily shown to be given by

$$\frac{M_0}{mlV_0^2}\theta_{1f} = \frac{1}{4} \quad \ldots\ldots [51]$$

As a check, we note that the initial kinetic energy of the beam is $V_0^2ml/2$. The energy absorbed at the central plastic hinge is $2M_0\theta_f = mlV_0^2/3$, while the work done in the interior of the two half-beams is $2M_0(\theta_{1f} - \theta_f) = mlV_0^2/6$. These energies balance.

Comparison of Solutions

In Figs. 8 to 11 are shown typical curves obtained from the elastic-plastic solution. They show the central angle θ (contained in the nondimensional quantity $EI\theta/M_0l$) as a function of the nondimensional time $\eta' = \pi^2(t - t_1)/4kl^2$, for the four values $S = 1, 2, 5$, and 13, respectively. It will be recalled that $S = mEIV_0^2/2M_0^2$, and hence S stands for the ratio of the initial kinetic energy $mlV_0^2/2$ to the quantity M_0^2l/EI which is an upper bound for the elastic-strain energy which can be stored in the beam.

The final plastic angle θ_f, as already stated, corresponds to the time η_f' when the slope of the curve of θ versus time first becomes zero. However, in certain cases, which are exemplified by Fig. 9, the first point of zero slope corresponds to a very weak relative maximum. It seems very likely that in such a case the angle corresponding to this relative maximum is not the maximum central angle, there being probably a second elastic-plastic phase following the second wholly elastic phase. No attempt has been made in this paper to determine the additional plastic flow in this second elastic-plastic phase, which would require a second sequence of eigenfunction solutions corresponding first to the wholly elastic beam and then to the beam with central plastic hinge.

In an attempt to bracket the maximum central angle and deflection, both the first maximum and the absolute maximum points were considered. Table 1 shows magnitudes obtained from Figs. 8 to 11, together with limiting values for very large S.

The last line of Table 1 gives the results obtained from the plastic-rigid analysis of this paper. In the next to the last line, figures are given for deformations computed from a drastically simplified plastic-rigid analysis in which plastic flow is assumed to occur only at the plastic hinge at the mid-point. Then the initial kinetic energy is completely absorbed by the work done at this hinge, and we can write

$$\left.\begin{aligned} \frac{1}{2}\,mlV_0^2 &= 2M_0\theta_f' \\ \frac{M_0\theta_f'}{mlV_0^2} &= \frac{M_0\delta_f'}{ml^2V_0^2} = \frac{1}{4} \end{aligned}\right\} \quad \ldots\ldots [52]$$

This is the "upper bound" method suggested by Bleich and Salvadori,[7] although in some problems a localization of plastic flow in this manner may furnish too low rather than too high values.

Table 1 includes also the values of R obtained from the elastic-plastic analysis. Since R is the ratio of plastic work done ($2M_0\theta_f$) to the upper limit of the elastic-strain energy (M_0^2l/EI), R is obtained simply by multiplying by 2 the values computed for $EI\theta_f/M_0l$.

Inspection of Table 1 shows that the value 0.167 of the nondimensional angular deformation parameter $M_0\theta_f/mlV_0^2$, furnished by the plastic-rigid analysis, is in poor agreement with the limiting value $24/\pi^4 \doteq 0.246$ from the elastic-plastic solution of this paper. The latter result also differs slightly from the value 0.25 obtained by the "single-hinge" rigid-plastic method. This small difference is evidently due to the fact that when plastic deformation ceases, in the elastic-plastic solution, the beam still has both kinetic energy and strain energy.

TABLE 1 COMPARISON OF RESULTS

First maximum of $\theta(\xi)$ curve						Absolute maximum					
S	R	$\frac{EI}{M_0 l}\theta_f$	$\frac{EI}{M_0 l^2}\delta_f$	$\frac{M_0\theta_f}{mlV_0^2}$	$\frac{M_0\delta_f}{ml^2V_0^2}$	S	R	$\frac{EI}{M_0 l}\theta_f$	$\frac{EI\theta_f}{M_0 l^2}$	$\frac{M_0\theta_f}{mlV_0^2}$	$\frac{M_0\delta_f}{ml^2V_0^2}$
1	0.568	0.284	0.654	0.142	0.327	1	0.568	0.284	0.654	0.142	0.327
2	1.24	0.62	0.998	0.155	0.249	2	1.64	0.82	1.168	0.205	0.292
5	4.0	2.00	2.34	0.200	0.234	5	4.68	2.34	2.64	0.234	0.264
13	11.9	5.96	6.27	0.229	0.241	13	12.6	6.30	6.59	0.242	0.254
∞	∞	$\frac{24}{\pi^4}(2S-1)$		$\frac{24}{\pi^4}=0.246$		∞	∞	$\frac{24}{\pi^4}(2S-1)$		0.246	0.246
Single-hinge plastic-rigid		$\frac{1}{4}\times 2S$	$\frac{1}{4}\times 2S$	0.25	0.25						
Plastic-rigid		$\frac{1}{6}\times 2S$	$\frac{0.239}{(2S)}$	0.167	0.239						

$S=\frac{mEIV_0^2}{2M_0^3}$; $R=2\frac{EI\theta_f}{M_0 l}$; $\frac{M_0\theta_f}{mlV_0^2}=\frac{EI\theta_f}{2SM_0 l}$, etc.

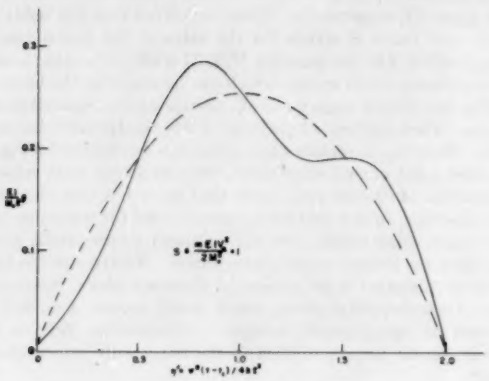

FIG. 8

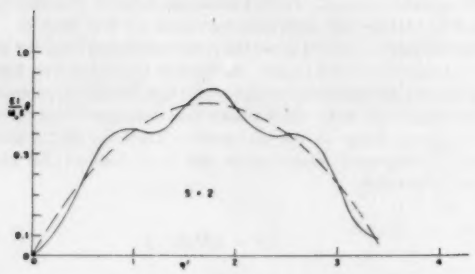

FIG. 9

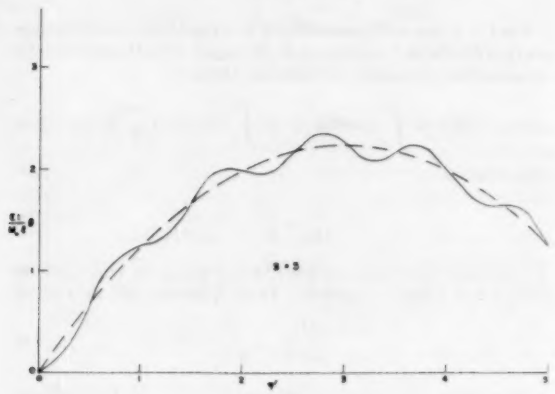

FIG. 10

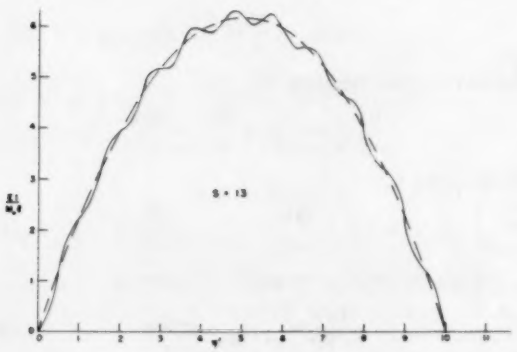

FIG. 11

Table 1 also shows that the displacement parameter $M_0\delta_f/ml^2V_0^2 = 0.239$ predicted by the plastic-rigid analysis agrees to within 5 per cent with that given by the single-hinge plastic-rigid solution (0.25) and the limiting value for very large S of the elastic-plastic solution (0.246).

For large S-values the present plastic-rigid solution presumably yields correct results for both the angular deformation and deflection. Comparison with corresponding results of an elastic-plastic solution will show the minimum value of the initial energy or the plastic work, above which the plastic-rigid solution is valid, only if the elastic-plastic solution itself is accurate. In the present elastic-plastic analysis the plastic-moment condition is explicitly satisfied at the beam mid-section but has not been used elsewhere in the beam. Thus the results can be taken as correct only if it is verified that the bending moment is everywhere no greater than M_0 in magnitude, for a given value of S.

In order to examine the bending-moment magnitudes the following approximate expressions may be used, obtained by retaining only the two terms with coefficients A_1, A_2 in the infinite series of Equation [23]

$$\frac{M}{M_0}=-\frac{EI}{M_0}\frac{\partial^2 y}{\partial x^2}=\frac{3}{2}\xi-\frac{1}{2}\xi^3+\sqrt{2S-1}\,\frac{\pi^2}{\sqrt{2}}\left\{\frac{-\sin a_1\sinh a_1\xi+\sin a_1\xi\sinh a_1}{a_1^3\left(1-\frac{\pi^4}{16a_n^4}\right)\sinh a_1}\sin\frac{4}{\pi^2}a_1^2\eta'\right.$$

$$\left.+\frac{\sin a_2\sinh a_2\xi-\sin a_2\xi\sinh a_2}{a_2^3\sinh a_2}\sin\frac{4}{\pi^2}a_2^2\eta'\right\}\quad\ldots\ldots[53]$$

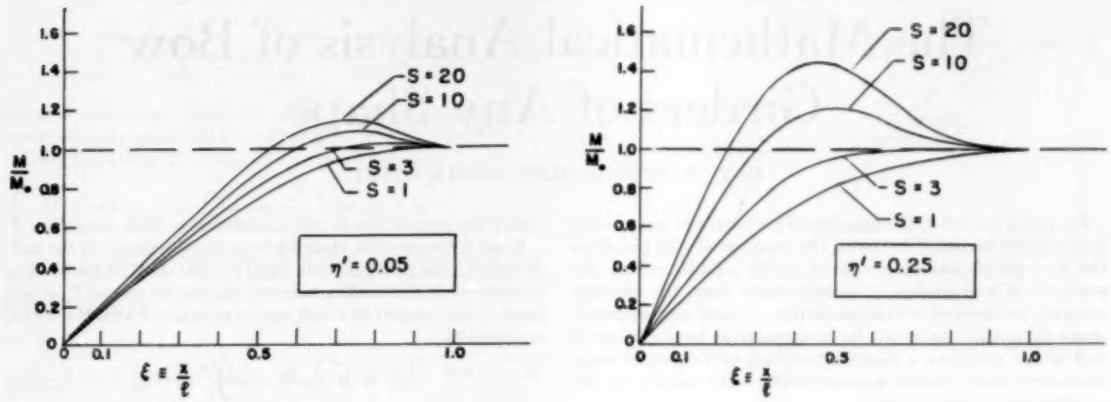

FIG. 12

where $\xi = x/l$, $a_1 = \pi + \pi/4$, $a_2 = 2\pi + \pi/4$. For example, choosing $\xi = 0.9$ and 0.5, the approximate formulas are

$$\xi = 0.9: \frac{M}{M_0} = 0.985 + \sqrt{2S - 1}[0.0111 \sin 6.25\eta' + 0.0080 \sin 20.25\eta'] \ldots\ldots [54a]$$

$$\xi = 0.5: \frac{M}{M_0} = 0.688 + \sqrt{2S - 1}\,[0.1263 \sin 6.25\eta' + 0.0081 \sin 20.25\eta'] \ldots\ldots [54b]$$

These indicate, roughly, that the limit moment will be exceeded at $\xi = 0.9$ when S is greater than about 1.2; and at $\xi = 0.5$ when S is greater than about 3.9. (The maximum values of the bracketed functions in Equations [54*a*, *b*] are about 0.013, 0.12, respectively.)

The curves plotted in Fig. 12 show the bending-moment ratios M/M_0 for various S-values and the two times $\eta' = 0.05$ and 0.25. It is clear that the present elastic-plastic solution must be unsatisfactory for S as large as 10, since at $\eta' = 0.25$ (which is long before the theoretical maximum deformations are attained) the limit moment is exceeded over about 70 per cent of the length of the beam.

Conclusion

Since the plastic-rigid solution can be expected to give good results only for values of S of the order of 10 or greater, it is clear that confirmation of the validity of the present plastic-rigid solution must await extension of the elastic-plastic solution so as to satisfy the moment-plasticity condition. Such an extension, in which the plasticity condition is exactly satisfied throughout the beam, involves serious analytical and computational difficulties. However, it may be possible to obtain adequate approximate solutions. For example, a central plastic zone whose length is chosen arbitrarily might be inserted at some stage of the deformation. This and other methods of approximation are now under study.

The Mathematical Analysis of Bow Girders of Any Shape

By M. M. ABBASSI,[1] ALEXANDRIA, EGYPT

By using parametric equations in which the parameter is the angle included between the tangent at any point on the bow girder and the tangent at the middle point, the analysis of bow girders of shapes other than the circular arc can be treated mathematically. Exact and approximate formulas are given for symmetrical bow girders of any shape carrying a distributed load or two equal concentrated loads placed symmetrically with respect to the middle point of the girder.

Introduction

THE subject of the beam curved in plan has been discussed in quite an interesting manner by Pippard.[2] He stated in his discussion that no general expressions can be given for certain lengths which he mentioned and which are associated with the normal at any point of the bow girder.

By using parametric equations in which the parameter is the angle included between the tangent at any point on the bow girder and the tangent at the middle point, these lengths can be easily expressed in terms of this parameter and the treatment of bow girders of shapes other than the circular arc is much simplified by this method.

It is well known that the bending moment and torque are dependent on the ratio $\lambda = (EI)/(NJ)$ where E = modulus of elasticity in tension or compression, I = moment of inertia of the cross section, N = modulus of rigidity, and NJ = torsional stiffness. In the present investigation an attempt has been made to obtain the necessary conditions for the bending moment and torque to be independent of this ratio, and a corresponding simple approximate formula is given.

Symmetrical Arc Bow Girder of Any Shape Carrying a Uniformly Distributed Load

Consider a symmetrical arc bow girder rigidly fixed at both ends carrying a uniformly distributed load w per unit length. The line of symmetry is taken as the y-axis; the tangent at the middle point of the girder is taken as the x-axis (Fig. 1). If the co-ordinates (x, y) of any point on the center line of the bow girder be expressed uniquely in terms of θ, the angle of inclination of the tangent at the point, then the parametric equations of the curve will be

$$x = x_\theta, \quad y = y_\theta, \quad \tan\theta = \frac{y_\theta'}{x_\theta'}$$

where the primes denote the differentiation with respect to θ.

From symmetry, the shearing force and the torque at the middle point of the girder are both equal to zero. If M_o is the bending moment at O, the bending moment M_s and the torque T_s at any point X, the tangent at which makes an angle θ with the x-axis, are given by

$$M_s = M_o \cos\theta - w\int_0^\theta CD\, ds_\phi \quad \ldots\ldots [1]$$

$$T_s = -M_o \sin\theta + w\int_0^\theta XD\, ds_\phi \quad \ldots\ldots [2]$$

where ds_ϕ is the elementary length referred to the parameter ϕ.

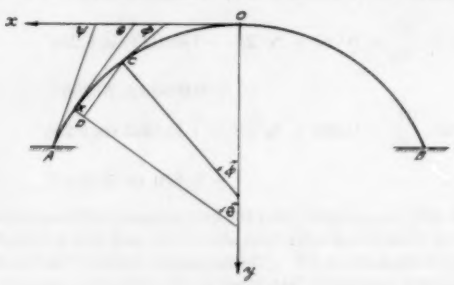

Fig. 1

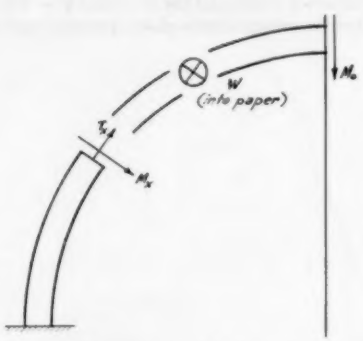

Fig. 2

The positive signs for the torque, moment, and load are shown in Fig. 2.

If U is the total strain energy, we have

$$\frac{\partial U}{\partial M_o} = 0$$

or

$$\frac{\partial U_B}{\partial M_o} + \frac{\partial U_T}{\partial M_o} = 0$$

where U_B is the strain energy due to bending and U_T is the strain energy due to torsion. It follows that

---

[1] Assistant Professor of Mathematics, Alexandria University.

[2] "The Analysis of Engineering Structures," by A. Pippard and J. Baker, Edward Arnold & Co., London, England, 1936, p. 395.

Presented at the National Applied Mechanics Division Conference, Urbana, Ill., June 14-16, 1956, of The American Society of Mechanical Engineers.

Discussion of this paper should be addressed to the Secretary, ASME, 29 West 39th Street, New York, N. Y., and will be accepted until January 10, 1957, for publication at a later date. Discussion received after the closing date will be returned.

Note: Statements and opinions advanced in papers are to be understood as individual expressions of their authors and not those of the Society. Manuscript received by ASME Applied Mechanics Division, January 7, 1955. Paper No. 56—APM-23.

$$\int_0^{\psi} M_s \frac{\partial M_s}{\partial M_o}\, ds + \lambda \int_0^{\psi} T_s \frac{\partial T_s}{\partial M_o}\, ds = 0 \ldots\ldots [3]$$

where ψ is the angle which the tangent at the end of the girder makes with the x-axis and $\lambda = (EI)/(NJ)$.

Using Equations [1] and [2], Equation [3] gives

$$\int_0^{\psi} M_s \cos^2\theta\, ds - w \int_0^{\psi} \left(\cos\theta \int_0^{\theta} CD\, ds_\phi\right) ds + \lambda \int_0^{\psi} M_s \sin^2\theta\, ds - \lambda w \int_0^{\psi} \left(\sin\theta \int_0^{\theta} XD\, ds_\phi\right) ds = 0$$

from which we get

$$M_o = \frac{\int_0^{\psi} \left(\cos\theta \int_0^{\theta} CD\, ds_\phi\right) ds + \lambda \int_0^{\psi} \left(\sin\theta \int_0^{\theta} XD\, ds_\phi\right) ds}{w \left\{\int_0^{\psi} \cos^2\theta\, ds + \lambda \int_0^{\psi} \sin^2\theta\, ds\right\}} \ldots\ldots [4]$$

Expression of XD, CD as Functions of θ and ϕ

The parametric equations of the curve, Fig. 3, are given by

$$x = x_\theta, \quad y = y_\theta$$

The equation of tangent at X is

$$y - y_\theta = \tan\theta(x - x_\theta)$$

or $$y - x\tan\theta - y_\theta + x_\theta \tan\theta = 0$$

If XD = length of perpendicular from $C(x_\phi, y_\phi)$ to the tangent at X then

$$XD = \frac{y_\phi - x_\phi \tan\theta - y_\theta + x_\theta \tan\theta}{\sec\theta}$$

or $$XD = (x_\theta - x_\phi)\sin\theta - (y_\theta - y_\phi)\cos\theta \ldots\ldots [5]$$

In our discussion, XD must be numerically positive; it is positive if

$$\frac{y_\theta - y_\phi}{x_\theta - x_\phi} < \tan\theta$$

or the slope of the chord CX is less than the slope of the tangent at X which is true. The equation of the normal at X is

$$y - y_\theta = -\cot\theta(x - x_\theta)$$

or $$-x\cot\theta - y + y_\theta + x_\theta \cot\theta = 0$$

If CD = length of perpendicular from $c(x_\phi, y_\phi)$ to the normal at X, then

$$CD = (x_\theta - x_\phi)\cos\theta + (y_\theta - y_\phi)\sin\theta \ldots\ldots [6]$$

It is evident that CD is positive since $x_\theta > x_\phi$, $y_\theta > y_\phi$, and θ is assumed to be less than $\pi/2$

$$\frac{\partial XD}{\partial\theta} = (x_\theta - x_\phi)\cos\theta + x_\theta' \sin\theta + (y_\theta - y_\phi)\sin\theta - y_\theta' \cos\theta$$

Since $y_\theta'/x_\theta' = \tan\theta$ or $x_\theta' \sin\theta = y_\theta' \cos\theta$, we have

$$\frac{\partial XD}{\partial\theta} = (x_\theta - x_\phi)\cos\theta + (y_\theta - y_\phi)\sin\theta = CD$$

and we obtain the relation

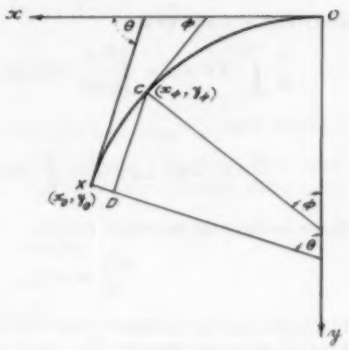

Fig. 3

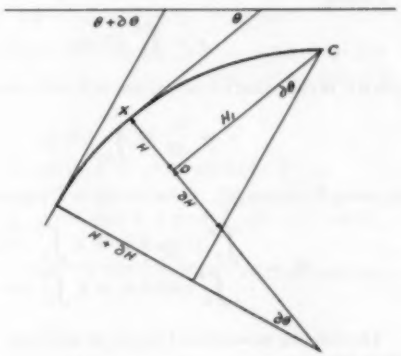

Fig. 4

$$\frac{\partial XD}{\partial\theta} = CD \ldots\ldots [7]^1$$

Differentiating Equation [2] with respect to θ we get

$$\frac{\partial T_s}{\partial\theta} = -M_o \cos\theta + w \frac{\partial}{\partial\theta} \int_0^{\theta} XD\, ds_\phi$$

By using the general rule of differentiation under the sign of integration, viz.

$$\frac{\partial}{\partial\theta}\int_a^b f(\phi,\theta)d\phi = \int_a^b \frac{\partial}{\partial\theta} f(\phi,\theta)d\phi + f(b,\theta)\frac{db}{d\theta} - f(a,\theta)\frac{da}{d\theta}$$

we get

$$\frac{\partial}{\partial\theta}\int_0^{\theta} XD\, ds_\phi = \int_0^{\theta} \frac{\partial}{\partial\theta}(XD)ds_\phi + f(\theta,\theta)\frac{d\theta}{d\theta} - f(o,\theta)\frac{do}{d\theta}$$

Since

$$\frac{do}{d\theta} = 0, \quad \frac{d\theta}{d\theta} = 1; \quad f(\phi,\theta) = XD = (x_\theta - x_\phi)\sin\theta - (y_\theta - y_\phi)\cos\theta$$

---

[1] This result can be proved geometrically as follows: Let $XD = H$, $CD = H_1$, Fig. 4; $H_1\partial\theta = \partial H$

$$\therefore \frac{\partial H}{\partial\theta} = H_1 \text{ or } \frac{\partial XD}{\partial\theta} = CD$$

then $f(\theta, \theta) = 0$ and we get

$$\frac{\partial}{\partial\theta}\int_0^\theta XD\,ds_\phi = \int_0^\theta \frac{\partial}{\partial\theta}(XD)\,ds_\phi = \int_0^\theta CD\,ds_\phi \ldots [8]$$

It follows that

$$\frac{\partial T_x}{\partial\theta} = -M_o\cos\theta + w\int_0^\theta CD\,ds_\phi = -M_x$$

Hence we have the important relation

$$\frac{\partial T_x}{\partial\theta} = -M_x \ldots\ldots [9]$$

It follows that the maximum torque occurs at the points of zero bending moments whatever the shape of the girder may be.

Putting

$$v = \int_0^\theta XD\,ds_\phi$$

(then it is clear that v is a function of θ only), we get

$$v' = \frac{dv}{d\theta} = \int_0^\theta CD\,ds_\phi$$

by using Equation [8]. Substituting in Equation [4] we get

$$M_o = w\,\frac{\int_0^\psi v'\cos\theta\,ds + \lambda\int_0^\psi v\sin\theta\,ds}{\int_0^\psi \cos^2\theta\,ds + \lambda\int_0^\psi \sin^2\theta\,ds} \ldots\ldots [10]$$

The bending moment and torque at any point of the girder are then given by

$$M_x = M_o\cos\theta - wv' \ldots\ldots [11]$$

$$T_x = -M_o\sin\theta + wv \ldots\ldots [12]$$

It is evident that the value of M_o is dependent on λ, therefore M_x, T_x at any point X are dependent on λ. If the tangent at the end of the beam makes an angle of 90 deg with the tangent at the middle point O, the end fixing moment will be equal to $M_o\cos 90 - wv' = -wv'$ which is independent of λ.

Condition Which Must Be Satisfied in Order That M_o Should Be Independent of λ

It is easy to prove that the value of the fraction $(a + b\lambda)/(c + d\lambda)$ is independent of λ if $a/b = c/d$.

From Equation [10], M_o is independent of λ if

$$\frac{\int_0^\psi v'\cos\theta\,ds}{\int_0^\psi v\sin\theta\,ds} = \frac{\int_0^\psi \cos^2\theta\,ds}{\int_0^\psi \sin^2\theta\,ds} \ldots\ldots [13]$$

If this condition is satisfied, the bending moment and the torque at any point are independent of λ. For a given curve, this condition is satisfied for a special value of ψ as will be seen from the examples.

If for a certain value of ψ, M_o is independent of λ, we can find a simple formula for determining M_o as follows

$$\frac{\int_0^\psi v'\cos\theta\,ds}{\int_0^\psi \cos^2\theta\,ds} = \frac{\int_0^\psi v\sin\theta\,ds}{\int_0^\psi \sin^2\theta\,ds} = k$$

or

$$\frac{\int_0^\psi (v'\cos\theta + v\sin\theta)ds}{s} = k$$

where s is half the perimeter of the girder. We get

$$\int_0^\psi \left\{\left[\cos\theta\left(\int_0^\theta (x_\theta - x_\phi)\cos\theta + (y_\theta - y_\phi)\sin\theta\right)\right]ds_\phi + \left[\sin\theta\left(\int_0^\theta (x_\theta - x_\phi)\sin\theta - (y_\theta - y_\phi)\cos\theta\right)\right]ds_\phi\right\}ds = ks$$

or

$$\int_0^\psi\int_0^\theta (x_\theta - x_\phi)ds_\phi\,ds = ks$$

From Equation [10], $M_o = wk$, hence

$$M_o = \frac{w}{s}\int_0^\psi\int_0^\theta (x_\theta - x_\phi)ds_\phi ds \ldots\ldots [14]$$

When putting $\lambda = 1$ in Equation [10] we get the foregoing value of M_o, and Equation [14] can be used also when $\lambda = 1$.

For reinforced-concrete beams with the usual permissible stresses, if $\lambda = 1$, $d/b = 1.1$ approx, i.e., about 1,[4] and the cross section will be nearly a square. It follows that Equation [14] can be used in the following cases:

1 When M_o is independent of λ for a certain value of ψ.
2 For all shapes of cross section if $\lambda = 1$.
3 When the cross section of the reinforced-concrete beam is nearly a square.

Position of Points of Zero Bending Moment

The position of points of zero bending moment must be determined, since the maximum torque occurs at such points and may be greater than that at the supports. If the tangent at a point of zero bending moment makes angle β with the x-axis, Equation [11] gives

$$0 = M_o\cos\beta - wv'$$

or

$$\cos\beta = \frac{wv'}{M_o} \ldots\ldots [15]$$

Symmetrical Bow Girder of Any Shape Carrying Two Equal Concentrated Loads Placed Symmetrically at the Girder

If the girder is carrying two equal concentrated loads W placed

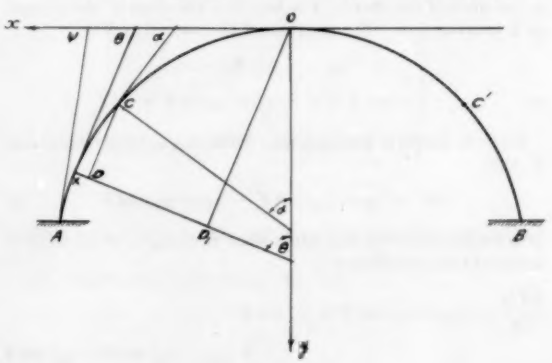

Fig. 5

symmetrically at C and C' for which the slope of the tangent is equal to α (Fig. 5), then

[4] "Design of Bow Girders in Reinforced Concrete," by W. Marshall, *Concrete and Constructional Engineering*, vol. 36, 1941, p. 467.

$$M_x = M_o \cos\theta - W \cdot CD \quad \ldots\ldots [16]$$

$$T_x = -M_o \sin\theta + W \cdot XD \quad \ldots\ldots [17]$$

$$\frac{\partial T_x}{\partial \theta} = -M_x$$

Since $\partial U/\partial M_o = 0$, we get

$$\int_0^\psi M_o \cos^2\theta ds - W\int_\alpha^\psi CD\cos\theta\, ds + \lambda\int_0^\psi M_o \sin^2\theta\, ds - W\lambda\int_\alpha^\psi XD\sin\theta\, ds = 0$$

whence

$$M_o = W\frac{\int_\alpha^\psi CD\cos\theta\, ds + \lambda\int_\alpha^\psi XD\sin\theta\, ds}{\int_0^\psi \cos^2\theta\, ds + \lambda\int_0^\psi \sin^2\theta\, ds}$$

If we put

$$XD = H, \quad CD = H' = \frac{dH}{d\theta}$$

we get

$$H = (x_\theta - x_\alpha)\sin\theta - (y_\theta - y_\alpha)\cos\theta$$

$$H' = (x_\theta - x_\alpha)\cos\theta + (y_\theta - y_\alpha)\sin\theta$$

and

$$M_o = W\frac{\int_\alpha^\psi H'\cos\theta\, ds + \lambda\int_\alpha^\psi H\sin\theta\, ds}{\int_0^\psi \cos^2\theta\, ds + \lambda\int_0^\psi \sin^2\theta\, ds} \quad \ldots\ldots [18]$$

M_o is independent of λ if

$$\frac{\int_\alpha^\psi H'\cos\theta\, ds}{\int_\alpha^\psi H\sin\theta\, ds} = \frac{\int_0^\psi \cos^2\theta\, ds}{\int_0^\psi \sin^2\theta\, ds}$$

If M_o is independent of λ or if $\lambda = 1$ we can easily find that

$$M_o = \frac{W}{s}\int_\alpha^\psi (x_\theta - x_\alpha)ds \quad \ldots\ldots [19]$$

The case commonly met with in practice is that of a beam carrying a single concentrated load W at its middle point O. In this case we have

$$M_o = \frac{W}{2}\frac{\int_0^\psi H'\cos\theta\, ds + \lambda\int_0^\psi H\sin\theta\, ds}{\int_0^\psi \cos^2\theta\, ds + \lambda\int_0^\psi \sin^2\theta\, ds} \quad \ldots\ldots [20]$$

where in this case, $H = XD_1 = x\sin\theta - y\cos\theta$

$$H' = OD_1 = x\cos\theta + y\sin\theta$$

If M_o is independent of λ or if $\lambda = 1$ we get

$$M_o = \frac{W}{2s}\int_0^\psi x\, ds \quad \ldots\ldots [21]$$

Position of Points of Zero Bending Moment

In the case of a single concentrated load W at the middle of the girder, if β is the inclination of the tangent at the point of zero bending moment, we get

$$0 = M_o\cos\beta - \frac{W}{2}OD_1$$

$$\cos\beta = \frac{WOD_1}{2M_o}$$

Illustrative Examples

1 Cycloidal Arc Bow Girder Carrying a Uniformly Distributed Load w Per Unit Length. The parametric equations of the curve are

$$x = a(2\theta + \sin 2\theta)$$

$$y = a(1 - \cos 2\theta)$$

$$ds = 4a\cos\theta d\theta$$

$$ds_\phi = 4a\cos\phi d\phi$$

$$XD = (x_\theta - x_\phi)\sin\theta - (y_\theta - y_\phi)\cos\theta$$

$$= a[(2\theta + \sin 2\theta)\sin\theta + \cos 2\theta\cos\theta] - a[(2\phi + \sin 2\phi)\sin\theta + \cos 2\phi\cos\theta]$$

$$v = \int_0^\theta XD\, ds_\phi$$

$$= 4a^2\{[(2\theta + \sin 2\theta)\sin\theta + \cos 2\theta\cos\theta]\sin\theta\}$$

$$- 4a^2\left[2\sin\theta\int_0^\theta \phi\cos\phi d\phi + 2\sin\theta\int_0^\theta \sin\phi\cos^2\phi d\phi + \cos\theta\int_0^\theta (1 - 2\sin^2\phi)\cos\phi d\phi\right]$$

which reduces to

$$v = \frac{16}{3}a^2\sin\theta\,(1 - \cos\theta)$$

$$v' = \frac{dv}{d\theta} = \frac{16}{3}a^2(1 + \cos\theta - 2\cos^2\theta)$$

$$\int_0^\psi v'\cos\theta\, ds = \frac{64}{3}a^3\int_0^\psi (\cos^2\theta + \cos^3\theta - 2\cos^4\theta)d\theta$$

$$= \frac{64}{3}a^3\left(-\frac{1}{4}\psi - \frac{1}{4}\sin 2\psi + \sin\psi - \frac{1}{3}\sin^3\psi - \frac{1}{16}\sin 4\psi\right)$$

$$\int_0^\psi v\sin\theta\, ds = \frac{64}{3}a^3\int_0^\psi (\cos\theta - \cos^2\theta - \cos^3\theta + \cos^4\theta)d\theta$$

$$= \frac{64}{3}a^3\left(-\frac{1}{8}\psi + \frac{1}{3}\sin^3\psi + \frac{1}{32}\sin 4\psi\right)$$

$$\int_0^\psi \cos^2\theta\, ds = 4a\int_0^\psi \cos^2\theta\, d\theta$$

$$= 4a\left(\sin\psi - \frac{1}{3}\sin^3\psi\right)$$

$$\int_0^\psi \sin^2\theta\, ds = 4a\int_0^\psi \sin^2\theta\cos\theta\, d\theta$$

$$= \frac{4a}{3}\sin^3\psi$$

Substituting the foregoing integrals in Equation [10] and putting

$$\frac{1}{3}\sin^3\psi = \frac{1}{4}\sin\psi - \frac{1}{12}\sin 3\psi$$

we get

$$M_o = \frac{16}{3} wa^2 \frac{(-3\psi + 9\sin\psi - 3\sin 2\psi + \sin 3\psi - 0.75\sin 4\psi) + \lambda(-1.5\psi + 3\sin\psi - \sin 3\psi + 0.375\sin 4\psi)}{(9\sin\psi + \sin 3\psi) + \lambda(3\sin\psi - \sin 3\psi)}$$

If M_o is independent from λ we get

$$\frac{-3\psi + 9\sin\psi - 3\sin 2\psi + \sin 3\psi - 0.75\sin 4\psi}{-1.5\psi + 3\sin\psi - \sin 3\psi + 0.375\sin 4\psi} = \frac{9\sin\psi + \sin 3\psi}{3\sin\psi - \sin 3\psi}$$

from which wet get

$$\cos\psi(24\psi\cos\psi - 8\sin\psi - 7\sin 3\psi + \sin 5\psi) = 0$$

Hence either $\cos\psi = 0$, i.e., $\psi = \pi/2$ (complete arc of a cycloid) or

$$24\psi\cos\psi - 8\sin\psi - 7\sin 3\psi + \sin 5\psi = 0$$

which gives $\psi = 0$ (straight beam), and $\psi = \pi/2$. Therefore for a complete arc of a cycloid ($\psi = \pi/2$) we get

$$M_o = \frac{16}{3} wa^2 \frac{\left(-3\frac{\pi}{2} + 8\right) + \lambda\left(-\frac{3\pi}{4} + 4\right)}{8 + 4\lambda} = \frac{1}{3} wa^2(16 - 3\pi)$$

If $\lambda = 1$, or approximately equals 1 for other values of λ, Equation [14] gives

$$M_o = \frac{w}{s}\int_0^{\psi}\int_0^{\theta}(x_\theta - x_\phi)ds_\phi\, ds$$

$$= \frac{w}{4a}\int_0^{\psi}\int_0^{\theta} a[2(\theta - \phi) + (\sin 2\theta - \sin 2\phi)]\, 4a\cos\phi \times 4a\cos\theta\, d\phi d\theta$$

$$= 4wa^2\int_0^{\psi}\left(\frac{4}{3}\cos\theta - \frac{4}{3}\cos^4\theta\right)d\theta$$

which reduces to

$$M_o = \frac{1}{6} wa^2(32\sin\psi - 12\psi - 8\sin 2\psi - \sin 4\psi)$$

When $\psi = \pi/2$, we get

$$M_o = \frac{1}{3} wa^2(16 - 3\pi)$$

2 Parabolic Arc Bow Girder Carrying a Concentrated Load W at the Middle. The parametric equations of the curve are

$$x = 2a\tan\theta$$

$$y = a\tan^2\theta$$

$$ds = 2a\sec^3\theta d\theta$$

$$H = x\sin\theta - y\cos\theta = a\frac{\sin^2\theta}{\cos\theta}$$

$$H' = \frac{dH}{d\theta} = a\frac{2\sin\theta - \sin^3\theta}{\cos^3\theta}$$

$$\int_0^{\psi} H'\cos\theta\, ds = 2a^2\int_0^{\psi}\left(\frac{2\sin\theta}{\cos^4\theta} - \frac{\sin^3\theta}{\cos^4\theta}\right)d\theta = \frac{2}{3}a^2(\sec^3\psi + 3\sec\psi - 4)$$

$$\int_0^{\psi} H\sin\theta\, ds = 2a^2\int_0^{\psi}\frac{\sin^3\theta}{\cos^4\theta}\, d\theta = \frac{2}{3}a^2(\sec^3\psi - 3\sec\psi + 2)$$

$$\int_0^{\psi}\cos^2\theta\, ds = 2a\int_0^{\psi}\sec\theta\, d\theta = 2a\log(\sec\psi + \tan\psi)$$

$$\int_0^{\psi}\sin^2\theta\, ds = 2a\int_0^{\psi}\frac{\sin^2\theta}{\cos^3\theta}\, d\theta = a[\sec\psi\tan\psi - \log(\sec\psi + \tan\psi)]$$

Substituting the foregoing integrals in Equation [20] we get

$$M_o = \frac{Wa}{3}\frac{(\sec^3\psi + 3\sec\psi - 4) + \lambda(\sec^3\psi - 3\sec\psi + 2)}{2\log(\sec\psi + \tan\psi) + \lambda[\sec\psi\tan\psi - \log(\sec\psi + \tan\psi)]}$$

It can be shown that M_o is not independent of λ for real values of ψ. If $\lambda = 1$ we get

$$M_o = \frac{2}{3} Wa\frac{\sec^3\psi - 1}{\sec\psi\tan\psi + \log(\sec\psi + \tan\psi)}$$

The foregoing value of M_o can be used approximately for other values of λ which are approximately equal to 1.

It also can be deduced from the simple Equation [21] that

$$M_o = W\frac{\int_0^{\psi} 4a^2\tan\theta\sec^3\theta\, d\theta}{2a\int_0^{\psi}\sec^3\theta\, d\theta} = \frac{2}{3} Wa\frac{\sec^3\psi - 1}{\sec\psi\tan\psi + \log(\sec\psi + \tan\psi)}$$

Other shapes of bow girders can be similarly treated.

Acknowledgments

The author owes a debt of gratitude to Dr. S. Bishara, Professor of Mathematics, Faculty of Engineering, University of Alexandria, and to Dr. I. A. Eldemirdash, Dean of the Faculty of Engineering, University of Cairo, for their help, advice, and guidance.

Thermal Stresses in Infinite Elastic Disks

By BRAHMADEV SHARMA,[1] RAJASTHAN, INDIA

A direct method of solving problems of thermal stress in a disk of finite thickness and infinite radius is discussed in this paper.

Nomenclature

The following nomenclature is used in the paper:

σ_x, σ_y, σ_z, τ_{xy}, τ_{xz}, τ_{yz} = Cartesian components of stress
σ_r, σ_θ, σ_z, $\tau_{r\theta}$, τ_{rz}, $\tau_{\theta z}$ = cylindrical components of stress
u, v, w = Cartesian components of displacement
u_r, u_θ, w = cylindrical components of displacement
$\Theta = \sigma_x + \sigma_y + \sigma_z = \sigma_r + \sigma_\theta + \sigma_z$
ν = Poisson's ratio
E = modulus of elasticity
G = modulus of elasticity in shear
$\mu = G$ = Lamé's constant
α = coefficient of linear expansion
ϵ_x, ϵ_y, ϵ_z = unit elongation in x, y, z-directions
γ_{xy}, γ_{xz}, γ_{yz} = shearing-strain components in rectangular coordinates
∇^2 = Laplacian operator
κ = coefficient of conductivity

Introduction

In this paper a direct method of finding thermal stresses in an elastic body due to any temperature distribution is presented. In the first section, the steady state is discussed and the results are applied to find stresses in a disk of thickness d and infinite radius attributable to axisymmetric temperature distribution. A second problem of a semi-infinite solid, in which the elastic properties change at a depth d, also is solved. Finally as a special case, a circular portion of the upper surface of the disk is supposed to be at a uniform temperature while the remainder of the surface is kept at zero temperature. Stress distribution and deformation on the surface for a semi-infinite solid also are found. In the second section, a general solution for an unsteady state is given.

SECTION 1

Method of Solution

If T is the temperature at any point in the solid, the stress-strain relations are (Timoshenko and Goodier)[2]

$$\left.\begin{aligned}\epsilon_x - \alpha T &= \frac{\partial u}{\partial x} - \alpha T = \frac{1}{E}[\sigma_x - \nu(\sigma_y + \sigma_z)]\\ \epsilon_y - \alpha T &= \frac{\partial v}{\partial y} - \alpha T = \frac{1}{E}[\sigma_y - \nu(\sigma_z + \sigma_x)]\\ \epsilon_z - \alpha T &= \frac{\partial w}{\partial z} - \alpha T = \frac{1}{E}[\sigma_z - \nu(\sigma_x + \sigma_y)]\end{aligned}\right\} \quad \ldots[1]\ (cont.)$$

and

$$\left.\begin{aligned}\gamma_{xy} &= \frac{\partial u}{\partial y} + \frac{\partial v}{\partial x} = \frac{2(1+\nu)}{E}\tau_{xy}\\ \gamma_{yz} &= \frac{\partial v}{\partial z} + \frac{\partial w}{\partial y} = \frac{2(1+\nu)}{E}\tau_{yz}\\ \gamma_{zx} &= \frac{\partial w}{\partial x} + \frac{\partial u}{\partial z} = \frac{2(1+\nu)}{E}\tau_{zx}\end{aligned}\right\} \quad \ldots\ldots[2]$$

Also the compatibility equations are

$$\frac{\partial^2 \epsilon_y}{\partial z^2} + \frac{\partial^2 \epsilon_z}{\partial y^2} = \frac{\partial^2 \gamma_{yz}}{\partial y \partial z} \quad \ldots\ldots[3a]$$

and two similar equations; and

$$2\frac{\partial^2 \epsilon_y}{\partial x \partial z} = \frac{\partial}{\partial y}\left[\frac{\partial \gamma_{yz}}{\partial x} - \frac{\partial \gamma_{zx}}{\partial y} + \frac{\partial \gamma_{xy}}{\partial z}\right] \quad \ldots\ldots[3b]$$

and two similar equations.

Substituting the values of ϵ_x, ϵ_y, ϵ_z, and γ_{xy}, γ_{yz}, γ_{zx} in Equations [3a] and with the help of the equations of equilibrium

$$\left.\begin{aligned}\frac{\partial \tau_{xz}}{\partial x} + \frac{\partial \tau_{yz}}{\partial y} + \frac{\partial \sigma_z}{\partial z} &= 0\\ \ldots\ldots\ldots\ldots\ldots\ldots\\ \ldots\ldots\ldots\ldots\ldots\ldots\end{aligned}\right\} \quad \ldots\ldots[4]$$

we get

$$(1+\nu)\left[\nabla^2\Theta - \nabla^2\sigma_z - \frac{\partial^2\Theta}{\partial z^2}\right] - \nu\left[\nabla^2\Theta - \frac{\partial^2\Theta}{\partial z^2}\right] + \alpha E\left[\nabla^2 T - \frac{\partial^2 T}{\partial z^2}\right] = 0 \quad \ldots\ldots[5]$$

and two similar equations.

Adding these equations we have

$$(1-\nu)\nabla^2\Theta + 2\alpha E\nabla^2 T = 0 \quad \ldots\ldots[6]$$

But in a steady state

$$\nabla^2 T = 0 \quad \ldots\ldots[7]$$

Hence

$$\nabla^2\Theta = 0 \quad \ldots\ldots[8]$$

By virtue of Equations [7] and [8], Equations [5] reduce to

$$\left.\begin{aligned}\nabla^2\sigma_z + \frac{1}{1+\nu}\frac{\partial^2}{\partial z^2}[\Theta + \alpha E T] &= 0\\ \ldots\ldots\ldots\ldots\ldots\ldots\\ \ldots\ldots\ldots\ldots\ldots\ldots\end{aligned}\right\} \quad \ldots\ldots[9]$$

Equations [3b] on using Equations [1], [2], and [4] give

---

[1] Lecturer in Mathematics, Birla College, Pilani.

[2] "Theory of Elasticity," by S. Timoshenko and J. N. Goodier, McGraw-Hill Book Company, Inc., New York, N. Y., second edition, 1951, p. 421.

Presented at the National Applied Mechanics Division Conference, Urbana, Ill., June 14–16, 1956, of The American Society of Mechanical Engineers.

Discussion of this paper should be addressed to the Secretary, ASME, 29 West 39th Street, New York, N. Y., and will be accepted until January 10, 1957, for publication at a later date. Discussion received after the closing date will be returned.

Note: Statements and opinions advanced in papers are to be understood as individual expressions of their authors and not those of the Society. Manuscript received by ASME Applied Mechanics Division, April 21, 1955. Paper No. 56—APM-19.

$$\left.\begin{aligned} &\nabla^2\tau_{xy} + \frac{1}{1+\nu}\frac{\partial^2}{\partial x \partial y}[\Theta + \alpha ET] = 0 \\ &\cdots\cdots\cdots\cdots\cdots\cdots\cdots\cdots\cdots\cdots \\ &\cdots\cdots\cdots\cdots\cdots\cdots\cdots\cdots\cdots\cdots \end{aligned}\right\} \ldots [10]$$

Solving equations involving τ_{xz}, τ_{yz}, and σ_z we get

$$\left.\begin{aligned} \tau_{xz} &= -\frac{1}{2(1+\nu)} z \frac{\partial}{\partial x}[\Theta + \alpha ET] + \phi_1 \\ \tau_{yz} &= -\frac{1}{2(1+\nu)} z \frac{\partial}{\partial y}[\Theta + \alpha ET] + \phi_2 \\ \sigma_z &= -\frac{1}{2(1+\nu)} z \frac{\partial}{\partial z}[\Theta + \alpha ET] + \phi_3 \end{aligned}\right\} \ldots [11]$$

where ϕ_1, ϕ_2, and ϕ_3 are harmonic functions to be determined by the boundary conditions.

Substituting these values of τ_{xz}, τ_{yz}, and σ_z in the equations of equilibrium, Equations [4]

$$\frac{\partial}{\partial z}[\Theta + \alpha ET] = 2(1+\nu)\left[\frac{\partial \phi_1}{\partial x} + \frac{\partial \phi_2}{\partial y} + \frac{\partial \phi_3}{\partial z}\right] \ldots [12]$$

whence Θ is determined by integration and constant of integration is determined by the conditions of the problem. Values of ϕ_1, ϕ_2, ϕ_3, and Θ being known, the stress components τ_{xz}, τ_{yz}, σ_z are completely determined. Then from Equations [1] and [2] it will, in general, be possible to determine the components of displacement. These will give the remaining stress components.

Solution for Symmetrical Distribution of Temperature

Suppose the plane boundary of the isotropic elastic solid is given by the plane $z = 0$, the axis of z being drawn into the body. The lower boundary is given by the plane $z = d$. The temperature is symmetrical about the z-axis; hence in steady state it satisfies the equation

$$\frac{\partial^2 T}{\partial r^2} + \frac{1}{r}\frac{\partial T}{\partial r} + \frac{\partial^2 T}{\partial z^2} = 0 \ldots\ldots\ldots\ldots [13]$$

This equation is clearly satisfied if we take

$$T = \int_0^\infty [M \cosh mz + N \sinh mz] J_0(mr) dm \ldots [14]$$

where M and N are arbitrary functions of m, and will be determined by the boundary conditions for temperature in particular problems. $J_0(mr)$ is the Bessel function of the first kind and 0th order.

Now, if the surface of the disk is free, in the present axisymmetric case we can put Equations [11] as

$$\left.\begin{aligned} \tau_{xz} &= -\frac{1}{2(1+\nu)} z \frac{\partial}{\partial x}(\Theta + \alpha ET) + \int_0^\infty A \sinh mz \frac{\partial}{\partial x}[J_0(mr)] dm \\ \tau_{yz} &= -\frac{1}{2(1+\nu)} z \frac{\partial}{\partial y}(\Theta + \alpha ET) + \int_0^\infty A \sinh mz \frac{\partial}{\partial y}[J_0(mr)] dm \\ \sigma_z &= -\frac{1}{2(1+\nu)} z \frac{\partial}{\partial z}(\Theta + \alpha ET) + \int_0^\infty Bm \sinh mz J_0(mr) dm \end{aligned}\right\} \ldots [15]$$

where A and B are arbitrary functions of m. These relations make $\tau_{xz} = \tau_{yz} = \sigma_z = 0$ on the plane $z = 0$. On substituting these values Equation [12] gives

$$\frac{\partial}{\partial z}(\Theta + \alpha ET) = 2(1+\nu)\int_0^\infty m^2[B \cosh mz - A \sinh mz] J_0(mr) dm$$

which is satisfied if we take

$$\Theta + \alpha ET = 2(1+\nu)\int_0^\infty m[B \sinh mz - A \cosh mz] J_0(mr) dm \ldots [16]$$

Substituting in Equations [15]

$$\left.\begin{aligned} \tau_{xz} &= \int_0^\infty [-mz(B \sinh mz - A \cosh mz) + A \sinh mz] \frac{\partial}{\partial x}[J_0(mr)] dm \\ \tau_{yz} &= \int_0^\infty [-mz(B \sinh mz - A \cosh mz) + A \sinh mz] \frac{\partial}{\partial y}[J_0(mr)] dm \\ \sigma_z &= \int_0^\infty [-m^2 z(B \cosh mz - A \sinh mz) + mB \sinh mz] J_0(mr) dm \end{aligned}\right\} \ldots [17]$$

From the first two equations in Equations [17] we get

$$\tau_{rz} = -\int_0^\infty m[-mz(B \sinh mz - A \cosh mz) + A \sinh mz] J_1(mr) dm \ldots [18]$$

With the help of Equations [17] the particular values of u, v, and w which satisfy Equations [1] and [2] can be found. As we are considering the axisymmetric case, it is of interest to find u_r and w which are

$$\left.\begin{aligned} u_r &= -\frac{1+\nu}{E}\int_0^\infty \Big\{A[2(1-\nu)\cosh mz + mz \sinh mz] - B[(1-2\nu)\sinh mz + mz \cosh mz] - \frac{\alpha E}{m}[M \cosh mz + N \sinh mz]\Big\} J_1(mr) dm \\ w &= \frac{1+\nu}{E}\int_0^\infty \Big\{A[mz \cosh mz - (1-2\nu)\sinh mz] + B[2(1-\nu)\cosh mz - mz \sinh mz] + \frac{\alpha E}{m}[M \sinh mz + N \cosh mz]\Big\} J_0(mr) dm \end{aligned}\right\} \ldots [19]$$

Also, in order to find the stress components σ_r, σ_θ we know the relations

$$\left.\begin{aligned} \sigma_r + \sigma_\theta &= \Theta - \sigma_z \\ \sigma_r - \sigma_\theta &= 2\mu\left[\frac{\partial u_r}{\partial r} - \frac{u}{r}\right] \end{aligned}\right\} \ldots\ldots [20]$$

Substituting the values of Θ, σ_z, and u_r from Equations [16], [17], and [19] we have

$$\left.\begin{aligned}\sigma_r + \sigma_\theta &= \int_0^\infty m\Big\{B[(1+2\nu)\sinh mz + mz\cosh mz] \\ &\quad - A[2(1+\nu)\cosh mz + mz\sinh mz] \\ &\quad - \frac{\alpha E}{m}[M\cosh mz + N\sinh mz]\Big\}J_0(mr)dm \\ \sigma_r - \sigma_\theta &= \int_0^\infty m\Big\{A[2(1-\nu)\cosh mz + mz\sinh mz] \\ &\quad - B[(1-2\nu)\sinh mz + mz\cosh mz] \\ &\quad - \frac{\alpha E}{m}[M\cosh mz + N\sinh mz]\Big\}J_2(mr)dm\end{aligned}\right\}\ldots[21]$$

which determine σ_r and σ_θ.

It can be seen readily that if the temperature distribution is known, the stresses and displacements are uniquely found from the foregoing equations, the arbitrary constants being determined by imposing two physically possible boundary conditions at the lower boundary.

As a particular case of the boundary conditions at the lower surface we consider that this infinite disk is a part of a semi-infinite solid, such that the elastic constants suddenly change at $z = d$. The temperature being in steady state will be given by the same Equation [14]. It must tend to zero at infinity, so we have

$$N = -M \ldots\ldots[22]$$

For $z > d$, let the stress components be marked with dash. The Equations [11] can be written as

$$\left.\begin{aligned}\tau_{zx}' &= -\frac{1}{2(1+\nu')}(z-d)\frac{\partial}{\partial x}[\Theta' + \alpha' E' T] \\ &\quad + \int_0^\infty Ce^{-m(z-d)}\frac{\partial}{\partial x}[J_0(mr)]dm \\ \tau_{yz}' &= -\frac{1}{2(1+\nu')}(z-d)\frac{\partial}{\partial y}[\Theta' + \alpha' E' T] \\ &\quad + \int_0^\infty Ce^{-m(z-d)}\frac{\partial}{\partial y}[J_0(mr)]dm \\ \sigma_z' &= -\frac{1}{2(1+\nu')}(z-d)\frac{\partial}{\partial z}[\Theta' + \alpha' E' T] \\ &\quad + \int_0^\infty mDe^{-m(z-d)}J_0(mr)dm\end{aligned}\right\}\ldots[23]$$

where C and D are as yet unspecified functions of m. The integrals involved are such that the stresses vanish at infinity.

Proceeding as in the first case we can easily get

$$\left.\begin{aligned}u_r' &= -\frac{1+\nu'}{E'}\int_0^\infty\Big\{[m(z-d)(C+D) \\ &\quad - (1-2\nu')(C+D) - C]e^{-m(z-d)} \\ &\quad - \frac{\alpha' E'}{m}Me^{-mz}\Big\}J_1(mr)dm \\ w' &= -\frac{1+\nu'}{E'}\int_0^\infty\Big\{[m(z-d)(C+D) \\ &\quad + (1-2\nu')(C+D) + D]e^{-m(z-d)} \\ &\quad + \frac{\alpha' E'}{m}Me^{-mz}\Big\}J_0(mr)dm\end{aligned}\right\}\ldots[24]$$

and

$$\left.\begin{aligned}\tau_{rz}' &= -\int_0^\infty m[C - m(z-d) \\ &\quad (C+D)]e^{-m(z-d)}J_1(mr)dm \\ \sigma_z' &= \int_0^\infty m[D + m(z-d) \\ &\quad (C+D)]e^{-m(z-d)}J_0(mr)dm \\ \sigma_r' + \sigma_\theta' &= \int_0^\infty m\Big\{(C+D)[2(1+\nu') \\ &\quad - m(z-d)] - D - \frac{\alpha' E'}{m}Me^{-mz}\Big\}e^{-m(z-d)}J_0(mr)dm \\ \sigma_r' - \sigma_\theta' &= \int_0^\infty m\Big\{[m(z-d)(C+D) \\ &\quad - (1-2\nu')(C+D) - C] - \frac{\alpha' E'}{m}Me^{-mz}\Big\} \\ &\quad e^{-m(z-d)}J_2(mr)dm\end{aligned}\right\}\ldots[25]$$

On the plane $z = d$, the stress and displacement must be continuous. In general it will be possible to determine the four constants introduced in Equations [15] and [23] by four equations of continuity in the axisymmetric case. It can be easily seen when $z = d$

$$\tau_{rz} = \tau_{rz}', \qquad \sigma_z = \sigma_z' \ldots\ldots[26]$$

if

$$\left.\begin{aligned}C &= A\sinh md - md\{B\sinh md - A\cosh md\} \\ D &= B\sinh md - md\{B\cosh md - A\sinh md\}\end{aligned}\right\}\ldots[27]$$

Substituting these values in Equations [24] and imposing the conditions

$$z = d; \qquad u_r = u_r'; \qquad w = w' \ldots\ldots[28]$$

we get

$$\left.\begin{aligned}&A[(p+qmd)\sinh md + (r+pmd)\cosh md] \\ &\quad + B[(s-pmd)\sinh md - qmd\cosh md] + \eta = 0 \\ &A[(s+pmd)\sinh md + qmd\cosh md] \\ &\quad + B[(p-qmd)\sinh md + (r-pmd)\cosh md] \\ &\quad + \eta = 0\end{aligned}\right\}\ldots[29]$$

where

$$\left.\begin{aligned}p &= \frac{2(1-\nu'^2)}{E'},\quad q = \frac{(1+\nu')(1-2\nu')}{E'} \\ &\quad + \frac{1+\nu}{E},\quad r = \frac{2(1-\nu^2)}{E} \\ s &= \frac{(1+\nu')(1-2\nu')}{E'} + \frac{(1+\nu)(1-2\nu)}{E} \\ \eta &= \frac{(1+\nu')\alpha' - (1+\nu)\alpha}{m}Me^{-md}\end{aligned}\right\}\ldots[30]$$

The values of A and B being known, the stresses and displacements in the disk and also in the lower portion of the solid are uniquely determined.

Finally, we consider a particular case of the temperature distribution. Suppose a circular area of radius a on the surface of the disk is at a uniform temperature V, while the rest of the surface is kept at zero temperature. That is

$$\left.\begin{array}{ll} z = 0 & \\ T = V & r \le a \\ = 0 & r > a \end{array}\right\} \quad \ldots\ldots\ldots\ldots\ldots [31]$$

and $T \to 0$ at infinity.

By Fourier-Bessel representation on the plane $z = 0$

$$T = \int_0^\infty J_0(mr)m\,dm \int_0^a VJ_0(m\lambda)\lambda\,d\lambda$$

$$= Va\int_0^\infty J_1(ma)J_0(mr)\,dm \ldots\ldots [32]$$

Hence comparing with Equation [14] we have

$$M = -N = VaJ_1(ma) \ldots\ldots\ldots\ldots\ldots [33]$$

M being known, from Equations [29]

$$\left.\begin{aligned} A &= \frac{\eta}{\Delta}\{[(p-s) + (p-q)md]\sinh md \\ &\qquad + [r - (p-q)md]\cosh md\} \\ B &= \frac{\eta}{\Delta}\{[-(p-s) + (p-q)md]\sinh md \\ &\qquad - [r + (p-q)md]\cosh md\} \\ \Delta &= (p\sinh md + r\cosh md)^2 - s^2\sinh^2 md \\ &\qquad + m^2d^2(q^2 - p^2) \\ \eta &= \frac{(1+\nu')\alpha' - (1+\nu)\alpha}{m} Va\varepsilon^{-md}J_1(ma) \end{aligned}\right\} \ldots [34]$$

It can be easily seen that all the integrals involved tend to zero at infinity and are convergent everywhere for these values of A and B.

Now, we find the numerical results for the simple and interesting case of $d = \infty$. In this case from Equations [34]

$$A = B = 0 \ldots\ldots\ldots\ldots\ldots [35]$$

From Equations [17], [18], and [21]

$$\tau_{rz} = \sigma_z = 0 \ldots\ldots\ldots\ldots\ldots [36]$$

and

$$\left.\begin{aligned} \sigma_r + \sigma_\theta &= -\alpha EVa\int_0^\infty e^{-mz}J_1(ma)J_0(mr)\,dm \\ \sigma_r - \sigma_\theta &= -\alpha EVa\int_0^\infty e^{-mz}J_1(ma)J_2(mr)\,dm \end{aligned}\right\} \ldots [37]$$

Hence

$$\left.\begin{aligned} &z > 0 \\ \sigma_r + \sigma_\theta &= -\frac{\alpha EVa^2}{z^2}\sum_{n=0}^{\infty}\frac{\Gamma(2n+2)}{n!\Gamma(n+2)} \\ &\qquad {}_2F_1\left(-n,\ -n\ -1;\ 1;\ \frac{r^2}{a^2}\right)\left(-\frac{1}{4}\frac{a^2}{z^2}\right)^n \\ \sigma_r - \sigma_\theta &= -\frac{\alpha EVa^2r^2}{2z^4}\sum_{n=0}^{\infty}\frac{\Gamma(2n+4)}{n!\Gamma(n+2)} \\ &\qquad {}_2F_1\left(-n,-n-1;\ 3;\ \frac{r^2}{a^2}\right)\left(-\frac{1}{4}\frac{a^2}{z^2}\right)^n \end{aligned}\right\} \ldots [38]$$

On the axis

$$\sigma_r = \sigma_\theta = -\alpha EV\left(1 - \frac{z}{\sqrt{a^2+z^2}}\right) \ldots\ldots [39]$$

Using the subscript 0 to denote the values of the stress on the plane $z = 0$ by evaluating the integrals in Equations [37] for $z = 0$

$$\sigma_{r,0} + \sigma_{\theta,0} = \left\{\begin{array}{ll} -\alpha EV & r < a \\ -\dfrac{\alpha EV}{2} & r = a \\ 0 & r > a \end{array}\right\} \ldots\ldots [40]$$

and

$$\sigma_{r,0} - \sigma_{\theta,0} = \left\{\begin{array}{ll} 0 & r < a \\ -\dfrac{\alpha EV}{2} & r = a \\ -\dfrac{\alpha EVa^2}{r^2} & r > a \end{array}\right\} \ldots\ldots [41]$$

From Equations [40] and [41]

$$\sigma_{r,0} = \left\{\begin{array}{ll} -\dfrac{\alpha EV}{2} & r \le a \\ -\dfrac{\alpha EVa^2}{2r^2} & r > a \end{array}\right\} \ldots\ldots\ldots [42]$$

and

$$\sigma_{\theta,0} = \left\{\begin{array}{ll} -\dfrac{\alpha EV}{2} & r < a \\ 0 & r = a \\ \dfrac{\alpha EVa^2}{2r^2} & r > a \end{array}\right\} \ldots\ldots\ldots [43]$$

So the radial normal stress on the surface is constant in the heated area and varies inversely proportional to the square of the distance from the origin. It is continuous throughout the plane. The tangential normal stress is equal to the normal radial stress in the heated region. It is zero at $r = a$ and changes its sign. They are equal but opposite in sign outside the heated region. The tangential normal stress is discontinuous at $r = a, z = 0$.

The surface deformation due to the temperature distribution can be found from the Equations [19]

$$u_{r,0} = V\alpha(1+\nu)a\int_0^\infty \frac{J_1(ma)J_1(mr)}{m}\,dm$$

$$= \frac{V\alpha(1+\nu)a}{2}\left\{\begin{array}{ll} \dfrac{r}{a} & r < a \\ 1 & r = a \\ \dfrac{a}{r} & r > a \end{array}\right\} \ldots\ldots [44]$$

and

$$w_0 = V\alpha(1+\nu)a\int_0^\infty \frac{J_1(ma)J_0(mr)}{m}\,dm$$

$$= V\alpha(1+\nu)a\left\{\begin{array}{ll} {}_2F_1\left(\dfrac{1}{2},-\dfrac{1}{2};\ 1;\ \dfrac{r^2}{a^2}\right) & r < a \\ \dfrac{2}{\pi} & r = a \\ \dfrac{a}{2r}\,{}_2F_1\left(\dfrac{1}{2},\dfrac{1}{2};\ 2;\ \dfrac{a^2}{r^2}\right) & r > a \end{array}\right\} \ldots [45]$$

Also, on the axis

$$w = V\alpha(1+\nu)\left(\sqrt{a^2+z^2}-z\right) \quad \ldots\ldots [46]$$

The radial displacement increases with r in the heated region and attains its maximum value at the boundary and then decreases slowly and tends to zero at infinity. The axial component of displacement is maximum at the origin and decreases as r increases. Both the components are continuous throughout the plane.

SECTION 2

Unsteady State

In the unsteady state, the temperature for axisymmetric distribution will satisfy the differential equation

$$\kappa\left[\frac{\partial^2 T}{\partial r^2}+\frac{1}{r}\frac{\partial T}{\partial r}+\frac{\partial^2 T}{\partial z^2}\right]=\frac{\partial T}{\partial t} \quad \ldots\ldots [47]$$

which is satisfied if we take

$$T = \Sigma e^{-\kappa(\lambda^2+m^2)t}(a_m \sin mz + b_m \cos mz) J_0(\lambda r) \ldots [48]$$

where a_m and b_m are arbitrary constants to be determined by the conditions of particular problems.

In this case Equations [5] by virtue of Equations [6] become

$$\left.\begin{aligned}&\nabla^2\left(\sigma_z+\frac{1}{1-\nu}\alpha ET\right)+\frac{1}{1+\nu}\frac{\partial^2}{\partial z^2}(\Theta+\alpha ET)=0\\ &\cdots\cdots\cdots\cdots\cdots\cdots\\ &\cdots\cdots\cdots\cdots\cdots\cdots\end{aligned}\right\} \ldots [49]$$

But Equations [10] remain unchanged.

Solutions of those equations in Equations [49] and [10] which contain τ_{zz}, τ_{yz}, σ_z can be put in the form

$$\left.\begin{aligned}\tau_{zz} &= -\frac{1}{2(1+\nu)} z\frac{\partial}{\partial z}(\Theta+\alpha ET)+\psi_1\\ \tau_{yz} &= -\frac{1}{2(1+\nu)} z\frac{\partial}{\partial y}(\Theta+\alpha ET)+\psi_2\\ \sigma_z &= -\frac{1}{2(1+\nu)} z\frac{\partial}{\partial z}(\Theta+\alpha ET)-\frac{1}{1-\nu}\alpha ET+\psi_3\end{aligned}\right\} \ldots [50]$$

where ψ_1, ψ_2, ψ_3 are some functions of r, z, and t.

Operating Equations [50] with the operator ∇^2 and comparing with the original equations, after a little reduction we get

$$\left.\begin{aligned}\nabla^2\psi_1 &= -\frac{\alpha E}{2(1-\nu)\kappa} z\frac{\partial^2 T}{\partial x\partial t}\\ \nabla^2\psi_2 &= -\frac{\alpha E}{2(1-\nu)\kappa} z\frac{\partial^2 T}{\partial y\partial t}\\ \nabla^2\psi_3 &= -\frac{\alpha E}{2(1-\nu)\kappa} z\frac{\partial^2 T}{\partial z\partial t}\end{aligned}\right\} \ldots\ldots [51]$$

(cont.)

Solving these equations and substituting the values of ψ_1, ψ_2, ψ_3, thus found, in Equations [50] we have

$$\left.\begin{aligned}\tau_{zz} &= -\frac{1}{2(1+\nu)} z\frac{\partial}{\partial x}(\Theta+\alpha ET)-\frac{\alpha E}{2(1-\nu)}\left(z\frac{\partial T}{\partial x}+\frac{2}{\lambda^2+m^2}\frac{\partial^2 T}{\partial x\partial z}\right)+\phi_1\\ \tau_{yz} &= -\frac{1}{2(1+\nu)} z\frac{\partial}{\partial y}(\Theta+\alpha ET)-\frac{\alpha E}{2(1-\nu)}\left(z\frac{\partial T}{\partial y}+\frac{2}{\lambda^2+m^2}\frac{\partial^2 T}{\partial y\partial z}\right)+\phi_2\\ \sigma_z &= -\frac{1}{2(1+\nu)} z\frac{\partial}{\partial z}(\Theta+\alpha ET)-\frac{1}{1-\nu}\alpha ET-\frac{\alpha E}{2(1-\nu)}\left(z\frac{\partial T}{\partial z}+\frac{2}{\lambda^2+m^2}\frac{\partial^2 T}{\partial z^2}\right)+\phi_3\end{aligned}\right\} \ldots [52]$$

where ϕ_1, ϕ_2, and ϕ_3 are harmonic functions to be determined by the boundary conditions.

Substituting these values of τ_{zz}, τ_{yz}, σ_z in the equation of equilibrium we get

$$\frac{\partial}{\partial z}[(1-\nu)\Theta+2\alpha ET]=2(1-\nu^2)\left[\frac{\partial\phi_1}{\partial x}+\frac{\partial\phi_2}{\partial y}+\frac{\partial\phi_3}{\partial z}\right] \quad \ldots\ldots [53]$$

The value of Θ being known from this relation on integration, we know completely the stress components τ_{zz}, τ_{yz}, σ_z. Substituting these values in the corresponding relations in Equations [1] and [2], on integration the components of displacement u, v, and w are uniquely determined, the constants of integration being determined by the conditions of the problem. We can find the rest of the stress components with the aid of the components of displacement thus determined and the Relations [1] and [2].

In general, in the axisymmetric case we can introduce four arbitrary constants through the harmonic functions ϕ_1, ϕ_2, and ϕ_3 and hence the stress distribution in a disk of finite thickness and infinite radius can be determined as we can satisfy the four boundary conditions involving stresses and/or displacements at both the surfaces. In the case of a semi-infinite solid the stresses tend to zero at infinity and there are two conditions at the plane boundary. Hence these four constants also will be sufficient to determine the stress distribution in a semi-infinite solid.

Acknowledgment

The author offers his grateful thanks to Dr. B. Sen for his kind help in the preparation of this paper.

Influence of Large Amplitudes on Free Flexural Vibrations of Rectangular Elastic Plates[1]

By HU-NAN CHU[2] AND GEORGE HERRMANN,[3] NEW YORK, N. Y.

In a recent paper (1)[4] a set of plate equations was derived, which governs motions with small elongations and shears, but moderately large rotations, valid for an isotropic material obeying Hooke's law. The resulting theory, which may be considered the dynamic analog of the von Karman plate theory, is applied presently to the study of free vibrations of a rectangular, elastic plate with hinged, immovable edges. The nonlinear equations are solved approximately by employing a perturbation procedure and also the principle of conservation of energy directly. The influence of large amplitudes on the period of free vibration and on the maximum normal stress is established. The free vibrations of a beam are studied as a special case and the resulting period compared with a previous investigation.

Nomenclature

The following nomenclature is used in the paper:

x, y, z = original co-ordinates of a particle (before deformation)
u, v, w = displacement components in the x, y, z-direction, respectively
u_0, v_0, w_0 = plate-displacement components (displacement of particle on middle surface of plate)
$\bar{u}, \bar{v}, \bar{w}$ = dimensionless displacement components defined by Equation [7]
h = plate thickness, beam depth
a, b = plate width and length, respectively
ξ, η = dimensionless space variables defined by Equation [6]
τ, ζ = dimensionless time defined by Equations [6] and [9], respectively
δ = perturbation parameter defined by Equation [5]
r = aspect ratio, $r = a/b$
ρ = density of plate material
ν = Poisson's ratio
c_p = phase velocity of compressional waves in a plate, $c_p = \sqrt{\dfrac{E}{\rho(1-\nu^2)}}$
c_b = phase velocity of compressional waves in a beam, $c_b = \sqrt{\dfrac{E}{\rho}}$
N_1, N_2, N_{12} = membrane forces
M_1, M_2, M_{12} = plate moments
D = flexural rigidity of plate
$u^{(0)}, v^{(0)}, w^{(1)}$ = lowest order perturbation components of displacement
F = stress function defined by Equation [15]
$H(\zeta), H(t)$ = time functions
T = kinetic energy
W = strain energy
i, j, m, n = indices of summation
σ_{1m} = maximum membrane stress
σ_{1b} = maximum bending stress
B = amplitude of vibration
$\beta = B/h$ = dimensionless amplitude of vibration
Z = time function, of dimensionless time ζ
S = dimensionless membrane stress defined by Equation [29]
$R = h/\sqrt{12}$
E = Young's modulus
K = complete elliptic integral of first kind
T^* = nonlinear period
ω^* = nonlinear frequency
T = linear period
ω = linear frequency

Introduction

The linear theories of motion of bodies, one or two of whose dimensions are small as compared to the third (beams, plates, and so on) are based, among others, on the assumption that the deflections are small in comparison with the beam depth or plate thickness. In most practical cases this implies in turn that the slopes (or rotations of the cross section) are small as compared to unity.

In a variety of circumstances of practical importance, however, motions may be excited, where this basic assumption is no longer valid; that is, the deflections have the order of magnitude of the thickness. It is of interest, therefore, to establish the influence of such large amplitudes on the salient parameters of the problem; e.g., the frequency of free vibrations.

Free vibrations with large amplitudes of elastic bodies, one or two of whose dimensions are small as compared to the third, have previously been studied, for example, by G. F. Carrier (2, 3) who investigated strings and by A. C. Eringen who dealt with beams (4) and circular membranes (5).

In the present paper, we propose to investigate free flexural vibrations of a rectangular elastic plate, supported by immovable hinges along all edges. The plate equations used for this purpose are those discussed in a previous paper (1). They may be considered the dynamic analog of the von Karman large-deflection plate theory of equilibrium, and are valid for moderately large amplitudes. These equations are also quite similar to those pre-

[1] This investigation was supported by the National Advisory Committee for Aeronautics, under Contract NAw-6366.

[2] Department of Civil Engineering and Engineering Mechanics, Institute of Flight Structures, Columbia University.

[3] Associate Professor of Civil Engineering, Institute of Flight Structures, Columbia University. Mem. ASME.

[4] Numbers in parentheses refer to the Bibliography at the end of the paper.

Presented at the National Applied Mechanics Division Conference, Urbana, Ill., June 14–16, 1956, of THE AMERICAN SOCIETY OF MECHANICAL ENGINEERS.

Discussion of this paper should be addressed to the Secretary, ASME, 29 West 39th Street, New York, N. Y., and will be accepted until January 10, 1957, for publication at a later date. Discussion received after the closing date will be returned.

NOTE: Statements and opinions advanced in papers are to be understood as individual expressions of their authors and not those of the Society. Manuscript received by ASME Applied Mechanics Division, January 9, 1956. Paper No. 56—APM-27.

viously obtained by Saint Venant.[5] If the body forces in Saint Venant's equations were taken to be the negative of the inertia forces and the transverse load were identified with the negative of the transverse inertia term, then they can be seen to be the same as Equations [1] of the present paper.

As in previous work by Carrier and Eringen, a perturbation procedure is used in the solution of the nonlinear problem. Since all the nonlinear terms are considered to be small throughout, only the lowest order equations of motion are solved. In addition, the problem was treated by direct energy considerations for the purpose of a verification. Graphs, indicating the influence of large amplitudes of vibration on the periodic time and on the maximum normal stress, have been plotted for various aspect ratios of the plate. Finally, the vibrating beam was considered as a special case, employing again a perturbation procedure, and furthermore, a procedure corresponding to Duffing's method (6) for a single lumped mass. The computed values are compared with those by A. C. Eringen (4). All the results obtained in this study reduce readily to those of the classical linear plate theory when the amplitudes of vibration tend to zero.

Statement of Problem

Considered are free vibrations of a flat rectangular plate of thickness h and edge lengths a and b. The edges are assumed to be hinged and immovable. The plate is referred to a Cartesian co-ordinate system $Oxyz$, the x,y-plane being in the middle plane of the plate and the origin O at a corner of the plate. We designate by subscripts 1 and 2 the directions of those fibers of the deformed plate which were in the x and y-directions, respectively, before deformation. The stress equations of free flexural motions of plates with moderately large amplitudes are

$$\left.\begin{aligned}
&\frac{\partial N_1}{\partial x}+\frac{\partial N_{12}}{\partial y}=\rho h\ddot{u}_0\\
&\frac{\partial N_2}{\partial y}+\frac{\partial N_{12}}{\partial x}=\rho h\ddot{v}_0\\
&\frac{\partial^2 M_1}{\partial x^2}+\frac{\partial^2 M_2}{\partial y^2}+2\frac{\partial^2 M_{12}}{\partial x\partial y}+\frac{\partial}{\partial x}\left(N_1\frac{\partial w_0}{\partial x}\right)\\
&\qquad+\frac{\partial}{\partial y}\left(N_2\frac{\partial w_0}{\partial y}\right)+\frac{\partial}{\partial x}\left(N_{12}\frac{\partial w_0}{\partial y}\right)\\
&\qquad+\frac{\partial}{\partial y}\left(N_{12}\frac{\partial w_0}{\partial x}\right)=\rho h\ddot{w}_0
\end{aligned}\right\}\ \ldots[1]$$

Dots indicate differentiation with respect to time t. In these equations u_0, v_0 designate the displacement of a particle in the middle plane of the plate in x and y-directions, respectively, while w_0 is the displacement of such particle normal to the middle plane. N_1, N_2, N_{12} are the membrane forces, characteristic of the state of stress in the middle plane of the plate. M_1, M_2, M_{12} are the usual moments of the classical linear plate theory. Subscripts 1 and 2 are used here to indicate that these forces and moments are taken with respect to fibers after deformation. If the inertia in the plane of the plate is neglected, that is, if the right-hand side of the first two equations of Set [1] is put equal to zero, the third equation may be simplified considerably. Set [1] becomes then

$$\left.\begin{aligned}
&\frac{\partial N_1}{\partial x}+\frac{\partial N_{12}}{\partial y}=0\\
&\frac{\partial N_2}{\partial y}+\frac{\partial N_{12}}{\partial x}=0
\end{aligned}\right\}\ \ldots[1a]$$

[5] See, for example, reference (7), p. 301.

$$\left.\begin{aligned}
&\frac{\partial^2 M_1}{\partial x^2}+\frac{\partial^2 M_2}{\partial y_2}+2\frac{\partial^2 M_{12}}{\partial x\partial y}+N_1\frac{\partial^2 w_0}{\partial x^2}+N_2\frac{\partial^2 w_0}{\partial y^2}\\
&\qquad+2N_{12}\frac{\partial^2 w_0}{\partial x\,\partial y}=\rho h\ddot{w}_0
\end{aligned}\right\}\ \ldots[1a]\ (cont.)$$

This set is identical to the static von Karman equations, if we consider the negative of the transverse load to be the transverse inertia. However, we note that a mere addition of longitudinal inertia terms to the first two equations of Set [1a] does not result in the original Set [1], because terms of the type

$$\frac{\partial N_1}{\partial x}\frac{\partial w_0}{\partial x}$$

the so-called "buoyancy" terms, would be missing.

The stress-displacement relations for an elastic, isotropic plate are given in (1, 7) as

$$\left.\begin{aligned}
N_1&=\frac{Eh}{1-\nu^2}\left[\frac{\partial u_0}{\partial x}+\frac{1}{2}\left(\frac{\partial w_0}{\partial x}\right)^2+\nu\frac{\partial v_0}{\partial y}+\frac{\nu}{2}\left(\frac{\partial w_0}{\partial y}\right)^2\right]\\
N_2&=\frac{Eh}{1-\nu^2}\left[\frac{\partial v_0}{\partial y}+\frac{1}{2}\left(\frac{\partial w_0}{\partial y}\right)^2+\nu\frac{\partial u_0}{\partial x}+\frac{\nu}{2}\left(\frac{\partial w_0}{\partial x}\right)^2\right]\\
N_{12}&=Gh\left(\frac{\partial u_0}{\partial y}+\frac{\partial v_0}{\partial x}+\frac{\partial w_0}{\partial x}\frac{\partial w_0}{\partial y}\right)\\
M_1&=-D\left(\frac{\partial^2 w_0}{\partial x^2}+\nu\frac{\partial^2 w_0}{\partial y^2}\right),\\
M_2&=-D\left(\frac{\partial^2 w_0}{\partial y^2}+\nu\frac{\partial^2 w_0}{\partial x^2}\right),\\
M_{12}&=-D(1-\nu)\frac{\partial^2 w_0}{\partial x\,\partial y}
\end{aligned}\right\}\ \ldots[2]$$

The occurrence of nonlinear terms in the first three relations is due to the fact that an element of the plate is not only sheared and elongated but also rotated about the x, y-axes, respectively, such that a fiber originally in the x-direction is after deformation in the 1-direction, the angle of rotation being given by $\partial w_0/\partial x$. A more complete discussion of these equations may be found in reference (1). The stress Equations of Motion [1] are converted to displacement equations of motion, using Relations [2]

$$\left.\begin{aligned}
&\frac{\partial^2 u_0}{\partial x^2}+\frac{\partial w_0}{\partial x}\frac{\partial^2 w_0}{\partial x^2}+\nu\left(\frac{\partial^2 v_0}{\partial x\partial y}+\frac{\partial w_0}{\partial y}\frac{\partial^2 w_0}{\partial x\,\partial y}\right)\\
&\qquad+\frac{1-\nu}{2}\left(\frac{\partial^2 u_0}{\partial y^2}+\frac{\partial^2 v_0}{\partial x\partial y}+\frac{\partial w_0}{\partial x}\frac{\partial^2 w_0}{\partial y^2}\right.\\
&\qquad\left.+\frac{\partial w_0}{\partial y}\frac{\partial^2 w_0}{\partial x\,\partial y}\right)=\frac{\ddot{u}_0}{c_p^2}\\
&\frac{1-\nu}{2}\left(\frac{\partial^2 u_0}{\partial x\partial y}+\frac{\partial^2 v_0}{\partial x^2}+\frac{\partial w_0}{\partial x}\frac{\partial^2 w_0}{\partial x\partial y}+\frac{\partial w_0}{\partial y}\frac{\partial^2 w_0}{\partial x^2}\right)\\
&\qquad+\frac{\partial^2 v_0}{\partial y^2}+\frac{\partial w_0}{\partial y}\frac{\partial^2 w_0}{\partial y^2}+\nu\left(\frac{\partial^2 u_0}{\partial x\partial y}+\frac{\partial w_0}{\partial x}\frac{\partial^2 w_0}{\partial x\partial y}\right)=\frac{\ddot{v}_0}{c_p^2}
\end{aligned}\right\}\ \ldots[3]$$

$$\left.\begin{aligned}&\frac{h^2}{12}\left(\frac{\partial^4 w_0}{\partial x^4}+2\frac{\partial^4 w_0}{\partial x^2\partial y^2}+\frac{\partial^4 w_0}{\partial y^4}\right)=\frac{\partial u_0}{\partial x}\frac{\partial^2 w_0}{\partial x^2}\\&+\frac{1}{2}\left(\frac{\partial w_0}{\partial x}\right)^2\frac{\partial^2 w_0}{\partial x^2}+\nu\left[\frac{\partial v_0}{\partial y}\frac{\partial^2 w_0}{\partial x^2}+\frac{1}{2}\left(\frac{\partial w_0}{\partial y}\right)^2\frac{\partial^2 w_0}{\partial x^2}\right]\\&+\frac{\partial v_0}{\partial y}\frac{\partial^2 w_0}{\partial y^2}+\frac{1}{2}\left(\frac{\partial w_0}{\partial y}\right)^2\frac{\partial^2 w_0}{\partial y^2}+\nu\left[\frac{\partial u_0}{\partial x}\frac{\partial^2 w_0}{\partial y^2}\right.\\&\left.+\frac{1}{2}\left(\frac{\partial w_0}{\partial x}\right)^2\frac{\partial^2 w_0}{\partial y^2}\right]+(1-\nu)\left(\frac{\partial u_0}{\partial y}\frac{\partial^2 w_0}{\partial x\partial y}+\frac{\partial v_0}{\partial x}\frac{\partial^2 w_0}{\partial x\partial y}\right.\\&\left.+\frac{\partial w_0}{\partial x}\frac{\partial w_0}{\partial y}\frac{\partial^2 w_0}{\partial x\partial y}\right)+\frac{\ddot{u}_0}{c_p^2}\frac{\partial w_0}{\partial x}+\frac{\ddot{v}_0}{c_p^2}\frac{\partial w_0}{\partial y}+\frac{\ddot{w}_0}{c_p^2}\end{aligned}\right\}\quad\ldots[3]\ (cont.)$$

where

$$c_p^2=\frac{E}{\rho(1-\nu^2)}$$

The boundary conditions of a rectangular plate, all four of whose edges are hinged and immovable, are

$$\left.\begin{aligned}&\text{at } x=0,a: \qquad u_0=w_0=\frac{\partial^2 w_0}{\partial x^2}=0\\&\text{at } y=0,b: \qquad v_0=w_0=\frac{\partial^2 w_0}{\partial y^2}=0\end{aligned}\right\}\quad\ldots\ldots[4]$$

Since only free vibrations are to be investigated, there is no need to specify the initial conditions.

Perturbation Procedure

A perturbation parameter δ is chosen, which depends only on the geometry of the plate and not on the type of motion. Letting, without loss of generality, $a \leq b$, we set

$$\delta=\frac{h}{a}\quad\ldots\ldots[5]$$

For convenience, the independent variables of the problem, x, y, and t are transformed to dimensionless quantities ξ, η, and τ, respectively, by

$$\xi=\frac{x}{a},\qquad \eta=\frac{y}{a},\qquad \tau=\frac{c_p t}{\sqrt{12}\,a}\quad\ldots\ldots[6]$$

and the dependent variables u_0, v_0, and w_0 are transformed to $\bar{u}$, $\bar{v}$, and $\bar{w}$ by

$$\bar{u}=\frac{u_0}{a},\qquad \bar{v}=\frac{v_0}{a},\qquad \bar{w}=\frac{w_0}{a}\quad\ldots\ldots[7]$$

Furthermore, the notation is introduced

$$r=\frac{a}{b}\quad\ldots\ldots[8]$$

$$\zeta=\delta\tau\quad\ldots\ldots[9]$$

This last substitution is performed in order to make all the terms of the classical linear plate theory of the same order in the parameter δ.

The Equations of Motion [3] may then be written as

$$\left.\begin{aligned}&\frac{\partial^2\bar{u}}{\partial\xi^2}+\frac{\partial\bar{w}}{\partial\xi}\frac{\partial^2\bar{w}}{\partial\xi^2}+\nu\left(\frac{\partial^2\bar{v}}{\partial\xi\partial\eta}+\frac{\partial\bar{w}}{\partial\eta}\frac{\partial^2\bar{w}}{\partial\xi\partial\eta}\right)\\&+\frac{1-\nu}{2}\left(\frac{\partial^2\bar{u}}{\partial\eta^2}+\frac{\partial^2\bar{v}}{\partial\xi\partial\eta}+\frac{\partial\bar{w}}{\partial\xi}\frac{\partial^2\bar{w}}{\partial\eta^2}+\frac{\partial\bar{w}}{\partial\eta}\frac{\partial^2\bar{w}}{\partial\xi\partial\eta}\right)\\&=\frac{\delta^2}{12}\frac{\partial^3\bar{u}}{\partial\zeta^2}\\&\frac{1-\nu}{2}\left(\frac{\partial^2\bar{u}}{\partial\xi\partial\eta}+\frac{\partial^2\bar{v}}{\partial\xi^2}+\frac{\partial\bar{w}}{\partial\xi}\frac{\partial^2\bar{w}}{\partial\xi\partial\eta}+\frac{\partial^2\bar{w}}{\partial\xi^2}\frac{\partial\bar{w}}{\partial\eta}\right)\\&+\frac{\partial^2\bar{v}}{\partial\eta^2}+\frac{\partial\bar{w}}{\partial\eta}\frac{\partial^2\bar{w}}{\partial\eta^2}+\nu\left(\frac{\partial^2\bar{u}}{\partial\xi\partial\eta}+\frac{\partial\bar{w}}{\partial\xi}\frac{\partial^2\bar{w}}{\partial\xi\partial\eta}\right)\\&=\frac{\delta^2}{12}\frac{\partial^3\bar{v}}{\partial\zeta^2}\\&\frac{\delta^2}{12}\left(\frac{\partial^4\bar{w}}{\partial\xi^4}+2\frac{\partial^4\bar{w}}{\partial\xi^2\partial\eta^2}+\frac{\partial^4\bar{w}}{\partial\eta^4}\right)\\&=\frac{\partial\bar{u}}{\partial\xi}\frac{\partial^2\bar{w}}{\partial\xi^2}+\frac{1}{2}\left(\frac{\partial\bar{w}}{\partial\xi}\right)^2\frac{\partial^2\bar{w}}{\delta\xi^2}\\&+\nu\left[\frac{\partial\bar{v}}{\partial\eta}\frac{\partial^2\bar{w}}{\partial\xi^2}+\frac{1}{2}\left(\frac{\partial\bar{w}}{\partial\eta}\right)^2\frac{\partial^2\bar{w}}{\partial\xi^2}\right]+\frac{\partial\bar{w}}{\partial\eta}\frac{\partial^2\bar{w}}{\partial\eta^2}\\&+\frac{1}{2}\left(\frac{\partial\bar{w}}{\partial\eta}\right)^2\frac{\partial^2\bar{w}}{\partial\eta^2}+\nu\left[\frac{\partial\bar{u}}{\partial\xi}\frac{\partial^2\bar{w}}{\partial\eta^2}+\frac{1}{2}\left(\frac{\partial\bar{w}}{\partial\xi}\right)^2\frac{\partial^2\bar{w}}{\partial\eta^2}\right]\\&+(1-\nu)\left[\frac{\partial\bar{u}}{\partial\eta}\frac{\partial^2\bar{w}}{\partial\xi\partial\eta}+\frac{\partial\bar{v}}{\partial\xi}\frac{\partial^2\bar{w}}{\partial\xi\partial\eta}+\frac{\partial\bar{w}}{\partial\xi}\frac{\partial\bar{w}}{\partial\eta}\frac{\partial^2\bar{w}}{\partial\xi\partial\eta}\right]\\&+\frac{\delta^2}{12}\frac{\partial\bar{w}}{\partial\xi}\frac{\partial^2\bar{u}}{\partial\zeta^2}+\frac{\delta^2}{12}\frac{\partial\bar{w}}{\partial\eta}\frac{\partial^2\bar{v}}{\partial\zeta^2}-\frac{\delta^2}{12}\frac{\partial^2\bar{w}}{\partial\zeta^2}\end{aligned}\right\}\quad\ldots[10]\ (cont.)$$

and the boundary conditions as

$$\left.\begin{aligned}&\text{at } \xi=0,1: \qquad \bar{u}=\bar{w}=\frac{\partial^2\bar{w}}{\partial\xi^2}=0\\&\text{at } \eta=0,\frac{1}{r}: \qquad \bar{v}=\bar{w}=\frac{\partial^2\bar{w}}{\partial\eta^2}=0\end{aligned}\right\}\quad\ldots\ldots[11]$$

Recognizing that the displacements $\bar{u}$ and $\bar{v}$, since they are omitted in classical linear theory, are of one order higher than the displacement $\bar{w}$ and noticing that $\bar{u}$ and $\bar{v}$ are even functions of δ, and that $\bar{w}$ is an odd function, the following perturbation series are used for these displacements

$$\left.\begin{aligned}\bar{u}&=\delta^2u^{(2)}+\delta^4u^{(4)}+\ldots\\\bar{v}&=\delta^2v^{(2)}+\delta^4v^{(4)}+\ldots\\\bar{w}&=\delta w^{(1)}+\delta^3w^{(3)}+\ldots\end{aligned}\right\}\quad\ldots\ldots[12]$$

Substituting the Series [12] into the Equations of Motion [10] and retaining terms of lowest order in δ only, the following equations of motion result

$$\left.\begin{aligned}&\frac{\partial^2u^{(2)}}{\partial\xi^2}+\frac{\partial w^{(1)}}{\partial\xi}\frac{\partial^2w^{(1)}}{\partial\xi^2}+\nu\left(\frac{\partial^2v^{(2)}}{\partial\xi\partial\eta}+\frac{\partial w^{(1)}}{\partial\eta}\frac{\partial^2w^{(1)}}{\partial\xi\partial\eta}\right)\\&+\frac{1-\nu}{2}\left(\frac{\partial^2u^{(2)}}{\partial\eta^2}+\frac{\partial^2v^{(2)}}{\partial\xi\partial\eta}+\frac{\partial w^{(1)}}{\partial\xi}\frac{\partial^2w^{(1)}}{\partial\eta^2}\right.\\&\left.+\frac{\partial w^{(1)}}{\partial\eta}\frac{\partial^2w^{(1)}}{\partial\xi\partial\eta}\right)=0\\&\frac{1-\nu}{2}\left(\frac{\partial^2u^{(2)}}{\partial\xi\partial\eta}+\frac{\partial w^{(1)}}{\partial\xi}\frac{\partial^2w^{(1)}}{\partial\xi\partial\eta}+\frac{\partial w^{(1)}}{\partial\eta}\frac{\partial^2w^{(1)}}{\partial\xi^2}+\frac{\partial^2v^{(2)}}{\partial\xi^2}\right)\\&+\frac{\partial^2v^{(2)}}{\partial\eta^2}+\frac{\partial w^{(1)}}{\partial\eta}\frac{\partial^2w^{(1)}}{\partial\eta^2}+\nu\left(\frac{\partial^2u^{(2)}}{\partial\xi\partial\eta}+\frac{\partial w^{(1)}}{\partial\xi}\frac{\partial^2w^{(1)}}{\partial\xi\partial\eta}\right)=0\\&\frac{1}{12}\left(\frac{\partial^4w^{(1)}}{\partial\xi^4}+2\frac{\partial^4w^{(1)}}{\partial\xi^2\partial\eta^2}+\frac{\partial^4w^{(1)}}{\partial\eta^4}\right)\end{aligned}\right\}\quad\ldots[13]$$

$$
\left.
\begin{aligned}
&= \frac{\partial u^{(2)}}{\partial \xi}\frac{\partial^2 w^{(1)}}{\partial \xi^2} + \frac{1}{2}\left(\frac{\partial w^{(1)}}{\partial \xi}\right)^2 \frac{\partial^2 w^{(1)}}{\partial \xi^2} \\
&+ \nu\left[\frac{\partial v^{(2)}}{\partial \eta}\frac{\partial^2 w^{(1)}}{\partial \xi^2} + \frac{1}{2}\left(\frac{\partial w^{(1)}}{\partial \eta}\right)^2 \frac{\partial^2 w^{(1)}}{\partial \xi^2}\right] \\
&+ \frac{\partial v^{(2)}}{\partial \eta}\frac{\partial^2 w^{(1)}}{\partial \eta^2} + \frac{1}{2}\left(\frac{\partial w^{(1)}}{\partial \eta}\right)^2 \frac{\partial^2 w^{(1)}}{\partial \eta^2} + \nu\left[\frac{\partial u^{(2)}}{\partial \xi}\frac{\partial^2 w^{(1)}}{\partial \eta^2}\right. \\
&\left. + \frac{1}{2}\left(\frac{\partial w^{(1)}}{\partial \xi}\right)^2 \frac{\partial^2 w^{(1)}}{\partial \eta^2}\right] + (1-\nu)\left(\frac{\partial u^{(2)}}{\partial \eta}\frac{\partial^2 w^{(1)}}{\partial \xi\,\partial \eta}\right. \\
&\left. + \frac{\partial v^{(2)}}{\partial \xi}\frac{\partial^2 w^{(1)}}{\partial \xi\,\partial \eta} + \frac{\partial w^{(1)}}{\partial \xi}\frac{\partial w^{(1)}}{\partial \eta}\frac{\partial^2 w^{(1)}}{\partial \xi\,\partial \eta}\right) - \frac{1}{12}\frac{\partial^2 w^{(1)}}{\partial \zeta^2}
\end{aligned}
\right\} \quad \ldots [13] \ (cont.)
$$

and, from Equations [11], the following boundary conditions

$$
\left.
\begin{aligned}
&\text{at } \xi = 0, 1: \qquad u^{(2)} = w^{(1)} = \frac{\partial^2 w^{(1)}}{\partial \xi^2} = 0 \\
&\text{at } \eta = 0, \frac{1}{r}: \qquad v^{(2)} = w^{(1)} = \frac{\partial^2 w^{(1)}}{\partial \eta^2} = 0
\end{aligned}
\right\} \quad \ldots . [14]
$$

Equations [13] represent a first-order approximation to the problem stated originally by Equation [1]. The only difference is the absence of longitudinal inertia terms, that is, Equations [13] are equivalent to Equations [1a]. Thus, Equations [13] may have been obtained by replacing in von Karman's equations the negative of the transverse loading term by transverse inertia. There would be no assurance, however, that all the terms of the same order are retained.

Similarly, as in the equilibrium case, a stress function F may now be introduced to replace the variables $u^{(2)}$ and $v^{(2)}$. Defining F as

$$
\left.
\begin{aligned}
\frac{\partial^2 F}{\partial \eta^2} &= \frac{\partial u^{(2)}}{\partial \xi} + \frac{1}{2}\left(\frac{\partial w^{(1)}}{\partial \xi}\right)^2 + \nu\left[\frac{\partial v^{(2)}}{\partial \eta} + \frac{1}{2}\left(\frac{\partial w^{(1)}}{\partial \eta}\right)^2\right] \\
\frac{\partial^2 F}{\partial \xi^2} &= \frac{\partial v^{(2)}}{\partial \eta} + \frac{1}{2}\left(\frac{\partial w^{(1)}}{\partial \eta}\right)^2 + \nu\left[\frac{\partial u^{(2)}}{\partial \xi} + \frac{1}{2}\left(\frac{\partial w^{(1)}}{\partial \xi}\right)^2\right] \\
-\frac{\partial^2 F}{\partial \xi\,\partial \eta} &= \frac{1-\nu}{2}\left(\frac{\partial u^{(2)}}{\partial \eta} + \frac{\partial v^{(2)}}{\partial \xi} + \frac{\partial w^{(1)}}{\partial \xi}\frac{\partial w^{(1)}}{\partial \eta}\right)
\end{aligned}
\right\} \quad \ldots [15]
$$

the first two of Equations [13] will be satisfied identically and the third equation becomes

$$
\frac{1}{12}\left(\frac{\partial^4 w^{(1)}}{\partial \xi^4} + 2\frac{\partial^4 w^{(1)}}{\partial \xi^2 \partial \eta^2} + \frac{\partial^4 w^{(1)}}{\partial \eta^4} + \frac{\partial^2 w^{(1)}}{\partial \zeta^2}\right) = \frac{\partial^2 F}{\partial \eta^2}\frac{\partial^2 w^{(1)}}{\partial \xi^2} + \frac{\partial^2 F}{\partial \xi^2}\frac{\partial^2 w^{(1)}}{\partial \eta^2} - 2\frac{\partial^2 F}{\partial \xi\,\partial \eta}\frac{\partial^2 w^{(1)}}{\partial \xi\,\partial \eta} \quad \ldots . [16a]
$$

Moreover, F has to satisfy the equation

$$
\frac{\partial^4 F}{\partial \xi^4} + 2\frac{\partial^4 F}{\partial \xi^2 \partial \eta^2} + \frac{\partial^4 F}{\partial \eta^4} = (1-\nu)\left[\left(\frac{\partial^2 w^{(1)}}{\partial \xi\,\partial \eta}\right)^2 - \frac{\partial^2 w^{(1)}}{\partial \xi^2}\frac{\partial^2 w^{(1)}}{\partial \eta^2}\right] \quad \ldots . [16b]
$$

as a consequence of its definition. F is related to the stress function F (for example, equation [e] of reference (7), p. 343)

$$
F = \frac{1-\nu^2}{Eh^2}\,F
$$

For the present purpose, it was found more convenient to continue to deal with Set [13] in three variables $u^{(2)}$, $v^{(2)}$, $w^{(1)}$, rather than with Set [16] in two variables F and $w^{(1)}$, largely because the Boundary Conditions [14] are in terms of $u^{(2)}$ and $v^{(2)}$.

Moreover, it appears that in a dynamic problem the use of the stress function F does not offer the advantages as in the corresponding static problem (8), because the time function is not separable from the space function. In fact, assuming the transverse displacement $w^{(1)}$ in the form

$$
w^{(1)} = \Pi(\zeta) \sum_{i,j \text{ odd}} a_{ij} \sin i\pi\xi \sin j\pi r\eta
$$

Equation [16b] determines the stress function F as

$$
F = \Pi^2 \sum f_{mn} \cos m\pi\xi \cos n\pi r\eta
$$

where

$$
\begin{aligned}
f_{mn} = \frac{(1-\nu^2)r^2}{4(m^2 + n^2r^2)^2}\Bigg\{ &\sum_{\substack{m>i \\ n>j}} [ij(m-i)(n-j) \\
&- i^2(n-j)^2]\, a_{ij}a_{(m-i)(n-j)} + \sum_{\substack{i>m \\ n>j}} [ij(i-m)(n-j) \\
&+ i^2(n-j)^2]a_{ij}a_{(i-m)(n-j)} + \sum_{\substack{m>i \\ j>n}} [ij(m-i)(j-n) \\
&+ i^2(j-n)^2]a_{ij}a_{(m-i)(j-n)} + \sum_{\substack{i>m \\ j>n}} [ij(i-m)(j-n) \\
&- i^2(j-n)^2]a_{ij}a_{(i-m)(j-n)}\Bigg\}
\end{aligned}
$$

Substitution of the foregoing expressions for $w^{(1)}$ and F into Equation [16a] results in

$$
\begin{aligned}
\frac{1}{12}\left[\Pi\pi^4 \sum a_{ij}(i^2 + j^2r^2)^2 \sin i\pi\xi \sin j\pi r\eta + \frac{d^2\Pi}{d\zeta^2}\sum a_{ij} \sin i\pi\xi \sin j\pi r\eta\right] \\
= \frac{\Pi^2\pi^4 r^2}{4}\Bigg\{ \sum_{\substack{i>m \\ j>n}} (i-m)^2n^2a_{(i-m)(j-n)} + \sum_{\substack{j>n \\ m>i}} (i+m)^2n^2a_{(i+m)(j-n)} + \sum_{\substack{i>m \\ n>j}} (i-m)^2n^2a_{(i-m)(j+n)} \\
+ \sum_{\substack{m>i \\ n>j}} (i+m)^2n^2a_{(i+m)(j+n)} + \sum_{\substack{i>m \\ j>n}} (j-n)^2m^2a_{(i-m)(j-n)} + \sum_{\substack{j>n \\ m>i}} (j-n)^2m^2a_{(i-m)(j-n)} + \sum_{\substack{i>m \\ n>j}} (j+n)^2m^2a_{(i-m)(j-n)} \\
+ \sum_{\substack{m>i \\ n>j}} (j+n)^2m^2a_{(i+m)(j+n)} - 2\sum_{\substack{i>m \\ j>n}} (i-m)(j-n)mna_{(i-m)(j-n)} + 2\sum_{\substack{j>n \\ m>i}} (i+m)(j-n)mna_{(i+m)(j-n)} \\
+ 2\sum_{\substack{i>m \\ n>j}} (i-m)(j+n)mna_{(i-m)(j+n)} - 2\sum_{\substack{m>i \\ n>j}} (i+m)(j+n)mna_{(i+m)(j+n)}\Bigg\} f_{mn} \sin i\pi\xi \sin j\pi r\eta
\end{aligned}
$$

The presence of the factors $(i^2 + j^2r^2)^2$ on the left-hand side of the foregoing expression precludes the possibility of separating the time function $\bar{H}(\zeta)$ from the space function.

Seeking now a solution of the perturbed problem, the transverse displacement $w^{(1)}$ is assumed in the form

$$w^{(1)} = \beta Z(\zeta) \sin \pi\xi \sin \pi r\eta \quad \ldots\ldots\ldots\ldots [17]$$

where β is the dimensionless amplitude and $z(\zeta) \leq 1$. As may be verified, $\beta = B/h$, where B is the actual amplitude. The first two equations of Set [13] are satisfied if the displacements $u^{(2)}$, $v^{(2)}$ are of the form

$$\left.\begin{aligned} u^{(2)} &= \frac{\beta^2 Z^2 \pi}{16} (\cos 2\pi r\eta - 1 + \nu r^2) \sin 2\pi\xi \\ v^{(2)} &= \frac{\beta^2 Z^2 \pi}{16} \left(r \cos 2\pi\xi - r + \frac{\nu}{r} \right) \sin 2\pi r\eta \end{aligned}\right\} \ldots [18]$$

The Expressions [17] and [18] satisfy the Boundary Conditions [14].

Substitution of Equations [17] and [18] into the third equation of Set [13] yields

$$\left\{ \frac{1}{12} \left[\pi^4 (1 + r^2)^2 Z + \frac{d^2 Z}{d\zeta^2} \right] \beta + \frac{1}{8} Z^3 \pi^4 \beta^3 \left[\left(\frac{3}{2} - \frac{\nu^2}{2} \right) (1 + r^4) + 2\nu r^2 \right] \right\} \sin \pi\xi \sin \pi r\eta + \frac{\beta^3 Z^3 \pi^4}{16} (1 - \nu^2) [\sin \pi\xi \sin 3\pi r\eta + r^4 \sin 3\pi\xi \sin \pi r\eta] = 0 \ldots [19]$$

It is noted that the nonlinearity of the problem introduces a coupling effect between the fundamental mode contained in the first term and the two higher modes contained in the second term of Equation [19]. Neglecting the effect of these higher modes, which is justified by observing that for small nonlinearities this effect will be small, we obtain the equation governing the time function $Z(\zeta)$

$$\frac{d^2 Z}{d\zeta^2} + \pi^4 (1 + r^2)^2 Z + 3\beta^2 \pi^4 Z^3 \left[\left(\frac{3}{4} - \frac{\nu^2}{4} \right) (1 + r^4) + \nu r^2 \right] = 0 \ldots [20]$$

Measuring the time ζ such that

$$(Z)_{\zeta=0} = 1, \quad \left(\frac{dZ}{d\zeta} \right)_{\zeta=0} = 0$$

solution of Equation [20] will be given in the form of an elliptic cosine c_n

$$Z = c_n(\omega^* \zeta, k) \quad \ldots\ldots\ldots\ldots [21]$$

where

$$\omega^* = \pi^2 \left\{ (1 + r^2)^2 + 3\beta^2 \left[\left(\frac{3}{4} - \frac{\nu^2}{4} \right) (1 + r^4) + \nu r^2 \right] \right\}^{1/2} \ldots [22]$$

$$k^2 = \left\{ 2 + \frac{2(1 + r^2)^2}{3\beta^2 \left[\left(\frac{3}{4} - \frac{\nu^2}{4} \right) (1 + r^4) + \nu r^2 \right]} \right\}^{-1} \quad \ldots\ldots [23]$$

The period T^* of $c_n(\omega^* \zeta, k)$ is

$$T^* = 4K \frac{\pi^2}{\omega^*} = \frac{4K}{\left\{ (1 + r^2)^2 + 3\beta^2 \left[\left(\frac{3}{4} - \frac{\nu^2}{4} \right) (1 + r^4) + \nu r^2 \right] \right\}^{1/2}} \ldots [24]$$

where $K(k)$ is the complete elliptic integral of the first kind.

The corresponding linear period is

$$T = \frac{2\pi}{(1 + r^2)} \quad \ldots\ldots\ldots\ldots [25]$$

T also may be deduced from Expression [24] for T^* by observing that as $\beta \to 0$, $\omega^* \to \pi^2(1 + r^2)$, $K \to \frac{\pi}{2}$. The ratio T^*/T is given by

$$\frac{T^*}{T} = \frac{2}{\pi} \left\{ (1 + r^2)^2 + 3\beta^2 \left[\left(\frac{3}{4} - \frac{\nu^2}{4} \right) (1 + r^4) + \nu r^2 \right] \right\}^{-1/2} (1 + r^2) K \ldots [26]$$

In Fig. 1 this ratio is plotted versus the dimensionless amplitude β, for various values of the aspect ratio r and for Poisson's ratio $\nu = 0.318$, which is typical for aluminum alloys. It is seen that the period, for any aspect ratio, decreases rapidly with increasing amplitude.

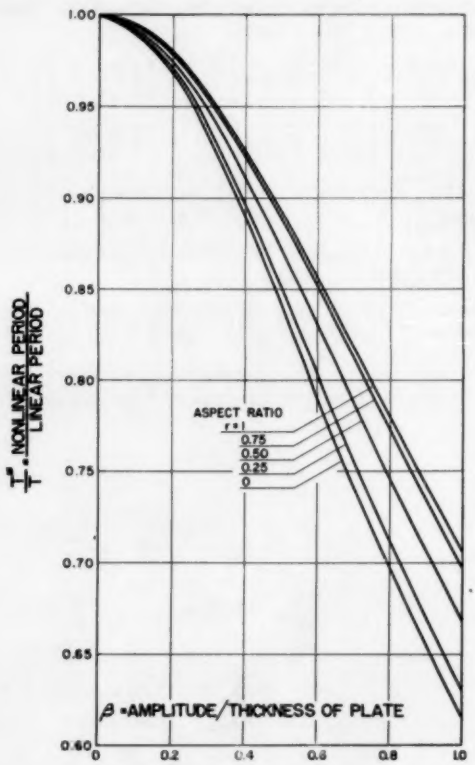

FIG. 1 INFLUENCE OF LARGE AMPLITUDES ON PERIOD OF VIBRATION OF A RECTANGULAR PLATE

Turning now our attention to the state of stress in the plate, we note that the occurrence of moderately large rotations manifests itself in the presence of membrane stresses, one of whose components is, by the first equation of Set [2]

$$\sigma_{1m} = \frac{N_1}{h} = \frac{E}{1-\nu^2}\left\{\frac{\partial u_0}{\partial x} + \frac{1}{2}\left(\frac{\partial w_0}{\partial x}\right)^2 + \nu\left[\frac{\partial v_0}{\partial y} + \frac{1}{2}\left(\frac{\partial w_0}{\partial y}\right)^2\right]\right\} \quad \ldots\ldots [27]$$

and which are absent in linear plate theory. The maximum value of σ_{1m} will be reached at the center of the plate, $x = a/2$, $y = b/2$. From Equations [17] and [18], the displacements u_0, v_0, w_0, are

$$\left.\begin{aligned} u_0 &= \frac{\beta^2 h^2 Z^2}{16a}\left(\cos\frac{2\pi y}{b} - 1 + \nu r^2\right)\sin\frac{2\pi x}{a} \\ v_0 &= \frac{\beta^2 h^2 Z^2}{16a}\left(r\cos\frac{2\pi x}{a} - r + \frac{\nu}{r}\right)\sin\frac{2\pi y}{b} \\ w_0 &= \beta h Z \sin\frac{\pi x}{a}\sin\frac{\pi y}{b} \end{aligned}\right\} \quad \ldots [28]$$

and σ_{1m} becomes, with $Z_{max} = 1$

$$\sigma_{1m} = \frac{E\pi}{8(1-\nu^2)}\left(\frac{\beta h}{a}\right)^2 (2 + \nu r^2 - \nu^2)$$

We define a dimensionless membrane stress S as

$$S = \frac{8\sigma_{1m}}{E\pi\left(\frac{h}{a}\right)^2} \quad \ldots\ldots [29]$$

which may be expressed, with a value of $\nu = 0.318$, as

$$S = \beta^2(2.11 + 0.353r^2) \quad \ldots\ldots [30]$$

For various values of aspect ratio r, this dimensionless membrane stress S is plotted versus the dimensionless amplitude β in Fig. 2. It is seen that the aspect ratio has a relatively small effect on the magnitude of the membrane stress.

It also may be of interest to establish the influence of the membrane stress on the total maximum stress, which will occur at the face of the plate at its center. This total maximum stress will be the sum of the membrane stress σ_{1m} computed above and the bending stress σ_{1b}

$$\left.\begin{aligned} \sigma_{1b} &= \frac{6M_1}{h} = -\frac{Eh}{2(1-\nu^2)}\left(\frac{\partial^2 w_0}{\partial x^2} + \nu\frac{\partial^2 w_0}{\partial y^2}\right) \\ &= \frac{E}{2}\left(\frac{h}{a}\right)^2 \pi^2\beta(1.111 + 0.353r^2) \end{aligned}\right\} \quad \ldots [31]$$

again with $Z_{max} = 1$ and $\nu = 0.318$.

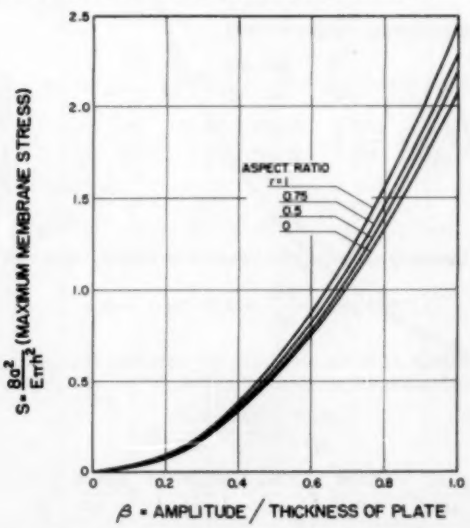

FIG. 2 INFLUENCE OF LARGE AMPLITUDES ON MAXIMUM MEMBRANE STRESS

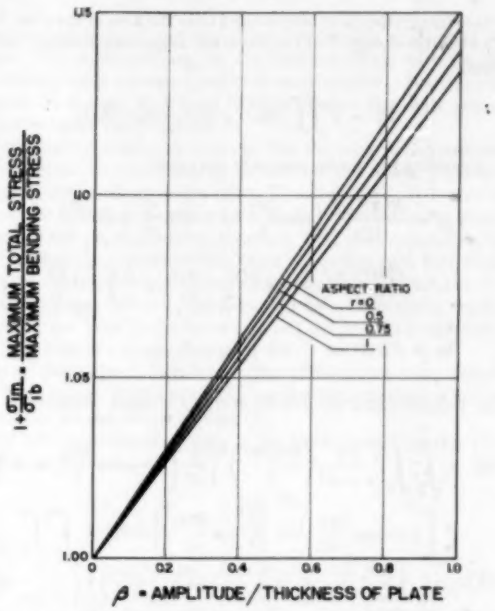

FIG. 3 INFLUENCE OF LARGE AMPLITUDES ON MAXIMUM TOTAL STRESS

For various aspect ratios r, the ratios of the total stress $\sigma_{1m} + \sigma_{1b}$ to the bending stress σ_{1b}, which is the only stress in classical plate theory, are plotted versus the dimensionless amplitude β in Fig. 3, in accordance with the relation

$$\frac{\sigma_{1b} + \sigma_{1m}}{\sigma_{1b}} = 1 + \frac{\beta(1.8989 + 0.318r^2)}{4\pi(1 + 0.318r^2)} \quad \ldots\ldots [32]$$

It is evident from the graph that, as a consequence of moderately large amplitudes, the total stress may be considerably larger than the stress predicted by the classical linear plate theory. However, it appears that percentagewise the large amplitudes affect the stress markedly less than the period of vibration.

PRINCIPLE OF CONSERVATION OF ENERGY

As an alternative, the same problem is studied in this section, using the principle of conservation of energy directly. The strain energy $\overline{W}$ in the present theory (1) is given by the expression

$$2\overline{W} = \iint\left\{N_1\left[\frac{\partial u_0}{\partial x} + \frac{1}{2}\left(\frac{\partial w_0}{\partial x}\right)^2\right] + N_2\left[\frac{\partial v_0}{\partial y} + \frac{1}{2}\left(\frac{\partial w_0}{\partial y}\right)^2\right] + N_{12}\left(\frac{\partial u_0}{\partial y} + \frac{\partial v_0}{\partial x} + \frac{\partial w_0}{\partial x}\frac{\partial w_0}{\partial y}\right) - M_1\frac{\partial^2 w_0}{\partial x^2} - M_2\frac{\partial^2 w_0}{\partial y^2} - 2M_{12}\frac{\partial^2 w_0}{\partial x \partial y}\right\} dxdy \quad \ldots [33]$$

where integration is to be extended over the area of the plate face. The kinetic energy $\bar{T}$ (1) is given by, neglecting rotatory inertia terms

$$2\bar{T} = \rho \iint (h\dot{u}_0^2 + h\dot{v}_0^2 + h\dot{w}_0^2)dxdy \quad \ldots\ldots [34]$$

Assuming the displacements in the form

$$\left.\begin{aligned} u_0 &= \frac{B^2H^2(t)\pi}{16a}\left(\cos\frac{2\pi y}{b} - 1 + \nu\frac{a^2}{b^2}\right)\sin\frac{2\pi x}{a} \\ v_0 &= \frac{B^2H^2(t)\pi}{16a}\left(\frac{a}{b}\cos\frac{2\pi x}{a} - \frac{a}{b} + \nu\frac{b}{a}\right)\sin^2\frac{\pi y}{b} \\ w_0 &= BH(t)\sin\frac{\pi x}{a}\sin\frac{\pi y}{b} \end{aligned}\right\} \ldots [35]$$

the potential and the kinetic energies become, respectively

$$\left.\begin{aligned} 2\bar{W} = &\int_0^a\int_0^b \frac{Eh}{1-\nu^2}\left(\frac{B^2H^2\pi^2}{8}\right)^2\left\{\frac{1}{a^4}\left[1-\cos\frac{2\pi y}{b}+\nu\frac{a^2}{b^2}\cos\frac{2\pi x}{a}\right]^2 + \frac{\nu}{a^2b^2}\left[1-\cos\frac{2\pi x}{a}+\nu\frac{b^2}{a^2}\cos\frac{2\pi y}{b}\right]\right. \\ &\left.\left[1-\cos\frac{2\pi y}{b}+\nu\frac{a^2}{b^2}\cos\frac{2\pi x}{a}\right]\right\}dxdy + \int_0^a\int_0^b \frac{Eh}{1-\nu^2}\left(\frac{B^2H^2\pi^2}{8}\right)^2\left\{\frac{1}{b^4}\left[1-\cos\frac{2\pi x}{a}+\nu\frac{b^2}{a^2}\cos\frac{2\pi y}{b}\right]^2\right. \\ &\left.+\frac{\nu}{a^2b^2}\left[1-\cos\frac{2\pi y}{b}+\nu\frac{a^2}{b^2}\cos\frac{2\pi x}{a}\right]\left[1-\cos\frac{2\pi x}{a}+\nu\frac{b^2}{a^2}\cos\frac{2\pi y}{b}\right]\right\}dxdy \\ &+\frac{Eh^3}{1-\nu^2}B^2H^2\pi^4\int_0^a\int_0^b \sin^2\frac{\pi x}{a}\sin^2\frac{\pi y}{b}\left(\frac{1}{a^4}+\frac{1}{b^4}+\frac{2}{a^2b^2}\right)dxdy = \frac{Eh}{1-\nu^2}\left(\frac{B^2H^2\pi^2}{8}\right)^2 \\ &\left\{\frac{b}{a^3}\left[\frac{3}{2}+\frac{\nu^2}{2}\frac{a^4}{b^4}\right]+\frac{2\nu}{ab}\left[1-\frac{\nu}{2}\frac{b^2}{a^2}-\frac{\nu}{2}\frac{a^2}{b^2}\right]+\frac{a}{b^3}\left[\frac{3}{2}+\frac{\nu^2}{2}\frac{b^4}{a^4}\right]\right\} + \frac{Eh^3}{12(H\nu^2)}\frac{B^2\pi^4H^2}{4}\left(\frac{1}{a^2}+\frac{1}{b^2}\right)^2 ab \end{aligned}\right\} \ldots [36]$$

$$2\bar{T} = \rho\left(\frac{B^2H\dot{H}\pi}{8}\right)^2\left[\frac{h}{a}b\left(\frac{3}{4}+\nu^2\frac{a^4}{b^4}-2\nu\frac{a^2}{b^2}\right) + \frac{h}{b}a\left(\frac{3}{4}+\nu^2\frac{b^4}{a^4}-2\nu\frac{b^2}{a^4}\right)\right] + \rho\frac{B^2\dot{H}^2}{4}abh \ldots [37]$$

The principle of conservation of energy is stated by requiring that

$$\frac{\partial}{\partial t}(\bar{T} + \bar{W}) = 0$$

Letting again $\delta = h/a$, $r = a/b$, and designating by p the corresponding linear frequency of the plate, given by (9)

$$p^2 = \frac{\pi^4}{a^4}\frac{E}{\rho}\frac{h^2}{12(1-\nu^2)}(1+r^2)^2$$

the result is, retaining terms of lowest power in δ only

$$\ddot{H} + p^2H + \frac{3}{2}p^2\left(\frac{B}{h}\right)^2H^3\left[\left(\frac{3}{2}-\frac{\nu^2}{2}\right)(1+r^4)+2\nu r^2\right](1+r)^{-2} = 0 \ldots [38]$$

This equation on $H(t)$ is identical to Equation [20] on $Z(\zeta)$ if the appropriate transformation of variables is performed.

A Special Case: Beam Vibrations

The stress equations of motion of a beam are obtained from the corresponding plate Equations [1] by letting $v_0 = 0$ and $\partial(\,)/\partial y = 0$

$$\left.\begin{aligned} \frac{\partial N_1}{\partial x} &= \rho h\ddot{u}_0 \\ \frac{\partial^2 M_1}{\partial x^2} + \frac{\partial}{\partial x}\left(N_1\frac{\partial w_0}{\partial x}\right) &= \rho h\ddot{w}_0 \end{aligned}\right\} \ldots [39]$$

For the sake of simplicity, but without loss of generality, a beam of rectangular cross section, of height h and unit width, is considered. The area of the cross section is thus given by h and the moment of inertia by $h^3/12$.

For the case of such a beam, the stress-displacement Relations [2] simplify to

$$N_1 = Eh\left[\frac{\partial u_0}{\partial x} + \frac{1}{2}\left(\frac{\partial w_0}{\partial x}\right)^2\right]$$

$$M_1 = -\frac{Eh^3}{12}\frac{\partial^2 w_0}{\partial x^2}$$

Using the same Transformations [6] and [7], where, however, the velocity c_p has to be replaced by the velocity of compressional waves in a beam

$$c_b = \sqrt{\frac{E}{\rho}}$$

the dimensionless equations result

$$\left.\begin{aligned} &\frac{\partial^2\bar{u}}{\partial\xi^2} + \frac{\partial\bar{w}}{\partial\xi}\frac{\partial^2\bar{w}}{\partial\xi^2} = \frac{\delta^2}{12}\frac{\partial^2\bar{u}}{\partial\zeta^2} \\ &\frac{\delta^2}{12}\left(\frac{\partial^4\bar{w}}{\partial\xi^4} + \frac{\partial^2\bar{w}}{\partial\zeta^2}\right) = \frac{3}{2}\frac{\partial^2\bar{w}}{\partial\xi^2}\left(\frac{\partial\bar{w}}{\partial\xi}\right)^2 + \frac{\partial^2\bar{w}}{\partial\xi^2}\frac{\partial\bar{u}}{\partial\xi} + \frac{\partial\bar{w}}{\partial\xi}\frac{\partial^2\bar{u}}{\partial\xi^2} \end{aligned}\right\} \ldots [40]$$

The boundary conditions for immovable, hinged, beam ends are

$$\bar{u} = \bar{w} = \frac{\partial^2\bar{w}}{\partial\xi^2} = 0 \qquad \text{at } \xi = 0, 1 \ldots\ldots [41]$$

Similarly, as in the plate case, the perturbation yields in first approximation the equations of motion

$$\left.\begin{aligned} &\frac{\partial^2 u^{(2)}}{\partial\xi^2} + \frac{\partial w^{(1)}}{\partial\xi}\frac{\partial^2 w^{(1)}}{\partial\xi^2} = 0 \\ &\frac{1}{12}\left(\frac{\partial^4 w^{(1)}}{\partial\xi^4} + \frac{\partial^2 w^{(1)}}{\partial\zeta^2}\right) = \frac{3}{2}\frac{\partial^2 w^{(1)}}{\partial\xi^2}\left(\frac{\partial w^{(1)}}{\partial\xi}\right)^2 + \frac{\partial^2 w^{(1)}}{\partial\xi^2}\frac{\partial u^{(2)}}{\partial\xi} + \frac{\partial w^{(1)}}{\partial\xi}\frac{\partial^2 u^{(2)}}{\partial\xi^2} \end{aligned}\right\} \ldots [42]$$

and the boundary conditions

$$u^{(2)} = w^{(1)} = \frac{\partial^2 w^{(1)}}{\partial \xi^2} = 0 \quad \text{at } \xi = 0, 1 \ldots\ldots\ldots [43]$$

With the aid of the boundary condition on $u^{(2)}$, the variable $u^{(2)}$ may be eliminated from the Equations of Motion [42], such that only one equation governing $w^{(1)}$ results

$$\frac{1}{12}\left(\frac{\partial^4 w^{(1)}}{\partial \xi^4} + \frac{\partial^4 w^{(1)}}{\partial \zeta^2}\right) = \frac{\partial^2 w^{(1)}}{\partial \xi^2}\int_0^1 \frac{1}{2}\left(\frac{\partial w^{(1)}}{\partial \xi}\right)^2 d\xi \ldots [44]$$

Assuming $w^{(1)}$ in the form

$$w^{(1)} = \beta Z(\zeta) \sin \pi\xi \ldots\ldots\ldots\ldots\ldots [45]$$

the time function will be governed by

$$\frac{d^2 Z}{d\zeta^2} + \pi^4 Z + 3\beta^2\pi^4 Z^3 = 0 \ldots\ldots\ldots\ldots [46]$$

whose solution may be given again in terms of elliptic functions. Similarly as in the case of plates, we evaluate the ratio of the nonlinear period T^* to the linear period T

$$\frac{T^*}{T} = \frac{2}{\pi}(1 + 3\beta^2)^{-1/2} K \ldots\ldots\ldots\ldots [47]$$

where K is again the complete elliptic integral of the first kind. This result, plotted in Fig. 4, is identical with the one obtained by A. C. Eringen (4), who, however, based his analysis on more exact equations than those used presently. The theory discussed in (4) describes rotations of any magnitude and strains which may be large. The present theory, on the contrary, deals with merely moderately large rotations and with small strains. It is thus of interest to observe that both theories predict the same period from first-order perturbations.

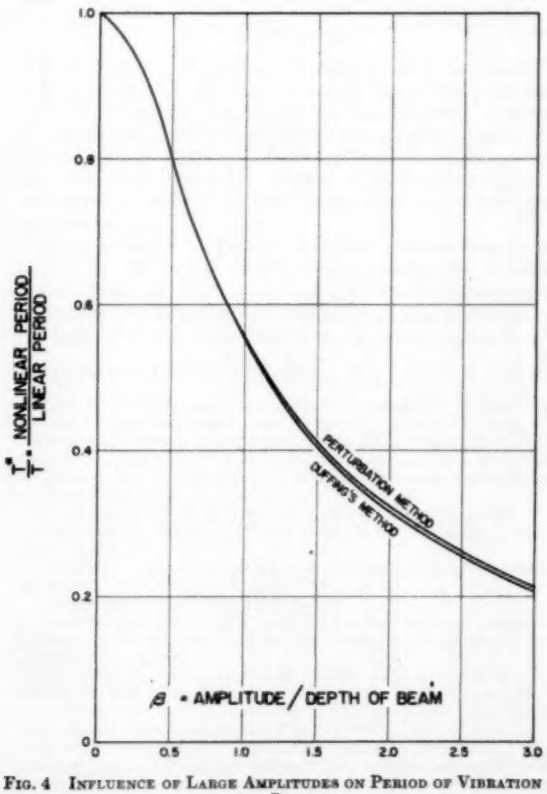

FIG. 4 INFLUENCE OF LARGE AMPLITUDES ON PERIOD OF VIBRATION OF A BEAM

Furthermore, it may be observed that the perturbed equations of motion can be solved exactly in the case of a beam, Equation [42], but not in the case of a plate, Equation [13]. It is also of interest to note that the ratio of the nonlinear period to the linear period of the plate, given by Equation [26], does not reduce to the corresponding relation of the beam, Equation [47], by letting the aspect ratio $r = 0$. This behavior may be made plausible by recognizing that the period is affected by terms containing $\partial v_0/\partial y$ which do not exist in the beam case but are present in the plate problem, even as r approaches zero.

As an alternative, a different solution of the same beam problem will be obtained, in the following, employing a method which is essentially the one due to Duffing (6).

The two equations of motion for the beam, from Equation [3], in dimensional form, are

$$\left.\begin{aligned} &\frac{\partial^2 u_0}{\partial x^2} - \frac{\ddot{u}_0}{c_0^2} = -\frac{\partial w_0}{\partial x}\frac{\partial^2 w_0}{\partial x^2} \\ &\frac{\partial^4 w_0}{\partial x^4} - \frac{1}{R^2}\left[\frac{3}{2}\left(\frac{\partial w_0}{\partial x}\right)^2\frac{\partial^2 w_0}{\partial x^2} + \frac{\partial w_0}{\partial x}\frac{\partial^2 u_0}{\partial x^2} + \frac{\partial^2 w_0}{\partial x^2}\frac{\partial u_0}{\partial x}\right] \\ &\qquad = -\frac{1}{c_0^2 R^2}\ddot{w}_0 \end{aligned}\right\} \ldots [48]$$

where

$$c_0^2 = \frac{E}{\rho}, \qquad R^2 = \frac{h^2}{12}$$

The transverse displacement w_0 is assumed in the form

$$w_0 = B(\omega^*) \sin\frac{\pi x}{a} \cos \omega^* t \ldots\ldots\ldots\ldots [49]$$

ω^* being the nonlinear frequency, and the longitudinal displacement u_0 is obtained from the first of Equations [48] as

$$u_0 = -\frac{1}{16}\frac{\pi}{a} B^2\left[1 + \frac{\cos 2\omega^* t}{1 - \left(\frac{\omega^* a}{c_0 \pi}\right)^2}\right] \sin\frac{2\pi x}{a} \ldots [50]$$

From the second of Equations [48] we obtain, after equating the coefficients of $\sin(\pi x/a)\cos\omega^* t$

$$\frac{B^2}{32R^2}\left[7 - \frac{1}{1 - \left(\frac{\omega^* a}{c_0\pi}\right)^2}\right]\left(\frac{\pi}{a}\right)^4 = \left(\frac{1}{c_0 R}\right)^2 \omega^{*4} - \left(\frac{\pi}{a}\right)^4 \ldots [51]$$

Noting that the frequency of the linear problem ω is (9)

$$\omega = \left(\frac{\pi}{a}\right)^2 c_0 R \ldots\ldots\ldots\ldots [52]$$

the ratio of the squares of the frequencies may be written as

$$\left(\frac{\omega^*}{\omega}\right)^2 = 1 + \frac{3}{8}\left(\frac{B}{h}\right)^2\left[7 - \frac{1}{1 - \frac{\pi^2}{12}\left(\frac{\omega^*}{\omega}\frac{h}{a}\right)^2}\right] \ldots [53]$$

Since for a beam $h/a \ll 1$, we may neglect the term $[(\omega^*/\omega)(h/a)]^2$ in comparison to unity. Relation [53] is then simplified to

$$\left(\frac{\omega^*}{\omega}\right)^2 = 1 + \frac{9}{4}\beta^2 \quad \ldots\ldots\ldots\ldots\ldots\ldots [54]$$

β stands, as before, for B/h, and the ratio of periods is given by

$$\frac{T^*}{T} = \left[1 + \left(\frac{3}{2}\beta\right)^2\right]^{-1/2} \quad \ldots\ldots\ldots\ldots [55]$$

This ratio is also plotted in Fig. 4 and it is seen that the agreement between the two solutions is excellent. Thus the conclusion is reached that in the present case the more elementary Duffing's approach yields practically the same result as a perturbation procedure followed by an integration involving elliptic functions.

In the case of a plate, however, Duffing's method would be rather tedious and no attempt was made to develop a solution by that method.

BIBLIOGRAPHY

1 "Influence of Large Amplitudes on Flexural Motions of Elastic Plates," by G. Herrmann, NACA TN 3578.

2 "On the Nonlinear Vibration Problem of the Elastic String," by G. F. Carrier, *Quarterly of Applied Mathematics*, vol. 3, 1945, p. 157.

3 "A Note on the Vibrating String," by G. F. Carrier, *Quarterly of Applied Mathematics*, vol. 7, 1949, p. 97.

4 "On the Nonlinear Vibration of Elastic Bars," by A. C. Eringen, *Quarterly of Applied Mathematics*, vol. 10, 1952, p. 361.

5 "On the Nonlinear Vibration of Circular Membrane," by A. C. Eringen, Proceedings of the First U. S. National Congress of Applied Mechanics, Chicago, Ill., 1951, p. 139.

6 "Nonlinear Vibrations," by J. J. Stoker, Interscience Publishers, Inc., New York, N. Y., 1950.

7 "Theory of Plates and Shells," by S. Timoshenko, McGraw-Hill Book Company, Inc., New York, N. Y., 1940.

8 "Large Deflection Theory for Rectangular Plates," by S. Levy, Proceedings of Symposia in Applied Mathematics, American Mathematical Society, New York, N. Y., vol. 1, 1949, p. 197.

9 "Vibration Problems in Engineering," by S. Timoshenko, D. Van Nostrand Company, Inc., New York, N. Y., 1937.

On the Transmission of a Concentrated Load Into the Interior of an Elastic Body[1]

By G. L. NEIDHARDT[2] and ELI STERNBERG,[3] CHICAGO, ILL.

An exact solution in series form is presented for the stresses and displacements in an elastic body bounded by one sheet of a two-sheeted hyperboloid of revolution, subjected to an axial concentrated load at the vertex. The problem is reduced to one governed by finite surface tractions with the aid of a scheme developed in (1),[4] and the solution is based on the Boussinesq stress functions referred to spheroidal co-ordinates. The corresponding known solutions appropriate to the half space and to the circular cone are obtained as limiting cases. Numerical results are given for the normal stress on planes perpendicular to the axis of symmetry, at points on this axis. These values are utilized in a discussion aimed at the influence of the curvature of the boundary at the load point upon the transmission of the load into the interior of the body; the results indicate that this influence may be considerable.

Introduction

THE concept of concentrated loads in the linear theory of elasticity was discussed extensively in (2) which contains an extension of the classical uniqueness theorem to mixed boundary-value problems involving concentrated internal and surface loads, in addition to distributed body forces and surface tractions. The theorem here referred to yields a formulation of such problems which is complete in the sense that it admits at most one solution.

It will suffice for our present purposes to cite this formulation merely for the second boundary-value problem for isotropic media. Moreover, we shall confine ourselves to the case in which body forces or internal concentrated loads are absent and assume the body to be subjected exclusively to concentrated surface loads[5] $\vec{L}_k$ applied at the load points Q_k $(k = 1, 2, \ldots n)$. If D, with the boundary B, is the regular region of space[6] occupied by the medium, the solution is uniquely characterized by the following requirements:

(a) The stresses, strains, and displacements must satisfy the field equations of the classical theory in D and must be continuous, as well as continuously differentiable, in any closed subregion of $D + B$ which excludes the load points. If D is not bounded

$$u_i = O(r^{-1}), \qquad \tau_{ij} = O(r^{-2}) \text{ as } r \to \infty \ldots\ldots [1]$$

where r is the distance from a fixed point of the space, whereas u_i and τ_{ij} denote the Cartesian components of displacement and stress.[7]

(b) The surface tractions must vanish identically on B except at the load points and at corners or edges of the boundary (where they are not defined).

(c) The solution must have singularities at the load points and the stress resultant of each singularity must equal the corresponding concentrated load. Thus, if $\Sigma_k(\delta)$ is the portion lying in D of a spherical surface of radius δ, centered at Q_k, and $\vec{T}$ is the resultant surface traction on that side of Σ_k which faces Q_k, then

$$\lim_{\delta \to 0} \int_{\Sigma_k(\delta)} \vec{T}\, dA = \vec{L}_k \qquad (k = 1, 2, \ldots n) \ldots\ldots [2]$$

(d) The order of the stress singularities at each load point must be characterized by

$$\tau_{ij} = O(r_k^{-2}) \text{ as } r_k \to 0 \qquad (k = 1, 2, \ldots n) \ldots\ldots [3]$$

where r_k is the distance from Q_k.

The foregoing formulation of concentrated-load problems derives its physical motivation from the definition of the solution through a limit process which may be described roughly as follows: Each of the concentrated loads is initially replaced with an arbitrary distribution of surface tractions ("replacement loadings") applied to finite surface elements ("load regions") surrounding the given points of application of the concentrated forces. The solution of the original concentrated-load problem is then defined as the limit of the solution to the modified problem, as the load regions are shrunk to the load points while the resultants of the replacement loadings are made to approach the corresponding prescribed concentrated loads. This limit process is spelled out precisely in Theorem 7.1 of reference (2), by virtue of which the

---

[1] The results contained in this paper were obtained in the course of an investigation conducted under Contract N7onr-32906, with the Office of Naval Research, Department of the Navy, Washington, D. C. One of the authors also is indebted to the American Steel Foundries in Chicago, Ill., for support of his activities in connection with the work described here.

[2] Assistant to the Vice-President, American Steel Foundries.

[3] Professor of Mechanics, Illinois Institute of Technology. Assoc. Mem. ASME.

[4] Numbers in parentheses refer to the Bibliography at the end of the paper.

[5] Letters carrying arrows denote vectors.

Presented at the National Applied Mechanics Division Conference, Urbana, Ill., June 14–16, 1956, of The American Society of Mechanical Engineers.

Discussion of this paper should be addressed to the Secretary, ASME, 29 West 39th Street, New York, N. Y., and will be accepted until January 10, 1957, for publication at a later date. Discussion received after the closing date will be returned.

Note: Statements and opinions advanced in papers are to be understood as individual expressions of their authors and not those of the Society. Manuscript received by ASME Applied Mechanics Division, January 12, 1956. Paper No. 56—APM-35.

[6] See Section 2 of reference (2) for a definition of a regular region of space. We merely note here that any region in which the divergence theorem holds is admissible. In particular, D need not be bounded or simply connected, and the boundary B may exhibit corners and edges.

[7] Although the conventional engineering notation, for the components of displacement and stress, will be used almost exclusively in this paper, we shall occasionally find it convenient to revert to indicial notation. The symbol "O," for "order of magnitude," throughout the paper will be employed only in its standard mathematical connotation. Thus, $f(x) = O(x^n)$ as $x \to \infty$ or $x \to 0$ means that $|f(x)/x^n|$ remains bounded in this limit.

limit solution so defined exists and is independent of the particular choice of the load regions as well as of the mode of distribution of the replacement loadings, provided these tractions on each load region are sufficiently smooth, parallel, and of the same sense.

According to Theorem 7.2 of (2), the limit solution conforms to requirements (*a*), (*b*), (*c*), (*d*), and thus—in view of the generalized uniqueness theorem cited earlier—the formulation of the problem in terms of conditions (*a*), (*b*), (*c*), (*d*) is equivalent to the limit formulation. On the other hand, as shown in reference (3), the traditional formulation of concentrated-load problems, which rests on conditions (*a*), (*b*), and (*c*) alone, is incomplete; it admits an infinity of "pseudo-solutions" which meet these *three* conditions but fail to coincide with the associated limit solution.

In order to arrive at practically useful representations of the solution to a concentrated-load problem, it is desirable to determine the relevant singularities in closed form. In reference (1) such a reduction of the problem to one which is regular, at least in the sense of being governed by finite and continuous surface tractions, was effected on the basis of conditions (*a*), (*b*), (*c*), (*d*) for a class of concentrated-load problems; i.e., the boundary, in a neighborhood of a typical load point, was assumed to be a sufficiently smooth, but otherwise arbitrary, surface of revolution, the axis of which coincides with the load axis. The reduction scheme developed in (1) is a generalization of a process first applied to the special problem of the sphere subjected to two equal and diametrically opposite concentrated loads (3).

The specific nature of the singularity—in contrast to its order—was found in reference (1) to depend on the curvature of the meridian of the boundary at the load point. It appears to be of interest, therefore, to solve explicitly a problem in which this local curvature may be varied, with a view toward gaining some quantitative insight into the effect of the local boundary curvature upon the transmission of the load into the interior of the body. This leads us to consider the problem of an elastic medium bounded by one sheet of a two-sheeted hyperboloid of revolution and subjected to an axial concentrated load at the vertex of the boundary.

Before turning to the particular problem which constitutes the main objective of the present paper, we briefly recall, in the succeeding section, the general reduction scheme given previously in reference (1). Moreover, since the problem at hand is most conveniently approached by means of spheroidal co-ordinates, its solution is preceded by a mainly expository section on spheroidal co-ordinates and harmonics, as well as by a discussion of certain particular solutions of the field equations of elasticity theory referred to spheroidal co-ordinates.

Spheroidal co-ordinates have previously been employed in the theory of elasticity in connection with problems involving hyperboloidal boundaries by Neuber (4) and spheroidal boundaries by Neuber (4), Sadowsky and Sternberg (5), Miyamoto (6 to 8), Edwards (9), Chih-Bing Ling (10), and Muki (11). A difficulty peculiar to the present application stems from the fact that there do not exist product solutions of Laplace's equation in spheroidal co-ordinates, which are regular in the region under consideration.

Boussinesq Stress Functions—Reduction of a Class of Concentrated-Load Problems to Regular Problems

Let (x, y, z) be Cartesian co-ordinates and (ρ, γ, z) be cylindrical co-ordinates, so that

$$\left.\begin{aligned} x &= \rho\cos\gamma, \qquad y = \rho\sin\gamma \\ 0 &\leq \rho < \infty \qquad 0 \leq \gamma < 2\pi \end{aligned}\right\} \quad \ldots\ldots\ldots [4]$$

Then every solution of the displacement equations of equilibrium which is characterized by torsionless axisymmetry about the z-axis, in the absence of body forces, admits the representation

$$\left.\begin{aligned} 2G[u_\rho, u_\gamma, u_z] &= \nabla(\phi + z\psi) - [0, 0, 4(1-\nu)\psi] \\ \nabla^2\phi(\rho, z) &= 0, \qquad \nabla^2\psi(\rho, z) = 0 \end{aligned}\right\} \quad \ldots [5]$$

Here, ϕ and ψ are the Boussinesq stress functions (12), $[u_\rho, u_\gamma, u_z]$ are the cylindrical components of displacement, G and ν designate the shear modulus and Poisson's ratio, respectively, while ∇ and ∇^2 denote the gradient and the Laplacian operators.

We now summarize, in a restricted form adapted to our present needs, the process developed in reference (1) for the reduction of a class of concentrated-load problems to problems governed by more regular boundary conditions. Thus consider an elastic body occupying a region D bounded by a surface of revolution B

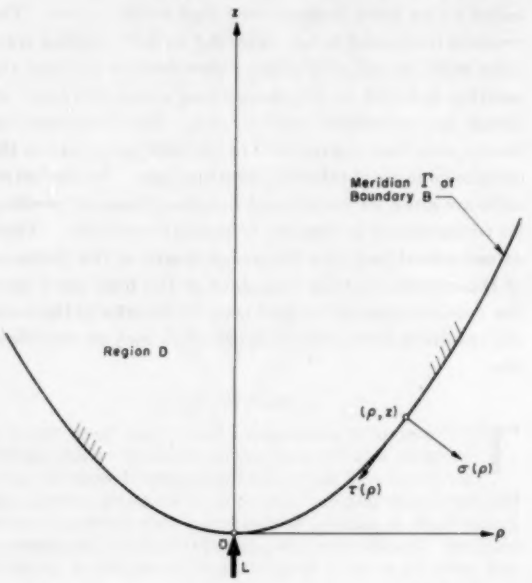

Fig. 1 Meridian of the Surface of Revolution Bounding the Elastic Body

which lies in the half space $z \geq 0$ and extends to infinity. Let the meridian Γ of B, Fig. 1, be given by

$$\Gamma: \qquad z = f(\rho), \qquad -\infty < \rho < \infty \ldots\ldots\ldots [6][8]$$

where $f(\rho)$ is an even analytic function

$$f(0) = 0, \quad \frac{df}{d\rho} > 0 \text{ for } \rho > 0$$

and

$$f(\rho) = O(\rho) \quad \text{as } \rho \to \infty \ldots\ldots\ldots\ldots [7][9]$$

Suppose that the body is subjected to a single concentrated load of magnitude $|L|$ applied at the vertex ($\rho = z = 0$) of B, parallel to the z-axis, and let $L > 0$ if the load is directed in the positive z-direction. The boundary B is assumed to be otherwise free from tractions. The stresses and displacements are to be determined throughout $D + B$.

[8] It is expedient to abandon the restriction $\rho \geq 0$ temporarily.

[9] The significance of this assumption will become apparent at the end of this section.

According to reference (1), the unique solution[10] $[S]$ to the problem, formulated in terms of the conditions (a), (b), (c), (d) listed in the Introduction, admits the alternative representations

$$[S] = [S_0] + [R_0] = [S_1] + [R_1] = [S_2] + [R_2] \quad \ldots\ldots [8]$$

Each of the component solutions $[S_0]$, $[S_1]$, $[S_2]$ contains, in closed form, leading terms of the singularity inherent in $[S]$. The component solutions appearing in Equations [8] are defined as follows with reference to the generating Boussinesq stress functions introduced in Equations [5]

$$\left.\begin{aligned} [S_0]: \quad \phi &= -\frac{L}{2\pi}(1-2\nu)\log\frac{r+z}{c} \\ \psi &= -\frac{L}{2\pi r} \end{aligned}\right\} \quad \ldots\ldots [9]$$

where

$$r = (x^2+y^2+z^2)^{1/2} = (\rho^2+z^2)^{1/2} \quad \ldots\ldots [10]$$

while c is an arbitrary parameter[11] which has the dimension of length. Solution $[S_0]$ is Boussinesq's solution (12)[12] corresponding to a concentrated load of magnitude $|L|$ applied at $r = 0$ to the plane boundary of a medium occupying the half space $z \geq 0$

$$[S_1] = [S_0] + \frac{(1-2\nu)\kappa_0 L}{2\pi}[E_0] \quad \ldots\ldots [11]$$

$$[S_2] = [S_1] + \frac{(1+12\nu-16\nu^2)\kappa_0^2 L}{16\pi}[E_1] \quad \ldots\ldots [12]$$

in which

$$\kappa_0 = \left.\frac{d^2 f}{d\rho^2}\right|_{\rho=0} \quad \ldots\ldots [13]$$

is the curvature of Γ at the load point $\rho = 0$ and

$$\left.\begin{aligned} [E_0]: \quad \phi &= 2(1-\nu)\left(z\log\frac{r+z}{c} - r\right) \\ \psi &= \log\frac{r+z}{c} \end{aligned}\right\} \quad \ldots\ldots [14]$$

$$\left.\begin{aligned} [E_1]: \quad \phi &= (1-\nu)\left[(3z^2-r^2)\log\frac{r+z}{c} - z^2 - 3rz + r^2\right] \\ \psi &= 2\left(z\log\frac{r+z}{c} - r\right) \end{aligned}\right\} \quad .[15][13]$$

The behavior of the displacements and stresses belonging to the singular solutions $[S_0]$, $[S_1]$, $[S_2]$, in the limit as $r \to 0$ or $r \to \infty$, is given by

$$\left.\begin{aligned} [S_0]: \quad & u_i = O(r^{-1}), \quad \tau_{ij} = O(r^{-2}) \\ [S_1]: \quad & u_i = O(\log r), \quad \tau_{ij} = O(r^{-1}) \\ [S_2]: \quad & u_i = O(r\log r), \quad \tau_{ij} = O(\log r) \end{aligned}\right\} \quad \ldots [16]$$

Each of the singular solutions satisfies conditions (a), (c), and (d), with the exception of the regularity requirement at infinity, Equation [1], which is violated by $[S_1]$ and $[S_2]$. On the other hand, all three singular solutions fail to clear the boundary B from tractions.

We turn next to $[R_0]$, $[R_1]$, $[R_2]$ in Equations [8], which denote the solutions of the "residual problems" associated with $[S_0]$, $[S_1]$, $[S_2]$. The characterization of these alternative residual problems follows from Equations [8], from conditions (a), (b), (c), (d), to be met by the complete solution $[S]$, and from the properties possessed by $[S_0]$, $[S_1]$, $[S_2]$. In particular, $[R_0]$, $[R_1]$, $[R_2]$ must satisfy the field equations in D and must annul the surface tractions arising on B from $[S_0]$, $[S_1]$, $[S_2]$, respectively; in addition, the behavior of $[R_0]$, $[R_1]$, $[R_2]$ at infinity must be such that $[S]$ conforms to Equation [1].[14]

The sequence of solutions $[R_0]$, $[R_1]$, $[R_2]$ of the complementary residual problems to which the sequence of singular solutions $[S_0]$, $[S_1]$, $[S_2]$ gives rise, is characterized by a progressively increasing regularity in the corresponding boundary conditions. Let $\sigma(\rho)$ and $\tau(\rho)$ be, respectively, the normal and shearing tractions on B, Fig. 1, belonging to the singular solutions. As shown in reference (1), $\sigma(\rho)$ is finite and continuous for all three singular solutions while the behavior of $\tau(\rho)$ as $\rho \to 0$, i.e., in the vicinity of the load point, is given by

$$\left.\begin{aligned} [S_0]: \quad \tau(\rho) &= \frac{L}{8\pi}\left[\frac{-4(1-2\nu)\kappa_0}{\rho} + (5-4\nu)\kappa_0^2\right] + O(\rho) \\ [S_1]: \quad \tau(\rho) &= \frac{\kappa_0^2 L}{8\pi}(1+12\nu-16\nu^2) + O(\rho) \\ [S_2]: \quad \tau(\rho) &= O(\rho) \end{aligned}\right\} \quad \ldots [17]$$

Thus the shearing tractions on B of $[S_0]$ become infinite as $\rho \to 0$, those of $[S_1]$ exhibit a finite-jump discontinuity at $\rho = 0$, while those of $[S_2]$ are finite and continuous at the load point. It should be emphasized, however, that $[S_2]$ contains the entire singularity inherent in the complete solution $[S]$ only if $\kappa_0 = 0$. In any event, the singularity at the load point depends upon the value of κ_0.

Finally, we observe in connection with Equation [7][15] that the regularity condition at infinity, Equation [1], is incompatible with the equilibrium of the body if the meridian Γ of B is such that $f(\rho)$ is of a higher order of magnitude[16] and not $O(\rho)$ as $\rho \to \infty$. Here, Equation [1] would imply that the resultant of the tractions acting on the circular cross sections of the body tends to zero as $z \to \infty$. In such an instance one needs to relax Condition [1], which, though sufficient for the uniqueness of $[S]$, is by no means necessary.[17]

---

[10] Capital letters in brackets denote either the displacement-vector field (within an arbitrary additive rigid displacement) or the stress-tensor field of a solution of the field equations. Equality, addition, and multiplication by a scalar are to be interpreted accordingly.

[11] See footnote 13.

[12] See also reference (13), p. 191.

[13] The stress functions associated with solutions $[S_0]$, $[E_1]$, and $[E_2]$ reduce to those generating the solutions bearing the same designations in (1) if we put $c = 1$. The introduction of c, which is expedient for future purposes, leaves unaltered $[S_0]$, as well as the stresses of $[E_0]$, and affects $[E_1]$ merely within an inessential additive plane-hydrostatic field of stress.

[14] The concluding remark in reference (1), to the effect that the representation $[S] = [S_2] + [R_2]$ becomes inadmissible for unbounded domains because of the behavior of $[S_2]$ at infinity, is unfounded.

[15] See footnote 9.

[16] E.g., if B is a paraboloid of revolution, $f(\rho) = O(\rho^2)$ as $\rho \to \infty$.

[17] The extent to which Condition [1] may be weakened without loss in uniqueness is apparently in need of investigation. The analogous question for the two-dimensional treatment of the plane problem was considered by Tiffen (14).

Spheroidal Co-Ordinates, Spheroidal Harmonics—Legendre Functions

Prolate spheroidal co-ordinates[18] (α, β, γ) may be defined in terms of the Cartesian co-ordinates (x, y, z) through the transformation

$$\left.\begin{aligned} x &= c \sinh \alpha \sin \beta \cos \gamma \\ y &= c \sinh \alpha \sin \beta \sin \gamma \\ z &= c \cosh \alpha \cos \beta \end{aligned}\right\} \quad \ldots\ldots\ldots [18]$$

or, in terms of the cylindrical co-ordinates (ρ, γ, z) introduced in Equations [4], through the conformal mapping

$$z + i\rho = c \cosh (\alpha + i\beta) \ldots\ldots\ldots [19]$$

where

$$0 \leq \alpha < \infty, \qquad 0 \leq \beta \leq \pi, \qquad 0 \leq \gamma < 2\pi \ldots [20]$$

and c is an arbitrary positive constant. With the reparameterization

$$p = \cos \beta, \qquad q = \cosh \alpha \ldots\ldots\ldots [21]$$

and the auxiliary notation

$$\hat{p} = (1 - p^2)^{1/2} = \sin \beta, \qquad \hat{q} = (q^2 - 1)^{1/2} = \sinh \alpha \ldots [22]$$

Equations [19], [20] are equivalent to

$$\rho = c\hat{p}\hat{q}, \qquad z = cpq \ldots\ldots\ldots [23]$$

$$-1 \leq p \leq 1, \qquad 1 \leq q < \infty, \qquad 0 \leq \gamma < 2\pi \ldots [24]$$

Equations [23] imply

$$\frac{z^2}{c^2p^2} - \frac{\rho^2}{c^2\hat{p}^2} = 1, \qquad \frac{z^2}{c^2q^2} + \frac{\rho^2}{c^2\hat{q}^2} = 1 \ldots\ldots [25]$$

The co-ordinate surfaces $p = \pm$ const and $q =$ const thus form a family of confocal and mutually orthogonal two-sheeted hyperboloids and spheroids, respectively, the traces of which, on a meridional half plane $\gamma =$ const, are shown in Fig. 2. The foci F_1 and F_2 are located on the z-axis, at $z = -c$ and $z = c$, respectively. The segment $-c \leq z \leq c$ of the axis is represented by $q = 1$ while the remainder of the axis is given by $p = \pm 1$. As is evident from Equations [23], [24], $p = p_0 \geq 0$ corresponds to a hyperboloidal sheet which lies in the half space $z \geq 0$. The vertex of such a sheet is situated at

$$z = h_0 = cp_0 \ldots\ldots\ldots [26]$$

and the curvature of its meridian at the vertex is

$$\kappa_0 = \frac{p_0}{c\hat{p}_0^2} \ldots\ldots\ldots [27]$$

For future convenience we also introduce the spherical co-ordinates (r, θ, γ) and the "displaced" spherical co-ordinates (r_1, θ_1, γ), referred to the origin and the lower focus F_1 as poles, respectively, Fig. 2. From Equations [23] we have for the radial distances r, r_1 and for the co-latitudes θ, θ_1 the relations

$$\left.\begin{aligned} r &= (\rho^2 + z^2)^{1/2} = c(q^2 - \hat{p}^2)^{1/2} \\ \cos \theta &= \frac{z}{r} = \frac{pq}{(q^2 - \hat{p}^2)^{1/2}} \end{aligned}\right\} \ldots [28]$$

$$\left.\begin{aligned} r_1 &= [\rho^2 + (z + c)^2]^{1/2} = c(p + q) \\ \cos \theta_1 &= \frac{z + c}{r_1} = \frac{1 + pq}{p + q} \end{aligned}\right\} \ldots [29]$$

[18] See (15), chapter x, and (16), chapter viii, for a discussion of this curvilinear co-ordinate system and of associated harmonic functions.

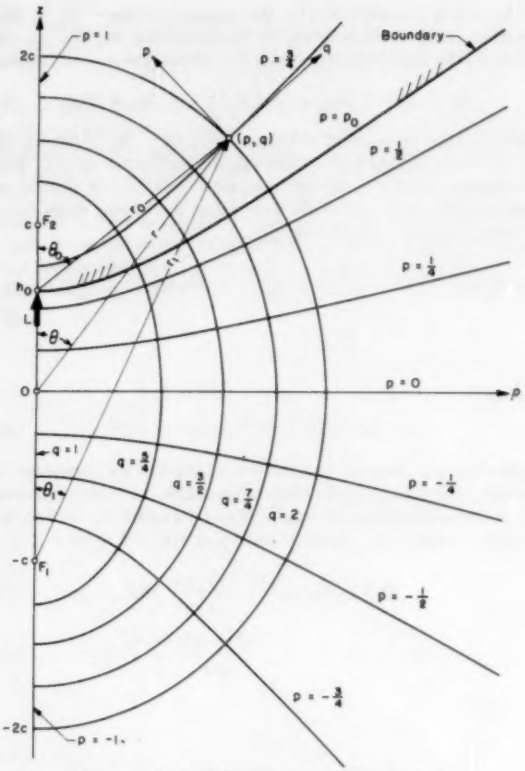

Fig. 2 Prolate Spheroidal Co-Ordinates: Trace of Surfaces $p =$ Const and $q =$ Const on a Half Plane $\gamma =$ Const

Laplace's equation in spheroidal co-ordinates, for a harmonic function U independent of γ, takes the form

$$\hat{p}^2U_{pp} - 2pU_p + \hat{q}^2U_{qq} + 2qU_q = 0 \ldots\ldots [30][19]$$

and Equation [30] admits the product solutions

$$U(p, q) = [P_n(p) \quad \text{or} \quad Q_n(p)][P_n(q) \quad \text{or} \quad Q_n(q)] \ldots [31]$$

Here P_n and Q_n are the Legendre functions[20] of the first and second kind, respectively.

In the particular problem to be considered later, we need harmonic functions which are regular for $z \geq 0$, that is, throughout the region $0 \leq p \leq 1$, $1 \leq q < \infty$, and which vanish at infinity. Since $P_n(q)$ does not tend to zero as $q \to \infty$ and $Q_n(q)$ has a logarithmic singularity at $q = 1$, i.e., along the segment joining the foci F_1 and F_2, it is clear from Equation [31] that the spheroidal product solutions of Laplace's equation do not possess the required regularity properties. For this reason we introduce the displaced exterior spherical harmonics, with the lower focus F_1 as the pole, and refer these to spheroidal co-ordinates. Indeed, the sequence of spherical harmonics

$$H_n(p, q) = c^{n+1}r_1^{-n-1}P_n(\cos \theta_1) \qquad (n \geq 0) \ldots [32][21]$$

[19] Subscripts attached to functions which originally bear no subscript, unless otherwise specified, denote differentiation with respect to the argument indicated.

[20] For extensive treatments of these functions, see references (15 to 18). See also the discussion toward the end of this section.

[21] See reference (15), p. 20. The letters j, k, m, and n henceforth denote integers. Thus P_n is the Legendre polynomial of degree n.

in view of Equations [29], assumes the form

$$H_n(p, q) = (p + q)^{-n-1} P_n\left(\frac{1 + pq}{p + q}\right) \qquad (n \geq 0) \ldots [33]$$

Since[22]

$$c\frac{\partial H_n}{\partial z} = -(n + 1)H_{n+1} \qquad (n \geq 0) \ldots\ldots\ldots [34]$$

the sequence H_n may be generated through successive differentiations with respect to z of its initial member

$$H_0 = \frac{1}{p + q} \ldots\ldots\ldots\ldots\ldots [35]$$

On the other hand, two successive integrations with respect to z of H_0 yield the harmonic functions

$$\left.\begin{aligned} H_{-1}(p, q) &= \log (1 + p)(q + 1) \\ H_{-2}(p, q) &= (1 + pq)\log (1 + p)(q + 1) - (p + q) \end{aligned}\right\} \ldots [36][23]$$

which are also needed in the subsequent analysis.

We now cite certain results in the theory of Legendre functions[24] to which we shall have to refer in what follows. The Legendre polynomials of degree $n \geq 0$, defined by

$$P_n(p) = \frac{1}{(-2)^n n!}\frac{d^n \hat{p}^{2n}}{dp^n}, \qquad (n \geq 0) \ldots\ldots\ldots [37]$$

satisfy Legendre's Equation

$$\hat{p}^2 P_n'' - 2pP_n' + n(n + 1)P_n = 0 \ldots\ldots\ldots [38][25]$$

and obey the recursion relations

$$\left.\begin{aligned} \hat{p}^2 P_n' &= (n + 1)(pP_n - P_{n+1}) \\ (n + 2)P_{n+2} &= (2n + 3)pP_{n+1} - (n + 1)P_n \end{aligned}\right\} \ldots [39]$$

Furthermore

$$P_n(1) = 1, \qquad P_{-n-1} = P_n \ldots\ldots\ldots\ldots [40]$$

The associated Legendre functions of the first kind, of degree n and order m, are defined by

$$\left.\begin{aligned} P_n^m(p) &= \hat{p}^m \frac{d^m P_n}{dp^m}, \qquad (n \geq 0, \quad m \geq 0) \\ P_n^{-m}(p) &= \frac{(-1)^m}{\hat{p}^m}\int_p^1 \cdots \int_p^1 P_n\, dp^m, \qquad (n \geq 0, \quad m \geq 0) \end{aligned}\right\} . [41][26]$$

We note, in particular, that

$$P_n^0 = P_n, \qquad P_n^m = 0, \qquad (m > n \geq 0) \ldots\ldots [42]$$

and recall Rodrigues' relation[27]

$$P_n^{-m} = (-1)^m \frac{(n - m)!}{(n + m)!} P_n^m, \qquad (-n \leq m \leq n) \ldots [43]$$

Next, we cite the recursion formulas

$$\left.\begin{aligned} &\hat{p}P_n^{m+1} - 2mpP_n^m \\ &\qquad + (n + m)(n - m + 1)\hat{p}P_n^{m-1} = 0 \\ &(n - m + 1)\hat{p}P_n^{m-1} - pP_n^m + P_{n-1}^m = 0 \end{aligned}\right\} \ldots [44]$$

which hold[28] for unrestricted values of m and n. Finally, with a view toward applications of Equation [33], we note the Taylor expansion

$$P_n(t) = \sum_{j=0}^{n} \frac{(t - p)^j}{j!} P_n^{(j)}(p) \ldots\ldots\ldots [45][29]$$

Now, let

$$t = \frac{1 + pq}{p + q} \ldots\ldots\ldots\ldots\ldots [46]$$

whence, from Equations [45], [41], and [22]

$$P_n\left(\frac{1 + pq}{p + q}\right) = \sum_{j=0}^{n} \frac{\hat{p}^j P_n^j(p)}{j!(p + q)^j} \ldots\ldots\ldots [47]$$

Particular Solutions of the Field Equations of Elasticity Theory in Spheroidal Co-Ordinates

As a last preliminary to the consideration of the main problem of this paper, we establish here certain relevant particular solutions of the field equations in the theory of elasticity, referred to spheroidal co-ordinates. To this end we first define the notion of translation of a solution to the field equations.

Suppose $[T]$ is a solution characterized by the displacement field

$$\vec{u} = \vec{U}(\rho, z) \ldots\ldots\ldots\ldots\ldots [48]$$

Then the solution whose displacement field is given by

$$\vec{u} = \vec{U}(\rho, z - h) \ldots\ldots\ldots\ldots\ldots [49]$$

is designated by $[T(h)]$ and, for $h > 0$, is said to be obtained from $[T]$ by a translation through a distance h in the positive z-direction; for brevity, we shall refer to $[T(h)]$ as the "translated form" of $[T]$. In view of Equations [5], if

$$\phi = \Phi(\rho, z), \qquad \psi = \Psi(\rho, z) \ldots\ldots\ldots\ldots [50]$$

are the stress functions generating $[T]$, then $[T(h)]$ is generated by

$$\phi = \Phi(\rho, z - h) - h\Psi(\rho, z - h), \qquad \psi = \Psi(\rho, z - h) \ldots [51]$$

In the next section we shall have to resort to the translated forms $[S_0(h_0)]$ and $[E_0(h_0)]$ of the solutions $[S_0]$ and $[E_0]$, defined by Equations [9] and [14]. Here h_0, the distance between the origin and the vertex of the hyperboloidal sheet $p = p_0 \geq 0$, is given by Equation [26], while c in Equations [9], [14] is now the focal distance of the spheroidal co-ordinate system (Fig. 2). The stress functions generating $[S_0(h_0)]$ and $[E_0(h_0)]$, in spheroidal co-ordinates, follow from Equations [9], [14], [50], [51] and from Equations [22], [23], [26].

---

[22] Reference (15), p. 16.

[23] The functions $H_{-1}(p, q)$, $H_{-2}(p, q)$, for $c = 1$, are the spheroidal transforms of $H_0(r_1, \cos\theta_1)$, $H_1(r_1, \cos\theta_1)$, where H_0 and H_1 are defined as in Equations [16] of (1) and should not be confused with H_0, H_1 of our Equation [32].

[24] See references (15 to 18).

[25] The primes denote differentiation with respect to p.

[26] This is Ferrer's definition; see reference (17), p. 323. It differs from Hobson's definition (15), p. 99, by a factor of $(-1)^m$.

[27] See (16), p. 361.

[28] See (18), p. 121.

[29] The superscript in parentheses denotes j-fold differentiation with respect to p. Observe that $P_n^{(j)}(p) = 0$ for $j > n$ since P_n is a polynominal of degree n.

$$[S_0(h_0)]: \quad \phi = \frac{L}{2\pi}\left[\frac{p_0}{s} - (1-2\nu)\log s(1+\omega)\right], \qquad \psi = -\frac{L}{2\pi cs} \qquad \ldots [52]$$

$$[E_0(h_0)]: \quad \phi = 2cs(1-\nu)[\omega \log s(1+\omega) - 1] - cp_0 \log s(1+\omega), \qquad \psi = \log s(1+\omega) \qquad \ldots [53]$$

The auxiliary symbols s and ω, appearing in Equations [52], [53], are defined by

$$s = [(q-p_0p)^2 - \beta_0^2\beta^2]^{1/2}, \qquad \omega = \frac{pq - p_0}{s} \ldots [54]$$

and admit a simple geometric interpretation. Indeed, according to Equations [22], [23], [26]

$$cs = r_0 = [\rho^2 + (z-h_0)^2]^{1/2}, \qquad \omega = \cos\theta_0 = \frac{z-h_0}{r_0} \ldots [55]$$

whence (r_0, θ_0, γ) are evidently displaced spherical co-ordinates, with the pole at the vertex $(\rho = 0, z = h_0)$ of the hyperboloidal sheet $p = p_0$ (Fig. 2).

The general Boussinesq Solution [5] was transformed into spheroidal co-ordinates in reference (5). Substitution of Equations [52], [53] into Equations [16], [18], [19], [21] of reference (5)[30] yields the spheroidal components of displacement and stress appropriate to $[S_0(h_0)]$ and $[E_0(h_0)]$. With the notation

$$\mu = (q^2 - p^2)^{1/2}, \qquad s_p \equiv \frac{\partial s}{\partial p} = \frac{p - p_0q}{s}, \qquad s_q \equiv \frac{\partial s}{\partial q} = \frac{q - p_0p}{s} \qquad \ldots [56]$$

and after voluminous routine computations, we reach for $[S_0(h_0)]$

$$u_p = \frac{L}{4\pi Gc\mu\beta s}[\beta^2 s_p\omega + (3-4\nu)q\beta^2 + (1-2\nu)(p-s_q)s]$$
$$u_q = \frac{L}{4\pi Gc\mu\beta s}[\beta^2 s_q\omega + (3-4\nu)p\beta^2 - (1-2\nu)(q-s_p)s] \qquad \ldots [57]^{31}$$

$$\sigma_p = \frac{-L}{2\pi c^2\mu^2\beta^2 s^2}[3\beta^4 s_p^2\omega - (1-2\nu)(1-\omega)p^2s^2]$$
$$\sigma_q = \frac{-L}{2\pi c^2\mu^2\beta^2 s^2}[3\beta^4 s_q^2\omega - (1-2\nu)(1-\omega)q^2s^2]$$
$$\sigma_\gamma = \frac{L(1-2\nu)}{2\pi c^2 s^2}\left[\omega - \frac{1}{1+\omega}\right]$$
$$\tau_{pq} = \frac{-L}{2\pi c^2\mu^2\beta^2 s^2}[3\beta^2\beta^2 s_p s_q\omega + (1-2\nu)(1-\omega)pqs^2] \qquad \ldots [58]^{31}$$

and for $[E_0(h_0)]$

$$u_p = \frac{1}{2G\mu\beta}[s\omega(s_q - p) + 2ps(1-\nu)(1-\omega) - (1-2\nu)q\beta^2 \log s(1+\omega)]$$
$$u_q = \frac{1}{2G\mu\beta}[s\omega(q - s_p) - 2qs(1-\nu)(1-\omega) - (1-2\nu)p\beta^2 \log s(1+\omega)] \qquad \ldots [59]$$

$$\sigma_p = \frac{1}{c\mu^2\beta^2 s}\{ps^2(1-\omega)[(1-2\nu)p - 2s_q] - \beta^4 s_p^2\}$$
$$\sigma_q = \frac{1}{c\mu^2\beta^2 s}\{qs^2(1-\omega)[(1-2\nu)q - 2s_p] - \beta^4 s_q^2\}$$
$$\sigma_\gamma = \frac{1}{cs(1+\omega)}\{(1-2\nu)\omega - 2\}$$
$$\tau_{pq} = \frac{1}{c\mu^2\beta\beta s}\{s^2(1-\omega)[ps_p + qs_q - (1-2\nu)pq] - \beta^2\beta^2 s_p s_q\} \qquad \ldots [60]$$

With reference to the harmonic functions given in Equations [33], [36], we now define the following two aggregates of particular solutions to the field equations.

$$[A_n]: \quad \phi = H_{n-1}, \qquad \psi = 0 \quad (n \geq -1) \ldots [61]$$

$$[B_{-1}]: \quad \phi = H_{-1} + (3-4\nu)H_{-2}, \quad \psi = \frac{1}{c}H_{-1}$$
$$[B_n]: \quad \phi = H_n, \qquad \psi = \frac{1}{c}H_n \quad (n \geq 0) \qquad \ldots [62]^{32}$$

We record the spheroidal components of displacement and stress belonging to solutions $[A_n]$, $[B_n]$ $(n \geq -1)$, which are obtained from the corresponding stress functions as indicated previously. For $[A_{-1}]$

$$u_p = \frac{\beta}{2Gc\mu}\left[q\log(1+p)(q+1) + p\frac{q-1}{1+p}\right]$$
$$u_q = \frac{\beta}{2Gc\mu}\left[p\log(1+p)(q+1) - q\frac{1-p}{q+1}\right] \qquad \ldots [63]$$

$$\sigma_p = \frac{1}{c^2\mu^2}\left(\frac{p+q}{1+p} - pq\right), \qquad \sigma_q = \frac{1}{c^2\mu^2}\left(pq - \frac{p+q}{q+1}\right)$$
$$\sigma_\gamma = \frac{-1}{c^2(1+p)(q+1)}, \qquad \tau_{pq} = \frac{(1-p)(q-1)(p+q+pq)}{c^2\mu^2\beta\beta} \qquad \ldots [64]$$

For $[A_0]$

$$u_p = \frac{\beta}{2Gc\mu(1+p)}, \qquad u_q = \frac{\beta}{2Gc\mu(q+1)} \ldots [65]$$

[30] The stress functions designated by ϕ and ψ are denoted in reference (5) by ϕ and λ, respectively.

[31] The displacement u_γ and the stresses $\tau_{p\gamma}$, $\tau_{q\gamma}$, which vanish for axisymmetric solutions, are suppressed in Equations [57], [58], and in all subsequent equations.

[32] In the definition of $[B_n]$ $(n \geq -1)$ we could have chosen $\phi = 0$; the particular choice made here yields simplifications in what follows.

$$\left.\begin{aligned}
\sigma_p &= \frac{1}{c^2\mu^2}\left(\frac{p}{1+p}-\frac{1}{p+q}\right) & \sigma_q &= \frac{1}{c^2\mu^2}\left(\frac{1}{p+q}-\frac{q}{q+1}\right)\\
\sigma_\gamma &= \frac{1}{c^2(1+p)(q+1)(p+q)} & \tau_{pq} &= \frac{-(1-p)(q-1)(1+p+q)}{c^2\mu^2\beta\gamma(p+q)}
\end{aligned}\right\} \quad [66]$$

With the aid of Equations [39], [33], we obtain for $[A_n]$ $(n \geq 1)$

$$\left.\begin{aligned}
u_p &= \frac{n}{2Gc\mu\beta}\,[pH_{n-1}-(p+q)H_n]\\
u_q &= \frac{-n}{2Gc\mu\gamma}\,[qH_{n-1}-(p+q)H_n]
\end{aligned}\right\} \quad \ldots\ldots [67]$$

$$\left.\begin{aligned}
\sigma_p &= \frac{n}{c^2\mu^2}\left\{\frac{1}{\beta^2}\,[H_{n-1}-(1+pq)H_n] - (n+1)[H_{n-1}-2H_n]\right\}\\
\sigma_q &= \frac{n}{c^2\mu^2}\left\{\frac{1}{\gamma^2}\,[H_{n-1}-(1+pq)H_n] + (n+1)[H_{n-1}-2H_n]\right\}\\
\sigma_\gamma &= \frac{n}{c^2\beta^2\gamma^2}\,\{(1+pq)H_n - H_{n-1}\}\\
\tau_{pq} &= \frac{n}{c^2\mu^2\beta\gamma}\,\{(1+pq)H_n - H_{n-1}\\
&\quad + (n+1)\,[(1-pq)H_{n-1} + (p^2+q^2-2)H_n]\}
\end{aligned}\right\} \quad [68]$$

For $[B_{-1}]$

$$\left.\begin{aligned}
u_p &= \frac{\beta}{2Gc\mu(1+p)}\,[1+p+4(1-\nu)(q-1)p]\\
u_q &= \frac{\gamma}{2Gc\mu(q+1)}\,[1+q-4(1-\nu)(1-p)q]
\end{aligned}\right\} \quad [69]$$

$$\left.\begin{aligned}
\sigma_p &= \frac{1}{c^2\mu^2}\left[p-q-\frac{\beta^2}{p+q}+\frac{2(1-\nu)(1-p)(p+q)}{1+p}\right]\\
\sigma_q &= \frac{1}{c^2\mu^2}\left[p-q-\frac{\gamma^2}{p+q}+\frac{2(1-\nu)(q-1)(p+q)}{q+1}\right]\\
\sigma_\gamma &= \frac{1}{c^2}\left[\frac{1-2\nu}{p+q}-\frac{4(1-\nu)}{(1+p)(q+1)}\right]\\
\tau_{pq} &= \frac{\beta\gamma}{c^2\mu^2}\left[\frac{-1}{p+q}+\frac{2(1-\nu)(p+q)}{(1+p)(q+1)}\right]
\end{aligned}\right\} \quad [70]$$

With recourse to Equations [39], [33], there results for $[B_n]$ $(n \geq 0)$

$$\left.\begin{aligned}
u_p &= \frac{1}{2Gc\mu\beta}\,\{(n+1)(1+pq)[pH_n-(p+q)H_{n+1}] - (3-4\nu)q\beta^2H_n\}\\
u_q &= \frac{1}{2Gc\mu\gamma}\,\{(n+1)(1+pq)[(p+q)H_{n+1}-qH_n] - (3-4\nu)p\gamma^2H_n\}
\end{aligned}\right\} \quad [71]$$

$$\left.\begin{aligned}
\sigma_p &= \frac{n+1}{c^2\mu^2}\left\{\frac{1+pq}{\beta^2}\,[H_n-(1+pq)H_{n+1}] - (n+2)(1+pq)[H_n-2H_{n+1}] + \mu^2H_{n+1} + (1-2\nu)[(p+q)^2H_{n+1}-2pqH_n]\right\}\\
\sigma_q &= \frac{n+1}{c^2\mu^2}\left\{\frac{1+pq}{\gamma^2}\,[H_n-(1+pq)H_{n+1}] + (n+2)(1+pq)[H_n-2H_{n+1}] + \mu^2H_{n+1} - (1-2\nu)\,[(p+q)^2H_{n+1}-2pqH_n]\right\}\\
\sigma_\gamma &= \frac{n+1}{c^2}\left\{\frac{1+pq}{\beta^2\gamma^2}\,[(1+pq)H_{n+1}-H_n] + 2\nu H_{n+1}\right\}\\
\tau_{pq} &= \frac{n+1}{c^2\mu^2\beta\gamma}\left\{(1+pq)[(1+pq)H_{n+1}-H_n] + (n+2)(1+pq)[(1-pq)H_n + (p^2+q^2-2)H_{n+1}] - (1-2\nu)[(2p^2q^2-p^2-q^2)H_n + (1-pq)(p+q)^2H_{n+1}]\right\}
\end{aligned}\right\} \quad [72]$$

Solutions $[S_0(h_0)]$, $[E_0(h_0)]$ are singular along the half of the z-axis $-\infty < z \leq h_0$, and are otherwise regular in the entire finite space. Their behavior at the vertex $\rho = 0$, $z = h_0$, and at infinity, i.e., as $r_0 \to 0$ and $r_0 \to \infty$, is

$$\left.\begin{aligned}
[S_0(h_0)]: &\quad u_i = O(r_0^{-1}), &\quad \tau_{ij} &= O(r_0^{-2})\\
[E_0(h_0)]: &\quad u_i = O(\log r_0), &\quad \tau_{ij} &= O(r_0^{-1})
\end{aligned}\right\} \quad [73][33]$$

where r_0, defined in Equations [55], is the distance from the vertex of the hyperboloidal sheet $p = p_0$.

Solution $[A_{-1}]$ is singular along the half of the z-axis $-\infty < z \leq -c$, and is otherwise regular in the finite space. Here we have, as $r_1 \to 0$ and $r_1 \to \infty$

$$[A_{-1}]: \qquad u_i = O(\log r_1), \qquad \tau_{ij} = O(r_1^{-1}) \ldots [74]$$

where r_1, defined in Equations [29], is the distance from the lower focus F_1.

The remaining members of the aggregates of solutions $[A_n]$, $[B_n]$ $(n \geq -1)$ are regular in the finite space, except for progressively stronger point singularities at the lower focus F_1. Their behavior as $r_1 \to 0$ and $r_1 \to \infty$ is characterized by

$$\left.\begin{aligned}
[B_{-1}]: &\quad u_i = O(1), &\quad \tau_{ij} &= O(r_1^{-1})\\
[A_n],\ [B_n]: &\quad u_i = O(r_1^{-n-1}), &\quad \tau_{ij} &= O(r_1^{-n-2}) \quad (n \geq 0)
\end{aligned}\right\} \quad [75]$$

[33] Cf. Equations [16].

It is also worth noting, with the aid of Equations [9], [14], [50], [51], [61], [62], that

$$\left.\begin{aligned}[S_0(-c)] &= \frac{-L}{2\pi}\{(1-2\nu)[A_0]+[B_0]\}\\ [E_0(-c)] &= -c\{(1-2\nu)[A_{-1}]-[B_{-1}]\}\end{aligned}\right\}\ldots.[76]$$

Solution of the Main Problem

We now turn to the particular problem which constitutes the primary objective of this investigation. Thus, consider an elastic body occupying a region D bounded by one sheet of a two-sheeted hyperboloid of revolution. With reference to the spheroidal coordinates (p, q) defined through Equations [18], [21], let the boundary B of D be given by $p = p_0\ (0 \leq p_0 < 1)$ and let an axial load of magnitude $|L|$ be applied at the vertex $\rho = 0$, $z = h_0$ of B, Fig. 2. Let $L > 0$ if the load acts in the positive z-direction, and suppose that B is otherwise free from tractions. The stresses and displacements are to be determined throughout $D + B$.

The solution $[S]$ is uniquely characterized by the conditions (a), (b), (c), (d) which were cited in the Introduction and applied in the second section to a class of problems that includes the present special case. Among the three alternative representations of $[S]$ listed in Equations [8], we adopt the intermediate one. This reduces the problem to a residual problem governed by finite and continuous normal surface tractions and by shearing tractions which are finite but exhibit a jump discontinuity at the load point.[34] The removal of the discontinuity in the shearing tractions, accomplished by the last of the Representations [8], in the present application would entail an additional amount of labor which does not appear to be justified by the corresponding gain in the regularity of the governing boundary conditions.

Recalling Equations [8], [48], [49], we thus assume $[S]$ in the form

$$[S] = [S_1(h_0)] + [R_1]\ldots\ldots\ldots\ldots\ldots\ldots[77]$$

where, according to Equations [11], [27]

$$[S_1(h_0)] = [S_0(h_0)] + \frac{(1-2\nu)p_0L}{2\pi c\hat{p}_0^2}[E_0(h_0)]\ldots\ldots[78]$$

while $[S_0(h_0)]$ and $[E_0(h_0)]$ are given by Equations [52] and [53], respectively. In view of conditions (a), (b), (c), (d), to be met by the complete solution $[S]$, and because of the properties of $[S_1]$, discussed previously, the solution $[R_1]$ to the residual problem is defined uniquely by the following requirements:

(A) Solution $[R_1]$ must satisfy the field equations in D, i.e., for $p_0 < p \leq 1$, $1 \leq q < \infty$, and must be regular in any closed subregion of $D + B$ which does not contain the vertex $p = p_0$, $q = 1$. $[R_1]$ must be such that for $[S]$

$$u_p, u_q = O(q^{-1}); \quad \sigma_p, \sigma_q, \sigma_\gamma, \tau_{pq} = O(q^{-2}) \text{ as } q \to \infty\ldots[79][35]$$

(B) For $[S]$

$$\sigma_p(p_0, q) = \tau_{pq}(p_0, q) = 0 \qquad (1 < q < \infty)\ldots\ldots[80]$$

(C) For $[R_1]$

$$\lim_{\delta \to 0}\int_{\Sigma(\delta)} \vec{T}\, dA = 0\ldots\ldots\ldots\ldots\ldots[81]$$

where $\Sigma(\delta)$ is the portion lying in D of a spherical surface of radius δ centered at the vertex $(p = p_0, q = 1)$, and $\vec{T}$ is as in Equation [2].

(D) For $[R_1]$

$$\sigma_p, \sigma_q, \sigma_\gamma, \tau_{pq} = O(r_0^{-2}) \quad \text{as } r_0 \to 0\ldots\ldots\ldots[82]$$

in which r_0 is the distance from the vertex, and is given by Equation [55].

Guided by conditions (A), (B), (C), (D), we take $[R_1]$ in the form

$$[R_1] = \sum_{n=-1}^{\infty}\{a_n[A_n] + b_n[B_n]\}\ldots\ldots\ldots\ldots[83]$$

where the component solutions $[A_n]$, $[B_n]$ $(n \geq -1)$ are defined by Equations [61], [62], and a_n, b_n are as yet undetermined coefficients of superposition. By virtue of the regularity properties of $[A_n]$, $[B_n]$, discussed at the end of the preceding section, each term in the Series [83] satisfies the requirements in the finite space stipulated in (A) and individually conforms to conditions (C), (D). Hence $[R_1]$ meets conditions (A), (B), (C), (D) provided the coefficients a_n, b_n $(n \geq -1)$ are determined in such a way that Equations [79], [80] hold for $[S]$ and that the infinite series in Equation [83], together with its first space derivatives, is uniformly convergent in the region $p_0 \leq p \leq 1, 0 < \epsilon \leq r_0 < \infty$.

With a view toward meeting the Boundary Conditions [80], we develop the surface tractions $\sigma_p(p_0, q)$ and $\tau_{pq}(p_0, q)$ of solutions $[A_n]$, $[B_n]$, and $[S_1(h_0)]$ into Laurent expansions in powers of $q + p_0$. These expansions are found to be of the form

$$\left.\begin{aligned}[A_n]:\quad \sigma_p(p_0, q) &= \frac{1}{c^2\mu_0^2}\sum_{k=n}^{\infty}\frac{\alpha_{nk}^{\sigma}}{(q+p_0)^k}\\ \tau_{pq}(p_0, q) &= \frac{1}{c^2\hat{p}_0\hat{q}(q-p_0)}\sum_{k=n}^{\infty}\frac{\alpha_{nk}^{\tau}}{(q+p_0)^k}\end{aligned}\right\}\ldots[84]$$

$$\left.\begin{aligned}[B_n]:\quad \sigma_p(p_0, q) &= \frac{1}{c^2\mu_0^2}\sum_{k=n}^{\infty}\frac{\beta_{nk}^{\sigma}}{(q+p_0)^k}\\ \tau_{pq}(p_0, q) &= \frac{1}{c^2\hat{p}_0\hat{q}(q-p_0)}\sum_{k=n}^{\infty}\frac{\beta_{nk}^{\tau}}{(q+p_0)^k}\end{aligned}\right\}\ldots[85]$$

$$\left.\begin{aligned}[S_1(h_0)]:\quad \sigma_p(p_0, q) &= \frac{1}{c^2\mu_0^2}\sum_{k=-1}^{\infty}\frac{\gamma_k^{\sigma}}{(q+p_0)^k}\\ \tau_{pq}(p_0, q) &= \frac{1}{c^2\hat{p}_0\hat{q}(q-p_0)}\sum_{k=-1}^{\infty}\frac{\gamma_k^{\tau}}{(q+p_0)^k}\end{aligned}\right\}\ldots[86]$$

where $\hat{p}_0$, μ_0 are the values[36] of $\hat{p}$, μ for $p = p_0$, and the Laurent coefficients are independent of q.

The Expansions [84], [85] are obtained from the formulas for σ_p and τ_{pq}, given in Equations [64], [66], [68], [70], and [72], with the aid of Equations [33], [44], and [47]. The results of these exceedingly tedious computations follow

[34] See the second of Equations [17].

[35] Cf. Equation [1]. Note from Equation [28] that $q = O(r)$ as $r \to \infty$.

[36] See Equations [22] and [56] for the definitions of $\hat{p}$ and μ.

$$\left.\begin{aligned}
&\alpha_{-1-1}{}^{\sigma} = \frac{1}{1+p_0} - p_0, \quad \alpha_{-10}{}^{\sigma} = p_0{}^2, \quad \alpha_{-1k}{}^{\sigma} = 0 \quad (k \geq 1)\\
&\alpha_{00}{}^{\sigma} = \frac{p_0}{1+p_0}, \quad \alpha_{01}{}^{\sigma} = -1, \quad \alpha_{0k}{}^{\sigma} = 0 \quad (k \geq 2)\\
&\alpha_{nk}{}^{\sigma} = -\frac{n(n+1)}{(k-n)!}\,\hat{p}_0{}^{k-n-1}\,[\hat{p}_0 P_{n-1}{}^{k-n} - (2k-2n-1)\,P_n{}^{k-n-1}] \quad (n \geq 1)
\end{aligned}\right\} \ldots [87]$$

$$\left.\begin{aligned}
&\alpha_{-1-1}{}^{\tau} = \hat{p}_0{}^2, \quad \alpha_{-10}{}^{\tau} = -(1-p_0)(1+2p_0+2p_0{}^2),\\
&\alpha_{-11}{}^{\tau} = p_0{}^2\hat{p}_0{}^2, \quad \alpha_{-1k}{}^{\tau} = 0 \quad (k \geq 2)\\
&\alpha_{00}{}^{\tau} = -(1-p_0), \quad \alpha_{01}{}^{\tau} = p_0(1-p_0),\\
&\alpha_{02}{}^{\tau} = \hat{p}_0{}^2, \quad \alpha_{0k}{}^{\tau} = 0 \quad (k \geq 3)\\
&\alpha_{nk}{}^{\tau} = \frac{n(n+1)}{(k-n)!}\,\hat{p}_0{}^{k-n}\,[(n-1)\hat{p}_0 P_{n-1}{}^{k-n-1} - (k-n)(2n+1)P_n{}^{k-n-2}] \quad (n \geq 1)
\end{aligned}\right\} \ldots [88]$$

$$\left.\begin{aligned}
&\beta_{-1-1}{}^{\sigma} = 2(1-\nu)\,\frac{1-p_0}{1+p_0} - 1, \quad \beta_{-10}{}^{\sigma} = 2p_0,\\
&\beta_{-11}{}^{\sigma} = -\hat{p}_0{}^2, \quad \beta_{-1k}{}^{\sigma} = 0\ (k \geq 2)\\
&\beta_{nk}{}^{\sigma} = \frac{n+1}{(k-n)!}\,\hat{p}_0{}^{k-n-1}\,\{[(n+4-4\nu)(1+n\hat{p}_0{}^2) - 2]\,P_n{}^{k-n-1} + [n(n+2)(n+3) + (n+3)(k-n)(k-n-1) + (2n+2-k)(2n+3-k)(1-2\nu)]\,\hat{p}_0 P_{n+1}{}^{k-n-2}\} \quad (n \geq 0)
\end{aligned}\right\} \ldots [89]$$

$$\left.\begin{aligned}
&\beta_{-1-1}{}^{\tau} = 2(1-\nu)(1-p_0), \quad \beta_{-10}{}^{\tau} = -(3-2\nu)\hat{p}_0{}^2,\\
&\beta_{-11}{}^{\tau} = 2p_0\hat{p}_0{}^2, \quad \beta_{-12}{}^{\tau} = \hat{p}_0{}^4, \quad \beta_{-1k}{}^{\tau} = 0 \quad (k \geq 3)\\
&\beta_{nk}{}^{\tau} = \frac{-(n+1)}{(k-n)!}\,\hat{p}_0{}^{k-n}\,\{[(n+2)(n+3k) + 4(k-2)(1-2\nu) + n(n-1)(n+4-4\nu)\hat{p}_0{}^2]\cdot P_n{}^{k-n-2} + [(n+2)(2n+3)(k-n)(k-n-1) + k(n+2)(n+3)(2n+4-k) + (n-2)\cdot(2n+3-k)(2n+4-k)(1-2\nu)]\hat{p}_0 P_{n+1}{}^{k-n-2}\} \quad (n \geq 0)
\end{aligned}\right\} \ldots [90]$$

The associated Legendre functions appearing in Equations [87] to [90] all have the argument p_0. Since the functions represented by the Laurent series in Equations [84], [85] are rational in $q + p_0$, the series terminate. This fact is confirmed by inspection of the Laurent coefficients just listed in view of the second of Identities [42].

Next, we sketch the determination of the Laurent coefficients $\gamma_k{}^{\sigma}$, $\gamma_k{}^{\tau}$ appropriate to solution $[S_1(h_0)]$. The surface tractions $\sigma_p(p_0, q)$ and $\tau_{pq}(p_0, q)$ of $[S_1(h_0)]$ are immediate from Equations [78], [58], [60]. In order to reach the Expansions [86], we need the Laurent series for $s_0{}^{-1}$, $s_0{}^{-2}$, $s_0{}^{-6}$, where s_0 is the value of s for $p = p_0$, s being given by Equation [55].

We first seek the auxiliary expansion

$$f(q) \equiv \frac{1}{s_0} = \frac{1}{\sqrt{[(q-1)(q+1-2p_0{}^2)]}} = \sum_{n=1}^{\infty} \frac{c_n}{(q+p_0)^n} \ldots [91]$$

The function $f(q)$, in the complex q-plane, is a two-valued function with branch points on the real axis at $q = 1$ and $q = 2p_0{}^2 - 1$. We cut the q-plane along the real segment joining the two branch points, splitting $f(q)$ into two branches, each analytic everywhere except on the cut. For our purposes, we must select that branch of $f(q)$ which assumes positive values for $q > 1$ on the real axis. From the general formula for Laurent coefficients[37] we have

$$c_{n+1} = \frac{1}{2\pi i}\int_C (z+p_0)^n f(z)\,dz \ldots [92]$$

where $z = x + iy$ temporarily denotes a dummy complex variable and the path of integration C is chosen as shown in Fig. 3.

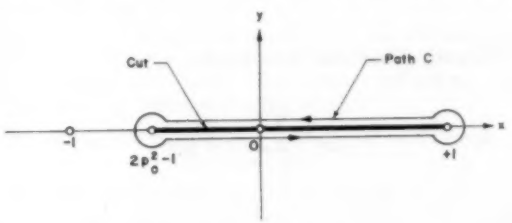

FIG. 3 INTEGRATION PATH IN CONNECTION WITH EQUATION [92]

From Equations [92], [91], and a trivial limit process, follows

$$c_{n+1} = \frac{1}{\pi}\int_{2p_0{}^2-1}^{1} \frac{(x+p_0)^n dx}{\sqrt{[(1-x)(x+1-2p_0{}^2)]}} \ldots [93]$$

which, with the aid of the transformation $\sin t = (x - p_0{}^2)\hat{p}_0{}^{-2}$ and of the binomial theorem, yields

$$\left.\begin{aligned}
c_{n+1} &= \frac{\hat{p}_0{}^{2n}}{\pi}\int_{-\pi/2}^{\pi/2}\left(\sin t + \frac{p_0}{1-p_0}\right)^n dt\\
&= \frac{\hat{p}_0{}^{2n}}{\pi}\sum_{m=0}^{n}\frac{n!}{m!(n-m)!}\left(\frac{p_0}{1-p_0}\right)^{n-m}\cdot\int_{-\pi/2}^{\pi/2}\sin^m t\,dt
\end{aligned}\right\} \ldots [94]$$

Equation [94], in view of Wallis' formula[38]

$$\int_0^{\pi/2}\sin^{2j} t\,dt = \frac{\pi(2j)!}{2^{2j+1}(j!)^2} \ldots [95]$$

finally leads to

$$c_{n+1} = n!(1+p_0)^n \sum_{j=0}^{[n/2]} \frac{(1-p_0)^{2j}p_0{}^{n-2j}}{2^{2j}j!j!(n-2j)!} \quad (n \geq 1) \ldots [96]$$

in which $[n/2]$ denotes the largest integer not exceeding $n/2$.

The Laurent expansion of $s_0{}^{-2}$ is most expediently obtained by noting, on the basis of Equation [91], the identity

[37] See reference (19), p. 119.
[38] See reference (20), p. 223.

$$\left.\begin{aligned}\frac{1}{s_0^3} &= \frac{-1}{\beta_0^2}\left[\frac{\partial}{\partial q}\left(\frac{1}{s_0}\right)+\frac{1}{2p_0}\frac{\partial}{\partial p_0}\left(\frac{1}{s_0}\right)\right]\\ &= \sum_{n=2}^{\infty}\frac{(n-1)(1+2p_0)c_{n-1}-\dfrac{dc_n}{dp_0}}{2p_0\beta_0^2(q+p_0)^n}\end{aligned}\right\}\ \ldots [97]$$

Substitution from Equation [96] for c_n yields, after elementary manipulations

$$\frac{1}{s_0^3} = \sum_{n=3}^{\infty}\frac{d_n}{(q+p_0)^n} \ldots\ldots [98]$$

where

$$\left.\begin{aligned}d_{n+1} &= n!(1+p_0)^{n-2}\sum_{j=1}^{[n/2]}\frac{(1-p_0)^{2j-2}p_0^{n-2j}}{2^{2j-1}j!(j-1)!(n-2j)!}\\ &\qquad (n\geq 2)\end{aligned}\right\}\ \ldots [99]$$

Similarly, we arrive at the expansion

$$\frac{1}{s_0^5} = \sum_{n=5}^{\infty}\frac{e_n}{(q+p_0)^n} \ldots\ldots [100]$$

where

$$\left.\begin{aligned}e_{n+1} &= \frac{n!}{3}(1+p_0)^{n-4}\sum_{j=2}^{[n/2]}\frac{(1-p_0)^{2j-4}p_0^{n-2j}}{2^{2j-2}j!(j-2)!(n-2j)!}\\ &\qquad (n\geq 4)\end{aligned}\right\}\ \ldots [101]$$

For future convenience we adjoin to Equations [99], [101] the definitions

$$d_1 = d_2 = e_1 = e_2 = e_3 = e_4 = 0 \ldots\ldots [102]$$

With the aid of the auxiliary Expansions [91], [98], [100], the Laurent coefficients γ_k^{σ} and γ_k^{τ} in Equations [86] follow after a cumbersome computation

$$\left.\begin{aligned}\gamma_{-1}^{\sigma} &= \frac{(1-2\nu)Lp_0^2}{2\pi\beta_0^2(1+p_0)}[(1-2\nu)p_0-2]\\ \gamma_0^{\sigma} &= \frac{(1-2\nu)Lp_0^2}{2\pi(1+p_0)}\\ \gamma_k^{\sigma} &= \frac{Lp_0^2}{2\pi}\Big\{3\beta_0^2[(1+p_0)^2e_k-3(1+p_0)^2e_{k+1}\\ &\quad +3(1+p_0)e_{k+2}-e_{k+3}]-(1-2\nu)[(1+p_0)^2d_k\\ &\quad -2(1+p_0)d_{k+1}+d_{k+2}]+\frac{1-2\nu}{\beta_0^4}\Big[[2\nu\\ &\quad +(3-4\nu)p_0](1+p_0)^3c_k-[3+(3-4\nu)p_0]\\ &\quad \cdot(1+p_0)c_{k+1}+(3-2\nu)c_{k+2}\Big]\Big\}\ (k\geq 1)\end{aligned}\right\}\ \ldots [103]$$

$$\left.\begin{aligned}\gamma_{-1}^{\tau} &= \frac{(1-2\nu)Lp_0}{2\pi(1+p_0)}[1-(1-2\nu)p_0]\\ \gamma_0^{\tau} &= \frac{(1-2\nu)Lp_0}{2\pi(1+p_0)}[2(1-\nu)p_0^2-1]\\ \gamma_1^{\tau} &= \frac{Lp_0^2(1-p_0)}{2\pi}[1-2\nu+(1+2\nu)\\ &\quad \cdot(1+\nu)(1+p_0)]\\ \gamma_k^{\tau} &= \frac{Lp_0^2}{2\pi}\Big\{3\beta_0^2[p_0\beta_0^2(1+p_0)^2e_{k-1}-(1+p_0\\ &\quad -4p_0^2)(1+p_0)^2e_k+2(1-3p_0)(1+p_0)^2e_{k+1}\\ &\quad +4p_0(2+p_0)(1+p_0)e_{k+2}-(2+5p_0\\ &\quad +p_0^2)e_{k+3}+e_{k+4}]-(1-2\nu)[p_0\beta_0^2(1+p_0)^2d_{k-1}\\ &\quad -(1-3p_0^2)(1+p_0)^2d_k+(1-4p_0\\ &\quad -3p_0^2)(1+p_0)d_{k+1}+(1+4p_0+p_0^2)d_{k+2}\\ &\quad -d_{k+3}]+\frac{1-2\nu}{\beta_0^2}\Big[[2\nu+(3-4\nu)p_0]\\ &\quad \cdot(1+p_0)^2p_0c_{k-1}-[2\nu+2(2-\nu)p_0\\ &\quad +2(3-4\nu)p_0^2](1+p_0)c_k+[2+6(1-\nu)p_0\\ &\quad +(3-4\nu)p_0^2]c_{k+1}-2(1-\nu)c_{k+2}\Big]\Big\}(k\geq 2)\end{aligned}\right\}\ \ldots [104]$$

The coefficients c_k, d_k, and e_k appearing in Equations [103], [104] were given in Equations [96], [99], [101], and [102].

The series in Equations [84], [85] terminate, as stated before, while the infinite series in Equations [86] are uniformly and absolutely convergent for $0 \leq p_0 \leq 1$, $1+\epsilon \leq q < \infty$ $(\epsilon > 0)$. From Equations [84], [85], [86], we obtain by superposition, in accordance with Equations [77], [83], the Laurent expansions of the boundary stresses for the complete solution [S]. In order that the Boundary Conditions [80] be satisfied, each Laurent coefficient in the expansions of $\sigma_p(p_0, q)$ and $\tau_{pq}(p_0, q)$ for [S] must vanish individually. This requirement yields an infinite system of linear algebraic equations for the unknown coefficients of superposition a_n, b_n

$$\left.\begin{aligned}\sum_{n=-1}^{k}(a_n\alpha_{nk}^{\sigma}+b_n\beta_{nk}^{\sigma}) &= -\gamma_k^{\sigma}\\ \sum_{n=-1}^{k}(a_n\alpha_{nk}^{\tau}+b_n\beta_{nk}^{\tau}) &= -\gamma_k^{\tau}\end{aligned}\right\}\ (k\geq -1) \ldots [105]$$

Equations [105] in matrix form appear as

$$\begin{bmatrix}\alpha_{-1-1}^{\sigma} & \beta_{-1-1}^{\sigma} & 0 & 0 & 0 & 0 & 0 & 0 & \cdots\\ \alpha_{-1-1}^{\tau} & \beta_{-1-1}^{\tau} & 0 & 0 & 0 & 0 & 0 & 0 & \cdots\\ \alpha_{-10}^{\sigma} & \beta_{-10}^{\sigma} & \alpha_{00}^{\sigma} & \beta_{00}^{\sigma} & 0 & 0 & 0 & 0 & \\ \alpha_{-10}^{\tau} & \beta_{-10}^{\tau} & \alpha_{00}^{\tau} & \beta_{00}^{\tau} & 0 & 0 & 0 & 0 & \\ \alpha_{-11}^{\sigma} & \beta_{-11}^{\sigma} & \alpha_{01}^{\sigma} & \beta_{01}^{\sigma} & \alpha_{11}^{\sigma} & \beta_{11}^{\sigma} & 0 & 0 & \\ \alpha_{-11}^{\tau} & \beta_{-11}^{\tau} & \alpha_{01}^{\tau} & \beta_{01}^{\tau} & \alpha_{11}^{\tau} & \beta_{11}^{\tau} & 0 & 0 & \\ \alpha_{-12}^{\sigma} & \beta_{-12}^{\sigma} & \alpha_{02}^{\sigma} & \beta_{02}^{\sigma} & \alpha_{12}^{\sigma} & \beta_{12}^{\sigma} & \alpha_{22}^{\sigma} & \beta_{22}^{\sigma} & \\ \alpha_{-12}^{\tau} & \beta_{-12}^{\tau} & \alpha_{02}^{\tau} & \beta_{02}^{\tau} & \alpha_{12}^{\tau} & \beta_{12}^{\tau} & \alpha_{22}^{\tau} & \beta_{22}^{\tau} & \\ \cdot & \cdot & \cdot & \cdot & & & & \cdot & \\ \cdot & \cdot & \cdot & \cdot & & & & \cdot & \\ \cdot & \cdot & \cdot & \cdot & & & & \cdot & \end{bmatrix}\begin{bmatrix}a_{-1}\\ b_{-1}\\ a_0\\ b_0\\ a_1\\ b_1\\ a_2\\ b_2\\ \cdot\\ \cdot\\ \cdot\end{bmatrix} = \begin{bmatrix}-\gamma_{-1}^{\sigma}\\ -\gamma_{-1}^{\tau}\\ -\gamma_0^{\sigma}\\ -\gamma_0^{\tau}\\ -\gamma_1^{\sigma}\\ -\gamma_1^{\tau}\\ -\gamma_2^{\sigma}\\ -\gamma_2^{\tau}\\ \cdot\\ \cdot\\ \cdot\end{bmatrix} \ldots [106]$$

Thus the first two equations involve the two unknowns a_{-1} and b_{-1}, while each succeeding pair of equations involves an additional pair of unknowns. Proceeding formally for the time being, we treat Equations [105] as a single pair of equations for any fixed k and solve for a_k and b_k, which leads us to the following recursion formulas for the solution of the system of Equations [105] or [106]

$$\left.\begin{aligned} a_k &= \frac{1}{\Delta_k}\left(\delta_k{}^{\sigma}\beta_{kk}{}^{\tau} - \delta_k{}^{\tau}\beta_{kk}{}^{\sigma}\right) \\ b_k &= \frac{1}{\Delta_k}\left(\alpha_{kk}{}^{\sigma}\delta_k{}^{\tau} - \alpha_{kk}{}^{\tau}\delta_k{}^{\sigma}\right) \end{aligned}\right\} (k \geq -1) \ldots [107][39, 40]$$

where

$$\left.\begin{aligned} \Delta_k &= \alpha_{kk}{}^{\sigma}\beta_{kk}{}^{\tau} - \alpha_{kk}{}^{\tau}\beta_{kk}{}^{\sigma} \\ \delta_k{}^{\sigma} &= -\gamma_k{}^{\sigma} - \sum_{n=-1}^{k-1}\left(a_n\alpha_{nk}{}^{\sigma} + b_n\beta_{nk}{}^{\sigma}\right) \\ \delta_k{}^{\tau} &= -\gamma_k{}^{\tau} - \sum_{n=-1}^{k-1}\left(a_n\alpha_{nk}{}^{\tau} + b_n\beta_{nk}{}^{\tau}\right) \end{aligned}\right\} (k \geq -1) \ldots [108]$$

and the sums in Equations [108] are defined to be zero for $k = -1$.

Setting $k = -1$ in Equations [107], [108], we reach, with recourse to Equations [87] to [90], [103], [104], the values

$$a_{-1} = \frac{(1-2\nu)^2 L p_0}{2\pi\rho_0{}^2}, \quad b_{-1} = -\frac{(1-2\nu)Lp_0}{2\pi\rho_0{}^2} \ldots [109]$$

For $k = 0$, the right-hand members of Equations [107] become indeterminate; the corresponding pair of Equations [105] is linearly dependent and, on substitution from Equations [109], [87] to [90], [103], [104], [41], [37], reduce to the single equation

$$\frac{a_0}{1-2\nu} - (1+p_0)b_0 = \frac{Lp_0(1+2\nu p_0)}{2\pi(1-p_0)} \ldots [110]$$

in the two unknowns a_0 and b_0. It might appear, therefore, that either a_0 or b_0 may be assigned arbitrarily. If we write a_0 in the form

$$a_0 = \frac{L(1-2\nu)}{2\pi(1-p_0)}\left[1 + 2(1-\nu)p_0 - \frac{(1+p_0)\lambda(\nu, p_0)}{1+2\nu p_0 + p_0{}^2}\right] \ldots [111][41]$$

where $\lambda(\nu, p_0)$ is as yet an arbitrary parameter, then Equation [110] yields, for the value of b_0

$$b_0 = \frac{L}{2\pi(1-p_0)}\left[1 - 2\nu p_0 - \frac{\lambda(\nu, p_0)}{1+2\nu p_0 + p_0{}^2}\right] \ldots [112]$$

The question remains whether λ can be assigned arbitrarily. That this is not possible can be seen as follows: Suppose the infinite series for $[R_1]$ in Equation [83] were suitably convergent for every choice of λ. Then, as will be shown in the next section, $[S]$ would meet the regularity requirements at infinity, given in Equations [79], regardless of the choice of λ. Hence $[R_1]$ for every value of λ would satisfy all of conditions (A), (B), (C), (D) by which it is *uniquely* characterized. On the other hand, $[R_1]$ depends on λ, as is most readily inferred from its behavior at infinity, which we establish in the following section. This dependence on λ, which is easily seen to be linear, contradicts the uniqueness of $[R_1]$. Consequently, there cannot be more than one value of λ for which the Representation [83] for $[R_1]$ is convergent.

In the next section we determine the value of λ from the condition that the solution $[S]$ must tend to the corresponding known closed solution for a cone under an axial concentrated load,[42] in the limit as the hyperboloidal boundary approaches a cone. This condition leads to the value

$$\lambda(\nu, p_0) \equiv 1 \ldots [113]$$

It follows from the discussion in the preceding paragraph that Equation [113] is at the same time a *necessary* condition for the convergence of the series for $[R_1]$. A proof that $\lambda = 1$ is also *sufficient* for the required convergence of the Series [83], does not appear to be manageable because of the unwieldy form of the coefficients a_n and b_n.

Taking $\lambda = 1$ in Equations [111], [112], the remaining coefficients a_n, b_n follow uniquely from Equation [107] with $k \geq 1$, provided $0 < p_0 < 1$. For $p_0 = 0$, i.e., for the half space $z \geq 0$, $[S]$ coincides with Boussinesq's solution[43] $[S_0]$.

Behavior of the Solution at Infinity—The Cone as a Limiting Case

The spheroidal co-ordinates (p, q, γ), defined in Equations [18], [21], pass over into the spherical co-ordinates (r, θ, γ) if we let

$$c \to 0 \ldots [114]$$

Taking this limit for arbitrary fixed r and θ, we find from Equations [28] that

$$q \to \infty, \qquad cq \to r, \qquad p \to \cos\theta \ldots [115]$$

As c tends to zero, the foci F_1, F_2, Fig. 2, coalesce, the hyperboloidal sheets $p = \text{const}$ approach the corresponding asymptotic cones of opening angle $2\theta = 2\cos^{-1}p$, while the spheroids $q = \text{const}$ go into spheres centered at the origin.

Consider a cone, coaxial with the z-axis, whose vertex is at the origin and whose generators are inclined at an angle $\theta_0 = \cos^{-1}p_0$ with respect to the axis; let the cone be subjected to an axial concentrated load L at the vertex. The well-known solution[44] to this problem, designated here by $[S^*]$, is generated by the Boussinesq stress functions

$$\left.\begin{aligned} \phi^* &= \frac{-(1-2\nu)(1+p_0)L}{2\pi(1-p_0)(1+2\nu p_0+p_0{}^2)}\log(r+z) \\ \psi^* &= \frac{-L}{2\pi(1-p_0)(1+2\nu p_0+p_0{}^2)r} \end{aligned}\right\} . [116]$$

If $[S^*(-c)]$ is the solution[45] corresponding to the same cone with its vertex at the lower focus F_1 ($\rho = 0$, $z = -c$), we reach with the aid of Equations [116], [50], [51], [23], [28], [61], [62], and [33], [36]

$$[S^*(-c)] = \frac{-L}{2\pi(1-p_0)(1+2\nu p_0+p_0{}^2)} \cdot \left\{(1-2\nu)(1+p_0)[A_0] + [B_0]\right\} \ldots [117]$$

[39] For $k = 0$ these forms are indeterminate; a_0 and b_0 are established later and are given by Equations [111] to [113].

[40] The summation convention for repeated indexes is not used in this paper.

[41] The expediency of this particular choice of a_0 will become evident in the next section where the arbitrary parameter λ will be found to admit a simple physical interpretation.

[42] See reference (13), p. 203.

[43] See Equations [9].

[44] See reference (13), p. 203.

[45] Cf. Equations [48], [49].

where $p_0 = \cos\theta_0$. Clearly

$$[S^*(-c)] \to [S^*] \text{ as } c \to 0 \quad \ldots\ldots\ldots\ldots [118]$$

We now examine the relation which the solution $[S]$ of the present problem bears to $[S^*]$ in the limit as $c \to 0$, i.e., as the hyperboloidal boundary $p = p_0$ tends to its asymptotic cone of opening angle $2\theta_0 = 2\cos^{-1} p_0$. To this end we note that, as $q \to \infty$

$$\left.\begin{aligned} &\frac{1}{\hat{q}} = \frac{1}{q} + O(q^{-3}), \qquad \frac{1}{\mu} = \frac{1}{q} + O(q^{-3}) \\ &s = q - p_0 p + O(q^{-1}), \quad \frac{1}{s} = \frac{1}{q} + \frac{p_0 p}{q^2} + O(q^{-3}) \\ &\log\frac{(1+p)(q+1)}{s + pq - p_0} = \frac{1+p_0}{q} + O(q^{-2}) \end{aligned}\right\} \quad [119]$$

in which $\hat{q}$, μ, and s are given by Equations [22], [56], and [54]. A lengthy computation, involving the foregoing auxiliary identities, Equations [77], [78], [83], [117], [57] to [60], [63] to [66], [69] to [72], [75], [29], and [109], [111], [112], finally yields

$$u_i = \lambda u_i^*(-c) + \frac{1}{cq} O(q^{-1}) \quad \text{as} \quad q \to \infty \ldots\ldots [120]$$

$$\tau_{ij} = \lambda \tau_{ij}^*(-c) + \frac{1}{c^2 q^2} O(q^{-1}) \quad \text{as} \quad q \to \infty \ldots\ldots [121]$$

Here u_i, τ_{ij}, and $u_i^*(-c), \tau_{ij}^*(-c)$ are the components of displacement and stress of solutions $[S]$ and $[S^*(-c)]$, respectively.

We conclude from Equations [75], [117], [120], and [121] that $[S]$, for every λ which yields convergence of the Series [83], conforms to the regularity requirement at infinity, stipulated in Equation [79]. This fact was appealed to in the preceding section.

On applying to Equations [120], [121] the limit process spelled out in Equations [114], [115], we find in view of Equation [118] that

$$\lim_{c \to 0} [S] = \lambda [S^*] \ldots\ldots\ldots\ldots\ldots [122]$$

The physical significance of the parameter λ, introduced in Equation [111], is now apparent. $[S]$ tends to the solution for the corresponding asymptotic cone as $c \to 0$ only if $\lambda = 1$, which accounts for the choice made in Equation [113].

Discussion. Numerical Results—Effect of Curvature on the Transmission of the Load

The complete solution $[S]$ of the problem solved in the preceding sections, according to Equations [77], [83], is of the form

$$[S] = [S_1(h_0)] + \sum_{n=-1}^{\infty} \{a_n[A_n] + b_n[B_n]\} \ldots\ldots [123]$$

For a fixed choice of the hyperboloidal boundary of the body, determined by specific values of the "shape parameter" p_0 and the "scale parameter" c, the dimensionless stresses $c^2\tau_{ij}/L$ appropriate to $[S]$ are found to depend exclusively on the dimensionless cylindrical co-ordinates ρ/c, z/c, as well as on Poisson's ratio ν. Here $|L|$ is the magnitude of the axial concentrated load at the vertex of the hyperboloid of revolution. Furthermore, we recall at this place the geometric significance of p_0 and c, inferred earlier from the first of Equations [25] which, for $p = p_0 \geq 0$, represents the meridional section of the boundary. Thus $0 \leq \cos^{-1} p_0 < \pi/2$ is half the opening angle of the asymptotic cone associated with the boundary, while c is the distance of its focus from the vertex of the asymptotic cone (i.e., from the origin). It will also be helpful to recall Equations [26], [27]

$$h_0 = cp_0, \quad \kappa_0 = \frac{1}{R_0} = \frac{p_0}{c(1 - p_0^2)} \ldots\ldots\ldots [124]$$

in which h_0 is the distance from the origin to the vertex of the boundary, whereas κ_0 denotes the curvature of the meridian at the vertex.

In discussing the stress distribution, we confine our attention to the normal stress $\sigma_z(\rho, z)$ at points along the axis of revolution $\rho = 0$. As is seen from Equations [23], [25] (see also Fig. 2), $\sigma_z(0, z)$ is related to the spheroidal stress components $\sigma_p(p, q)$ and $\sigma_q(p, q)$ according to the formulas

$$\sigma_z(0, z) = \left\{\begin{aligned} &\sigma_p\left(\frac{z}{c}, 1\right) \quad \text{for} \quad h_0 \leq z < c \\ &\sigma_q\left(1, \frac{z}{c}\right) \quad \text{for} \quad z > c \end{aligned}\right\} \ldots [125]$$

For the sake of convenience we list here the special formulas for $\sigma_z(0, z)$ appropriate to each of the component solutions entering Equations [123]. From Equations [33], [40], [58], [60], [64], [66], [68], [70], [72], and [78] we find with the aid of Equations [125]

For $[S_1(h_0)]$

$$\frac{c^2\sigma_z(0, z)}{L} = -\frac{3\hat{p}_0^2 + (1 - 2\nu)p_0(z/c - p_0)}{2\pi(z/c - p_0)^2\hat{p}_0^2} \ldots [126]$$

For $[A_{-1}]$

$$c^2\sigma_z(0, z) = \frac{1}{1 + z/c}$$

for $[A_0]$

$$c^2\sigma_z(0, z) = \frac{-1}{(1 + z/c)^2}$$

for $[A_n]$

$$c^2\sigma_z(0, z) = \frac{n(n+1)}{(1 + z/c)^{n+2}} \quad (n \geq 1)$$

$\ldots [127]$

For $[B_{-1}]$

$$c^2\sigma_z(0, z) = \frac{-2\nu}{1 + z/c}$$

for $[B_n]$

$$c^2\sigma_z(0, z) = \frac{(n+1)(n+4-2\nu)}{(1 + z/c)^{n+2}} \quad (n \geq 0)$$

$. [128]$

Similarly, we obtain from Equation [116] for $[S^*]$

$$\frac{c^2\sigma_z(0, z)}{L} = \frac{-3 + (1 - 2\nu)p_0}{2\pi(z/c)^2(1 - p_0)(1 + 2\nu p_0 + p_0^2)} \ldots [129]$$

where $[S^*]$ is the solution corresponding to a cone with the opening angle $2\theta_0$ and $0 \leq \theta_0 = \cos^{-1} p_0 \leq \pi$. If, in particular, we set $p_0 = 0$ in Equation [129], we reach the formula appropriate to the half space[48] $z \geq 0$.

The coefficients of superposition a_n, b_n appearing in Equation [123] are proportional to the load L and otherwise are functions of ν and p_0 alone. These coefficients were determined numerically

[48] Both $[S^*]$ and $[S]$, for $p_0 = 0$, coincide with Boussinesq's solution $[S_0]$.

for $-1 \leq n \leq 13$, $\nu = 1/4$, and for various values of the shape parameter p_0 needed in the subsequent discussion. The corresponding highly voluminous computations were carried out on the basis of Equations [107] to [109], [111] to [113], [87] to [90], [103], [104], with the aid of Equations [37], [39], [41] to [44], and tables of Legendre functions (21), (22). The values of a_n and b_n thus obtained,[7] together with Equation [123] and Formulas [126] to [129], now yield the numerical values of the axial normal stress $\sigma_z(0, z)$ for $\nu = 1/4$ and various shapes of the boundary. Fig. 4 shows an illustrative graph of $\sigma_z(0, z)$ for $p_0 = 0.9$.

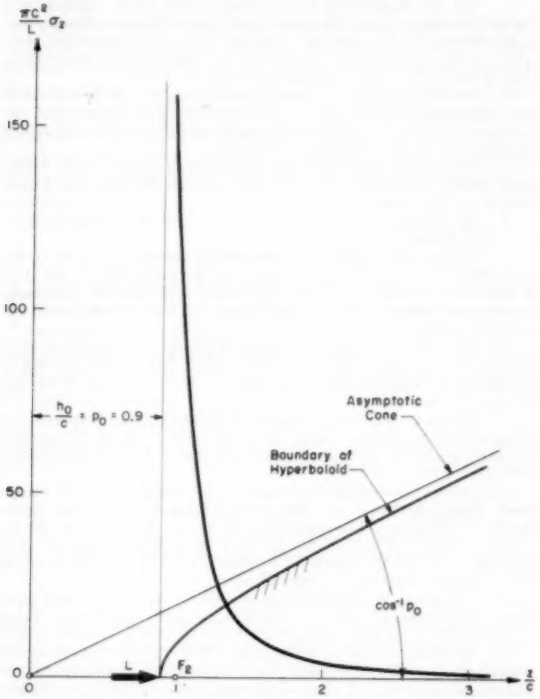

FIG. 4 AXIAL NORMAL STRESS IN THE HYPERBOLOID $p_0 = 0.9$

As demonstrated in reference (1) and reflected in Equations [11], [12], the curvature of the boundary at the load point affects the singularity at that point. We now attempt to examine the influence of this local curvature upon the stresses in the interior, which constitutes the main motivation of the investigation described in this paper. It is not possible to isolate completely the effect of the curvature at the point of application of the load, since any change in the curvature there is necessarily accompanied by a change in the shape of the entire boundary if the latter is an analytic surface as in the present case.

To cope with this difficulty, we observe first that for a given ν, the normal stress $\sigma_z(0, z)$ at a point on the axis of the hyperboloid must depend on the area of the cross section at that point, on the distance of the point from the load point (vertex), as well as on the load. Moreover, if these three factors are held fixed while the curvature of the boundary at the vertex is varied, any change in the interior stress $\sigma_z(0, z)$ should be primarily attributable to the variation of the curvature at the load point.

[7] As a partial check on the accuracy of the computed coefficients a_n, b_n, the vanishing of both boundary tractions was confirmed numerically at two separate points of the boundary, for each value of the shape parameter p_0 that was employed in the computation.

Guided by the foregoing considerations, we compare the values of $\sigma_z(0, z)$, holding fixed the load L, the distance $\zeta_* = z - h_0$ from the vertex of the hyperboloid (load point), and the radius ρ_* of the circular cross section at $z = h_0 + \zeta_*$, while varying the radius of curvature R_0 at the vertex. With these definitions of ζ_* and ρ_*, Equations [25] to [27] yield

$$\left.\begin{aligned} p_0 &= \left[1 + \left(\frac{\rho_*}{\zeta_*}\right)^2 - \frac{2R_0}{\zeta_*}\right]^{-1/2} \\ c &= \frac{p_0 R_0}{1 - p_0^2} \\ z &= \zeta_* + cp_0 \end{aligned}\right\} \quad \ldots\ldots [130]$$

Equations [130] reveal that each specific choice of the ratio ρ_*/ζ_* gives rise to a one-parameter family of hyperboloids with R_0 as the parameter; once R_0 is selected, the values of p_0 and c follow and the boundary is uniquely determined. It should be noted, however, that R_0 cannot be varied indefinitely for fixed ρ_*/ζ_*. Indeed, the first of Equations [130], subject to Equations [24], implies that R_0 is confined to the range

$$0 \leq R_0 \leq \rho_*^2/2\zeta_* \quad \ldots\ldots [131]$$

The lower limit of Inequality [131] corresponds to a cone of opening angle

$$2\theta_0 = 2 \tan^{-1}(\rho_*/\zeta_*)$$

while the upper limit corresponds to the paraboloid

$$\rho_*^2(z - h_0) = \zeta_* \rho^2$$

Fig. 5 depicts three of the one-parameter families of hyperboloids just described, corresponding to $\rho_*/\zeta_* = 1/2, 1, 2$.

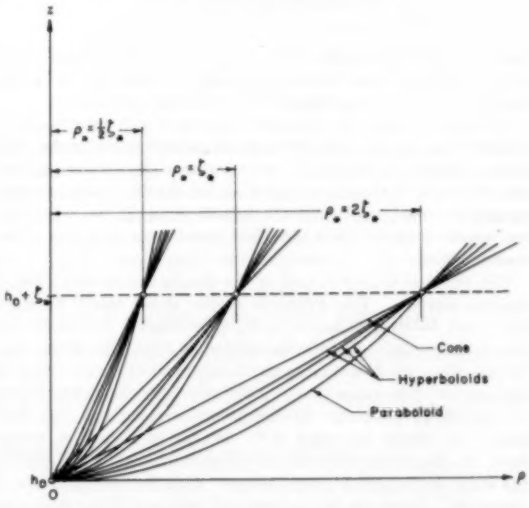

FIG. 5 FAMILIES OF HYPERBOLOIDS USED IN STUDY OF CURVATURE EFFECT

We now proceed as follows: For each of the three ratios ρ_*/ζ_* underlying Fig. 5, we choose values of R_0 within the Range [131] and compute the corresponding values of p_0, c, and z from Equations [130]. Using further the numerical values of a_n, b_n belonging to the values of p_0 just obtained, we compute $\sigma_z(0, z)$ from Equation [123] with the aid of Equations [126] to [129]. This procedure yields the three curves in Fig. 6 which show the de-

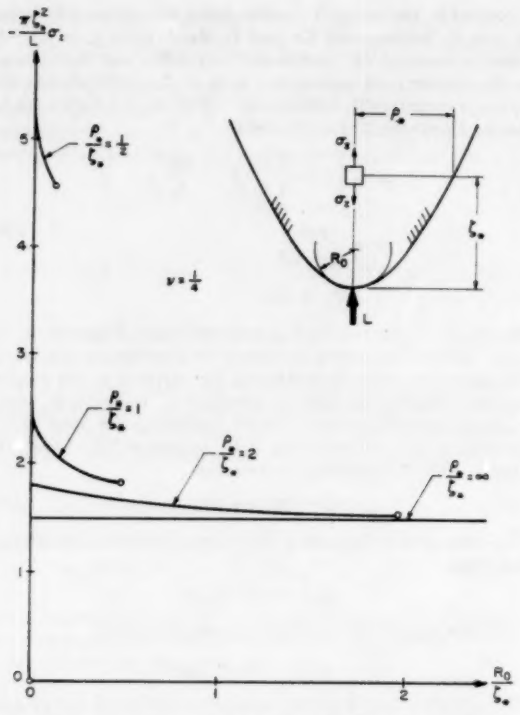

FIG. 6 EFFECT OF CURVATURE AT LOAD POINT ON AXIAL NORMAL STRESS IN INTERIOR OF BODY

pendence upon R_0 of $\sigma_z(0, z)$ for $\rho_*/\zeta_* = 1/2, 1, 2$. The left end-point of each of these curves corresponds to a limiting cone while the right end point corresponds to a limiting paraboloid.[48]

In order to render the representations on Fig. 6 dimensionless, $-L/\pi\zeta_*^2$ and ζ_* were chosen as the respective units for the axial normal stress and the radius of curvature. If, instead, ρ_* had been chosen as the normalizing parameter, the dimensionless axial normal stress $\pi\rho_*^2\sigma_z/L$ would be infinite for $\rho_*/\zeta_* = \infty$ and the half space could not have been included in the diagrams under consideration.

The physical interpretation of the results contained in Fig. 6 requires caution. The difference in the stress values for fixed R_0/ζ_* but different values of ρ_*/ζ_* is principally due to the difference in the area of the cross section at which the stress acts. On the other hand, confining the comparison of stress values to one and the same value of ρ_*/ζ_*, we note two effects which may be attributed primarily to the local curvature at the load point: (*a*) Stress increases with decreasing radius of curvature. (*b*) Sensitivity of stress to curvature-changes rises; that is, the slope of the graph grows steeper, with decreasing radius of curvature. Moreover, the quantitative influence of the curvature at the load point may be appreciable; thus at $\rho_*/\zeta_* = 1$ the stress value for the limiting paraboloid with $R_0 = \zeta_*/2$ is less than 80 per cent of the corresponding value for the limiting cone with $R_0 = 0$.

Finally, we note that as $\rho_*/\zeta_* \to \infty$, the stress curves approach that appropriate to the half space and thus the stress becomes independent of the radius of curvature at the load point. This observation is accounted for by recalling once more that the solutions for the hyperboloid and for the cone depend continuously on p_0; as $p_0 \to 0$, while R_0 is held fixed, both the hyperboloid and the cone (with $R_0 = 0$) approach the half space.

[48] See the remarks following Inequality [131].

ACKNOWLEDGMENT

The authors are greatly indebted to Mrs. Katherine Gandy who skillfully performed and valiantly survived the voluminous numerical computations involved in this investigation.

BIBLIOGRAPHY

1 "On the Singularity at a Concentrated Load Applied to a Curved Surface," by E. Sternberg and R. A. Eubanks, Proceedings of the Second U. S. National Congress of Applied Mechanics, Ann Arbor, Mich., THE AMERICAN SOCIETY OF MECHANICAL ENGINEERS, New York, N. Y., June, 1954, pp. 237–245.

2 "On the Concept of Concentrated Loads and an Extension of the Uniqueness Theorem in the Linear Theory of Elasticity," by E. Sternberg and R. A. Eubanks, *Journal of Rational Mechanics and Analysis*, vol. 4, no. 1, 1955, pp. 135–138.

3 "The Elastic Sphere Under Concentrated Loads," by E. Sternberg and F. Rosenthal, JOURNAL OF APPLIED MECHANICS, Trans. ASME, vol. 74, 1952, pp. 413–421.

4 "Kerbspannungslehre," by H. Neuber, J. W. Edwards Bros., Inc., Ann Arbor, Mich., 1944.

5 "Stress Concentration Around an Ellipsoidal Cavity in an Infinite Body Under Arbitrary Plane Stress Perpendicular to the Axis of Revolution of the Cavity," by M. A. Sadowsky and E. Sternberg, JOURNAL OF APPLIED MECHANICS, Trans. ASME, vol. 69, 1947, pp. A-191 to A-201.

6 "Stress Concentration Around a Heterogeneous Insertion of an Ellipsoid in an Infinite Elastic Body," by H. Miyamoto, *Journal of the Society of Applied Mechanics* (Japan), vol. 3, no. 13, 1950, pp. 15–19.

7 "Stress Concentration Around a Heterogeneous Insertion of a Spheroid in an Elastic Body—III. (Torsion)," by H. Miyamoto, Proceedings of the First Japanese Congress of Applied Mechanics, 1951, pp. 43–46.

8 "Stress Concentration Around a Spheroidal Cavity in an Infinite Elastic Body," by H. Miyamoto, Transactions of the Japan Society of Mechanical Engineering, vol. 19, no. 87, 1953, pp. 60–66.

9 "Stress Concentrations Around Spheroidal Inclusions and Cavities," by R. H. Edwards, JOURNAL OF APPLIED MECHANICS, Trans. ASME, vol. 73, 1951, pp. 19–30.

10 "On Symmetrical Strain in Solids of Revolution in Curvilinear Coordinates," by Chih-Bing Ling and Kuo-Liang Yang, *Annals of the Academia Sinica*, Taipei, Formosa, vol. 1, 1954, p. 507.

11 "Thermal Stress in a Spheroid With Steady Axisymmetric Distribution of Temperature," by R. Muki, Proceedings of the Faculty of Engineering, Keio University, vol. 6, 1953, pp. 10–26.

12 "Application des potentiels à l'étude de l'équilibre et du mouvement des solides élastiques," by J. Boussinesq, Gauthier-Villars, Paris, France, 1885.

13 "A Treatise on the Mathematical Theory of Elasticity," by A. E. H. Love, Dover Publications, New York, N. Y., 1944.

14 "Uniqueness Theorems of Two-Dimensional Elasticity Theory," by R. Tiffen, *Quarterly Journal of Mechanics and Applied Mathematics*, vol. 5, no. 2, 1952, pp. 237–252.

15 "The Theory of Spherical and Ellipsoidal Harmonics," by E. W. Hobson, University Press, Cambridge, England, 1931.

16 "Partial Differential Equations of Mathematical Physics," by H. Bateman, Dover Publications, New York, N. Y., 1944.

17 "A Course of Modern Analysis," by E. T. Whittaker and G. N. Watson, fourth edition, University Press, Cambridge, England, 1935.

18 "Higher Transcendental Functions," Staff of the Bateman Manuscript Project (California Institute of Technology), McGraw-Hill Book Company, Inc., New York, N. Y., vol. 1, 1953.

19 "Theory of Functions," by Konrad Knopp, Dover Publications, New York, N. Y., part 1, 1945.

20 "Differential and Integral Calculus," by R. Courant, Nordemann Publishing Company, New York, N. Y., vol. 1, 1937.

21 "Tafeln der Kugelfunktionen $P_n(x)$ und ihrer abgeleiteten Funktionen," by A. H. Hj. Tallqvist, Acta Societatis Scientiarum Fennicae, Finska Vetenskaps-Societeten, Helsingfors, vol. 32, no. 6, 1906, 27 pages.

22 "Tafeln der Abgeleiteten und zugeordneten Kugelfunktionen erster Art," by A. H. Hj. Tallqvist, Acta Societatis Scientiarum Fennicae, Finska Vetenskaps-Societeten, Helsingfors, vol. 33, no. 9, 1908, 67 pages.

On the Stresses in a Strip Under Tension and Containing Two Equal Circular Holes Placed Longitudinally

By A. ATSUMI,[1] SENDAI, JAPAN

A problem of determining the stresses in an infinite strip of finite breadth under tension and containing two equal circular holes placed on the longitudinal axis is studied theoretically. Stresses are calculated by a perturbation method, in each case the radius of the circle and the distance between the centers of two holes being varied. From consideration of the results obtained, some conclusions are made regarding the effects of the straight boundaries and the holes.

Introduction

IT IS well known that the presence of a hole in a stressed plate has a very great influence upon the maximum stress, and a number of investigations, both mathematical and experimental, have been directed toward determining the exact extent of this influence. When the hole is isolated and the boundaries of the plate are distant, the mathematical method of finding the stresses in its neighborhood is elementary. But the presence of adjacent boundaries introduces great complications. The problem has been solved by Jeffery (1)[2] for a circular hole near a single straight boundary, and by Howland and others (2) for a hole between two straight boundaries. And the problems have been solved by Howland, Green, Chih-Bing Ling, and others (3) for a group of holes closely placed together so as to influence each other in a plate of indefinite extent. Excepting the investigations that have been made by Howland and Knight, and Green (4) on stresses in a perforated strip, of finite breadth, containing circular holes, there appears, however, to have been no theoretical investigation which gives much information as to numerical aspects of the problem for some particular cases. The purpose of this paper, therefore, is to determine theoretically the stresses in the problem mentioned and to give, with the aid of some other studies, some consideration of the effects of proximity of the straight edges and the circular holes.

Method of Analysis

Let the strip of isotropic and elastic material be bounded in the x, y-plane by the lines $y = \pm b$, and perforated by two holes of equal radius $a(<b)$, with the centers at the points $O_1(h, 0)$, $O_2(-h, 0)$. Polar co-ordinates (r, θ) will be used, taking the initial line O_1y_1 and the positive direction of θ clockwise as shown in Fig. 1.

Then the relation between these co-ordinates is

$$\left.\begin{aligned} x &= r\sin\theta + h \\ y &= r\cos\theta \end{aligned}\right\} \quad \ldots\ldots\ldots\ldots\ldots [1]$$

We express the formulas in terms of dimensionless variables as follows

$$\left.\begin{aligned} &\xi = x/b, \quad \eta = y/b, \quad \rho = r/b \\ &\lambda = a/b, \quad \beta = h/b \end{aligned}\right\} \quad \ldots\ldots\ldots [2]$$

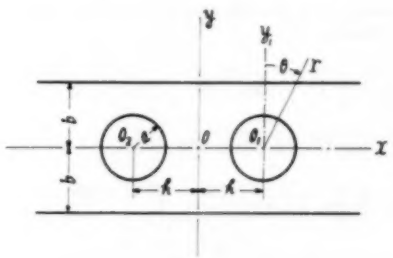

Fig. 1

The present problem is to determine the distribution of stresses in the perforated strip, shown in Fig. 1, under a uniform tension T applied parallel to the straight edges in its plane.

Under the usual conditions of generalized plane stress, the mean values taken throughout the thickness of the plate of the stresses are derivable from a single stress function χ satisfying the biharmonic equation

$$\nabla^4\chi = \partial^4\chi/\partial x^4 + 2\partial^4\chi/\partial x^2\partial y^2 + \partial^4\chi/\partial y^4 = 0 \quad \ldots\ldots [3]$$

The stress components relative to Cartesian co-ordinates are

$$\sigma_x = \frac{1}{b^2}\frac{\partial^2\chi}{\partial\eta^2}, \quad \sigma_y = \frac{1}{b^2}\frac{\partial^2\chi}{\partial\xi^2}, \quad \tau_{xy} = -\frac{1}{b^2}\frac{\partial^2\chi}{\partial\xi\partial\eta} \quad \ldots\ldots [4]$$

Those relative to the polar co-ordinates are

$$\left.\begin{aligned} &\sigma_r = \frac{1}{b^2}\left(\frac{1}{\rho^2}\frac{\partial^2\chi}{\partial\theta^2} + \frac{1}{\rho}\frac{\partial\chi}{\partial\rho}\right), \quad \sigma_\theta = \frac{1}{b^2}\frac{\partial^2\chi}{\partial\rho^2} \\ &\tau_{r\theta} = -\frac{1}{b^2}\frac{\partial}{\partial\rho}\left(\frac{1}{\rho}\frac{\partial\chi}{\partial\theta}\right) \end{aligned}\right\} \quad \ldots [5]$$

Then the problem is that of finding a solution of Equation [3] satisfying the following equations for the boundary conditions

(a) On the lines

$$\eta = \pm 1, \quad \sigma_y = \tau_{xy} = 0 \quad \ldots\ldots\ldots\ldots [6]$$

[1] Assistant Professor of Mechanical Engineering, Tohoku University.

[2] Numbers in parentheses refer to the Bibliography at the end of the paper.

Presented at the National Applied Mechanics Division Conference, Urbana, Ill., June 14–16, 1956, of The American Society of Mechanical Engineers.

Discussion of this paper should be addressed to the Secretary, ASME, 29 West 39th Street, New York, N. Y., and will be accepted until January 10, 1957, for publication at a later date. Discussion received after the closing date will be returned.

Note: Statements and opinions advanced in papers are to be understood as individual expressions of their authors and not those of the Society. Manuscript received by ASME Applied Mechanics Division, May 31, 1955. Paper No. 56—APM-12.

(*b*) On the circles

$$\sqrt{(\xi \mp \beta)^2 + \eta^2} = \lambda, \quad \sigma_r = \tau_{r\theta} = 0 \ldots\ldots\ldots [7]$$

(*c*) At infinity

$$\xi \to \pm\infty, \quad \sigma_x = T, \quad \sigma_y = \tau_{xy} = 0 \ldots\ldots\ldots [8]$$

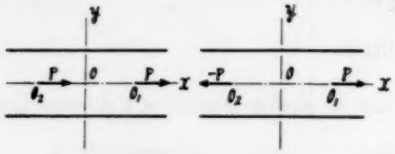

FIG. 2

We start with the fundamental stress functions χ_a and χ_b, shown in Fig. 2, representing the solutions for the infinite strip under forces P at the centers of the circles.

χ_a is the stress function for the case of two equal isolated forces acting at the points O_1 and O_2 in the direction $\overrightarrow{Ox}$. χ_b is the one for the case where one force is taken in the direction $\overrightarrow{Ox}$ and the other in the opposite direction.

These are given in the following by using the stress functions found by Howland (5)

$$\chi_a = \frac{Pb}{4\pi(1-\nu)}\left[(1-2\nu)\left\{(\xi-\beta)\log\sqrt{(\xi-\beta)^2+\eta^2}\right.\right.$$
$$\left. + (\xi+\beta)\log\sqrt{(\xi+\beta)^2+\eta^2}\right\} + 2(1-\nu)\eta\left(\tan^{-1}\frac{\xi-\beta}{\eta}$$
$$\left.\left. + \tan^{-1}\frac{\xi+\beta}{\eta}\right)\right] + \frac{Pb}{\pi(1-\nu)}\int_0^\infty\left[\frac{u\eta sS-(s+uc)C}{u^2\Sigma}\right.$$
$$\left.\{u-(1-2\nu)\}\,e^{-u} + \frac{sC-\eta cS}{u\Sigma}\{2(1-\nu)-u\}\,e^{-u}\right]$$
$$\sin u\xi\cos u\beta du \ldots\ldots [9]$$

$$\chi_b = \frac{Pb}{4\pi(1-\nu)}\left[(1-2\nu)\left\{(\xi-\beta)\log\sqrt{(\xi-\beta)^2+\eta^2}\right.\right.$$
$$\left. - (\xi+\beta)\log\sqrt{(\xi+\beta)^2+\eta^2}\right\} + 2(1-\nu)\eta\left(\tan^{-1}\frac{\xi-\beta}{\eta}$$
$$\left.\left. - \tan^{-1}\frac{\xi+\beta}{\eta}\right)\right] - \frac{Pb}{\pi(1-\nu)}\int_0^\infty\left[\frac{u\eta sS-(s+uc)C}{u^2\Sigma}\right.$$
$$\left.\{u-(1-2\nu)\}\,e^{-u} + \frac{sC-\eta cS}{u\Sigma}\{2(1-\nu)-u\}\,e^{-u}\right]$$
$$\cos u\xi\sin u\beta du \ldots\ldots [10]$$

where ν is the modified value of Poisson's ratio occurring in the theory of "generalized plane stress," and the other new symbols are defined as follows

$$\left.\begin{aligned} &s = \sinh u, \quad c = \cosh u, \quad S = \sinh \eta u, \quad C = \cosh \eta u \\ &\Sigma = \sinh 2u + 2u \end{aligned}\right\} \ldots [11]$$

Now we must consider the expansions of these functions about the singular point $O_1(h, 0)$. The problem is not difficult but involves a fair amount of algebraic manipulation; hence only the final results will be given.

χ_a is given by the equation

$$\chi_a = \frac{Pb}{4\pi(1-\nu)}\left\{(1-2\nu)\rho\sin\theta\log\rho + 2(1-\nu)\theta\rho\cos\theta\right.$$
$$\left. + \sum_{n=0}^{\infty}\left[(A_{2n}+A_{2n}'\rho^2)\rho^{2n}\cos 2n\theta\right.\right.$$
$$\left.\left. + (B_{2n+1}+B_{2n+1}'\rho^2)\rho^{2n+1}\sin(2n+1)\theta\right]\right\} \ldots\ldots [12]$$

where

$$\left.\begin{aligned} A_{2n} &= \frac{1}{(2n)!}\left\{-2I_{2n} + 2nI_{2n-1} - n(I_{2n-2}+J_{2n-2})\right. \\ &\quad \left. + (1-2\nu)[2I_{2n-1} - (2n-1)I_{2n-2} - J_{2n-2}]\right\} \\ &\quad - (1-2\nu)l_{2n} - 2(1-\nu)l_{2n}' \\ A_{2n}' &= \frac{1}{(2n+1)!}\left[I_{2n+1} - \frac{1}{2}(I_{2n}+J_{2n})\right. \\ &\quad \left. - (1-2\nu)I_{2n}\right] - (1-2\nu)m_{2n} - 2(1-\nu)m_{2n}' \\ B_{2n+1} &= \frac{1}{(2n+1)!}\left\{-2(I_{2n+1}+I_{2n+1}')\right. \\ &\quad + (2n+1)(I_{2n}+I_{2n}') - \frac{2n+1}{2}(I_{2n-1}+I_{2n-1}' \\ &\quad + J_{2n-1}+J_{2n-1}') + (1-2\nu)[2(I_{2n}+I_{2n}') \\ &\quad \left. - 2n(I_{2n-1}+I_{2n-1}') - (J_{2n-1}+J_{2n-1}')]\right\} \\ &\quad - (1-2\nu)n_{2n+1} - 2(1-\nu)n_{2n+1}' \\ B_{2n+1}' &= \frac{1}{(2n+2)!}\left[(I_{2n+2}+I_{2n+2}')\right. \\ &\quad - \frac{1}{2}(I_{2n+1}+I_{2n+1}'+J_{2n+1}+J_{2n+1}') \\ &\quad \left. - (1-2\nu)(I_{2n+1}+I_{2n+1}')\right] - (1-2\nu)p_{2n+1} \\ &\quad - 2(1-\nu)p_{2n+1}' \end{aligned}\right\} \ldots [13]$$

The new symbols denote

$$\left.\begin{aligned} I_n &= \int_0^\infty \frac{u^n}{\Sigma}du, \quad I_n' = \int_0^\infty \frac{u^n}{\Sigma}\cos 2u\beta du, \\ &\qquad I_n = \int_0^\infty \frac{u^n}{\Sigma}\sin 2u\beta du \\ J_n &= \int_0^\infty \frac{u^n e^{-2u}}{\Sigma}du, \quad J_n' = \int_0^\infty \frac{u^n e^{-2u}}{\Sigma}\cos 2u\beta du, \\ &\qquad J_n = \int_0^\infty \frac{u^n e^{-2u}}{\Sigma}\sin 2u\beta du \end{aligned}\right\} \ldots [14]$$

and

$$\left.\begin{aligned} l_{2n} &= \frac{(-)^{n+1}(1-n)}{2n(2n-1)(2\beta)^{2n-1}}, \\ &\qquad l_{2n}' = \frac{(-)^{n+1}}{2(2n-1)(2\beta)^{2n-1}} \\ m_{2n} &= \frac{(-)^{n+1}}{2(2n+1)(2\beta)^{2n+1}} = -m_{2n}', \\ &\qquad n_{2n+1} = \frac{(-)^{n+1}(2n-1)}{4n(2n+1)(2\beta)^{2n}} \end{aligned}\right\} \ldots [15]$$

$$n_{2n+1}' = \frac{(-)^n}{4n(2\beta)^{2n}}$$

$$p_{2n+1} = \frac{(-)^n}{4(n+1)(2\beta)^{2n+2}} = -p_{2n+1}' \quad \left.\right\} \ldots [15] \text{ (cont.)}$$

χ_b is given by the same expression as χ_a, provided the signs of the integrals I_n', J_n', I_n, J_n, and the constants l_{2n}, m_{2n}, . . . n_{2n+1}', p_{2n+1}' in Equations [13] are all reversed.

χ_a and χ_b are biharmonic functions for all vaulues of ν and satisfy the Condition [6], but we consider cases when ν has special values. This is justifiable since the functions derived are giving single-valued displacements.

First, let χ_a', χ_b' be a function taking $Pb/2\pi = 1$ and $\nu \to \infty$ in χ_a and χ_b, respectively. Next, make χ_a'', χ_b'' taking $\nu = 1/2$. As the stress system in the present problem should be symmetrical about the y-axis, we have to find the even functions in x, which may be obtained by differentiating χ_a' and χ_a'' an odd number of times and χ_b' and χ_b'' an even number of times with respect to ξ. These are defined as follows

$$\left.\begin{aligned} U_0 &= \frac{-\partial\chi_a'}{\partial\xi}, \quad U_{2s} = \frac{(-)^s\partial^{2s}U_0}{(2s-1)\partial\xi^{2s}} \quad (s \geq 1) \\ V_0' &= \frac{2\partial\chi_a''}{\partial\xi}, \quad V_{2s} = \frac{(-)^s\partial^{2s}V_0'}{2s\,\partial\xi^{2s}} \quad (s \geq 1) \\ U_1 &= \frac{\partial^2\chi_b'}{\partial\xi^2}, \quad U_{2s+1} = \frac{(-)^s\partial^{2s}U_1}{2s\,\partial\xi^{2s}} \quad (s \geq 1) \\ V_{2s+1} &= \frac{(-)^{s+1}\partial^{2s+2}\chi_b''}{(2s+1)\partial\xi^{2s+2}} (s \geq 0) \end{aligned}\right\} \ldots [16]$$

In order to find the limiting values of the stresses at $x \to \pm\infty$, we first find the values of χ_a and χ_b at $x \to \pm\infty$. And we obtain

$$\sigma_x = \mp\frac{P}{2b}, \quad \sigma_y = \tau_{xy} = 0$$

from χ_a and $\sigma_x = \sigma_y = \tau_{xy} = 0$ from χ_b. But from a differentiated function of χ_a with respect to ξ, we obtain the residual stress $\sigma_x = 0$ at $x \to \pm\infty$. Then our standard Functions [16] show no contribution to the stresses at infinity.

Now detailed expressions of [16] are shown in the following

$$U_0 = -\log\rho + \sum_{n=0}^{\infty} ({}^0A_{2n} + {}^0A_{2n}'\rho^2)\rho^{2n}\cos 2n\theta + \sum_{n=0}^{\infty} ({}^0B_{2n+1} + {}^0B_{2n+1}'\rho^2)\rho^{2n+1}\sin(2n+1)\theta \ldots\ldots [17]$$

$$U_{2s} = \rho^{-2s}\cos 2s\theta + \sum_{n=0}^{\infty} ({}^{2s}A_{2n} + {}^{2s}A_{2n}'\rho^2)\rho^{2n}\cos 2n\theta + \sum_{n=0}^{\infty} ({}^{2s}B_{2n+1} + {}^{2s}B_{2n+1}'\rho^2)\rho^{2n+1}\sin(2n+1)\theta \ldots\ldots [18]$$

where, for $s \geq 0$

$$\left.\begin{aligned} {}^{2s}A_{2n} &= -[2(I_{2n+2s} + I_{2n+2s}') - (2n-1)(I_{2n+2s-1} + I_{2n+2s-1}') - (J_{2n+2s-1} + J_{2n+2s-1}')]/(2s-1)!(2n)! \\ &\quad + (-)^{n+s}\binom{2n+2s-1}{2n}\Big/(2\beta)^{2n+2s} \end{aligned}\right\} \ldots [19]$$

$$\left.\begin{aligned} {}^{2s}A_{2n}' &= (I_{2n+2s+1} + I_{2n+2s+1}')/(2s-1)!(2n+1)! \\ {}^{2s}B_{2n+1} &= (2I_{2n+2s+1} - 2nI_{2n+2s} - J_{2n+2s})/(2s-1)!(2n+1)! \\ &\quad + (-)^{n+s+1}\binom{2n+2s}{2n+1}\Big/(2\beta)^{2n+2s+1} \\ {}^{2s}B_{2n+1}' &= -I_{2n+2s+2}/(2s-1)!(2n+2)! \end{aligned}\right\} \ldots [19] \text{ (cont.)}$$

for $s = 0$ the last terms of ${}^0A_{2n}$ and ${}^0B_{2n+1}$ are defined by $(-)^n/2n(2\beta)^{2n}$ and $(-)^{n+1}/(2n+1)(2\beta)^{2n+1}$, respectively.

$$V_0' = \cos 2\theta + \sum_{n=0}^{\infty} ({}^0\bar{C}_{2n} + {}^0\bar{C}_{2n}'\rho^2)\rho^{2n}\cos 2n\theta + \sum_{n=0}^{\infty} ({}^0\bar{D}_{2n+1} + {}^0\bar{D}_{2n+1}'\rho^2)\rho^{2n+1}\sin(2n+1)\theta \ldots\ldots [20]$$

$$V_{2s} = \rho^{-2s}[\cos(2s+2)\theta + \cos 2s\theta] + \sum_{n=0}^{\infty} ({}^{2s}C_{2n} + {}^{2s}C_{2n}'\rho^2)\rho^{2n}\cos 2n\theta + \sum_{n=0}^{\infty} ({}^{2s}D_{2n+1} + {}^{2s}D_{2n+1}'\rho^2)\rho^{2n+1}\sin(2n+1)\theta \ldots\ldots [21]$$

where, for $s \geq 0$

$$\left.\begin{aligned} {}^{2s}C_{2n} &= [-4(I_{2n+2s+1} + I_{2n+2s+1}') + 4n(I_{2n+2s} + I_{2n+2s}') - 2n(I_{2n+2s-1} + I_{2n+2s-1}' + J_{2n+2s-1} + J_{2n+2s-1}')]/(2s)!(2n)! \\ &\quad + (-)^{n+s+1}\binom{2n+2s-1}{2n-1}\Big/(2\beta)^{2n+2s} \\ {}^{2s}C_{2n}' &= [2(I_{2n+2s+2} + I_{2n+2s+2}') - (I_{2n+2s+1} + I_{2n+2s+1}' + J_{2n+2s+1} + J_{2n+2s+1}')]/(2s)!(2n+1)! \\ &\quad + (-)^{n+s}\binom{2n+2s+1}{2n+1}\Big/(2\beta)^{2n+2s+2} \\ {}^{2s}D_{2n+1} &= [4I_{2n+2s+2} - (4n+2)I_{2n+2s+1} + (2n+1)(I_{2n+2s} + J_{2n+2s})]/(2s)!(2n+1)! \\ &\quad + (-)^{n+s}\binom{2n+2s}{2n}\Big/(2\beta)^{2n+2s+1} \\ {}^{2s}D_{2n+1}' &= [-2I_{2n+2s+3} + I_{2n+2s+2} + J_{2n+2s+2}]/(2s)!(2n+2)! \\ &\quad + (-)^{n+s+1}\binom{2n+2s+2}{2n+2}\Big/(2\beta)^{2n+2s+3} \end{aligned}\right\} \ldots [22]$$

${}^0\bar{C}_{2n}, \ldots, {}^0\bar{D}_{2n+1}'$ in Equation [20] are given by ${}^0C_{2n}, \ldots, {}^0D_{2n+1}'$ in Equation [22] with $s = 0$

$$U_{2s+1} = \rho^{-(2s+1)}\sin(2s+1)\theta + \sum_{n=0}^{\infty} ({}^{2s+1}A_{2n} + {}^{2s+1}A_{2n}'\rho^2)\rho^{2n}\cos 2n\theta + \sum_{n=0}^{\infty} ({}^{2s+1}B_{2n+1} + {}^{2s+1}B_{2n+1}'\rho^2)\rho^{2n+1}\sin(2n+1)\theta \ldots\ldots [23]$$

for $s \geq 0$

$$\left.\begin{aligned} {}^{2s+1}A_{2n} &= [2I_{2n+2s+1} - (2n-1)I_{2n+2s} - J_{2n+2s}]/(2s)!(2n)! \\ &\quad + (-)^{n+s-1}\binom{2n+2s}{2n}\Big/(2\beta)^{2n+2s+1} \end{aligned}\right\} \ldots [24]$$

$$
\left.
\begin{aligned}
{}^{2s+1}A_{2n}' &= -I_{2n+2s+2}/(2s)!(2n+1)! \\
{}^{2s+1}B_{2n+1} &= -[2(I_{2n+2s+2} - I_{2n+2s+2}') \\
&\quad - 2n(I_{2n+2s+1} - I_{2n+2s+1}') - (J_{2n+2s+1} \\
&\quad - J_{2n+2s+1}')]/(2s)!(2n+1)! \\
&\quad + (-)^{n+s}\binom{2n+2s+1}{2n+1}\Big/(2\beta)^{2n+2s+2} \\
{}^{2s+1}B_{2n+1}' &= (I_{2n+2s+3} - I_{2n+2s+3}')/(2s)!(2n+2)!
\end{aligned}
\right\} \quad \text{..[24] (cont.)}
$$

$$
\begin{aligned}
V_{2s+1} &= \rho^{-(2s+1)}[\sin(2s+3)\theta + \sin(2s+1)\theta] \\
&\quad + \sum_{n=0}^{\infty}({}^{2s+1}C_{2n} + {}^{2s+1}C_{2n}'\rho^2)\rho^{2n}\cos 2n\theta \\
&+ \sum_{n=0}^{\infty}({}^{2s+1}D_{2n+1} + {}^{2s+1}D_{2n+1}'\rho^2)\rho^{2n+1}\sin(2n+1)\theta \quad \text{..... [25]}
\end{aligned}
$$

for $s \geq 0$

$$
\left.
\begin{aligned}
{}^{2s+1}C_{2n} &= [4I_{2n+2s+2} - 4nI_{2n+2s+1} \\
&\quad + 2n(I_{2n+2s} + J_{2n+2s})]/(2s+1)!(2n)! \\
&\quad + (-)^{n+s}\binom{2n+2s}{2n-1}\Big/(2\beta)^{2n+2s+1} \\
{}^{2s+1}C_{2n}' &= [-2I_{2n+2s+3} + I_{2n+2s+2} \\
&\quad + J_{2n+2s+2}]/(2s+1)!(2n+1)! \\
&\quad + (-)^{n+s+1}\binom{2n+2s+2}{2n+1}\Big/(2\beta)^{2n+2s+3} \\
{}^{2s+1}D_{2n+1} &= [-4(I_{2n+2s+3} - I_{2n+2s+3}') \\
&\quad + (4n+2)(I_{2n+2s+2} - I_{2n+2s+2}') \\
&\quad - (2n+1)(I_{2n+2s+1} - I_{2n+2s+1}' + J_{2n+2s+1} \\
&\quad - J_{2n+2s+1}')]/(2s+1)!(2n+1)! \\
&\quad + (-)^{n+s+1}\binom{2n+2s+1}{2n}\Big/(2\beta)^{2n+2s+2} \\
{}^{2s+1}D_{2n+1}' &= [2(I_{2n+2s+4} - I_{2n+2s+4}') \\
&\quad - (I_{2n+2s+3} - I_{2n+2s+3}' + J_{2n+2s+3} \\
&\quad - J_{2n+2s+3}')]/(2s+1)!(2n+2)! \\
&\quad + (-)^{n+s}\binom{2n+2s+3}{2n+2}\Big/(2\beta)^{2n+2s+4}
\end{aligned}
\right\} \quad \text{..[26]}
$$

Further, it is found that it will be more convenient to take, for our standard stress functions, V_{2s}' and V_{2s+1}', which are defined by the equations

$$
\left.
\begin{aligned}
V_{2s}' &= V_{2s} - U_{2s}\ (s \geq 1) = \rho^{-2s}\cos(2s+2)\theta \\
&\quad + \sum_{n=0}^{\infty}({}^{2s}\bar{C}_{2n} + {}^{2s}\bar{C}_{2n}'\rho^2)\rho^{2n}\cos 2n\theta \\
&\quad + \sum_{n=0}^{\infty}({}^{2s}\bar{D}_{2n+1} + {}^{2s}\bar{D}_{2n+1}'\rho^2)\rho^{2n+1}\sin(2n+1)\theta \\
V_{2s+1}' &= V_{2s+1} - U_{2s+1}(s \geq 0) \\
&\quad = \rho^{-(2s+1)}\sin(2s+3)\theta \\
&\quad + \sum_{n=0}^{\infty}({}^{2s+1}\bar{C}_{2n} + {}^{2s+1}\bar{C}_{2n}'\rho^2)\rho^{2n}\cos 2n\theta \\
&\quad + \sum_{n=0}^{\infty}({}^{2s+1}\bar{D}_{2n+1} + {}^{2s+1}\bar{D}_{2n+1}'\rho^2)\rho^{2n+1}\sin(2n+1)\theta
\end{aligned}
\right\} \quad \text{..[27]}
$$

Then we finally take as a complete stress function

$$
\begin{aligned}
\tilde{\chi} &= T\left[b^2\rho^2(1+\cos 2\theta)/4\right. \\
&\quad \left. + \sum_{s=0}^{\infty}(a_{2s}U_{2s} + b_{2s}V_{2s}' + c_{2s+1}U_{2s+1} + d_{2s+1}V_{2s+1}')\right] \quad \text{..... [28]}
\end{aligned}
$$

The first term in this equation is the stress function expressing the uniform tension applied and satisfying the Condition [6]. Therefore $\tilde{\chi}$ is a solution of Equation [3] satisfying the Conditions [6] and [8]. Then we have to determine the unknown constants $a_{2s}, \ldots, d_{2s+1}$ so the Boundary Condition [7] is satisfied. As $\tilde{\chi}$ is an even function in both x and y, if the boundary condition on the circumference $\rho = \lambda$ on the circle is satisfied, it is also satisfied on the other circle automatically. Equating σ_{rr} $\tau_{r\theta}$ of $\tilde{\chi}$ to zero after setting $\rho = \lambda$, we obtain the following equations to determine the unknown constants

$$
\left.
\begin{aligned}
\frac{b^2\lambda^2}{2} &= a_0 - 2\sum_{s=0}^{\infty}(a_{2s}{}^{2s}A_0' + b_{2s}{}^{2s}\bar{C}_0' \\
&\quad + c_{2s+1}{}^{2s+1}A_0' + d_{2s+1}{}^{2s+1}\bar{C}_0')\lambda^2 \\
\frac{-b^2\lambda^2}{2} &= b_0 + 2\sum_{s=0}^{\infty}(a_{2s}{}^{2s}A_2 + b_{2s}{}^{2s}\bar{C}_2 \\
&\quad + c_{2s+1}{}^{2s+1}A_2 + d_{2s+1}{}^{2s+1}\bar{C}_2)\lambda^2 \\
&\quad + 3\sum_{s=0}^{\infty}(a_{2s}{}^{2s}A_2' + b_{2s}{}^{2s}\bar{C}_2' + c_{2s+1}{}^{2s+1}A_2' \\
&\quad + d_{2s+1}{}^{2s+1}\bar{C}_2')\lambda^4 \\
\frac{b^2\lambda^4}{4} &= a_2 - \sum_{s=0}^{\infty}(a_{2s}{}^{2s}A_2 + b_{2s}{}^{2s}\bar{C}_2 \\
&\quad + c_{2s+1}{}^{2s+1}A_2 + d_{2s+1}{}^{2s+1}\bar{C}_2)\lambda^4 \\
&\quad - 2\sum_{s=0}^{\infty}(a_{2s}{}^{2s}A_2' + b_{2s}{}^{2s}\bar{C}_2' + c_{2s+1}{}^{2s+1}A_2' \\
&\quad + d_{2s+1}{}^{2s+1}\bar{C}_2')\lambda^6 \\
0 &= a_{2n} - \sum_{s=0}^{\infty}a_{2s}[(2n-1)^{2s}A_{2n} + 2n^{2s}A_{2n}'\lambda^2]\lambda^{4n} \\
&\quad - \sum_{s=0}^{\infty}b_{2s}[(2n-1)^{2s}\bar{C}_{2n} + 2n^{2s}\bar{C}_{2n}'\lambda^2]\lambda^{4n} \\
&\quad - \sum_{s=0}^{\infty}c_{2s+1}[(2n-1)^{2s+1}A_{2n} + 2n^{2s+1}A_{2n}'\lambda^2]\lambda^{4n} \\
&\quad - \sum_{s=0}^{\infty}d_{2s+1}[(2n-1)^{2s+1}\bar{C}_{2n} \\
&\quad + 2n^{2s+1}\bar{C}_{2n}'\lambda^2]\lambda^{4n}(n \geq 2) \\
0 &= b_{2n} + \sum_{s=0}^{\infty}a_{2s}[(2n+2)^{2s}A_{2n+2} \\
&\quad + (2n+3)^{2s}A_{2n+2}'\lambda^2]\lambda^{4n+2} \\
&\quad + \sum_{s=0}^{\infty}b_{2s}[(2n+2)^{2s}\bar{C}_{2n+2} + (2n+3)^{2s}\bar{C}_{2n+2}'\lambda^2]\lambda^{4n+2} \\
&\quad + \sum_{s=0}^{\infty}c_{2s+1}[(2n+2)^{2s+1}A_{2n+2} \\
&\quad + (2n+3)^{2s+1}A_{2n+2}'\lambda^2]\lambda^{4n+2} \\
&\quad + \sum_{s=0}^{\infty}d_{2s+1}[(2n+2)^{2s+1}\bar{C}_{2n+2} \\
&\quad + (2n+3)^{2s+1}\bar{C}_{2n+2}'\lambda^2]\lambda^{4n+2}(n \geq 1)
\end{aligned}
\right\} \quad \text{..[29]}
$$

$$0 = c_{2n+1} - \sum_{s=0}^{\infty} a_{2s}[2n^{2s}B_{2n+1} + (2n+1)^{2s}B_{2n+1}'\lambda^2]\lambda^{4n+2} - \sum_{s=0}^{\infty} b_{2s}[2n^{2s}\bar{D}_{2n+1} + (2n+1)^{2s}\bar{D}_{2n+1}'\lambda^2]\lambda^{4n+2} - \sum_{s=0}^{\infty} c_{2s+1}[2n^{2s+1}B_{2n+1} + (2n+1)^{2s+1}B_{2n+1}'\lambda^2]\lambda^{4n+2} - \sum_{s=0}^{\infty} d_{2s+1}[2n^{2s+1}\bar{D}_{2n+1} + (2n+1)^{2s+1}\bar{D}_{2n+1}'\lambda^2]\lambda^{4n+2} \quad (n \geq 0)$$

$$0 = d_{2n+1} + \sum_{s=0}^{\infty} a_{2s}[(2n+3)^{2s}B_{2n+3} + (2n+4)^{2s}B_{2n+3}'\lambda^2]\lambda^{4n+4} + \sum_{s=0}^{\infty} b_{2s}[(2n+3)^{2s}\bar{D}_{2n+3} + (2n+4)^{2s}\bar{D}_{2n+3}'\lambda^2]\lambda^{4n+4} + \sum_{s=0}^{\infty} c_{2s+1}[(2n+3)^{2s+1}B_{2n+3} + (2n+4)^{2s+1}B_{2n+3}'\lambda^2]\lambda^{4n+4} + \sum_{s=0}^{\infty} d_{2s+1}[(2n+3)^{2s+1}\bar{D}_{2n+3} + (2n+4)^{2s+1}\bar{D}_{2n+3}'\lambda^2]\lambda^{4n+4} \quad (n \geq 0)$$

. . [29] (*cont.*)

Determination of Coefficients

It seems more convenient to solve Equation [29] by a perturbation method in which λ is the perturbation parameter. We then seek for the solution in the forms

$$a_0 = \sum_{p=0}^{\infty} a_0^{(2p+2)}\lambda^{2p+2}, \quad a_2 = \sum_{p=0}^{\infty} a_2^{(2p+4)}\lambda^{2p+4}$$

$$b_0 = \sum_{p=0}^{\infty} b_0^{(2p+2)}\lambda^{2p+2}, \quad c_1 = \sum_{p=1}^{\infty} c_1^{(2p+4)}\lambda^{2p+4}$$

$$a_{2n} = \sum_{p=1}^{\infty} a_{2n}^{(4n+2p)}\lambda^{4n+2p} \quad (n \geq 2),$$

$$b_{2n} = \sum_{p=1}^{\infty} b_{2n}^{(4n+2p+2)}\lambda^{4n+2p+2} \quad (n \geq 1)$$

$$c_{2n+1} = \sum_{p=1}^{\infty} c_{2n+1}^{(4n+2p+2)}\lambda^{4n+2p+2} \quad (n \geq 1),$$

$$d_{2n+1} = \sum_{p=1}^{\infty} d_{2n+1}^{(4n+2p+4)}\lambda^{4n+2p+4} \quad (n \geq 0)$$

. . [30]

where $a_0^{(2p+2)}, \ldots, d_{2n+1}^{(4n+2p+4)}$ are independent of λ. Substituting Equations [30] in [29], and equating the coefficients of the various powers of λ on both sides, we have the following equations

$$a_0^{(2)} = b^2/2, \quad a_2^{(4)} = b^2/4, \quad b_0^{(2)} = -b^2/2$$

$$a_0^{(2p+2)} = 2\sum_{s=0}^{p} [a_{2s}^{(2p)}\,{}^{2s}A_0' + b_{2s}^{(2p)}\,{}^{2s}\bar{C}_0' + c_{2s+1}^{(2p)}\,{}^{2s+1}A_0' + d_{2s+1}^{(2p)}\,{}^{2s+1}\bar{C}_0']$$

. . [31]

$$a_2^{(2p+6)} = \sum_{s=0}^{p} [a_{2s}^{(2p+2)}\,{}^{2s}A_2 + b_{2s}^{(2p+2)}\,{}^{2s}\bar{C}_2 + c_{2s+1}^{(2p)}\,{}^{2s+1}A_2 + d_{2s+1}^{(2p)}\,{}^{2s+1}\bar{C}_2] + 2\sum_{s=0}^{p} [a_{2s}^{(2p)}\,{}^{2s}A_2' + b_{2s}^{(2p)}\,{}^{2s}\bar{C}_2' + c_{2s+1}^{(2p)}\,{}^{2s+1}A_2' + d_{2s+1}^{(2p)}\,{}^{2s+1}\bar{C}_2']$$

$$a_{2n}^{(4n+2p+2)} = \sum_{s=0}^{p} \{(2n-1)[a_{2s}^{(2p+2)}\,{}^{2s}A_{2n} + b_{2s}^{(2p+2)}\,{}^{2s}\bar{C}_{2n} + c_{2s+1}^{(2p+2)}\,{}^{2s+1}A_{2n} + d_{2s+1}^{(2p+2)}\,{}^{2s+1}\bar{C}_{2n}] + 2n\,[a_{2s}^{(2p)}\,{}^{2s}A_{2n}' + b_{2s}^{(2p)}\,{}^{2s}\bar{C}_{2n}' + c_{2s+1}^{(2p)}\,{}^{2s+1}A_{2n}' + d_{2s+1}^{(2p)}\,{}^{2s+1}\bar{C}_{2n}']\}$$

$$b_0^{(2p+4)} = -2\sum_{s=0}^{p} [a_{2s}^{(2p+2)}\,{}^{2s}A_2 + b_{2s}^{(2p+2)}\,{}^{2s}\bar{C}_2 + c_{2s+1}^{(2p+2)}\,{}^{2s+1}A_2 + d_{2s+1}^{(2p+2)}\,{}^{2s+1}\bar{C}_2] - 3\sum_{s=0}^{p} [a_{2s}^{(2p)}\,{}^{2s}A_2' + b_{2s}^{(2p)}\,{}^{2s}\bar{C}_2' + c_{2s+1}^{(2p)}\,{}^{2s+1}A_2' + d_{2s+1}^{(2p)}\,{}^{2s+1}\bar{C}_2']$$

. . [31] (*cont.*)

$$b_{2n}^{(4n+2p+4)} = -\sum_{s=0}^{p} \{(2n+2)[a_{2s}^{(2p+2)}\,{}^{2s}A_{2n+2} + b_{2s}^{(2p+2)}\,{}^{2s}\bar{C}_{2n+2} + c_{2s+1}^{(2p+2)}\,{}^{2s+1}A_{2n+2} + d_{2s+1}^{(2p+2)}\,{}^{2s+1}\bar{C}_{2n+2}] + (2n+3)[a_{2s}^{(2p)}\,{}^{2s}A_{2n+2}' + b_{2s}^{(2p)}\,{}^{2s}\bar{C}_{2n+2}' + c_{2s+1}^{(2p)}\,{}^{2s+1}A_{2n+2}' + d_{2s+1}^{(2p)}\,{}^{2s+1}\bar{C}_{2n+2}']\}$$

$$c_{2n+1}^{(4n+2p+4)} = \sum_{s=0}^{p} \{2n\,[a_{2s}^{(2p+2)}\,{}^{2s}B_{2n+1} + b_{2s}^{(2p+2)}\,{}^{2s}\bar{D}_{2n+1} + c_{2s+1}^{(2p+2)}\,{}^{2s+1}B_{2n+1} + d_{2s+1}^{(2p+2)}\,{}^{2s+1}\bar{D}_{2n+1}] + (2n+1)[a_{2s}^{(2p)}\,{}^{2s}B_{2n+1}' + b_{2s}^{(2p)}\,{}^{2s}\bar{D}_{2n+1}' + c_{2s+1}^{(2p)}\,{}^{2s+1}B_{2n+1}' + d_{2s+1}^{(2p)}\,{}^{2s+1}\bar{D}_{2n+1}']\}$$

$$d_{2n+1}^{(4n+2p+6)} = -\sum_{s=0}^{p} \{(2n+3)[a_{2s}^{(2p+2)}\,{}^{2s}B_{2n+3} + b_{2s}^{(2p+2)}\,{}^{2s}\bar{D}_{2n+3} + c_{2s+1}^{(2p+2)}\,{}^{2s+1}B_{2n+3} + d_{2s+1}^{(2p+2)}\,{}^{2s+1}\bar{D}_{2n+3}] + (2n+4)[a_{2s}^{(2p)}\,{}^{2s}B_{2n+3}' + b_{2s}^{(2p)}\,{}^{2s}\bar{D}_{2n+3}' + c_{2s+1}^{(2p)}\,{}^{2s+1}B_{2n+3}' + d_{2s+1}^{(2p)}\,{}^{2s+1}\bar{D}_{2n+3}']\}$$

This solution is much easier than the successive approximation, one which requires troublesome calculations to determine the unknown constants. Though it is necessary to prove the convergency of Equations [30], we do not give it. But it may be seen later in the numerical equations that this method gives results to any required degree of approximation.

Numerical Examples

The numerical calculations have been carried out for the cases $\beta = 0.25, 0.50$, and 1.00. The values of σ_θ at the point $\theta = 0$ deg on the circle have been given for these three cases, and also the values of σ_θ along the periphery of hole have been given for $\beta = 1.0$ and λ varying from 0.1 to 0.5.

First, an evaluation of the integrals I_n', J_n', $\bar{I}_n$, and $\bar{J}_n$ is to be discussed, while the integrals I_n and J_n have been calculated by Howland (2). It may be shown that these integrals have the following asymptotic values

$$\left.\begin{aligned} I_n' &\sim n!\cos[(n+1)\tan^{-1}\beta]/2^n(1+\beta^2)^{\frac{n+1}{2}} \\ J_n' &\sim n!\cos[(n+1)\tan^{-1}\beta/2]/2^n(4+\beta^2)^{\frac{n+1}{2}} \\ I_n &\sim n!\sin[(n+1)\tan^{-1}\beta]/2^n(1+\beta^2)^{\frac{n+1}{2}} \\ J_n &\sim n!\sin[(n+1)\tan^{-1}\beta/2]/2^n(4+\beta^2)^{\frac{n+1}{2}} \end{aligned}\right\} \quad [32]$$

For larger values of n, Expressions [32] give a more rapid method than the numerical computation of the integrals. For n from 1 to 20 the values were obtained by direct computation. The integrals for values for u from 0 to 9 with intervals 0.25 were computed by Weddle's rule (6). The integrals for $u = 9$ to ∞ were computed by replacing Σ by $e^{2u}/2$. For $n = 19$, 20 both methods were used, and the results are in good agreement. For the case $\beta = 0.25$, the values of integrals were evaluated directly by the equation

$$\left.\begin{aligned} I_n' &= \sum_{q=0}^{\infty}(-)^q\frac{(2\beta)^{2q}}{(2q)!}I_{2q+n}, \qquad J_n' = \sum_{q=0}^{\infty}(-)^q\frac{(2\beta)^{2q}}{(2q)!}J_{2q+n} \\ I_n &= \sum_{q=0}^{\infty}(-)^q\frac{(2\beta)^{2q+1}}{(2q+1)!}I_{2q+n+1}, \qquad J_n = \sum_{q=0}^{\infty}(-)^q\frac{(2\beta)^{2q+1}}{(2q+1)!}J_{2q+n+1} \end{aligned}\right\} \quad [33]$$

Using these values of I_n', J_n', I_n, and J_n the coefficients in U_{2n}, V_{2n}', U_{2n+1}, V_{2n+1}' were calculated and finally the unknown constants a_{2n}, b_{2n}, c_{2n+1}, d_{2n+1} were determined. Then the stress σ_θ obtained using Equation [28] was expanded in series using Equations [30] and was calculated numerically. Tables of these values of the integrals and the constants for each case are omitted here, while some numerical expressions for σ_θ calculated by using these values are given.

The expression for σ_θ along the periphery of circular hole for $\beta = 1.0$ is

$$\begin{aligned} &\sigma_\theta(\beta = 1.0, \rho = \lambda)/T \\ &= 1 + 3.0886\times10^{-1}\lambda^2 + 1.3372\times10^{-1}\lambda^4 + 5.2888\times10^{-1}\lambda^6 - 2.1051\times10^{-1}\lambda^8 - 1.3834\lambda^{10} + 2.1715\lambda^{12} \\ &+ (2 + 2.4081\lambda^2 - 3.2896\times10^{-1}\lambda^4 + 3.6967\times10^{-1}\lambda^6 + 1.1930\times10\lambda^8 - 9.2089\lambda^{10} - 4.0372\times10\lambda^{12})\cos 2\theta \\ &+ (7.5712\lambda^4 - 3.4537\lambda^6 - 9.4489\lambda^8 + 3.8521\times10\lambda^{10} - 3.2907\times10\lambda^{12})\cos 4\theta \\ &+ (2.3239\lambda^6 - 4.2893\lambda^8 - 1.7242\lambda^{10} + 5.9716\times10\lambda^{12})\cos 6\theta \\ &+ (1.9970\lambda^8 - 3.1973\lambda^{10} - 3.3629\lambda^{12})\cos 8\theta \\ &+ (4.7858\times10^{-1}\lambda^{10} - 1.6276\lambda^{12})\cos 10\theta \\ &+ (3.4353\times10^{-1}\lambda^{12})\cos 12\theta \\ &+ (3.0440\times10^{-2}\lambda^3 + 3.4784\times10^{-1}\lambda^5 - 1.4803\lambda^7 - 3.8108\times10^{-1}\lambda^9 - 1.1021\lambda^{11})\sin\theta \\ &+ (2.0995\lambda^3 + 5.5643\times10^{-2}\lambda^5 + 2.5061\lambda^7 - 1.4693\times10\lambda^9 + 2.6903\times10\lambda^{11})\sin 3\theta \\ &+ (-1.8996\lambda^5 + 1.6870\times10^{-2}\lambda^7 + 1.3108\times10\lambda^9 - 1.4530\times10\lambda^{11})\sin 5\theta \\ &+ (5.8748\times10^{-1}\lambda^7 - 1.0223\times10^{-1}\lambda^9 + 5.5805\lambda^{11})\sin 7\theta \\ &+ (-2.5410\times10^{-1}\lambda^9 + 6.3811\times10^{-2}\lambda^{11})\sin 9\theta \\ &+ (1.3116\times10^{-1}\lambda^{11})\sin 11\theta \qquad [34] \end{aligned}$$

The expressions for σ_θ at the point $\theta = 0$ deg on the circle for $\beta = 0.25, 0.50, 1.00$ are

$$\begin{aligned} &\sigma_\theta(\beta = 1.0, \rho = \lambda, \theta = 0°)/T = 3.0 + 2.7170\lambda^2 + 7.3760\lambda^4 - 2.3129\times10^{-1}\lambda^6 - 2.1746\times10^{-2}\lambda^8 + 2.3486\times10\lambda^{10} - 1.5988\times10\lambda^{12} \qquad [35] \\ &\sigma_\theta(\beta = 0.5, \rho = \lambda, \theta = 0°)/T = 3.0 - 3.4614\lambda^2 + 5.3462\times10\lambda^4 - 1.8864\times10^2\lambda^6 + 1.4943\times10^3\lambda^8 + 1.1013\times10^3\lambda^{10} - 1.8262\times10^3\lambda^{12} \qquad [36] \\ &\sigma_\theta(\beta = 0.25, \rho = \lambda, \theta = 0°)/T = 3.0 - 2.6160\times10\lambda^2 + 9.9949\times10^2\lambda^4 - 1.7607\times10^4\lambda^6 + 1.2050\times10^5\lambda^8 + 3.0549\times10^5\lambda^{10} \qquad [37] \end{aligned}$$

TABLE 1 VALUES OF σ_θ/T AT RIM OF HOLE FOR $\beta = 1.0$

θ/λ deg	0.1	0.2	0.3	0.4	0.5
90	−1.02	−1.09	−1.19	−1.31	−1.45
75	−0.75	−0.81	−0.90	−1.02	−1.17
60	−0.01	−0.04	−0.10	−0.20	−0.35
45	1.00	1.01	1.02	0.99	0.90
30	2.02	2.07	2.16	2.28	2.41
15	2.76	2.85	3.01	3.29	3.72
0	3.03	3.12	3.30	3.63	4.17
−15	2.76	2.82	2.94	3.13	3.40
−30	2.01	2.04	2.05	2.02	1.91
−45	1.00	0.99	0.93	0.77	0.47
−60	−0.01	−0.04	−0.11	−0.24	−0.44
−75	−0.75	−0.79	−0.82	−0.83	−0.77
−90	−1.02	−1.05	−1.07	−1.01	−0.82

TABLE 2 VALUES OF σ_θ/T AT THE POINT $\theta = 0$ DEG ON THE PERIPHERY OF HOLE

β/λ	0	0.05	0.10	0.125	0.15	0.20	0.25	0.30	0.40	0.50
1.0	3.00	3.01	3.03	3.04	3.06	3.12	3.20	3.30	3.63	4.17
0.50	3.00	2.99	2.97	2.96	2.95	2.94	2.95	3.00	....	....
0.25	3.00	2.94	2.82	2.78	2.75	....	....	....	....	....

The results given by Equations [34] to [37] are shown in Tables 1 and 2. In Fig. 3 and Fig. 4, the values of σ_θ/T in the last two columns of Table 1 and the values of stress-concentration factor $\sigma_\theta(1-\lambda)/T$ calculated from the values in Table 2 are compared with those calculated by Howland (2) for the single circular hole which is shown in dotted lines. The relations between the values of σ_θ shown in Table 2 and those of $\lambda/2\beta$ are given in Fig. 5. Curves (I), (II), (III) in this figure show values given in a paper by C. B. Biezeno (7) on the stress in an infinite strip containing an infinite row of holes. (I) gives the stress for the infinite plate; (II) and (III) give the stresses for $\lambda = 0.2$ and 0.4. Further, the dot-dash curve gives the stress in an infinite plate containing two circular holes as given by Chih-Bing Ling (3). The relations between the stress-concentration factor and $\lambda/2\beta$ are given in Fig. 6, curves (I), (II), (III) being omitted.

Conclusions

From a consideration of the results given in this paper the following conclusions seem to be justified:

1 The values of stress-concentration factor for the case treated in this paper are smaller than the values for the case of a single hole of the same geometry given by Howland (2). This is shown in Fig. 4.

Further, as the two circular holes come close together, the values of the stress-concentration factor decrease. This is shown in Fig. 6.

2 Through the whole range of $\lambda < 0.15$ the rate of decrease of the stress-concentration factor with increase in $\lambda/2\beta$ is the same as in the case of an infinite plate containing two circular

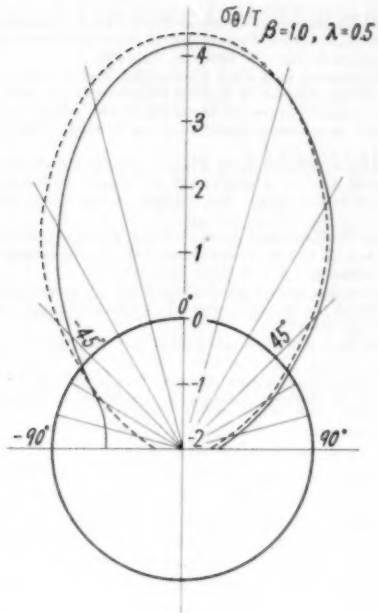

FIG. 3(a)

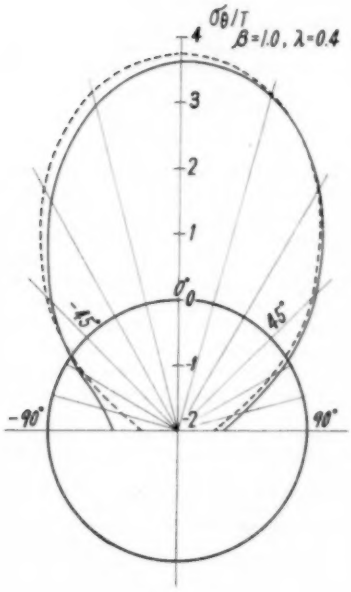

FIG. 3(b)

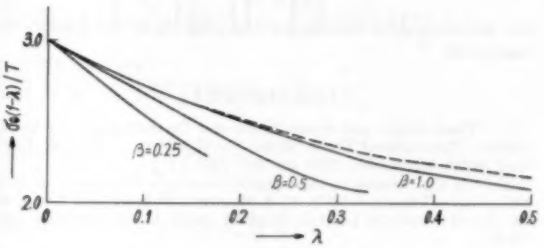

FIG. 4

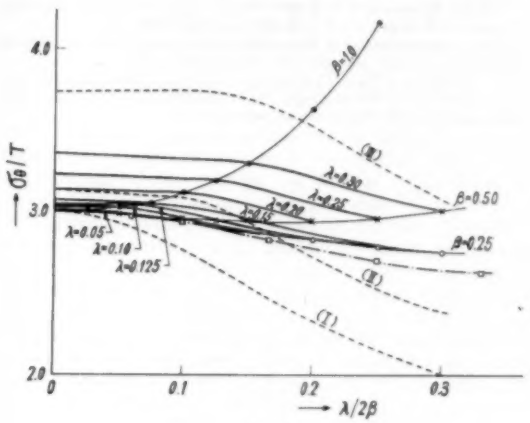

FIG. 5

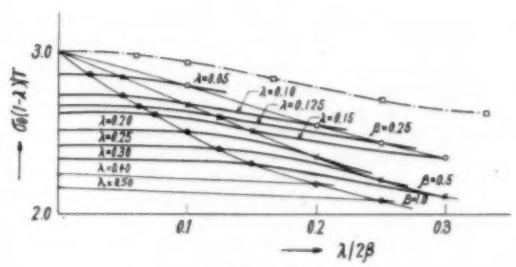

FIG. 6

holes. This means that the effect of the straight edges is negligible through this range (Fig. 6).

3 Through the range of $\lambda = 0.20 \sim 0.30$ the rate of decrease becomes larger than that just mentioned, especially at $\lambda = 0.20$, where it is the largest (Fig. 6).

4 Beyond this range, it seems that the rate of decrease of the stress-concentration factor again becomes lower. This shows that there is no considerable decrease provided that two holes are not too close together. This is probably due to the fact that the stress concentrations between the holes and the straight edges, which are near to each other when λ becomes large, cancel the decrease of the factors for $\lambda > 0.3$.

5 The decrease of the stress-concentration factor for the case of two holes considered here is smaller than for the case of a large number of circular holes (Fig. 5).

6 Stresses along the periphery near the other hole are smaller than those for a single hole as given by Howland (2), while the stresses along the other side of the periphery are larger. Therefore the points of maximum stress are found at positive θ $\doteqdot$ 0 deg at the edge of each hole (Fig. 3).

ACKNOWLEDGMENT

The author wishes to express his hearty thanks to Prof. Emeritus Seiichi Higuchi of the Tohoku University for his advice

and encouragement throughout the progress of the present investigation.

BIBLIOGRAPHY

1 "Plane Stress and Strain in Bipolar Co-Ordinates," by G. B. Jeffery, Philosophical Trans. of the Royal Society of London, England, series A, vol. 221, 1920, pp. 265–293.

2 "On the Stresses in the Neighborhood of a Circular Hole in a Strip Under Tension," by R. C. J. Howland, Philosophical Trans. of the Royal Society of London, England, series A, vol. 229, 1930, pp. 49–86.

"Bi-Harmonic Analysis in a Perforated Strip," by R. C. J. Howland and A. C. Stevenson, Philosophical Trans. of the Royal Society of London, England, series A, vol. 232, 1933, pp. 155–222.

"On the Stresses in a Perforated Strip," by R. C. Knight, *Quarterly Journal of Mathematics*, vol. 5, 1934, pp. 255–268.

"Photoelastic Studies in Stress Concentrations," by M. M. Frocht, *Mechanical Engineering*, vol. 58, 1936, pp. 485–489.

3 "Stress in a Plate Containing an Infinite Row of Holes," by R. C. J. Howland, Proceedings of the Royal Society of London, England, series A, vol. 148, 1935, pp. 471–491.

"General Bi-Harmonic Analysis for a Plate Containing Circular Holes," by A. E. Green, Proceedings of the Royal Society of London, England, series A, vol. 176, 1940, pp. 121–139.

"On the Stresses in a Plate Containing Two Circular Holes," by Chih-Bing Ling, *Journal of Applied Physics*, vol. 19, 1948, pp. 77–82.

"Stress Peaks in Perforated Metal Plates and Strips," by A. Hutter, *Zeitschrift für angewandte Mathematik und Mechanik*, vol. 22, 1942, pp. 322–335.

4 "Stress Functions for a Plate Containing Groups of Circular Holes," by R. C. J. Howland and R. C. Knight, Philosophical Trans. of the Royal Society of London, England, series A, vol. 238, 1939, pp. 357–392.

"General Bi-Harmonic Analysis for a Plate Containing Circular Holes," by A. E. Green, Proceedings of the Royal Society of London, England, series A, vol. 176, 1940, pp. 121–139.

5 "Stress Systems in an Infinite Strip," by R. C. J. Howland, Proceedings of the Royal Society of London, England, series A, vol. 124, 1929, pp. 89–119.

6 "The Calculus of Observations," by Whittaker and Robinson, 175.

7 "Survey of Papers on Elasticity Published in Holland 1940–1946," by C. B. Biezeno, *Advances in Applied Mechanics*, vol. 1, 1948 pp. 105–170.

Three-Dimensional and Shell-Theory Analysis of Axially Symmetric Motions of Cylinders[1]

By GEORGE HERRMANN[2] and I. MIRSKY,[3] NEW YORK, N. Y.

The frequency (or phase velocity) of axially symmetric free vibrations in an elastic, isotropic, circular cylinder of medium thickness is studied on the basis of the three-dimensional linear theory of elasticity and several different shell theories. To be in good agreement with the solution of the three-dimensional equations for short wave lengths, an approximate theory has to include the influence of rotatory inertia and transverse shear deformation, for example, in a manner similar to Mindlin's plate theory. A shell theory of this (Timoshenko) type is deduced from the three-dimensional elasticity theory. From a comparison of phase velocities it appears that, to a good approximation, membrane and curvature effects on one hand, and on the other hand, flexural, rotatory-inertia, and shear-deformation effects are mutually exclusive in two ranges of wave lengths, separated by a "transition" wave length. Thus, in the full range of wave lengths, the associated lowest phase velocities may be determined on the basis of the membrane shell theory (for wave lengths larger than the transition wave length) and on the basis of Mindlin's plate theory (for wave lengths smaller than the transition wave length).

Introduction

In the course of reconsideration and refinement of proposed theories of shells, in particular that of Love (1),[4] various objections have been raised as to the method of deriving a shell theory and the resulting equations. It was emphasized by Vlasov (2), for example, that certain shell theories are in contradiction to the principle of conservation of energy and, also, that the approximations, introduced in the course of the development, are sometimes dealt with subsequently in a nonconsistent manner.

Systematic procedures for deducing shell theories of various degrees of accuracy, starting from three-dimensional equations, were discussed by a number of authors; for example, Hildebrand, Reissner, and Thomas (3), and by Kennard (4, 5). The latter based his development on the work of Epstein (6).

Several such theories have been compared with one another recently by Naghdi and Berry (7) in a qualitative manner. However, solutions obtained by different shell theories should be compared not only on a relative basis, but also with solutions of the three-dimensional equations of elasticity.[5] The present paper is intended to be a first contribution in this direction and, naturally the simplest problem possible was selected for consideration; namely, that of free motions in an infinite shell.

Longitudinal motions of a cylinder on the basis of the three-dimensional theory were first considered by Ghosh (10), however, without numerical evaluation or any discussion. Recently, an analysis of traveling waves in a circular cylinder on the basis of the same theory was carried out by Fay (11). His results were not used, however, because it was noticed that an error was committed in his development. Thus the derivation of the frequency equation is briefly outlined in the first section of this paper. A discussion of the transition to the two limiting cases of a flat plate [Rayleigh-Lamb solution (12, 13)] and of a solid rod [Pochhammer solution (14)], is taken up by the present authors in a separate paper (15).

Free motions in a cylinder using shell theories were analyzed by Rayleigh (16), and more recently by Baron and Bleich (17) and by Junger and Rosato (18). Since only membrane effects or, in addition, bending effects were taken into account, the results cannot be expected to be valid for the full frequency range, that is, for very short wave lengths. Lin and Morgan (19), therefore, took account of rotatory inertia and transverse-shear effects. Their study, however, does not contain any comparison between the approximate and exact solutions. In addition, their equations were derived in a different manner than those established in the present paper. They are similar, but not identical to those advanced presently. This difference arises from the fact that Lin and Morgan considered from the start a shell element, while the authors employed the basic relations of the three-dimensional theory of elasticity.

Being guided by the work of Mindlin (20) in the theory of plates, an analogous shell theory was deduced for axially symmetric motions in a cylinder from the three-dimensional theory of elasticity. Thus, in addition to the terms of "classical" shell theories, the effect due to transverse-shear deformation, introduced previously into more general shell equations (3), and the effect of rotatory inertia are included.

---

[1] This investigation was supported by the United States Air Force, through the Office of Scientific Research of the Air Research and Development Command, under Contract AF 18(600)-1247.

[2] Associate Professor of Civil Engineering, Institute of Flight Structures, Columbia University. Mem. ASME.

[3] Research Staff, Department of Civil Engineering and Engineering Mechanics, Columbia University.

[4] Numbers in parentheses refer to the Bibliography at the end of the paper.

Presented at the National Applied Mechanics Division Conference, Urbana, Ill., June 14–16, 1956, of The American Society of Mechanical Engineers.

Discussion of this paper should be addressed to the Secretary, ASME, 29 West 39th Street, New York, N. Y., and will be accepted until January 10, 1957, for publication at a later date. Discussion received after the closing date will be returned.

Note: Statements and opinions advanced in papers are to be understood as individual expressions of their authors and not those of the Society. Manuscript received by ASME Applied Mechanics Division, January 9, 1956. Paper No. 56—APM-32.

[5] Reviewing recently a controversial paper by Hwang (8) on the subject of shell theories, where the correctness of various approaches was questioned, Truesdell (9) appraised the situation by stating that in his opinion "all work on this subject is purely formal, and the various results obtained by different perturbation processes cannot be shown to be right or wrong by the *a priori* arguments always employed. What is lacking is a mathematical theorem making precise the status of solutions of any given set of proposed equations with respect to corresponding solutions of the three-dimensional theory."

Computations of the lowest wave velocity as a function of the wave length were made for a shell of thickness-to-radius ratio of 1/30 and Poisson's ratio $\nu = 0.30$. It was found that excellent agreement between the approximate and the exact solution may be reached for the full frequency range by including in a shell theory all the effects mentioned above.

Two fairly distinct types of shell behavior were established. For wave lengths larger than a certain transition (relative) length, the membrane theory gives good results. For wave lengths smaller than this transition length, the shell behaves essentially like a plate and, for good results, calls for inclusion of bending, transverse-shear deformation, and rotatory-inertia effects. Thus the use of a shell-bending theory is not advantageous in this connection. In the full frequency range, vibrations of a shell may be described with good accuracy by the membrane theory and by Mindlin's plate theory.

Since interest concentrated at present on free-vibration solutions, no attention was given to terms arising from external loading and no energy functions were constructed, which would permit the establishment of necessary initial and boundary conditions. Furthermore, attention was restricted to the lower mode only, and no mode shapes were investigated.

Three-Dimensional Theory

The circular cylindrical shell of inner radius a and outer radius b is referred to cylindrical co-ordinates r, θ, x, the x-axis coinciding with the axis of the shell. In the case of axially symmetric motions and for a homogeneous, isotropic shell material obeying Hooke's law, the linear elasticity equations of motion may be given in the form

$$\left.\begin{aligned}(\lambda + 2\mu)\frac{\partial \Delta}{\partial r} + 2\mu\frac{\partial \omega_\theta}{\partial x} &= \rho\frac{\partial^2 u_r}{\partial t^2}\\ (\lambda + 2\mu)\frac{\partial \Delta}{\partial x} - \frac{2\mu}{r}\frac{\partial}{\partial r}(r\omega_\theta) &= \rho\frac{\partial^2 u_x}{\partial t^2}\end{aligned}\right\} \quad \ldots\ldots [1]$$

where u_r, u_x are the displacement components and Δ, ω_θ are dilatation and rotation components, respectively

$$\Delta = \frac{1}{r}\frac{\partial (ru_r)}{\partial r} + \frac{\partial u_x}{\partial x} \quad \ldots\ldots [2]$$

$$\omega_\theta = \frac{1}{2}\left(\frac{\partial u_r}{\partial x} - \frac{\partial u_x}{\partial r}\right) \quad \ldots\ldots [3]$$

λ, μ are Lamé's constants and ρ is the mass density.

Since the shell is assumed to be free from surface tractions, the boundary conditions, to be imposed on the cylindrical surfaces of the shell, are as follows:

For $r = a, b$

$$\left.\begin{aligned}\lambda\Delta + 2\mu\frac{\partial u_r}{\partial r} &= 0\\ \mu\left(\frac{\partial u_r}{\partial x} + \frac{\partial u_x}{\partial r}\right) &= 0\end{aligned}\right\} \quad \ldots\ldots [4]$$

Assuming the motion to be harmonic, the Equations of Motion [1], together with the Boundary Conditions [4], give rise to a characteristic equation of the form

$$\begin{aligned}f(K) = {} & [K_{10}(\beta)K_{01}(\gamma) + K_{01}(\beta)K_{10}(\gamma) + (8/\pi^2\beta\gamma ab)\\ & + FK_{11}(\gamma)K_{00}(\beta) + (1/F)K_{11}(\beta)K_{00}(\gamma)]\\ & + [(1 + \bar{B})^2/F\gamma^2 ab]K_{11}(\beta)K_{11}(\gamma)\\ & -[(1 + \bar{B})/\gamma ab][aK_{11}(\gamma)K_{10}(\beta) + bK_{11}(\gamma)K_{01}(\beta)]\\ & -[(1 + \bar{B})/F\gamma ab][aK_{11}(\beta)K_{10}(\gamma) + bK_{11}(\beta)K_{01}(\gamma)]\\ & = 0 \quad \ldots [5]\end{aligned}$$

where

$$\left.\begin{aligned}K_{mn}(z) &= J_m(zb)Y_n(za) - J_n(za)Y_m(zb)\\ \beta^2 &= \alpha^2\left(\frac{c^2}{c_c^2} - 1\right)\\ \gamma^2 &= \alpha^2\left(\frac{c^2}{c_s^2} - 1\right)\\ \bar{B} &= \frac{c^2}{2c_s^2} - 1\\ F &= \frac{\alpha^2\bar{B}^2}{\beta\gamma}\\ c_c^2 &= (\lambda + 2\mu)/\rho\\ c_s^2 &= \mu/\rho\end{aligned}\right\} \quad \ldots\ldots [6]$$

In these relations α is the wave number and J_m, Y_m are Bessel functions, in the notation of Watson (21). It may be of interest to note that the last three terms of the characteristic Equation [5] appear to have been omitted by Fay (11).

Let c designate the phase velocity, L the wave length, and h the thickness of the shell. Solving Equation [5], the phase velocity $s = \frac{c}{c_s}$ versus $\delta = h/L$ (with Poisson's ratio $\nu = 0.3$) is plotted as curve ① in Fig. 1.

The limiting velocities may be evaluated directly from Equation [5] by a limiting process. For very long waves, $\delta \to 0$, the limiting velocity is found to be $s^2 = 2(1 + \nu)$, that is, $c^2 = E/\rho$. This is the "bar" velocity as given by the elementary bar theory and obtained by Pochhammer (14) for the analogous limiting case in his study of motion of solid cylinders (see also reference 22). For very short waves, $\delta \to \infty$, and the limiting velocity is the root of

$$\sqrt{[(n^2 - s^2)(1 - s^2)]} = n(s^2/2 - 1)^2 \; 0 < s < 1 \ldots [7]$$

where

$$n^2 = 2(1 - \nu)/(1 - 2\nu) \quad \ldots\ldots [8]$$

Expression [7] is the equation for the velocity of Rayleigh surface waves. Thus very short waves are propagated in the shell with the same velocity as in a plate, the latter case having been investigated by Lamb (13).

Approximate Shell Theories

In the theory of shells, it is customary to employ a co-ordinate system, formed by two axes in the middle surface of the shell and the third axis normal to the middle surface. Thus the co-ordinates will now be taken as x, θ, z, x being still in the axial direction of the cylindrical shell and the new z-co-ordinate being

$$z = r - R \quad \ldots\ldots [9]$$

where $R = (a + b)/2$ is the mean radius of the shell.

Stress Equations of Motion. For the case of axial symmetry, the stress equations of motion may then be written as

$$\left.\begin{aligned}\frac{\partial \sigma_{xx}}{\partial x} + \frac{\partial \sigma_{zx}}{\partial z} + \frac{\sigma_{zx}}{R + z} &= \rho\frac{\partial^2 u_x}{\partial t^2}\\ \frac{\partial \sigma_{xz}}{\partial z} + \frac{\partial \sigma_{zz}}{\partial x} + \frac{\sigma_{zz} - \sigma_{\theta\theta}}{R + z} &= \rho\frac{\partial^2 u_z}{\partial t^2}\end{aligned}\right\} \quad \ldots\ldots [10]$$

The displacements u_z, u_x of the three-dimensional theory are now approximated by $\bar{u}_z$, $\bar{u}_x$, which are taken in the form

$$\left.\begin{aligned} \hat{u}_x &= u(x, t) + z\psi_x(x, t) \\ \hat{u}_z &= w(x, t) \end{aligned}\right\} \quad \ldots\ldots\ldots\ldots [11]$$

The shell stress equations of motion are obtained by substituting $\hat{u}_x$, $\hat{u}_z$ for u_x, u_z respectively, in Equations [10], multiplying the first and the second by $(R + z)$ and the second of Equations [10] by $z(R + z)$ and integrating through the shell thickness h. The justification for this multiplication stems from energy considerations. The resulting equations are

$$\left.\begin{aligned} N_{xx}' &= \rho h\left(\ddot{u} + \frac{h^2}{12R}\ddot{\psi}_x\right) \\ Q_x' - \frac{1}{R}N_{\theta\theta} &= \rho h\ddot{w} \\ M_{xx}' - Q_x &= \frac{\rho h^3}{12}\left(\ddot{\psi}_x + \frac{1}{R}\ddot{u}\right) \end{aligned}\right\} \quad \ldots\ldots [12]$$

where use has been made of the fact that the shell is free from surface tractions. Primes and dots indicate differentiation with respect to x and t, respectively.

The stress resultants (or shell stresses) are defined by the following integrals

$$\left.\begin{aligned} N_{xx} &= \int_{-h/2}^{h/2} \sigma_{xx}\left(1 + \frac{z}{R}\right) dz \\ N_{\theta\theta} &= \int_{-h/2}^{h/2} \sigma_{\theta\theta}\, dz \\ Q_x &= \int_{-h/2}^{h/2} \sigma_{xz}\left(1 + \frac{z}{R}\right) dz \\ M_{xx} &= \int_{-h/2}^{h/2} \sigma_{xx}\left(1 + \frac{z}{R}\right) z dz \end{aligned}\right\} \quad \ldots\ldots [13]$$

In case of equilibrium, Equations [12] represent a special case of a more general shell theory, deduced by Hildebrand, Reissner, and Thomas (3). If the radius of curvature R tends to infinity, that is, if the shell approaches a flat plate, the last two equations reduce to those derived by Mindlin (20), which govern flexural motions of plates, including the influence of rotatory inertia and shear deformation. The first equation represents longitudinal motions of the plate, which are not coupled to flexural motions. The terms with ρh^3 represent the influence of rotatory inertia.

Stress-Displacement Relations. The relation between the shell stresses, defined by the Set [13] and shell displacements, introduced by Equations [11], may be derived from the stress-strain relations of an isotropic three-dimensional solid obeying Hooke's law. Eliminating the component of normal strain in the radial direction e_{zz} the stress-strain relations for the other two normal stress components may be written in the form

$$\left.\begin{aligned} \sigma_{xx} &= \frac{E}{(1 - \nu^2)}\left[e_{xx} + \nu e_{\theta\theta}\right] + \frac{\nu}{1 - \nu}\sigma_{zz} \\ \sigma_{\theta\theta} &= \frac{E}{(1 - \nu^2)}\left[e_{\theta\theta} + \nu e_{xx}\right] + \frac{\nu}{1 - \nu}\sigma_{zz} \end{aligned}\right\} \quad \ldots\ldots [14]$$

This procedure is justified by observing that e_{zz} would vanish on the basis of the form given for the transverse displacement w. On the other hand, unrestrained Poisson's ratio effect will take place in the z-direction in an actual shell. These two mutually exclusive requirements may be reconciled, by eliminating e_{zz} from the stress-strain relations in the manner described previously.

In addition to the normal stresses, the shear stress σ_{xz} is needed, which is related to the shear deformation γ_{xz} by

$$\sigma_{xz} = G\gamma_{xz} \quad \ldots\ldots [15]$$

where G is the shear modulus.

With the aid of the strain-displacement relations

$$\left.\begin{aligned} e_{xx} &= \frac{\partial u_x}{\partial x} \\ e_{\theta\theta} &= u_x/(R + z) \\ \gamma_{xz} &= \frac{\partial u_z}{\partial x} + \frac{\partial u_x}{\partial z} \end{aligned}\right\} \quad \ldots\ldots [16]$$

the approximate strains are evaluated using Assumptions [11]. These strains are then substituted in the stress-strain Relations [14], [15] and integrations are carried out as specified by the Forms [13]. The results are modified in three respects: (*a*) The integrals containing σ_{zz} are omitted, just as in the classical beam or plate theories; (*b*) the integral containing σ_{xz} is multiplied by a constant κ^2 (the shear coefficient), to be determined later; (*c*) logarithmic terms occurring in the integration are expanded in series of ascending powers of h/R, and terms higher than the cubic one are neglected. The resulting shell stress-dispacement relations are

$$\left.\begin{aligned} N_{xx} &= \frac{Eh}{(1 - \nu^2)}\left[u' + \nu\frac{w}{R} + \frac{h^2}{12R}\psi_x'\right] \\ N_{\theta\theta} &= \frac{Eh}{(1 - \nu^2)}\left[\nu u' + \frac{w}{R}\left(1 + \frac{h^2}{12R^2}\right)\right] \\ Q_x &= \kappa^2 Gh[\psi_x + w'] \\ M_{xx} &= D\left[\psi_x' + \frac{u'}{R}\right] \end{aligned}\right\} \quad \ldots [17]$$

where $D = Eh^3/12(1 - \nu^2)$ is the plate flexural modulus.

Substituting the stress-displacement Relations [17] into the stress Equations of Motion [12], displacement equations of motion are obtained, which may be put into the form

$$\left.\begin{aligned} &\left[\frac{D\partial^2}{\partial x^2} - \kappa^2 Gh - \rho I\frac{\partial^2}{\partial t^2}\right]\psi_x - \left[\kappa^2 Gh\frac{\partial}{\partial x}\right]w \\ &\qquad + \left[\frac{D}{R}\frac{\partial^2}{\partial x^2} - \frac{\rho I}{R}\frac{\partial^2}{\partial t^2}\right]u = 0 \\ &-\left[\kappa^2 Gh\frac{\partial}{\partial x}\right]\psi_x + \left[\frac{E_p}{R^2} + \frac{D}{L^4} - \kappa^2 Gh\frac{\partial^2}{\partial x^2}\right. \\ &\qquad \left. + \rho h\frac{\partial^2}{\partial t^2}\right]w + \left[E_p\frac{\nu}{R}\frac{\partial}{\partial x}\right]u = 0 \\ &\left[\frac{D}{R}\frac{\partial^2}{\partial x^2} - \frac{\rho I}{R}\frac{\partial^2}{\partial t^2}\right]\psi_x + \left[E_p\frac{\nu}{R}\frac{\partial}{\partial x}\right]w \\ &\qquad + \left[E_p\frac{\partial^2}{\partial x^2} - \rho h\frac{\partial^2}{\partial t^2}\right]u = 0 \end{aligned}\right\} \quad \ldots [18]$$

$I = h^3/12$ is the moment of inertia, and $E_p = Eh/(1 - \nu^2)$ is the plate compressional modulus.

This form is convenient for the discussion of the physical significance of the various terms influencing the motion. There are

three stiffnesses involved, D representing the influence of flexural, E_p of compressional, and G of transverse-shear stiffness, respectively. In addition, there are three inertia terms involved, ρI representing the influence of rotatory inertia, ρh in the second equation representing transverse inertia, and ρh in the third equation representing longitudinal inertia. The nature of the coupling effects is apparent from inspection of Equations [18].

For a thin shell, terms with D/R and I/R may be omitted. The suppression of flexural stiffness and rotatory-inertia effects implies the assumption of a thin shell, but not vice versa, because in the first bracket of the first Equation [18], D and I-terms are unaffected by the curvature $1/R$. For a thin shell, there is no direct coupling between ψ_x and u. Going one step further, the shell can be made to approach a flat plate, $R \to \infty$. The first two equations reduce to Mindlin's plate theory (20) and the last, not coupled to the first two, is the classical equation for compressional motions in a plate.

Wishing to suppress the influence of transverse shear, we may not set the terms with G simply equal to zero, because these terms represent the transverse-shear force, while we wish to neglect the transverse-shear deformation. This is effected by setting $\psi_x = -w'$. There will be thus only two displacement components left and the terms with G and ψ_x may be eliminated. The result is

$$\left.\begin{aligned}&\left[D\frac{\partial^4}{\partial x^4} + \frac{D}{R^4} + \frac{E_p}{R^2} + \rho h\frac{\partial^2}{\partial t^2} - \rho I\frac{\partial^4}{\partial x^2\partial t^2}\right]w \\ &\quad + \left[\frac{-D}{R}\frac{\partial^3}{\partial x^3} + \frac{E_p\nu}{R}\frac{\partial}{\partial x} + \frac{\rho I}{R}\frac{\partial^3}{\partial x\partial t^2}\right]u = 0 \\ &\left[\frac{-D}{R}\frac{\partial^3}{\partial x^3} + \frac{E_p\nu}{R}\frac{\partial}{\partial x} + \frac{\rho I}{R}\frac{\partial^3}{\partial x\partial t^2}\right]w \\ &\quad + \left[E_p\frac{\partial^2}{\partial x^2} - \rho h\frac{\partial^2}{\partial t^2}\right]u = 0\end{aligned}\right\} \quad [19]$$

In these equations, the stiffness terms are those of the bending theory of shells; see, for example, Flügge (23) or Vlasov (2). For thin shells, we may again set $D/R = 0, I/R = 0$. If the rotatory-inertia term is neglected and the transition to a flat plate is performed, $R \to \infty$, the two motions in w and u again become uncoupled. The motion of w will be governed by the classical bending theory of plates and the motion of u will be again that of classical compression theory. If, instead, the rotatory-inertia term and the flexural stiffness term are neglected, in Equation [19] we obtain the familiar membrane theory of shells.

Wave Solutions. We consider again free harmonic motions and seek solutions of shell equations in the form

$$\left.\begin{aligned}\psi_x(x, t) &= \Psi e^{i(\omega t - \alpha x)} \\ w(x, t) &= We^{i(\omega t - \alpha x)} \\ u(x, t) &= Ue^{i(\omega t - \alpha x)}\end{aligned}\right\} \quad [20]$$

The natural frequency ω and the wave number α are related to the phase velocity c, by $\omega = 2\pi c/L$, $\alpha = 2\pi/L$ where L is the wave length. Introducing, further, the notation $m = h/R$, $N = 1/(1-\nu)$, and substituting Forms [20] into the shell Equations [18], the characteristic equation is calculated to be

$$\left.\begin{aligned}&\frac{1}{3}s^2(2N - s^2)^2\left[4\pi^2\kappa^2\delta^2 - 4\pi^2 s^2\delta^2 + 2Nm^2\left(1 + \frac{m^2}{12}\right)\right]\left(1 - \frac{m^2}{12}\right) \\ &+ (2N - s^2)\left[\frac{2N}{\pi^2}\kappa^2 m^2\left(1 + \frac{m^2}{12}\right) - 4\kappa^2 s^2\delta^2 - \frac{4}{3}\nu\kappa^2 N\delta^2 m^2 - \frac{4}{3}\nu^2 N^2\delta^2 m^2\right] \\ &- 4\frac{N^2\nu^2}{\pi^2}\kappa^2 m^2 = 0\end{aligned}\right\} \quad [21]$$

There are thus three roots for s^2, but attention will be given only to the smallest one. In the whole range, $0 < \delta < \infty$, the values obtained differed only slightly from those obtained by the solution of three-dimensional equations, and cannot be observed on the scale of Fig. 1. Thus curve ① in Fig. 1 represents also a solution of Equation [21]. Numerically, largest discrepancies between the two solutions were obtained in the neighborhood of the minimum value, which may be due to a coupling effect with purely radial vibrations. The limiting velocities may be evalu-

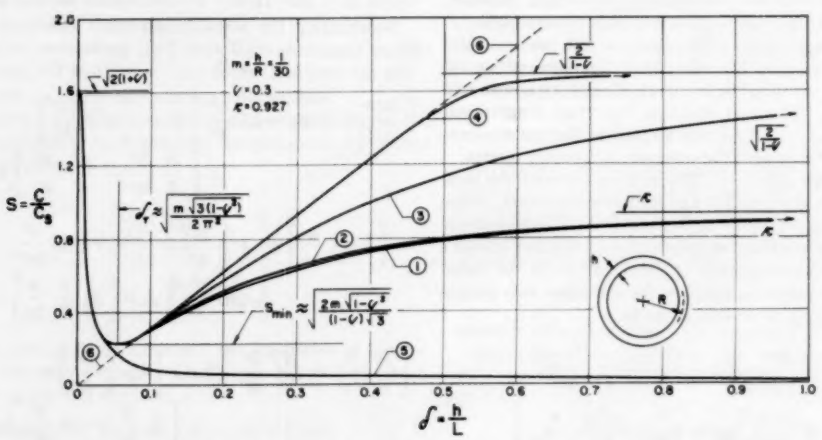

FIG. 1 AXIAL PHASE VELOCITY (LOWEST MODE) AS A FUNCTION OF WAVE LENGTH

① Exact solution of three-dimensional equation, and present shell theory (including membrane, bending, rotatory, inertia, and shear deformation effects)
② Present shell theory, neglecting rotatory-inertia effect
③ Present shell theory, neglecting shear-deformation effect
④ Shell bending theory
⑤ Shell membrane theory
⑥ Classical plate theory

ated directly from Equation [21]. For very long waves, $\delta \to 0$, the limiting velocity is

$$s^2 = \left[2(1+\nu) + \frac{m^2}{6(1-\nu)}\right] \Big/ \left(1 + \frac{m^2}{12}\right) \ldots\ldots [22]$$

If m is small as compared to unity, as in the present case

$$s^2 = 2(1+\nu) \ldots\ldots [23]$$

which coincides with the exact solution, given by the limit of Equation [5]. For very short waves, $\delta \to \infty$, Equation [21] reduces to

$$(2N - s^2)^2(\kappa^2 - s^2) = 0 \ldots\ldots [24]$$

whatever the shell parameter m.

The double root $s^2 = 2N$ belongs to the two higher modes and will not be discussed in the present paper. The root $s^2 = \kappa^2$ belongs to the lower mode and the coefficient κ may now be determined, precisely as in Mindlin's plate theory (20), by matching the velocity obtained in the foregoing with that obtained from a solution of the three-dimensional theory given by Equation [7]. An appropriate value of κ^2 is therefore the lowest root of

$$\sqrt{[(n^2 - \kappa^2)(1 - \kappa^2)]} = n\left(\frac{1}{2}\kappa^2 - 1\right)^2 \quad 0 < \kappa < 1. [25]$$

Thus, κ^2 depends upon Poisson's ratio ν and ranges from $\kappa^2 = 0.76$ for $\nu = 0$ to $\kappa^2 = 0.91$ for $\nu = 0.5$. For $\nu = 0.3$, $\kappa^2 = 0.86$. As $m \to 0$, the shell approaches a flat plate and Equation [21] reduces, in part, to the one obtained by Mindlin (20).

Neglecting Rotatory Inertia. Omitting now the terms with ρI in Equations of Motion [18], the wave Solutions [20] lead to the characteristic equation

$$\begin{aligned}(2N - s^2)\Big[&\frac{8}{3}N\kappa^2\pi^4\delta^4 - \frac{8}{3}N\pi^4\delta^4 s^2 - 4\pi^2\kappa^2 s^2\delta^2 \\ &+ 2N\kappa^2 m^2 + \frac{4}{3}N^2\pi^2\delta^2 m^2\left(1 + \frac{m^2}{12}\right)\Big] \\ + \Big[&\frac{4}{9}N^2\pi^4\delta^4(s^2 - \kappa^2)m^2 - \frac{2}{9}N^2\pi^2\delta^2 m^4\left(1 + \frac{m^2}{12}\right) \\ - &\frac{8}{3}N^2\nu\kappa^2\pi^2\delta^2 m^2 - 4\nu^2 N^2\kappa^2 m^2 - \frac{8}{3}\nu^2 N^2\pi^2\delta^2 m^2\Big] = 0 \ldots. [26]\end{aligned}$$

Its solution is plotted as curve ② in Fig. 1. For long waves, $(\delta \to 0)$, $s^2 = 2(1+\nu)$, and for short waves $(\delta \to \infty)$, $s^2 = \kappa^2$. As $m \to 0$, Equation [26] reduces, in part, to the corresponding case of a flat plate, discussed by Mindlin (20).

Neglecting Shear Deformation. Using Equations of Motion [19], the membrane effect, flexural stiffness, and rotatory inertia are included. The motion will consist of just two modes and the characteristic equation is

$$\begin{aligned}(2N - s^2)\Big[&-\frac{8}{3}\pi^4 N\delta^4 + \frac{2}{9}\pi^4 N\delta^4 m^2 \\ &+ \frac{4}{3}\pi^4 s^2\delta^4 - \frac{1}{9}\pi^4 m^2 s^2\delta^4 + 4\pi^2 s^2\delta^2 \\ &+ \frac{2}{3}N\nu\pi^2\delta^2 m^2 - 2Nm\left(1 + \frac{m^2}{12}\right)\Big] \\ &+ 2\nu N m^2\left[\frac{2}{3}\pi^2 N\delta^2 - \frac{\pi^2}{3}s^2\delta^2 + 2\nu N\right] = 0 \ldots\ldots [27]\end{aligned}$$

The solution of Equation [27] is plotted as curve ③ in Fig. 1. For long waves $(\delta \to 0)$ the lower velocity is

$$s^2 = \left[2(1+\nu) + \frac{m^2}{6(1-\nu)}\right] \Big/ \left(1 + \frac{m^2}{12}\right) \ldots\ldots [28]$$

which reduces to $s^2 = 2(1+\nu)$ if m is small. For short waves $(\delta \to \infty)$ the lower wave velocity is $s^2 = 2/(1-\nu)$ which is identical to the one obtained by Mindlin (20) in the corresponding case, and is much too large as compared to the Rayleigh wave velocity. If $m = 0$, again Mindlin's corresponding result for a flat plate is obtained.

Bending Theory. The bending theory of shells, Equations [19], with $I = 0$, leads to the characteristic equation

$$\begin{aligned}(2N - s^2)&\left[4\pi^2 s^2\delta^2 - 2Nm^2\left(1 + \frac{m^2}{12}\right) - \frac{8}{3}N\pi^4\delta^4\right] \\ &+ 4N^2 m^2\left(\nu + \pi^2\frac{\delta^2}{3}\right)^2 = 0 \ldots\ldots [29]\end{aligned}$$

whose solution is plotted as curve ④ in Fig. 1. For long waves the lower limiting velocity is

$$s^2 = \left[2(1+\nu) + \frac{m^2}{6(1-\nu)}\right] \Big/ \left(1 + \frac{m^2}{12}\right) \ldots\ldots [30]$$

which simplifies, for small m, to $s^2 = 2(1+\nu)$. For short waves $(\delta \to \infty)$

$$s^2 = \frac{2}{1-\nu} - \frac{m^2}{6(1-\nu)}$$

which simplifies for small m to $s^2 = 2/(1-\nu)$. With $m = 0$, Equation [29] reduces, in part, to the result of the classical plate theory.

Membrane Theory. The classical membrane theory of shells gives rise to the characteristic equation

$$2\pi^2 s^4\delta^2 - 4N\pi^2 s^2\delta^2 - Ns^2 m^2 + 2Nm^2(1+\nu) = 0 \ldots [31]$$

which still contains two modes. The solution of Equation [31] is plotted as curve ⑤ in Fig. 1. For long waves $(\delta \to 0)$ the lower mode has a velocity $s^2 = 2(1+\nu)$ and for short waves $(\delta \to \infty)$ the lower mode has a vanishing velocity.

Discussion of Results

The essential results of the present study are visible from Fig. 1. The important conclusion which can be drawn is to the effect that it is possible to deduce a relatively simple shell theory, which predicts for the full range of wave lengths practically the same phase velocities of propagated waves (or frequencies of free vibration), as the three-dimensional theory.

Furthermore, it is seen that, for large wave lengths, $\delta < 0.035$, the elementary membrane shell theory, as expected, yields good results. From this value on, that is, if the wave length L is smaller than the mean radius of the shell R [since $\delta = (h/R)(R/L)$ and h/R was taken as 1/30], the shell bending theory must be used, which predicts a minimum of the phase velocity. An approximate value for this minimum may be obtained by observing that since bending is important in this region the effect of axial inertia may be neglected.

The minimum velocity is then found to be

$$s_{\min}^2 = \frac{2m\sqrt{1-\nu^2}}{(1-\nu)\sqrt{3}} \ldots\ldots [32]$$

and the corresponding value of δ is

$$\delta_T^2 = \frac{m\sqrt{3(1-\nu^2)}}{2\pi^2} \ldots\ldots [33]$$

which gives

$$\frac{L^2}{R^2} = m\,\frac{2\pi^2}{\sqrt{3(1-\nu)^2}} \qquad [34]$$

The expression for the minimum velocity, suggested by Junger and Rosato (18), differs markedly from the one given by Equation [32]. For wave lengths larger than those given by Equation [33], that is, if L is smaller than, say, twice the radius R, the curvature terms are practically of no importance and the shell behaves like a flat plate, but rotatory inertia and, much more so, transverse-shear-deformation effects become very significant.

In summarizing, it may be stated that in propagating a harmonic wave, a thin shell behaves in a different manner in two regions, depending upon whether the wave length is smaller or larger than the transition length given by Equation [34].

For wave lengths larger than the transition length, the shell may be well described by the membrane theory, because all bending effects are negligible and curvature terms are predominant. For wave lengths smaller than the transition length, the shell behaves like a flat plate, since curvature terms become negligible. Thus it appears that actually in the problem on hand, no advanced shell theory is necessary. The full range may be described by the membrane shell theory (for large wave lengths) and by the Mindlin plate theory (for short wave lengths).

An analogous behavior occurs in hydrodynamics for the case of capillary waves taking gravity into account (24). For small wave lengths, the motion is governed by cohesion, while for larger wave lengths gravity preponderates. Both the separate and joint effects of these forces lead qualitatively to the same velocity-wave length curves as in the present case.

The existence of a minimum may be made plausible physically by observing that as the wave length becomes smaller the contribution of radial displacements to the motion becomes larger and therefore the coupling with purely radial vibrations becomes stronger, exhibiting in the minimum a certain resonance effect. After a further decrease of wave length, the motion becomes essentially flexural and the coupling gets weaker. A certain improvement of the shell theory offered in this paper may be achieved, by matching the frequency of purely radial vibrations obtained from the present theory, with the one determined by McFadden from the three-dimensional theory (25). This would necessitate the appropriate introduction of an additional constant in the stress-displacement Relations [17] of the present shell theory, which would play a role similar to the constant κ^2.

In conclusion, it should be emphasized that the foregoing remarks are valid only for lower phase velocities and are not necessarily true for velocities of higher modes, mode shapes, stress in the shell, or group velocities. Neither are they necessarily valid for nonaxially symmetric motions, which will be investigated by the authors in a forthcoming paper.

BIBLIOGRAPHY

1 "A Treatise on the Mathematical Theory of Elasticity," by A. E. H. Love, fourth edition, Dover Publications, New York, N. Y., 1944, Chapter 24.

2 "Basic Differential Equations in General Theory of Elastic Shells," by V. Z. Vlasov, NACA TN 1241 Translation, 1951.

3 "Notes on the Foundations of the Theory of Small Displacements of Orthotropic Shells," by F. B. Hildebrand, E. Reissner, and G. B. Thomas, NACA TN 1833, 1949.

4 "The New Approach to Shell Theory: Circular Cylinders," by E. H. Kennard, JOURNAL OF APPLIED MECHANICS, Trans. ASME, vol. 75, 1953, pp. 33–40.

5 "Cylindrical Shells: Energy, Equilibrium, Addenda, and Erratum," by E. H. Kennard, JOURNAL OF APPLIED MECHANICS, Trans. ASME, vol. 77, 1955, pp. 111–116.

6 "On the Theory of Elastic Vibrations in Plates and Shells," by P. S. Epstein, *Journal of Mathematics and Physics*, vol. 21, 1942, pp. 198–208.

7 "On the Equations of Motion of Cylindrical Shells," by P. M. Naghdi and J. G. Berry, JOURNAL OF APPLIED MECHANICS, Trans. ASME, vol. 76, 1954, pp. 160–166.

8 "General Elastic Theory of Thin Plates and Shells With Small Deflections," by K. C. Hwang, *Academia Sinica Science Record*, vol. 5, 1952, pp. 88–124.

9 Review of paper (8), by C. Truesdell, *Mathematical Reviews*, vol. 15, 1954, p. 579.

10 "Longitudinal Vibrations of a Hollow Cylinder," by J. Ghosh, *Bulletin Calcutta Mathematical Society*, vol. 14, 1923, pp. 31–40.

11 "Waves in Liquid-Filled Cylinders," by R. D. Fay, *Journal of the Acoustical Society of America*, vol. 24, 1952, pp. 459–462.

12 "On the Free Vibrations of an Infinite Plate of Homogeneous Isotropic Elastic Matter," by Lord Rayleigh, Proceedings of the London Mathematical Society, London, England, vol. 10, 1889, pp. 225–234.

13 "On Waves in an Elastic Plate," by H. Lamb, Proceedings of the Royal Society of London, England, series A, vol. 93, 1917, pp. 114–128.

14 "Über die Fortpflanzungsgeschwindigkeiten kleiner Schwingungen in einem unbegrensten isotropen Kreiscyclinder," by L. Pochhammer, *Journal für Mathematik* (Crelle), vol. 81, 1876, p. 324.

15 "Axially-Symmetric Motions of Thick Shells," by I. Mirsky and G. Herrmann, Office of Scientific Research, Air Research and Development Command, U. S. Air Force, Contract AF 18(600)-1247, Columbia University, Technical Note No. 2, New York, N. Y., November, 1955.

16 "The Theory of Sound," by Lord Rayleigh, Dover Publications, New York, N. Y., 1945.

17 "Table of Frequencies and Modes of Free Vibration of Infinitely Long Thin Cylindrical Shells," by M. L. Baron and H. H. Bleich, JOURNAL OF APPLIED MECHANICS, Trans. ASME, vol. 76, 1954, pp. 178–184.

18 "The Propagation of Elastic Waves in Thin-Walled Cylindrical Shells," by M. C. Junger and F. J. Rosato, *Journal of the Acoustical Society of America*, vol. 26, 1954, pp. 709–713.

19 "A Study of Axisymmetric Vibrations of Cylindrical Shells as Affected by Rotatory Inertia and Transverse Shear," by T. C. Lin and G. W. Morgan, JOURNAL OF APPLIED MECHANICS, Trans. ASME, vol. 78, 1956, pp. 255–261.

20 "Influence of Rotatory Inertia and Shear on Flexural Motions of Isotropic Elastic Plates," by R. D. Mindlin, JOURNAL OF APPLIED MECHANICS, Trans. ASME, vol. 73, 1951, pp. 31–38.

21 "A Treatise on the Theory of Bessel Functions," by G. N. Watson, second edition, Cambridge University Press, London, England, 1952.

22 "A One-Dimensional Theory of Compressional Waves in an Elastic Rod," by R. D. Mindlin and G. Herrmann, Proceedings of the First National Congress of Applied Mechanics, ASME, 1952.

23 "Statik und Dynamik der Schalen," by W. Flügge, Edwards Brothers, Inc., Ann Arbor, Mich.

24 "Hydrodynamics," by H. Lamb, sixth edition, Dover Publications, New York, N. Y., 1945, p. 458.

25 "Radial Vibrations of Thick-Walled Hollow Cylinders," by J. A. MacFadden, *Journal of the Acoustical Society of America*, vol. 26, 1954, 714–715.

Effect of Imperfections on Buckling of Thin Cylinders Under External Pressure[1]

By L. H. DONNELL,[2] CHICAGO, ILL.

The buckling of thin cylinders under external pressure is studied by finite-deflection theory, assuming the same type of imperfections as had been assumed in a previous study of buckling under axial compression (3).[3] Unlike the axial compression case only a small elastic postbuckling reduction in resistance is found, and this only for long cylinders. However, if reasonable imperfections are assumed, failure loads initiated by yielding are found to be of the same order as those indicated by experiments.

Nomenclature

The following nomenclature is used in the paper:

l, r, t = length, mean radius, wall thickness of cylinder
E, μ, σ_y = Young's modulus, Poisson's ratio, yield point of material
p = hydraulic pressure on cylinder wall and end bulkheads
x, s = axial, circumferential co-ordinates, Fig. 1
w, u, v = radial, axial, circumferential displacement under load, Fig. 1
w_0 = equivalent initial radial deviation from cylindrical shape
n, m = number of circumferential waves, ratio of circumferential to axial wave length
a, a_0, b = parameters defining amplitudes of w, w_0, and secondary deflection
f = stress function of membrane stresses
$K = 1 + 2w_0/w = 1 + 2a_0/a$
U = unevenness factor, assumed to depend only on material and manufacturing process, Equation [2]
$\nu = Katn^2/2r$

$$L = \frac{l}{\sqrt{(rt)}}, \quad V = \frac{\text{(volume decrease)}}{(rt)^{3/2}}, \quad P = \frac{r^{3/2}l}{t^{5/2}}\frac{p}{E}$$

Introduction

The simplest and probably the most practically important type of shell for buckling studies is the right circular cylinder, of isotropic material and of uniform wall thickness, which is thin enough compared to the radius to justify certain theoretical simplifications and to make at least the initial stages of buckling elastic. The most basic loadings which can produce buckling are those causing uniform axial compressive stress, uniform circumferential compressive stress combined with axial compressive stress produced by all-around hydraulic pressure, and uniform shear stress produced by torsion. The simplest boundary conditions are those corresponding to complete cylinders having hinged or fixed end edges; these at least "bracket" the end conditions of most cylinder applications. Until such basic cases have been satisfactorily solved there does not seem much point in studying more special cases.

"Classical" solutions to most of these basic cases, satisfying with probably adequate accuracy the conditions for neutral stability of ideally perfect specimens, have been known for many years. The most nearly complete experimental check of these theories available is perhaps for the case of torsion of fixed-edge cylinders. Experiments on cylinders having a very wide range of proportions and materials check the theoretical buckling shape closely, and give failure strengths from 60 to nearly 100 per cent of those predicted, over this whole range. It is customary in such cases to attribute the discrepancy in strength to "defects always present in actual specimens." However, we can hardly be satisfied with this "explanation" when the experimental failure strengths are only 15 to 60 per cent of the theoretical value and give a poor check with theoretical buckling shape, as is the case for axial compression. And even for the torsion case it is highly desirable to know just how defects reduce strength, and perhaps to be able to predict strengths in individual cases within closer limits. The check between experiments and the classical theory for the case of buckling under hydraulic pressure seems to be intermediate between the cases of torsion and axial compression.

In 1941 von Karman and Tsien (1) studied the case of axial compression of a perfect cylinder with an approximate finite-deflection theory developed by the author in 1934 (2). They found an almost catastrophic drop-off in resistance after buckling, a condition radically different from the constant resistance predicted by the classical theory, and one which suggests great sensitivity to defects for this case.

In 1950 the author and C. C. Wan (3) studied the effect of defects in the axial-compression case by the finite-deflection theory, and found that the assumption of reasonable defects could indeed explain the experimental behavior and give some insight into the strength reduction to be expected in individual cases. In a recently published paper, T. T. Loo (4) studies the case of torsion by similar methods, and finds that defects of about the same magnitude as were assumed for the axial-compression case, which gave large strength reductions for that case, produce the much smaller reductions indicated by experiments when assumed for the torsion case.

The present paper describes a similar study, by the finite-deflection theory, of the effect of defects in the case of buckling of a thin cylinder with hinged end edges under all-around hydraulic pressure.

---

[1] This work was carried out under a contract with the Office of Naval Research sponsored by the David Taylor Model Basin.

[2] Research Professor of Mechanics, Illinois Institute of Technology. Mem. ASME.

[3] Numbers in parentheses refer to the Bibliography at the end of the paper.

Presented at the National Applied Mechanics Division Conference, Urbana, Ill., June 14–16, 1956, of The American Society of Mechanical Engineers.

Discussion of this paper should be addressed to the Secretary, ASME, 29 West 39th Street, New York, N. Y., and will be accepted until January 10, 1957, for publication at a later date. Discussion received after the closing date will be returned.

Note: Statements and opinions advanced in papers are to be understood as individual expressions of their authors and not those of the Society. Manuscript received by ASME Applied Mechanics Division, October 24, 1955. Paper No. 56—APM-39.

Assumptions Made

Fig. 1 shows the co-ordinate system and the symbols which will be used for displacements, cylinder dimensions, and loads. The radial deflection w under load is assumed to be

$$w = at\left[\cos\frac{ns}{r}\cos\frac{mnx}{r} + b\left(\cos\frac{mnx}{r} + 0.3\cos\frac{3mnx}{r}\right)\right] \quad (-l/2 < x < l/2) \ldots\ldots [1]$$

where a (the amplitude of the deflection), n (the number of circumferential waves), and b are three parameters to be determined

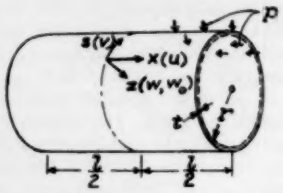

Fig. 1 Co-Ordinates, Displacements, Etc., Used in Theory

from energy considerations, and $m = \pi r/nl$ is the ratio between the circumferential and axial half wave length (assumed equal to l, as it is in tests) of the primary buckling deflection.

Expression [1] satisfies the conditions on w for hinged end edges

$$x = \pm l/2: \quad w = 0, \quad M_x = [Et^3/12(1-\mu^2)](\partial^2 w/\partial x^2 + \mu\partial^2 w/\partial s^2) = 0$$

where E, μ are the elastic modulus and the Poisson's ratio of the material, respectively. The first term of Expression [1] is the deflection satisfying the differential equations of small-deflection classical theory, and will be called the "primary" deflection.

The "secondary" deflection, represented by the last two terms, serves a double purpose. First, it can represent the inward deflection of the cylinder, due to the pressure, before buckling occurs; this has been neglected in most previous theories for this case. It has about the right shape for this purpose in the practically important case of a bay which forms one of many bays separated by rigid bulkheads, to which a continuous skin is hinged.[4] In such a case the primary buckling wave would be inward in one bay and outward in the adjoining bay, with a node between; on the other hand, the axisymmetric secondary deflection would be inward in both bays, with a horizontal tangent between. For the bay studied a horizontal tangent would require the coefficient of the third term to be $^1/_4$; the value of 0.3 represents a compromise with the conditions which would prevail in a single bay, or at one end of an end bay in a series of bays, where a value of around zero for this coefficient could be expected.

The second and most important purpose of the secondary deflection is to represent the axisymmetric inward deflection, with a shape approximately proportional to squares of the primary deflections, which experience shows to be very important in finite-deflection theories to partially cancel the finite-displacement circumferential strains which otherwise greatly increase the strain energy. Of course such a secondary displacement also involves bending energy, and the use of a value of 0.3 instead of $^1/_4$ for the coefficient of the third term is in the direction of the compromise which these conflicting energy trends will result in, in an actual specimen. It would of course be better to use an arbitrary parameter for the coefficient of the third term, but this would greatly increase the computational difficulties.

The initial radial deviation from true cylindrical shape, w_0, must have the same shape as the deflection under load w in order to satisfy the requirements of the theory used, that is $w_0 = (a_0/a)w$, where a_0 is the amplitude of deviation.[5] This means that only this one component of the actual deviation can be taken into consideration; however, experience with buckling problems indicates that such a component is more important than any other component of the deviation. Moreover, a_0 is to be regarded as not merely the amplitude of this component of the actual geometric deviation of the specimen, but as the amplitude of an equivalent component which would have the same effect, in so far as possible, as the combined effects of this and of "neighboring" components (components of nearly the same shape) as well as of other kinds of defects (such as those due to irregularities of elastic properties due to crystal orientation, inclusions, etc.)

The amplitude a_0 of this "equivalent initial deviation" from cylindrical shape will certainly vary from specimen to specimen, even for specimens which are "identical" as far as manufacturing methods can make them. Nevertheless, its average value for a group of such identical specimens will differ from the average value for another such group in which the proportions, material, or manufacturing process is different. These average values can be expected to be some more or less definite function of the proportions, material, and manufacturing process.

In the 1950 paper previously cited on the axial compression case (3) this function was, for reasons discussed in that paper, assumed to be of the form

$$a_0 = (U/\pi^2)l_x^{1.5}l_s^{0.5}/t^2 = Ur^2/m^{1.5}n^2t^2 \ldots\ldots [2]$$

where l_x and l_s are the half wave lengths of the primary buckling waves in the axial and circumferential directions, and U is an "unevenness" factor assumed to depend only upon the material and manufacturing process.[6] We will assume the same relation in the present case, and we will then be able to compare the effect of defects corresponding to the same values of U upon the two types of loading.

Membrane Stresses and Displacements

In the previously mentioned paper of 1934 (2) the following relation was developed between the deflection w and the stress function of the membrane stresses f

$$(\nabla^2)^2 f = EK\left[\left(\frac{\partial^2 w}{\partial x \partial s}\right)^2 - \frac{\partial^2 w}{\partial x^2}\frac{\partial^2 w}{\partial s^2}\right] - \frac{E}{r}\frac{\partial^2 w}{\partial x^2} \ldots [3]$$

where ∇^2 is the operator $\partial^2/\partial x^2 + \partial^2/\partial s^2$ and $K = 1 + 2w_0/w = $ const. The nonlinear terms on the right-hand side correspond to membrane stresses due to finite displacements and are the same as in von Karman's finite-displacement theory for flat plates (6). The last term on the right-hand side corresponds to membrane stresses due to curvature, and is obtained by using the same approximations as were used in the approximate small-deflection cylinder theory first developed by the author for studying the problem of buckling under torsion (7).

In the present case

$$K = 1 + 2w_0/w = 1 + 2a_0/a \ldots\ldots [4]$$

where a_0 is defined by Equation [2]. We will use the new parameter ν defined as

[4] Ring stiffeners riveted to the skin but of open cross section, so that they are flexible in torsion but stiff against radial displacement, would approximate this condition.

[5] A different theoretical method would have to be used to investigate such questions as the possible relative importance of axisymmetric and nonaxisymmetric parts of the initial deviation.

[6] Measurements of columns have since indicated the suitability of this type of relation for the case of columns (5). It is hoped to make further studies of this question for the case of cylinders.

$$w = \frac{Katn^2}{2r} = \frac{atn^2}{2r} + \frac{a_0tn^2}{r} = \frac{atn^2}{2r} + \frac{Ur^2}{m^{1.5}n^2l^2}\frac{tn^2}{r} = \frac{atn^2}{2r} + \frac{Ur}{m^{1.5}l} \quad [5]$$

Substituting the Expression [1] for w into Equation [3], using Equation [5], and simplifying, we obtain

$$(\nabla^2)^2 f = \frac{Eatm^2n^2}{r^2}\left[-\nu\left(\cos\frac{2mnx}{r} + \cos\frac{2ns}{r}\right) - \nu b\cos\frac{ns}{r}\left(1 + 3.7\cos\frac{2mnx}{r} + 2.7\cos\frac{4mnx}{r}\right) + \cos\frac{ns}{r}\cos\frac{mnx}{r} + b\left(\cos\frac{mnx}{r} + 2.7\cos\frac{3mnx}{r}\right)\right]$$

A particular solution for f is

$$f = \frac{Eatl^2m^4}{\pi^2 r}\left[-\nu\left(\frac{1}{16m^4}\cos\frac{2mnx}{r} + \frac{1}{16}\cos\frac{2ns}{r}\right) - \nu b\cos\frac{ns}{r}\left(1 + \frac{3.7}{(1+4m^2)^2}\cos\frac{2mnx}{r} + \frac{2.7}{(1+16m^2)^2}\cos\frac{4mnx}{r}\right) + \frac{1}{(1+m^2)^2}\cos\frac{ns}{r}\cos\frac{mnx}{r} + \frac{b}{m^4}\left(\cos\frac{mnx}{r} + \frac{1}{30}\cos\frac{3mnx}{r}\right)\right] + C_x s^2 + C_s x^2 \quad [6]$$

The last two terms of Equation [6] are part of the general solution of the homogeneous equation obtained by setting the right-hand side of Equation [3] equal to zero, which can be added to the particular solution to obtain the general solution for f. Besides such power-function solutions, trigonometric-hyperbolic solutions of the homogeneous equation such as

$$\cos\frac{ns}{r}\left(A\cosh\frac{nx}{r} + B\frac{nx}{r}\sinh\frac{nx}{r}\right) + \cos\frac{2ns}{r}\left(C\cosh\frac{2nx}{r} + D\frac{2nx}{r}\sinh\frac{2nx}{r}\right) \quad [7]$$

can also be added to the expression for f. If the Expressions [7] are added, the constants of integration A, B, C, D can be determined so as to satisfy end conditions on the "membrane displacements" u, v or the membrane stresses

$$\sigma_x = \partial^2 f/\partial s^2, \quad \sigma_s = \partial^2 f/\partial x^2, \quad \tau_{xy} = -\partial^2 f/\partial x \partial s,$$

describing complete fixity against u, v displacements or complete freedom of u, v displacements

$$x = \pm l/2: \quad u = v = 0, \text{ or } \sigma_x = \tau_{xy} = 0 \quad [8]$$

or related end conditions.

Because of the greatly increased work of computation which their use would have involved, the Terms [7] were not used, and the expression for f was taken as that given in Equation [6]. As a result, the solution obtained does not satisfy any simple end conditions for membrane displacements or stresses. This is probably not important in the early stages of buckling but must become important in later stages. Further study of this question would certainly be desirable.

Returning to Expression [6] for the membrane stress function f, the constant of integration C_x can be determined from the condition of equilibrium in the axial direction of one end of the cylinder. Assuming the hydraulic pressure to act upon the entire end bulkhead, this requires that

$$-\pi r^2 p = \int_0^{2\pi r} t\sigma_x ds = t\int_0^{2\pi r} (\partial^2 f/\partial s^2) ds$$

On using Expression [6] for f this reduces to

$$-\pi r^2 p = 4\pi r t C_x, \quad C_x = -\tfrac{1}{4}pr/t \quad [9]$$

The constant of integration C_x can be determined from the requirement that the circumferential displacement v must be continuous. It is shown in the 1934 paper previously mentioned (2) that the u and v displacements have the following relations to w and f

$$\left.\begin{aligned} \frac{\partial u}{\partial x} &= \frac{1}{E}\left(\frac{\partial^2 f}{\partial s^2} - \mu\frac{\partial^2 f}{\partial x^2}\right) - \frac{K}{2}\left(\frac{\partial w}{\partial x}\right)^2 \\ \frac{\partial v}{\partial s} &= \frac{1}{E}\left(\frac{\partial^2 f}{\partial x^2} - \mu\frac{\partial^2 f}{\partial s^2}\right) - \frac{K}{2}\left(\frac{\partial w}{\partial s}\right)^2 + \frac{w}{r} \\ \frac{\partial u}{\partial s} + \frac{\partial v}{\partial x} &= -\frac{2(1+\mu)}{E}\frac{\partial^2 f}{\partial x \partial s} - K\frac{\partial w}{\partial x}\frac{\partial w}{\partial s} \end{aligned}\right\} \quad [10]$$

Substituting Expressions [1] and [6] for w and f into Equations [10], integrating, eliminating functions of integration, and determining constants of integration by assuming $u = v = 0$ at $x = 0$, $s = 0$, we find

$$u = \frac{2}{E}(C_x - \mu C_s)x - \frac{atm}{n}\left\{\frac{\nu mn}{4r}x + \frac{\nu}{8}\sin\frac{2mnx}{r}\left(\frac{\mu}{m^2} - 1 - \cos\frac{2ns}{r}\right) + \frac{\nu b}{2}\cos\frac{ns}{r}\left[\left(\frac{3.7(4\mu m^2 - 1)}{(1+4m^2)^2} - 0.1\right)\sin\frac{2mnx}{r} + \left(\frac{1.35(16\mu m^2 - 1)}{(1+16m^2)^2} - 0.45\right)\sin\frac{4mnx}{r}\right] + \frac{1 - \mu m^2}{(1+m^2)^2}\cos\frac{ns}{r}\sin\frac{mnx}{r} - \frac{\mu b}{m^2}\left(\sin\frac{mnx}{r} + 0.1\sin\frac{3mnx}{r}\right) + \frac{\nu b^2}{4}\left(\frac{3.62mn}{r}x + 0.8\sin\frac{2mnx}{r} - 0.9\sin\frac{4mnx}{r} - 0.27\sin\frac{6mnx}{r}\right)\right\} \quad [11]$$

$$v = \frac{2}{E}(C_s - \mu C_x)s - \frac{al}{n}\left\{\frac{\nu n}{4r}s + \frac{\nu}{8}\sin\frac{2ns}{r}\left(\mu m^2 - 1 - \cos\frac{2mnx}{r}\right) + m^2\nu b\sin\frac{ns}{r}\left[\mu + \frac{3.7(\mu - 4m^2)}{(1+4m^2)^2}\cos\frac{2mnx}{r} + \frac{2.7(\mu - 16m^2)}{(1+16m^2)^2}\cos\frac{4mnx}{r}\right] - \frac{1 + (2+\mu)m^2}{(1+m^2)^2}\sin\frac{ns}{r}\cos\frac{mnx}{r}\right\} \quad [12]$$

It can be seen that in order for v to be continuous, the terms linear in s in Equation [12] must vanish, or

$$\frac{2}{E}(C_s - \mu C_x) - \frac{al}{n}\frac{\nu n}{4r} = 0$$

By using the Value [9] for C_x this gives

$$C_s = \frac{a\nu El}{8r} - \frac{\mu r}{4t}p \quad [13]$$

Volume-Pressure Relation

We wish to determine the relation between the external loading and the deformation of the cylinder. The loading is of course fully described by the hydraulic pressure p, while the deformation corresponding to such loading can best be characterized by the volume decrease under load, which we will designate by ΔV. The volume change can be taken without serious error to be that due to radial displacements of the cylinder wall, plus that due to the general axial displacements of the end bulkheads, or

$$\Delta V = \pi r^2(u_{z=-l/2} - u_{z=l/2}) + \int_{-\frac{l}{2}}^{\frac{l}{2}} dx \int_0^{2\pi r} w ds. \quad [14]$$

where terms periodic in s in the expression for u can be neglected, since their effect on volume change would cancel out. By using Expressions [1] and [11], the resulting relation can be written

$$(1-\mu^2)\frac{p}{E} = \frac{2t\Delta V}{\pi r^2 l} - \frac{at^2}{r^2}\left[\frac{3.6(2-\mu)b}{\pi} + \frac{p}{2}(\mu + m^2 + 3.62m^2b^2)\right] \quad [15]$$

Energy Relations

The internal strain energy $\mathbf{E}$ is

$$\mathbf{E} = \frac{Et^3}{24(1-\mu^2)}\int_{-\frac{l}{2}}^{\frac{l}{2}} dx \int_0^{2\pi r} ds \left\{(\nabla^2 w)^2 + 2(1-\mu)\left[\left(\frac{\partial^2 w}{\partial x \partial s}\right)^2 - \frac{\partial^2 w}{\partial x^2}\frac{\partial^2 w}{\partial s^2}\right]\right\} + \frac{t}{2E}\int_{-\frac{l}{2}}^{\frac{l}{2}} dx \int_0^{2\pi r} ds \left\{(\nabla^2 f)^2 + 2(1+\mu)\left[\left(\frac{\partial^2 f}{\partial x \partial s}\right)^2 - \frac{\partial^2 f}{\partial x^2}\frac{\partial^2 f}{\partial s^2}\right]\right\} \quad [16]$$

We will use the new dimensionless parameters

$$L = \frac{l}{\sqrt{rt}}, \quad V = \frac{\Delta V}{(rt)^{1.5}}, \quad P = \frac{r^{1.5}l}{t^{2.5}}\frac{p}{E} \quad [17]$$

together with m and ν previously defined

$$\left.\begin{aligned} m &= \pi r/nl \\ \nu &= \frac{atn^2}{2r} + \frac{Ur}{m^{1.5}t} = \frac{\pi^2 a}{2m^2L^2} + \frac{Ur}{m^{1.5}t}\end{aligned}\right\} \quad [18]$$

By using Expressions [1] and [6] for w, f, Expression [9] and [13] for C_m, C_n eliminating p, n, and a by means of Relations [15] and [18], and taking $\mu = 0.3$, the strain energy $\mathbf{E}$ can be written

$$\frac{\pi^2 r^3}{Etl^3}\mathbf{E} = \left(3.3\frac{V}{L^3}\right)^2 - \frac{V}{L^3}\left(m^2\nu - \frac{Ur}{t}m^{1/2}\right)[13.5b + \nu(A + Bb^2)] + \left(m^2\nu - \frac{Ur}{t}m^{1/2}\right)^2\left[\frac{8.92}{L^4}\left(\frac{1}{C} + 16.58b^2\right) + (C + 6.35b^2) + \nu b(D + Fb^2) + \nu^2(G + Hb^2 + Jb^4)\right] \quad [19]$$

Where $A, B, \ldots, J$ are the following functions of m

$$A = 3.45m^2 + 1.04, \quad B = 12.5m^2, \quad C = \left(\frac{m^2}{1+m^2}\right)^2,$$

$$D = 2.14m^2 - 1.16 + C\left[0.76m^2 - 2.55 - \frac{3.14(1 + 8.9m^2 + 4m^4)}{(1+4m^2)^2} + \frac{0.46(1 + 36.5m^2 + 16m^4)}{(1+16m^2)^2}\right]$$

$$F = 7.74m^2, \quad G = 0.4(1+m^4) + 0.165m^2$$

$$H = 0.6m^2 + 4m^4\left[1 + \frac{3.43}{(1+4m^2)^2} + \frac{1.83}{(1+16m^2)^2}\right], \quad J = 3.6m^4$$

For a given cylinder, U and L will be given. If the volume change ΔV, and hence V, is held constant (as in a test in which the cylinder is surrounded by an incompressible fluid in a tight, rigid tank) there will be no external work done by the pressure p during virtual displacements produced by small changes in m, b, and ν. By the law of virtual work, therefore, the partial derivatives, $\mathbf{E}_m$, $\mathbf{E}_b$, $\mathbf{E}_\nu$, of $\mathbf{E}$ with respect to m, b, and ν must be zero. This is equivalent to minimization with respect to the original parameters n, b, and a. The three equations thus obtained are most conveniently taken in the form

$$m\mathbf{E}_m - 2\nu\mathbf{E}_\nu = 0, \quad \nu\mathbf{E}_\nu = 0, \quad \text{and } b\mathbf{E}_b = 0$$

Dividing by $(m^2\nu - m^{1/2}Ur/t)$, since the solution $m^{3/2}\nu = Ur/t$ seems meaningless here, we obtain, treating V as a constant

$$\left.\begin{aligned} 0 &= \frac{V}{L^3}\left\{\frac{0.5(Ur/t)m^{1/2}}{m^2\nu - (Ur/t)m^{1/2}}[13.5b + \nu(A + Bb^2)] + 2.07\nu\right\} - \frac{Ur}{t}m^{1/2}\left\{\frac{8.92}{L^4}\left(\frac{1}{C} + 16.58b^2\right) + (C + 6.35b^2) + \nu b(D + Fb^2) + \nu^2(G + Hb^2 + Jb^4)\right\} + \left(m^2\nu - \frac{Ur}{t}m^{1/2}\right)\left\{mC_m\left(1 - \frac{8.92}{L^4C^2}\right) + \nu b(mD_m - 2D) + \nu^2[(mG_m - 4G) + (mH_m - 4H)b^2]\right\} \\ 0 &= -\frac{V}{L^3}\left\{\frac{m^2\nu}{m^2\nu - (Ur/t)m^{1/2}}[13.5b + \nu(A + Bb^2)] + \nu(A + Bb^2)\right\} + 2m^2\nu\left\{\frac{8.92}{L^4}\left(\frac{1}{C} + 16.58b^2\right) + (C + 6.35b^2) + \nu b(D + Fb^2) + \nu^2(G + Hb^2 + Jb^4)\right\} + \left(m^2\nu - \frac{Ur}{t}m^{1/2}\right)\{\nu b(D + Fb^2) + 2\nu^2(G + Hb^2 + Jb^4)\} \\ 0 &= -\frac{V}{L^3}(13.5b + 2\nu Bb^2) + \left(m^2\nu - \frac{Ur}{t}m^{1/2}\right)\left\{\frac{17.84}{L^4}16.58b^2 + 12.7b^2 + \nu b(D + 3Fb^2) + 2\nu^2 b^2(H + 2Jb^2)\right\}\end{aligned}\right\} \quad [20]$$

By using the foregoing parameters, the Relation [15] between the loading and deformation of the cylinder can be put in the form

$$P = 0.7V - L^3\left(m^3\nu - \frac{Ur}{t}\,m^{1/3}\right)[0.44b + 0.032(A + Bb^2)] \quad \ldots\ldots [21]$$

The load-deformation, or P versus V curve, for a cylinder having a certain value of Ur/t and L can theoretically now be determined by assuming values of V, solving Equations [20] for m, b, and ν, and then finding P from Equation [21].

Since it is actually quite impractical to solve Equations [20] explicitly for m, b, and ν, solutions have been obtained as follows: The third of Equations [20] is used to eliminate V/L^3 from the other two, which are solved for L. Sets of values of Ur/t, m, b, and ν are assumed, and each of the two values found for L is plotted against b. The intersection of the two curves gives a combination of values of Ur/t, m, b, ν, and L satisfying Equations [20]. For given values of Ur/t and m, the quantities L and b are plotted against ν, and sets of values of Ur/t, m, b, ν are determined corresponding to certain specific values of L. For each of these sets of values, V can then be determined from the third of Equations [20] and P from Equation [21].

Fig. 2 shows P versus V curves thus calculated for four values, 1.7, 3.1, 5.5, and 9.7, of the cylinder shape constant L, and for several values of Ur/t. It will be noticed that for the largest value of L, 9.7 (corresponding to relatively long or thin cylinders), there is some drop-off of resistance after buckling, both for perfect specimens ($Ur/t = 0$) and for those with small imperfections. The peaks of the P versus V curves give values of the resistance to a purely elastic type of failure. However, for some proportions and materials, yielding of the material may occur at certain points in the specimen before these elastic buckling peaks are reached, and experience indicates that in such cases (except for extremely stocky, stable shapes) complete buckling failure initiated by yielding will occur at only slightly higher loads.

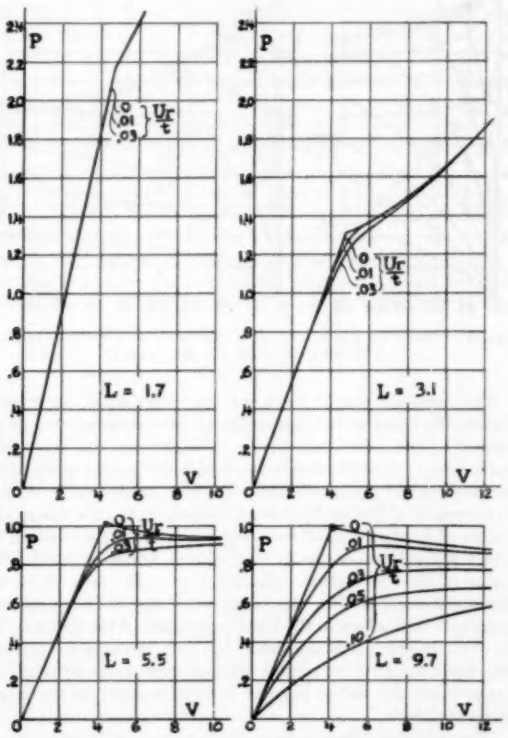

FIG. 2 PRESSURE FACTOR P VERSUS VOLUME-CHANGE FACTOR V FOR VARIOUS SHAPE FACTORS L AND UNEVENNESS FACTORS Ur/t, UNDER ELASTIC CONDITIONS

For $L = 5.5$ the drop-off in resistance after elastic buckling is much smaller, and for the lower values of L the drop-off is eliminated entirely. For $L = 1.7$ the change in slope of the P versus V curve after buckling is comparatively slight. For these shorter or thicker cylinders there is thus apparently no purely elastic ultimate buckling strength, and all complete buckling *failures* must be initiated by yielding.

The value of m, which determines the number of circumferential waves n, is found to be nearly constant for a given value of L. Fig. 3 shows the value of n and of P at the point of buckling of a perfect specimen ($Ur/t = 0$), as functions of the shape factor L, compared to the classical von Mises theory (8).

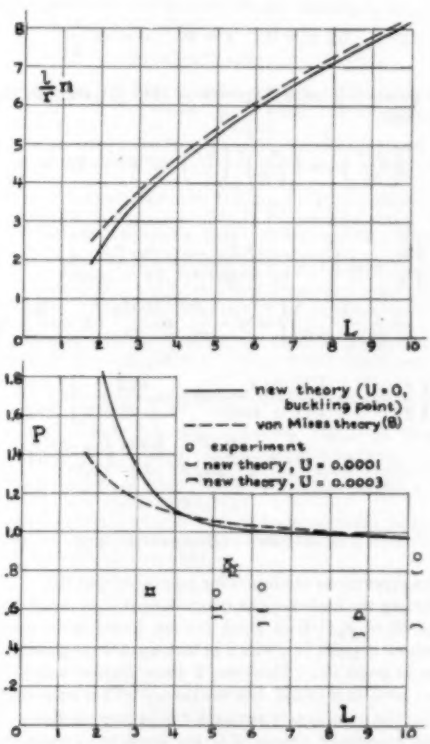

FIG. 3 NUMBER OF CIRCUMFERENTIAL WAVES n AND PRESSURE FACTOR P AT POINT OF BUCKLING OF A PERFECT SPECIMEN VERSUS SHAPE FACTOR L

It is shown in the 1950 paper (3) that, according to the shear-energy theory, yielding will occur when the yield point of the material σ_y reaches the value

$$\sigma_y = \sqrt{\sigma_x^2 - \sigma_x\sigma_s + \sigma_s^2 + 3\tau_{xs}^2} \quad \ldots\ldots [22]$$

where

$$\sigma_x = \frac{\partial^2 f}{\partial s^2} - \frac{Ez}{(1-\mu^2)}\left(\frac{\partial^2 w}{\partial x^2} + \mu\,\frac{\partial^2 u}{\partial s^2}\right)$$

$$\sigma_s = \frac{\partial^2 f}{\partial x^2} - \frac{Ez}{(1-\mu^2)}\left(\frac{\partial^2 w}{\partial s^2} + \mu\frac{\partial^2 w}{\partial x^2}\right)$$

$$\tau_{xs} = -\frac{\partial^2 f}{\partial x \partial s} - \frac{Ez}{(1+\mu)}\frac{\partial^2 w}{\partial x \partial s}$$

Points where yielding seems most likely to occur first are on the inside or outside surfaces where the maximum flexural stress occurs: (*a*) at the nodes of the primary deflection, where the twist is a maximum, and (*b*) at the outside peaks of the primary deflection, or (*c*) at the inside peaks of the primary deflection, where the bending stresses are a maximum. Co-ordinates of such points are, respectively

$$\left.\begin{aligned}
&(a)\ x = \frac{l}{2}, \quad s = \frac{\pi r}{2n}, \quad z = \pm\frac{t}{2}\\
&(b)\ x = 0, \quad s = \frac{\pi r}{n}, \quad z = \pm\frac{t}{2}\\
&(c)\ x = 0, \quad s = 0, \quad z = \pm\frac{t}{2}
\end{aligned}\right\} \quad \ldots\ldots [23]$$

For points (*c*), using Expressions [1], [6], etc., in Equation [22] we find

$$\left(\frac{\sigma_y r}{Et}\right)^2 = \left(\frac{\sigma_y}{UE}\right)^2\left(\frac{Ur}{t}\right)^2 = X^2 - XS + S^2 \ldots [24]$$

where

$$X = \left\{\frac{\nu}{4} + \nu b\left(1 + \frac{3.7}{(1+4m^2)^2} + \frac{2.7}{(1+16m^2)^2} - \frac{1}{(1+m^2)^2}\right)\right\} m^2 a - \frac{P}{2L} \pm \frac{5.43a}{L^2}\left(1 + \frac{0.3}{m^2} + 3.7b\right)$$

$$S = \left\{\frac{\nu}{2} + m^4\nu b\left[\frac{14.8}{(1+4m^2)^2} + \frac{43.2}{(1+16m^2)^2}\right] - C - 1.3b\right\} a - \frac{0.3P}{2L} \pm \frac{5.43a}{L^2}\left(\frac{1}{m^2} + 0.3 + 1.11b\right)$$

and

$$a = [m^2\nu - (Ur/t)m^{1/2}]L^2/4.94$$

Similar expressions are found for points (*a*) and (*b*).

Selecting the higher of the two values at each point, the values of $\sigma_y r/Et$ or σ_y/UE at point (*c*) are found to be about twice the values at point (*b*), which in turn are always greater than the values at point (*a*). However, if these highest values, at point (*c*), are used, it is found that the theory is "too successful" in explaining the reduction in strength due to imperfections. That is, for any reasonable values of U the predicted pressure at which yielding starts seems to be unreasonably far below the experimental failure pressure.

A clue to the reason for this is found in the experimental results. These indicate that yielding actually occurs first at point (*b*) instead of at point (*c*), and that the reason this is so is that the primary deflection shape is actually not a simple sinusoidal one in the circumferential direction, as was assumed in the theory. The primary deflection shape indicated by experiments seems to contain a strong second-harmonic component which greatly increases the circumferential bending at point (*b*), at the same time decreasing the circumferential bending at point (*c*).

This means that the values found for $\sigma_y r/Et$ or σ_y/UE by this theory at point (*c*) are too large, and those found at point (*b*) are too small. In the absence of the more complex theory which would be required to analyze these trends completely, it appears that the best estimate which can be obtained from the present theory of the values of $\sigma_y r/Et$ or σ_y/UE at which substantial yielding will occur is the average of the values of these quantities found at points (*b*) and (*c*).

Fig. 4 shows such average values of these quantities plotted against P and Ur/t, for each of the four values of L previously used. According to the theory, experimental points for groups of specimens made of the same material and by the same manufacturing process should lie along one of the constant σ_y/UE lines, since this quantity would be the same for all such specimens.

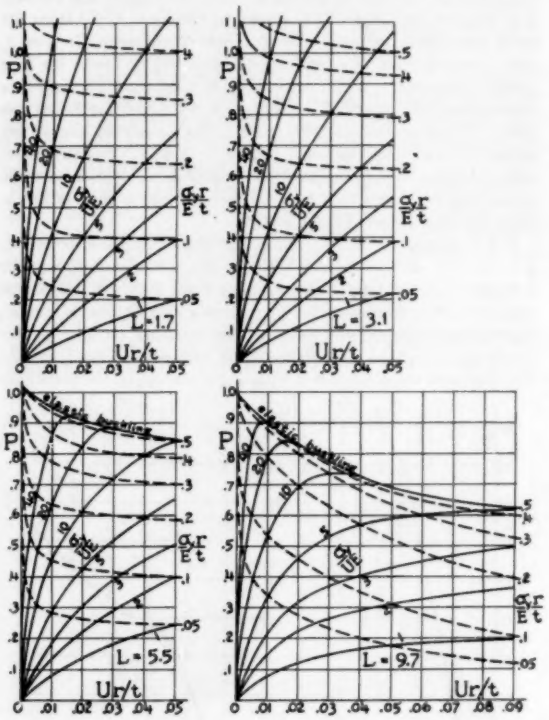

FIG. 4 PRESSURE FACTOR P AS A FUNCTION OF Ur/t FOR VARIOUS VALUES OF σ_y/UE, $\sigma_y r/ET$, AND L

The constant $\sigma_y r/Et$ lines, on the other hand, show more clearly the effect of the magnitude of the imperfections, as described by the co-ordinate Ur/t. It can be seen that for a given value of $\sigma_y r/Et$ and L, that is, for cylinders of a given material and dimensions, the predicted failure pressure, measured by P, falls very rapidly at first as Ur/t increases from zero. For the smaller values of L, after a small threshold value of Ur/t is reached, the effect of further increase in Ur/t is comparatively small. The value of Ur/t for actual cylinders is probably well above this threshold value and in the range where the failure pressure is relatively insensitive to the exact magnitude of the defects. For $L = 9.7$ the picture is somewhat different, but even for this case the values of Ur/t for actual cylinders are certainly above the range where the failure pressure is most sensitive to the magnitudes of defects.

The predicted failure pressure for any given cylinder can be determined from Fig. 4 as follows: A value of U is first selected, corresponding to the care which was taken in all the manufacturing operations to reduce deviations from perfect shape and other

TABLE 1 COMPARISON OF THEORY WITH DAVID TAYLOR MODEL BASIN TESTS

DTMB model no.	$\frac{L}{\sqrt{(rt)}}$	$\frac{r}{t}$	$\frac{1000\sigma_y}{E}$	P				n	
				von Mises	Test	Present theory $U = 0.0001$	Present theory $U = 0.0003$	Test	Present theory
32	9.38	158	1.11	0.97	0.83	0.65	0.49	11	10.5
33	6.21	156	1.11	1.03	0.67	0.59	0.53	13 to 14	12.3
44	6.20	155	1.57	1.03	0.64	0.67	0.62	13	12.3
46	6.24	157	1.29	1.03	0.84	0.62	0.58	13	12.2
48	4.75	163	1.39	1.07	0.71	0.64	0.62	13 to 14	13.7
50	3.33	178	1.39	1.13	0.69	0.71	0.68	19	15.5
55	7.90	251	1.04	1.01	0.75	0.68	0.57	14	14.3
60	5.67	130	1.22	1.04	0.64	0.57	0.53	14	12.0
66	10.10	104	1.29	0.97	0.86	0.64	0.49	8 to 9	8.4
71	8.72	77	1.47	0.99	0.56	0.56	0.47	...	7.5
73	9.40	89	1.21	0.97	0.70	0.56	0.44	...	7.8
BR1	5.33	208	2.06	1.05	0.82	0.85	0.80	15	14.9
BR4	5.06	102	1.69	1.06	0.68	0.60	0.56	10	10.5
BR5	5.43	217	1.81	1.05	0.81	0.82	0.77	14	15.0

defects. In the study of the axial compression case (3) values of U from 0.0001 up to 0.0005 or even a little higher were required to explain experimental results from a large number of specimens made in a very wide range of proportions, materials, and manufacturing processes. These values seemed reasonable since similar values were required to explain the strength of columns as predicted by commonly accepted column formulas. The largest values of U required corresponded to specimens which were very small scale and which were rolled from thin "shim stock," a material which has large deviations from flatness. The values of U required for specimens made from sheet stock which had been subjected to standard flattening process ranged from about 0.0001 to 0.0003, with an average value of about 0.00015.

With the dimensions and properties of the material known, values of Ur/t and of σ_y/UE or $\sigma_y r/Et$ can then be calculated, and values of P read from each of the four charts, corresponding to four values of L. A curve of P versus L is then plotted with these four values, from which the value of P can be read corresponding to the actual L of the specimen (this is not difficult since the variation of P with L is not great). The value of p can then be determined from the definition of P.

A number of specimens tested by the David Taylor Model Basin (9) were analyzed by this method, using values for U of 0.0001 and 0.0003. The results of these calculations are shown in Table 1 and also have been plotted in Fig. 3. It can be seen that, with the assumption of reasonable defects, the theory can easily explain the observed reductions of actual buckling pressures below those predicted by the classical theory of von Mises (8). In some cases the theory predicts too low a buckling pressure. This may be due to the fact that the ultimate pressure which was measured in the tests can somewhat exceed the pressure at which yielding starts, and to the fact that the end conditions in most of the tests were probably closer to the fixed-end than to the hinged-end condition. Further study of the effect of end conditions is planned.

Acknowledgment

The author wishes to thank Drs. Kennard and Wenk and other members of the staff of David Taylor Model Basin for their interest and suggestions, and to acknowledge the help of Mr. C. W. Lee, who carried out most of the calculations.

BIBLIOGRAPHY

1 "The Buckling of Thin Cylindrical Shells Under Axial Compression," by Th. von Karman and H. S. Tsien, *Journal of the Aeronautical Sciences*, vol. 8, June, 1941, p. 303.

2 "A New Theory for the Buckling of Thin Cylinders Under Axial Compression and Bending," by L. H. Donnell, Trans. ASME, vol. 56, 1934, p. 795.

3 "Effect of Imperfections on Buckling of Thin Cylinders and Columns Under Axial Compression," by L. H. Donnell and C. C. Wan, JOURNAL OF APPLIED MECHANICS, Trans. ASME, vol. 72, 1950, p. 73.

4 "Effects of Large Deflections and Imperfections on the Elastic Buckling of Cylinders Under Torsion and Axial Compression," by T. T. Loo, Proceedings of the Second U. S. National Congress of Applied Mechanics, THE AMERICAN SOCIETY OF MECHANICAL ENGINEERS, New York, N. Y., 1955.

5 "A Universal Column Formula for Load at Which Yielding Starts," by L. H. Donnell and V. C. Tsien, NACA Technical Note No. 3415.

6 Th. von Karman, *Encyklopädie der Math. Wiss.*, vol. 4, article 27, 1910, p. 349.

7 "Stability of Thin Cylinders in Torsion," by L. H. Donnell, NACA Report No. 479, 1933.

8 "The Critical External Pressure of Cylindrical Tubes Under Uinform Radial and Axial Load," by R. von Mises, Stodola's Festschrift, Zurich, Switzerland, 1929, p. 418.

9 "Collapse by Instability of Thin Cylindrical Shells Under External Pressure," by D. F. Windenburg and Charles Trilling, Trans. ASME, vol. 56, 1934, pp. 819–825.

Minimum Weight Design of Cylindrical Shells[1]

By WALTER FREIBERGER,[2] PROVIDENCE, R. I.

The theory of collapse and minimum weight design of cylindrical shells by Onat and Prager[3,4] is applied in this paper to the development of a method for designing the variable wall thickness of a cylindrical shell under axial loading and arbitrary pressures to give maximum economy of material. The design is such that the shell does not fail plastically in the sense used in limit analysis.[5] It will be assumed that the shell is supported at the ends by inextensible rings so that the circumferential strain rates vanish there.

Nomenclature

The following nomenclature is used in the paper:

x, φ = axial and circumferential co-ordinates
R = radius of mid-surface of shell
h = wall thickness of shell
N_x, N_φ = axial and circumferential membrane forces
M_x = axial bending moment
S = shear force
N_0, M_0 = fully plastic membrane force and bending moment
p, q = radial and axial loads

Note: N_x, N_φ, M_x, S, N_0, and M_0 are specified per unit length of line element in the mid-surface of the shell, and p, q per unit area of the mid-surface. The membrane forces and axial load are positive for tension, the loading moments are positive if they produce concave curvature in the axial direction, referred to the outside of the shell, and shear force and radial load are positive radially outward.

Q = applied axial force per unit length of shell perimeter, positive for tension
σ_0 = yield limit of shell material in simple tension
ω = $\sqrt{(2\sigma_0/QR)}$ for positive Q
l = half-length of shell
n_φ, n_x, m_x = nondimensional quantities N_φ/N_0, N_x/N_0, M_x/M_0

Primes denote ordinary differentiation with respect to x.

With the foregoing notation the equilibrium of the shell elemen in Fig. 1 demands

$$S' + \frac{N_\varphi}{R} = p, \quad N_x' = -q, \quad M_x' = S \qquad [1]$$

so that

$$M_x'' + \frac{N_\varphi}{R} = p \qquad [2]$$

The fully plastic membrane force and bending moment per unit length are

$$N_0 = \sigma_0 h, \quad M_0 = \frac{1}{4}\sigma_0 h^2 \qquad [3]$$

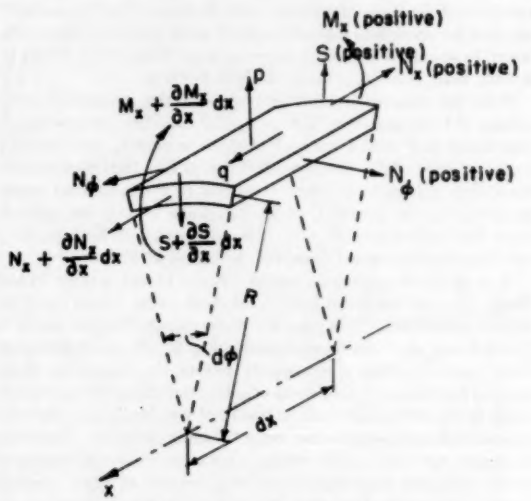

Fig. 1 Element of Shell

Design for Minimum Weight

The theory and philosophy on which minimum weight design in the sense of limit analysis is based are discussed by Onat and Prager.[4] Fig. 2 shows the yield surface of cylindrical shells developed by Onat.[3] It consists of a number of intersecting planes and surfaces to make up a convex surface in space, and it is shown[4] that for maximum economy of material the generic point of the stress state of the shell must move on the edges separating the various domains of the yield surface. This result is a consequence of the argument that, to achieve minimum weight, the shell must be designed in such a manner that any admissible collapse mode is a linear combination of a number of independent collapse modes, this number being equal to the number of independent variables at the designer's disposal. For a shell with continuously varying wall thickness the number is infinite.

Depending on the signs of n_x, n_φ, m_x, four edges of the yield surface are admissible regimes, viz.

I Positive n_φ and n_x

$$m_\varphi = 1, \quad m_x = 2n_x(1 - n_x) \qquad [4]$$

---

[1] The results presented in this paper were obtained in the course of research sponsored by the Ballistic Research Laboratories of Aberdeen Proving Ground under Contract DA-19-020-ORD-798.

[2] Assistant Professor of Applied Mathematics, Brown University.

[3] "The Plastic Collapse of Cylindrical Shells Under Axially Symmetrical Loading," by E. T. Onat, *Quarterly of Applied Mathematics*, vol. 13, April, 1955, pp. 63–72.

[4] "Limit of Economy of Material in Shells," by E. T. Onat and W. Prager, *De Ingenieur*, vol. 67, 1955, pp. 46–49.

[5] "Extended Limit Design Theorems for Continuous Media," by D. C. Drucker, W. Prager, and H. J. Greenberg, *Quarterly of Applied Mathematics*, vol. 9, 1952, pp. 381–389.

Presented at the National Applied Mechanics Division Conference, Urbana, Ill., June 14–16, 1956, of The American Society of Mechanical Engineers.

Discussion of this paper should be addressed to the Secretary, ASME, 29 West 39th Street, New York, N. Y., and will be accepted until January 10, 1957, for publication at a later date. Discussion received after the closing date will be returned.

Note: Statements and opinions advanced in papers are to be understood as individual expressions of their authors and not those of the Society. Manuscript received by ASME Applied Mechanics Division, February 20, 1956. Paper No. 56—APM-33.

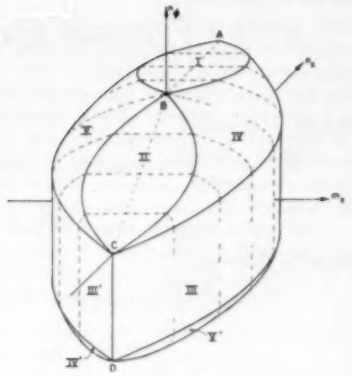

FIG. 2 YIELD SURFACE

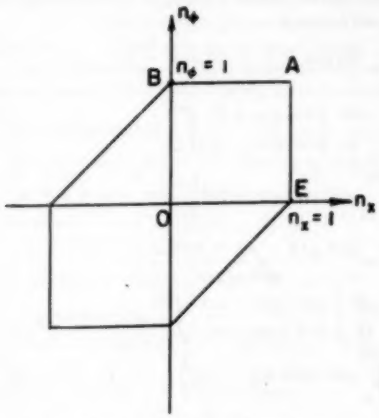

FIG. 3 SECTION $m_x = 0$ OF YIELD SURFACE

or $$m_x = -2n_x(1 - n_x) \quad [5]$$

according to the sign of the bending moment. These are the parabolas bounding face I in Fig. 2. The section $m_x = 0$ of the yield surface is shown in Fig. 3. Also admissible for case I is the edge AE in Fig. 3; there, $m_x = 0$, $n_x = 1$, and $0 \leq n_\varphi \leq 1$.

II Positive n_φ, negative n_x

$$n_\varphi - n_x = 1, \quad m_x = \pm 2n_x(1 + n_x)$$

These are the parabolas bounding face II in Fig. 2.

III Negative n_φ, positive n_x

$$n_x - n_\varphi = 1, \quad m_x = \pm 2n_x(1 - n_x)$$

IV Negative n_φ, negative n_x

$$n_\varphi = -1, \quad m_x = \pm 2n_x(1 - n_x), \quad \text{plus line } n_x = -1, \quad m_x = 0$$

The edges III and IV are hidden in Fig. 2.

Case I is appropriate to axial tension and internal pressure, Case II to axial compression and internal pressure, Case III to axial tension and external pressure, Case IV to axial compression and external pressure. By proper choice of the regime for each shell point any loading condition can be analyzed. The following discussion will be confined to Case I.

Substituting Equations [2] and [3] into [4] gives, for positive bending moment, the relation

$$N_\varphi = \sigma_0 h, \quad M_x = \frac{N_x}{2\sigma_0}(\sigma_0 h - N_x) \quad [6]$$

and into Equation [5], for negative bending moment

$$N_\varphi = \sigma_0 h, \quad M_x = -\frac{N_x}{2\sigma_0}(\sigma_0 h - N_x) \quad [7]$$

The problem to be discussed is indicated in Fig. 5; namely, the determination of the wall thickness $h(x)$ of a shell under constant axial tension Q per unit length of shell perimeter and arbitrary internal pressure $p(x)$. Hence $N_x = Q$ in Equations [6] and [7], and

$$M_x'' = \frac{1}{2} Qh'' \quad [8]$$

or

$$M_x'' = -\frac{1}{2} Qh'' \quad [9]$$

Substituting the first of Equations [6] and [7], and Equations [8] and [9], into Equation [1] gives, finally

$$h'' + \omega^2 h = \frac{2p(x)}{Q} \quad [10]$$

for positive bending moment, and

$$h'' - \omega^2 h = -\frac{2p(x)}{Q} \quad [11]$$

for negative bending moment, where

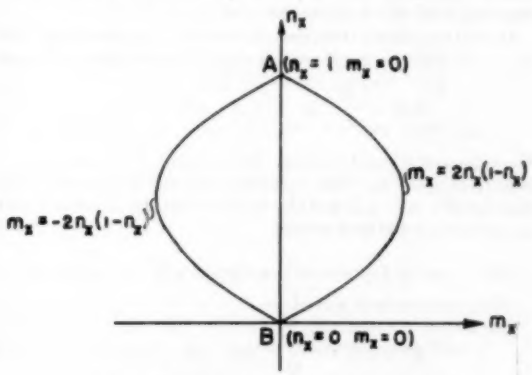

FIG. 4 SECTION $n_\varphi = 1$ OF YIELD SURFACE

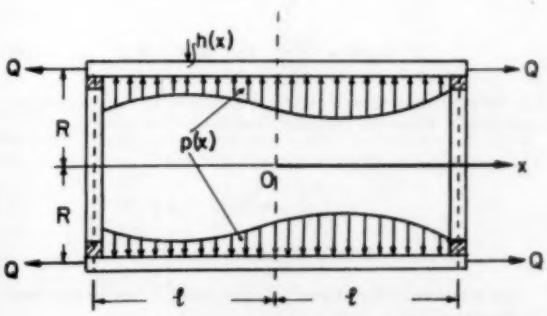

FIG. 5 LONGITUDINAL SECTION OF SHELL

$$\omega^2 = \frac{2\sigma_0}{QR} \quad \ldots\ldots [12]$$

The boundary conditions on h at the ends $x = \pm l$ follow from the condition that the shell is supported by inextensible rings; i.e., that the circumferential strain ϵ_φ vanishes there. By inspection of Figs. 3 and 4 it is seen that the end points $x = \pm l$ must correspond to point A on the yield surface where a vanishing of the circumferential strain rate is possible under the assumption of a discontinuity in n_φ; viz., that a transition from point A to point E ($n_\varphi = 0$) takes place at $x = \pm l$. This jump in the value of n_φ from 1 to 0 is permissible because it does not violate equilibrium or yield conditions.

Clearly, from Equations [6] and [7], $M_x = 0$ leads to the following boundary condition on h

$$h(x) = \frac{Q}{\sigma_0} \quad \text{for} \quad x = \pm l \quad \ldots\ldots [13]$$

The solution of the problem consists in the determination of a function $h(x)$ satisfying Equation [10] at points of positive and Equation [11] at points of negative bending moment, and Boundary Conditions [13].

In general, it may be expected that there will be a range $x_1 \leq x \leq x_2$ in which the bending moment will be negative, and that the bending moment will be positive in the remaining parts $-l \leq x \leq x_1$, $x_2 \leq x \leq l$ of the shell. Let $h(x) = h_2(x)$ in the former, and $h_1(x)$, $h_3(x)$, respectively, in the latter. If this assumption is not justified in a particular case, and nevertheless made, it will lead to an impossible answer such as that $h(x) < Q/\sigma_0$ at some points of the shell. A different assumption about the sections at which the bending moment changes sign—one suggested by physical reasoning—and application of the same technique as that here outlined will then lead to the correct solution.

It will be assumed, then, that the bending moment changes sign at $x = x_1$ and $x = x_2$; it must therefore be zero there and hence

$$h(x) = \frac{Q}{\sigma_0} \quad \text{at} \quad x = x_1 \quad \text{and} \quad x = x_2$$

the same as at the end sections. Furthermore, $h'(x)$ must be continuous at x_1 and x_2. These conditions are sufficient to determine $h(x)$ for all x in $(-l, l)$ and also to determine the values of x_1 and x_2, as shown in the next section.

Solution of Equations for Optimum Wall Thickness

The equations to be solved are

$$h'' + \omega^2 h = \frac{2p(x)}{Q} \quad \text{for} \quad -l \leq x \leq x_1 \quad \ldots\ldots [14]$$

$$h'' - \omega^2 h = -\frac{2p(x)}{Q} \quad \text{for} \quad x_1 \leq x \leq x_2 \quad \ldots\ldots [15]$$

$$h'' + \omega^2 h = \frac{2p(x)}{Q} \quad \text{for} \quad x_2 \leq x \leq l \quad \ldots\ldots [16]$$

Let the solution of these equations be denoted by h_1, h_2, and h_3, respectively. Then the boundary conditions are given by

$$\left.\begin{aligned} h_1(-l) = h_1(x_1) = h_2(x_1) = h_2(x_2) \\ = h_3(x_2) = h_3(l) = \frac{Q}{\sigma_0} \\ h_1'(x_1) = h_2'(x_1), \quad h_2'(x_2) = h_3'(x_2) \end{aligned}\right\} \quad \ldots [17]$$

The solutions of Equations [14], [15], and [16] can be expressed in the form

$$h_1(x) = A_1 \sin \omega x + A_2 \cos \omega x + \frac{2}{\omega Q}\int_{-l}^{x} p(t) \sin \omega(x - t)dt \quad \ldots\ldots [18]$$

$$\text{for} \quad -l \leq x \leq x_1$$

$$h_2(x) = B_1 \sinh \omega x + B_2 \cosh \omega x - \frac{2}{\omega Q}\int_{x_1}^{x} p(t) \sinh \omega(x - t)dt \quad \ldots\ldots [19]$$

$$\text{for} \quad x_1 \leq x \leq x_2$$

$$h_3(x) = C_1 \sin \omega x + C_2 \cos \omega x + \frac{2}{\omega Q}\int_{x_1}^{x} p(t) \sin \omega(x - t)dt \quad \ldots\ldots [20]$$

$$\text{for} \quad x_2 \leq x \leq l$$

where A_1, A_2, B_1, B_2, C_1, C_2 are constants to be determined by the Boundary Conditions [17]; the latter are eight equations for these six constants and the values x_1 and x_2. The following expressions for h_1, h_2, and h_3 result

$$\frac{\sigma_0}{Q} h_1(x) = \frac{\sin \omega(x + l) + \sin \omega(x_1 - x)}{\sin \omega(x_1 + l)} - \frac{\omega R}{Q}\left\{\frac{\sin \omega(x + l)}{\sin \omega(x_1 + l)}\int_{-l}^{x_1} p(t) \sin \omega(x_1 - t)dt - \int_{-l}^{x} p(t) \sin \omega(x - t)dt\right\} \quad \text{for} \quad -l \leq x \leq x_1 \quad \ldots\ldots [21]$$

$$\frac{\sigma_0}{Q} h_2(x) = \frac{\sinh \omega(x - x_1) + \sinh \omega(x_2 - x)}{\sinh \omega(x_2 - x_1)} + \frac{\omega R}{Q}\left\{\frac{\sinh \omega(x - x_1)}{\sinh \omega(x_2 - x_1)}\int_{x_1}^{x_2} p(t) \sinh \omega(x_2 - t)dt - \int_{x_1}^{x} p(t) \sinh \omega(x - t)dt\right\} \quad \text{for} \quad x_1 \leq x \leq x_2 \quad \ldots\ldots [22]$$

$$\frac{\sigma_0}{Q} h_3(x) = \frac{\sin \omega(x - x_2) + \sin \omega(l - x)}{\sin \omega(l - x_2)} - \frac{\omega R}{Q}\left\{\frac{\sin \omega(x - x_1)}{\sin \omega(l - x_2)}\int_{x_1}^{l} p(t) \sin \omega(l - t)dt - \int_{x_1}^{x} p(t) \sin \omega(x - t)dt\right\} \quad \text{for} \quad x_2 \leq x \leq l \quad \ldots\ldots [23]$$

where the functions $p(x)$ are given and x_1 and x_2 are determined from the following two equations

$$\frac{-1 + \cos \omega(x_1 - l)}{\sin \omega(x_1 + l)} + \frac{\omega R}{Q}\int_{-l}^{x} p(t) \frac{\sin \omega(l + t)}{\sin \omega(x_1 + l)}\, dt = \frac{1 - \cosh \omega(x_2 - x_1)}{\sinh \omega(x_2 - x_1)} - \frac{\omega R}{Q}\int_{x_1}^{x_2} p(t) \frac{\sinh \omega(x_2 - t)}{\sinh \omega(x_2 - x_1)}\, dt \quad \ldots [24]$$

and

$$\frac{-1 + \cosh \omega(x_2 - x_1)}{\sinh \omega(x_2 - x_1)} - \frac{\omega R}{Q}\int_{x_1}^{x_2} p(t) \frac{\sinh \omega(t - x_1)}{\sinh \omega(x_2 - x_1)}\, dt = \frac{1 - \cos \omega(l + x_2)}{\sin \omega(l - x_2)} - \frac{\omega R}{Q}\int_{x_2}^{l} p(t) \frac{\sin \omega(l - t)}{\sin \omega(l - x_2)}\, dt \quad \ldots\ldots [25]$$

Simplification in Particular Cases

In particular cases simplification will result when along portion of the shell the optimum thickness may be chosen as constant and

equal to its value at the extremities of the shell. This will occur, for instance, when a certain part of the wall is stress-free, and in other cases. The examples discussed here are a band of uniform pressure and a distribution of linearly increasing pressure.

Band of Pressure. Let the band occupy the region $a \leq x \leq b$ of the shell and the internal pressure along this length be p = const per unit area and zero everywhere else. The axial tension is Q/unit length of shell perimeter. If a thickness distribution can be found such that at points $x = x_1$ and $x = x_2$ where $x_1 < a, x_2 > b$ the bending moment and shearing force both vanish, then a uniform thickness $h(x) = h(x_1) = h(x_2) = Q/\sigma_0$ can be taken as the optimum distribution for $-l \leq x \leq x_1$ and $x_2 \leq x \leq l$. In other words, the equations to be solved are

$$h'' - \omega^2 h = 0 \quad \text{for} \quad x_1 \leq x \leq a, \quad b \leq x \leq x_2 \ldots [26]$$

$$h'' - \omega^2 h = -\frac{2p}{Q} \quad \text{for} \quad a \leq x \leq b \ldots\ldots\ldots [27]$$

under the boundary conditions $h(x_1) = h(x_2) = Q/\sigma_0$, $h'(x)_1 = h'(x_2) = 0$. Then this solution, together with $h(x) = Q/\sigma_0$ for $-l \leq x \leq x_1$, $x_2 \leq x \leq l$ will give the optimum design. It can be seen readily, as a special case of the solution of the previous section, or independently, that the following solution satisfies these conditions

$$\frac{\sigma_0}{Q} h(x) = \cosh \omega(x_1 - x) \quad \text{for} \quad x_1 \leq x \leq a \ldots\ldots [28]$$

$$\frac{\sigma_0}{Q} h(x) = \cosh \omega(x_1 - x) - \frac{pR}{Q} \{\cosh \omega(a - x) - 1\} \quad \text{for} \quad a \leq x \leq b \ldots\ldots [29]$$

$$\frac{\sigma_0}{Q} h(x) = \cosh \omega(x_2 - x) \quad \text{for} \quad b \leq x \leq x_2 \ldots\ldots [30]$$

where x_1 and x_2 are found from the equations

$$x_1 + x_2 = a + b \ldots\ldots\ldots\ldots\ldots [31]$$

$$\sinh \omega(x_1 - \xi) = \frac{pR}{Q} \sinh \omega(a - \xi) \ldots\ldots\ldots [32]$$

where $\xi = (a + b)/2$ and the solution is valid only if $pR/Q \geq 1$. Clearly

$$\frac{\sigma_0}{Q} h_{\max} = \frac{\sigma_0}{Q} h(\xi) = \cosh \omega(x_1 - \xi) - \frac{pR}{Q} \cosh \omega(a - \xi) + \frac{pR}{Q} \ldots\ldots [33]$$

In this case n_φ is discontinuous at the sections $x = x_1$ and $x = x_2$, viz., it suffers a unit jump there, and the situation is the same as that previously discussed in connection with the end points $x = \pm l$.

Fig. 6 shows the optimum thickness distribution for a cylindrical shell with two bands of internal pressure: One at $a/l = -0.7$, $b/l = -0.5$, the other at the end of the shell, $a/l = 0.8$, $b/l = 1.0$. The boundary conditions for the band at the extremity of the shell are slightly different from those given previously but the modifications in the analysis are trivial. The following numerical values are assumed in the diagram.

$$\frac{pR}{Q} = 2, \quad \frac{l}{R} = 4, \quad \frac{\sigma_0 R}{Q} = 10 \ldots\ldots\ldots [34]$$

Since x_2 for the left-hand band is smaller than x_1 for the right-hand band, the design procedures for the two bands are independent of each other. Since x_1 differs only slightly from a and x_2 from b this will, in general, be true when the bands are not too close together.

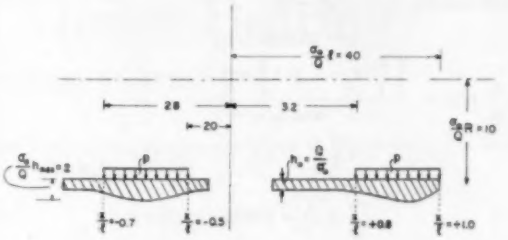

FIG. 6 OPTIMUM THICKNESS DISTRIBUTION FOR BANDS OF CONSTANT PRESSURE

LINEARLY INCREASING PRESSURE DISTRIBUTION

In this case the solution of the preceding section applies, with

$$p(x) = \frac{P}{2}\left(1 - \frac{x}{l}\right) \ldots\ldots\ldots\ldots [35]$$

where P is the pressure per unit area at the extremity $x = -l$ of the shell; the pressure tapers to zero at $x = l$.

It is found that a point x_1 can be chosen such that the bending moment and shearing force vanish there; i.e.

$$h(x_1) = \frac{Q}{\sigma_0}, \quad h'(x_1) = 0 \ldots\ldots\ldots\ldots [36]$$

and that the optimum wall-thickness distribution is given by the solution of

$$h'' - \omega^2 h = -\frac{2}{Q} p(x) = -\frac{P}{Q}\left(1 - \frac{x}{l}\right) \ldots [37]$$

in the region $-l \leq x \leq x_1$ under the boundary conditions

$$h(-l) = h(x_1) = \frac{Q}{\sigma_0}, \quad h'(x_1) = 0 \ldots\ldots\ldots [38]$$

and by

$$h(x) = \frac{Q}{\sigma_0} \ldots\ldots\ldots\ldots\ldots [39]$$

in the region $x_1 \leq x \leq l$. For the latter solution to be statically admissible one must have, from the equilibrium equations

$$\frac{N_\varphi}{R} = p(x) \ldots\ldots\ldots\ldots\ldots [40]$$

i.e.

$$n_\varphi = \frac{pR}{Q} = \frac{PR}{2Q}\left(1 - \frac{x}{l}\right) \quad \text{for} \quad x_1 \leq x \leq l \ldots [41]$$

In other words, as the generic point x moves from x_1 to l on the shell, the generic stress point on the yield locus moves on AE in Fig. 3. At x_1, n_φ jumps from the value 1 to the value

$$\frac{PR}{2Q}\left(1 - \frac{x_1}{l}\right)$$

then, as $x_1 \to l$, $n_\varphi \to 0$ on AE.

It follows that with

$$p(x) = \frac{P}{2}\left(1 - \frac{x}{l}\right)$$

and putting $(RP)/(2Q) = k$

$$\frac{\sigma_0}{Q} h(x) = \frac{(1-2k)\sinh\omega(x_1 - x) + \left(\frac{x_1}{l}k - k + 1\right)\sinh\omega(l+x)}{\sinh\omega(x_1+l)} - k\left(\frac{x}{l} - 1\right) \quad \text{for} \quad -l \le x \le x_1 \quad [42]$$

$$\frac{\sigma_0}{Q} h(x) = 1 \quad \text{for} \quad x_1 \le x \le l$$

with x_1 given by

$$\left(\frac{x_1}{l}k - k + 1\right)\cosh\omega(l+x_1) - \frac{k}{\omega l}\sinh\omega(l+x_1) + 2k - 1 = 0 \quad [43]$$

As a numerical example, we take again $Q/PR = 0.5$ (therefore $k = 1$), $l/R = 4$, $\sigma_0 R/Q = 10$.

The equation for x_1 becomes, for $k = 1$

$$\frac{1}{\omega l}\sinh\omega(l+x_1) - \frac{x_1}{l}\cosh\omega(l+x_1) = 1$$

In the present case

$$\omega l = \sqrt{\left(\frac{2\sigma_0}{QR}\right)} l = \sqrt{\left(2\frac{\sigma_0 R}{Q}\right)}\frac{l}{R} = 4\sqrt{20}$$

so that for the order of magnitude of ωl considered

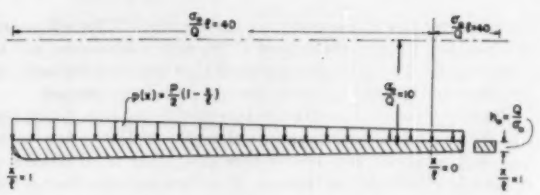

FIG. 7 OPTIMUM THICKNESS DISTRIBUTION FOR LINEARLY INCREASING PRESSURE

$$\sinh\omega l \backsimeq \cosh\omega l \backsimeq \frac{1}{2}e^{\omega l}$$

hence

$$\frac{1}{\omega l} - \frac{x_1}{l} \backsimeq 2e^{-\omega(l+x_1)}$$

Since $e^{-4\sqrt{20}} = 6.5 \times 10^{-7}$, this is negligible compared to $1/\omega l$ and so

$$\frac{x_1}{l} \backsimeq \frac{1}{\omega l} = 0.056$$

The optimum wall-thickness distribution is plotted in Fig. 7.

ACKNOWLEDGMENT

The author is indebted to Prof. W. Prager for helpful discussion and advice.

The Tapered-Land Thrust Bearing

By C. F. KETTLEBOROUGH,[1] MELBOURNE, AUSTRALIA

Neglecting side leakage the maximum load capacity which can be carried per unit width is obtained when there is a stepped convergence to the oil film. However, when side leakage is considered the stepped bearing is only slightly better than the tilting-pad bearing, this being due to the fact that the maximum oil pressure occurs at the step where the oil-film thickness is a maximum and hence there is easy means of escape for oil. The tapered-land bearing does not suffer from this disadvantage and computations have been carried out which show that the maximum load this bearing is capable of supporting is about 14 per cent greater than the maximum load capable of being supported by the tilting-pad bearing, both cases not neglecting side leakage. Some numerical calculations are made.

Nomenclature

The following nomenclature is used in the paper:

b = slope of tapered film = $\dfrac{h_1 - h_2}{h_2(1 - R)}$
L = width of pad
C_f = friction criterion
C_p = load criterion
f = coefficient of friction
F = friction force
h = film thickness
h_1 = inlet-film thickness
h_2 = outlet-film thickness
$\bar{h}$ = $(h_1 - h_2)$
H = nondimensional film thickness = h/h_2
k = film ratio (h_1/h_2)
B = length of pad in direction of motion
p = oil-film pressure
P = nondimensional pressure parameter
R = fractional length of parallel portion (see Fig. 1)
U = linear velocity of moving boundary
W = total load
x, z = co-ordinate axes in plane of bearing
X, Z = nondimensional co-ordinate
μ = viscosity

Introduction

Lord Rayleigh (1)[2] analyzed in detail the simple slider, neglecting side leakage and found the maximum load capacity per unit width perpendicular to the direction of motion was produced when there was a stepped convergence to the oil film. For this case Rayleigh showed that

$$W_{max} = 0.206 \frac{\mu U B^2}{h_2^2} \quad [1]$$

This constitutes an increase in load-carrying capacity of 29 per cent as compared with the maximum load per unit width which can be supported by a tilting-pad bearing, also neglecting side leakage, in which case

$$W_{max} = 0.160 \frac{\mu U B^2}{h_2^2} \quad [2]$$

When side leakage is considered, the constants in Equations [1] and [2] become 0.0725 and 0.072, respectively, for maximum load capacity. The advantage of the stepped slider over the tilting pad is considerably reduced. As pointed out by Archibald (2), this is due to the fact that the maximum oil pressure occurs at the step where the oil-film thickness is a maximum and hence there is easy means of escape for oil.

Bower (3) has demonstrated that, for the composite slider shown in Fig. 1, the maximum load per unit width, neglecting side leakage is

$$W_{max} = 0.192 \frac{\mu U B^2}{h_2^2} \quad [3]$$

when $R = 0.2$ and $k = 2.25$. This is only about 7 per cent less than the maximum load carried by the stepped pad. However, when side leakage takes place, the tapered-land bearing does not suffer from the same disadvantage as the stepped bearing.

Computations have been made and it is found that the maximum load capacity of the tapered-land bearing is 14 per cent greater than that carried by the tilting-pad bearing, side leakage being considered.

Analysis

The composite slider, Fig. 1, consists of two regions; region 2,

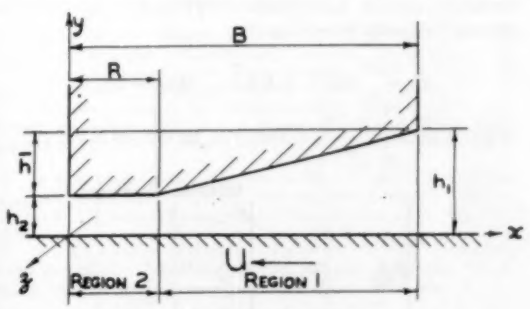

Fig. 1 Tapered-Land Bearing

where the oil-film thickness is h_2, and region 1, where the oil-film thickness increases linearly from h_2 to h_1.

The governing equation over region 1 is Reynolds equation

$$\frac{\partial}{\partial x}\left(\frac{h^3}{\mu}\frac{\partial p}{\partial x}\right) + \frac{\partial}{\partial z}\left(\frac{h^3}{\mu}\frac{\partial p}{\partial z}\right) = 6U\frac{dh}{dx} \quad [4]$$

---

[1] Senior Lecturer, School of Engineering, University of Melbourne.

[2] Numbers in parentheses refer to the Bibliography at the end of the paper.

Presented at the National Applied Mechanics Division Conference, Urbana, Ill., June 14–16, 1956, of The American Society of Mechanical Engineers.

Discussion of this paper should be addressed to the Secretary, ASME, 29 West 39th Street, New York, N. Y., and will be accepted until January 10, 1957, for publication at a later date. Discussion received after the closing date will be returned.

Note: Statements and opinions advanced in papers are to be understood as individual expressions of their authors and not those of the Society. Manuscript received by ASME Applied Mechanics Division, November 8, 1954. Paper No. 56—APM-21.

Over region 2 where the film thickness is constant this reduces to

$$\frac{\partial^2 p}{\partial x^2} + \frac{\partial^2 p}{\partial z^2} = 0 \quad \ldots\ldots [5]$$

The pressure on the exterior boundaries is zero. The boundary condition between the two regions is determined by equating the oil flow out of region 1 to the oil flow into region 2, i.e.

$$\frac{h_1^3}{12\mu}\left(\frac{\partial p}{\partial x}\right)_1 + \frac{Uh_1}{2} = \frac{h_2^3}{12\mu}\left(\frac{\partial p}{\partial x}\right)_2 + \frac{Uh_2}{2} \quad \ldots\ldots [6]$$

where $(\partial p/\partial x)_1$ and $(\partial p/\partial x)_2$ are the slopes of the pressure distribution for regions 1 and 2, respectively, at the common boundary. Since $h_2 = h_1$, at this boundary Equation [6] reduces to

$$\left(\frac{\partial p}{\partial x}\right)_1 = \left(\frac{\partial p}{\partial x}\right)_2 \quad \ldots\ldots [7]$$

Equations [4], [5], and [6] are made nondimensional by the following substitutions

$$p = \frac{6\mu UB}{h_2^2} \cdot P; \; z = ZB; \; x = XB$$

$$h = Hh_2$$

where $H = [1 + b(X - R)]$ over region 1

$$\frac{\partial}{\partial X}\left[H^3 \frac{\partial p}{\partial X}\right] + \frac{\partial}{\partial Z}\left[H^3 \frac{\partial P}{\partial Z}\right] = \frac{\partial H}{\partial X} \quad \ldots\ldots [8]$$

$$\frac{\partial^2 P}{\partial X^2} + \frac{\partial^2 P}{\partial Z^2} = 0 \quad \ldots\ldots [9]$$

$$\left(\frac{\partial P}{\partial X}\right)_1 = \left(\frac{\partial P}{\partial X}\right)_2 \quad \ldots\ldots [10]$$

The resultant pressure distribution over the bearing surface is determined by relaxation techniques. The application of Equation [8] over region 1 has been given by Christopherson (4). Equation [9] applied over region 1 is the simple (1,1,1,1, —4) relaxation operator, and Equation [10], used to determine the common boundary pressure, gives

$$P_0 = \frac{1}{6}\,[4(P_1)_2 + 4(P_1)_1 - (P_2)_2 - (P_2)_1]$$

where P_0, $(P_1)_2$, $(P_1)_1$, $(P_2)_2$, and $(P_2)_1$, are defined in Fig. 2.

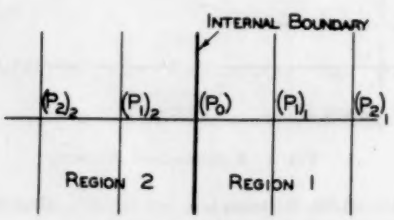

FIG. 2

Having determined the pressure distribution, all the important operating characteristics can be computed:

Total load

$$W = \frac{6\mu UB^3}{h_2^2}\int_0^1 \int_0^{L/B} P\,dX\,dZ$$

Load criterion

$$C_p = \left(\frac{W}{\mu U}\right)\left(\frac{h_2^2}{B^2}\right) = 6\int_0^1 \int_0^{L/B} P\,dX\,dZ$$

Friction force

$$F = \frac{\mu UB^2}{h_2}\left[R\,\frac{L}{B} + \frac{L}{bB}\log_e\,[1 + b(1 - R)] + 3b\int_R^1 \int_0^{L/B} P\,dX\,dZ\right]$$

Friction criterion

$$C_f = \left(\frac{F}{\mu U}\right)\left(\frac{h_2}{B^2}\right) = \left[R\,\frac{L}{B} + \frac{L}{bB}\log_e\,[1 + b(1 - R)] + 3b\int_R^1 \int_0^{L/B} P\,dX\,dZ\right]$$

Coefficient of Friction Criterion. This equals

$$\frac{\text{Friction criterion}}{\text{Load criterion}} = f\,\frac{B}{h_2}$$

Calculated Results

A square slider was considered ($B/L = 1$), and the pressure distribution was determined for values of $R = 0$, 0.125, 0.25, 0.375, and 0.50. The load criterion is plotted in Fig. 3 for these conditions. A value of $R = 0.25$ appears to give the maximum load-carrying capacity for all values of the film ratio. This value is greater than the load carried by the tilting pad for which $R = 0$. Fig. 3 gives the variation of the load criterion against film ratio for $R = 0.25$, extra computations being made for values of k between 2 and 3. The maximum load capacity is now

$$0.0823\,\frac{\mu UB^3}{h_2^2} \quad \ldots\ldots [11]$$

at a film ratio of 2.3. This is 14 per cent increase on the load of the simple tilting slider.

Some Numerical Calculations

It must be noted that the tapered-land and tilting thrust bearings behave differently. The film ratio under which the tilting pad operates is controlled by the pivot location. An increase in the load causes a decrease in the minimum film thickness, while the film ratio remains constant, the pad tilting about some axis ahead of the trailing edge; hence the difference between the inlet and outlet-film thicknesses decreases. In the tapered-land bearing the difference between the inlet and outlet-film thicknesses remains constant. An increase in the load causes the minimum film thickness to decrease and the film ratio to increase. Hence Fig. 3 is not entirely suitable for the solution of fixed-tapered thrust bearings as this graph shows the variation in load capacity for different film ratios for constant outlet-film thickness, this implying a progressively increasing value of $(h_1 - h_2)$ which is physically impossible. The load-criterion curve has been replotted in Fig. 3, introducing $\bar{h} = (h_1 - h_2)$, instead of h_2 in the load-criterion formula so that the load criterion based on $\bar{h}$ is

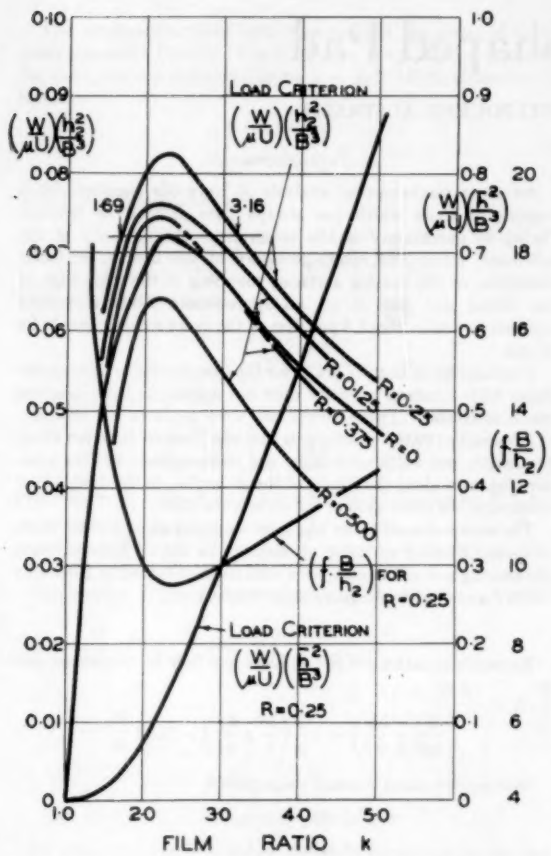

FIG. 3 LOAD CRITERION AND COEFFICIENT OF FRICTION CRITERION CURVES FOR TAPERED-LAND BEARING

$$\left(\frac{W}{\mu U}\right)\left(\frac{\bar{h}^2}{B^2}\right) = (k-1)^2 C_p$$

Similarly

$$\left(\frac{F}{\mu U}\right)\left(\frac{\bar{h}}{B^2}\right) = (k-1)C_f$$

and

$$\frac{\text{Friction criterion}}{\text{Load criterion}} = f\frac{B}{\bar{h}}$$

The following example illustrates the behavior of the tapered-land bearing as compared with the tilting-pad bearing:

(*a*) A tilting-pad bearing, 1 in. × 1 in., operates at 100 fps and a minimum oil-film thickness of 0.001 in. at a load of 200 psi. The pivot position is to be chosen so that the optimum conditions may be obtained.

The charts of Muskat, Morgan, and Meres (5) have been used. The pivot must be located 0.6 in. from the inlet edge, the film ratio is 2.33, an oil viscosity of 2.36×10^{-6} reyns is necessary, and the coefficient of friction is 0.00997. For the same oil viscosity and pivot position, operating values have been computed for different loads as given in Table 1.

(*b*) A tapered-land bearing was then considered. The initial conditions were taken as in the foregoing case at 200 lb load ($h_1 = 0.001$ in., $h_2 = 0.00233$ in., $\bar{h} = 0.00133$ in., $U = 100$ fps).

When $k = 2.33$, and using Fig. 3

$$\frac{W\bar{h}^2}{\mu U B^2} = 0.148$$

from which the operating viscosity $= 1.99 \times 10^{-6}$ reyns. Using this oil viscosity and assuming $\bar{h}$ remains constant at 0.00133 in., the minimum film thickness, the film ratio, and coefficient of friction have been computed for several applied loads, using the graphs in Fig. 3, and tabulated in Table 1.

(*c*) As another example of its operation, a tapered-land bearing was considered with $\bar{h} = 0.001$ in. and $\mu = 2.1 \times 10^{-6}$ reyns. Details are given in Table 1.

TABLE 1 TYPICAL CALCULATED OPERATING CONDITIONS

		Load, psi				
		100	200	300	400	500
Tilting pad	h_2	0.0014	0.0010	0.00082	0.00071	0.00063
$k = 2.33$	f	0.0141	0.0100	0.0081	0.0071	0.0063
Tapered-land pad	h_2	0.0014	0.0010	0.00079	0.00067	0.00058
$\bar{h} = 0.00133$ in.	f	0.0144	0.0096	0.0077	0.0066	0.0060
	k	1.96	2.33	2.68	2.99	3.29
Tapered-land pad	h_2	0.0014	0.0010	0.00084	0.00072	0.00064
$\bar{h} = 0.001$ in.	f	0.0158	0.0102	0.0082	0.0069	0.0061
	k	1.73	2.00	2.19	2.38	2.57

The results clearly indicate that a nontilting bearing of the tapered-land type can be designed to operate with a comparable efficiency to that of the more complicated tilting-pad bearing over a certain range of operating conditions. However, the tilting-pad bearing, by reason of its adjustability, can maintain optimum conditions for all values of the $\mu N/W$ criterion. Referring to Fig. 3, the load capacity of the tapered-land bearing with $R = 0.25$ is greater than the maximum load capacity for the tilting-pad bearing ($R = 0$) over a range of film ratio from 1·69 to 3·16. Hence, during the starting and stopping cycle, when k is very large or under light loads when k is small, the tilting-pad bearing has the advantage.

BIBLIOGRAPHY

1 "Notes on the Theory of Lubrication," by Lord Rayleigh, *Philosophical Magazine and Journal of Science*, vol. 35, 1918, pp. 1–12.

2 "A Simple Hydrodynamic Thrust Bearing," by F. R. Archibald, Trans. ASME, vol. 72, 1950, pp. 393–400.

3 Discussion of paper by A. Fogg entitled, "Film Lubrication of Parallel Thrust Surfaces," by G. S. Bower, Proceedings of The Institution of Mechanical Engineers, London, England, vol. 155, 1946, p. 49.

4 "A New Mathematical Method for the Solution of Film Lubrication Problems," by D. G. Christopherson, Proceedings of The Institution of Mechanical Engineers, London, England, vol. 146, 1941, p. 126.

5 "The Lubrication of Sliders of Finite Width," by M. Muskat, F. Morgan, and M. W. Meres, *Journal of Applied Physics*, vol. 2, 1940, p. 208.

The Sector-Shaped Pad

By C. F. KETTLEBOROUGH,[1] MELBOURNE, AUSTRALIA

Boegli's simplifying assumptions for the solution of the rectangular pad has been applied to the sector-shaped pad and extended to the case of varying viscosity. The process of obtaining the operating characteristics is very rapid and yields results comparable with those obtained by longer numerical methods.

Nomenclature

The following nomenclature is used in the paper:

$\bar{A} = (6\omega\lambda_o r_o^2\phi)/h_o^2$
A, B, C = constants of integration
b = (film ratio —1)
c = (viscosity ratio —1)
D = load function, Equation [7]
F = friction force
f = film ratio
h = film thickness
h_o = outlet film thickness
K_1, K_2 = constants in solution of Equation [4]
M = defined in Equation [4a]
$N = \phi/\rho$
$n = \sqrt{-M/N^2}$
p = pressure
r = radius
r_o = inner radius
r_1 = nondimensional radius
r_2 = outer radius
r_f = radial breadth
r_m = radius at which $F(r_1)$ has a maximum value
v = viscosity ratio
w = oil-film velocity in direction of motion
y = co-ordinate perpendicular to plane of motion
$F(\theta_1)$ = nondimensional pressure parameter in direction of motion
$F(r_1)$ = nondimensional pressure parameter in radial direction
θ = circumferential co-ordinate
θ_1 = nondimensional circumferential co-ordinate
θ_m = value of θ_1, where $F(\theta_1)$ has a maximum value
$\bar{\theta}$ = position of center of pressure
ϕ = angle subtended by radial edges of pad
β = film-thickness function $= (1 + b\theta_1)$
ϵ = viscosity function $= (1 + c\theta_1)$
ρ = $\log_e r_2/r_o$, from $r = r_o e^{\rho r_1}$
λ = viscosity
λ_o = inlet viscosity
λ_m = mean viscosity
ω = angular velocity
μ = coefficient of friction

[1] Senior Lecturer, School of Engineering, University of Melbourne.

Presented at the National Applied Mechanics Division Conference, Urbana Ill., June 14–16, 1956, of The American Society of Mechanical Engineers.

Discussion of this paper should be addressed to the Secretary, ASME, 29 West 39th Street, New York, N. Y., and will be accepted until January 10, 1957, for publication at a later date. Discussion received after the closing date will be returned.

Note: Statements and opinions advanced in papers are to be understood as individual expressions of their authors and not those of the Society. Manuscript received by ASME Applied Mechanics Division, November 8, 1954. Paper No. 56—APM-22.

Introduction

An exact mathematical analysis of Reynolds equation for a bearing of finite width has always been difficult or tedious. Owing to uncertainty of the behavior of the viscosity of the lubricant, micro and macro-geometry of the bearing surfaces, distortion of the bearing surfaces, rounding of the inlet edge of the tilting pad, and so on, an approximate solution yielding answers to within about 5 per cent of the exact solution would be of use.

The solution of Boegli (1947)[2] for the case of a finite rectangular slider with constant viscosity does not appear to have received much attention. Two assumptions were made in his analysis: (1) Boswall's (1928)[3] assumption that the pressure function along the length and width of a slider are independent; (2) the pressure function along the length of the slider, i.e., in the direction of motion, is the same as that for an infinite slider.

The sector-shaped slider has been analyzed along similar lines, assuming a linear variation of viscosity as the oil flows through the bearing and values compared with those obtained by Boswall's (1928)[3] and Christopherson's (1941)[4] solutions.

Analysis

Reynolds equation for two-dimensional flow for the sector pad is

$$\frac{\partial}{\partial\theta}\left(\frac{h^3}{\lambda}\frac{\partial p}{\partial\theta}\right) + r\frac{\partial}{\partial r}\left(\frac{h^3}{\lambda}r\frac{\partial p}{\partial r}\right) = 6\omega r^2\frac{dh}{d\theta}$$

Making the usual Boswall assumptions

$$\theta = \phi\theta_1;\quad r = r_o e^{\rho r_1}$$
$$h = h_o\beta = h_o(1 + b\theta_1)$$
$$\lambda = \lambda_o\epsilon = \lambda_o(1 + c\theta_1)$$

the foregoing equation becomes

$$\frac{\partial}{\partial\theta_1}\left(\frac{\beta^3}{\epsilon}\frac{\partial p}{\partial\theta_1}\right) + N^2\frac{\beta^3}{\epsilon}\frac{\partial^2 p}{\partial r_1^2} = \bar{A}e^{2\rho r_1}\cdot\frac{d\beta}{d\theta_1} \quad \ldots\ldots [1]$$

Following Boswall's assumption the pressure at any point can be expressed as the product of two independent functions. Hence, substituting

$$p = \bar{A}e^{2\rho r_m}F(\theta_1)F(r_1)$$

$$\frac{\partial}{\partial\theta_1}\left[\frac{\beta^3}{\epsilon}F(r_1)\frac{\partial F(\theta)_1}{\partial\theta_1}\right] + N^2\frac{\beta^3}{\epsilon}F(\theta_1)\frac{\partial^2 F(r_1)}{\partial r_1^2} = e^{2\rho(r_1 - r_m)}\frac{d\beta}{d\theta_1} \quad \ldots\ldots [2]$$

To solve for $F(\theta_1)$, i.e., pressure function in direction of motion. $F(\theta_1)$ is assumed to be the same form as that for a pad neglecting side leakage. Under this condition Equation [1] reduces to

$$\frac{d}{d\theta_1}\left(\frac{\beta^3}{\epsilon}\frac{dp}{d\theta_1}\right) = \bar{A}e^{2\rho r_1}\frac{d\beta}{d\theta_1} \quad \ldots\ldots\ldots\ldots [3]$$

[2] "The Hydrodynamic Lubrication of Finite Sliders," by C. P. Boegli, *Journal of Applied Physics*, vol. 18, 1947, p. 482.

[3] "Theory of Film Lubrication," by R. O. Boswall, Longmans, Green and Company, New York, N. Y., 1928.

[4] "A New Mathematical Solution of Film Lubrication Problems," by D. G. Christopherson, Proceedings of The Institution of Mechanical Engineers, London, England, vol. 146, 1941, p. 126.

The pressure functions both pass through the point of maximum pressure. For $F(\theta_1)$ this is where $r_1 = r_m$. Hence, considering the r_m-section and substituting $p = Ae^{2\rho r_m}F(\theta)$, Equation [3] becomes

$$\frac{d}{d\theta_1}\left[\frac{\beta^3}{\epsilon}\frac{dF(\theta_1)}{d\theta_1}\right] = \frac{d\beta}{d\theta_1} \quad \ldots\ldots\ldots\ldots\ldots\ldots [4]$$

which on differentiation gives

$$\frac{\beta^3}{\epsilon}\frac{d^2F(\theta_1)}{d\theta_1^2} + \frac{dF(\theta_1)}{d\theta_1}\frac{d}{d\theta_1}\left(\frac{\beta^3}{\epsilon}\right) = \frac{d\beta}{d\theta_1}$$

when $F(\theta_1)$ is a maximum, i.e.

$$\frac{dF(\theta_1)}{d\theta_1} = 0$$

this equation shows that

$$\left[\frac{d^2F(\theta_1)}{d\theta_1^2}\right]_{\theta_m} = \left(\frac{\epsilon}{\beta^3}\frac{d\beta}{d\theta_1}\right)_{\theta_m}$$

where $\theta_m = \theta_1$ when $F(\theta_1)$ is a maximum. Dividing by $F(\theta_m)$

$$\left[\frac{1}{F(\theta_1)}\frac{d^2F(\theta_1)}{d\theta_1^2}\right]_{\theta_m} = \left[\frac{\epsilon}{\beta^3}\frac{d\beta}{d\theta_1}\frac{1}{F(\theta_1)}\right]_{\theta_m} = M, \text{ say} \ldots [4a]$$

The solution of Equation [4] is given by Boswall[5]

$$F(\theta_1) = \frac{1}{b^2}\left[c\log_e(1+b\theta_1) - \frac{(b-c)}{(1+b\theta_1)} + K_1\frac{(b+c+2bc\theta_1)}{2(1+b\theta_1)^2} + K_2\right]$$

$$K_1 = \frac{2(1+b)^2}{b^2(b+c+2)}\left[c\log_e(1+b) + \frac{b(b-c)}{(1+b)}\right]$$

$$K_2 = (b-c) - K_1(b+c)/2 \quad \text{and} \quad \theta_m = (K_1 - 1)/b$$

To solve for $F(r_1)$—pressure function perpendicular to the direction of motion. $F(r_1)$[6] is solved along the line where $F(\theta_1)$ is a maximum, i.e.

$$\frac{dF(\theta_1)}{d\theta_1} = 0$$

Equation [2] gives

$$\frac{d^2F(r_1)}{dr_1^2} + \frac{\left[\frac{1}{F(\theta_1)}\frac{d^2F(\theta_1)}{d\theta_1^2}\right]_{\theta_m}}{N^2}F(r_1) = \frac{\left[\frac{\epsilon}{\beta^3}\frac{d\beta}{d\theta_1}\frac{1}{F(\theta_1)}\right]_{\theta_m}}{N^2}e^{2\rho(r_1-r_m)}$$

$$\therefore \frac{d^2F(r_1)}{dr_1^2} + \frac{M}{N^2}F(r_1) = \frac{M}{N^2}e^{2\rho(r_1-r_m)}$$

The solution of this is

$$F(r_1) = Ae^{nr_1} + Be^{-nr_1} + Ce^{2\rho r_1} \quad \ldots\ldots\ldots\ldots [5]$$

where

$$A = C\left(\frac{e^{-n} - e^{2\rho}}{e^n - e^{-n}}\right); \quad B = C\left(\frac{e^{2\rho} - e^n}{e^n - e^{-n}}\right);$$

$$C = \left(\frac{M}{M + 4\rho^2}\right)e^{-2\rho r_m}$$

The value of r_m is required. This is the value of r_1 when $F(r_1)$ is a maximum.

[5] Boswall, loc. cit., pp. 40–41.

[6] The maximum value of the radial pressure function is not necessarily equal to unity, as in Boswall's solution.

This condition is obtained from Equation [5]

$$\frac{dF(r_1)}{dr_1} = An e^{nr_m} - Bne^{-nr_m} + 2\rho Ce^{2\rho r_m} = 0 \ldots [5a]$$

Friction and Friction Criterion

It is necessary to apply a tangential force to overcome the shear stress in the layer of film in contact with the rotating disk. The fluid exerts a drag force on the stationary surface chiefly in the direction of motion. The intensity of the tangential force T across any oil section is given by

$$T = -\lambda\left(\frac{dw}{dy}\right)$$

where

$$w = \frac{1}{r\lambda}\frac{dp}{d\theta}y\frac{(y-h)}{2} - \omega r\frac{(y-h)}{h}$$

$$F = \text{frictional force} = \iint Tr d\theta\, dr$$

Substituting for p, r, h, θ, and λ and simplifying

$$F = \pm Ae^{2\rho r_m}r_0\frac{h_0}{2}\rho\int_0^1\int_0^1 F(\theta_1)\frac{d\beta}{d\theta_1}e^{\rho r_1}F(r_1)d\theta_1 dr_1 + \frac{\lambda_0\omega\phi}{h_0}r_0^3\left[\frac{\left(1+\frac{r_b}{r_0}\right)^3 - 1}{3}\right]\int_0^1\frac{\epsilon}{\beta}d\theta_1$$

The coefficient of friction μ is given by F/W and defining the friction criterion as

$$\left(\frac{\mu}{r_0}\right)\left(\frac{W}{\lambda_0\omega}\right)^{1/2}$$

$$\left(\frac{\mu}{r_0}\right)\left(\frac{W}{\lambda_0\omega}\right)^{1/2} = \left(\frac{1}{6D}\right)^{1/2}\left\{\left[\frac{\left(1+\frac{r_b}{r_0}\right)^3 - 1}{3}\right]\int_0^1\frac{\epsilon}{\beta}d\theta_1 \pm 3\rho e^{2\rho r_m}\int_0^1\int_0^1\frac{d\beta}{d\theta_1}F(\theta_1)F(r_1)e^{\rho r_1}dr_1 d\theta_1\right\} \ldots [6]$$

The positive sign is for the stationary surface; the negative sign is for the moving surface. Examination shows that μ is greatest for the moving surface; $F(\theta_1)$ is actually negative. Considering the first integral

$$\int_0^1\frac{\epsilon}{\beta}d\theta_1 = E$$

This integral has been evaluated for different values of c and b by Boswall[7]

The second integral becomes

$$\pm 3b\rho e^{2\rho r_m}\int_0^1 F(\theta_1)d\theta_1\int_0^1 F(r_1)e^{\rho r_1}dr_1$$

The integral $\int_0^1 F(\theta_1)d\theta_1$ is the same as that for a pad with side leakage neglected and has been evaluated for different conditions by Boswall.[7] (This is actually the table headed D.) The integral $\int_0^1 F(r_1)e^{\rho r_1}dr_1$ is solved numerically.

Total Load. Following the method of Boswall

[7] Boswall, loc. cit., p. 42.

TABLE 1 EXAMPLES

Ratio f, v		Film criterion		Friction criterion		$\bar{\theta}$	
		This method	Previous method	This method	Previous method	This method	Previous method
2	1	0.390	0.393[a]	3.21	3.16[a]	0.432	0.42
3	1	0.407	0.397[b]	2.60	2.65[b]	0.392	0.375
3	2	0.381	0.391[b]	2.57	2.57[b]	0.416	0.394

[a] Determination by Boswall's approximate method.
[b] Determination by Christopherson's method.

$$W = \iint prd\theta\, dr = \bar{A} r_0^2 \phi D \quad \ldots\ldots\ldots\ldots [7]$$

where

$$D = \rho e^{2\rho r_m} \int_0^1 F(\theta_1) d\theta_1 \int_0^1 F(r_1) e^{2\rho r_1} dr_1$$

Film-Thickness Criterion. This is defined as

$$\left(\frac{h_0}{\phi r_0^2}\right)\left(\frac{W}{\lambda_0 \omega}\right)^{1/2} = (6D)^{1/2} \quad \ldots\ldots\ldots\ldots [8]$$

on rearranging Equation [7].

Center of Pressure. (Defined as $\bar{\theta}$.) The value of $\bar{\theta}$ depends on the values of b and c and is equal to $\bar{\theta}$ for a pad neglecting side leakage. The error introduced is only small, particularly as the equivalent (length/breadth) ratio is normally in the region of 1.

Numerical Problem

The case will be considered where the film ratio (f) is 3, i.e., $b = 2$ and $c = 1$; i.e., viscosity ratio is 2. Substituting in the given formulas, $K_1 = 1.589$, $(\theta_m) = 0.294$, $F(\theta_m) = -0.060$

$$\beta_m = 1 + b\theta_m = 1.59$$
$$\epsilon_m = 1 + c\theta_m = 1.29$$

The value of M is calculated from the expression on the right-hand side of Equation [4a], $M = -10.74$.

In some research carried out at Sheffield University the pads had the following dimensions: Inner radius $1\frac{1}{8}$ in.; outer radius $2\frac{1}{16}$ in.; angle subtended by pad, 35° 16′. The values of ρ and N are 0.606 and 1.107, respectively, and hence $n = 3.22$.

From Equation [5a] r_m is found to be 0.592 and $e^{2\rho r_m} = 2.050$. The constants required to determine $F(r_1)$ become

$$A = -0.077, \quad B = -0.493, \quad C = 0.568$$

$F(r_1)$ is determined for $r_1 = 0$ to 1.0 for 10 intervals whence

$$\int_0^1 F(r_1) e^{2\rho r_1} dr_1 = 0.803$$

From Boswall, $\int_0^1 F(\theta_1) d\theta_1 = 0.0368$,

whence D becomes 0.0366 and the film-thickness criterion based on the mean viscosity (λ_m)

$$\left(\frac{h_0}{\phi r_0^2}\right)\left(\frac{W}{\omega \lambda_m}\right)^{1/2} = (6D)^{1/2}\left(\frac{2}{c+2}\right)^{1/2} = 0.381$$

Friction Criterion. Briefly

$$\int_0^1 e^{\rho r_1} F(r_1) dr_1 = 0.55; \quad \int_0^1 F(\theta_1) d\theta_1 = 0.0368;$$

$$\int_0^1 \frac{\epsilon}{\beta} d\theta_1 = 0.775$$

whence

$$\left(\frac{\mu}{r_0}\right)\left(\frac{W}{\omega \lambda_0}\right)^{1/2} = 3.16; \quad \left(\frac{\mu}{r_0}\right)\left(\frac{W}{\omega \lambda_m}\right) = 2.57$$

From Boswall[5] $\bar{\theta} = 0.416$.

Examples which have been solved are given in Table 1. The agreement between the two sets of results is very close and appears to justify the assumptions made. The chief advantage is the time saved. The method described requires the use of a slide rule only, whereas Boswall's and Christopherson's methods require a calculating machine.

[5] Boswall, loc. cit., table 11, p. 43.

The Boundary Layer Inside a Conical Surface Due to Swirl

By H. E. WEBER,[1] EMERYVILLE, CALIF.

An analysis of the axially symmetric boundary layer on the inside of a conical surface due to swirl flow about the conical axis is presented. The momentum integrals of the boundary layer are derived, and both the laminar and turbulent boundary-layer solutions are obtained numerically. In the free stream the flow is assumed to be a potential vortex. A comparison between theory and experiment is made by using the particle paths on the conical surface of a cyclone dust separator.

Nomenclature

The following nomenclature is used in the paper:

c_3, c_4 = constants in series expansion of the dependent variables in boundary-layer solution for swirl flow near a conical surface
E = proportionality factor in assumed expression for u-velocity, where $E = E(x)$
m = mass rate of flow
p = static pressure
R = radius in spherical co-ordinates with origin at vertex of cyclone cone with R lying on conical surface
R_0 = distance between vertex and base of a cone measured along R
R_1 = nondimensional spherical radius on conical surface where $R_1 = R/R_0$
r_w = radius of conical wall in cylindrical co-ordinates
u, v, w = fluid velocities in boundary-layer analysis for swirl flow in x, θ, y co-ordinates, respectively
v_δ = θ-velocity in free stream at edge of boundary layer on cone wall
X = acute angle between path of particle on conical surface and spherical radius R
x, θ, y = co-ordinates in boundary-layer analysis with x and y in a meridian plane and parallel and perpendicular, respectively, to cone wall and θ in direction perpendicular to a meridian plane
α, α' = acute cone angles where $\alpha' = -\alpha$
δ = boundary-layer thickness as defined by momentum integrals of boundary layer
δ_1 = nondimensional boundary-layer thickness defined in text
η = nondimensional y-co-ordinate where $\eta = y/\delta$
ρ = density of fluid
μ = viscosity of fluid
ν = kinematic viscosity of fluid
τ_w = shear stress on fluid at wall
τ_{xw}, $\tau_{\theta w}$ = shear stress on fluid at wall in x and θ-directions
Γ = free-stream vortex strength, $\Gamma = v_\delta r = \text{const}$ for a potential vortex

Introduction

In a cyclone dust separator the tangential-velocity components are much greater than the axial and radial-velocity components except in a region near the cyclone axis and in the boundary layers near the walls. Therefore, as a first approximation, the flow outside of the wall boundary layer on the conical surface of the cyclone may be considered as a two-dimensional vortex; i.e., the component of velocity parallel to the wall in a meridian plane may be assumed zero. In addition, it may be assumed that the vortex in the free stream is a potential vortex about the axis of the cone and outside of central fluid core.

The data of Ter Linden[2] on experimentally measured velocity profiles show that this approximation for the tangential velocity component in the free stream is reasonable. In addition, the data show that the core of solid-body rotation continually decreases in diameter with the decrease in cone diameter, and the potential type of vortex exists outside of the boundary layer as far down the cone as the measurements were taken which was $^3/_4$ of the cone depth. In the cyclone used by Ter Linden the hole to the collecting hopper was formed by cutting the cone at 85 per cent of its depth. Hence we shall assume that the potential vortex exists outside of the wall boundary layer over the entire axial depth of the conical surface.

The free-stream vortex creates a pressure gradient with pressure decreasing radially inward. This pressure gradient has a component parallel to the cone wall. In the free stream the pressure gradient is balanced by the radial acceleration of the fluid, but in the boundary layer the pressure gradient causes fluid which is retarded by the wall and has a smaller radial acceleration to acquire a component of velocity in a meridian plane. However, the total velocity is zero at the wall. In the free stream the component of velocity in a meridian plane is zero by the assumed flow conditions. Therefore this component of velocity is zero at the surface of the boundary layer and at the wall of the cone and attains a maximum value somewhere in the boundary layer.

Finally, the customary boundary-layer assumptions are made. The velocity normal to the wall is assumed negligible as compared with the velocity parallel to the wall. The variations in pressure through the boundary layer in the direction normal to the wall are assumed negligible as compared with these variations in the direction parallel to the wall. In addition, the boundary-layer thickness is assumed to be small compared with the radius of the cone. In this analysis the momentum integrals of the boundary layer are employed,[3] and both laminar and turbulent boundary-layer solutions are obtained.

---

[1] Shell Development Company; formerly, Instructor of Mechanical Engineering, Massachusetts Inst. of Technology, Cambridge, Mass.

Presented at the National Applied Mechanics Division Conference, Urbana, Ill., June 14–16, 1956, of The American Society of Mechanical Engineers.

Discussion of this paper should be addressed to the Secretary, ASME, 29 West 39th Street, New York, N. Y., and will be accepted until January 10, 1957, for publication at a later date. Discussion received after the closing date will be returned.

Note: Statements and opinions advanced in papers are to be understood as individual expressions of their authors and not those of the Society. Manuscript received by ASME Applied Mechanics Division, February 17, 1956. Paper No. 56—APM-31.

[2] "Investigations Into Cyclone Dust Separators," by A. J. Ter Linden, Proceedings of The Institution of Mechanical Engineers, London, England, vol. 160, no. 2, 1949, p. 233.

[3] G. I. Taylor has solved this problem for the laminar boundary layer by transforming the Navier-Stokes equations into integral equations and using the Karman-Pohlhausen method. "The Boundary Layer in the Converging Nozzle of a Swirl Atomizer," by G. I. Taylor, *Quarterly Journal of Mechanics and Applied Mathematics*, vol. 3, 1950, p. 129.

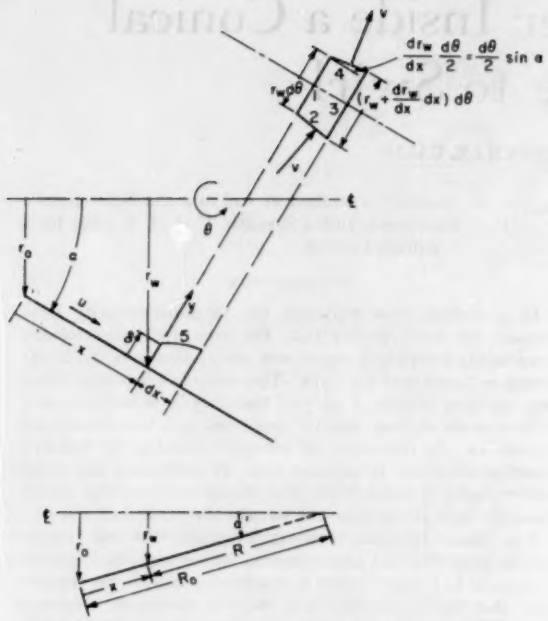

FIG. 1 · ELEMENTARY CONTROL VOLUME FOR BOUNDARY LAYER

MOMENTUM INTEGRAL EQUATIONS OF BOUNDARY LAYER FOR AXIALLY SYMMETRIC FLOW

In Fig. 1 is shown an elementary portion of the boundary layer on the conical surface which diverges in the positive x-direction. In the cyclone the cone converges in the positive x-direction and the angle α becomes negative, but the same equations are applicable in either case. Since the velocity u, parallel to the wall in a meridian plane, is assumed negligible outside of the boundary layer, a momentum influx occurs across surface 1 in the positive x-direction and across surface 2 with a component in the positive x-direction as shown in Fig. 1. Neglecting second-order differentials this influx of momentum in the positive x-direction can be written as

$$M_{in} = \int_0^\delta \rho u^2 r d\theta dy + \int_0^\delta \rho v^2 \sin\alpha\, dx \frac{d\theta}{2}\, dy \quad [1]$$

where $\sin(d\theta/2)$ is approximated by $d\theta/2$.

An efflux of momentum occurs across surface 3 in the positive x-direction and across surface 4 with a component in the negative x-direction. Again neglecting second-order differentials this efflux of momentum in the positive x-direction can be written as

$$M_{out} = \int_0^\delta \rho u^2 r d\theta dy + \frac{d}{dx}\left[\int_0^\delta \rho u^2 r d\theta dy\right] dx - \int_0^\delta \rho v^2 \sin\alpha dx \frac{d\theta}{2} dy \quad [2]$$

The net force acting on the elementary control volume of Fig. 1 in the positive x-direction is composed of the pressure forces and the wall shear force. This net force in the positive x-direction is given as

$$F_x = -\delta r_w d\theta \frac{dp}{dx} dx - \tau_{xw} r_w d\theta dx \quad [3]$$

The net efflux of momentum in the positive x-direction is equal to the net force in this direction. Therefore, by subtracting Equation [1] from Equation [2], equating this difference to Equation [3], and dividing by $d\theta\, dx$ we obtain the momentum equation for the x-direction as

$$\frac{d}{dx}\left[\int_0^\delta \rho u^2 r dy\right] - \int_0^\delta \rho v^2 \sin\alpha\, dy = -\delta r_w \frac{dp}{dx} - \tau_{xw} r_w \quad [4]$$

In addition to the linear momentum equation just derived we can derive the moment-of-momentum equation about the axis of the cone for the elementary control volume of Fig. 1. In a manner similar to that used in the derivation of the linear-momentum-equation, the net efflux of moment of momentum about the axis of the cone from surfaces 1, 2, 3, and 4 can be expressed as

$$MM_{1234} = \frac{d}{dx}\left[\int_0^\delta \rho v u r^2 d\theta dy\right] dx \quad [5]$$

However, although the x-momentum carried in by the mass flow through surface 5 is assumed negligible because of a negligible value of u in the free stream, the moment of momentum carried in by the mass flow across this top surface of the boundary layer is not negligible. This moment-of-momentum influx is written as

$$MM_5 = v_\delta (r_w - \delta) dm \cong v_\delta r_w dm \quad [6]$$

where dm is the mass rate of flow across surface 5. The quantity dm can be related to the u-velocity in the boundary layer by the continuity equation for the elementary control volume considered. The net efflux of mass from surfaces 1, 2, 3, and 4 can be expressed as

$$\frac{d}{dx}\left[\int_0^\delta \rho u r\, d\theta dy\right] dx \quad [7]$$

In the steady state with no sources or sinks in the boundary layer, this efflux of mass must be equal to the influx of mass across the top surface of the boundary layer (surface 5), or

$$dm = \frac{d}{dx}\left[\int_0^\delta \rho u r\, d\theta dy\right] dx \quad [8]$$

The net efflux of moment of momentum from the control volume about the axis of the cone must be equal to the torque acting on the control volume about the same axis. The torque on the control volume is due to the wall shear stress in the tangential direction. This torque, positive in the direction of efflux of moment of momentum, is expressed as

$$T = -\tau_{\theta w} r_w^2 d\theta\, dx \quad [9]$$

Combining Equations [5], [6], [8], and [9] we obtain the moment-of-momentum equation for the control volume of Fig. 1 as

$$\frac{d}{dx}\left[\int_0^\delta \rho v u r^2\, dy\right] - v_\delta r_w \frac{d}{dx}\left[\int_0^\delta \rho u r\, dy\right] = -\tau_{\theta w} r_w^2 \quad [10]$$

In order to solve Equations [4] and [10] for the boundary-layer thickness δ the velocities u and v are assumed as functions of y and the shear stresses at the wall τ_{xw} and $\tau_{\theta w}$ are expressed in terms of these velocities or their derivatives and hence also in terms of y. In the following sections the laminar and turbulent boundary-layer solutions for Equations [4] and [10] are obtained.

LAMINAR BOUNDARY LAYER

To solve the momentum Equations [4] and [10] for the growth of the boundary layer and the acceleration of the flow along the wall of the cone appropriate velocity profiles must

be assumed across the boundary layer. In addition, the wall shear stresses must be determined. The velocity profiles for u and v must satisfy the essential boundary conditions

$$\left.\begin{aligned} u &= 0, \quad v = 0 \text{ at } y = 0 \\ \text{and} \qquad u &= 0, \quad v = v_\delta \text{ at } y = \delta \end{aligned}\right\} \quad \ldots\ldots\ldots [11]$$

If the radius of the cone is large compared with the thickness of the boundary layer, the foregoing boundary conditions and the equations of motion for a real fluid require the normal derivatives of u and v to be a constant at the wall. Furthermore, the velocity asymptotically approaches the free-stream velocity as the distance from the wall increases. Hence the derivatives of u and v in the direction normal to the wall are made zero at the edge of the boundary layer. Finally, it is assumed that u, the velocity in meridian planes, can be expressed as the product of a function of x and a power series in y. For simplicity we take the power series in y to be a cubic such that the Boundary Conditions [11] are satisfied. Finally, u must approach zero as v_δ approaches 0. Hence u and v are expressed as

$$\left.\begin{aligned} u &= v_\delta E(\eta - 2\eta^2 + \eta^3) \\ v &= v_\delta(2\eta - \eta^2) \end{aligned}\right\} \quad \ldots\ldots\ldots [12]$$

where $\eta = y/\delta$, and where $E = E(x)$ and $E(0) = 0$, since $u = 0$ at $x = 0$.

With the assumed velocity profiles for u and v the wall shear stresses may be expressed in terms of δ by evaluating the gradients of u and v in the y-direction at the cone wall. Hence the wall shear stress in the x-direction is given by

$$\tau_{x_w} = \mu \left(\frac{\partial u}{\partial y}\right)_{y=0} = \frac{\mu}{\delta}\left(\frac{\partial u}{\partial \eta}\right)_{\eta=0} \quad \ldots\ldots\ldots [13]$$

From the velocity profile assumed for u this shear stress becomes

$$\tau_{x_w} = \mu v_\delta E/\delta \quad \ldots\ldots\ldots [14]$$

If the radius r_w of the conical surface is large compared with δ, the wall shear stress in the θ-direction is given by

$$\tau_{\theta_w} = \mu \left(\frac{\partial v}{\partial y}\right)_{y=0} = \frac{\mu}{\delta}\left(\frac{\partial v}{\partial \eta}\right)_{\eta=0} \quad \ldots\ldots\ldots [15]$$

and from Equation [12] this shear stress becomes

$$\tau_{\theta_w} = 2\mu v_\delta/\delta \quad \ldots\ldots\ldots [16]$$

Substituting the assumed velocity profiles and the shear stresses of Equations [14] and [16] into the momentum integral Equations [4] and [10], we obtain after integration

$$\frac{1}{105}\frac{d}{dx}(\delta E^2 v_\delta^2 r) - \frac{8}{15}\delta v_\delta^2 \sin\alpha = -\delta\frac{r_w}{\rho}\frac{dp}{dx} - \frac{\nu v_\delta r_w E}{\delta} \quad \ldots\ldots\ldots [17]$$

and

$$\frac{1}{20}\frac{d}{dx}(\delta E v_\delta^2 r^2) - \frac{v_\delta r_w}{12}\frac{d}{dx}(\delta E v_\delta r) = -\frac{2\nu v_\delta r_w^2}{\delta} \quad \ldots [18]$$

The boundary-layer thickness was assumed to be small compared with the radius of the cone, and in the free stream the velocity distribution was assumed to be a potential vortex. Therefore

$$v_\delta r_w = \Gamma = \text{const} \quad \ldots\ldots\ldots [19]$$

Also, r_w is related to x by the cone angle as shown in Fig. 1 and is given as

$$r_w = r_0 + x\sin\alpha \quad \ldots\ldots\ldots [20]$$

and for the converging cone

$$r_w = r_0 - x\sin\alpha' \quad \ldots\ldots\ldots [21]$$

where $\alpha' = -\alpha$.

The pressure gradient in the boundary layer in the x-direction is obtained from the free-stream pressure gradient. Fluid shear is assumed negligible in the free stream, and the pressure gradient is obtained from the equations of motion of an inviscid fluid. Hence we obtain

$$\frac{dp}{dx} = \frac{dp}{dr_w}\frac{dr_w}{dx} \quad \ldots\ldots\ldots [22]$$

and with Equation [21] and the equations of motion for an inviscid fluid

$$\frac{dp}{dx} = -\rho v_\delta^2 \sin\alpha'/r_w \quad \ldots\ldots\ldots [23]$$

Using these relations and performing the indicated differentiation we may write Equations [17] and [18] for the converging cone as

$$\delta^2\frac{dE^2}{dx} + \frac{1}{2}E^2\frac{d\delta^2}{dx} = -\frac{\delta^2 E^2}{r_w}\sin\alpha' + 49\frac{\delta^2}{r_w}\sin\alpha' - 105\frac{\nu E r_w}{\Gamma} \quad \ldots [24]$$

$$\delta^2\frac{dE^2}{dx} + E^2\frac{d\delta^2}{dx} = 120\frac{\nu E r_w}{\Gamma} \quad \ldots\ldots\ldots [25]$$

It is somewhat more convenient to put these equations in terms of spherical co-ordinates as shown in Fig. 1. The required relations are

$$\left.\begin{aligned} x &= R_0 - R \\ dx &= -dR \\ r_w &= R\sin\alpha' \end{aligned}\right\} \quad \ldots\ldots\ldots [26]$$

With these substitutions Equations [24] and [25] are expressed in spherical co-ordinates as

$$\delta^2\frac{dE^2}{dR} + \frac{1}{2}E^2\frac{d\delta^2}{dR} = \frac{\delta^2 E^2}{R} - 49\frac{\delta^2}{R} + 105\frac{\nu E R\sin\alpha'}{\Gamma} \quad \ldots [27]$$

$$\delta^2\frac{dE^2}{dR} + E^2\frac{d\delta^2}{dR} = -120\frac{\nu E R\sin\alpha'}{\Gamma} \quad \ldots\ldots [28]$$

Finally, the equations may be simplified and put into dimensionless form with the following substitutions

$$\delta^2 = \delta_1^2\,\nu R_0^2\sin\alpha'/\Gamma \quad \ldots\ldots\ldots [29]$$

$$R_1 = R/R_0 \quad \ldots\ldots\ldots [30]$$

In dimensionless form Equations [27] and [28] are written as

$$\delta_1^2\frac{dE^2}{dR_1} + \frac{1}{2}E^2\frac{d\delta_1^2}{dR_1} = \frac{\delta_1^2 E^2}{R_1} - 49\frac{\delta_1^2}{R_1} + 105\,ER_1 \quad \ldots [31]$$

$$\delta_1^2\frac{dE^2}{dR_1} + E^2\frac{d\delta_1^2}{dR_1} = -120\,ER_1 \quad \ldots\ldots [32]$$

with the initial conditions

$$E = 0, \qquad \delta_1 = 0 \text{ at } R_1 = 1$$

and $1 \geqslant R_1 \geqslant 0$.

These equations may be solved by numerical computation.

However, to start the equations numerically, another combination of the variables E and δ_1 are required, since Equations [31] and [32] are identically zero at $R_1 = 1$. With the variables E^2 and $E\delta_1^2$ these equations can be put into a form suitable for computation. The resulting equations are

$$\frac{dE^2}{dR_1} = \frac{2E^2}{R_1} - \frac{98}{R_1} + \frac{330E^2R_1}{E\delta_1^2} \quad \ldots\ldots [33]$$

$$\frac{d(E\delta_1^2)}{dR_1} = -\frac{E\delta_1^2}{R_1} + \frac{49E\delta_1^2}{E^2R_1} - 285\,R_1 \quad \ldots\ldots [34]$$

and $E\delta_1^2 = 0$, $E^2 = 0$ at $R_1 = 1$.

To start these equations from $R_1 = 1$ we expand E^2 and $E\delta_1^2$ in a power series about R_1 and assume that for a small change in R_1 the first term of the series is valid. Hence we can start these equations by taking $dR_1 = \Delta R_1 = -0.005$ and expressing the variables E^2 and $E\delta_1^2$ as

$$\left.\begin{aligned} E^2 &= c_3(1 - R_1) \\ E\delta_1^2 &= c_4(1 - R_1) \end{aligned}\right\} \quad \ldots\ldots [35]$$

Substituting these quantities into Equations [33] and [34] we can solve for c_3 and c_4 and obtain in this way the values of E^2 and $E\delta_1^2$ at $R_1 = 0.995$. From then on Euler's finite-difference forms of Equations [33] and [34] are employed and the solution obtained stepwise to $R_1 = 0.05$. The numerical solution is plotted in Fig. 2 as a function of R_1.

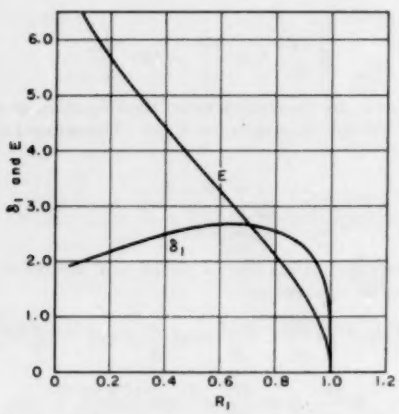

FIG. 2 LAMINAR BOUNDARY-LAYER THICKNESS AND PROPORTIONALITY FACTOR OF u-VELOCITY PROFILE

It is of interest for comparison with experimental data to determine the angle X between a tangent to a streamline and the radius R in spherical co-ordinates at the conical surface. A line on the conical surface which at every point makes this angle with R is the path traced by a small particle on the surface under the action of the fluid-drag forces. Analytically, this angle is given as

$$X = \tan^{-1}\left(\frac{v}{u}\right)_{\eta \to 0} \quad \ldots\ldots [36]$$

and from the velocity profiles of Equation [12]

$$X = \tan^{-1}\left(\frac{2}{E}\right) \quad \ldots\ldots [37]$$

The angle X is plotted as a function of R_1 in Fig. 3. A line making this angle with the radius R_1 is drawn as its projection on a flat plate in Fig. 4.

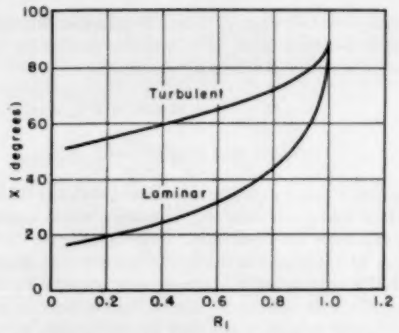

FIG. 3 STREAMLINE ANGLE AT CONICAL SURFACE

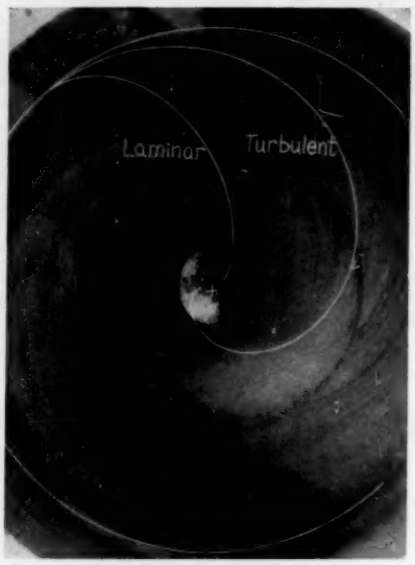

FIG. 4 LAMPBLACK STREAKS ON CONICAL SURFACE OF A CYCLONE DUST SEPARATOR COMPARED WITH THEORETICAL STREAKS

It is doubtful that the boundary layer on the conical surface of a cyclone is laminar in designs usually encountered. Hence we shall solve the turbulent boundary-layer flow employing again the momentum Equations [4] and [10].

TURBULENT BOUNDARY LAYER

Again, to make use of the integral equations of the boundary layer, velocity distributions are assumed for u and v normal to the wall. The essential boundary conditions, Equations [11], must be satisfied by these distributions. If the boundary-layer thickness is small compared to the cone radius, the one-seventh power distribution is suitable for v, the velocity in planes normal to the axis of the cone. Hence this velocity profile is assumed to be

$$v = v_\delta \eta^{1/7} \quad \ldots\ldots [38]$$

In the boundary layer near the wall it is assumed that u, the velocity in meridian planes, also varies as the one-seventh power of the distance from the wall. This velocity reaches a maximum at some distance from the wall and decreases again to zero at the edge of the boundary layer. The greatest percentage of the loss of angular momentum in the boundary layer as indicated by v oc-

curs very near the wall. Hence the maximum value of u probably occurs at a smaller value of η than in the case of the laminar boundary layer. Again it is assumed that u can be expressed as the product of a function of x and a power series in y or η. In addition, u must approach zero as v_δ approaches zero. Therefore, for lack of other data u is assumed to be given simply as

$$u = v_\delta E(\eta^{1/7} - \eta) \quad [39]$$

The profile assumed for u has its maximum value at about $\eta = 0.1$.

The wall shear stresses cannot be determined from the gradients of u and v, because these gradients are infinite at the wall ($\eta = 0$). However, from theoretical considerations and pipe-flow data the shear stress at the wall can be expressed in terms of the velocity and distance from the wall as

$$\tau_w = 0.0225\rho V^{7/4}(\nu/y)^{1/4} \quad [40]$$

It should be noted that this shear stress is independent of y for the one-seventh power velocity distributions. In the x-direction (direction of u) the component of the shear stress decreases as the distance from the wall increases. This component goes through zero at the point of maximum u. Since the x and θ-components of the shear stress at the wall are required, the behavior of the total velocity near the wall is used in evaluating the shear stress. Near the wall η approaches zero and both assumed components of velocity, u and v, vary as the one-seventh power of the distance from the wall. The x and θ-components of the wall shear stress may be expressed in terms of u and v with Equation [40] and the relation

$$u^2 + v^2 = V^2 \quad [41]$$

Then with the velocity profiles given in Equations [38] and [39] we obtain

$$\tau_{\theta w} = 0.0225\rho v_\delta^{7/4}\left(\frac{\nu}{\delta}\right)^{1/4}(1 + E^2)^{5/8} \quad [42]$$

and

$$\tau_{xw} = 0.0225\rho(v_\delta E)^{7/4}\left(\frac{\nu}{\delta}\right)^{1/4}\left(1 + \frac{1}{E^2}\right)^{5/8} \quad [43]$$

The wall shear stresses as given by Equations [42] and [43] and the assumed velocity profiles are now substituted into the momentum integral Equations [4] and [10]. Performing the indicated integration we obtain

$$\frac{8}{45}\frac{d}{dx}(\rho\delta r_w v_\delta^2 E^2) - \frac{7}{8}\rho\delta v_\delta^2 \sin\alpha = -\delta r_w\frac{dp}{dx} - 0.0225\rho r_w(v_\delta E)^{7/4}\left(\frac{\nu}{\delta}\right)^{1/4}\left(1 + \frac{1}{E^2}\right)^{5/8} \quad [44]$$

and

$$\frac{14}{45}\frac{d}{dx}(\rho\delta r_w^2 v_\delta^2 E) - \frac{3}{8}v_\delta r_w\frac{d}{dx}(\rho\delta r_w v_\delta E) = -0.0225\rho r_w^2 v_\delta^{7/4}\left(\frac{\nu}{\delta}\right)^{1/4}(1 + E^2)^{5/8} \quad [45]$$

Equations [19], [21], and [23] of the previous section on Laminar Boundary Layer may be used to express the foregoing equations in the form

$$\frac{8}{45}\frac{d}{dx}(\delta E^2) = -\frac{8}{45}\frac{\delta E^2}{r_w}\sin\alpha' + \frac{1}{8}\frac{\delta}{r_w}\sin\alpha' - 0.0225E^{7/4}\left(\frac{r_w\nu}{\delta\Gamma}\right)^{1/4}\left(1 + \frac{1}{E^2}\right)^{5/8} \quad [46]$$

and

$$\frac{d}{dx}(\delta E) = 0.352\left(\frac{r_w\nu}{\delta\Gamma}\right)^{1/4}(1 + E^2)^{5/8} \quad [47]$$

For convenience spherical co-ordinates are employed as shown in Fig. 1 and as given by Equation [26]. In addition, the equations may be simplified and put into dimensionless form with the following substitutions

$$\delta = \delta_1 R_0\left(\frac{\nu\sin\alpha'}{\Gamma}\right)^{1/5} \quad [48]$$

$$R_1 = R/R_0 \quad [49]$$

With these variables Equations [46] and [47] become

$$\frac{8}{45}\frac{d}{dR_1}(\delta_1 E^2) = \frac{8}{45}\frac{E^2\delta_1}{R_1} - \frac{\delta_1}{8R_1} + 0.0225E^{7/4}\left(\frac{R_1}{\delta_1}\right)^{1/4}\left(1 + \frac{1}{E^2}\right)^{5/8} \quad [50]$$

and

$$\frac{d}{dR_1}(\delta_1 E) = -0.352\left(\frac{R_1}{\delta_1}\right)^{1/4}(1 + E^2)^{5/8} \quad [51]$$

with the following initial conditions

$$\delta_1 = 0, \qquad E = 0 \text{ at } R_1 = 1$$

and

$$1 \geqslant R_1 \geqslant 0$$

As in the previous section on the Laminar Boundary Layer, numerical methods are required to obtain the solution to these equations. But to start the equations numerically with $E = \delta_1 = 0$ at $R_1 = 1$ an appropriate combination of E and δ_1 is required as variables. If Equations [50] and [51] are put in terms of the variables E^2 and $E\delta_1^{5/4}$, the numerical method described in the Laminar Boundary Layer is easily applied to the solution. The resulting equations suitable for numerical computation are as follows

$$\frac{dE^2}{dR_1} = \frac{2E^2}{R_1} - \frac{1.406}{R_1} + 0.957\frac{E^2(E^2 + 1)^{5/8}}{E\delta_1^{5/4}}R_1^{1/4} \quad [52]$$

and

$$\frac{d}{dR_1}(E\delta_1^{5/4}) = -0.560\,R_1^{1/4}(E^2 + 1)^{5/8} - 0.250\frac{E\delta_1^{5/4}}{R_1} + 0.176\frac{E\delta_1^{5/4}}{E^2R_1} \quad [53]$$

The solution is plotted in Fig. 5. The angle X which the stream-

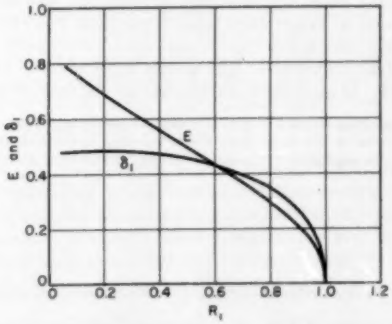

FIG. 5 TURBULENT BOUNDARY-LAYER THICKNESS AND PROPORTIONALITY FACTOR OF u-VELOCITY PROFILE

lines make with the spherical radius R as the conical surface is approached (i.e., as η approaches zero) is given by Equation [36]. For the turbulent boundary layer X is obtained from this equation and the velocity profiles given by Equations [38] and [39] as

$$X = \tan^{-1}\left(\frac{1}{E}\right) \quad \text{[54]}$$

The angle X is plotted as a function of R_1 in Fig. 3. A line making this angle with the radius R_1 is drawn as its projection on a flat plate (90-deg cone angle) in Fig. 4 for comparison with the same line obtained for the laminar boundary layer.

Discussion

Without probing the boundary layer on the conical surface of a cyclone separator a comparison of the theoretical results with an actual flow can be obtained by the measurement of the angle X. As was discussed previously, the line traced by a small particle on the conical surface makes the angle X with the radius R_1. These lines obtained by the preceding analysis for laminar and turbulent boundary layern are shown in Fig. 4 as their projections on a flat plate.

For comparison with the theory the projected particle paths are superimposed on a photograph of lampblack streaks on the conical surface of the experimental cyclone shown in Fig. 4. The streaks were obtained from the evaporation of a solution of lampblack and kerosene which was painted on the conical surface. The photograph does not represent exactly a projection of the conical surface on a flat plate because of the effect of perspective from the cone base to the central hole. However, this effect was made as small as possible and makes the central hole appear only about 10 per cent smaller than an actual projection. From the fact that the experimental streaks begin tangent to the base circle of the cone, it would appear that the u-velocity in the free stream is very small compared with the v-velocity as was assumed in the analysis.[4] The correspondence between the lampblack streaks and the theoretical particle path for the turbulent boundary layer may be fortuitous, at least in the region near the apex of the cone. We shall see that this is true by an examination of the theoretical boundary-layer thickness.

The ratio of maximum boundary-layer thickness to the radius of the cylindrical portion of the cyclone is shown in Fig. 6 as a function of the cone angle using air at 70 F. In addition Fig. 7 shows the ratio of boundary-layer thickness to the cone radius as a function of R_1. This latter figure shows that the boundary-layer thickness in swirl flow rapidly becomes 10 per cent of the cone radius when the boundary layer begins with zero thickness at the base of the cone which is the radius of the cyclone cylinder. In fact, for small cone angles as shown in Fig. 7 the boundary layer theoretically "fills" the cone near its lower end, and the assumption of small boundary-layer thickness as compared with the cone radius is invalidated in this region. The cyclone used in the experimental program has a 30-deg cone angle with the cone cut at $R_1 = 0.18$. In all of the experimental runs the product of the inlet velocity and inlet-port radius was about 50 sq ft per sec which is equal to Γ, if loss of angular momentum of the fluid after entry is negligible. Thus at the edge of the hole in the cone which opens to the dust-collecting hopper, Fig. 7 shows the boundary-layer thickness to be 35 per cent of the cone radius for $\Gamma = 50$ sq ft per sec.

[4] As the extension of the cyclone exhaust pipe is increased, approaching the plane of the cone base, the u-velocity in the free stream may no longer be negligible and must be taken into account in the analysis.

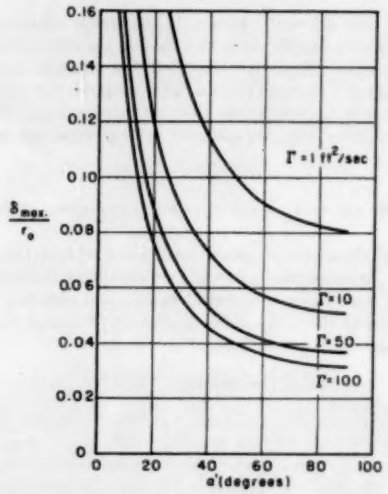

Fig. 6 Ratio of Maximum Boundary-Layer Thickness to Radius of Cone Base

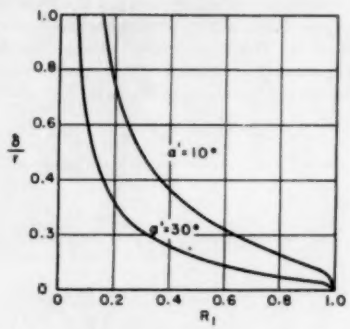

Fig. 7 Ratio of Boundary-Layer Thickness to Radius of Cone in Cylindrical Co-Ordinates

In conclusion it is pointed out that this analysis was performed as a part of the over-all determination of the flow in a vortex chamber or cyclone separator. The boundary-layer mechanics are important, since it is the flow near the wall that carries the dust to the hopper.

Acknowledgment

The work reported herein was sponsored by Jabez Burns and Sons, Inc., of New York, N. Y.

A Theory for Base Pressures in Transonic and Supersonic Flow[1]

By H. H. KORST,[2] URBANA, ILL.

A physical flow model is devised based on the concepts of interaction between the dissipative shear flow and the adjacent free stream and the conservation of mass in the wake. Four flow components are integrated in the model; namely, the flow approaching the trailing edge, the expansion around the trailing edge, the mixing within the free-jet boundary, and the recompression at the end of the wake. A unique and stable solution results for the base pressure. Theoretical results obtained for thin approaching boundary layer do not require empirical information and are, therefore, best suited to evaluate the merits of the theory. Here emphasized is the case of isoenergetic constant-pressure mixing in the turbulent free-jet boundary and agreement is found between theory and experimental data.

Nomenclature

The following nomenclature is used in the paper:

A = area
g_c = gravitational constant
G_b = mass rate per unit width at which air is added externally to the wake
G_s = mass rate per unit width flowing between jet-boundary streamline and streamline s
H = step height
$\sum_n \frac{l_i}{L}$ = n significant length proportions assuring geometrical similarity
L = reference length
P = absolute pressure
$\mathbf{R}$ = gas constant
T = absolute temperature
u = velocity component in x-direction
x, y = co-ordinates in the intrinsic co-ordinate system
X, Y = co-ordinates in the reference co-ordinate system
β = dummy variable
δ = boundary-layer thickness
ϵ = eddy viscosity
θ = streamline angle
ρ = density

Subscripts

1, 2, 3, 4 refers to conditions at cross sections indicated in Fig. 2
a refers to conditions in the free stream adjacent to the dissipative regions
d refers to conditions along the discriminating streamline
i = floating index
j refers to conditions along the jet-boundary streamline
m refers to co-ordinate shift due to momentum integral
0 refers to stagnation value
red refers to reduced approach conditions
R refers to large co-ordinate reference value
s refers to streamline defined by Equation [19]

Superscripts

* refers to conditions where $\mathbf{M} = 1.0$
′ refers to lower stream past blunt trailing edge

Dimensionless Groups

$\mathbf{C} = u/u_{max}$, Crocco number
$k = c_p/c_v$, ratio of specific heats
$\mathbf{M}$ = Mach number
P_2/P_1 = base pressure ratio
Re = Reynolds number
$\zeta = y/\delta_2$, dimensionless y-co-ordinate
$\zeta_1 = y/\delta_1$, dimensionless y-co-ordinate
$\eta = \zeta\eta_P$, dimensionless co-ordinate
$\eta_P = 1/(2\sqrt{\xi})$, position parameter
ξ = transformed dimensionless x-co-ordinate
H = dimensionless bleed number
φ = dimensionless velocity
$\bar{\psi} = x/\delta_2$, dimensionless x-co-ordinate
σ = similarity parameter for homogeneous co-ordinate y/x.

Introduction

The study of base-pressure problems has been pursued by both analytical and experimental methods over a long period of time so that a noticeable amount of information is available in the literature (1)[3, 4] pertinent to external and internal-flow configurations. Here considered are cases in which the flow approaching the base is sonic or supersonic and remains supersonic after the wake, as they are applicable to various practical problems in external and internal aerodynamics, some of which are depicted schematically in Fig. 1.

While analytical approaches did not keep pace with the need for reliable design data, a great number of experimental investigations helped establish the significant parameters influencing the base pressure for a given geometrical configuration, such as Mach number, Reynolds number, type and configuration of the bound-

[1] Research carried out under partial support by the U. S. Air Force under Contract AF 18(600)-392, "Transonic and Supersonic Flow of a Real Fluid at Abrupt Increase in Cross Section," monitored by the Office of Scientific Research, Fluid Dynamics Division.

[2] Professor of Mechanical Engineering, University of Illinois.

Presented at the National Applied Mechanics Division Conference, Urbana, Ill., June 14–16, 1956, of The American Society of Mechanical Engineers.

Discussion of this paper should be addressed to the Secretary, ASME, 29 West 39th Street, New York, N. Y., and will be accepted until January 10, 1957, for publication at a later date. Discussion received after the closing date will be returned.

Note: Statements and opinions advanced in papers are to be understood as individual expressions of their authors and not those of the Society. Manuscript received by ASME Applied Mechanics Division, March 7, 1956. Paper No. 56—APM-30.

[3] Numbers in parentheses refer to the Bibliography at the end of the paper.

[4] A comprehensive Bibliography of unclassified references appears in reference (1).

ary layer approaching the base, heating of the forebody, and at the base (2).

Recently, a theoretical analysis of the base-pressure problem, based on a flow model exhibiting interaction between the dissipative flow region and the nearly isentropic free stream, was advanced by L. Crocco and L. Lees (3). Their results reflect qualitatively the influences of Mach number and Reynolds number but depend, for quantitative interpretation, on empirical information concerning the jet-mixing component of the model. The importance of the interaction concept had already been recognized and D. R. Chapman (4) devised such a flow model, although for qualitative reasoning only, while depending on a semiempirical correlation of experimental data.

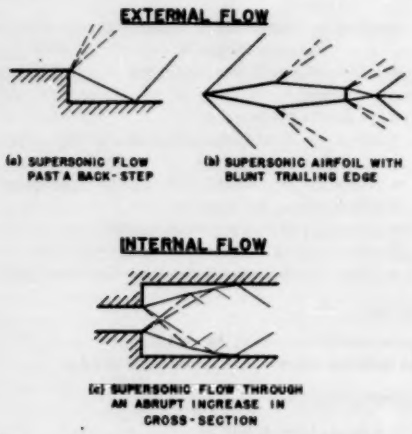
EXTERNAL FLOW
(a) SUPERSONIC FLOW PAST A BACK-STEP
(b) SUPERSONIC AIRFOIL WITH BLUNT TRAILING EDGE
INTERNAL FLOW
(c) SUPERSONIC FLOW THROUGH AN ABRUPT INCREASE IN CROSS-SECTION

FIG. 1 TYPICAL FLOW CONFIGURATIONS FOR TWO-DIMENSIONAL BASE-PRESSURE PROBLEMS

In the present analysis a theoretical treatment of the base-pressure problem is given which utilizes, essentially, D. R. Chapman's model, but includes one additional flow component which makes the system of equations complete and yields a quantitative, stable solution for the base pressure. The additional information is obtained by relating the physical requirement of conservation of mass in the wake to an "escape concept" applied to a particular streamline in the mixing region, thus formulating an energetic criterion for penetration into the high-pressure region created by the recompression at the end of the wake (5). A prerequisite for determining the level of mechanical energy along streamlines in the jet-mixing region was to study first the problem of compressible jet mixing at constant pressure under consideration of initial mixing profile disturbances (6, 7). The latter influence is easily recognized as providing the mechanism for Reynolds-number effects as the free jet boundary itself would not contribute any significant reference length. An asymptotic solution of the jet-mixing problem corresponds to a fully developed jet boundary in which any influence of an initial disturbance in the jet-mixing profile (boundary-layer configuration developed upstream of the tailing edge) has vanished.

Application of this asymptotic jet-mixing solution to the base-pressure problem, specified as "restricted theory," is consistent with physical conditions where the thickness of the boundary layer approaching the trailing edge is thin as compared to the length of the wake. Results obtained with this restriction represent lowest limiting base-pressure values as they are approached with increasing Reynolds numbers for a given configuration and approach Mach number. It is of special significance that some base-pressure problems of practical importance can be treated by the restricted theory without the use of empirical information; others by utilizing a single proportionality factor σ which is reasonably well defined by previous experimental investigations on turbulent compressible jet boundaries. Results of the restricted theory are emphasized in this paper as they are best suited for an evaluation of the merits of this base-pressure theory. A comprehensive treatment of the initially disturbed turbulent jet-mixing problem going beyond mere qualitative aspects in comparison with the restricted theory would require empirical information which is presently not available in sufficient detail.

The use of an isoenergetic two-dimensional turbulent jet-mixing concept reduces the scope of this paper to adiabatic, two-dimensional wakes.[5]

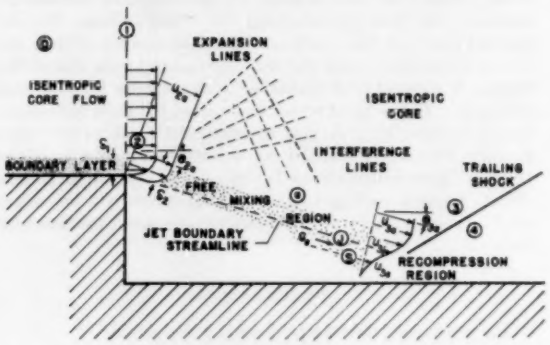

FIG. 2 FLOW MODEL FOR TWO-DIMENSIONAL BASE-PRESSURE PROBLEM

MODEL OF FLOW MECHANISM

The general principle underlying the analysis is to consider the interaction between dissipative and adjacent free-stream domains together with information concerning the mechanical energy distribution within the compressible jet boundary, in order to satisfy quantitatively the conservation of mass in the wake. The model of the flow mechanism, exemplified for the two-dimension case, is illustrated in Fig. 2, depicting the following flow regions:

(*a*) Flow approaching the trailing edge, between cross sections 0 and 1.

(*b*) Flow expanding around the trailing edge, between 1 and 2.

(*c*) Flow along the wake, with constant pressure mixing within the compressible jet boundary, between 2 and 3.

(d) Recompression at the end of the wake; e.g., by a plane shock between 3 and 4.

The flow mechanism is formulated in the following five points:

(i) The flow in the dissipative shear-flow domain has its static pressure impressed by the adjacent, nearly uniform free stream

$$\frac{P_i}{P_{i_e}} = 1 \qquad [1]$$

(ii) The expansion of the free stream, between cross sections 1 and 2, follows the Prandtl-Meyer solution for the simple wave, here functionally expressed by

$$\frac{P_2}{P_1} = \frac{P_2}{P_1}(M_{1e}, \theta_{2e} - \theta_{1e}) \qquad [2]$$

[5] Extension to some axially symmetric configurations was given in reference (1), and an extension to nonadiabatic wakes has meanwhile been made by R. H. Page and H. H. Korst (8).

$$M_{2s} = M_{2s}(M_{1s}, \theta_{2s} - \theta_{1s}) \quad [3]$$

In the dissipative domain, between 1 and 2, one may formally express

$$\varphi_2(\zeta) = \varphi_2\left[\varphi_1(\zeta_1), M_{1s}, \frac{P_2}{P_1}\right] \quad [4]$$

$$\frac{\delta_2}{\delta_1} = \frac{\delta_2}{\delta_1}\left[\varphi_1(\zeta_1), M_{1s}, \frac{P_2}{P_1}\right] \quad [5]$$

(iii) The mixing process in the jet boundary, between cross sections 2 and 3, occurs at constant pressure, so that

$$\frac{P_3}{P_2} = 1 \quad [6]$$

which generally will require that the thickness of the dissipative region remains small as compared to any significant length in the wake, such as step height, or any radius of curvature related to the jet boundary. Under this condition, and in restricting to the isoenergetic turbulent jet boundary, the results of the previously mentioned mixing theory (6, 7) become applicable, the main points of which are briefly summarized for convenience:

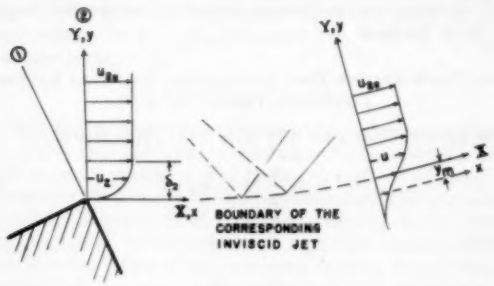

FIG. 3 SYSTEM OF CO-ORDINATES EMPLOYED IN JET MIXING COMPONENT OF TWO-DIMENSIONAL BASE-PRESSURE MODEL

The mixing theory introduces a reference system of co-ordinates (X, Y) as an orthogonal and generally curvilinear system of co-ordinates which follows the boundary of the corresponding inviscid jet, Fig. 3. The latter is defined as the hypothetical frictionless jet which has the same approach Mach number M_{1s}, expands through the same pressure ratio P_2/P_1, and is influenced by the same geometry of physical boundaries

$$\sum_n \frac{l_i}{L}$$

as the actual viscous jet. The angular deviation of the reference system of co-ordinates from the uniform flow approaching cross section 1 is

$$\Delta\theta_s = \theta_s - \theta_{1s} = \Delta\theta_s\left(M_{1s}, P_2/P_1, \sum_n \frac{l_i}{L}\right) \quad [7]$$

as resulting from potential flow theory. Also specified is an intrinsic system of co-ordinates (x, y) which is displaced from the reference system of co-ordinates in the Y-direction, so that, as the angle between the two co-ordinate systems will be small, $X \approx x$ and $Y = y - y_m(x)$, while $y_m(0) = 0$. Essentially, the mixing theory is a momentum-integral method which utilizes a highly simplified equation of motion

$$\frac{\partial u}{\partial x} = \frac{\epsilon}{u_{2s}}\frac{\partial^2 u}{\partial y^2} \quad [8]$$

with the turbulent viscosity expressed in a modified form of Prandtl's exchange coefficient ϵ, so that, after introducing the dimensionless variables

$$\varphi = \frac{u}{u_{2s}}, \quad \psi = \frac{x}{\delta_2}, \quad \zeta = \frac{y}{\delta_2}$$

$$\epsilon = \frac{1}{2\sigma^2}\psi\delta_2 u_{2s} f(\psi) \quad [9]$$

where $f(\psi) \to 1$ as $\psi \to \infty$

and by the transformation

$$\xi = \frac{1}{2\sigma^2}\int_0^{\psi} \psi f(\psi) d\psi \quad [10]$$

The following formulation of the mixing problem is obtained

$$\frac{\partial\varphi}{\partial\xi} = \frac{\partial^2\varphi}{\partial\zeta^2}$$

$$\left.\begin{aligned} &\varphi(0, \zeta) \equiv 0 \quad \text{for} \quad -\infty < \zeta < 0 \\ &\varphi(0, \zeta) = \varphi_2(\zeta) \quad \text{for} \quad 0 < \zeta < 1 \\ &\varphi(0, \zeta) \equiv 1 \quad \text{for} \quad 1 < \zeta < +\infty \\ &\varphi(\xi, -\infty) \to 0 \quad \text{for} \quad \xi > 0 \\ &\varphi(\xi, +\infty) \to 1 \quad \text{for} \quad \xi > 0 \end{aligned}\right\} \quad [11]$$

The resulting approximate solutions for the velocity distributions satisfy the initial and boundary conditions in both the intrinsic and reference systems of co-ordinates, but are interpreted as valid within the intrinsic system

$$\varphi = \varphi[\varphi_2(\zeta), \eta_P; \eta]$$
$$= \frac{1}{2}[1 + \operatorname{erf}(\eta - \eta_P)] + \frac{1}{\sqrt{\pi}}\int_{\eta-\eta_P}^{\eta} \varphi_2\left(\frac{\eta - \beta}{\eta_P}\right) e^{-\beta^2} d\beta \quad [12]$$

where η_P, the position parameter, is given by

$$\eta_P = 1/(2\sqrt{\xi}) \quad [13]$$

and

$$\eta = \zeta\eta_P \quad [14]$$

Subsequently, the momentum integral is used to localize the intrinsic system with respect to the reference system of co-ordinates. For isoenergetic conditions in the mixing region, here restricting the treatment to adiabatic wakes

$$\frac{T_0}{T_{0s}} = 1 \quad [15]$$

As a matter of expediency, the dimensionless velocity $C = u/u_{max}$ is introduced to replace Mach number to which it is related by

$$C = \left[1 + \frac{2}{(k-1)M^2}\right]^{-1/2} \quad [16]$$

The displacement of the intrinsic system with respect to the reference system $\eta_m = (y_m\eta_P)/\delta_2$ is expressed by

$$\eta_m = \eta_m[\varphi_2(\zeta), \eta_P, C_{2s}]$$
$$= \eta_R - \eta_P + [1 - C_{2s}^2]\left[\eta_P\int_0^1 \frac{\varphi_2^2 d\zeta}{1 - C_{2s}^2\varphi_2^2} - \int_{-\infty}^{\eta_R} \frac{\varphi^2 d\eta}{1 - C_{2s}^2\varphi^2}\right] \quad [17]$$

where η_R is a reference value, chosen large enough, so that

$$1 - \varphi[\varphi_2(\zeta), \quad \eta_P; \quad \eta_R] < t$$

t being a small quantity.

By the use of the continuity equation, the location η_s of the streamline s, defined by

$$\int_{\eta_s}^{\eta_R} \frac{\varphi d\eta}{1 - C_{2a}{}^2\varphi^2} + \frac{\eta_P G_s}{\delta_2 \rho_{2a} u_{2a}(1 - C_{2a}{}^2)} = -\int_{-\infty}^{\eta_R} \frac{\varphi^2 d\eta}{1 - C_{2a}{}^2\varphi^2} + \eta_P \int_0^1 \frac{\varphi_2(1 - \varphi_2)d\zeta}{1 - C_{2a}{}^2\varphi_2{}^2} \quad [18]$$

where

$$G_s = \int_{y_i}^{y_s} \rho u \, dy \quad [19]$$

is obtained, and the velocity along any streamline may be calculated, according to Equation [12]. The jet-boundary streamline j at location η_j, which separates the fluid of the approaching stream from the fluid in the "dead-air" region, is specified by $G_s = 0$

$$\int_{\eta_j}^{\eta_R} \frac{\varphi d\eta}{1 - C_{2a}{}^2\varphi^2} = \int_{-\infty}^{\eta_R} \frac{\varphi^2 d\eta}{1 - C_{2a}{}^2\varphi^2} + \eta_P \int_0^1 \frac{\varphi_2(1 - \varphi_2)d\zeta}{1 - C_{2a}{}^2\varphi_2{}^2} \quad [20]$$

(iv) The pressure increase in the recompression region at the end of the wake is determined by the flow conditions in the adjacent free stream, according to point (i), and the free-stream compression has to be specified; e.g., by a plane angle shock between cross sections 3 and 4. Thus the static pressure in the dissipative region behind the shock may be found if approach conditions of the free stream are given and the deflection angle $(\theta_{3a} - \theta_{4a})$ is sufficiently defined

$$\frac{P_4}{P_3} = \frac{P_4}{P_3}(M_{3a}, \quad \theta_{3a} - \theta_{4a}) \quad [21]$$

(v) The requirement of conservation of mass in the dead-air region is to be satisfied. A discriminating streamline d, at location η_d within the mixing region is defined such that it has a level of mechanical energy, expressed by the stagnation pressure at cross section 3, P_{03d}, so that recompression to the static pressure in cross section 4, P_4, is possible by the complete conversion of the kinetic energy; that is

$$\frac{P_{03d}}{P_3} = \frac{P_4}{P_3} \quad [22]$$

where, using the reversible adiabatic relation

$$\frac{P_{03d}}{P_3} = \left(1 + \frac{k-1}{2} M_{3d}{}^2\right)^{\frac{k}{k-1}} \quad [23]$$

This expresses the escape criterion satisfied by the streamline d. Fluid along streamlines having $P_{03}/P_4 < 1$ will not be able to penetrate into the region where the static pressure P_4 prevails, while fluid along streamlines with $P_{03}/P_4 > 1$ will pass through the recompression zone.

An "open wake" is defined as referring to those cases where mass is added to the dead-air region, at the rate G_b, either by direct mass injection or by backflow from the high-pressure region behind the recompression zone. The continuity of mass in the wake requires that

$$G_b + G_s = 0 \quad [24]$$

and

$$\frac{P_{03s}}{P_{03d}} = \frac{P_{03s}}{P_4} = 1 \quad [25]$$

A "closed wake" specifies the case where both G_b and G_s are individually equal to zero and

$$\frac{P_{03j}}{P_{03d}} = \frac{P_{03j}}{P_4} = 1 \quad [26]$$

While there are, strictly speaking, no closed wakes (considering the possibility of backflow in the dissipative domain near the trailing shock), there are a number of configurations of practical interest where the model of a closed wake may be applied successfully.

The system of equations listed under points (i) through (v) is principally sufficient to determine the solution of the base-pressure problem. However, it must be stressed that exact theoretical solutions have not yet been obtained for Equations [4] and [5]. It is now fortunate that the case of thin approaching boundary layers $(\eta_P \to 0)$ eliminates these two relationships entirely and, at the same time, will not require any empirical information concerning the mixing component in the case of a closed wake, while, for an open wake only one empirical coefficient, namely σ, has to be known. It shall be noticed that as $\varphi(\eta_P > 0; \ \eta_j) < \varphi(\eta_P = 0, \eta_j)$, the restricted base pressure theory $(\eta_P = 0)$ establishes the lower limit for base pressures obtained with a finite approaching boundary-layer thickness.

Base Pressures for Thin Approaching Boundary Layers—Restricted Theory $(\eta_P = 0)$

As $\eta_P \to 0$, Equations [12], [17], [18], [19] reduce to

$$\varphi = \frac{1}{2}(1 + \operatorname{erf} \eta) \quad [27]$$

where

$$\eta = \sigma \frac{y}{x}$$

$$\eta_m = \eta_R - (1 - C_{2a}{}^2) \int_{-\infty}^{\eta_R} \frac{\varphi^2 d\eta}{1 - C_{2a}{}^2\varphi^2} \quad [28]$$

$$\int_{\eta_s}^{\eta_R} \frac{\varphi d\eta}{1 - C_{2a}{}^2\varphi^2} + \frac{\sigma G_s}{x\rho_{2a}u_{2a}(1 - C_{2a}{}^2)} = \int_{-\infty}^{\eta_R} \frac{\varphi^2 d\eta}{1 - C_{2a}{}^2\varphi^2} \quad [29]$$

and

$$\int_{\eta_j}^{\eta_R} \frac{\varphi d\eta}{1 - C_{2a}{}^2\varphi^2} = \int_{-\infty}^{\eta_R} \frac{\varphi^2 d\eta}{1 - C_{2a}{}^2\varphi^2} \quad [30]$$

The integrals

$$\int_{-\infty}^{\eta} \frac{\varphi d\eta}{1 - C_{2a}{}^2\varphi^2} = I_1(C_{2a}; \ \eta)$$

and

$$\int_{-\infty}^{\eta} \frac{\varphi^2 d\eta}{1 - C_{2a}{}^2\varphi^2} = I_2(C_{2a}; \ \eta)$$

where $\varphi = \varphi(\eta)$, according to Equation [27], have been tabulated[6] as functions of the upper limit for 21 values of the parameter C_{2a} together with the values for $\eta_m(C_{2a})$, $\eta_j(C_{2a})$, and $\varphi_j(C_{2a})$ (9). A graphical presentation of $\varphi_j = \varphi_j(C_{2a})$ is given in Fig. 4.

[6] The calculations were carried out on the ILLIAC, Electronic Digital Computer, Engineering Research Laboratory, University of Illinois.

Application of the Restricted Theory to Closed Wakes

With $G_b = G_s = 0$ and a given geometry and approach Mach number, the base pressure is uniquely determined, as shall be shown in the case of supersonic flow past a back step, Fig. 5(*a*).

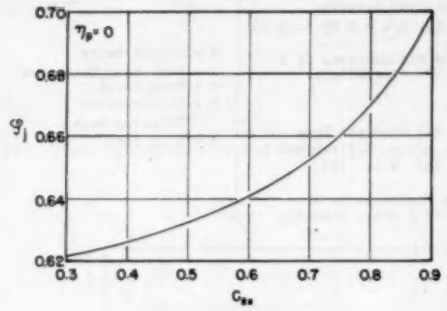

IG. 4 Dimensionless Velocity Along Jet-Boundary Streamline ($\eta_P = 0$)

A trial-and-error solution can be avoided if one selects M_{2s} as the independent variable, determines C_{2s} (Equation [16]), φ_j (Fig. 4), $P_{t2j}/P_3 = P_4/P_3$ (Equation [23]), and solves the angle shock relation for $\theta_{1s} - \theta_{4s}$ (Equation [21]). As $\theta_{2s} = \theta_{3s}$ for a straight jet boundary

$$\theta_{3s} - \theta_{1s} = \theta_{3s} - \theta_{4s}$$

and M_{1s} may be found from the Prandtl-Meyer expansion (Equation [3]) so that P_2/P_1 will be determined by the reversible adiabatic pressure relations. The results of such calculations are compared with experimental base-pressure values obtained for high Reynolds numbers by D. R. Chapman, et al. (10), and H. Eggink (11), Fig. 5(*b*). It is significant to note that Eggink reported lower limiting values of base pressures as being asymptotically reached for an increasing height of the back step, while the other parameters were left unchanged, so that the conditions of the restricted theory were met. The limiting character of the $\eta_P = 0$ solution is also well borne out for the higher Mach-number range in Fig. 6, showing test data of various sources originally compiled by K. L. Goin (12). Support for the validity of the theoretical solution in the lower supersonic Mach-number range was found by studying internal-flow problems with $M_{1s} = 1$ (1, 5, 13), Fig. 7.

A generalization of the back-step problem is possible which includes the effects of upstream and downstream wall inclinations in a unified treatment by introducing a reduced Mach number (M_{red}) concept, Fig. 8(*a*). Defining a streamline angle θ_s^* which gives the direction of the critical flow ($M_s = 1$) from which the flow condition (M_{1s}, θ_{1s}) would be produced by a Prandtl-Meyer expansion

$$M_{1s} = M_{1s}(\theta_{1s} - \theta_s^*)$$

this reduced Mach number is

$$M_{red} = M_{red}(\theta_{4s} - \theta_s^*) \equiv M_{red}[(\theta_{1s} - \theta_s^*) - (\theta_{1s} - \theta_{4s})] \quad [31]$$

which is now interpreted as an approach Mach number for the simple back-step configuration of Fig. 5(*a*) where $\theta_{1s} = \theta_{4s} = (0)$. In order to reduce the test data obtained by H. Eggink (11) for two approach Mach numbers, 1.85 and 2.48, and for various downstream wall inclinations, θ_{4s}, so that they can be compared with the theoretical solution presented in Fig. 5(*b*), one uses the identity

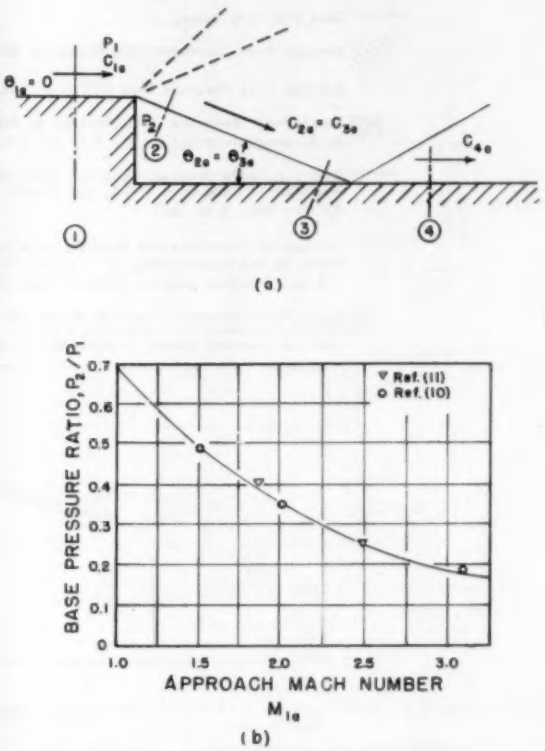

Fig. 5 Supersonic Flow Past a Back Step
(*a*, Flow configuration. *b*, Comparison of theory and experimental data.)

$$\frac{P_2}{P_{red}} = \frac{P_2}{P_1}\,\frac{P_1/P_{0s}}{P_{red}/P_{0s}}$$

where P_1/P_{0s} and P_{red}/P_{0s} are reversible, adiabatic pressure functions of M_{1s} and M_{red}, respectively. The apparent validity of the reduced Mach-number concept is illustrated by Fig. 8(*b*).

A further generalization of the back-step problem permits the treatment of the base-pressure problem produced by two streams approaching a blunt trailing edge with generally different Mach numbers M_{1s} and M_{1s}', and different streamline angles θ_{1s} and θ_{1s}', but identical stagnation pressures and stagnation temperatures. Introducing, in the same way as before, θ_s^* and $\theta_s^{*\prime}$, one obtains

$$\theta_{4s} = \frac{1}{2}(\theta_s^* - \theta_s^{*\prime}) \quad [32]$$

and

$$M_{red} = M_{red}(\theta_{4s} - \theta_s^*) \quad [33]$$

so that the results given previously for the generalized back step can be applied.[7]

It shall be noted that Equation [7] completely contains the effects of interference between disturbances in the adjacent free stream and the jet boundary. This is of special importance for configurations where expansion fans or shocks originate from opposite boundaries, limiting the range of a direct comparison of base-

[7] To include the effects of appreciable angles of attack (different stagnation pressures in the free streams on both sides of the trailing edge), the concept of open wakes must be used; see next section.

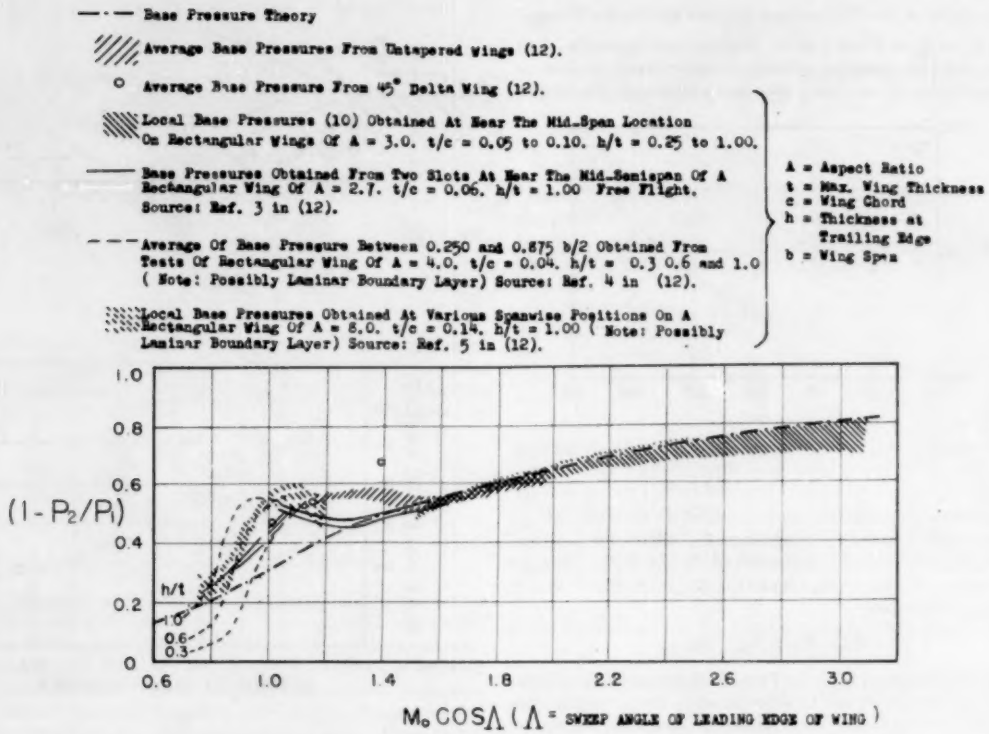
Base Pressure Theory
Average Base Pressures From Untapered Wings (12).
Average Base Pressure From 45° Delta Wing (12).
Local Base Pressures (10) Obtained At Near The Mid-Span Location On Rectangular Wings Of A = 3.0. t/c = 0.05 to 0.10. h/t = 0.25 to 1.00.
Base Pressures Obtained From Two Slots At Near The Mid-Semispan Of A Rectangular Wing Of A = 2.7. t/c = 0.06. h/t = 1.00 Free Flight. Source: Ref. 3 in (12).
Average Of Base Pressure Between 0.250 and 0.875 b/2 Obtained From Tests Of Rectangular Wing Of A = 4.0. t/c = 0.04. h/t = 0.3 0.6 and 1.0 (Note: Possibly Laminar Boundary Layer) Source: Ref. 4 in (12).
Local Base Pressures Obtained At Various Spanwise Positions On A Rectangular Wing Of A = 8.0. t/c = 0.14. h/t = 1.00 (Note: Possibly Laminar Boundary Layer) Source: Ref. 5 in (12).
A = Aspect Ratio
t = Max. Wing Thickness
c = Wing Chord
h = Thickness at Trailing Edge
b = Wing Span
(1 - P2/P1)
h/t
1.0
0.6
0.3
M0 COS Λ (Λ = SWEEP ANGLE OF LEADING EDGE OF WING)

FIG. 6 COMPARISON OF BASE-PRESSURE DATA AS PRESENTED BY K. L. GOIN (12) AND THEORY ($\eta_P = 0$)

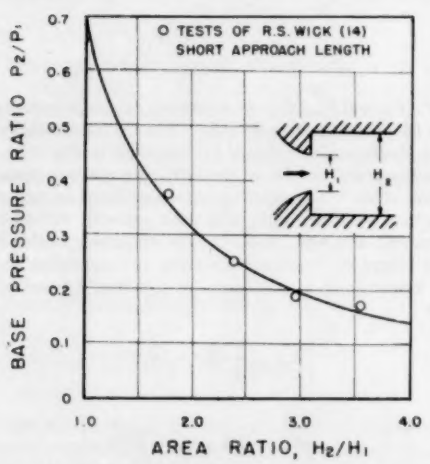

FIG. 7 EXPERIMENTAL BASE-PRESSURE RATIOS FOR SONIC FLOW THROUGH AN ABRUPT CROSS-SECTIONAL AREA CHANGE COMPARED WITH THEORETICAL SOLUTION

pressure values obtained in internal and external flow (1). A two-dimensional base-pressure problem of the internal-flow type was studied by R. S. Wick (14) for sonic flow approaching a sudden enlargment in cross section, and the results of this experimental investigation were discussed in the light of the present theory (5, 13), Fig. 7.

APPLICATION OF THE RESTRICTED THEORY TO OPEN WAKES

Open wakes, with $G_b \neq 0$ and $\eta_d \neq \eta_j$ will generally require information on σ, an empirical quantity, the numerical value of which is well established as 12 for low velocities ($\mathbf{M} \to 0$) (15), but on which information in the compressible flow region is meager (1).

Here discussed is the case of a supersonic flow past a back step with bleeding into the wake; see Fig. 9(*a*). The bleeding air has the same stagnation temperature[8] as the main stream and is added slowly into the wake at a rate G_b, which is considered to be the independent variable since the effectiveness of bleeding as a means of base pressure control shall be studied.

Defining a dimensionless *bleed number* H

$$\mathrm{H} = \frac{G_b\sqrt{T_{0a}}}{HP_{0a}}\sqrt{\left(\frac{\mathbf{R}}{g_c k}\right)} \qquad [34]$$

where H is the height of the step and $\mathbf{R}$ the gas constant, one obtains

$$\mathrm{H} = \left(\frac{2}{k+1}\right)^{\frac{k+1}{2(k-1)}} \frac{[I_1(\mathbf{C}_{2a};\ \eta_j) - I_1(\mathbf{C}_{2a};\ \eta_s)]}{\frac{T_{0a}}{T_{2a}}\frac{A_{2a}}{A_a{}^*}\ \sigma \sin(\theta_{2a} - \theta_{1a})} \qquad [35]$$

where T_{0a}/T_{2a} and $A_{2a}/A_a{}^*$ are the reversible adiabatic relations of the absolute-temperature ratio and the area ratio, respectively, for $\mathbf{M}_{2a}$. Shown in Fig. 9(*b*) are the results of the theoretical cal-

[8] For an extension of the theory to treat the case of bleeding of hot air, see reference (8).

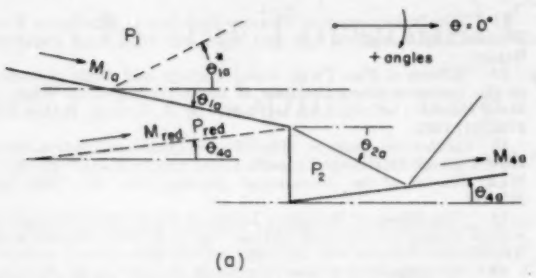

FIG. 8(a) FLOW CONFIGURATION FOR A GENERALIZED BACK STEP

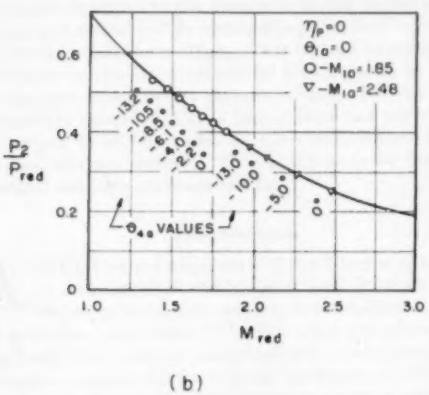

FIG. 8(b) REDUCED MACH-NUMBER PLOT OF H. EGGINK'S EXPERIMENTS WITH INCLINED DOWNSTREAM WALLS

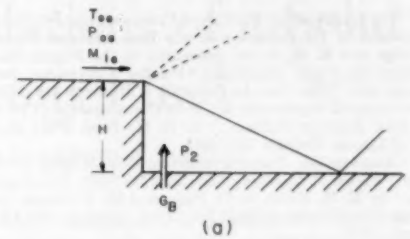

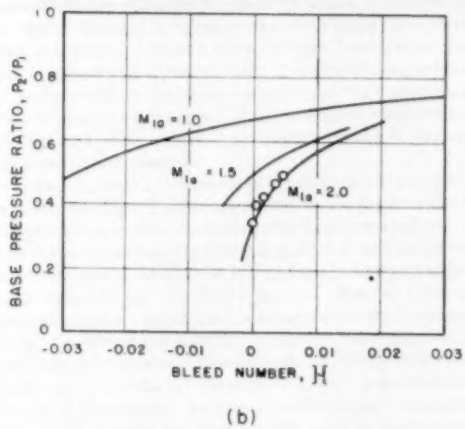

FIG. 9 SUPERSONIC FLOW PAST A BACK STEP WITH BLEEDING INTO THE WAKE

(a, Flow configuration. b, Theoretical effects of mass bleeding for M_{1a} = 1.0, 1.5, and 2.0, and experimental data for M_{1a} = 2.0.)

culations, based on a value of $\sigma = 12$, together with experimental data obtained at the University of Illinois for $M_{1a} = 2.00$. It is noteworthy to point out the high sensitivity of the base-pressure ratio to small rates of bleeding at higher supersonic Mach numbers. A discussion of the stability of the base-pressure solution can be based on the monotonous character of the curves as shown in Fig. 9(*b*) (1).

The flow past blunt trailing edges (or supersonic separation wakes) on airfoils in transonic and supersonic flow with dissimilar Mach numbers and dissimilar stagnation pressures (but identical stagnation temperatures, according to the restriction imposed in this paper, Equation [15], as occur at appreciable angles of attacks, also can be treated by the theory of open wakes.[9]

CONCLUSIONS

The simplified flow model devised to study the base-pressure problem in supersonic and transonic flow is apparently suited to explain the main influencing parameters, in this case, Mach number, and, in a limiting consideration, Reynolds number.

Asymptotic results which would apply to cases where the approaching turbulent boundary layer is relatively thin, that is, for high Reynolds numbers, predict lowest limiting base-pressure values.

These limiting base-pressure values, calculated for closed wakes without the use of empirical information, are in good agreement with experimental data obtained at high Reynolds numbers.

The theoretical treatment of mass bleeding into the wake requires the use of one empirical coefficient. Agreement between theoretical results and experimental data was obtained for a value of $\sigma = 12$, which value has been established previously, although for low-speed mixing.

BIBLIOGRAPHY

1 "A Theory for Base Pressures in Transonic and Supersonic Flow," by H. H. Korst, R. H. Page, and M. E. Childs, University of Illinois, ME-TN-392-2, OSR-TN-55-89, Contract No. AF 18(600)-392, March, 1955.

2 "Inter-Relationship Between Boundary Layer and Base Pressure," by H. H. Kurzweg, *Journal of the Aeronautical Sciences*, vol. 18, 1951, pp. 743–748.

3 "A Mixing Theory for the Interaction Between Dissipative Flows and Nearly Isentropic Streams," by L. Crocco and L. Lees, *Journal of the Aeronautical Sciences*, vol. 19, 1952, pp. 649–676.

4 "An Analysis of Base Pressure at Supersonic Velocities and Comparison With Experiment," by D. R. Chapman, NACA TN 2137, 1950; also, NACA Report 1051, 1951.

5 "Comments on the Effect of Boundary Layer on Sonic Flow Through an Abrupt Cross-Sectional Area Change," by H. H. Korst, *Journal of the Aeronautical Sciences*, vol. 21, 1954, pp. 568–569.

6 "Auflösung eines ebenen Freistrahlrandes bei Berücksichtigung der ursprünglichen Grenzschichtströmung," by H. H. Korst, *Österreichisches Ingenieur-Archiv*, vol. 7, no. 2, 1954.

7 "Compressible Two-Dimensional Jet Mixing at Constant Pressure," by H. H. Korst, R. H. Page, and M. E. Childs, University of Illinois, ME-TN-392-1, OSR-TN-54-82, Contract No. AF 18(600)-392, April, 1954.

[9] A detailed discussion of this problem was given in a thesis proposal by W. Tripp: "The base pressure behind a blunt trailing edge for supersonic two-dimensional flow in which the approaching streams have the same stagnation temperature, but have dissimilar Mach numbers and stagnation pressures," submitted to the Mechanical Engineering Graduate Studies Chairman, University of Illinois, October, 1954, and will be presented, together with the results of the experimental phase of this investigation, in a forthcoming PhD thesis.

8 "Non-Isoenergetic Turbulent Compressible Jet Mixing With Consideration of Its Influence on the Base Pressure Problem," by R. H. Page and H. H. Korst, presented at the Fourth Midwestern Conference on Fluid Mechanics, Purdue University, September, 1955; see also "The Non-Isoenergetic Turbulent Jet Mixing of a Two-Dimensional Supersonic Jet With Consideration of Its Influence on the Base Pressure Problem," by R. H. Page, PhD thesis, University of Illinois, Urbana, Ill., 1955.

9 "Compressible Two-Dimensional Jet Mixing at Constant Pressure—Tables of Auxiliary Functions for Fully Developed Mixing Profiles," by H. H. Korst, R. H. Page, and M. E. Childs, University of Illinois, ME-TN-392-3, OSR-TN-55-99, Contract No. AF 18(600)-392, April, 1955.

10 "Experimental Investigations of Base Pressures on Blunt-Trailing-Edge Wings at Supersonic Velocities," by D. R. Chapman, W. R. Wimbrow, and R. H. Kester, NACA TN 2611, 1952.

11 "The Improvement in Pressure Recovery in Supersonic Wind Tunnels," by H. Eggink, Rep. and Mem. No. 2703, ARC Technical Report.

12 "Effects of Plan Form, Airfoil Section, and Angle of Attack on the Pressures Along the Base of Blunt-Trailing-Edge Wings at Mach Numbers of 1.41, 1.62, and 1.96," by K. L. Goin, NACA RM L52D21, 1952.

13 Further comments on "The Effect of Boundary Layer on Sonic Flow Through an Abrupt Cross-Sectional Area Change," by R. S. Wick, *Journal of the Aeronautical Sciences*, vol. 22, 1955, pp. 135–137.

14 "The Effect of Boundary Layer on Sonic Flow Through an Abrupt Cross-Sectional Area Change," by R. S. Wick, *Journal of the Aeronautical Sciences*, vol. 20, 1953, pp. 675–682.

15 "Investigations on Free Turbulent Mixing," by H. W. Liepmann and J. Laufer, NACA TN 1257, 1947.

On the Torsional Oscillations of a Solid Sphere in a Viscous Fluid[1]

By G. F. CARRIER[2] and R. C. DI PRIMA,[3] CAMBRIDGE, MASS.

Most treatments of the torsional oscillations of solid bodies assume that the velocity field is circumferential. In this paper the motion in planes containing the axis of oscillation is also considered. An expansion in terms of the angular displacement ϵ (assumed small) is made. The first approximation to the circumferential velocity is computed, and then used in computing the first approximation to the pumping motion. This is used to compute the correction to the circumferential velocity and, in particular, the correction to the viscous torque. For the range of parameters considered it is found that the correction to the torque is of the order of $0.04\epsilon^2|N_0|$, where N_0 is the classical viscous torque. This problem is of interest in practical viscosity measurements.

Introduction

A STUDY of the oscillations of small bodies of revolution in a viscous fluid was initiated with the work of G. G. Stokes in his memoir relating to the motion of spherical and cylindrical pendulums (1).[4] This work was primarily concerned with the transverse oscillations of the body, though Stokes does give a solution for the torsional oscillation of a finite disk (and could have given the solution for the torsional oscillation of a sphere). The torsional oscillations of spheres and cylinders were then discussed both theoretically and experimentally by Helmholtz and Piotrowski (2). They were primarily interested in this problem as a possible method of measuring the viscosity of various fluids, the idea being that the kinematic viscosity of the fluid can be deduced from the period of oscillation, and from the logarithmic decrement of the torsional oscillations of the system. In recent years such methods have been suggested for measuring the viscosity of gases, in particular at high temperatures and pressures. For a discussion of the work that has been done along these lines as well as an extensive bibliography, see Kestin and Persen (3, 4) and Kestin (5). Finally, we mention that the transverse, as well as the torsional oscillations of a prolate spheroid were treated by J. Buchanan in 1891 (6). Accounts and some additions to the early work on the oscillations of bodies of revolution in a viscous fluid may be found in Basset (7) and Lamb (8).

In this paper we shall center our attention on the torsional oscillations of a solid sphere in a viscous fluid which extends to infinity in all directions. In all of the afore-mentioned papers dealing with this problem, it has been assumed that the fluid moves in concentric circles whose centers lie on the axis of rotation. It is clear that if account is taken of the centrifugal force that this cannot be the case. Actually, since the centrifugal force is greatest in the neighborhood of the equator of the oscillating sphere, the fluid particles will recede from the sphere at the equator and approach it again at the poles. Thus, combined with the motion about the axis, there will be a circulatory motion in planes containing the axis of rotation.

It is the purpose of this paper to compute the first approximation to this circulatory motion, and then to use these results to obtain a correction to the viscous torque acting on the sphere. First, the circumferential velocity, assuming there is no circulatory motion, is computed. This result is then used in computing the first approximation to the circulatory motion. Both of these results appear in a rather complicated manner in the nonhomogeneous term in the differential equation governing the correction to the circumferential velocity. This differential equation is solved in the case that $a = R(2\omega/\nu)^{1/2}$ is large.[5] Here R is the radius of the sphere, ω is the angular frequency, and ν is the kinematic viscosity. If N_0 denotes the torque which must be supplied, on the assumption of only concentric flow in order that the sphere perform harmonic torsional oscillations of amplitude ϵ, it is found that the correction to N_0 is the order of $0.04\epsilon^2|N_0|$ for the range of a considered. Hence for small values of ϵ the correction is quite small. It is particularly interesting to note that, since both N_0 and the correction torque are proportional to a plus terms of order one, increasing a does not decrease the correction to the viscous torque.

Equations of Motion

The equations of motion of a viscous, incompressible fluid are

$$\operatorname{div} \vec{v} = 0$$

$$\rho(\partial \vec{v}/\partial t + \vec{v} \operatorname{grad} \vec{v}) + \operatorname{grad} p = -\mu \operatorname{curl}^2 \vec{v} \quad \ldots [1]$$

It is most convenient to use the spherical co-ordinates r, θ, ϕ, where r is the radial co-ordinate, θ is the latitudinal angle, and ϕ is the longitudinal angle. Let the unit vectors $\mathbf{i}$, $\mathbf{j}$, and $\mathbf{k}$ be associated with the r, θ, ϕ directions, respectively. For a sphere performing torsional oscillations about the ϕ-axis, we seek a solution of Equations [1] independent of ϕ. Consequently, in line with the discussion in the introduction we take v to be of the form[6]

$$\left.\begin{aligned}\vec{v}(r, \theta, t) &= \mathbf{k}v(r, \theta, t) + \operatorname{curl} \{\mathbf{k}\psi(r, \theta, t)\} \\ &= \mathbf{i}(r \sin \theta)^{-1}(\psi \sin \theta)_\theta - \mathbf{j}r^{-1}(r\psi)_r + \mathbf{k}v\end{aligned}\right\} \quad \ldots [2]$$

The term $\mathbf{k}v(r, \theta, t)$ gives the flow in planes perpendicular to the

---

[1] The present paper is a report on work done under the sponsorship of the Office of Naval Research, under Contract No. N5-ORI-07666, with Harvard University.

[2] Gordon McKay Professor of Mechanical Engineering, Harvard University. Assoc. Mem. ASME.

[3] Research Fellow, Harvard University.

[4] Numbers in parentheses refer to the Bibliography at the end of the paper.

Presented at the National Applied Mechanics Division Conference, Urbana, Ill., June 14–16, 1956, of The American Society of Mechanical Engineers.

Discussion of this paper should be addressed to the Secretary, ASME, 29 West 39th Street, New York, N. Y., and will be accepted until January 10, 1957, for publication at a later date. Discussion received after the closing date will be returned.

Note: Statements and opinions advanced in papers are to be understood as individual expressions of their authors and not those of the Society. Manuscript received by ASME Applied Mechanics Division, January 9, 1956. Paper No. 56—APM-29.

[5] In certain experiments being performed at Brown University by Prof. J. Kestin, values of a in the range 20–30 occur; hence taking a large is not impractical.

[6] The symbols r, θ, t, v, x used as subscripts denote differentiation with respect to that variable. It will be clear from the content whether partial or ordinary differentiation is implied.

axis of oscillation, and the term curl $\{\mathbf{k}\psi(r, \theta, t)\}$ gives the flow in planes containing the axis of oscillation. The k-components of the momentum equation and the curl of the momentum equation will yield two equations for v and ψ. Carrying out these lengthy but straightforward computations we obtain

$$\left.\begin{aligned} v_t + \nu L(v) &= -\nu(r^2 \sin\theta)^{-1}\{(rv)_r(\psi \sin\theta)_\theta \\ &\qquad - (r\psi)_r(v \sin\theta)_\theta\} \\ L(\psi_t) + \nu L^2(\psi) &= -\nu r^{-1}\{(v^2 \cot\theta)_r - (v^2/r)_\theta \\ &\qquad - [rQ_1(\psi)L(\psi)]_r - [Q_2(\psi)L(\psi)_\theta\} \end{aligned}\right\} \quad \ldots [3]$$

where the operators L, Q_1, and Q_2 are defined by

$$\left.\begin{aligned} L(v) &= -\frac{1}{r}\left\{(rv)_{rr} + \frac{1}{r}\left[\frac{(v \sin\theta)_\theta}{\sin\theta}\right]_\theta\right\} \\ Q_1(\psi) &= r^{-1}(\psi \sin\theta)_\theta, \quad Q_2(\psi) = -r^{-1}(r\psi)_r \end{aligned}\right\} \quad \ldots [4]$$

We shall assume that the motion of the sphere is harmonic; that is, we assume that the angular velocity Ω of the sphere is given by $\Omega = \epsilon\omega \exp(i\omega t)$.[7] Here ω is the angular frequency, and ϵ is the angular displacement amplitude, which we assume to be small. (Our problem might now be stated as: What torque is required to maintain this harmonic oscillation when the sphere is surrounded by a viscous fluid?) Let R be the radius of the sphere, and introduce the following dimensionless variables

$$\tau = \omega t, \quad x = r/R, \quad \sigma^2 = \mu/R^2\rho\omega = \nu/R^2\omega,$$
$$v = \omega\epsilon RF(x, \theta, \tau), \quad \psi = \omega\epsilon R^2\chi(x, \theta, \tau)$$

Then Equations [3] become

$$\left.\begin{aligned} F_\tau + \sigma^2 L(F) &= -\epsilon^2(x^2 \sin\theta)^{-1}\{(xF)_x \\ &\qquad (\chi \sin\theta)_\theta - (x\chi)_x(F \sin\theta)_\theta\} \\ L(\chi_\tau) + \sigma^2 L^2(\chi) &= x^{-1}\{\cot\theta(F^2)_x - x^{-1}(F^2)_\theta\} \\ &\qquad - \epsilon^2 x^{-1}\{[xQ_1(\chi)L(\chi)]_x + [Q_2(\psi)L(\chi)]_\theta\} \end{aligned}\right\} \quad \ldots [5]$$

where now L, Q_1, and Q_2 are the operators defined by Equations [4] with r replaced by x.

It would be a hopeless task to try and solve Equations [5] as they now stand. However, if F and χ are expanded as series in the small parameter ϵ^2

$$F(x, \theta, \tau) = \sum_{n=0}^{\infty} \epsilon^{2n} F_n(x, \theta, \tau), \quad \chi(x, \theta, \tau) = \sum_{n=0}^{\infty} \epsilon^{2n}\chi_n(x, \theta, \tau) \quad \ldots\ldots [6]$$

we obtain the following system of equations for F_0, χ_0, and F_1 which are amenable to treatment

$$(F_0)\tau + \sigma^2 L(F_0) = 0 \ldots\ldots\ldots\ldots\ldots [7a]$$

$$L(\chi_0)_\tau + \sigma^2 L^2(\chi_0) = x^{-1}\{\cot\theta(F_0^2)_x - x^{-1}(F_0^2)_\theta\} \ldots [7b]$$

$$(F_1)_\tau + \sigma^2 L(F_1) = -(x^2 \sin\theta)^{-1}\{(xF_0)_x(\chi_0 \sin\theta)_\theta - (x\chi_0)_x(F_0 \sin\theta)_\theta\} \ldots\ldots [7c]$$

The boundary conditions that the F_n and χ_n must satisfy are obtained from the requirement that there be no slip at the surface of the sphere, and that the velocity at infinity be zero. They are

$$\left.\begin{aligned} &F_0(x, \theta, \tau) = \sin\theta e^{i\tau}, \quad F_{n+1} = \chi_n = (\chi_n)_x = 0 \\ &\text{at } x = 1, \text{ and as } x \text{ approaches infinity} \\ &F_n = \chi_n = (\chi_n)_x = 0 \end{aligned}\right\} \quad \ldots [8]$$

for $n \geq 0$. If we had assumed that the flow took place in concentric circles about the axis of oscillation, and also had neglected the nonlinear terms in the equations of motion, we would have obtained only Equation [7a]. Once we know the solution of Equation [7a] we can solve Equation [7b] for χ_0 which is the first approximation to the circulatory motion. Then, knowing F_0 and χ_0, we can solve Equation [7c] for F_1 and hence obtain a correction to the circumferential velocity, and the torque acting on the sphere.

In order to solve the foregoing systems of equations it is necessary to investigate more closely the differential operator L. It is easy to deduce that the derivatives of the Legendre polynomials $P_n(\cos\theta)$ which we denote by $T_n(\theta)$ (and we have factored out a constant so that the coefficient of the leading term is 1), are eigenfunctions of the differential equation

$$\frac{d}{d\theta}\left\{\frac{1}{\sin\theta}\frac{d}{d\theta}[\sin\theta\, T_n(\theta)]\right\} + k_n T_n(\theta) = 0$$

and hence the $T_n(\theta)$ are factors of the operator L (reference 9). It follows immediately from the form of the Legendre polynomials that for n odd the $T_n(\theta)$ are simply polynomials in $\sin\theta$, while for n even they are polynomials in $\sin\theta$ times a factor $\sin 2\theta$. In particular, the first few T_n are

$$T_0(\theta) = 0, \qquad T_2(\theta) = \sin 2\theta$$

$$T_1(\theta) = \sin\theta \qquad T_3(\theta) = \sin\theta - (5/4)\sin^3\theta$$

The orthogonality relation which the T_n satisfy is

$$\int_0^\pi T_n(\theta)T_m(\theta) \sin\theta d\theta = 0 \qquad m \neq n$$

and for $n = 1$ this becomes

$$\int_0^\pi T_m(\theta) \sin^2\theta d\theta = 0$$

This relation is important for the following reason.

The tangential stress S which opposes the motion of the sphere is given by $S = -\mu(v/r)_r$ evaluated at $r = R$. The torque N which acts on the sphere is $SR \sin\theta$ integrated over the sphere. Then, substituting for v and carrying out the integration in ϕ, we obtain

$$N = -2\pi\mu\omega\epsilon R^3 \int_0^\pi \left.\frac{\partial(F/x)}{\partial x}\right|_{x=1} \sin^2\theta d\theta$$

In analogy with the expansion of F in a powers series in ϵ^2 we may write

$$N = \sum_{n=0}^{\infty} \epsilon^{2n} N_n, \quad N_n = -2\pi\mu\omega\epsilon R^3 \int_0^\pi \left.\frac{\partial(F_n/x)}{\partial x}\right|_{x=1} \sin^2\theta d\theta \quad \ldots\ldots [9]$$

Thus if the $F_n(x, \theta, \tau)$ are expanded in terms of the $T_m(\theta)$ [actually in terms of the odd $T_m(\theta)$ because of the geometry of the problem], it is clear from Equation [9] and the foregoing orthogonality relation that only the first mode in θ can give a nonzero viscous torque.

Now let us return to Equation [7a]. From the form of the boundary conditions and the discussion it is evident that we should take

$$F_0(x, \theta, \tau) = f(x) \sin\theta e^{i\tau} \ldots\ldots\ldots\ldots [10]$$

in which case Equation [7a] becomes

$$L_1(f) - z^2 f = 0 \ldots\ldots\ldots\ldots [11]$$

[7] It is to be understood that here and throughout the rest of this paper, where complex representations are used, we are actually referring to their real parts.

where

$$L_1(f) = x^{-1}\{(xf)_{xx} - 2x^{-1}f\}, \quad z^2 = i/\sigma^2$$

or

$$\varepsilon = (1+i)\alpha \text{ and } \alpha = R(\omega/2\nu)^{1/2}$$

Solving this equation we obtain

$$\left.\begin{aligned} F_0(x,\theta,\tau) &= \frac{1+zx}{(1+z)x^2}\, e^{-\varepsilon(x-1)} \sin\theta e^{i\tau} \\ &= \left(\frac{1+2\alpha x+2\alpha^2x^2}{x^4\beta}\right)^{1/2} e^{-\alpha(x-1)} \\ &\qquad \sin\theta e^{i\{\tau-\alpha(x-1)+\eta_1(x)\}} \end{aligned}\right\} \quad [12]$$

where $\beta = (1+2\alpha+2\alpha^2)$ and $\eta_1(x) = \arctan\{\alpha(x-1)/(1+\alpha+\alpha x+2\alpha^2 x)\}$. Using Equation [9] and carrying out the indicated computations we find that

$$\left.\begin{aligned} N_0 &= -\frac{8\pi\mu R^3}{3}\,\frac{(3+6\alpha+6\alpha^2+2\alpha^3)+i(1+\alpha)2\alpha^2}{\beta}\,\omega\epsilon e^{i\omega t} \\ &= -\frac{8\pi\mu R^3}{3}\,\frac{(8\alpha^6+32\alpha^5+64\alpha^4+84\alpha^3+72\alpha^2+36\alpha+9)^{1/2}}{\beta}\,\omega\epsilon e^{i\omega t} \end{aligned}\right\} \quad [13]$$

where $\eta_2 = \arctan[2\alpha^2(1+\alpha)/(3+6\alpha+6\alpha^2+2\alpha^3)]$. The phase advance in N_0 for large α is $\arctan(1-2/\alpha)$, and as $\alpha \to \infty$ this is $\pi/4$, which is the well-known result for the skin friction of an infinite lamina oscillating in a viscous incompressible fluid. The results given in Equations [12] and [13] are in agreement with those given by Lamb (8); however, the notation is quite different.

Finally, we point out that if one wished to consider an initial value problem, instead of the steady-state problem considered here, and had used the method of Laplace transforms to solve the resulting problem he would find that the transform of $F_0(x,\theta,\tau)$ is given by the first of Equations [12] where now $z^2 = s/\sigma^2$ (s being the transform variable with respect to t). See (4) for a more complete discussion of the nonsteady-state problem.

The Circulatory Motion

Since $F_0(x,\theta,\tau)$ is proportional to $\exp(i\tau)$, the quadratic nonhomogeneous term in Equation [7b] will consist of a time-independent term plus a term which is proportional to $\exp(2i\tau)$. Using Equation [12] we obtain after substituting in Equation [7b] the following differential equation for χ_0

$$\begin{aligned} &L(\chi_0)_\tau + \sigma^2 L^2(\chi_0) \\ &\quad = -\sin 2\theta\,\frac{3+6\alpha x+6\alpha^2x^2+2\alpha^3x^3}{2\beta x^6}\, e^{-2\alpha(x-1)} \\ &\quad - \sin 2\theta\,\frac{3+6zx+4z^2x^2+z^2x^3}{2(1+z)^2x^6}\, e^{-2z(x-1)}e^{2i\tau} \end{aligned} \quad [14]$$

The form of this equation suggests that we take

$$\chi_0(x,\theta,\tau) = \sin 2\theta\{g(x)+G(x)e^{2i\tau}\} \quad [15]$$

in which case we obtain the two ordinary differential equations

$$L_2^2(g) = -\frac{(3+6\alpha x+6\alpha^2x^2+2\alpha^3x^3)}{2\sigma^2\beta x^6}\, e^{-2\alpha(x-1)} \quad [16a]$$

$$\begin{aligned} &L_2^2(G) - 2z^2 L_2(G) \\ &\quad = -\frac{(3+6zx+4z^2x^2+z^2x^3)}{2\sigma^2(1+z)^2x^6}\, e^{-2z(x-1)} \end{aligned} \quad [16b]$$

where $L_2(g) = x^{-1}\{d^2(xg)/dx^2 - 6x^{-1}g\}$

The boundary conditions on g and G are that they and their first derivatives vanish at $x = 1$, and as $x \to \infty$.

Solutions of Equations [16a] and [16b] which satisfy the boundary conditions at infinity may be obtained by the usual method of variation of parameters. They are

$$\begin{aligned} g(x) = \frac{A_1}{x} + \frac{A_2}{x^3} - \frac{1}{40\sigma^2\beta}\Big\{ & e^{-\alpha(x-1)}\left(\frac{3}{\alpha x^3}+\frac{1}{2x^2}-\frac{\alpha}{6x}+\frac{\alpha^2}{12}-\frac{\alpha^2 x}{12}\right) \\ & + \frac{\alpha^4 e^\alpha x^3}{12}E(\alpha x)\Big\} \end{aligned} \quad [17a]$$

$$\begin{aligned} G(x) = \frac{B_1}{x^3} + B_2 h(x,\delta) - \frac{1}{4\sigma^2(1+z)^2}\Big\{ & e^{-2z(x-1)}\,\frac{3+zx}{8zx^3} \\ & - \frac{M(x,\delta)-M(x,-\delta)}{16\delta}\Big\} \end{aligned} \quad [17b]$$

where $a = 2\alpha$, $\delta^2 = 2z^2$, and

$$M(x,\delta) = h(x,\delta)E[(2x-\delta)x]e^{-(\delta-2x)}$$

$$h(x,\delta) = \frac{3+3\delta x+\delta^2x^2}{x^3}\, e^{-\delta(x-1)}$$

$$E(x) = \int_x^\infty \frac{e^{-s}}{s}\,ds$$

The constants A_1, A_2, B_1, and B_2 are determined by requiring that $g(x)$ and $G(x)$ and their first derivatives are zero at $x = 1$. We obtain the following results

$$\left.\begin{aligned} A_1 &= \frac{-1}{32\sigma^2\beta}\left\{1+\frac{a}{3}-\frac{a^2}{6}+\frac{a^3}{6}-\frac{a^4e^aE(a)}{6}\right\} \\ A_2 &= \frac{1}{80\sigma^2\beta}\left\{\frac{6}{a}+\frac{7}{2}+\frac{a}{2}-\frac{a^2}{4}+\frac{a^3}{4}-\frac{a^4e^aE(a)}{4}\right\} \\ B_1 &= \left(\frac{1}{4z}-\frac{1}{2z^2}+\frac{3}{8z^3}\right)K - \frac{(3+3\delta+\delta^2)(z^3-2z^2+11z-78)K}{4z(1+\delta)} \\ B_2 &= \frac{(z^3-2z^2+11z-78)K}{4z^3(1+\delta)} \end{aligned}\right\} \quad [18]$$

where

$$K = a^2/8(1+z)^2$$

As has been pointed out previously, as the sphere performs torsional oscillations, fluid will be sucked in along the axis of oscillation and then thrown out along the equatorial plane of the sphere. A measure of the amount of steady pumping (i.e., the d-c pumping) can be found in the following manner: Let V be the steady component of velocity in the θ-direction; then using Equations [2] and [15] we see that

$$V = -\frac{\omega\epsilon^2 R}{x}\sin 2\theta\,\frac{d(xg)}{dx} \quad [19]$$

A careful analysis of $d(xg)/dx$ shows that it only vanishes at $x = 1$ and $x = \infty$; hence V is one signed. Let

$$Q = \int_R^\infty 2\pi r V dr \quad [20]$$

Then Q is essentially the amount of fluid which is pumped across a surface of a cone of apex angle θ outside of a sphere of radius R. Q is clearly the product of a velocity times an area. Upon using Equations [19], [17a], and [18] we may evaluate Equation [20] obtaining the result

$$Q = \frac{\pi\omega\epsilon^2R^3a^3\sin 2\theta}{16P}\left\{1 + \frac{a}{3} - \frac{a^2}{6} + \frac{a^3}{6} - \frac{a^4E(a)}{6}\right\} \quad \ldots [21]$$

where $P = (2 + 2a + a^2)$. As is to be expected, the pumping is proportional to the square of the angular displacement. Its dependence on the other parameters is more complicated; however, it is possible to consider the limiting cases of a large and small.

When a is large, $E(a)$ may be replaced by its asymptotic form

$$[E(a) \sim (1/a - 1/a^2 + 2!/a^3 + \ldots)\exp(-a)]$$

and we obtain

$$Q = \frac{\pi\omega\epsilon^2R^3\sin 2\theta}{8}\left\{1 - \frac{4}{a} + 0\left(\frac{1}{a^2}\right)\right\} \quad \ldots [22]$$

If we denote the maximum peripheral velocity by $V_1 = \epsilon\omega R\sin\theta$, and the area of the sphere by $A = 4\pi R^2$ we can rewrite Equation [22] as

$$Q = \frac{V_1A\epsilon\cos\theta}{16}\left\{1 - \frac{4}{a} + 0\left(\frac{1}{a^2}\right)\right\} \quad \ldots [23]$$

For fixed values of θ, V_1, and A the pumping decreases linearly with ϵ. On the other hand, if we keep θ, ϵ, and V_1 fixed it is clear that Q varies as the square of R. If one is running an experiment at large values of a and wishes to keep the pumping small it is desirable to keep ϵ and particularly R small.

The limiting case in which the sphere rotates with constant angular velocity Ω_0 can be obtained by dividing Equation [21] by ω^2 and then letting $\omega \to 0$; i.e., $a \to 0$. The reason for this is that in our formulation of the problem the circumferential velocity is proportional to $\epsilon\omega\exp(i\omega t)$ while χ is proportional to the square of the circumferential velocity. Carrying out this operation and noting that ϵ becomes Ω_0 we obtain

$$Q = \frac{\pi\Omega_0^2R\sin 2\theta}{8\nu} \quad \ldots [24]$$

Just as in the previous case, if we let $V_0 = \Omega_0R\sin\theta$ we can write Equation [24] as

$$Q = V_0A\left(\frac{\Omega_0R^2\cos\theta}{16\nu}\right) \quad \ldots [25]$$

where the quantity Ω_0R^2/ν is a dimensionless quantity. Again, just as before, it is clear that the most important factor in decreasing Q is to decrease R. For intermediate values of a, Q can be computed from Equation [21].

Finally, in the next section we shall require asymptotic representations of $g(x)$, $G(x)$ and their first derivatives when a is large. These representations can be obtained from Equations [17a] and [17b] by replacing the exponential integrals by their asymptotic representations. We obtain

$$\left.\begin{aligned} g(x) &\sim \frac{a^2}{16P}\left\{\frac{A_1'}{x} + \frac{A_2'}{x^2} - e^{-a(x-1)}\left(\frac{2}{ax^2} - \frac{4}{a^2x^4} + \frac{24}{a^3x^5} + \ldots\right)\right\} \\ G(x) &\sim \frac{B_1}{x^3} + B_2h(x,\delta) - Ke^{-2a(x-1)}\left(\frac{1}{4ax^3} - \frac{1}{2a^2x^4} + \frac{3}{a^3x^4} + \ldots\right)\Big\} \\ A_1' &\sim -\left(1 - \frac{2}{a} + \frac{10}{a^2} - \frac{60}{a^3} + \ldots\right), \\ B_1 &\sim \frac{K}{4z}\left\{\left(1 - \frac{\delta}{z}\right) - \frac{4}{z} + \frac{4}{\delta}\right\} \\ A_2' &\sim 1 + \frac{6}{a^2} - \frac{36}{a^3} + \ldots, \\ B_2 &\sim \frac{K}{4z^2\delta}\left(1 - \frac{2}{z} - \frac{1}{\delta}\right) \end{aligned}\right\} \quad \ldots [26] \text{ (cont.)}$$

Asymptotic representations of the derivatives of g and G can be obtained by differentiating Equations [26]. However, the highest-order terms must be neglected; i.e., in dg/dx the terms of $0(1/a^2)$ would not be correct if the representation of $g(x)$ given in Equation [26] is used. It is not too difficult to obtain more accurate expressions, but the accuracy we shall acquire in the next section will allow us to drop terms $0(1/a^2)$ against 1 so the accuracy in Equation [26] is sufficient. Actually, terms $0(1/a^2)$ have already been neglected in the expressions for B_1 and B_2 given previously.

Corrections to the Viscous Torque

Now, knowing F_0 and χ_0, we can compute the nonhomogeneous term in Equation [7c] obtaining

$$(F_1)_\tau + \sigma^2L(F_1) = e^{i\tau}\{H_{11}(x)T_1(\theta) + H_{13}(x)T_3(\theta)\} + e^{3i\tau}\{H_{31}(x)T_1(\theta) + H_{33}(x)T_3(\theta)\} \quad \ldots [27]$$

where

$$H_{11}(x) = (1/20x^2)\{26(xg)_xf + 6(xf)_xg + 13(xG)_xf^* + 3(xf^*)_xG\}$$

$$H_{13}(x) = (4/5x^2)\{4(xf)_xg - 6(xg)_xf + 2(xf^*)_xG - 3(xG)_xf^*\}$$

$$H_{31}(x) = (1/20x^2)\{13(xG)_xf + 3(xf)_xG\}$$

$$H_{33}(x) = (4/5x^2)\{2(xf)_xG - 3(xG)_xf\}$$

An asterisk is used to denote the complex conjugate. Unfortunately, because of the complexity of the differential equation, the notation which is employed must become more complicated. However, the method of attack, in theory, is still straightforward.

Recalling our earlier discussion about the operator L, and noting the form of the nonhomogeneous term in Equation [27], it is clear that we should take

$$F_1(x,\theta,\tau) = e^{i\tau}\{f_{11}(x)T_1(\theta) + f_{13}(x)T_3(\theta)\} + e^{3i\tau}\{f_{31}(x)T_1(\theta) + f_{33}(x)T_3(\theta)\} \quad \ldots [28]$$

Now we are primarily interested in determining the correction to the first harmonic of the viscous torque, so we need only determine $f_{11}(x)$ and $f_{13}(x)$; but because of the orthogonality relation for the $T_m(\theta)$, $f_{13}(x)$ cannot contribute to N_1. Hence we need only determine $f_{11}(x)$; the equation for this function is

$$if_{11} - \sigma^2x^{-1}\{(xf_{11})_{xx} - 2x^{-1}f_{11}\} = H_{11}(x) \quad \ldots [29]$$

The boundary conditions are $f_{11}(1) = f_{11}(\infty) = 0$. Now the function $H_{11}(x)$, as defined previously, is an extremely complex function involving products of five different exponentials and polynomials in $1/x$ as well as exponential integrals. It is clear that solving Equation [29] exactly and extracting numerical information is an extremely laborious task.

However, in computing N_1 we only need $d(f_{11}/x)/dx$ evaluated at $x = 1$. Hence we need only determine a solution of Equation [29] which is accurate in the neighborhood of $x = 1$. Now in the case that a is large (the only case which we shall consider) the behavior of $H_{11}(x)$ is the following: It starts at zero at $x = 1$, rises quickly to its maximum in a distance of the order of $1/a$, and then dies out exponentially as exp $\{a(x - 1)\}$. Hence $H_{11}(x)$ can be approximated quite well in the region of particular interest by letting $x = 1 + \xi/a$, where $\xi/a < 1$ and then neglecting terms $0(1/a^2)$. To the same order of accuracy the term $2\sigma^2 x^{-1} f_{11}$ can be neglected against $ixf_{11}(x)$. This is essentially an approximation of the boundary-layer type.

Letting $p(x) = xf_{11}(x)$ Equation [29] reduces to

$$\frac{d^2p}{d\xi^2} - bp = (c_1 + d_1\xi + e_1\xi^2)e^{-\gamma_1\xi} + \sum_{i=2}^{5} (c_i + d_i\xi)e^{-\gamma_i\xi} \quad \ldots\ldots [30]$$

where $b = z^2/a^2$. The γ_i are, respectively, z/a, $(z + a)/a$, $(z^* + \delta)/a$, $(2z + z^*)/a$, and z^*/a; the c_i and d_i and e_i are functions of a of the form $U_1 + U_2/a$ where U_1 and U_2 are, in general, complex constants. To solve this equation still requires a considerable amount of work, but this work is very small indeed compared to that required to solve the original problem. Carrying out the necessary computations we obtain

$$N_1 = -\frac{8\pi\mu R^3\omega\epsilon}{3} \frac{85.556a}{3200} \left(1 - \frac{4.173}{a}\right) e^{i(\omega t + \eta_4 + \pi/2)} \quad [31]$$

where

$$\eta_4 = \arctan \{(0.356 + 7.502/a)\}$$

To the same order of accuracy Equation [13] reduces to

$$N_0 = -\frac{8\pi\mu R^3\omega\epsilon}{3} \frac{a}{2^{1/2}} \left(1 + \frac{2}{a}\right) e^{i(\omega t + \eta_3)} \quad \ldots\ldots [32]$$

where $\eta_3 = \arctan (1 - 4/a)$. It is interesting to note that both N_0 and N_1 are proportional to the dimensionless parameter $a = R(2\omega/\nu)^{1/2}$. Hence, forgetting about the extremely slight effect of the terms $0(1/a)$ compared to 1, it is clear that increasing a will not decrease the correction to the viscous torque. However, because of the extremely small coefficient in N_1 the correction will not be too large as long as ϵ is small. Combining Equations [31] and [32] we obtain

$$N_0 + \epsilon^2 N_1 = -\frac{8\pi\mu R^3\omega\epsilon a}{3(2)^{1/2}} \left\{\left(1 + \frac{2}{a}\right) \cos(\omega t + \eta_3) - 0.038\epsilon^2 \left(1 - \frac{4.173}{a}\right) \sin(\omega t + \eta_4) + 0\left(\frac{1}{a^2}\right)\right\}$$

So if ϵ is one radian the correction is about 4 per cent, but for a more reasonable value of ϵ, say $\epsilon = 1/4$ radian, the correction is only about 0.23 per cent and hence should affect only extremely accurate measurements. Hence for very accurate viscosity measurements ϵ should be kept as small as possible.

ACKNOWLEDGMENT

The authors would like to express their appreciation to Mr. Harvey Greenspan who checked independently almost all of the calculations involved in computing $f_{11}(x)$ and N_1.

BIBLIOGRAPHY

1 "On the Effect of the Internal Friction on the Motion of Pendulums," by G. G. Stokes, Transactions of the Cambridge Philosophical Society, vol. 9, 1856, pp. 8–150 (read in 1850).

2 "Wissenschaftliche Abhandlungen," by H. Helmholtz and Piotrowski, J. A. Barth, Leipzig, Germany, 1882, p. 172.

3 "Slow Oscillations of an Infinite Plate and an Infinite Disk in a Viscous Fluid," by J. Kestin and L. N. Persen, Brown University Report AF-891/1 Contract AF 18(600)-891.

4 "Small Oscillations of Bodies of Revolution in a Viscous Fluid," by J. Kestin and L. N. Persen, Brown University Report AF-891/2 Contract AF 18(600)-891.

5 "Three Papers on the Oscillating Cup Viscometer: Translated and Condensed," by J. Kestin, Brown University Report AF-891/4 Contract 18(600)-891.

6 "The Oscillations of a Spheroid in a Viscous Liquid," by J. Buchanan, Proceedings of the London Mathematical Society, vol. 22, 1891–1892, pp. 181–214.

7 "A Treatise on Hydrodynamics," by A. B. Basset, Deighton, Bell and Co., London, England, vol. 2, 1888, chapters 26 and 27.

8 "Hydrodynamics," by H. Lamb, Dover Publications, New York, N. Y., sixth edition, 1945, p. 642.

9 "The Mathematics of Physics and Chemistry," by H. Margenau and G. M. Murphy, D. Van Nostrand Co., Inc., New York, N. Y., 1943, p. 68.

An Experimental Investigation of Beam Stresses Produced by Oblique Impact of a Steel Sphere[1]

By D. M. CUNNINGHAM[2] and WERNER GOLDSMITH,[3] BERKELEY, CALIF.

An experimental investigation designed to study the phenomena incident to the oblique collision of 1/2-in-diam steel spheres with mild-steel and annealed drill-rod beams at oblique angles of incidence has been undertaken. Initial ball velocities ranged from 30 ft/sec to 150 ft/sec, beam sizes varied from 1/4 in. × 1/4 in. to 3/4 in. × 3/4 in., angles of incidence were chosen from 85 deg to normal incidence, and simply supported, clamped, and free beams were employed. Information is reported concerning the values of maximum bending stress at various positions along the beam as function of the angle of incidence and as a function of beam size for various angles of incidence. The progressive dispersion of the initial transient has been examined in detail. The effect of end supports, effective beam length, and repetitive shots into the same hole upon stress are described.

Introduction

PREVIOUS theoretical and experimental investigations of the transverse impact of spheres on beams have been limited to the case of normal impact at low initial velocities resulting in essentially elastic collisions. In many important applications, however, the impact will occur at oblique incidence and may produce considerable plastic flow at the contact point, whereas the structure as a whole will not be permanently deformed. The present investigation was undertaken to ascertain the effect of oblique impact and crater formation on various parameters which were believed to describe most effectively the resistance of the beam to the collision. The primary variables involved are the peak stresses and deformations encountered in the beam. In terms of a damage criterion for the structure, the dimensions of the crater, the duration of contact, and the wave-propagation effects are also important.

The present paper is the second of a sequence of four describing the phenomena incident to the oblique impact of steel spheres upon steel beams. The first paper (1)[4] described the equipment and procedure employed in the present experimental investigation and delineated the analysis of a typical test run. The current publication contains the results for the entire stress investigation of approximately 130 runs and a discussion of these data. A forthcoming paper will present parallel information on the kinetic history of the process, including data relative to beam deflections, contact deformations, durations of contact, and wave-propagation characteristics. The final paper of this sequence will deal with a theoretical prediction of the variables and a comparison of such calculated values with a selected number of data.

The parameters employed in this investigation are summarized as follows:

Ball: 1/2-in-diam steel ball bearing, approximately 68 Rockwell C hardness

Beams: (*a*) Simply supported between 30-in. centers:

1/4-in. × 1/4-in., 1/4 × 1/2, 1/2 × 1/2, 1/2 × 3/4, 3/4 × 3/4-in. mild cold-rolled steel, 1/2-in. × 1/2-in. annealed drill-rod steel (0.95/1.05 C, 0.20/40 Mn, 0.10/0.25 Si)

(*b*) Clamped over a 2-in. distance at both ends with a span of 22 in.: 1/2-in. × 1/2-in. mild cold-rolled steel

1/4-in. × 1/4-in., 3/8 × 1/2, 1/2 × 1/2, and 3/4 × 3/4-in. annealed drill-rod steel

(*c*) Free-free ends with a length of 36 in.

Superficial hardness of mild cold-rolled steel was about 95 Rockwell B and that of annealed drill rod about 90 Rockwell B. Stress-strain curves for both materials are shown in Fig. 1.

Impact velocities: 30 to 150 fps

Angles of incidence: From 85 deg to normal incidence

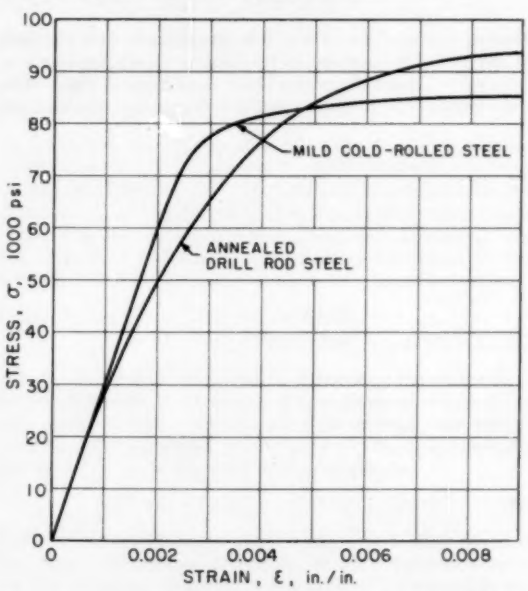

FIG. 1 STATIC STRESS-STRAIN CURVES FOR COLD-ROLLED MILD STEEL AND ANNEALED DRILL ROD. 1/4-IN. × 1/4-IN. × 2-IN. TEST SECTION

[1] Work supported by Mechanics Branch, USNOTS, China Lake.

[2] Associate Professor, Division of Engineering Design, University of California. Assoc. Mem. ASME.

[3] Associate Professor, Division of Engineering Design, University of California. Assoc. Mem. ASME.

[4] Numbers in parentheses refer to the Bibliography at the end of the paper.

Presented at the West Coast Conference of the Applied Mechanics Division, Pasadena, Calif., June 11–13, 1956, of THE AMERICAN SOCIETY OF MECHANICAL ENGINEERS.

Discussion of this paper should be addressed to the Secretary, ASME, 29 West 39th Street, New York, N. Y., and will be accepted until January 10, 1957, for publication at a later date. Discussion received after the closing date will be returned.

NOTE: Statements and opinions advanced in papers are to be understood as individual expressions of their authors and not those of the Society. Manuscript received by ASME Applied Mechanics Division, March 8, 1956. Paper No. 56—APM-41.

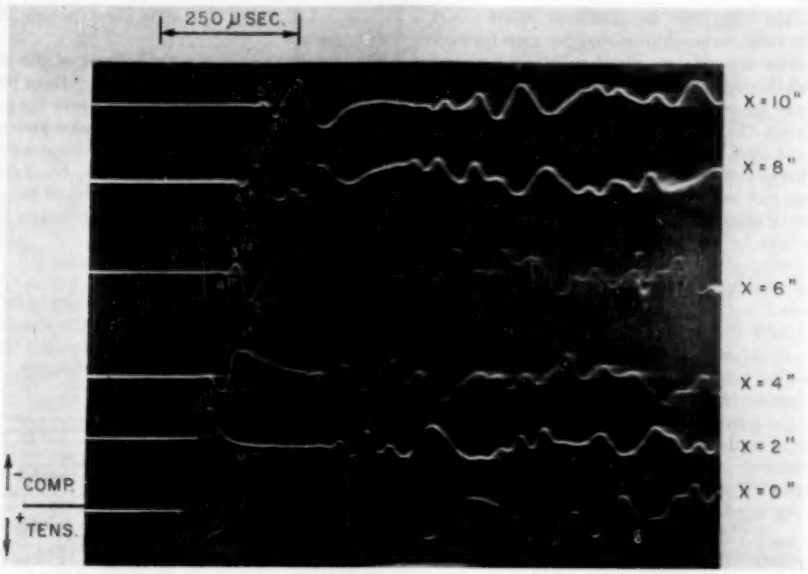

FIG. 2 STRESS PROPAGATION IN A 3/8-IN. × 1/2-IN. × 22-IN. CLAMPED, ANNEALED, DRILL-ROD BEAM SHOT AT AN INITIAL VELOCITY OF 30 FPS. ANGLE OF INCIDENCE 7 DEG

(MP = major pulse. Numbers refer to number of precursor.)

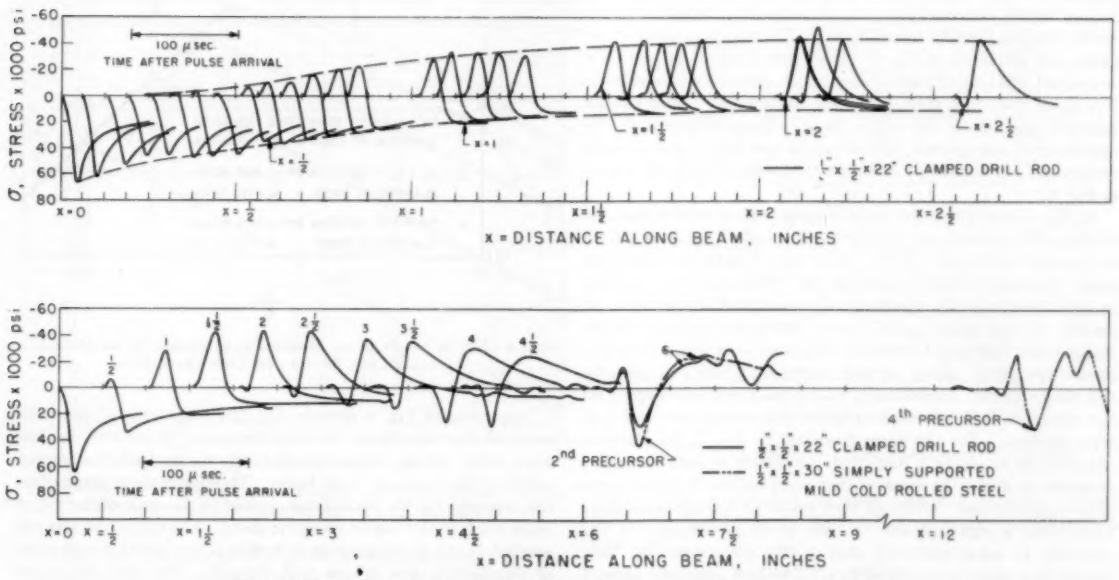
σ, STRESS x 1000 psi
100 μ sec.
TIME AFTER PULSE ARRIVAL
x = 1/2
x = 1
x = 1 1/2
x = 2
x = 2 1/2
1/2" x 1/2" x 22" CLAMPED DRILL ROD
x = 0
x = 1/2
x = 1
x = 1 1/2
x = 2
x = 2 1/2
x = DISTANCE ALONG BEAM, INCHES
σ, STRESS x 1000 psi
100 μ sec.
TIME AFTER PULSE ARRIVAL
2nd PRECURSOR
4th PRECURSOR
1/2" x 1/2" x 22" CLAMPED DRILL ROD
1/2" x 1/2" x 30" SIMPLY SUPPORTED MILD COLD ROLLED STEEL
x = 0
x = 1/2
x = 1 1/2
x = 3
x = 4 1/2
x = 6
x = 7 1/2
x = 9
x = 12
x = DISTANCE ALONG BEAM, INCHES

FIG. 3 METAMORPHOSIS OF MAJOR PULSE OF LONGITUDINAL BENDING STRESS

RESULTS

The transient-stress peaks have been labeled in accordance with a scheme of successive appearance of these pulses. The strain transient at the impact point, called the major pulse, consists of a single pulse which disperses along the rod with continued inversion of amplitude and increasing number of wavelets, or precursors. The number of each precursor represents the number of strain inversions of the pulse since its initiation at the impact point. The terminology is illustrated in Fig. 2 which is an actual strain record representing the propagation of a stress pulse in a 3/8 in. × 1/2-in. annealed drill-rod beam, with gages spaced at 2 in. intervals from center. The detailed structure of such a pulse is shown in Fig. 3 where the stress history was measured at 1/16-in. intervals.

Each beam was used for several shots, and an attempt was made to prevent overlapping of successive craters. However, a tabulation of the stresses obtained from some of the initial runs indicated a high degree of inconsistency which was later attrib-

uted to the fact that the shots were scattered too widely about the central gage. In order to obtain one shot per gage for each beam, avoid any scatter or overlapping, and yet retain a central impact, it was expedient to run a series of tests with a new end connection. This was accomplished by using clamped-clamped supports at the ends of a 22-in. span on a 36-in. bar with a clamping distance of 2 in. at each end. The characteristic of this connection was such that it permitted a longitudinal shifting of the beam between shots, and incidentally prevented a vibration of the overhanging parts of the beam. It was ascertained that neither length nor type of end connection—simply supported, fixed-fixed, or free—affected the major pulse region of the gage behind the point of impact provided this position was not too close to the span ends.

Metamorphosis of the Major Pulse. In previous investigations (2 to 4) a number of strain-gage records have been exhibited showing the stress-time histories for various positions along a beam subjected to central impact. In all instances the spacing of the gages was far too great to permit an analysis of the growth and decay of any of the predominant wave groups of the transient as a function of distance along the beam. The phase of the investigation described in this section was designed to resolve this question by providing an effective gage spacing of $^1/_{16}$ in. along the beam.

A number of tests were conducted on a simply supported $^1/_2$-in. $\times$ $^1/_2$-in. annealed drill-rod beam with a $^1/_2$-in. gage spacing for a distance of $2^1/_2$ in. from the beam center. Impact points were chosen judiciously so that their location relative to the several gage positions varied by $^1/_{16}$-in. increments. The gun was moved longitudinally with respect to the beam up to a distance 2 in. off center, resulting in noncentral impact. The results of this investigation are exhibited in Fig. 3. The upper diagram is primarily concerned with the decay of the major pulse and covers only $2^1/_2$ in. of the beam span, while the lower figure shows a more complete picture for the entire beam. These diagrams clearly demonstrate the growth and decay of the predominant wave groups and substantiate the basis of the nomenclature presented in Fig. 2.

At the center, the major pulse begins with a rapid linear rise of about 10 microsec and decays "exponentially" until the arrival of the reflected wave. As the pulse moves along the beam, its peak diminishes until its shape has been distorted beyond recognition at a point approximately four beam depths from the center. In the interim, the energy contained originally in the major pulse has been transferred primarily to a single predominant wave group, called the first precursor, which just precedes this major pulse. Periodically, additional precursors appear on the record and each in turn becomes the predominant pulse at some position. For the beam described by Fig. 3, the distance required for attaining a maximum amplitude of each successive precursor is about the same as that observed for the diminution of the major pulse. Although each precursor reaches a maximal value with a sign opposite to that of its predecessor, it was observed in some instances that a few precursors had their genesis in a pulse of identical sign. The first precursor appears to attain a maximum value corresponding to 75 per cent of the stress reached by the major pulse at the center, and all subsequent precursors are smaller.

Although the impact produces both flexural and tensile wave components in the beam, the former completely control the shape of the major pulse. A separate series of tests indicated that the peak tensile-wave strain never exceeded 7 per cent of the maximum flexural-wave strain, and hence the strain pulses observed can be considered to be almost entirely of flexural character. The presence of the tensile component is manifested by a small disturbance on the flat portion of the major pulse, as shown in Figs. 2 and 3, which represents the reflection of this wave from the supports.

The distribution of the peak stress of the major pulse as a function of distance along the beam for three beams is shown in dimensionless co-ordinates in Fig. 4 where the parameter σ/σ_0 is plotted against x/h. σ is the major pulse stress at any station, σ_0 is the peak major pulse stress at the impact point, x represents the distance traveled, and h denotes the beam depth. An essentially linear relationship may be observed to exist between the dimensionless terms, represented most nearly by the empirical equation

$$\sigma = \sigma_0(1.79)^{-x/h}$$

The applicability of this equation appears to be restricted to the range $0 \leq x/h \leq 2$. The major pulse is obscured or disappears beyond the upper limit of this parameter, and the accuracy of the stress measurement decreases proportionally.

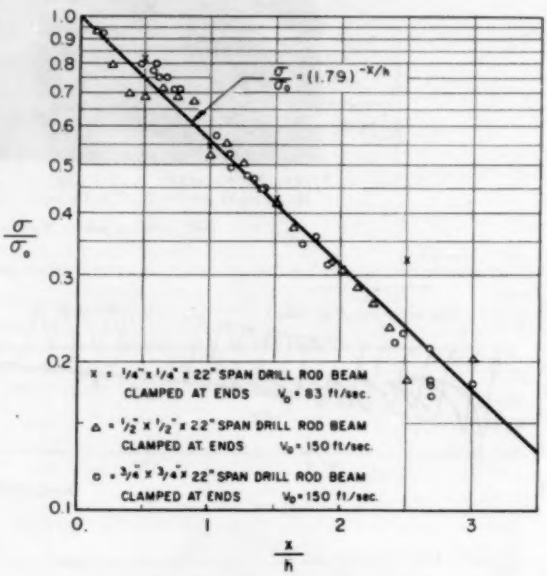

FIG. 4 DECAY OF PEAK OF MAJOR PULSE STRESS WITH DISTANCE x FOR THREE BEAMS AND TWO VELOCITIES

Inspection of Fig. 4 reveals that the magnitude of the peak stress of the major pulse would be indicated 25 per cent too low when measured by a gage located only $^1/_4$ in. from the impact point for the $^1/_2$-in. $\times$ $^1/_2$-in. beam. This discrepancy emphasizes the necessity for the corrections applied to the peak of the major pulse stress in the case of eccentric shots. The correction was not applied to any of the precursors in view of the fact that such a law of distribution was not as well defined. However, the stress magnitude of the precursors at any given position is not nearly as sensitive to the position of the impact as that of the major pulse.

A study of the effect of velocity on peak stresses at normal incidence was undertaken by shooting a $^3/_4$-in. $\times$ $^1/_2$-in. $\times$ 22-in. clamped-clamped drill-rod beam at velocities ranging from 30 to 150 fps. An essentially linear relationship was found to exist between peak stresses of the major pulse at positions $x = 0$ and $x = 2$ in., the first precursor at $x = 2$ and $x = 4$ in., and the second precursor at $x = 4$ in.

Effect of Repetitive Shots Over the Same Spot. It was believed that some of the craters in the distributed tests were spaced so close

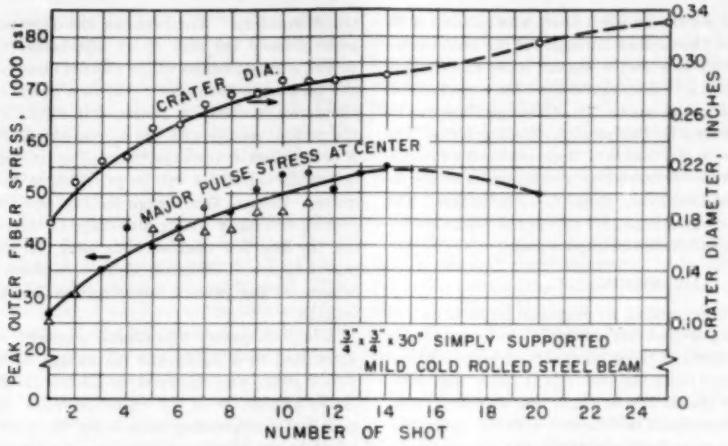
PEAK OUTER FIBER STRESS, 1000 psi
CRATER DIAMETER, INCHES
NUMBER OF SHOT
CRATER DIA.
MAJOR PULSE STRESS AT CENTER
3/4" x 3/4" x 30" SIMPLY SUPPORTED
MILD COLD ROLLED STEEL BEAM

FIG. 5 CRATER DIAMETER AND MAJOR PULSE STRESS AT CENTER AFTER REPEATED SHOTS

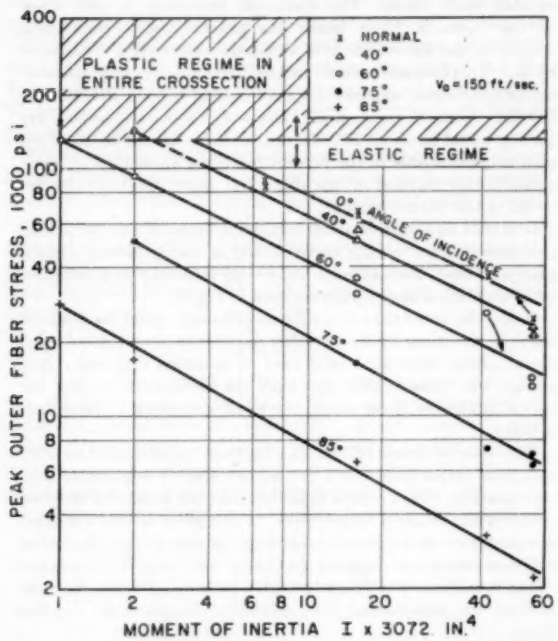

FIG. 6 EFFECT OF BEAM CROSS SECTION ON PEAK CENTRAL MAJOR PULSE STRESS FOR VARIOUS ANGLES OF INCIDENCE

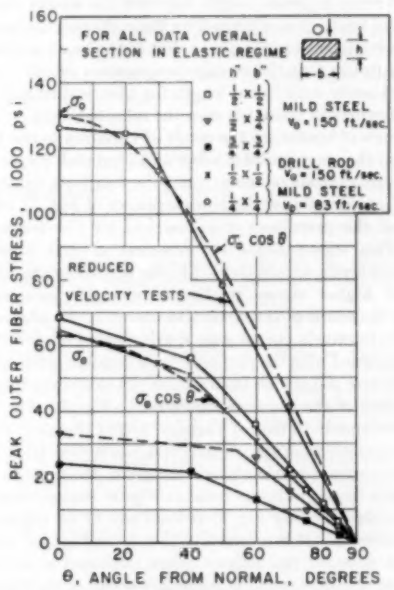
FOR ALL DATA OVERALL SECTION IN ELASTIC REGIME
MILD STEEL V0 = 150 ft./sec.
DRILL ROD V0 = 150 ft./sec.
MILD STEEL V0 = 83 ft./sec.
REDUCED VELOCITY TESTS
PEAK OUTER FIBER STRESS, 1000 psi
θ, ANGLE FROM NORMAL, DEGREES

FIG. 7 PEAK OF MAJOR PULSE VARIATION WITH ANGLE

together that the stress level produced by the second shot was not independent of the previous history. A series of controlled shots over the same station indicated a pronounced effect. Fig. 5 describes the variation of the major pulse stress at the center and the diameter of the crater as a function of the number of repeated shots for a $^3/_4$-in. × $^3/_4$-in. × 30-in. simply supported mild-steel beam. The stress nearly doubles after about fifteen shots and levels off subsequently, with the largest single increase (about 18 per cent) observed between the first and second shots. The curve representing crater diameter follows a similar trend.

Effect of Beam Size. Fig. 6 represents the variation of the peak of the central major pulse stress with beam stiffness for various angles of incidence at a constant initial velocity of about 150 fps. Both mild steel and drill rod were used in these tests. All data below a critical stress appear to follow an exponential law of the form

$$\sigma = k(I)^{-n}$$

where n varies from 0.48 to 0.57 and I is the moment of inertia of the beam. The critical stress seems to be associated with the dynamic elastic limit of the material and represents a value of 130,000 psi. This compares with a static elastic limit of 80,000 to 90,000 psi for the materials employed. The empirical law described is restricted to the present experimental conditions and depends on the velocity, geometry, and material of the striking mass.

Effect of Angle. The variation of stress with angle of incidence has been portrayed in Fig. 7. With the exception of the $^1/_4$-in. × $^1/_4$-in. beam, the tests were conducted at an initial velocity of 150

fps; the impact velocity for the smallest beam was reduced to 83 fps to avoid the onset of plastic flow throughout the entire cross section. For comparison, two cosine curves have been superposed on these data. It may be observed that the experimental data conform quite well to the cosine law, although they can be more adequately represented by two straight-line segments. The excellent correspondence in the trends of these curves for two different materials also may be observed by a comparison of the results for the mild-steel and drill-rod $^1/_2$-in. $\times$ $^1/_2$-in. beams. The knee evident in the experimental data for the central positions disappears at stations removed from the impact point.

Discussion

Comparison of the stress pattern for identical impacts on two beams with different lengths and end conditions indicates clearly that neither parameter governs the motion at a given point until arrival of a reflected wave from the end. It is likely that some small-amplitude pulses travel faster than the observed wave velocity; but these pulses cannot be detected with the equipment employed, and consequently their effect will not appear in the strain histories reproduced in this paper.

The difference in beam lengths between the simply supported and clamped beams is emphasized by the earlier occurrence of the reflected wave in the same ratio as that of the beam spans. This also demonstrates that the average propagation velocity does not vary significantly with beam length for identical impact velocities. Differences in phase between the reflected wave portions of the two types of beams are the result of variation in the mode of reflection of the wave striking a free and fixed end, respectively.

The metamorphosis of the major pulse has been detailed previously in conjunction with the description of Fig. 3. A faster build-up of the precursors was observed for the more flexible beams. This substantiates the observation that successively higher stress levels were activated in the smaller beams and indicates that higher stress amplitudes change character more rapidly as the result of the dispersive nature of the phenomenon.

Owing to relatively coarse gage spacing, previous investigators (2 to 4) concerned with the propagation of bending pulses resulting from transverse impact on beams have not described the successive inversion of the pulse as indicated in Fig. 3. The present work differs from both that of Vigness (3) and Dengler (4) in that permanent craters were always achieved, while their tests featured only elastic contact mechanisms. However, their strain records at successive beam positions indicated quite similar characteristics to that described by Fig. 3, at least within the regime of the transient stresses. It is interesting to note in Vigness' tests that the closest gage to the impact point indicated a much more gradual rise (2 millisec) and much longer decay of the major pulse than observed under the present conditions. However, the pattern of the precursors shown in his diagrams is virtually indistinguishable from the records presented here. The limited number of strain records given in reference (4) appear to be much more irregular than the present data, but a quantitative comparison of these strain-time histories with those presented in this paper cannot be effected in view of the difference in the imposed conditions. A recent publication (6) describing the production of bending waves in rods by means of unsymmetrical end impact of balls also indicates a similar propagation mechanism.

On the basis of identical initial momenta, the strain records obtained by reference (2) for an 8-oz ball-pointed steel hammer striking a 15-ft, $^1/_4$-in. $\times$ $^1/_2$-in. steel beam should be comparable to the transient strains obtained in the present experiments on beams of identical cross section when the $^1/_4$-in. ball was fired at an initial velocity of about 160 fps. The records shown exhibit similar tendencies concerning the metamorphosis of the major pulse, but are spaced too far apart to indicate the details of this transformation. Furthermore, the decaying portion of the major pulse crossed the zero strain axis before the arrival of reflected waves, a phenomenon which was not observed on any of the tests in the present investigation. In view of the empirical nature of the theoretical correlation proposed in reference (2), a comparison of the present results with the suggested analysis was not attempted. A correlation of the experimental strains with more rigorous analytical formulations will be provided in the fourth paper of this series. Central strain-gage records obtained by Hoppmann (7) also agreed fairly well in the shape of the initial major pulse during the first few microseconds after contact; however, reflected waves appeared to distort his records much more rapidly than observed in the present investigation for beams of comparable lengths.

A high-frequency vibrational transient, whose amplitude often amounted to a significant percentage of the peak stress of the major pulse, was observed for all central strain records of appreciable amplitude on the $^3/_4$-in. $\times$ $^3/_4$-in. beams, but did not appear on corresponding records for the more flexible beams. The effect is apparently produced by the successive reflections of the dilatational wave created by the impact between the two vertical beam faces. The measured frequency of this wave for the $^3/_4$-in. $\times$ $^3/_4$-in. beam was 130,000 cps, corresponding roughly to the traverse time of an elastic wave over a distance of 1.5 in. This frequency would still be detectable by the Hathaway equipment, whose response drops off rapidly beyond 100,000 cps. For the $^1/_4$-in. $\times$ $^1/_4$-in. beam, however, the corresponding frequency would be about 500,000 cps, and this cannot be observed with gains available in the present recording apparatus. Consequently, the traverse of the dilational wave could not be detected in the thinner beams.

It should be noted that the maximum value of any particular precursor did not usually occur at any of the artificially chosen gage positions. Such extreme values can thus only be determined by interpolation from a diagram such as Fig. 3.

It may be noted that virtually no difference could be observed either in the stress level or in other parameters investigated upon use of either cold-rolled mild steel or annealed drill rod. Any scatter was considerably less than the deviations existing between successive stress-strain curves of specimens of these materials.

The observed linear relationship between initial impact velocity and peak major pulse stress for normal impact is partially substantiated by Fig. 7 which indicates that the variation of stress with angle is nearly a cosine curve. For a given beam, this effect demonstrates the exclusive dependence of this stress upon initial ball momentum and suggests that the process of crater formation either is subject to a linear law with velocity or else is not significant in determining the maximum longitudinal bending stress.

Repetitive shots over the same crater, Fig. 5, cause work hardening of the surface along with associated enlargement of crater diameter. This permits the establishment of a greater total force of contact and consequent increase in the transfer of momentum to the beam, resulting in larger bending stresses.

Indicated stresses beyond the corresponding value of 130,000 psi cannot be considered as a reliable measure of the strain since a permanent set was observed to exist in all such instances. This condition was manifested by a terminal unbalance of the strain-gage amplifier amounting to several millivolts in extreme instances. However, a quantitative determination of the permanent set from the magnitude of the unbalance would be highly speculative and consequently was not attempted. Visual evidence of the formation of a central plastic hinge for the $^1/_4$-in. $\times$ $^1/_4$-in. beam was obtained for a number of runs at velocities of about 150 fps and nearly normal angles of incidence upon examination of the

beam at the conclusion of each test. The beams had been bent into a V-shape through angles ranging from a fraction of a degree to several degrees. However, permanent bending for the next larger beam ($^1/_4$ in. × $^1/_2$ in.) was visible only after a large number of repetitive impacts, even though the unbalance of the amplifier indicated a permanent set after the first shot. The present case corresponds to that described by Duwez, et al. (5) for constant-velocity impact of long beams with a horizontal plastic stress-strain curve when the impact velocity was in the lower plastic range and produced a V-shaped yield hinge.

The majority of the data of peak major pulse stress as a function of the angle of incidence, Fig. 7, could be plotted more consistently as two straight lines than as a cosine curve. The location of the knee varied between the limits of 30 and 60 deg. The deviation from a cosine law must be ascribed to the effects of the tangential-velocity component of the ball, since a linear stress variation with initial velocity was observed for normal impact. The more rapid reduction of peak stress at higher angles of incidence might be explained by the appearance of mounds surrounding the craters. The energy required to produce this flow phenomenon would not be transmitted in the form of the oscillating dilatational wave at the center, and would result in a corresponding reduction of stress over cases of identical normal velocity, but at zero angle of incidence. The disappearance of the knee at positions removed from the impact point lends some support to the hypothesis that the crater formation does have some influence on the magnitude of the peak stress of the major pulse. This stress will be even more drastically affected by the formation of a plastic hinge.

The exponential relationship observed within the elastic range between peak stress and moment of inertia of the beam was not expected. According to a very elementary model, stress should vary inversely with beam depth. The information presented shows that the stress is inversely proportional to approximately the square root of the moment of inertia. No simple relationship could be found between the peak stress and any other beam parameter.

Conclusions

(*a*) The metamorphosis of the initial transient upon propagation along the beam involves a continued periodic inversion of stress with the addition of a successively greater number of precursors. The build-up of the precursors to a maximum value occurs over approximately the same distance as the decay of the major pulse, about four or five times the beam depth. The major pulse diminishes with distance according to an exponential law

$$\sigma = \sigma_0(1.79)^{-s/h}$$

(*b*) Beyond a dynamic elastic limit of approximately 130,000 psi the impact produced a plastic hinge in the beam, resulting in a permanent set of the gage. Readings above this value cannot be considered as reliable. At normal incidence, this threshold is reached at initial velocities of about 85 fps for the $^1/_4$-in. × $^1/_8$-in. beam and about 130 fps for the $^1/_4$-in. × $^1/_2$-in. beam.

(*c*) A high-frequency vibrational transient exhibited on a number of central strain-gage records corresponds to the frequency of dilatational waves traversing between the faces of the beam.

(*d*) Variation of the major pulse and precursor stresses with initial velocity was linear.

(*e*) Repetitive shots over the same spot produced increases in both stress and crater diameter. A constant plateau for both parameters was reached after a number of impacts at nearly twice the initial value.

(*f*) The peak stress of the major pulse varied approximately as the inverse square root of the moment of inertia within the elastic range.

(*g*) The variation of peak stress with angle of incidence yielded two straight lines rather than a cosine curve. This is attributed to the crater formation.

Acknowledgment

The authors wish to acknowledge the technical aid of Mr. Myron Harvey, Mr. Robert Keller, and Mr. William Tumlin in maintaining the electronic equipment and assisting in the conduct of the experimental investigation.

BIBLIOGRAPHY

1 "An Experimental Investigation of the Oblique Impact of Spheres Upon Simply Supported Beams," by W. Goldsmith and D. M. Cunningham, Proceedings of the Society for Experimental Stress Analysis, vol 14, no. 1, p. 179.

2 "Transverse Impact Transients," by C. O. Dohrenwend, D. C. Drucker, and P. Moore, Proceedings of the Society for Experimental Stress Analysis, vol. 1, no. 2, 1943, p. 1.

3 "Propagation of Transverse Waves in Beams," by I. Vigness, NRL Report F-3476, 1949.

4 "Propagation of Elastic Impact in Beams in Bending," by M. Goland, P. D. Wickersham, and M. E. Dengler, Journal of Applied Mechanics, Trans. ASME, vol. 77, 1955, p. 1.

5 "The Behavior of Long Beams Under Impact Loading," by P. E. Duwez, D. S. Clark, and H. F. Bohnenblust, Journal of Applied Mechanics, Trans. ASME, vol. 72, 1950, p. 27.

6 "Measurements of Short Bending Wave Pulses in Steel Bars," by E. A. Ripperger, University of Texas, Defense Research Laboratory, DRL-367, CM-838, 1955.

7 "Impulsive Loads on Beams," by W. H. Hoppmann, II, Proceedings of the Society for Experimental Stress Analysis, vol. 10, no. 1, 1952, p. 157.

Kinematic Phenomena Observed During the Oblique Impact of a Sphere on a Beam[1]

By WERNER GOLDSMITH[2] and D. M. CUNNINGHAM,[3] BERKELEY, CALIF.

Experimental data relating to the kinetics of oblique impact of a 1/2-in-diam steel sphere upon steel beams at initial velocities ranging from 30 to 150 fps are presented. The variation of beam deflection, contact duration, trajectory of the sphere, and contour topography with angle of incidence, beam size, and initial velocity have been determined, and the velocity of propagation of several waves has been ascertained.

Introduction

THE current paper is the third of a sequence of articles describing the results of an experimental investigation of the oblique impact of steel sphere upon steel beams. The first of these papers contained an account of the instrumentation and delineated the analysis of a typical run (1)[4] while the second summarized the information collected for bending stresses of the beam (2). The present work pertains to data delineating the kinematic history of the ball and beam as well as to wave-propagation measurements deduced from strain gages placed longitudinally at various positions on the distal side of the beam. Beam deflections, duration of contact, initial and terminal ball velocities, crater topography, and wave velocities have been examined in detail.

Mild-steel and drill-rod beams employed in this investigation varied in cross section from 1/4 in. × 1/4 in. to 3/4 in. × 3/4 in. and were either simply supported with a span of 30 in. or clamped at the ends with a 22-in. span. A Rockwell hardness of about 95 B was obtained for both materials. A standard 1/2-in. steel ball bearing with a surface hardness of 68 Rockwell C, traveling in a horizontal plane containing the central axis of the beam at initial velocities ranging from 30 to about 150 fps, was employed as the projectile. Angles of incidence ranged from 85 deg to normal. A mild-steel block screwed onto a rigid foundation also was used as a target for comparative purposes in the phase of the tests dealing with contact times.

Results

Beam Deflections Resulting From the Collision. Successive peak center deflections of the fundamental mode of vibration of several simply supported beams were determined by means of a Fastax camera. A typical record, shown in Fig. 1, for a 1/8-in. × 1/8-in. beam, clearly indicates the excitation of higher vibrational modes. The peak center deflection ranged from 1.04 in. for the 1/8-in. × 1/8-in. beam to 0.06 in. for the 3/8-in. × 3/8-in. beam at normal incidence and an initial projectile velocity of 150 fps, and varied as the cosine of the angle of incidence.

Duration of Contact. A set of separate experiments was performed to determine the time of contact between a 1/2-in-diam ball bearing and simply supported mild steel beams of various cross section with a 30-in. span. Similar tests were conducted to ascertain the contact time upon a fully supported mild-steel block. The duration of contact was measured by a Hewlitt-Packard timer through the closing of a circuit composed of the beam (or block), a Litz wire attached to the ball, and a battery. Fig. 2 shows the results of this investigation for normal incidence. It may be observed that the contact time decreased markedly with velocity and increased slightly with stiffness. Fig. 3 shows the variation of contact time with angle of incidence and various initial ball velocities for a 1/2-in. × 1/2-in. beam. It may be observed that the contact duration for this case increases much more rapidly with angle than the corresponding reduction of the normal component of velocity would indicate.

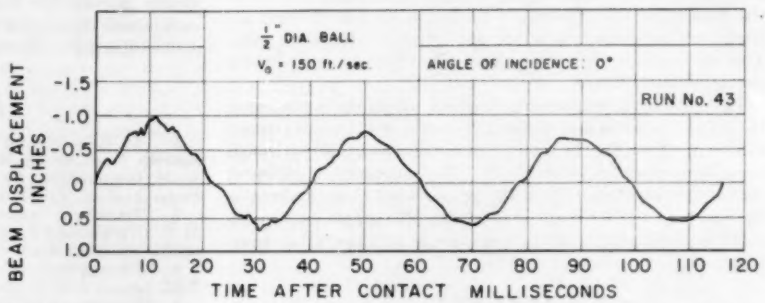

Fig. 1 Center Deflection of a 1/8-In. × 1/8-In. × 30-In. Simply Supported Beam Versus Time
(Data obtained with the Fastax camera.)

Crater Analysis. Fig. 4 shows the variation of the ratio of width to length for these craters as a function of angle for various beam sizes. Fig. 5 portrays the calculated penetration depth based on the chord of the circle of the measured width and the actual depth for one beam measured by means of a profilometer as a function of the angle of incidence.

Profilometer measurements of the craters in a 1/2-in. × 1/2-in. drill-rod beam shot at various angles of incidence are shown in Fig. 6. The measured depth is based upon the penetration relative to the flat surface of the beam. It was observed that in some

[1] Work sponsored by Mechanics Branch, USNOTS, China Lake, Calif.

[2] Associate Professor of Engineering Design, University of California. Assoc. Mem. ASME.

[3] Associate Professor of Engineering Design, University of California. Assoc. Mem. ASME.

[4] Numbers in parentheses refer to the Bibliography at the end of the paper.

Presented at the West Coast Conference of the Applied Mechanics Division, Pasadena, Calif., June 11–13, 1956, of The American Society of Mechanical Engineers.

Discussion of this paper should be addressed to the Secretary, ASME, 29 West 39th Street, New York, N. Y., and will be accepted until January 10, 1957, for publication at a later date. Discussion received after the closing date will be returned.

Note: Statements and opinions advanced in papers are to be understood as individual expressions of their authors and not those of the Society. Manuscript received by ASME Applied Mechanics Division, March 8, 1956. Paper No. 56—APM-40.

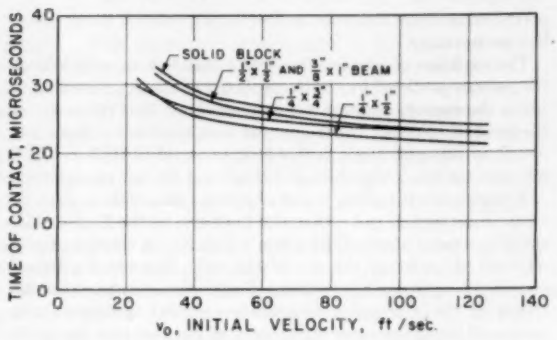

FIG. 2 VARIATION OF TIME OF CONTACT OF A 1/2-IN-DIAM BALL BEARING WITH INITIAL VELOCITY FOR VARIOUS BEAMS AND A SOLID BLOCK AT NORMAL INCIDENCE. BEAMS ARE SUPPORTED ON A 30-IN. SPAN

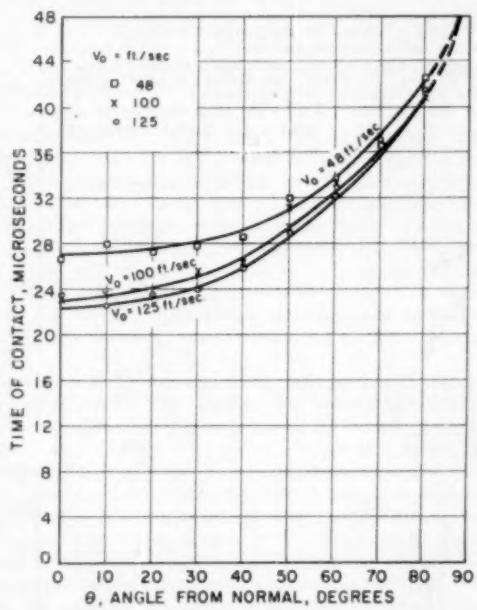

FIG. 3 VARIATION OF CONTACT TIME FOR A 1/2-IN-DIAM STEEL BALL AGAINST A 1/2-IN. × 1/2-IN. × 30-IN. SIMPLY SUPPORTED BEAM FOR VARIOUS ANGLES OF INCIDENCE AND SEVERAL INITIAL VELOCITIES

instances the raised surface produced by the transfer of metal in the generation of the crater extends as far as one crater diameter. This uplift extends to the beam edge in the transverse direction in all beams 1/2-in. wide or smaller.

Fig. 6 also shows the width of these craters as a function of angle of incidence measured at the lip of the crater and at the beam plane, respectively. The former is that observed on contour photographs, and corresponds to the information presented in Fig. 5; however, the data relative to the beam plane are generally better defined. The difference between these measured widths amounts to approximately 20 per cent.

Wave Characteristics. The strain-gage measurements described in reference (2) were related to a common time base and could thus be employed to ascertain arrival times of successive pulses. The arrival time of the earliest measurable signal at various gage stations for a 3/4-in. × 3/4-in. × 30-in. simply supported beam is portrayed in Fig. 7. The velocity of propagation of the initial disturbance for this and other tests averaged to a value of 17,900 fps. Since the instrumentation was not specifically designed to measure these velocities, the accuracy of these data is not as great as that of other results, with a possible error of ±10 per cent.

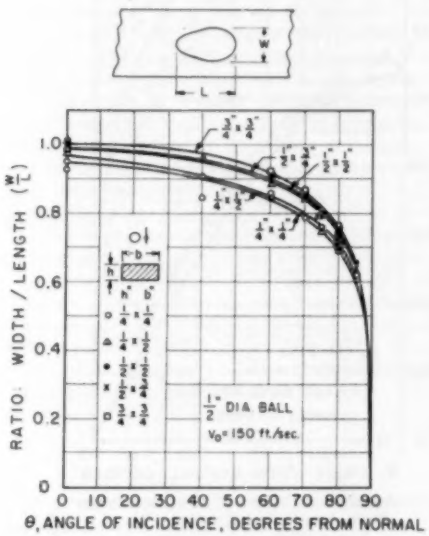

FIG. 4 WIDTH-TO-LENGTH RATIO OF CRATERS AS A FUNCTION OF ANGLE OF INCIDENCE FOR VARIOUS BEAM SIZES

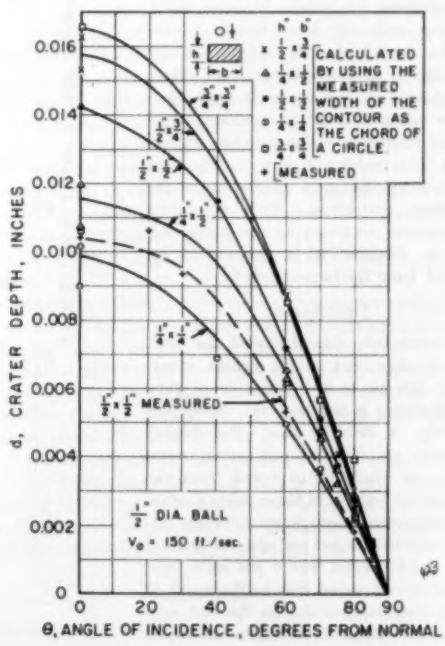
CALCULATED BY USING THE MEASURED WIDTH OF THE CONTOUR AS THE CHORD OF A CIRCLE
MEASURED
1/2" x 1/2" MEASURED
1/2" DIA. BALL
V0 = 150 ft./sec.
d, CRATER DEPTH, INCHES
θ, ANGLE OF INCIDENCE, DEGREES FROM NORMAL

FIG. 5 CALCULATED AND MEASURED CRATER DEPTHS AS A FUNCTION OF ANGLE OF INCIDENCE FOR VARIOUS BEAM SIZES

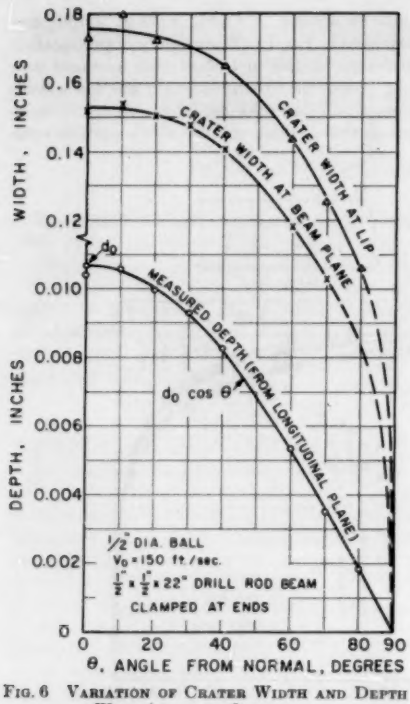

FIG. 6 VARIATION OF CRATER WIDTH AND DEPTH WITH ANGLE OF INCIDENCE

The rise time of the major pulse at the center of the 30-in. beam averaged 18 ± 2 microsec for beams 1/4 and 1/2-in. thickness, while the decay time until the arrival of the reflected waves from the supports averaged about 220 microsec. Both time intervals did not appear to vary significantly either with beam cross section or angle of incidence. The number of precursors observable at any station was governed by the gain employed in the strain-gage amplifiers. With maximum amplification, as many as nine precursors could be detected at a position 12 in. removed from the impact point.

DISCUSSION

The extremely slow decay of the peak beam displacement of all beams investigated attests to the presence of very little damping in the system. Nevertheless, Fig. 1 reveals that the higher harmonics are damped out much more rapidly, as would be expected from the lower energy content of these mode shapes. The maximum discrepancy between observed and calculated periods of vibration of the fundamental was 4 per cent; the lower observed period may be the result of a slight restraining action at the end supports. The harmonic variation of center deflection with angle of incidence indicates that over-all response to the collision as portrayed by beam deflection is directly proportional to the initial ball momentum.

The variation of contact time with initial ball velocity follows the pattern predicted by the Hertz theory of contact according to which the contact duration varies inversely as the fifth power of the incident velocity. In the present case, the contact times predicted on the solid block in this fashion would be 20.7 and 28.6 microsec for initial velocities of 150 fps and 30 fps, respectively.

A calculation involving a Euler-type of beam with a 1/2-in. × 1/2-in. cross section and a Hertzian force law by the Timoshenko small-increment method (3) yields a duration of contact of 19.9 microsec at an initial velocity of 150 fps. This result substantiates once again the observations of other investigators that the theory of Hertz provides remarkably excellent agreement with measured impact parameters in spite of the fact that its applicability is restricted to elastic contacts.

A small, but nevertheless noticeable reduction of contact duration was observed when the flexibility of the struck member was

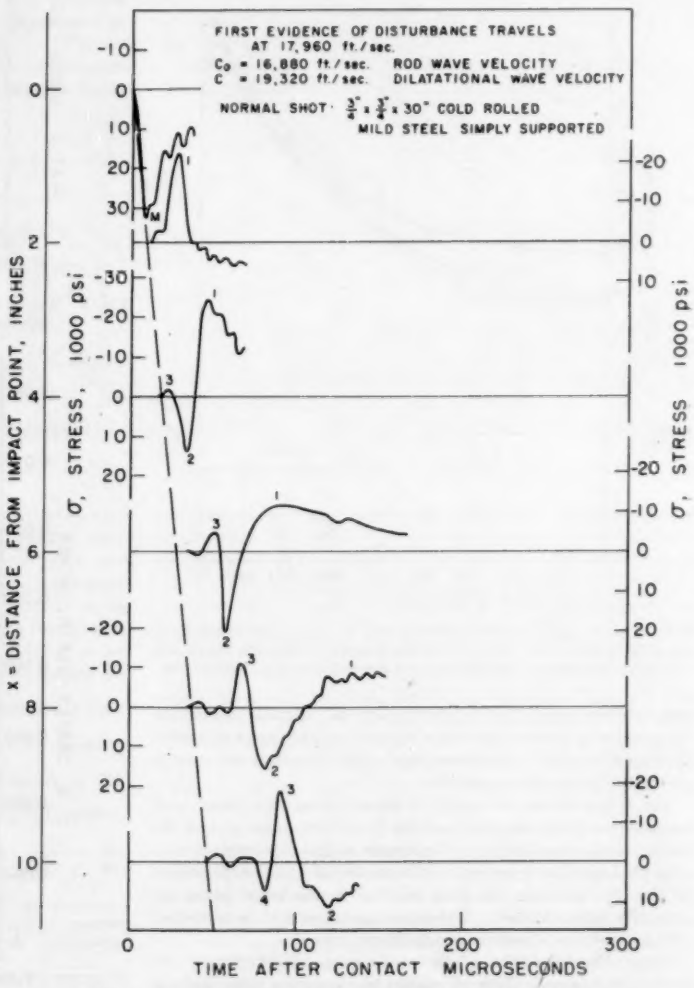
FIRST EVIDENCE OF DISTURBANCE TRAVELS AT 17,960 ft./sec.
C_0 = 16,880 ft./sec. ROD WAVE VELOCITY
C = 19,320 ft./sec. DILATATIONAL WAVE VELOCITY
NORMAL SHOT · 3/4" x 3/4" x 30" COLD ROLLED MILD STEEL SIMPLY SUPPORTED
x = DISTANCE FROM IMPACT POINT, INCHES
σ, STRESS, 1000 psi
TIME AFTER CONTACT MICROSECONDS

FIG. 7 WAVE-VELOCITY PATTERN, WHERE M = MAJOR PULSE

(Numbers on peak refer to the number of the precursor.)

increased. This observation corresponds to the fact that the more flexible beams exhibited smaller crater diameters for identical impact conditions and that the total contact time was consequently shorter in view of the smaller observed penetration. This can be explained in terms of a more rapid acceleration of the lighter beams and a consequent faster separation of ball and beam. The change in contact time with angle of incidence, shown in Fig. 3, is also much more rapid than would be warranted solely by the reduction of initial velocity. This effect can be attributed to the lengthening of the plastic crater and the mound formation of the material at its edge in the direction of motion of the ball.

The observed percentage reduction in tangential ball velocity never exceeded 10 per cent, indicating that only a small fraction of the energy transferred to the beam will appear in the form of a wave generated by friction. The disturbance appearing during the decaying portion of the major pulse, described in references (1) and (2), which travels with longitudinal wave velocity, cannot be the result of the action of the tangential impulse since this disturbance also appears in the case of normal impact. Furthermore, the amplitude of this disturbance is independent of angle of incidence. It must be concluded that any energy transfer due to friction is completely obscured by the lateral vibrations created by the bending action when single longitudinal gages are employed for strain measurements.

The reduction of the width-to-length ratio of the craters with increasing beam flexibility in Fig. 4 and failure to achieve a unit value of this parameter at normal incidence may be attributed both to the initiation of beam motion during the impact and the fact that the flow created by crater formation produced a mound extending to the beam edge in the transverse direction for all beams $^1/_2$-in. wide or smaller. This latter phenomenon also would lead to the prediction of a lower stress based on crater geometry than would be deduced from identical crater dimensions in a solid block where the raised surface did not extend to an edge.

The difference in the values of the apparent and median-plane depths is emphasized by Figs. 5 and 6. Fig. 5 shows the variation of calculated penetration depths based on the measured crater diameter at the crater lip as a function of angle of incidence for various sizes of beams. These curves approximate a cosine law, and the crater depth decreases with beam flexibility for reasons cited previously. The depths measured with a profilometer for the $^1/_2$-in. × $^1/_2$ in. beam are based on the median plane of the beam and are approximately 35 per cent below the values computed from the apparent diameters. The difference of 20 per cent between the apparent and median crater widths, shown in Fig. 6, would translate into a difference of 36 per cent if the depths are computed on the basis of these two diameters, respectively. This calculation is based on a rigid ball, in which case $\alpha D = (^1/_2 d)^2$ where α is the crater depth, D the ball diameter, and d the diameter of the crater.

Fig. 6 also indicates that the crater width does not vary as a cosine with the angle of incidence, whereas the measured depth closely approximates such a curve. This may be explained by the hypothesis that the latter dimension is not affected nearly as much by the piling-up process, which occurs primarily during rebound after the maximum penetration has been achieved.

As indicated previously, the measurements of wave velocities over the relatively short beam lengths are not as accurate as might be obtained with more suitable instrumentation. The velocity of propagation of the earliest measurable signal is approximately 17,900 fps. When based upon the return of the reflected waves to any gage as determined by the end of the transient period of the record, the velocity of propagation of these waves appears to average around 10,000 fps. These values substantiate the data presented in reference (1). It should be reiterated that these velocities were based on measurements from single strain gages located on the side of the beams in a longitudinal direction.

A number of theoretical investigations (4 to 13) have been concerned with the propagation of flexural waves in beams, utilizing either the exact three-dimensional equations of elasticity or the one-dimensional approximation including the effects of rotatory inertia and shear. Calculations performed on the exact equations for a single flexural mode (5) indicate the dispersive nature of the bending wave and lead to a group velocity pattern rising from zero at infinite wave lengths to a relatively constant plateau, whose limiting value at infinitely short wave lengths approaches the Rayleigh surface wave, $c_R = 0.580$, $c_0 = 9860$ fps, where c_0 is the rod wave. These results have been applied to circular bars of comparable lengths to those used in the present experiments (4) to predict that the maximum group velocity of flexurable waves has a value of $0.64c_0$ while the maximum phase velocity is only $0.582c_0$ regardless of the frequency of the wave. Prescott (6) points out the possibility of the existence of other flexural-wave velocities, including some branches exhibiting velocities higher than c_0. However, little importance is attached to these branches since most of the energy is presumed to be transmitted by the basic mode. When the coefficients of the Timoshenko beam equation are rewritten in terms of a longitudinal and a shear wave velocity (11), it was shown that an impulsive moment is transmitted with velocity c_0 and an impulse shear is carried with velocity

$$c_s = \frac{\sqrt{(k'G)}}{\rho}$$

where k' is a factor relating total shear across a section to average shear and depends only on the shape of the beam (7, 8).

The gages employed in the present experiments were attached in a manner such that they would measure an elongation in the longitudinal direction (also, due to Poisson effect, they would measure a transverse strain but this is irrelevant to the present argument). Consequently, these gages cannot differentiate between a pure flexural wave and tensile or compressive wave. Strain gages at the same location on opposite faces of the beam could have been suitably connected to read only bending stresses, but this was not done during the present sequence of tests.

Examination of Fig. 7 reveals further the nature of the energy transfer between the precursors from one station to the next. If the maximum strain at any location can be regarded as the predominant group, the average velocity of propagation of this high-energy group is approximately 13,500 fps, a value still in excess of the maximum velocity of flexural waves of the basic mode of transmission.

It may be assumed that, in view of the pronounced continued inversion of stress from the beginning of the signal at any station, the entire subsequent process during the transient period is activated by flexural behavior due to the action of an applied impulsive moment. The initial signal is limited, of course, by gain of the amplifier, but the earliest measurable arrival time corresponds closely to the rod-wave velocity in bars.

Some recent measurements by Ripperger (14) using strain gages to measure bending pulses indicate a propagation velocity in the range of 11,000 fps. However, these values are based on admittedly indefinite disturbances, and the author does not attribute much qualitative significance to these data.

Conclusions

The following conclusions may be drawn from the experimental investigation of the contact phenomena and kinematic history of the oblique impact of spheres upon simply supported beams:

(a) The magnitude of successive beam deflections indicated the

presence of little damping in the system. Computed and observed frequencies of beam vibration are in good accord. The magnitude of the center deflection varies as the cosine of the angle of incidence.

(*b*) Contact durations decrease with increased beam flexibility and decrease with increased velocity for normal incidence in a manner similar to that predicted by the Hertz theory of contact. Variation with angle of incidence is more rapid than would be expected on the basis of the normal velocity component.

(*c*) Considerable deviation exists between crater dimensions measured at the crater lip and the median plane of the beam. In neither case does crater width vary as a cosine with angle of incidence, while penetration depth conforms to this law. Depths and width-to-length ratios of craters decrease with increasing beam flexibility.

(*d*) The earliest measurable signal propagates at a velocity corresponding to that of longitudinal waves in rods. The pulse of maximum strain in the current tests exhibits a velocity of propagation halfway between that of rod waves and Rayleigh surface waves.

Acknowledgment

The authors wish to acknowledge the technical aid of Mr. Myron Harvey and Mr. Robert Keller in maintaining the electronic equipment and assisting in the conduct of the experimental investigation.

BIBLIOGRAPHY

1 "An Experimental Investigation of the Oblique Impact of Spheres Upon Simply Supported Beams," by Werner Goldsmith and D. M. Cunningham, Proceedings of the Society for Experimental Stress Analysis, vol. 14, no. 1, p. 179.

2 "An Experimental Investigation of Beam Stresses Produced by Oblique Impact of a Steel Sphere," by D. M. Cunningham and Werner Goldsmith, JOURNAL OF APPLIED MECHANICS, Trans. ASME, this issue, pp. 606–611.

3 "Zur Frage Nach der Wirkung eines Stosses auf einen Balken," by S. Timoshenko, *Zeitschrift für, Mathematik und Physik*, vol. 62, 1913, p. 198.

4 "A Critical Study of the Hopkinson Pressure Bar," by R. M. Davies, Philosophical Transactions of the Royal Society of London, London, England, series A, vol. 240, 1948, p. 451.

5 "Dispersion of Elastic Waves in Solid Circular Cylinders," by G. E. Hudson, *Physical Review*, vol. 63, 1943, p. 46.

6 "Elastic Waves and Vibrations of Thin Rods," by J. Prescott, *Philosophical Magazine*, series 7, vol. 33, 1942, p. 703.

7 "Transverse Impact of Long Beams, Including Rotatory Inertia and Shear Effects," by M. A. Dengler and M. Goland, Proceedings of the First U. S. National Congress of Applied Mechanics, 1952, p. 179.

8 "Flexural Waves in Beams According to the More Exact Theory of Bending," by J. Miklowitz, USNOTS, China Lake, NOTS 741, NAVORD Report 2049, 1953.

9 "An Approximate Theory of Lateral Impact on Beams," by B. A. Boley, JOURNAL OF APPLIED MECHANICS, Trans. ASME, vol. 77, 1955, p. 69.

10 Discussion of "Effect of Shear in Transverse Impact on Beams," by R. N. Arnold, Proceedings of The Institution of Mechanical Engineers, London, England, vol. 165, 1951, p. 184.

11 "Über Biegewellen in Staben," by H. Schirmer, *Ingenieur-Archiv*, vol. 20, 1952, p. 247.

12 "Bemerkungen zur Ausbrietung von Biegewellen in Staben und Platten," by L. Cremer, *Zeitschrift für angewandte Mathematik und Mechanik*, vol. 23, 1943, p. 291.

13 "Flexural Vibrations in Uniform Beams According to the Timoshenko Theory," by R. A. Anderson, JOURNAL OF APPLIED MECHANICS, Trans. ASME, vol. 75, 1953, p. 504.

14 "Measurements of Short Bending Wave Pulses in Steel Bars," by E. A. Ripperger, University of Texas, Defense Research Laboratory, DRL-367, CM-838, 1955.

The Influence of Blast Characteristics on the Final Deformation of Circular Cylindrical Shells[1]

By P. G. HODGE, JR.,[2] BROOKLYN, N. Y.

The final maximum deformation of a reinforced circular cylindrical shell caused by a briefly applied, intense loading is considered. The maximum deformation is obtained in a form which requires a double quadrature of the pressure where the limits of the integration are determined from side conditions. Attempts are made to find a simple analytic approximation, but the attempts are unsuccessful for loads of practical importance. A straightforward graphical-numerical method of solution is devised. Several examples are considered in support of the conclusions. The shell is assumed to be infinitely long, so that end effects may be neglected. The load is assumed to be applied to the entire shell simultaneously. The shell is assumed a perfect cylinder, and the reinforcements are taken as rigid. Finally, the shell is assumed to be made of an ideal rigid-plastic material which satisfies a certain simplified yield condition and the associated flow rule.

Introduction

ACCORDING to the classical elasticity theory, the maximum loads which a given statically indeterminate structure can support are the smallest loads which produce inelastic behavior at the most highly stressed portion of the structure. However, it is well known that if the structure is made of a ductile material, then it may still be serviceable under considerably greater loads. Essentially, this is due to the relieving of stress concentrations by the mechanism of plastic flow. If the loads are still further increased, there will exist a more or less sharply defined point at which small load increments will produce large deformations. The load for which this first occurs is called the "collapse load."

The question arises as to the behavior of structures under loads greater than the collapse load. The quasistatic analysis used in determining the collapse load states that if the collapse load is maintained indefinitely, arbitrarily large deformations may ensue. Further, the collapse load is the largest load for which the structure can support an equilibrium state of stress. It follows that under a load larger than the collapse load, the elements of the structure must accelerate and a dynamic analysis is necessary. Obviously, if such a load is maintained for an appreciable length of time, the deformations will increase until the structure becomes unserviceable. However, if the load is applied very briefly, as in an explosion, the deformations may be so small that the usefulness of structure is not impaired.

Under such load conditions, the detailed analysis of a real structure made of a real material is prohibitively difficult for all but the very simplest cases. However, it may be that some useful information can be gained by a drastic simplification of the problem. To this end, the real material is replaced by a rigid-plastic material. In simple tension such material is rigid at stresses less than the yield stress, and flows without strain hardening if the stress equals the yield stress. The behavior under general stress states will be discussed in the next section.

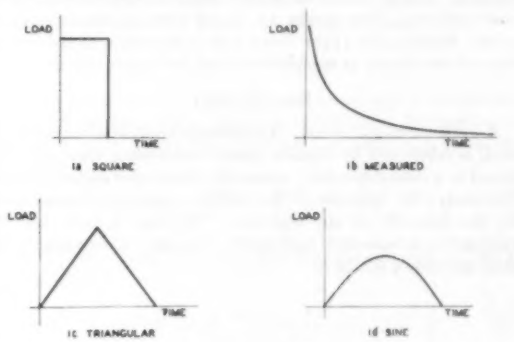

FIG. 1 PRESSURE PULSES

In an earlier investigation (1)[3] this problem was solved for the particular case of a circular cylindrical shell subjected to a step function load-time relation; i.e., the load was zero except for a given time interval during which it had a prescribed constant value, Fig. 1(*a*). This choice of load shape made it possible to obtain a closed-form solution. However, one practical situation in which a briefly applied excess load is experienced is in the neighborhood of an explosive blast. In this situation the pressure rises rapidly (almost instantaneously) to a peak value and then decays rapidly. Fig. 1(*b*) shows a typical experimentally measured (but smoothed) curve.[4] Obviously, this bears little resemblance to the step curve in Fig. 1(*a*).

In the case of a free-free beam, subjected to a concentrated dynamic load at its mid-point, Symonds (3) has postulated that the final deformation for any load shape is well approximated by considering a step function with the same peak load and the same total impulse as the given wave. In support of this conjecture he presents computations for a triangular wave, Fig. 1(*c*), and a sine wave, Fig. 1(*d*).

---

[1] The results presented in this paper were obtained in the course of research conducted under contract with the Office of Naval Research.

[2] Professor of Applied Mechanics, Department of Aeronautical Engineering, Polytechnic Institute of Brooklyn. Mem. ASME.

Presented at the West Coast Conference of the Applied Mechanics Division, Pasadena, Calif., June 11–13, 1956, of THE AMERICAN SOCIETY OF MECHANICAL ENGINEERS.

Discussion of this paper should be addressed to the Secretary, ASME, 29 West 39th Street, New York, N. Y., and will be accepted until January 10, 1957, for publication at a later date. Discussion received after the closing date will be returned.

NOTE: Statements and opinions advanced in papers are to be understood as individual expressions of their authors and not those of the Society. Manuscript received by ASME Applied Mechanics Division, February 11, 1955. Paper No. 56—APM-25.

[3] Numbers in parentheses refer to the Bibliography at the end of the paper.

[4] Reference (2), p. 155.

It might appear reasonable to expect the same conclusion to be valid for circular cylindrical shells. However, in a particular example investigated (4), this was found not to be the case.

The present paper is concerned with a general investigation of this problem. It will be found that the blast characteristics have a profound effect on the final deformation for peak loads slightly exceeding the collapse load, but that the percentage effect decreases as the load increases. This may be qualitatively explained by observing that for very high loads the greater part of the deformation occurs after the load is removed and hence may be expected to be less dependent on the loading details. However, based upon the experience indicated in reference (4), it appears that these high loads have little practical interest as applied to cylindrical shells. Therefore, for this problem it is necessary to pay attention to the details of the blast characteristics.

In an effort to make the paper reasonably self-contained, the basic equations are all stated in the next section, together with some of the reasoning which leads to them. More complete derivations may be found in references (1) and (4).

The next sections are concerned with demonstrating the inapplicability of Symonds' approximation to shell problems. Problems considered include a monotonically decreasing load of arbitrary magnitude, the effect of the load-rise-shape, and "medium" loads which rise to a peak and then decay. Next, a simple graphical-numerical procedure which enables the final deformation to be easily computed for any arbitrary blast shape is developed. This is illustrated by an example and compared with an exact solution. The results are found to be in excellent agreement. Finally, the paper closes with a discussion of the limitations of the theory as applied to actual physical problems.

Basic Theory

A Statement of Problem. An infinitely long circular cylindrical shell is reinforced by equally spaced reinforcing rings and subjected to a time-dependent, uniformly distributed radial pressure. Obviously, the behavior of the shell is completely characterized by the behavior of any one bay. The bay in turn may be analyzed as a finite shell built in at either end. Dimensions of the shell are shown in Fig. 2.

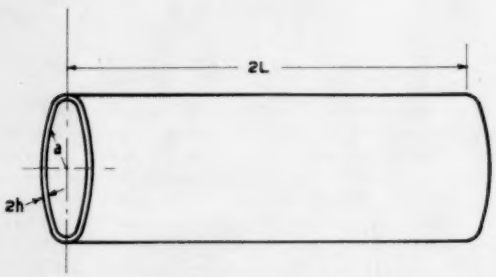

Fig. 2 Dimensions of Shell

B List of Unknowns. The problem is to be treated as one in shell theory, whereby the stress distributions across the thickness of the shell are replaced by their resultant direct stresses, bending moments, and shears. It can be shown (1, 5, 6) that the present problem can be formulated in terms of only two of these resultants; namely, the circumferential direct stress N_φ and the axial bending stress M_x. For purposes of analysis it is convenient to replace these resultants by dimensionless quantities defined by

$$n = N_\varphi/2Yh, \qquad m = M_x/Yh^2 \ldots\ldots\ldots\ldots [1]$$

where Y is the tensile yield stress.

Under the usual assumptions that normals to the centroidal surface of the shell remain straight and normal to the deformed surface, all the displacements in the shell are determined by the displacements of the centroidal surface. The only displacement of interest in the present problem is the radial displacement w, which is considered positive when directed inward. Again, it is convenient to replace w by the dimensionless displacement

$$W = ws a/2Yht_0^2 \ldots\ldots\ldots\ldots [2]$$

where s is the surface density and t_0 some representative time.

C Yield Condition. When the yield condition is expressed in terms of the resultants n and m, a more or less complex interaction curve is obtained, depending upon the yield criterion. For purposes of analysis this curve will be replaced by the ideal "square" curve, shown in Fig. 3. Remarks on the relation between this curve and the true interaction curve may be found in references (4) and (5).

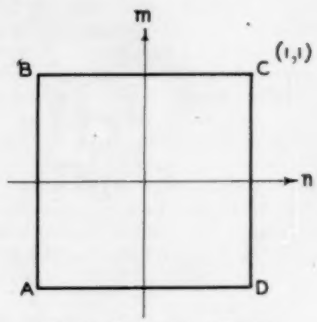

Fig. 3 Interaction Curve

D Equations of Motion. The two equations of motion are obtained by adding the appropriate inertia terms to the equations of equilibrium in the radial direction and for axial bending. Radial shear may then be eliminated between these two equations to obtain a single second-order equation

$$(d^2M_x/dx^2) + (N_\varphi/a) + p = s(d^2w/dt^2)$$

where x is the distance along a generator and p is the difference between the exterior and interior pressure. In terms of Equations [1] and [2], together with further dimensionless variables defined by

$$y = x/L, \quad \tau = t/t_0, \quad c = L/\sqrt{ah}, \quad P = pa/2Yh \ldots [3]$$

the equation of motion may be written

$$(m''/2c^2) + n + P - \ddot{W} = 0 \ldots\ldots\ldots\ldots [4]$$

Here primes indicate differentiation with respect to y and dots with respect to τ.

E Flow Rule. As discussed in references (6) and (7), the stress and velocity resultants must be related by the plastic potential flow rule. In the present case this states that the "strain-rate vector" defined by

$$\dot{\mathbf{E}} = (-\dot{W}, -\dot{W}''/2c^2) \ldots\ldots\ldots\ldots [5]$$

must be normal to the interaction curve and directed outward. Thus, if the stress point is on side AB of Fig. 3, the velocity must satisfy

$$\dot{W} \geq 0, \quad \dot{W}'' = 0 \ldots\ldots\ldots\ldots [6a, b]$$

At a corner the strain-rate vector can have any direction between the limiting normals, so that at B the requirement is

$$\dot{W} \geq 0, \quad \dot{W}'' \leq 0 \ldots\ldots\ldots\ldots\ldots [7a, b]$$

F Continuity. In a complete solution for a real material there may exist certain regions of rapid change of some quantities. For the ideal material here considered, these regions may become arbitrarily narrow and hence the quantities in question may become discontinuous. However, it can be shown (6) that even in the ideal case the quantities m, m', W, and $\dot{W}$ must be continuous. Further, it also can be shown that the velocity slope $\dot{W}'$ can be discontinuous only if $m = \pm 1$. Circumferences where this is so are termed "hinge circles" in analogy to the "yield hinges" in framework theory.

G Boundary Conditions. At the built-in end ($y = 0$), slope and displacement must vanish while at the center, symmetry demands that slope and shear vanish. However, the conditions on slope need not hold if there is a hinge circle. Since the rotation and applied moment at a hinge circle must be in the same direction, the boundary conditions may thus be written

$$\left.\begin{array}{l} \text{at } y = 0, \quad W = \dot{W} = 0 \text{ and either} \\ \qquad\qquad W' = \dot{W}' = 0 \quad \text{or} \quad m = -1 \\ \text{at } y = 1, \quad m' = 0 \text{ and either } W' \\ \qquad\qquad = \dot{W}' = 0 \quad \text{or} \quad m = +1 \end{array}\right\} \ldots [8]$$

H Initial Conditions. Initially, the shell is at rest in an undeformed state so that at

$$\tau = 0, \quad W = \dot{W} = 0 \ldots\ldots\ldots\ldots\ldots [9]$$

Further, it is evident that W and $\dot{W}$ must both be continuous functions of time. No initial or time-continuity conditions are required on the stress quantities n and m since they are uniquely determined as time-functions from the pressure-time relation.

I Static Collapse. The static collapse load is defined as the smallest load for which the plastic-rigid material can deform. It turns out (1) that the velocity slope at incipient collapse is discontinuous at the center and support so that the Boundary Conditions [8] are

$$m(0) = -1, \quad m(1) = +1, m'(1) = 0 \ldots\ldots [10]$$

Therefore, the "stress profile" (the image in the stress-resultant plane, Fig. 3, of the stress resultants along a typical generator of the shell) goes from A at $y = 0$ to B at $y = 1$.

If n is set equal to -1 and the inertia term equal to zero in Equation [4], the resulting solution satisfying the boundary conditions at $y = 1$ is

$$m = 1 - c^2(P - 1)(1 - y)^2$$

The boundary condition at $y = 0$ then requires that P be equal to the static collapse load

$$P_0 = 1 + 2/c^2 \ldots\ldots\ldots\ldots\ldots [11]$$

Decaying Loads

In the present section the pressure is assumed to be given as a monotonically nonincreasing positive function of time. Such a function may be written

$$P = P_0 \rho f(\tau) \ldots\ldots\ldots\ldots\ldots [12a]$$

where

$$f(0) = 1, \quad f'(\tau) \leq 0, \quad f(\tau) \geq 0 \ldots\ldots [12b]$$

For $\rho < 1$ there will obviously be no plastic flow, while for $\rho > 1$ but sufficiently small it is reasonable to expect the stress profile to go from A to B as in the static case. Under this hypothesis the complete solution is given (1) by

$$m = \frac{P_0 \rho f - 1}{P_0 - 1}(y^3 - 2y^2 + y) - (y^3 - 3y + 1)$$

$$n = -1, \quad \dot{W} = (3P_0/2)(\rho f - 1)y \ldots\ldots\ldots [13]$$

It is readily verified that this solution satisfies Equations [4] and [6b] and the Boundary Conditions [10]. However, it also must be shown that the stress point actually lies on AB, rather than on AB extended, and that the strain-rate vector is directed outward. If m is plotted as a function of y, it follows from Equations [10] that the resulting curve will go through the point $(0, -1)$ and will have a horizontal tangent at the point $(1, 1)$. Obviously, a necessary condition that m be between -1 and $+1$ in the interval $0 \leq y \leq 1$ is that the slope be nonnegative at $y = 0$ and the curvature nonpositive at $y = 1$. Since m is a cubic in y these conditions are also sufficient. The resulting restrictions on the pressure can be written

$$\frac{4 - 3P_0}{P_0} \leq \rho f \leq \frac{3P_0 - 2}{P_0} \ldots\ldots\ldots [14]$$

Throughout the analysis to follow, it will be assumed that the left-hand Inequality [14] is always satisfied. In view of Equation [11], this will automatically be true if the shell dimensions are such that $c^2 \leq 6$. So far as the right-hand Inequality [14] is concerned, since f is assumed to be nonincreasing, it is sufficient for this to be satisfied at $\tau = 0$. Therefore, for the shells considered, the solution is given by Equations [13] provided

$$\rho \leq (3P_0 - 2)/P_0 \ldots\ldots\ldots\ldots\ldots [15]$$

The last requirement is that the strain-rate vector be directed outward; i.e. Inequality [6a] must also be met. Integration of the last Equation [13] together with the initial Condition [9] furnishes

$$\dot{W} = (3P_0/2)\left(\rho \int_0^\tau f d\tau - \tau\right) y \ldots\ldots\ldots [16]$$

In view of the restrictions on f there is a unique positive time τ_2 defined by

$$\rho \int_0^{\tau_2} f d\tau = \tau_2 \ldots\ldots\ldots\ldots\ldots [17]$$

such that $\dot{W}$ is positive for $0 < \tau < \tau_2$. Therefore the solution given by Equations [13] is valid for $0 \leq \tau \leq \tau_2$. At $\tau = \tau_2$ the velocity is zero and the applied load is less than the collapse load so that there is no further deformation.

Finally, Equation [16] may be integrated to obtain the displacement. Since this will be linear in y and increasing in τ, the maximum displacement W_m occurs at the center of the shell at time $\tau = \tau_2$

$$W_m = (3P_0/2)\left[\rho \int_0^{\tau_2} \int_0^\tau f(d\tau)^2 - (\tau_2^2/2)\right], \quad 0 < \rho < 3 - 2/P_0 \ldots\ldots [18]$$

where τ_2 is defined by Equation [17].

In the event that ρ is larger than $(3P_0 - 2)/P_0$, it is found that the stress profile consists of plastic regime AB for $0 < y < v$, and plastic regime B for $v < y < 1$, where v is to be determined. A solution similar to Equations [13] can easily be constructed for $0 < y < v$ by introducing $\dot{W} = \alpha y$, $n = -1$ into Equation [4], integrating with respect to y, and using the continuity of m and m' at $y = v$ together with $m(0) = -1$ to determine α and the constants of integration. This solution will satisfy Equation [6b] and the Boundary Conditions [8] where $y = 1$ is replaced by $y = v$. For $v < y < 1$ where $m = 1$, the solution is immediately given by Equation [4] and will satisfy Equation [7b]. It will subse-

quently be shown that this two-piece solution also satisfies Equations [6a] and [7a]. The solution is as follows

$$0 < y < v: \quad m = \left(\frac{P_0\rho f - 1}{P_0 - 1}\, v^2 - 1\right)\left(\frac{y}{v}\right)^3 - 2\,\frac{P_0\rho f - 1}{P_0 - 1}\, v^2 \left(\frac{y}{v}\right)^2 + \left(\frac{P_0\rho f - 1}{P_0 - 1}\, v^2 + 3\right)\left(\frac{y}{v}\right) - 1$$

$$n = -1, \quad \dot{W} = 3\,\frac{(P_0 - 1)}{2v^3}\left[\frac{P_0\rho f - 1}{P_0 - 1}\, v^2 - 1\right] y$$

$$v < y < 1: \; m = 1, \quad n = -1, \quad \dot{W} = P_0\rho f - 1 \ldots [19a]$$

The division point v must now be determined so that $\dot{W}$ is continuous; hence v must satisfy

$$\frac{3v}{2}\int_0^\tau \frac{1}{v^3}\left[\frac{P_0\rho f - 1}{P_0 - 1}\, v^2 - 1\right] d\tau = \int_0^\tau \frac{P_0\rho f - 1}{P_0 - 1}\, d\tau$$

Division by v and differentiation with respect to τ yields the equation

$$\frac{3}{2v^3}\left[\frac{P_0\rho f - 1}{P_0 - 1}\, v^2 - 1\right] = \frac{1}{v}\,\frac{P_0\rho f - 1}{P_0 - 1} - \frac{\dot{v}}{v^3}\int_0^\tau \frac{P_0\rho f - 1}{P_0 - 1}\, d\tau$$

the solution of which is readily verified to be

$$v^2 \int_0^\tau \frac{P_0\rho f - 1}{P_0 - 1}\, d\tau - 3\tau = \text{const}$$

Since this relation must hold for some range of τ starting at $\tau = 0$, the constant is zero. Thus

$$v^2 = \frac{3(P_0 - 1)\tau}{P_0\rho \int_0^\tau f d\tau - \tau} \ldots [19b]$$

At $\tau = 0$, Equation [19b] shows that $v^2 = 3(P_0 - 1)/(P_0\rho - 1)$ and hence $v(0)$ is always between zero and 1 for ρ not satisfying Expression [15]. Further, it follows from the restrictions on f (Equations [12b]) that $d(v^2)/d\tau > 0$ and hence v^2 is an increasing function of time and will, in general, reach 1 at a time τ_1 defined by

$$\frac{\rho}{\tau_1}\int_0^{\tau_1} f d\tau = \frac{3P_0 - 2}{P_0} \ldots [20]$$

Again, it follows from Equations [12] and [20] that ρf, evaluated at $\tau = \tau_1$, satisfies the right-hand Inequality [14]. Therefore, for $\tau > \tau_1$, the solution is again given by Equations [13].

The velocity may now be obtained by integrating the appropriate Equations [19] and [13]

$$0 < \tau < \tau_1, \quad 0 < y < v: \quad \dot{W} = \frac{3}{2}(P_0 - 1) y \int_0^\tau \frac{1}{v^3}\left[\frac{P_0\rho f - 1}{P_0 - 1}\, v^2 - 1\right] d\tau \ldots [21a]$$

$$v < y < 1: \quad \dot{W} = P_0\rho \int_0^\tau f d\tau - \tau \ldots [21b]$$

$$\tau_1 < \tau, \quad 0 < y < 1: \quad \dot{W} = \dot{W}(\tau_1) + (3P_0/2) y \left[\rho \int_{\tau_1}^\tau f d\tau - (\tau - \tau_1)\right] \ldots [21c]$$

Thus, for $0 < \tau < \tau_1$ the velocity is linear in y for $0 < y < v$ and independent of y for $v < y < 1$, while for $\tau_1 < \tau$ it is everywhere linear in y. Therefore the velocity Inequalities [6a] and [7a] will be everywhere satisfied provided $\dot{W}$ is positive at $y = 1$. In view of Equation [19b], Equation [21b] can be written $\dot{W} = 3(P_0 - 1)\tau/v^2$; hence $\dot{W}$ is always positive for $0 < \tau < \tau_1$. Therefore the terminal time τ_2 must be greater than τ_1. If $\dot{W}(\tau_2)$ is set equal to zero in Equation [21c] and then y is replaced by 1 and $\dot{W}(\tau_1)$ is introduced from Equation [21b], it will be seen that the terminal time τ_2 is still given by Equation [17] after the expression is simplified by Equation [20]. With τ_2 known, the maximum displacement is found by integrating Equation [21c], setting $y = 1$, $\tau = \tau_2$ and using Equation [21b] to furnish $\dot{W}(\tau_1)$ and $W(\tau_1)$. Thus

$$W_\infty = \frac{P_0}{4}\left[6\rho \int_0^{\tau_1}\int_0^\tau f(d\tau)^2 - 2\rho \int_0^{\tau_1}\int_0^\tau f(d\tau)^2 - 3\tau_2^2 + \frac{3P_0 - 2}{P_0}\,\tau_1^2\right], \quad \rho > 3 - 2/P_0 \ldots [22]$$

where τ_1 and τ_2 are defined by Equations [20] and [17], respectively.

Example of Decaying Loads

Since an exponential curve closely approximates the pressure-time relation actually observed in underwater explosions (2), the function

$$f(\tau) = e^{-\tau} \ldots [23]$$

was chosen for an example. The integrals in Equations [18] and [22] can then be evaluated easily in closed form. A numerical or graphical procedure is still necessary to determine τ_1 and τ_2 for a given ρ from Equations [20] and [17]. In order to obtain numerical results, the particular value $P_0 = 1.40$, corresponding to $c = 2.24$ was chosen. The resulting values for W_∞ as a function of ρ are shown as the heavy curve in Fig. 4(*b*).

It is desired to compare these displacements with those due to a square wave. The latter is defined by

$$f(\tau) = \left\{\begin{array}{l} 1, \; 0 < \tau < I/P_0\rho \\ 0, \; I/P_0\rho < \tau \end{array}\right\} \ldots [24]$$

where I is the impulse. Various square waves may be compared with the exponential curve by choosing different values for the impulse I. The total impulse of the exponential pressure wave is

$$I_0 = P_0\rho \ldots [25a]$$

However, it is evident that a portion of this wave reaches the shell after the plastic deformation has stopped and hence has no effect. To obtain a more realistic comparison, various partial impulses for the exponential wave are defined as follows, Fig. 4(*a*)

Impulse to $\tau = \tau_1$:

$$I_1 = \left[\begin{array}{l} 0, \; \rho < (3P_0 - 2)/P_0 \\ (3P_0 - 2)\tau_1, \; \rho > (3P_0 - 2)/P_0 \end{array}\right] \ldots [25b]$$

Impulse to $\tau = \tau_2$: $\quad I_2 = P_0\tau_2 \ldots [25c]$

Impulse to $P = 3P_0 - 2$:

$$I_3 = \left[\begin{array}{l} 0, \; \rho < (3P_0 - 2)/P_0 \\ P_0\rho - 3P_0 + 2, \; \rho > (3P_0 - 2)/P_0 \end{array}\right] \ldots [25d]$$

Impulse to $P = P_0$: $\quad I_4 = P_0(\rho - 1) \ldots [25e]$

In each case the final deformation is easily computed from Equations [18] and [22]. The results are shown as light curves in Fig.

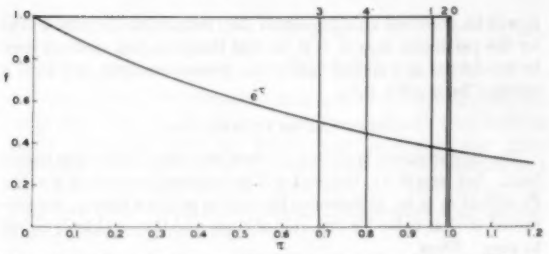

FIG. 4(*a*) COMPARISON OF EXPONENTIAL AND SQUARE WAVES
($P_0 = 1.40$, $\rho = 5$, $\tau_1 = 3.035$, $\tau_2 = 4.965$.)

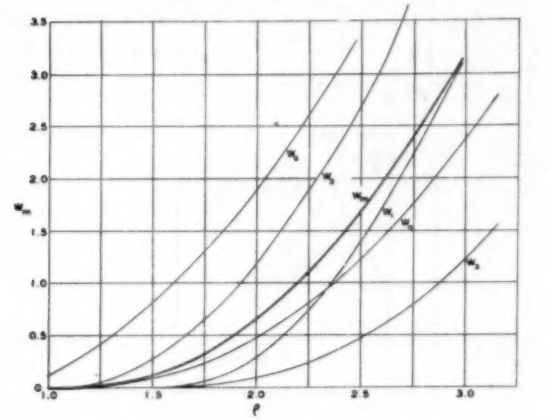

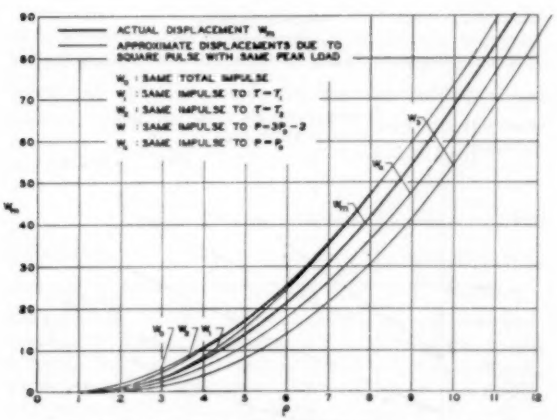
ACTUAL DISPLACEMENT W_m
APPROXIMATE DISPLACEMENTS DUE TO SQUARE PULSE WITH SAME PEAK LOAD
W_0 : SAME TOTAL IMPULSE
W_1 : SAME IMPULSE TO $T = T_1$
W_2 : SAME IMPULSE TO $T = T_2$
W_3 : SAME IMPULSE TO $P = 3P_0 - 2$
W_4 : SAME IMPULSE TO $P = P_0$

FIG. 4(*b*) MAXIMUM DISPLACEMENT FOR $P = P_0\rho e^{-\tau}$

4(*b*), with subscripts corresponding to those on the impulses.

Fig. 4(*b*) was drawn in two sections to bring out the different degrees of approximation for different magnitudes of ρ. Generally, it is evident that for large values of ρ all approximations appear to be reasonably adequate, but for small values none of them is. The approximations would therefore appear to be valuable only for initial pressures of the order of many times the collapse loads.

In reference (4), some specific examples using reasonable design values for the shell parameters were computed. In every case the displacement had become such as to render the shell unserviceable for a maximum load less than 3 times the static collapse load. It would appear, then, that for practical purposes, an approximation method which furnished good results only for very large pressures was of little value. Therefore, the remainder of this paper will be devoted to "medium" values of the load which are of the same order of magnitude as the collapse load.

Specifically, a medium load will be defined as one which satisfies Inequality [15]. Since Equation [18] for the maximum displacement can be used in this case, the actual dependence of W_m upon P_0 is simply multiplicative. Therefore, if the dimensionless displacement is redefined by

$$\omega_m = \frac{2W_m}{3P_0} = \frac{w_m sa}{Yht_0^2(1 + 2/c^2)} \quad \ldots\ldots\ldots [26]$$

the analysis becomes independent of P_0 and hence of the shell dimensions. However, it follows from Inequality [15] that the maximum value of ρ for which the solution so obtained is valid does depend upon P_0, but in no case can be greater than 3.

In view of the relatively simpler form of Equation [18] and the extreme divergence shown by the approximations in Fig. 4, for small ρ, some further approximations have been attempted. The results are shown in Fig. 5(*b*). The heavy curve shows the actual solution while ω_2 and ω_4 represent the best approximations discussed in Fig. 4 (observe that the change in scale is due to the change in dependent variable).

The remaining curves, Fig. 5(*a*) represent more complex pulses. The displacement ω_6 corresponds to a trapezoidal wave

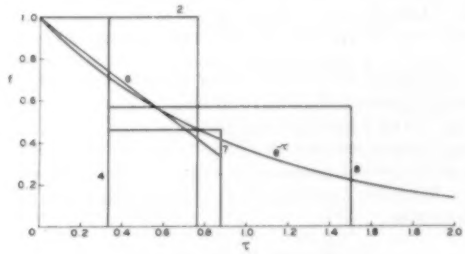

FIG. 5(*a*) COMPARISON OF EXPONENTIAL AND OTHER WAVES
($\rho = 1.5$, $\tau_2 = 0.875$.)

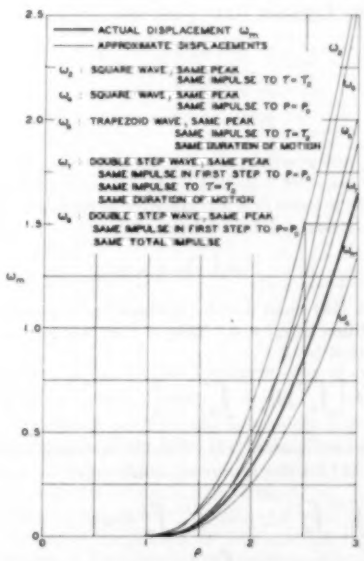
ACTUAL DISPLACEMENT ω_m
APPROXIMATE DISPLACEMENTS
ω_2 : SQUARE WAVE, SAME PEAK, SAME IMPULSE TO $T = T_2$
ω_4 : SQUARE WAVE, SAME PEAK, SAME IMPULSE TO $P = P_0$
ω_6 : TRAPEZOID WAVE, SAME PEAK, SAME IMPULSE TO $T = T_2$, SAME DURATION OF MOTION
ω_7 : DOUBLE STEP WAVE, SAME PEAK, SAME IMPULSE IN FIRST STEP TO $P = P_0$, SAME IMPULSE TO $T = T_2$, SAME DURATION OF MOTION
ω_8 : DOUBLE STEP WAVE, SAME PEAK, SAME IMPULSE IN FIRST STEP TO $P = P_0$, SAME TOTAL IMPULSE

FIG. 5(*b*) MAXIMUM DISPLACEMENT FOR $P = P_0\rho e^{-\tau}$

$$= \left\{ \begin{array}{ll} 1 - \alpha\tau, & 0 < \tau < \tau_2 \\ 0, & \tau_2 < \tau \end{array} \right\} \quad \ldots\ldots\ldots [27]$$

where α is chosen so that the total impulse of the trapezoidal wave will match the impulse of the exponential wave to time τ_2, and τ_2 is given by Equation [17]. The curve for ω_7 represents a two-step pressure wave defined by

$$f = \left\{ \begin{array}{ll} 1, & 0 < \tau < \alpha \\ \lambda, & \alpha < \tau < \beta \\ 0, & \beta < \tau \end{array} \right\} \quad \ldots\ldots\ldots\ldots [28]$$

Here α, β, and λ were determined so that (a) the impulse of the first step of the step wave is equal to the impulse to $P = P_0$ of the exponential wave, (b) the total impulse of the step wave is equal to the impulse of the exponential wave to $\tau = \tau_2$, and (c) the motion caused by the step wave stopped when the wave passed. It turns out that the duration of the motion produced by both waves is also the same. Finally, ω_8 is the displacement due to the same two-step wave except that the total impulse of the step wave is equal to the total impulse of the exponential wave rather than its impulse to $\tau = \tau_2$.

Fig. 5(b) is perhaps a little misleading, owing to the steep slopes of all the curves which tend to make them look close together. Actually, at $\rho = 2$ the closest approximation (ω_7) is in error by over 18 per cent. Further, the computations for ω_2, ω_6, and ω_7 require a knowledge of the actual termination time—a quantity which, in general, is not known. The best of the remaining approximations (ω_4) is in error by 30 per cent.

While better approximations certainly could be obtained by taking multistep functions, it will be shown later that a complete graphical-numerical procedure is easily set up for an arbitrary pulse. Therefore there appears to be no advantage to a complex approximation.

Medium Peaked Loads

The present section will consider loads which rise to a peak and then decay, the maximum load satisfying Inequality [14]. Thus P is given by Equation [12] where f now satisfies the conditions

$$\left. \begin{array}{l} f' \geq 0 \text{ for } 0 < \tau \leq \bar{\tau} \\ f' \leq 0 \text{ for } \bar{\tau} < \tau \\ f(\bar{\tau}) = 1 \end{array} \right\} \quad \ldots\ldots\ldots\ldots [29]$$

for some $\bar{\tau}$, and ρ satisfies Inequality [15]. The solution in this case is still given by Equations [13], but only after the pressure has reached the value $P = P_0$. In view of Equation [12a], then, plastic flow starts at a time τ_0 defined by

$$\rho f(\tau_0) - 1 = 0 \quad \ldots\ldots\ldots\ldots\ldots\ldots [30]$$

Equation [16] must now be modified to take account of the initial condition $\dot{W}(\tau_0) = 0$. This, in turn, will lead to a terminal time τ_2 defined by

$$\rho \left[\int_0^{\tau_2} f d\tau - \int_0^{\tau_0} f d\tau \right] - (\tau_2 - \tau_0) = 0 \quad \ldots\ldots [31]$$

rather than by Equation [17]. Finally, in view of Equation [26], Equation [18] for the maximum displacement is replaced by

$$\omega_m = \rho \left[\int_0^{\tau_1} \int_0^{\tau} f(d\tau)^2 - \int_0^{\tau_0} \int_0^{\tau} f(d\tau)^2 - (\tau_2 - \tau_0) \int_0^{\tau_0} f d\tau - (\tau_2 - \tau_0)^2/(2\rho) \right] \quad \ldots\ldots [32]$$

It will be observed that Equation [32] reduces to Equation [18] for the particular case $\tau_0 = 0$, so that the preceding sections may be considered as a special case of the present analysis, provided ρ satisfies Inequality [15].

Examples of Peaked Loads

The first example is chosen to show the effect of the increasing load. For simplicity, the load will be assumed to start at a value P_0 so that $\tau_0 = 0$. It increases linearly to ρP_0 in a time α, is maintained at that value for one unit of time, and then suddenly drops to zero. Thus

$$f = \left\{ \begin{array}{ll} [1 + (\rho - 1)\tau/\alpha]/\rho, & 0 < \tau < \alpha, \\ 1, & \alpha < \tau < \alpha + 1 \\ 0, & \alpha + 1 < \tau \end{array} \right\} \quad \ldots [33]$$

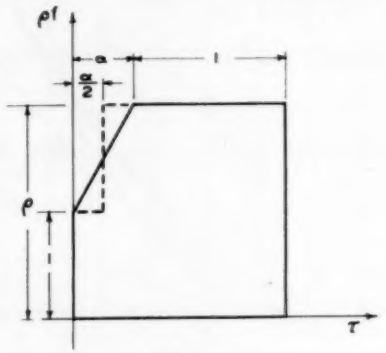

———Linear increase
.....Step increase

Fig. 6 Pressure Pulse to Show Effect of Load Rise

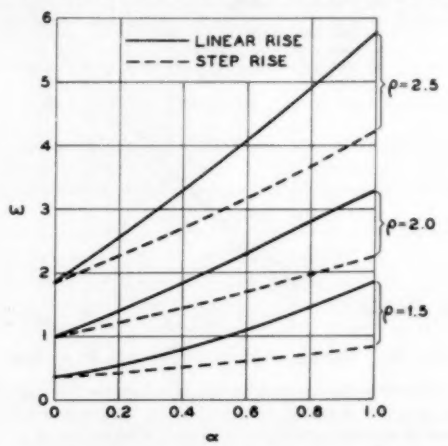

Fig. 7 Displacement Due to Pressure Pulses Shown in Fig. 6

The pressure-time curve is shown as the solid curve in Fig. 6. The dashed curve gives the corresponding square wave of the same impulse. The resulting displacements as functions of the rise time α are shown in Fig. 7 for typical values of ρ. It is seen that the displacement is quite sensitive to α, particularly for large ρ. Further, the reasonable appearing step approximation is in considerable error for even moderately large α.

A second example is the triangle wave, Fig. 1(c), considered by Symonds (3)

$$f(\tau) = \left\{ \begin{array}{ll} \tau & 0 < \tau < 1 \\ 2 - \tau & 1 < \tau < 2 \\ 0 & 2 < \tau \end{array} \right\} \quad \ldots\ldots\ldots [34]$$

This is compared with two matching square waves, each with the same peak load. If the square wave has the same total impulse as the triangular wave the displacement is considerably overestimated. On the other hand, if the square wave is chosen so that the two waves have the same impulse due to that part of the pressure which exceeds P_0, the displacement is quite a bit too low. The results are shown in Fig. 8.

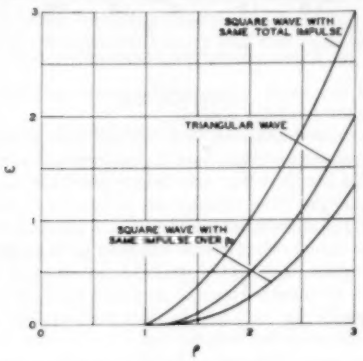

FIG. 8 COMPARISON OF DISPLACEMENTS DUE TO TRIANGULAR AND SQUARE WAVES

DIRECT SOLUTION AND EXAMPLE

Since none of the simple approximations suggested gives adequate results for medium values of ρ, it is desirable to develop techniques for a direct solution. The suggested procedure is as follows: Curves of $f(\tau)$ and $\int_0^\tau f(\tau)d\tau$ are accurately drawn to a convenient scale. With reference to the curve for $f(\tau)$, τ_0 is easily determined from Equation [30] for any value of ρ. Equation [31] is then written in the form

$$\int_0^{\tau_2} f d\tau = (\tau_2/\rho) + (\tau_0/\rho) + \int_0^{\tau_0} f d\tau \ldots\ldots [35]$$

If τ_2 is replaced by τ, the right-hand side of Equation [35] may be drawn as a straight line on the same graph as $\int_0^\tau f d\tau$, since τ and ρ are both known. The termination value τ_2 is then determined as the abscissa of the point of intersection of the straight line with the integral curve. Finally, with τ_0 and τ_2 known, ω_m is easily found from Equation [32] by either numerical or graphical integrations.

In order to discuss the accuracy of the foregoing procedure the following function for which an analytic solution could also be obtained was chosen

$$= \left\{ \begin{array}{ll} 10\tau & 0 < \tau < 0.1 \\ e^{-(\tau - 0.1)} & 0.1 < \tau \end{array} \right\} \quad \ldots\ldots\ldots [36]$$

Fig. 9 shows the pressure curve, together with the level lines $1/\rho$ for various values of ρ used to determine τ_0. The curve $\int_0^\tau f(\tau)d\tau$ (computed numerically) is shown in Fig. 10, together with the straight lines used in determining τ_2. Fig. 11 shows the curve of

$$\int_0^\tau \int_0^\tau f(\tau)(d\tau)^2$$

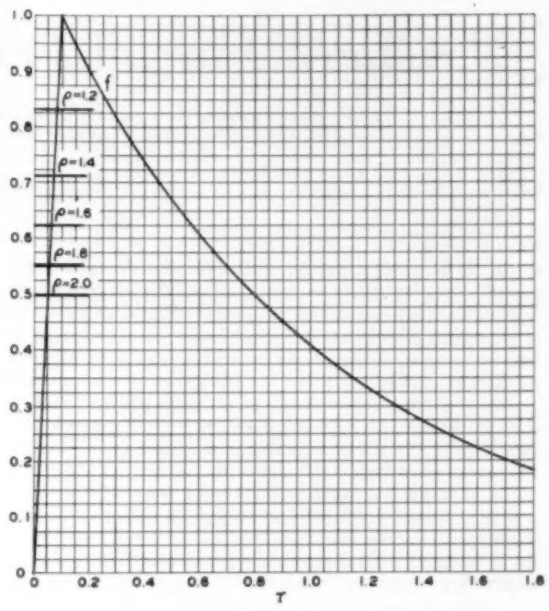

FIG. 9 $f(\tau)$ AND DETERMINATION OF τ_0

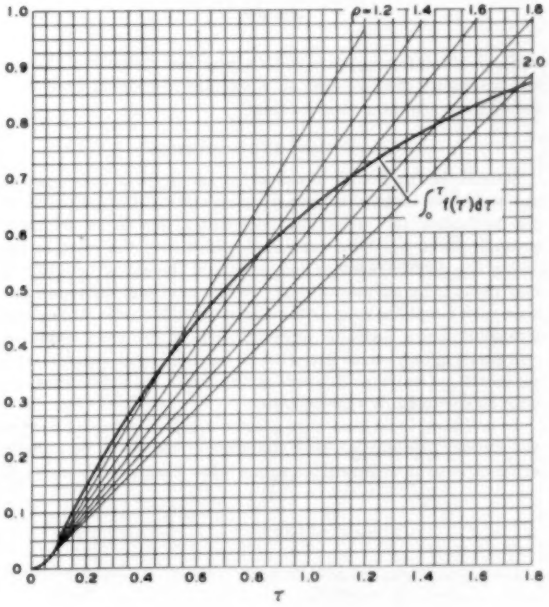

FIG. 10 $\int_0^\tau f(\tau)d\tau$ AND DETERMINATION OF τ_2

This curve was used to evaluate the integrals in Equation [32]. The resulting displacement is shown as the solid curve in Fig. 12.

The same problem was also solved analytically, using Newton's method to solve the transcendental equation for τ_2. The results are shown as the dashed curve in Fig. 12. In view of the fact that all computations were carried out by slide rule, the agreement is felt to be excellent. Therefore the proposed graphical-numerical

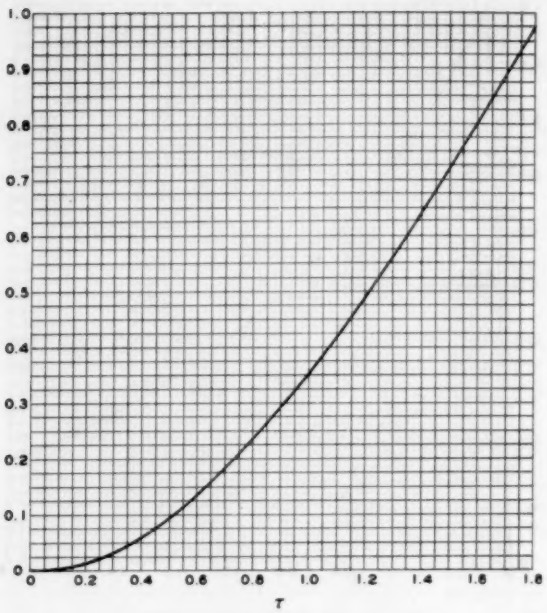

FIG. 11 $\int_0^\tau \int_0^\tau f(\tau)(d\tau)^2$

method of solution appears to be a practical method for finding the maximum displacement in a circular cylindrical shell subjected to an arbitrary blast loading.

CONCLUSIONS AND LIMITATIONS

Within the framework of the initial assumptions of the paper, the conclusion is obvious; namely, that a straightforward method for computing the maximum deformation due to an arbitrary pressure wave has been presented. However, the relation between the displacement so computed and the actual behavior of real shells is by no means clear. While it is reasonable to hope that such simplifications as the neglect of the elastic strains and strain hardening and the approximation of the yield condition will result in only small errors in the resulting predictions, it is by no means certain that this will be the case. Such questions can only be answered by experiments.

In addition, there is an even greater source of potential error in the implicit assumption that the shell continues to be radially symmetric as it deforms. It seems quite likely that buckling in some form will occur. This possibility has not been taken into account in the foregoing analysis.

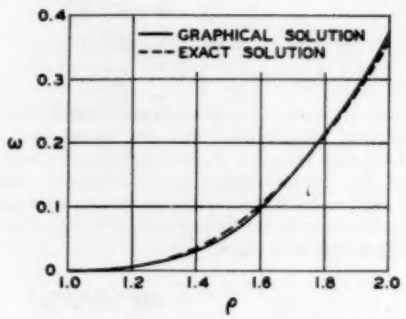

FIG. 12 DISPLACEMENT FOR PRESSURE PULSE OF FIG. 9

Despite these limitations, it is believed that symmetric solutions of idealized problems have a certain practical value in addition to the fact that they may help to point the way to a more realistic analysis. The assumptions of no elastic strains, radial symmetry, and approximate yield condition are all nonconservative in that the actual deformations will tend to be larger than predicted. Further, the effect of strain hardening can always be accounted for by suitable choice of an average yield stress. Therefore the results may certainly be used in the following negative sense: If the predicted deformations are excessive the shell will not remain serviceable under the given pressure wave. On the other hand, if the predicted deformations are not excessive, it is still possible that the shell will become unserviceable due to buckling or some other cause.

BIBLIOGRAPHY

1 "Impact Pressure Loading of Rigid-Plastic Cylindrical Shells," by P. G. Hodge, Jr., *Journal of the Mechanics and Physics of Solids*, vol. 3, 1955, pp. 176–188.

2 "Underwater Explosions," by R. H. Cole, Princeton University Press, Princeton, N. J., 1948.

3 "Dynamic Load Characteristics in Plastic Bending of Beams," by P. S. Symonds, JOURNAL OF APPLIED MECHANICS, Trans. ASME, vol. 75, 1953, pp. 475–481.

4 "Ultimate Dynamic Load of a Circular Cylindrical Shell," by P. G. Hodge, Jr., Polytechnic Institute of Brooklyn, PIBAL Report No. 265, 1954. Proceedings of the Second Midwest Conference on Solid Mechanics (to be published).

5 "Limit Analysis of Cylindrical Shells Under Axially Symmetric Loading," by D. C. Drucker, Proceedings of the First Midwest Conference on Solid Mechanics, 1953, pp. 158–163.

6 "The Rigid-Plastic Analysis of Symmetrically Loaded Cylindrical Shells," by P. G. Hodge, Jr., JOURNAL OF APPLIED MECHANICS, Trans. ASME, vol. 76, 1954, pp. 336–342.

7 "The Plastic Collapse of Cylindrical Shells Under Axially Symmetrical Loading," by E. T. Onat, *Quarterly of Applied Mathematics*, vol. 13, 1955, pp. 63–72.

Axisymmetrical Buckling of Circular Cones Under Axial Compression

By PAUL SEIDE,[1] LOS ANGELES, CALIF.

The axisymmetrical buckling of right circular cones under axial compression is investigated. A simple expression is obtained for long cones of constant thickness, relating the cone buckling load to the buckling load of a long cylinder of equal thickness and the cone semivertex angle.

Nomenclature

The following nomenclature is used in the paper:

- D = bending stiffness per unit width of shell wall $\left(D = \frac{Et^3}{12(1 - \nu^2)}\right)$
- E = Young's modulus
- M = additional middle-surface force per unit width due to buckling
- N_{s_0} = membrane force per unit width prior to buckling, in direction of cone generator $\left(N_{s_0} = -\frac{P}{\pi s \sin 2\alpha}\right)$
- Q = additional shear force per unit width due to buckling
- P = critical axial load
- $P_{cyl\ \infty}$ = axisymmetric axial-buckling load of infinite cylinder with constant-thickness walls $\left\{P_{cyl\ \infty} = \frac{2Et^2\pi}{\sqrt{[3(1 - \nu^2)]}}\right\}$
- r = radius of cone cross section ($r = s \sin \alpha$)
- s = distance from vertex
- t = wall thickness, constant around circumference
- u = additional middle-surface displacement in direction of cone generator due to buckling
- w = additional middle-surface displacement normal to cone wall due to buckling
- α = semivertex angle of cone
- ϵ = additional middle-surface strain due to buckling
- ν = Poisson's ratio
- χ = additional change in curvature due to buckling

Subscripts

- s = in direction of cone generator
- θ = circumferential

Introduction

While considerable information of varying degrees of rigor is available on the axial buckling loads of circular cylinders, little or no similar information is available for the more general problem of the right circular cone. In view of the extreme complexity of the differential equations involved, it appears practical to consider the axisymmetrical mode of buckling of circular cones in an attempt to obtain some idea of the effects of taper.

In deriving the differential equations to be solved, two approaches are possible. One such approach is given by Pflueger (1)[3] where both stress and strain vary nonlinearly across the thickness of the cone. Furthermore, force components take into account the varying circumferential size of the element as a function of distance from the middle surface. A second approach given by Timoshenko for cylinders and spheres in reference (2) neglects such refinements. While the first approach can be shown to be necessary to satisfy all the equations of equilibrium of forces on an element of the shell consistently, Timoshenko's method has been found to yield adequate results with much simpler equations. Accordingly, the latter method of derivation is used in the present paper.

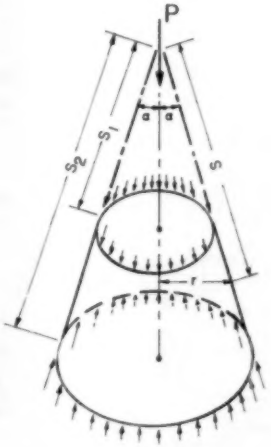

Fig. 1 Cone Subjected to Axial Load

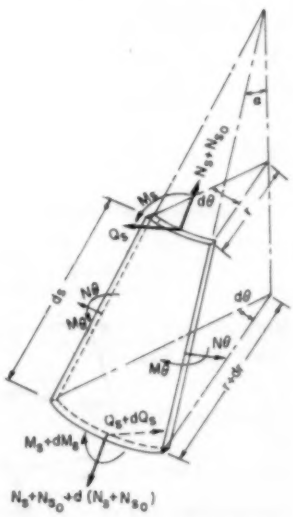

Fig. 2 Forces and Moments on Element of Cone

Equilibrium and Stress-Strain Relations

The stress state in the cone prior to buckling can be approximated satisfactorily by the membrane stresses given by (see Fig. 1)

[1] Member of Technical Staff, The Ramo-Wooldridge Corporation.

Presented at the West Coast Conference of the Applied Mechanics Division, Pasadena, Calif., June 11–13, 1956, of The American Society of Mechanical Engineers.

Discussion of this paper should be addressed to the Secretary, ASME, 29 West 39th Street, New York, N. Y., and will be accepted until January 10, 1957, for publication at a later date. Discussion received after the closing date will be returned.

Note: Statements and opinions advanced in papers are to be understood as individual expressions of their authors and not those of the Society. Manuscript received by ASME Applied Mechanics Division, February 7, 1956. Paper No. 56—APM-36.

[3] Numbers in parentheses refer to the Bibliography at the end of the paper.

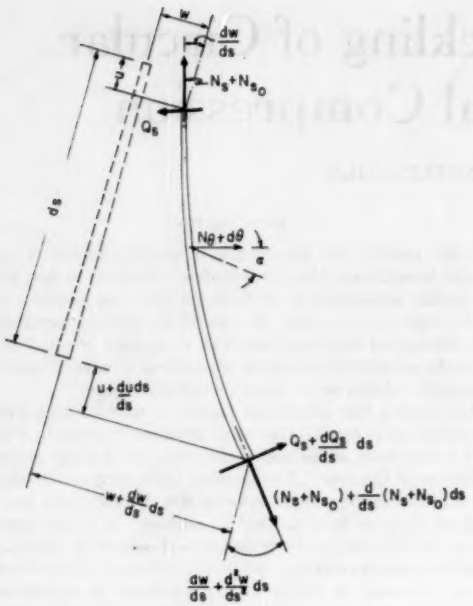

FIG. 3(a) FORCE-EQUILIBRIUM DIAGRAM

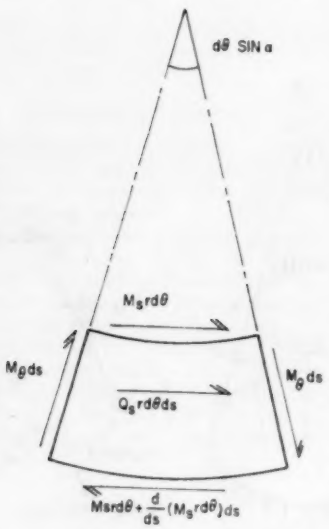

FIG. 3(b) MOMENT-EQUILIBRIUM DIAGRAM

$$\left.\begin{aligned} M_s &= M_\theta = Q_s = N_\theta = 0 \\ N_s &= \frac{-P}{2\pi s \sin\alpha \cos\alpha} = N_{s_0} \end{aligned}\right\} \quad \ldots\ldots [1]$$

Additional forces and moments per unit width acting on an element of the cone are shown in Fig. 2. The equilibrium relations for these can be read from Figs. 3(a) and 3(b) as

$$\frac{d}{ds}(sN_s) - N_\theta = 0 \quad \ldots\ldots [2a]$$

$$\frac{d}{ds}\left(\frac{-P}{\pi \sin 2\alpha}\frac{dw}{ds}\right) + N_\theta \cot\alpha + \frac{d}{ds}(sQ_s) = 0 \quad \ldots\ldots [2b]$$

$$\frac{d}{ds}(sM_s) - M_\theta - sQ_s = 0 \quad \ldots\ldots [2c]$$

where only first-order terms have been included.

Stress-strain relations are given by

$$\left.\begin{aligned} N_s &= \frac{Et}{1-\nu^2}(\epsilon_s + \nu\epsilon_\theta) \\ N_\theta &= \frac{Et}{1-\nu^2}(\epsilon_\theta + \nu\epsilon_s) \\ M_s &= -D(\chi_s + \nu\chi_\theta) \\ M_\theta &= -D(\chi_\theta + \nu\chi_s) \end{aligned}\right\} \quad \ldots\ldots [3]$$

where (see reference 3)

$$\left.\begin{aligned} \epsilon_s &= du/ds \\ \epsilon_\theta &= \frac{u - w\cot\alpha}{s} \\ \chi_s &= d^2w/ds^2 \\ \chi_\theta &= 1/s\,\frac{dw}{ds} \end{aligned}\right\} \quad \ldots\ldots [4]$$

The displacements u and w are assumed to be measured from the equilibrium position of the cone prior to buckling.

By the addition of Equation [2b] and Equation [2a] multiplied by cot α, an equation of equilibrium of load in the vertical direction is obtained

$$\frac{d}{ds}\left(sN_s\cot\alpha - \frac{P}{\pi\sin 2\alpha}\frac{dw}{ds} + sQ_s\right) = 0 \quad \ldots\ldots [5]$$

Noting that the vertical component of the edge stress is assumed not to change after buckling

$$sN_s\cot\alpha - \frac{P}{\pi\sin 2\alpha}\frac{dw}{ds} + sQ_s = 0 \quad \ldots\ldots [6]$$

The addition of Equations [6] and [2c] then yields

$$\frac{d}{ds}(sM_s) - M_\theta + sN_s\cot\alpha - \frac{P}{\pi\sin 2\alpha}\frac{dw}{ds} = 0 \quad \ldots\ldots [7]$$

Substitution of Equations [3] and [4] into Equations [2a] and [7] results finally in the following simultaneous differential equations for the unknown displacements u and w

$$\frac{d}{ds}\left\{t\left[s\frac{du}{ds} + \nu(u - w\cot\alpha)\right]\right\} - t\left[1/s(u - w\cot\alpha) + \nu\frac{du}{ds}\right] = 0 \quad \ldots\ldots [8a]$$

$$\frac{d}{ds}\left[t^3\left(s\frac{d^2w}{ds^2} + \nu\frac{dw}{ds}\right)\right] - t^3\left(1/s\frac{dw}{ds} + \nu\frac{d^2w}{ds^2}\right) - 12t\cot\alpha\left[s\frac{du}{ds} + \nu(u - w\cot\alpha)\right] + \frac{12P(1-\nu^2)}{\pi E\sin 2\alpha}\frac{dw}{ds} = 0 \quad \ldots\ldots [8b]$$

Boundary conditions for these equations for the case of simple support at the edges and rigid rings are

$$\left.\begin{aligned} &\frac{d^2w}{ds^2} + \frac{\nu}{s}\frac{dw}{ds} = 0 \\ &u \sin\alpha - w\cos\alpha = 0 \end{aligned}\right\} \text{ at } s = s_1, s_2 \ldots\ldots\ldots [9]$$

CONSTANT-THICKNESS CONE

When the wall thickness t is constant, Equations [8] can be reduced to

$$s\frac{d^2u}{ds^2} + \frac{du}{ds} - \frac{u}{s} + \left(\frac{w}{s} - \nu\frac{dw}{ds}\right)\cot\alpha = 0 \ldots [10a]$$

$$\frac{1}{s}\frac{d^2}{ds^2}\left(s\frac{dw}{ds}\right) - \frac{1}{s^2}\frac{d}{ds}\left(s\frac{dw}{ds}\right) + \frac{P}{\pi D\sin 2\alpha}\frac{1}{s^2}\left(s\frac{dw}{ds}\right) + \frac{12\nu\cot^2\alpha}{t^2}\frac{w}{s} - \frac{12\cot\alpha}{t^2}\left(\frac{du}{ds} + \nu\frac{u}{s}\right) = 0 \ldots [10b]$$

The operation $\left[s^2\frac{d^2(\ )}{ds^2} + 3s\frac{d(\ )}{ds}\right]$

is now performed on Equation [10b] and leads to

$$s\frac{d^4}{ds^4}\left(s\frac{dw}{ds}\right) + \frac{12P(1-\nu^2)}{\pi Et^3\sin 2\alpha}\left[\frac{d^2}{ds^2}\left(s\frac{dw}{ds}\right) - \frac{1}{s}\frac{d}{ds}\left(s\frac{dw}{ds}\right)\right] + \frac{12\nu\cot^2\alpha}{t^2}\left[\frac{d}{ds}\left(s\frac{dw}{ds}\right) - \frac{w}{s}\right] - \frac{12\cot\alpha}{t^2}\left\{\frac{d}{ds}\left[s\left(s\frac{d^2u}{ds^2} + \frac{du}{ds} - \frac{u}{s}\right)\right] + \nu\left(s\frac{d^2u}{ds^2} + \frac{du}{ds} - \frac{u}{s}\right)\right\} = 0 \ldots [11]$$

Substitution of Equation [10a] into Equation [11] then yields a single equation for w

$$s^2\frac{d^4Z}{ds^4} + \frac{P/D}{\pi\sin 2\alpha}\left(s\frac{d^2Z}{ds^2} - \frac{dZ}{ds}\right) + \frac{12(1-\nu^2)\cot^2\alpha}{t^2}Z = 0 \ldots [12]$$

where $$Z = s\frac{dw}{ds}$$

Equation [12] can be easily integrated if it is differentiated once more with respect to s. Then

$$s^2\frac{d^4f}{ds^4} + 2s\frac{d^3f}{ds^3} + \frac{P}{\pi D\sin 2\alpha}s\frac{d^2f}{ds^2} + \frac{12(1-\nu^2)\cot^2\alpha}{t^2}f = 0 \ldots [13]$$

where $$f = \frac{dZ}{ds} = \frac{d}{ds}\left(s\frac{dw}{ds}\right)$$

This equation can be expressed as

$$\left(s\frac{d^2}{ds^2} + \frac{P}{2\pi D\sin 2\alpha}\right)\left(s\frac{d^2f}{ds^2} + \frac{P}{2\pi D\sin 2\alpha}f\right) - \left(\frac{P}{2\pi D\sin 2\alpha}\right)^2\left[1 - \left(\frac{P_{cyl\ \infty}}{P}\cos^2\alpha\right)^2\right]f = 0 \ldots [14]$$

so that the complete solution for f is given by the solutions of the two second-order equations

$$\left.\begin{aligned} &s\frac{d^2f}{ds^2} + b_1 f = 0 \\ &s\frac{d^2f}{ds^2} + b_2 f = 0 \end{aligned}\right\} \ldots\ldots\ldots\ldots [15]$$

where

$$b_{1,2} = \frac{P}{2\pi D\sin 2\alpha}\left\{1 \pm \sqrt{\left[1 - \left(\frac{P_{cyl\ \infty}}{P}\cos^2\alpha\right)^2\right]}\right\} \ldots [16]$$

The solution of Equations [15] can be found in reference (4) as

$$f = \frac{d}{ds}\left(s\frac{dw}{ds}\right) = -b_1\{C_1[2\sqrt{(b_1s)}]J_1[2\sqrt{(b_1s)}] + C_2[2\sqrt{(b_1s)}]Y_1[2\sqrt{(b_1s)}]\} - b_2\{C_3[2\sqrt{(b_2s)}]J_1[2\sqrt{(b_2s)}]_1 [J2(b_2s)] + C_4[2\sqrt{(b_2s)}]Y_1[2\sqrt{(b_2s)}]\} \ldots [17]$$

Where $J_p(x)$ and $Y_p(x)$ are Bessel functions of the first and second kinds, respectively. Integration of Equation [17] yields the general solution for w

$$w = C_1\{2J_0[2\sqrt{(b_1s)}] + [2\sqrt{(b_1s)}]J_1[2\sqrt{(b_1s)}]\} + C_2\{2Y_0[2\sqrt{(b_1s)}] + [2\sqrt{(b_1s)}]Y_1[2\sqrt{(b_1s)}]\} + C_3\{2J_0[2\sqrt{(b_2s)}] + [2\sqrt{(b_2s)}]J_1[2\sqrt{(b_2s)}]\} + C_4\{2Y_0[2\sqrt{(b_2s)}] + [2\sqrt{(b_2s)}]Y_1[2\sqrt{(b_2s)}]\} + C_5 \ldots [18]$$

Solution of Equation [10a], which can be written as

$$\frac{d}{ds}\left[s^3\frac{d}{ds}\left(\frac{u}{s}\right)\right] = \left(\nu s\frac{dw}{ds} - w\right)\cot\alpha \ldots\ldots [19]$$

yields the corresponding expression for the displacement u

$$u = 2\cot\alpha\left[C_1\left\{2\frac{J_1[2\sqrt{(b_1s)}]}{2\sqrt{(b_1s)}} + \nu J_2[2\sqrt{(b_1s)}]\right\} + C_2\left\{2\frac{Y_1[2\sqrt{(b_1s)}]}{2\sqrt{(b_1s)}} + \nu Y_2[2\sqrt{(b_1s)}]\right\} + C_3\left\{2\frac{J_1[2\sqrt{(b_2s)}]}{2\sqrt{(b_2s)}} + \nu J_2[2\sqrt{(b_2s)}]\right\} + C_4\left\{2\frac{Y_1[2\sqrt{(b_2s)}]}{2\sqrt{(b_2s)}} + \nu Y_2[2\sqrt{(b_2s)}]\right\}\right] + C_5\cot\alpha \ldots [20]$$

It should be noted that, although there are five unknown constants of integration, only four boundary conditions are needed to determine the buckling load since the constant C_5 in both u and w corresponds to a rigid body translation in the direction of the cone axis.

Substitution of Equations [18] and [20] into the Boundary Conditions [9] yields, after some manipulation, the following criterion for instability of the cone

$$\begin{vmatrix} x_{11}^2J_2'(x_{11}) + 2\nu x_{11}^2J_2(x_{11}) & x_{11}^2Y_2'(x_{11}) + 2\nu x_{11}^2Y_2(x_{11}) & x_{21}^2J_2'(x_{21}) + 2\nu x_{21}^2J_2(x_{21}) & x_{21}^2Y_2'(x_{21}) + 2\nu x_{21}^2Y_2(x_{21}) \\ x_{11}J_2'(x_{11}) - 2\nu J_2(x_{11}) & x_{11}Y_2'(x_{11}) - 2\nu Y_2(x_{11}) & x_{21}J_2'(x_{21}) - 2\nu J_2(x_{21}) & x_{21}Y_2'(x_{21}) - 2\nu Y_2(x_{21}) \\ x_{12}^2J_2'(x_{12}) + 2\nu x_{12}^2J_2(x_{12}) & x_{12}^2Y_2'(x_{12}) + 2\nu x_{12}^2Y_2(x_{12}) & x_{22}^2J_2'(x_{22}) + 2\nu x_{22}^2J_2(x_{22}) & x_{22}^2Y_2'(x_{22}) + 2\nu x_{22}^2Y_2(x_{22}) \\ x_{12}J_2'(x_{12}) - 2\nu J_2(x_{12}) & x_{12}Y_2'(x_{12}) - 2\nu Y_2(x_{12}) & x_{22}J_2'(x_{22}) - 2\nu J_2(x_{22}) & x_{22}Y_2'(x_{22}) - 2\nu Y_2(x_{22}) \end{vmatrix} = 0 \ldots [21]$$

where

$$\left.\begin{aligned} x_{11} &= 2\sqrt{(b_1 s_1)} \\ x_{12} &= 2\sqrt{(b_1 s_2)} \\ x_{21} &= 2\sqrt{(b_2 s_1)} \\ x_{22} &= 2\sqrt{(b_2 s_2)} \end{aligned}\right\} \quad \ldots\ldots\ldots\ldots\ldots [22]$$

and the primes indicate differentiation with respect to x.

The stability determinant given by Equation [21] is rather complicated but gives a much simplified result when Poisson's ratio ν is set equal to zero. For this special case Equation [23] yields the two criteria

$$\left.\begin{aligned} &J_2'[2\sqrt{(b_1 s_2)}]Y_2'[2\sqrt{(b_1 s_1)}] \\ &\qquad - J_2'[2\sqrt{(b_1 s_1)}]Y_2'[2\sqrt{(b_1 s_2)}] = 0 \\ &J_2'[2\sqrt{(b_2 s_2)}]Y_2'[2\sqrt{(b_2 s_1)}] \\ &\qquad - J_2'[2\sqrt{(b_2 s_1)}]Y_2'[2\sqrt{(b_2 s_2)}] = 0 \end{aligned}\right\} \quad \ldots [23]$$

It can be argued that buckling loads are usually not sensitive to Poisson's ratio so that Equations [23] should be adequate for other values of ν.

The solution of Equations [23] can be expressed as

$$2\sqrt{(b_{1,2} s_1)} = X_n \left[\sqrt{\frac{s_2}{s_1}}\right] \qquad n = 1, 2, 3$$

which expands to, from either equation

$$\frac{P}{P_{cyl\,\infty}\cos^2\alpha} = \frac{1}{2}\left[\frac{X_n^2}{(8s_1/t)\sqrt{[3(1-\nu^2)]}\cot\alpha} + \frac{(8s_1/t)\sqrt{[3(1-\nu^2)]}\cot\alpha}{X_n^2}\right] n = 1, 2, 3 \ldots\ldots [24]$$

The value of X_n to be used is that which yields the lowest value of P. For large values of the parameter

$$(8s_1/t)\sqrt{[3(1-\nu^2)]}\cot\alpha$$

minimization of Equation [24] with respect to

$$\frac{(8s_1/t)\sqrt{[3(1-\nu^2)]}\cot\alpha}{X_n^2}$$

yields

$$\frac{P}{P_{cyl\,\infty}\cos^2\alpha} = 1 \quad \ldots\ldots\ldots\ldots\ldots [25]$$

It is interesting to note that this is the buckling load of a cylinder having a thickness equal to the projection of the cone thickness on a plane perpendicular to the longitudinal axis.

Discussion

Although a particular mode of buckling has been assumed, the results of the present paper should be useful in determining the actual buckling load of cones of moderate length. The investigation of reference (5) indicates that the theoretical axial buckling load of relatively long cylinders is equal to the axisymmetric buckling load and that the actual buckling load can be expressed as

$$P_{act} = C\left(\frac{r}{t}\right)P_{cyl\,\infty} \quad \ldots\ldots\ldots\ldots\ldots [26a]$$

where r is the radius of the cylinder. This circumstance suggests that it may be possible to approximate axial buckling loads of long cones by

$$P = C\left(\frac{\bar{r}}{t}\cos\alpha\right)P_{cyl\,\infty}\cos^2\alpha \quad \ldots\ldots\ldots [26b]$$

where $\bar{r}$ is some average radius of the cone cross sections. For the cylinder, the corresponding values of r/t and C are approximately as follows (5)

r/t	600	800	1000	1200	1400
C	0.337	0.289	0.248	0.218	0.197
r/t	1600	1800	2000	2400	
C	0.183	0.169	0.158	0.140	

and can be represented by

$$C \approx 23.8\left(\frac{t}{r}\right)^{0.66} \quad \ldots\ldots\ldots\ldots\ldots [27]$$

Example

Given a cone having the following properties, what is the critical load

$$\begin{aligned} \alpha &= 30 \text{ deg} \\ r_1 &= 10 \text{ in.} \\ r_2 &= 30 \text{ in.} \\ E &= 30 \times 10^6 \text{ psi} \\ t &= 0.02 \text{ in.} \\ \nu &= 1/3 \end{aligned}$$

$$P_{cyl\,\infty} = \frac{2\pi Et^2}{\sqrt{[3(1-\nu^2)]}} = \frac{2\pi \times 30 \times 10^6 \times 4 \times 10^{-4}}{\sqrt{(3 \times 8/9)}} = 46{,}100 \text{ lb}$$

Then, from Equation [25]

$$P = 46{,}100 \times \left(\frac{\sqrt{3}}{2}\right)^3 = 34{,}600 \text{ lb}$$

With $\bar{r}/t$ taken as the average value of r/t for the cone, or

$$r/t\cos\alpha = \frac{20}{0.02}\frac{2}{\sqrt{0.3}} = 1155$$

$$C \approx 0.227 \text{ and } P_{act} \approx 0.227 \times 34{,}600 = 7580 \text{ lb}$$

BIBLIOGRAPHY

1 "Stability of Thin Conical Shells," by A. Pflueger, *Ingenieur-Archiv*, vol. 8, no. 3, 1937. Available as translation prepared under Contract N123S-80065, task order No. 3, between Naval Ordnance Test Station, Pasadena, Calif., and the University of Michigan.

2 "Theory of Elastic Stability," by S. Timoshenko, McGraw-Hill Book Company, Inc., New York, N. Y., 1936, pp. 419–497.

3 "Theory of Plates and Shells," by S. Timoshenko, McGraw-Hill Book Company, Inc., New York, N. Y., 1940, pp. 452–453.

4 "Tables of Functions," by E. Jahnke and F. Emde, Dover Publications, New York, N. Y., 1945, p. 147.

5 "Critical Stresses of Thin-Walled Cylinders in Axial Compression," by S. B. Batdorf, M. Schildcrout, and M. Stein, NACA TN 1343, 1947.

Electronic Analog Computer Solutions of Nonlinear Vibratory Systems of Two Degrees of Freedom

By C. P. ATKINSON,[1] BERKELEY, CALIF.

The main contribution of this paper is its account of the use of an electronic differential analyzer for solving the exact differential equations of certain two-degree-of-freedom nonlinear vibrating systems, and the comparison of the differential-analyzer solutions with the approximate analytical solutions obtained from a single-term harmonic approximation (Ritz approximation). The results of these two methods for solving nonlinear differential equations compare favorably over much of the ranges of variables. Where discrepancies arise between the results of the two methods the value of the differential-analyzer approach can be practically appreciated. For example, in the region where superharmonics might be expected, the single-term harmonic approximation ignores them, while the analyzer solutions contain the superharmonic components of the exact solution. A secondary contribution of the paper is the account of the use of the differential analyzer for verification of suspected stability criteria for two-degree-of-freedom nonlinear vibrating systems. Analytical solutions that were reproducible on the analyzer were considered stable; those that were not reproducible were considered unstable. This paper also can be considered as a call for further application of modern computer techniques to the problems of nonlinear mechanics. Since the computer solves the exact or complete differential equations, the results are the complete solutions including transient phenomena, steady state, subharmonics, superharmonics, and so on. These exact solutions are produced as functions of time which are analogous to the actual vibrations of the physical system studied.

Nomenclature

The following nomenclature is used in the paper:

- A = arbitrary constant in multiplier circuit
- c_i = spring constant, coefficient of algebraic expression for restoring force
- D_i = coefficient of damping term
- IC = initial conditions on integrators
- m_i = mass
- $\bar{m}$ = mass ratio m_2/m_1
- p = the ratio P/m_1
- P = amplitude of harmonic disturbing force
- Q_i = dimensionless displacement amplitude of mass m_i
- q_i = dimensionless dependent variable of dimensionless differential equations of motion ($q_i = \sqrt{3/4}\mu_i x_i$)
- s = ratio $\dfrac{P}{m_1 k_1^2} = \dfrac{P}{c_1}$
- $\bar{s}$ = dimensionless disturbance amplitude $\sqrt{3/4}\mu_i s$
- t = time, independent variable
- V = generalized variable of multiplier circuit
- x_i = instantaneous displacement of mass m_i
- z = spring extension
- Ω = circular frequency of harmonic disturbing force
- η = frequency ratio Ω/K_1
- K_i^2 = ratio c_i/m_i
- $\bar{K}^2$ = ratio K_2^2/K_1^2
- μ_i^2 = coefficient of nonlinear term in algebraic expression for restoring force. μ_i has the units of reciprocal length L^{-1}

Code Words for Different Systems

HOLO = free vibration of system with a hardening main spring and a linear coupling spring.

HILO = forced vibrations of system with a hardening main spring and a linear coupling spring. The disturbing force acts on the main mass.

SOLO = free vibrations; softening main spring; linear coupling spring.

SILO = forced vibrations; softening main spring; linear coupling spring; disturbing force acts on the main mass.

LOHO = free vibrations; linear main spring; hardening coupling spring.

LIHO = forced vibrations; linear main spring; hardening coupling spring; disturbing force acts on main mass.

LOSO = free vibrations; linear main spring; softening coupling spring.

LISO = forced vibrations; linear main spring; softening coupling spring; disturbing force acts on main mass.

1 Introduction

This paper is an account of the results of the use of an electronic differential analyzer[2] for solving the exact differential equations of certain two-degree-of-freedom nonlinear vibrating systems. The differential equations are of the Duffing type; that is, the nonlinearities are in the form of nonlinear springs. The restoring forces in the springs are represented as polynomials of the form $c(z \pm \mu^2 z^3)$ where z is the spring extension. The springs can thus be linear, hardening or softening depending on μ and the $\pm$ sign. For a further account of the systems studied refer to the next section. This paper can be considered further as experimental verification for the response curves of the systems as obtained by

[1] Assistant Professor of Engineering Design, University of California.

Presented at the West Coast Conference of the Applied Mechanics Division, Pasadena, Calif., June 11–13, 1956, of The American Society of Mechanical Engineers.

Discussion of this paper should be addressed to the Secretary, ASME, 29 West 39th Street, New York, N. Y., and will be accepted until January 10, 1957, for publication at a later date. Discussion received after the closing date will be returned.

Note: Statements and opinions advanced in papers are to be understood as individual expressions of their authors and not those of the Society. Manuscript received by ASME Applied Mechanics Division, December 9, 1955. Paper No. 56—APM-38.

[2] The electronic differential analyzer used is a Beckman EASE computer located at the Timoshenko Laboratory, Stanford University, Stanford, Calif.

the approximate analytical method known as the Ritz averaging method.

The results of the application of the Ritz approximation to these systems are presented, in part, in a paper by F. R. Arnold (1)[2] and more fully in his doctoral dissertation at Stanford University (2).

The use of an electronic differential analyzer for the solutions of these nonlinear differential equations emphasizes its value as a scientific tool for the solution of the mathematically untractable equations arising in nonlinear mechanics. The analyzer solutions presented in this paper verify the analytical results gotten by the single-term harmonic approximation over much of the ranges of variables but go further to show where the harmonic approximation is deficient in depicting the true solution of the differential equations. The differential-analyzer solutions present the exact (within the accuracy of the analyzer) solutions of the vibrating systems studied. These solutions produced as functions of time indicate the nature of the vibrations and show, in the cases studied, the modified elliptic functions which are the solutions to the differential equations of the systems. In certain regions where the analyzer results differ from the analytical results the analyzer solutions show superharmonic components along with the fundamental response given by the single-term harmonic approximation. In other regions where the analytical results predict stable solutions the analyzer is unable to produce them, but only yields transients whose amplitudes increase with time, thus indicating instability of the vibrating systems. It is where the approximate analytical results do not tell the whole story of the vibrating system, that the differential-analyzer techniques prove most valuable. Modern analog computers are now available with accuracies of better than 1 per cent for the generation of nonlinear functions. (The analyzer used in this paper can claim an accuracy of no better than 5 per cent.) The speed of the generation of solutions and the ease of reproducibility of solutions are additional factors for greater use of analyzer techniques for solving nonlinear vibration problems.

The analyzer results in this paper are presented as points in a plane whose co-ordinates are amplitude versus a squared frequency ratio (abscissa). The amplitude for analyzer results represent $q(t)_{max}$ of the analyzer solution. The analytical results are presented as response curves in the plane of amplitude versus squared frequency ratio. The analyzer results are thus compared with the analytical results over the frequency range of interest in the particular system studied.

The remainder of Part 1 describes the systems to be studied; presents the differential equations solved by the computer and defines the notation used in the paper. Part 2 presents the computer results and compares them with the analytical results. In Part 3 suspected stability criteria for two-degree-of-freedom nonlinear systems are presented and the analyzer results are studied to confirm or refute these criteria. Part 4 is a general discussion of the analyzer results as compared with the analytical results with special emphasis on the discrepancies between the two methods of solution.

(*a*) *Systems Studied.* The generalized system studied in this paper can be represented in mechanical notation as shown in Fig. 1(*a*). The figure shows two masses and two springs with a harmonic disturbing force acting on the left-hand mass. The left-hand mass is referred to as the "main" mass, the left-hand spring the main spring. The right-hand spring is the "coupling" spring, the right-hand mass the "absorber" mass. The springs in this system will exhibit the nonlinearities. A spring which gets stiffer with stretching will be referred to as a hardening spring, Fig. 1(*b*). One that gets less stiff with stretching will be called a softening spring. Thus a spring may be linear, hardening, or softening and will be symbolized by the letters L, H, or S in the code word for any particular system. The code word (developed for reference 2) will be a group of four letters which will characterize the system as to type of spring, and whether or not a disturbing force is acting on the system. As an example, consider a system in which the main spring is a hardening spring, the coupling spring is linear, and the system is vibrating freely; the code word for the system is HOLO. Forced vibrations of this system with the disturbing force acting on the main mass is indicated HILO. Systems with a disturbing force acting on the absorber mass will not be considered. The nonlinearity assumed present in the systems to be treated is the cubic restoring force commonly associated with Duffing's equation of single-degree-of-freedom systems. The possibility that a spring may be nonlinear is represented in Fig. 1(*a*) by the constants μ_1^2 and μ_2^2. Fig. 1(*b*)

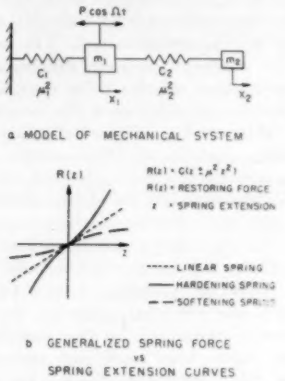

FIG. 1 MODEL OF MECHANICAL SYSTEM AND SPRING FORCE VERSUS SPRING EXTENSION CURVES

gives the expression for a nonlinear restoring force as $c(z \pm \mu^2 z^3)$ where z is the spring extension.

Applying Newton's second law to the system shown in Fig. 1(*a*) the most general equations of motion are as follows

$$m_1\ddot{x}_1 + c_1(x_1 \pm \mu_1^2 x_1^3) - c_2[(x_2 - \quad) \pm \mu_2^2(x_2 - x_1)^3] = P\cos\Omega t$$

$$m_2\ddot{x}_2 + c_2[(x_2 - x_1) \pm \mu_2^2(x_2 - x_1)^3] = 0 \ldots\ldots [1]$$

The coefficients c_1 and c_2 are the usual spring constants, and μ_4 is the square root of the constant coefficient of the nonlinear term and has the units of reciprocal length L^{-1}. Note that with $\mu_1^2 = \mu_2^2 = 0$ the system is reduced to the linear vibration-absorber system with the code words LOLO or LILO representing it. The positive sign used before μ_4^2 indicates a hardening spring, the negative sign a softening one. With $\mu_2^2 = 0$, $\mu_1^2 \neq 0$, and the negative sign used before μ_1^2 the system would be referred to as SOLO for free vibrations, or SILO for forced vibrations. The systems to be studied in this paper are:

1 HOLO, HILO, SOLO, SILO.
2 LOHO, LIHO, LOSO, LISO.

Other systems representable by different letter combinations are not considered herein (e.g., SISO).

(*b*) *Dimensionless Differential Equations Solved by Computer.* The specific differential equations of motion of each system were derived from the general Equations [1] by the choice of the coefficients of the nonlinear terms. These specific equations were then made dimensionless and solved on the electronic analog computer. Mr. Arnold's results were presented by plotting his calculated values of $\bar{Q}_i$, a dimensionless amplitude, versus η^2, a

[2] Numbers in parentheses refer to the Bibliography at the end of the paper.

squared-frequency ratio. To verify these results the amplitudes of the computer solutions $q_i(t)$ are compared with the $\bar{Q}_i$ of the calculated results for corresponding values of η^2.

The dimensionless differential equations solved by the computer for the particular systems are as follows; first for HILO and SILO we have

$$\left.\begin{aligned} &\frac{\ddot{q}_1}{K_1^2} + q_1 \pm \frac{4}{3} q_1^3 - \bar{K}^2\bar{m}(q_2 - q_1) = \bar{s}\cos\Omega t \\ &\frac{\ddot{q}_2}{K_1^2} + \bar{K}^2(q_2 - q_1) = 0 \end{aligned}\right\} \quad \ldots\ldots [2]$$

in which the use of the positive sign before the nonlinear term in the first equation yields the equations for HILO; the negative sign gives the equations for SILO. For free vibrations $\bar{s} = 0$.

Then

$$\left.\begin{aligned} &\frac{\ddot{q}_1}{K_1^2} + q_1 - \bar{m}\bar{K}^2\left[(q_2 - q_1) \pm \frac{4}{3}(q_2 - q_1)^3\right] = \bar{s}\cos\Omega t \\ &\frac{\ddot{q}_2}{K_2^2} + (q_2 - q_1) \pm \frac{4}{3}(q_2 - q_1)^3 = 0 \end{aligned}\right\} \quad \ldots [3]$$

for systems LIHO and LISO, depending on whether the upper or lower sign is used.

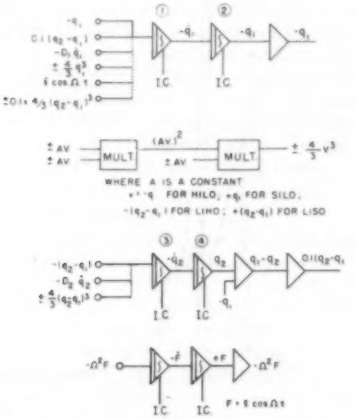

FIG. 2 GENERALIZED COMPUTER CIRCUIT

The computer solved these reduced equations for $\bar{m} = 0.1$, $K_1^2 = K_2^2 = \bar{K}^2 = 1$, $\bar{s} = 0.1$. (System LISO is solved for $\bar{s} = 0.1$ and $\bar{s} = 0.03$.)

A generalized computer circuit is shown in Fig. 2.

2 COMPUTER RESULTS

(*a*) *Computer Results for HILO and HOLO.* Fig. 3 presents the calculated "response" curves for system HILO and HOLO (these are the code words for a system with a hardening main spring and a linear coupling spring). The computer results are indicated by small circles ($\bar{Q}_1$) and crosses ($\bar{Q}_2$) for forced vibrations and by squares ($\bar{Q}_1$) and triangles ($\bar{Q}_2$) for free vibrations. The crosshatched curves indicate that such curves are suspected to be unstable. This will be considered in Part 3.

The computer results for free vibration (HOLO) are in agreement with the calculated results.

The computer results for forced vibrations (HILO) confirm the calculated results in the following ranges, see Fig. 3:

1 $0 < \eta^2 < 0.7$. Computer solutions were obtained for this range of η^2. The amplitudes of these solutions are seen to check the calculated amplitudes quite well in this range.

2 The range of resonance $0.75 < \eta^2 < 0.85$ was avoided.

3 $0.85 < \eta^2 < 1.0$. In this range three possible values for $\bar{Q}_1$ and $\bar{Q}_2$ are calculated. The computer produced results corresponding to the lower branch of calculated response curve, marked 2.

4 $1 < \eta^2 < 3.0$ for curves 2. Computer solutions were obtained for this range of η^2. For η^2 above 1.7 the computer results indicate an amplitude from 10 to 20 per cent greater than the calculated results.

5 $1.65 < \eta^2 < \infty$. In this range three possible solutions are indicated; the curves 2 and the looped curves 3. The computer produced solutions for the curves 2 (mentioned previously) and for the lower loops only of the curves 3.

(*b*) *Computer Results for SILO and SOLO.* Fig. 4 presents the calculated response curves for system SILO (and SOLO). (These are the code words for a system with a softening main spring and a linear coupling main spring.) The computer results are represented by circles ($\bar{Q}_1$) and crosses ($\bar{Q}_2$) for forced vibrations, and squares ($\bar{Q}_1$) and triangles ($\bar{Q}_2$) for free vibrations. The results for free vibrations can be summarized as follows:

Response curves for free vibrations are calculated for the range $0.2 < \eta^2 < 0.73$ and $1.12 < \eta^2 < 1.37$. The computer would produce no stable free vibrations for $\eta^2 < 0.56$. The computer results obtained for the remainder of the range of η^2 fall 10 to 20 per cent below the calculated response curves.

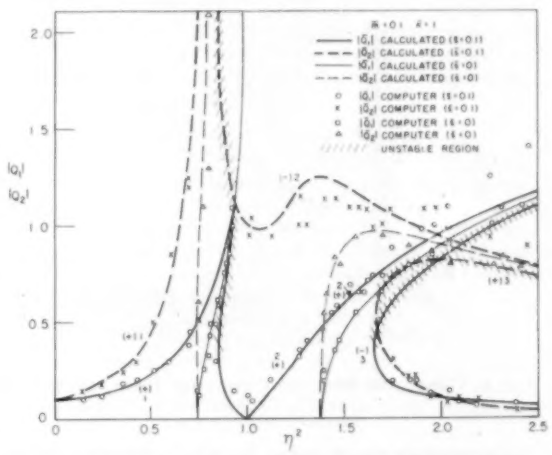

FIG. 3 CALCULATED RESPONSE CURVES AND COMPUTER RESULTS FOR THE HILO SYSTEM
(Hardening main spring.)

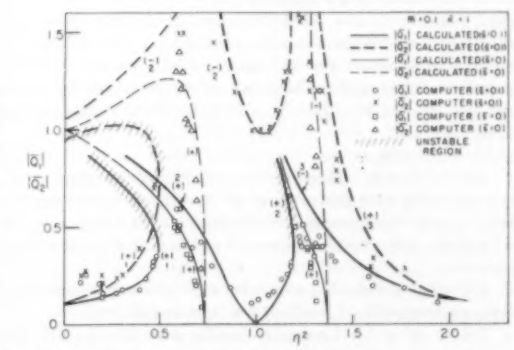

FIG. 4 CALCULATED RESPONSE CURVES AND COMPUTER RESULTS FOR THE SILO SYSTEM
(Softening main spring.)

The computer results for forced vibrations of SILO are as follows:

1 $0 < \eta^2 < 0.5$. Three possible amplitudes for an η^2 are given by the calculated results in the range. They are looped curves 1 and the curves 2. Computer results were obtained for only the lower loop of curves 1. Computer results for curves 2 could not be obtained for $\eta^2 < 0.6$. Note that this corresponds to the range for which free vibrations could not be produced.

2 $0.6 < \eta^2 < 1.0$. The computer produced solutions through this range. A damping term $0.1\,\dot{q}_i$ was required to go through the region of the resonance for Q_2.

3 $1.0 < \eta^2 < 1.2$. Three possible solutions are calculated for this range. The computer produced only the lower branches of curves 2.

4 $1.2 < \eta^2 < 2$. The computer produced results corresponding to curves 3. A damping term was needed in the range of resonance. The computer results fall 20 per cent below the calculated response curves.

(*c*) *Computer Results for LIHO and LOHO.* Fig. 5 presents the calculated response curves and the computer results for system LIHO and LOHO. (This system has a linear main spring and a hardening coupling spring.) The notation is similar to that in Figs. 3 and 4.

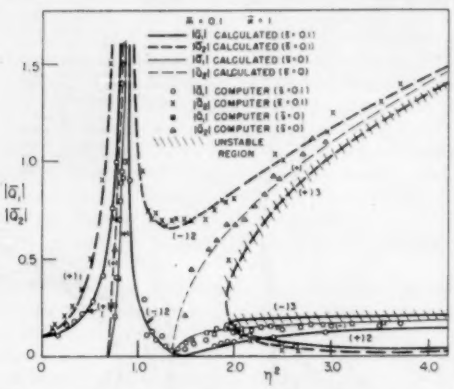

FIG. 5 CALCULATED RESPONSE CURVES AND COMPUTER RESULTS FOR THE LIHO SYSTEM
(Hardening coupling spring.)

The computer results confirm the calculated results over the range from $0 < \eta^2 < 1.96$. Above $\eta^2 = 1.96$ there are three response curves. The computer produced solutions for curves 2 and the lower branches of curves 3.

(*d*) *Computer Results for LISO and LOSO.* The calculated response curves and the computer results for LISO (LOSO) are given in Fig. 6 for an $\bar{s} = 0.1$ and in Fig. 7 for an $\bar{s} = 0.03$. Computer results could not be obtained for free vibrations for the range $1 < \eta^2 < 1.16$. The results for forced vibrations are as follows:

(*a*) $\bar{s} = 0.1$, Fig. 6.

1 $0 < \eta^2 < 0.5$. Three pairs of calculated response curves are given in Fig. 6 for this range of η^2. Computer results were obtained for only the lower branches of the looped response curves marked curves 2. Neither curves 1 nor curves 3 could be produced.

2 $0.5 < \eta^2 < 1.4$. No computer solutions were obtained in this range even with a damping term $0.1\dot{q}_i$ in the circuit.

3 $1.4 < \eta^2 < 3$. Computer results were obtained in this range to correspond with curves 3.

(*b*) $\bar{s} = 0.03$, Fig. 7.

1 $0 < \eta^2 < 0.6$. Three pairs of calculated response curves

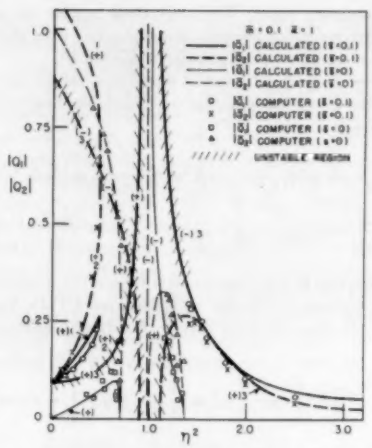

FIG. 6 CALCULATED RESPONSE CURVES AND COMPUTER RESULTS FOR THE LISO SYSTEM
(Softening coupling spring, with $\bar{s} = 0.1$.)

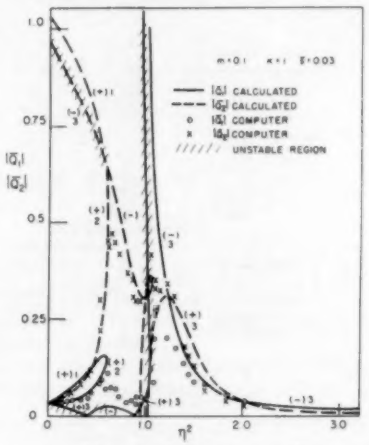

FIG. 7 CALCULATED RESPONSE CURVES AND COMPUTER RESULTS FOR THE LISO SYSTEM
(Softening coupling spring, with $\bar{s} = 0.03$.)

are given for this range of η^2. Computer results were obtained for only the curves marked 2+.

2 $0.6 < \eta^2 < 0.98$. In this range of η^2 only one pair of calculated curves is given. Computer solutions were found to correspond to these curves in this range. The magnitudes of the computer results for $q_1(t)_{max}$ are as much as twice the calculated values however. A damping term of $0.1\dot{q}_i$ was used in this range.

3 $0.98 > \eta^2 < 1.20$. All solutions failed in this range unless a damping term $0.1\dot{q}_i$ was used.

4 $1.20 < \eta^2 < 3.0$. The computer results gotten for this range verify the calculated curves.

3 SUSPECTED CRITERIA FOR NONLINEAR SYSTEMS FOR TWO DEGREES OF FREEDOM

(*a*) *Stability Criteria.* The stability criterion for nonlinear systems of a single degree of freedom requires that the partial derivative of the form $\partial|\bar{Q}|/\partial\bar{s}$ be larger than zero. The suspected stability criteria for nonlinear systems of two degrees of freedom are $\partial|\bar{Q}_i|/\partial\bar{s} > 0$; that is, the partial derivative of each amplitude $\bar{Q}_1$ and $\bar{Q}_2$ with respect to $\bar{s}$ must be positive. If one

(or both) of the partial derivatives is (are) negative the system is suspected to be unstable.

Figs. 3 to 7 which contain the calculated response curves have some of these curves with crosshatch lines over them. This crosshatching indicates that the particular response curve is suspected to be unstable. The remainder of this part of the paper will discuss the computer results in the light of the suspected stability criteria.

(*b*) *Stability of System HILO* (hardening main spring). The suspected unstable response curves for system HILO are indicated by the crosshatched lines in Fig. 3. These are the upper loops of curves 2 ($0.85 < \eta^2 < 1.0$; $\partial \left| \bar{Q}_{1.2} \right| / \partial \bar{s} < 0$) and the upper loops of curves 3 ($1.65 < \eta^2 < \infty$; $\partial \left| \bar{Q}_{1.2} \right| / \partial \bar{s} < 0$). No computer results were obtained to correspond with any of these response curves which are suspected to be unstable. Computer results were obtained to correspond with the remainder of the response curves, all of which are suspected to be stable.

(*c*) *Stability of the System SILO* (softening main spring). The crosshatched curves in Fig. 4 indicate that those response curves are suspected to be unstable. The upper loops of curves 1 ($0.17 < \eta^2 < 0.6$; $\partial \left| \bar{Q}_{1.2} \right| / \partial \bar{s} < 0$) and the upper loops of curves 2 ($1.11 < \eta^2 < 1.26$; $\partial \left| \bar{Q}_{1.2} \right| / \partial \bar{s} < 0$) are so marked. No computer results were obtained for these ranges of η^2.

The free vibrations for this system (SOLO) are of interest with regard to stability criteria because computer solutions for free vibrations for the range $\eta^2 < 0.56$ could not be produced. No reason is suggested for this lack of free vibrations and no suspected stability criterion for free vibrations is presented. This fact is mentioned because forced vibrations could not be produced for nearly the same range of suspected stable curves 2 ($0.3 < \eta^2 < 0.6$) for which free vibrations could not be produced.

The remainder for the computer results for system SILO bear out the suspected stability criteria.

(*d*) *Stability for System LIHO* (hardening coupling spring). The crosshatched response curves in Fig. 5 indicate that the upper loops of curves 3 ($1.94 < \eta^2 < \infty$; $\partial \left| \bar{Q}_{1.2} \right| / \partial \bar{s} < 0$) are suspected to be unstable. No computer solutions could be obtained to correspond with these response curves. Stable computer results were obtained, however, to confirm the suspected stability criteria for the remainder of the response curves.

(*e*) *Stability of System LISO* (softening coupling spring):

1 $\bar{s} = 0.1$, Fig. 6. The crosshatched response curves in Fig. 6 marked 3+ in the range $0 < \eta^2 < 1.4$, are suspected to be unstable since $\partial \left| \bar{Q}_1 \right| / \partial \bar{s} > 0$; $\partial \left| \bar{Q}_2 \right| / \partial \bar{s} < 0$. No computer results were obtained to correspond with response curves 3 in the suspected unstable range. Although the remainder of the response curves are suspected to be stable no computer results could be obtained for the curves 1 ($\eta^2 < 0.5$ to the point where the relative displacement is greater than 0.866).

Computer results could not be produced for free vibrations of this system (LOSO) for the range $1.0 < \eta^2 < 1.16$.

2 $\bar{s} = 0.03$, Fig. 7. The crosshatched response curves marked 3+ in Fig. 7 for the range $0 < \eta^2 < 0.6$ are suspected to be unstable since $\partial \left| \bar{Q}_1 \right| / \partial \bar{s}\, \partial > 0$ and $\partial \left| \bar{Q}_2 \right| / \partial \bar{s} < 0$. No computer results were obtained for these curves. No computer results were obtained for curves 1 although they represent stable vibrations as long as the relative displacement is less than 0.866.

In the range $0.96 < \eta^2 < 1.04$ the upper branches of the curves 3 are unstable. The computer results in the range were obtained only for the lower branches of the curves 3. The range $0.96 < \eta^2 < 1.1$ is a resonance band in which a damping term was needed to produce a computer response. The computer solutions are unstable without damping because the spring extension exceeds the limit of $(\bar{Q}_1 + \bar{Q}_2) = 0.866$. However, the unstable range extended to $\eta^2 = 1.20$ for computer solutions.

Summary of Comparisons Between Suspected Stability Criteria and Computer Results

The suspected stability criteria for nonlinear systems of two degrees of freedom are $\partial \left| \bar{Q}_1 \right| / \partial \bar{s} > 0$; $\partial \left| \bar{Q}_2 \right| / \bar{s} > 0$.

Unstable response curves were suspected if one or both of these criteria did not hold. The following summary relates computer results with suspected stability regions:

(*a*) For system HILO there is complete correspondence between computer results and the suspected stability criteria.

(*b*) For system SILO there is considerable correspondence between the computer results and the suspected stability criteria. The only discrepancy occurs along "curves 2" of Fig. 4 for the range $0.28 < \eta^2 < 0.6$ where response curves are suspected to be stable. No computer results were obtained. Note that this corresponds closely with the range where free vibrations (SOLO) could not be obtained.

(*c*) For system LIHO there is complete correspondence between the computer results and the suspected stability criteria.

(*d*) For system LISO with $\bar{s} = 0.1$ there were no computer results for curves 1 of Fig. 6 although they were suspected to be stable. Free vibrations (LOSO) could not be produced for the range $1.0 < \eta^2 < 1.16$. The computer confirmed the suspected stability criteria for the rest of the response curves.

(*e*) For system LISO with $\bar{s} = 0.03$ there were no computer results for the curves 1 of Fig. 7 although they were suspected to be stable. Except for the resonance range of η^2, the computer confirmed the suspected stability criteria for the remainder of the calculated response curves.

4 Discussion of Computer Results

(*a*) The computer results for the HILO system (hardening main spring) as given in Fig. 3, compare favorably with the calculated response curves. The reason that computer results for both Q_1 and Q_2 are larger than the analytical results for $\eta^2 > 1.7$ is not too clear. It is interesting to note that Mr. Sethna (5) had similar results for a similar system. The fact that the computer results for Q_2 are less than the analytical results in the range $1 < \eta^2 < 1.7$ can only be explained by saying that single-term harmonic approximation yields too large an amplitude. The fact that the analyzer results for free vibration in the range $\eta^2 > 1.3$ follow the calculated results quite well indicates (to the author) that the analyzer results for forced vibrations are close to the true amplitudes.

In the range $0.1 < \eta^2 < 0.4$ superharmonic components are produced on the analyzer solutions. For $\bar{s} = 0.1$ the amplitude of these components is less than 10 per cent of the fundamental. When $\bar{s}$ was increased to 1.0, superharmonics with amplitudes equal to 50 per cent of the fundamental were produced. These are not indicated in Fig. 3. It might also be stated that these harmonics were of third, fifth, and higher orders depending on η^2.

(*b*) The computer results for SILO (softening main spring) given in Fig. 4 for $\eta^2 < 0.2$ show Q_1 and Q_2 at least 50 per cent greater than the calculated response curve. This can be accounted for by harmonic components generated in this range. The computer solutions produce these harmonic components. No obvious reason can be given for the fact that free vibrations cannot be produced by the computer in the range $\eta^2 < 0.6$. It is noted that for both cases of softening springs presented here, in SILO and LISO, that no free vibrations are produced beyond the maximum point in the Q_2-curve for free vibrations. Further investigation into the energy relationships in the systems might clear up these problems.

(*c*) The LIHO system of Fig. 5 has no discrepancies to discuss. The computer results and the calculated response curves are in good agreement. There is some computer evidence of superharmonics for $\eta^2 < 0.3$.

(*d*) The LISO system of Figs. 6 and 7 presents some evidence concerning the "danger zones" and "forbidden regions" sometimes mentioned when considering the LISO system as a nonlinear vibration absorber system. Roberson (6) has defined forbidden regions as starting at such amplitudes where the tangent to the softening spring-characteristic curve becomes horizontal. Arnold (2) allows the softening spring to be extended further to the point of negative restoring force, thus producing a narrower forbidden region than Roberson.

Computer results of Fig. 6 with $\beta = 0.1$ indicate that no solutions are producible for the range $0.5 < \eta^2 < 1.4$ even with heavy damping. Arnold's work indicates a forbidden region of $0.9 < \eta^2 < 1.15$. Computer results indicate that Roberson's forbidden regions are closer to the computer results than Arnold's. Similarly, in Fig. 7 for the LISO system with $\beta = 0.03$ the computer's forbidden region is from $0.6 < \eta^2 < 1.2$ since damping was required to produce a stable solution, whereas Arnold's forbidden region is $0.98 < \eta^2 < 1.08$.

The results of this paper indicate the value of an analog computer for solving the nonlinear-vibration problems arising in nonlinear mechanics. The fact that the computer can easily solve the mathematically untractable differential equations and produce exact solutions as functions of time make such a computer valuable not only for experimental verification of analytical results but also as a tool for probing the unknown areas of the vast field of nonlinear problems.

Acknowledgment

The investigation of nonlinear systems presented in this paper was made under the direction of Prof. Karl Klotter of Stanford University. The subject matter of the paper is part of the results presented in a thesis for the Degree of Engineer received at Stanford University, 1955.

BIBLIOGRAPHY

1 "Steady-State Behavior of Systems Provided With Nonlinear Dynamic Absorbers," by F. R. Arnold, JOURNAL OF APPLIED MECHANICS, Trans. ASME, vol. 77, 1955, pp. 487–492.

2 "Steady-State Oscillations in Nonlinear Systems of Two Degrees of Freedom," by F. R. Arnold, PhD thesis, Stanford University, 1953.

3 "Nonlinear Vibrations in Mechanical and Electrical Systems," by J. J. Stoker, Interscience Publishers, Inc., New York, N. Y., 1950.

4 "A Comprehensive Stability Criterion for Forced Vibrations in Nonlinear Systems," by K. Klotter and E. Pinney, JOURNAL OF APPLIED MECHANICS, Trans. ASME, vol. 75, 1953, pp. 9–12.

5 "Steady-State Motion of One and Two Degrees of Freedom Vibrating Systems With a Nonlinear Restoring Force," by Pathrasp Rustomji Sethna, Proceedings of the Second U. S. National Congress of Applied Mechanics, ASME, 1954, pp. 69–78.

6 "Synthesis of a Nonlinear Dynamic Vibration Absorber," by R. E. Roberson, *Journal of The Franklin Institute*, vol. 254, 1952, no. 3, pp. 205-220.

7 "Analysis of a Nonlinear Dynamic Vibration Absorber," by L. A. Pipes, JOURNAL OF APPLIED MECHANICS, Trans. ASME, vol. 75, 1953, pp. 515–518.

Transient Response of a Nonlinear System by a Bilinear Approximation Method

By E. I. ERGIN[1]

A line-segment approximation for a nonlinear elastic force has been developed which makes it possible to obtain analytical solutions to a number of transient-load problems which formerly could be solved only by graphical or numerical methods. It is shown that for many problems involving even large nonlinearities, two line segments only are sufficient to give satisfactory accuracy. For some problems where the classical analytical approximate methods of Lindstedt or of Kryloff and Bogoliuboff can be applied, it is shown that the bilinear method leads to an improved accuracy.

Nomenclature

The following nomenclature is used in the paper:

- x = displacement
- a = transition constant
- k_1, k_2 = first and second spring constants of bilinear approximation
- x_t = transition amplitude
- t_t = transition time
- $g_1(x)$ = k_1x
- $g_2(x)$ = $k_2x + x_t(k_1 - k_2)$
- $h(x)$ = nonlinear portion of the spring force
- $g(x)$ = linear plus nonlinear spring force: $k_1x + h(x)$
- ϵ = nonlinear parameter
- x_0 = or $x(0)$, initial amplitude
- $\dot{x}_0$ = or $\dot{x}(0)$, initial velocity
- $F(t)$ = forcing function
- τ = pulse length
- ϕ = phase angle
- x_m = maximum deflection
- x_1 = approximate displacement for $|x| < x_t$
- x_2 = approximate displacement for $|x| > x_t$
- r = transition velocity (v_t)
- ω_0 = linear frequency

Introduction

Steady-state forced vibrations of nonlinear systems have been treated by many investigators and a number of special features, such as jump phenomena, ultra and subharmonic resonances, which cannot be found in linear systems, have been discussed. At present, however, no analytical method exists for the treatment of a large class of problems involving transient motions. The present investigation was undertaken primarily to find a procedure for solving pulse-excitation problems in nonlinear systems, and to develop a method which would combine the advantages of engineering accuracy with ease of application. Numerical and graphical methods are, of course, available for such problems. These numerical methods, however, are not only long and tedious to work out, but they almost never exhibit answers in a general form so that the effect of parameter changes can readily be seen.

It is a well-known principle that any function can be approximated by a number of straight line segments. Each line can be determined by its slope and a point through which it passes; this point can be picked to be the transition point where two segments meet. The slopes and the transition points can be determined such that the mean square error between the function and the series of line segments is minimized within a range of variables. The application of this idea to the solution of nonlinear equations is a direct one. Any nonlinearity, which is a function of the dependent variable only, can be described by a number of line segments which are determined to approximate the nonlinear function as closely as possible. The problem, then, resolves itself to the solution of the same number of linear equations as there are line segments, with the proper matching of displacement and velocity at the transition points. The determination of the optimum slopes and the transition points for n line segments requires the solution of $(2n - 1)$ nonlinear algebraic simultaneous equations.

There are certain simplifications which bring this method of linear approximations within the realm of practicability. Most functions encountered in practice can be approximated satisfactorily by two line segments only. In addition, it is possible to choose the slope of the first line segment as the slope of the function at the origin without appreciable loss of accuracy. This simplifies the problem to the determination of the second slope and the transition point only, by minimizing the mean square error.

It will be shown that for any nonlinearity which can be expressed as a power in the dependent variable, the second slope and the transition point are simple functions of the maximum amplitude. It also will be shown that for small nonlinearities the solution of the problem in many cases is insensitive to the exact choice of the maximum deflection used to calculate the parameters of the bilinear approximation, and hence the choice of the linear maximum amplitude for this purpose gives satisfactory results.

One of the significant applications of the concept of the line-segment approximation is in the field of electric analog computing. It has always been difficult to synthesize exactly nonlinear functions for the purposes of electrical analog computations, and approximation by straight line segments has been one of the common ways of handling the problem. The studies of the present paper indicate that, for many such problems, line-segment approximations of a simple form will give results which are well within the accuracy of an analog computer.

The Bilinear Method

A differential equation of the following form will be investigated

$$\frac{d^2x}{dt^2} + k_1x + h(x) = F(t) \quad \ldots\ldots\ldots\ldots [1]$$

[1] At present with Beckman Instruments, Inc., Fullerton, Calif.

Presented at the West Coast Conference of the Applied Mechanics Division, Pasadena, Calif., June 11–16, 1956, of The American Society of Mechanical Engineers.

Discussion of this paper should be addressed to the Secretary, ASME, 29 West 39th Street, New York, N. Y., and will be accepted until January 10, 1957, for publication at a later date. Discussion received after the closing date will be returned.

Note: Statements and opinions advanced in papers are to be understood as individual expressions of their authors and not those of the Society. Manuscript received by ASME Applied Mechanics Division, January 18, 1956. Paper No. 56—APM-37.

It will be shown that Equation [1] can be approximated by two linear equations

$$\frac{d^2x}{dt^2} + g_1(x) = F(t) \quad \text{for } |x| < x_t \ldots\ldots [2]$$

$$\frac{d^2x}{dt^2} + g_2(x) = F(t) \quad \text{for } |x| > x_t \ldots\ldots [3]$$

where $g_1(x)$ and $g_2(x)$ are linear functions of x, and x_t is the transition amplitude where the linear restoring force changes from $g_1(x)$ to $g_2(x)$.

For purposes of simplification $g_1(x)$ is taken to be equal to k_1x. In other words $g_1(x)$ will have a spring constant which is the slope of the nonlinear restoring force at the origin. Then

$$g_1(x) = k_1x, \qquad g_2(x) = k_2x + x_t(k_1 - k_2) \ldots\ldots [4]$$

where x_t and k_2 are as yet undetermined constants. This form of $g_2(x)$ guarantees that at $x = x_t$, $g_1(x) = g_2(x)$; in other words, at the transition point the spring force is continuous.

Terms x_t and k_2 will be determined such that the mean square error ($\overline{E^2}$) between the nonlinear spring force and the bilinear spring force is a minimum. Hence

$$\overline{E^2} = \frac{1}{x_m}\left\{\int_0^{x_t} [g_1(x) - g(x)]^2\,dx + \int_{x_t}^{x_m} [g_2(x) - g(x)]^2\,dx\right\}$$

where $g_1(x)$ and $g_2(x)$ are defined by Equations [4], and x_m is the maximum amplitude of the oscillations. Later on the exact nature of x_m and its importance in the solution of the equation will be discussed more fully.

The condition that $\overline{E^2}$ has an extremum is

$$\frac{\partial(\overline{E^2})}{\partial x_t} = 0 \ldots\ldots [5]$$

and

$$\frac{\partial(\overline{E^2})}{\partial k_2} = 0 \ldots\ldots [6]$$

Since $g_1(x)$ and $g(x)$ are not functions of x_t, Equation [5] becomes

$$\frac{\partial(\overline{E^2})}{\partial x_t} = \frac{1}{x_m}\left\{[g_1(x_t) - g(x_t)]^2 + 2\int_{x_t}^{x_m} [g_2(x) - g(x)]\frac{\partial g_2(x)}{\partial x_t}\,dx - [g_2(x_t) - g(x_t)]^2\right\} = 0$$

Since $g_1(x_t) = g_2(x_t)$ by definition, and

$$\frac{\partial g_2(x)}{\partial(x_t)}$$

is a constant with respect to x, the foregoing equation becomes

$$\int_{x_t}^{x_m} [g_2(x) - g(x)]\,dx = 0 \ldots\ldots [7]$$

Condition [6] will give the equation

$$\int_{x_t}^{x_m} [g_2(x) - g(x)]\frac{\partial g_2(x)}{\partial k_2}\,dx = 0$$

but

$$\frac{\partial g_2(x)}{\partial k_2} = x - x_t$$

hence

$$\int_{x_t}^{x_m} [g_2(x) - g(x)]\,(x - x_t)dx = 0$$

and because of Equation [7] one gets

$$\int_{x_t}^{x_m} [g_2(x) - g(x)]x\,dx = 0 \ldots\ldots [8]$$

Putting the value of $g_2(x)$ in from the Equation [4] and letting $g(x) = k_1(x) + h(x)$, Equations [7] and [8] will simplify to

$$k_2 - k_1 = \frac{2}{(x_m - x_t)^2}\int_{x_t}^{x_m} h(x)dx \ldots\ldots [9]$$

and

$$k_2 - k_1 = \frac{6}{(x_m - x_t)^2(2x_m + x_t)}\int_{x_t}^{x_m} h(x)x\,dx \ldots [10]$$

Simultaneous solution of Equations [9] and [10] will give the required values of k_2 and x_t. If $h(x)$ is a single power in x instead of being a polynomial, the problem can be solved quite easily. Let $h(x) = \epsilon x^n$ where $n > 1$, and let

$$x_t = ax_m \ldots\ldots [11]$$

where a is a proportionality constant. Then Equation [9] becomes

$$k_2 - k_1 = \frac{2\epsilon x_m^{n-1}(1 - a^{n+1})}{(1 - a)^2(n + 1)} \ldots\ldots [12]$$

and Equation [10] becomes

$$k_2 - k_1 = \frac{6\epsilon x_m^{n-1}(1 - a^{n+2})}{(1 - a)^2(a + 2)(n + 2)} \ldots\ldots [13]$$

Solving for a from Equations [12] and [13]

$$a + 2 = \frac{3(n + 1)}{n + 2}\frac{1 - a^{n+2}}{1 - a^{n+1}} \ldots\ldots [14]$$

Since $a < 1$ and $n > 1$, one can take

$$\frac{1 - a^{n+2}}{1 - a^{n+1}} \sim 1$$

in which case Equation [14] simplifies to

$$a = \frac{n - 1}{n + 2} \ldots\ldots [15]$$

where n is the power of the nonlinear term. With this value of a, k_2 can be calculated from Equation [12].

Applications of Method

An equation with cubic nonlinearity in the spring force will now be solved by the bilinear method for various transient exciting functions, and the results will be compared with solutions of known accuracy formed by analytical, numerical, or graphical methods.

The differential equation to be solved is

$$\ddot{x} + k_1x + \epsilon x^3 = F(t) = F_0 = \text{const} \ldots\ldots [16]$$

where $\ddot{x}$ is the second derivative of x with respect to time, and the mass of the system is taken as unity for simplification of the algebra.

Equation [16] will be approximated by the two linear differential equations

$$\ddot{x}_1 + k_1x_1 = F_0 \quad |x| < x_t \ldots\ldots [17]$$

and

$$\ddot{x}_2 + k_2x_2 + x_t(k_1 - k_2) = F_0 \quad |x| > x_t \ldots\ldots [18]$$

The initial conditions for x_1 will be
At $t = 0$

$$x_1(0) = \dot{x}_1(0) = 0$$

and the conditions for x_2 at $t = t_i$

$$x_2(t_i) = x_1(t_i) \quad \text{and} \quad \dot{x}_2(t_i) = \dot{x}_1(t_i) \ldots\ldots\ldots [19]$$

Terms x_i and k_2 are determined from Equations [11] and [12], respectively, and the constant a used in Equations [11] and [12] is given by Equation [15]. The solution of Equation [17] satisfying the initial conditions will be

$$x_1 = \frac{F_0}{k_1}(1 - \cos \omega_1 t) \ldots\ldots\ldots\ldots [20]$$

where $\omega_1 = \sqrt{k_1}$, since mass was taken as unity.
For $x_1 = x_i$

$$x_i = \frac{F_0}{k_1}(1 - \cos \omega_1 t_i)$$

or

$$t_i = \frac{1}{\omega_1} \cos^{-1}\left[1 - \frac{k_1 x_i}{F_0}\right] \ldots\ldots\ldots\ldots [21]$$

hence

$$\dot{x}_1(t_i) = \frac{F_0 \omega_1}{k_1} \sin \omega_1 t_i = \sqrt{F_0 x_i \left(2 - \frac{k_1 x_i}{F_0}\right)} \ldots\ldots [22]$$

The solution of Equation [18] is

$$x_2 = \frac{F_0 + x_i(k_2 - k_1)}{k_2} + A \cos(\omega_2 t + \phi) \ldots\ldots [23]$$

where $\omega_2 = \sqrt{k_2}$.
In order to satisfy the conditions of Equation [19]

$$x_i = \frac{F_0 + x_i(k_2 - k_1)}{k_2} + A \cos(\omega_2 t_i + \phi) \ldots\ldots [24]$$

$$\dot{x}_1(t_i) = \sqrt{\left[F_0 x_i \left(2 - \frac{k_1 x_i}{F_0}\right)\right]} = -A\omega_2 \sin(\omega_2 t_i + \phi) \ldots\ldots [25]$$

A and ϕ are found by solving the two simultaneous Equations [24] and [25]. Thus

$$A = \frac{F_0}{k_2} \sqrt{\left[1 + (k_2 - k_1)\left(2\frac{x_i}{F_0} - k_1 \frac{x_i^2}{F_0^2}\right)\right]} \ldots [26]$$

and

$$\phi = \left\{\tan^{-1} \sqrt{\frac{k_2 \frac{x_i}{F_0}\left(2 - \frac{x_i}{F_0}\right)}{1 - k_1 \frac{x_i}{F_0}}}\right\} - \omega_2 t_i \ldots\ldots [27]$$

So far nothing has been said about the choice of maximum deflection x_m from which the second slope k_2 and the transition amplitude x_i are determined. It will be shown that this choice is not very critical and an error relationship for the maximum deflection for any power of nonlinearity will be derived.

Assume that the actual maximum deflection $\bar{x}_m$, as found from the solution of the bilinear equations, differs by an amount δ from the assumed maximum deflection x_m such that $\delta/\bar{x}_m \ll 1$. Hence

$$x_m = \bar{x}_m + \delta \quad \text{and} \quad x_m^s = \bar{x}_m^s \left(1 + s\frac{\delta}{\bar{x}_m}\right) \ldots\ldots [28]$$

where s is any power.

The differential equations of motion were given by Equations [17] and [18]. Letting $\dot{x}_1 = v_1$ and $\dot{x}_2 = v_2$ and integrating Equation [17] between the limits of $0 < x_1 < x_i$, and Equation [18] between $x_i < x_2 < \bar{x}_m$ where $\bar{x}_m$ is the maximum deflection defined by the point where the velocity is zero, we obtain

$$\frac{1}{2} v_i^2 + \frac{k_1}{2} x_i^2 = F_0 x_i \ldots\ldots\ldots\ldots [29]$$

(since the initial displacement and the velocity are zero), and

$$-\frac{1}{2} v_i^2 + \frac{k_2}{2}(\bar{x}_m^2 - x_i^2) - x_i(k_2 - k_1)(\bar{x}_m - x_i) = F_0(\bar{x}_m - x_i) \ldots\ldots [30]$$

Combining Equations [29] and [30] and putting the value of $(k_2 - k_1)$ in from Equation [12], the value of

$$x_i = a x_m = a\bar{x}_m\left(1 + x\frac{\delta}{\bar{x}_m}\right)$$

and

$$(1 - a^{n+1})\left\{\frac{2 + a}{(1 - a)^2}\frac{\delta}{\bar{x}_m} + 1\right\}\frac{\epsilon \bar{x}_m^n}{n + 1} + \frac{k_1}{2}\bar{x}_m - F_0 = 0 \ldots\ldots [31]$$

Equation [31] clearly shows that any small change in δ will not affect the value of $\bar{x}_m$ as found from this equation as long as $\delta/\bar{x}_m < 1$, or better yet, is of the order of ϵ. This means that the original assumption of $\bar{x}_m$ can be made quite freely as long as it is in the neighborhood of the correct deflection.

This suggests that one can choose, for example, the linear maximum deflection in order to calculate the second slope k_2 and the transition point x_i without any appreciable loss of accuracy. For very large nonlinearities where the actual maximum deflection may be very different from the linear one, an iterative procedure can be developed.

If δ is taken as zero in Equation [31]

$$(1 - a^{n+1})\frac{\epsilon \bar{x}_m^n}{n + 1} + \frac{k_1}{2}\bar{x}_m - F_0 = 0 \ldots\ldots [32]$$

is obtained. This is the best that can be done by the bilinear approximation. In other words, the maximum deflection calculated from Equation [32] will be the most accurate possible using the bilinear method. The exact maximum-deflection equation can be obtained, in this particular case, by integrating the original nonlinear Equation [16]. This integration will give

$$\frac{\epsilon}{n + 1} x_m^n + \frac{k_1}{2} x_m - F_0 = 0 \ldots\ldots [33]$$

From the comparison of Equations [32] and [33] the difference is seen to be

$$-\frac{\epsilon}{n + 1} a^{n+1} \bar{x}_m^n$$

Since $a < 1$, as n gets large the foregoing difference will approach zero. This means that for a given maximum deflection the accuracy of the solution will increase with increasing powers of nonlinearity.

For a cubic nonlinearity ($n = 3$) the two amplitude equations are of the form

$$0.50\epsilon x_m^3 + k_1 x_m - 2F_0 = 0 \text{ (exact)} \ldots\ldots [34]$$

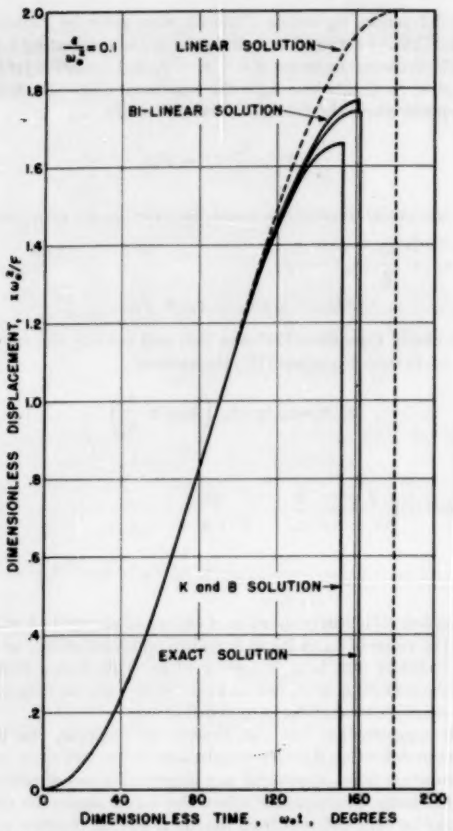

FIG. 1 COMPARATIVE HALF-PERIOD SOLUTIONS OF THE DIFFERENTIAL EQUATION $\ddot{x} + \omega_0^2 x + \epsilon x^3 = F$

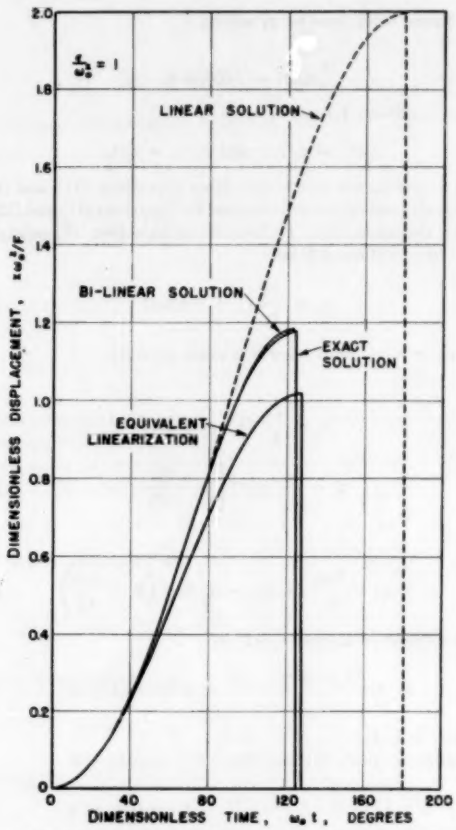

FIG. 2 COMPARATIVE HALF-PERIOD SOLUTIONS OF THE DIFFERENTIAL EQUATION $\ddot{x} + \omega_0^2 x + \epsilon x^3 = F$

$$0.487\epsilon x_m^3 + k_1 x_m - 2F_0 = 0 \text{ (bilinear)} \quad \ldots\ldots\ldots [35]$$

It is seen that even for very large nonlinearities such that the linear term $k_1 x_m$ can be neglected compared to the nonlinear term ϵx_m^3, the error in maximum amplitude is only about 1 per cent.

In the step-function response, then, for any power n and coefficient ϵ of the nonlinearity, the error in maximum deflection will always be less than

$$\frac{a^{n+1}}{3} \times 100 \text{ per cent}$$

Two numerical examples have been worked out for this case, and the results for a quarter period are shown in Figs. 1 and 2. These figures also include the linear solution, the exact solution, a solution obtained by the Kryloff procedure (1),[3] and a solution obtained by the method of equivalent linearization (2) for comparative purposes. In Fig. 1

$$\frac{\epsilon}{k_1} = \frac{\epsilon}{\omega_0^2} = 0.1$$

and in Fig. 2

$$\frac{\epsilon}{k_1} = \frac{\epsilon}{\omega_0^2} = 1 \text{ (large nonlinearity)}$$

[3] Numbers in parentheses refer to the Bibliography at the end of the paper.

In both of these instances the bilinear approximation follows the exact solution very closely.

The exact solution is obtained by performing a numerical integration of the integral

$$t = \int_0^x \frac{dx}{\sqrt{\left(2F_0 x - k_1 x^2 - \frac{\epsilon}{2} x^4\right)}}$$

It is interesting to note that if the exact maximum amplitude of 1.74 (for $k_1 = 1$, $\epsilon = 0.1$, and $F_0 = 1$) is used to determine the parameters of the bilinear approximation, the calculated maximum amplitude will be 1.75. If, however, instead of the exact maximum amplitude of 1.74, the linear maximum amplitude of 2 is used to calculate the parameters of the bilinear approximation, the resulting equations will give a maximum deflection of 1.73, which is still within 1 per cent of the exact maximum deflection. This fact numerically illustrates the flexibility in the choice of the maximum amplitude upon which the parameters of the bilinear approximation are based.

From the foregoing solution we also may obtain the solution to the square pulse-excitation problem. Suppose that $F(t)$ in Equation [16] is replaced by

$$F(t) = F = \text{const} \quad \text{for} \quad 0 < t < \tau = \frac{\pi}{\omega_0}$$

$$F(t) = 0 \quad \text{for} \quad t > \tau = \frac{\pi}{\omega_0}$$

The treatment of this rectangular pulse is quite simple since the step-function response and the homogeneous solutions are readily available. A particular example has been solved and the results are shown in Fig. 3 (3). For comparison purposes the linear solution is drawn on the same graph. The effect of nonlinearity on both the frequency and the amplitude becomes quite apparent.

Half-Sine Pulse Excitation

We next replace $F(t)$ in Equation [16] by

$$F(t) = \sin \omega t \quad \text{for} \quad 0 < t < \tau$$

$$F(t) = 0 \quad \text{for} \quad t > \tau$$

Here the bilinear method is expanded into a region where no analytic solution, approximate or otherwise, has been obtained. The only available tool for such problems as these has been the use of graphical integration or numerical iteration methods, both of which are very time consuming (4, 5).

To check the results obtained by the bilinear approximation, exact solutions to the problems are obtained by numerical iteration of the differential equations.

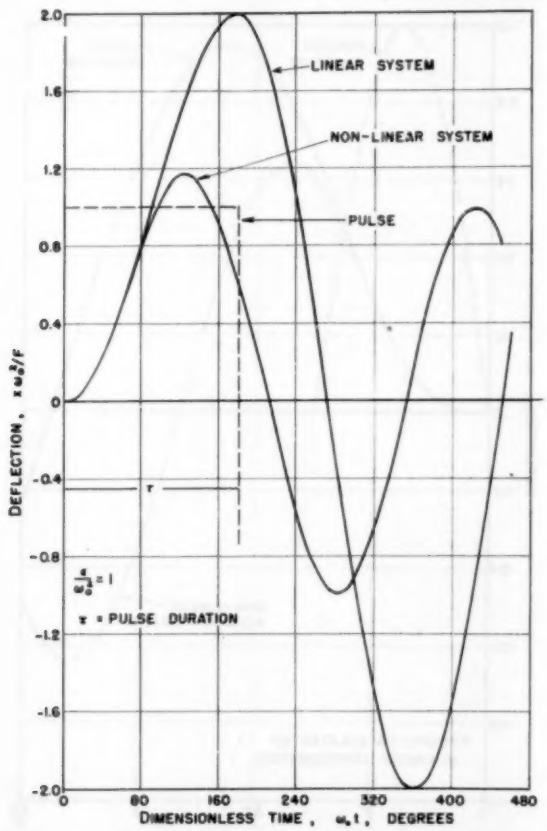

Fig. 3 Effect of Nonlinearity on the Rectangular Pulse Response of the Differential Equation

$$\ddot{x} + \omega_0^2 x + \epsilon x^3 = \begin{cases} F & 0 < t < \frac{\pi}{\omega_0} \\ 0 & t > \frac{\pi}{\omega_0} \end{cases}$$

Let the differential equation of motion be

$$\ddot{x} + k_1 x + \epsilon x^3 = \sin \omega t \quad 0 < t < \frac{\pi}{\omega} \qquad [36]$$

$$\ddot{x} + k_1 x + \epsilon x^3 = 0 \qquad t > \frac{\pi}{\omega} \qquad [37]$$

For $t = \pi/\omega$ the solutions of the differential Equations [36] and [37] must correspond. The initial conditions are

At $t = 0$

$$x(0) = \dot{x}(0) = 0 \qquad [38]$$

Since an exact solution of Equation [37] exists, the main interest lies in finding an approximation to the differential Equation [36] such that the motion during the pulse can be obtained. The complete analysis requires the solution of a transcendental equation and hence cannot be done in a general form.

In the following example a numerical solution will be worked out by the bilinear method to show the amount of work involved in such a calculation.

Let the differential equation be

$$\ddot{x} + x + x^3 = \begin{cases} \sin 2t & 0 < t < \frac{\pi}{2} \\ 0 & t > \frac{\pi}{2} \end{cases} \qquad [39]$$

For a cubic nonlinearity the transition amplitude was calculated to be

$$x_t = 0.4 x_m \qquad [40]$$

and the second slope

$$k_2 = k_1 + 1.35 x_m^2 = 1 + 1.35 x_m^2 \qquad [41]$$

(x_m) is calculated as the maximum amplitude of the linear solution of Equation [39], hence

$$\ddot{x} + x = \sin 2t$$

The solution with the required initial conditions will be

$$x = \frac{1}{3}(2 \sin t - \sin 2t) \qquad [42]$$

The maximum value of x in Equation [42] is $x_m = 0.667$. Hence

$$x_t = 0.267 \text{ and } k_2 = 1.60 \qquad [43]$$

The two bilinear equations to be solved are

$$\ddot{x}_1 + x_1 = \sin 2t; \quad x_1(0) = \dot{x}_1(0) = 0 \quad \text{for} \quad |x| < x_t \qquad [44]$$

$$\ddot{x}_2 + 1.6 x_2 - 0.16 = \sin 2t; \quad x_2(t_t) = x_1(t_t); \quad \dot{x}_2(t_t) = \dot{x}_1(t_t) \qquad [45]$$

where t_t is the transition time, the time which it takes x_1 to reach the value x_t. The solution of Equation [44] is

$$x_1 = \frac{1}{3}(2 \sin t - \sin 2t) \qquad [46]$$

from which the transition parameters can be determined as

$$x_1(t_t) = x_t = 0.267, \quad t_t = 58°, \quad \dot{x}_1(t_t) = 0.646 \qquad [47]$$

The solution of Equation [45] which satisfies the conditions

$x_2(t_1) = 0.267$ and $\dot{x}_2(t_1) = 0.646$ is

$$x_2 = 0.1 + 0.582 \sin(\sqrt{1.6}\, t - 4.8^0) - \frac{1}{2.4} \sin 2t \ldots [48]$$

The displacement and the velocity at the end of the pulse can be calculated by letting $t = \pi/2$

$$\left.\begin{aligned} x_2\left(\frac{\pi}{2}\right) &= 0.651 \\ \text{and} \\ \dot{x}_2\left(\frac{\pi}{2}\right) &= 0.592 \end{aligned}\right\} \ldots\ldots\ldots\ldots [49]$$

The values obtained by numerical iteration to four-place accuracy are

$$x\left(\frac{\pi}{2}\right) = 0.6518 \quad \text{and} \quad \dot{x}\left(\frac{\pi}{2}\right) = 0.6001$$

The approximate results obtained are within about $^1/_2$ per cent of the exact amplitude and $1^1/_2$ per cent of the exact velocity when the nonlinear force is about 60 per cent of the linear one at the maximum deflection point.

If more than one cycle of the system occurs during the pulse, a cycle-by-cycle analysis is necessary to obtain the complete solution. In the following example the nonlinearity is increased to investigate its effect on the accuracy of the solution.

Let the differential equation of motion be

$$\left.\begin{aligned} \ddot{x} + x + 5x^3 &= \sin 2t \quad 0 < t < \frac{\pi}{2} \\ &= 0 \qquad t > \frac{\pi}{2} \end{aligned}\right\} \ldots\ldots [50]$$

Since the effect of nonlinearity is to decrease the maximum amplitude, x_m will be assumed to be 0.60 instead of 0.667 which was the linear maximum displacement. This helps the results to converge faster, and, as it will be shown later, makes it possible to get an accurate answer after only one step.

Then

$$x_1 = 0.24 \quad \text{and} \quad k_2 = 3.5 \ldots\ldots\ldots\ldots [51]$$

If one goes through the process of solving the two linear equations

$$\ddot{x}_1 + x_1 = \sin 2t \quad |x| < x_1 \ldots\ldots\ldots\ldots [52]$$

$$\ddot{x}_2 + 3.5x_2 + 0.6 = \sin 2t \quad |x| > x_1 \ldots\ldots\ldots [53]$$

and matching the boundary conditions at $t = t_1$ (the transition point) the solutions are found to be

$$x_1 = \frac{1}{3}(2 \sin t - \sin 2t) \quad 0 < t < t_1 \ldots\ldots\ldots [54]$$

$$x_2 = 1.98 \sin(\sqrt{3.5}\, t - 1^0) + 0.172 - 2 \sin 2t$$

$$t_1 < t < \frac{\pi}{2} \ldots\ldots [55]$$

where $t_1 = 55.5^0$. The conditions at the end of the pulse are determined by letting $t = \pi/2$ and finding the displacement and the velocity from Equation [55]. Hence

$$x\left(\frac{\pi}{2}\right) = 0.581 \quad \text{and} \quad \dot{x}\left(\frac{\pi}{2}\right) = 0.38 \ldots\ldots [56]$$

It is seen that the increased nonlinearity has caused a reduction of about 13 per cent in amplitude and 47 per cent in velocity at the end of the pulse.

The accuracy of the results at any point can be checked readily without the necessity of obtaining an exact solution to the differential Equation [50]. Since Equations [54] and [55] satisfy the initial conditions, their value at any point can be substituted into the differential equation and an error in acceleration at that particular point calculated.

For the example solved above at $t = \pi/2$ the error in the differential Equation [50] is about 2 per cent; this means that the error in displacement must necessarily be less than this.

Fig. 4 shows a comparison of the bilinear and the exact solutions for the case just treated. The linear solution is also indicated on the graph for comparison purposes.

For any pulse shape and duration, of course, one can theoretically always solve the problem by the use of numerical or graphical integration methods. The solution by the bilinear approximation is also theoretically possible, but becomes more complicated than it was for the simpler cases treated above. However, by making the bilinear approximation before resorting to a graphical solution, the work can be considerably reduced, and the accuracy of the solution can be improved (6).

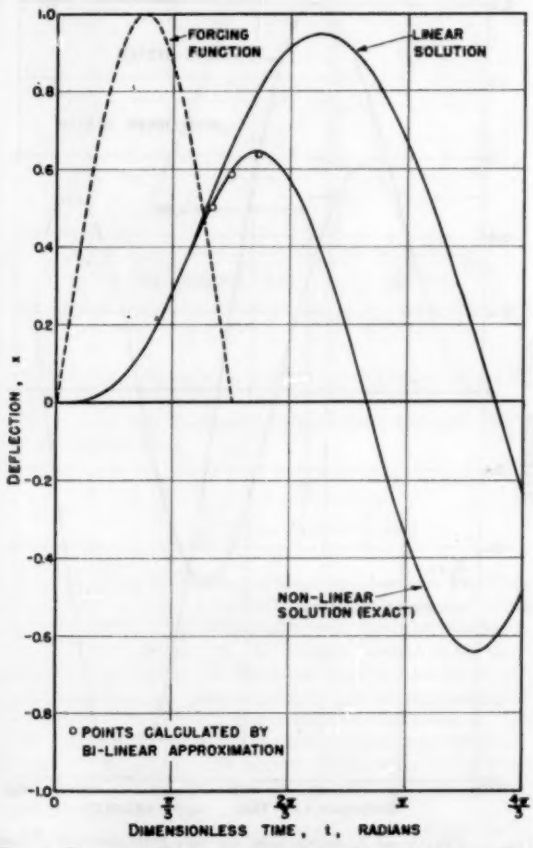

FIG. 4 EFFECT OF NONLINEARITY ON THE SOLUTION OF THE DIFFERENTIAL EQUATION

$$\ddot{x} + x + 5x^3 = \begin{cases} \sin 2t & 0 < t < \frac{\pi}{2} \\ 0 & t > 0 \end{cases}$$

Conclusions

The foregoing examples have shown that for certain types of nonlinear problems, the bilinear approximation gives more accurate results than the classical perturbation methods, and may be easier to apply. The accuracy obtained by the bilinear method is for many problems not significantly decreased for large nonlinearities. For the pulse-excitation problems solved the bilinear method is faster than graphical or numerical methods, and the limitations on the size of the nonlinearities are not severe. The method may also be adapted to an iterative procedure if an improvement in accuracy is desired.

Acknowledgment

The author wishes to thank Drs. D. E. Hudson and T. K. Caughey of the Division of Engineering, California Institute of Technology, for patient guidance and many helpful suggestions in the execution of the work and the final preparation of this paper.

BIBLIOGRAPHY

1 "Introduction to Non-Linear Mechanics," by N. Kryloff and N. Bogoliuboff, Princeton University Press, Princeton, N. J., 1947.

2 "Introduction to Non-Linear Mechanics," by N. Minorsky, J. W. Edwards Bros., Inc., Ann Arbor, Mich., 1947.

3 "Transient Response of a Non-Linear Spring-Mass System," by E. I. Ergin, PhD thesis, California Institute of Technology, Pasadena, Calif., 1954.

4 "On a General Method of Solving Second-Order Ordinary Differential Equations by Phase-Plane Displacements," by L. S. Jacobsen, Journal of Applied Mechanics, Trans. ASME, vol. 74, 1952, pp. 543–553.

5 "An Iterative Numerical Method for Nonlinear Vibrations," by J. E. Brock, Journal of Applied Mechanics, Trans. ASME, vol. 73, 1951, pp. 1–11.

6 "Response of an Elastically Non-Linear System to Transient Disturbances," by R. L. Evaldson, R. S. Ayre, and L. S. Jacobsen, *Journal of the Franklin Institute*, vol. 248, 1949, pp. 548–562.

Design Data and Methods

It is important that the data contained in technical papers be made readily available to designing engineers. In order to satisfy these needs of industry, this section of the Journal includes a concise presentation of data and information drawn chiefly from papers previously published by the Applied Mechanics Division of The American Society of Mechanical Engineers.

Biezeno Pressure Vessel Heads

By R. A. STRUBLE,[1] CHICAGO, ILL.

The equation of thin-walled pressure vessel heads with constant maximum shear stress throughout is derived. Such heads, used on cylindrical vessels with uniform internal pressure, were first conceived by Biezeno[2] in 1922 who gave a semigraphical prescription for determining the head shape.

Introduction

HEADS for cylindrical vessels are generally surfaces of revolution about the vessel axis joined tangentially to the vessel at one end while closing smoothly at the other. A plane containing the axis of revolution is called a meridional plane and the trace of the head in a meridional plane is referred to as the *shape* of the head. The radius of curvature of the head at a point P, Fig. 1, in a meridional plane will be denoted by R_2. A plane that is normal to the meridional plane in the direction of R_2 will be called a circumferential plane. The radius of curvature of the head at P in this plane will be denoted by R_1. For thin-walled vessels with bending stresses neglected, the principal tangential stresses are given by the formulas[3]

$$\sigma_1 = \frac{pR_1}{2h}\left(2 - \frac{R_1}{R_2}\right) \quad [1]$$

$$\sigma_2 = \frac{pR_1}{2h} \quad [2]$$

where σ_1 is the circumferential plane stress, σ_2 the meridional plane stress, h the head thickness, and p the internal pressure. The stresses σ_1 and σ_2 are tensile when positive and compressive when negative. The radii of curvature R_1 and R_2 are positive as shown in Fig. 1, and are positive throughout convex heads. Thus σ_2 is always tensile while σ_1 is tensile only for $R_1 < 2R_2$ and compressive for $R_1 > 2R_2$. When σ_1 is compressive, the maximum

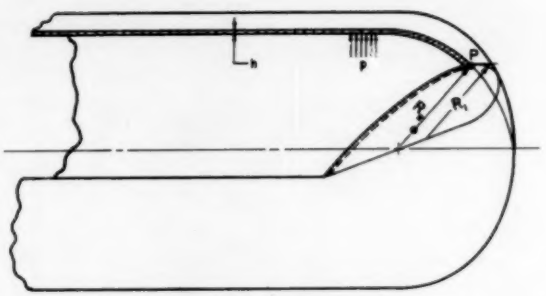

Fig. 1 Nomenclature of a Pressure Vessel Head

shear stress at P is given[3] by one half the difference between the two principal stresses

$$\sigma_s = \frac{1}{2}(\sigma_2 - \sigma_1) = \frac{pR_1}{4h}\left(\frac{R_1}{R_2} - 1\right) \quad [3]$$

When both principal stresses are tensile, the maximum shear stress is one half the maximum of the principal stresses. In particular, the maximum shear stress in the cylindrical portion of the vessel is

$$(\sigma_s)_{cyl} = \frac{pR}{2h} \quad [4]$$

where R is the vessel radius.

Biezeno Heads

A Biezeno head is defined as a thin-walled vessel head of constant thickness with a shape such that under uniform internal pressure, the maximum shear stress throughout the head is constant. In the following, it will be seen that a Biezeno head consists of a knuckle and a cap. The cap will be spherical, while the knuckle will be a transition section joining the spherical cap to the cylindrical vessel. The Biezeno head thus resembles the torispherical head which is a spherical cap with a knuckle of constant meridional curvature. Discontinuities in the meridional curvature occur at the vessel-knuckle juncture and at the knuckle-cap juncture introducing, in practice, secondary bending stresses near these points.

Derivation of the Equation of Biezeno Heads

The equation of the knuckle is obtained from Equation [3] which may be written

[1] Assistant Professor of Mathematics, Illinois Institute of Technology.

[2] "Bijdrage tot de berckening van ketelfronten," by C. B. Biezeno, *Ingenieur*, Haag 37, 1922, pp. 781–784.

[3] "Advanced Strength of Materials," by J. P. den Hartog, McGraw-Hill Book Company, Inc., New York, N. Y., 1952.

Discussion of this paper should be addressed to the Secretary, ASME, 29 West 39th Street, New York, N. Y., and will be accepted until January 10, 1957, for publication at a later date. Discussion received after the closing date will be returned.

Note: Statements and opinions advanced in papers are to be understood as individual expressions of their authors and not those of the Society. Manuscript received by ASME Applied Mechanics Division, April 13, 1956.

$$\frac{4h\sigma_s}{p} = \frac{R_1^2}{R_2} - R_1 \quad [5]$$

where $4h\sigma_s/p$ is maintained constant. In terms of the rectangular co-ordinates of Fig. 2, with

$$R_2 = -\frac{\left[1 + \left(\frac{dy}{dx}\right)^2\right]^{3/2}}{\frac{d^2y}{dx^2}} \text{ and } R_1 = y\sqrt{1 + \left(\frac{dy}{dx}\right)^2}$$

Equation [5] becomes

$$-\frac{4h\sigma_s}{yp} = \sqrt{1 + \left(\frac{dy}{dx}\right)^2} + \frac{y\,\frac{d^2y}{dx^2}}{\sqrt{1 + \left(\frac{dy}{dx}\right)^2}} \quad [6]$$

The right-hand member of Equation [6] may be recognized as the y-derivative of

$$R_1 = y\sqrt{1 + \left(\frac{dy}{dx}\right)^2}$$

and hence upon integration we have

$$-\frac{4h\sigma_s}{p}\ln y = y\sqrt{1 + \left(\frac{dy}{dx}\right)^2} + c \quad [7]$$

where c is a constant. The boundary conditions at the vessel juncture, $dy/dx = 0$ for $y = R$, require that

$$c = -R - \frac{4h\sigma_s}{p}\ln R$$

so that Equation [7] becomes

$$\frac{R_1}{R} = \frac{y}{R}\sqrt{1 + \left(\frac{dy}{dx}\right)^2} = 1 - 4\,\frac{h\sigma_s}{Rp}\ln\frac{y}{R}$$
$$= 1 - \beta\ln\left(\frac{y}{R}\right)^2 \quad [8]$$

The quantity

$$\beta = \frac{2h\sigma_s}{Rp} = \frac{\sigma_s}{(\sigma_s)_{cyl}}$$

is the ratio of the maximum shear stress in the knuckle to the maximum shear stress in the cylindrical vessel of the same thickness. The variables in Equation [8] may be separated to yield

$$dx = \frac{-\frac{y}{R}\,dy}{\sqrt{\left[1 - \beta\ln\left(\frac{y}{R}\right)^2\right]^2 - \left(\frac{y}{R}\right)^2}} \quad [9]$$

Integration of Equation [9] results in the equation of the knuckle

$$\frac{x}{R} = \frac{1}{2}\int_{\left(\frac{y}{R}\right)^2}^{1} \frac{dt}{\sqrt{(1 - \beta\ln t)^2 - t}} \quad [10]$$

where $t = (y/R)^2$. The knuckle extends to a point E, Fig. 2, where the circumferential plane stress σ_1 becomes tensile so that the maximum shear stress is no longer given by Equation [3]. This point is determined by the condition

$$R_1 = 2R_2 \quad [11]$$

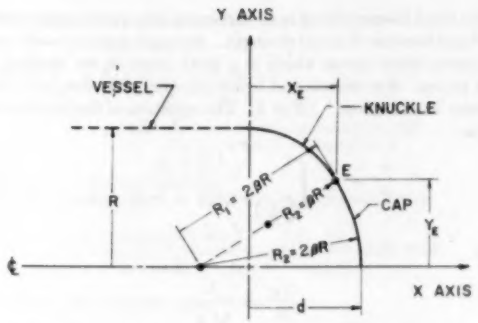

FIG. 2 GEOMETRY OF A BIEZENO PRESSURE VESSEL HEAD

or from Equation [5], by the condition

$$\frac{R_1}{R} = \frac{4h\sigma_s}{Rp} = 2\beta \quad [12]$$

The y-co-ordinate of E is given by Equations [8] and [12] as

$$\frac{y_E}{R} = \frac{1}{e^{\left(1 - \frac{1}{2\beta}\right)}} \quad [13]$$

The ratio β may vary from 1/2 to $+\infty$. The limiting value $\beta = 1/2$ corresponds to a vanishing knuckle, $y_E/R = 1$, where the head becomes simply a hemisphere of radius R. The limiting value $\beta = +\infty$ corresponds in some sense to a largest knuckle with $y_E/R = 1/e$ but such that the entire head becomes a flat disk. Hence, Biezeno heads vary in depth from a maximum of R represented by the hemisphere to a minimum of zero represented by the flat disk. The head is completed by adjoining a spherical cap of thickness h and of radius $R_1 = 4h\sigma_s/p$ at the point E. This value of R_1 is the limiting value of the circumferential radius on the knuckle side of E so that the tangent is continuous across the juncture. In addition, the maximum shear stress in the spherical cap is given by

$$(\sigma_s)_{cap} = \frac{pR_1}{4h} = \sigma_s$$

Hence the maximum shear stress is maintained constant throughout the entire head. The meridional radius of curvature at E jumps from a value of $R_2 = R_1/2 = \beta R$, Equations [11], [12], on the knuckle side to a value of $R_2 = R_1 = 2\beta R$ on the cap side. The principal stresses σ_1 and σ_2 in the knuckle are given through Equations [1], [2], [3], and [8] and may be written

$$\frac{\sigma_1}{(\sigma_s)_{cyl}} = -\left[2\beta + \beta\ln\left(\frac{y}{R}\right)^2 - 1\right]$$

$$\frac{\sigma_2}{(\sigma_s)_{cyl}} = 1 - \beta\ln\left(\frac{y}{R}\right)^2$$

In the spherical cap, the principal stresses are, of course, constant and given by

$$\frac{\sigma_1}{(\sigma_s)_{cyl}} = \frac{\sigma_2}{(\sigma_s)_{cyl}} = 2\beta$$

THE IDEAL BIEZENO HEAD

An ideal Biezeno head is defined as a Biezeno head with its maximum shear stress equal to that of the maximum shear stress in the cylindrical vessel to which it is joined.

The ideal Biezeno head is of particular importance since vessel and head become of equal strength. Strength here is based upon maximum shear stress which is a good criterion for yielding in steel plates. For vessels and heads of equal thickness, the ideal Biezeno head is given by $\beta = 1$. The equation of the knuckle becomes

$$\frac{x}{R} = \frac{1}{2}\int_{\left(\frac{y}{R}\right)^2}^{1} \frac{dt}{\sqrt{(1 - \ln t)^3 - t}} \quad [14]$$

with

$$\frac{y_E}{R} = \frac{1}{\sqrt{e}}$$

The integral in Equation [14] is not tabulated but may be evaluated by standard numerical methods. The singularity at $t = 1$ may be removed by the substitution

$$t = \cos\theta$$

so that Equation [14] becomes

$$\frac{x}{R} = \frac{1}{2}\int_{0}^{\arccos\left(\frac{y}{R}\right)^2} \frac{\sin\theta}{\sqrt{(1 - \ln\cos\theta)^3 - \cos\theta}} d\theta \quad [15]$$

The integrand in Equation [15] is now finite throughout with the limiting value $\sqrt{2/3}$ for $\theta \to 0$. A plot of the integrand is given in Fig. 3, together with a plot of the quantity

$$0.30 + 0.52\cos\theta \quad [16]$$

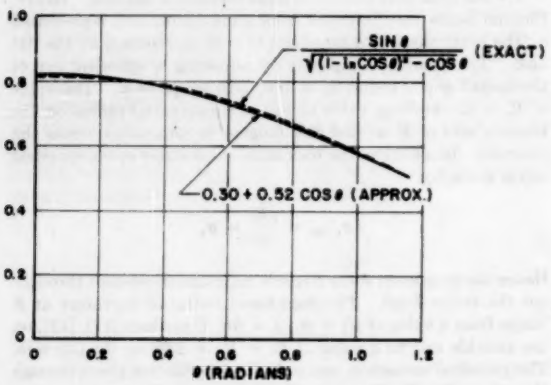

FIG. 3 EXACT AND APPROXIMATE INTEGRAND IN EQUATION [15]

which is an excellent approximation to the integrand. Using Equation [16] in [15] and integrating, there results

$$\frac{x}{R} = 0.15 \arccos\left(\frac{y}{R}\right)^2 + 0.26\sqrt{1 - \left(\frac{y}{R}\right)^4} \quad [17]$$

Equation [17] is accurate to within ½ per cent for the range of interest

$$\frac{1}{\sqrt{e}} \leq \frac{y}{R} \leq 1$$

In particular, the depth of the knuckle is given by

$$\frac{x_E}{R} = 0.421$$

From Fig. 2 it is seen that the spherical cap adds to the depth of the head by an amount equal to

$$2R - R\sqrt{4 - \frac{1}{e}} = 0.094\,R$$

Hence the over-all depth of the ideal Biezeno head is given by

$$\frac{d}{R} = 0.515 \quad [18]$$

Fig. 4 gives a plot of the ideal Biezeno head together with plots of an ellipsoidal head and optimum torispherical[4] head of depth $d = 0.5R$. Extensive tests in the past have repeatedly demonstrated[5] the desirability of the latter two for the reduction of yielding in the knuckle region. It appears now that this is because of the pronounced similarity with the ideal Biezeno head which is indicated by Fig. 4 and Table 1.

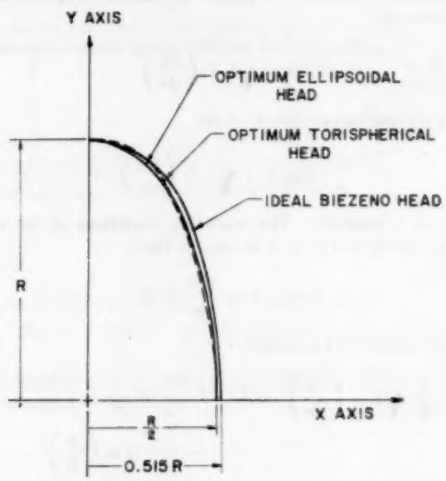

FIG. 4 SIMILARITY OF THREE PRESSURE VESSEL HEADS

TABLE 1 DATA FOR VARIOUS HEADS

	Ideal Biezeno head	Optimum torispherical head	Optimum ellipsoidal head
Depth	$d = 0.515R$	$d = 0.5R$	$d = 0.5R$
Minimum radius of curvature	$\frac{R}{3} = 0.333R$	$\frac{1}{2}\frac{\sqrt{5}}{\sqrt{5}+1}R = 0.345R$	$\frac{R}{4} = 0.25R$
Maximum radius of curvature	$2R$	$\frac{\sqrt{5}}{\sqrt{5}-1}R = 1.81R$	$\frac{5}{4}\sqrt{5}R = 2.79R$
Discontinuity in radius of curvature at knuckle - cap juncture	R	$\frac{\sqrt{5}}{8}(\sqrt{5}+3)R = 1.47R$	0

AREA AND VOLUME OF IDEAL BIEZENO HEAD

The volume of the ideal Biezeno head as measured from the vessel-knuckle juncture within the knuckle is given by

$$V = \pi\int_0^x y^2 dx = \pi\int_1^y y^2\frac{dx}{dy}\,dy \quad [19]$$

[4] "Optimum Torispherical Pressure Vessel Heads," by H. C. Boardman, *The Water Tower*, vol. 35, 1949, pp. 8–9.

[5] "Report on the Design of Pressure Vessel Heads," *Welding Journal*, vol. 32, 1953, Welding Research Supplement, pp. 31s–52s.

where dx/dy is given by Equation [9] with $\beta = 1$. With $t = (y/r)$,[3] Equation [19] becomes

$$V = \frac{1}{2}\pi R^3 \int_{\left(\frac{y}{R}\right)^3}^{1} \frac{t\,dt}{\sqrt{(1 - \ln t)^2 - t}} \quad \ldots\ldots [20]$$

Using the substitution $t = \cos\theta$ and the Approximation [16], there results upon integration

$$\frac{V}{\pi R^3} = 0.13 \arccos\left(\frac{y}{R}\right)^3 + 0.13\left(\frac{y}{R}\right)^2\sqrt{1 - \left(\frac{y}{R}\right)^4} + 0.15\sqrt{1 - \left(\frac{y}{R}\right)^4} \quad \ldots\ldots [21]$$

which is accurate to within $^1/_2$ per cent. The volume contributed by the spherical cap can be obtained from well-known formulas.

The surface area of the knuckle may be written

$$S = 2\pi \int_y^1 y\sqrt{1 + \left(\frac{dx}{dy}\right)^2}\,dy = \pi R^2 \int_{\left(\frac{y}{R}\right)^2}^{1} \frac{1 - \ln t}{\sqrt{(1 - \ln t)^2 - t}}\,dt \quad \ldots\ldots [22]$$

With the substitution $t = \cos\theta$ and the approximation

$$\frac{(1 - \ln\cos\theta)\sin\theta}{\sqrt{(1 - \ln\cos\theta)^2 - \cos\theta}} = 1.08 - 0.26\cos\theta$$

Equation [22] becomes, upon integration

$$\frac{S}{\pi R^2} = 1.08 \arccos\left(\frac{y}{R}\right)^2 - 0.26\sqrt{1 - \left(\frac{y}{R}\right)^4}$$

which is also accurate to within $^1/_2$ per cent.

Brief Notes*

On the recommendations of the Executive Committee of the ASME Applied Mechanics Division, it has been decided to initiate a section devoted to brief notes on technical matters in mechanics. These notes must not be longer than 750 words (about $2^1/_2$ double-spaced typewritten pages, including figures) and will be subject to the usual review procedure prior to publication. After approval such notes will be published in the next issue of the Journal. The notes should be submitted to the Secretary of the ASME Applied Mechanics Division.

Approximate Energy and Equilibrium Equations for Cylindrical Shells

By E. H. KENNARD,[1] WASHINGTON, D. C.

In a recent paper (1)[2] additional results were reported for cylindrical shells of uniform thickness h, obtained by the method of systematic expansion in powers of h (2, 3). The expressions thus obtained are so lengthy, however, that their chief practical value seems to lie in checking the precision of simpler approximate expressions.

Elastic Energy

THE expression for the energy U per unit area of the median surface as given in reference (1), which will be denoted by C, appears to be complete through terms of order h^2 except for h^2-terms involving applied shearing stresses. A much simpler formula, denoted hereinafter by BD, was proposed by Bleich and DiMaggio (4). It is difficult to invent a case in which the difference between BD and C exceeds a per cent or two. Sometimes this is because, in the h^2-terms, the principal bending terms U_{b1} predominate, and these terms are the same in all formulas. More often, the membrane part of the energy U_m, being proportional to h, greatly predominates, so that relatively large errors in the h^2-terms cause only a trivial error in U. The case is different, of course, if $U_m = 0$; but then BD agrees exactly with C!

Other simplified forms can be derived, however, which differ less from C and which likewise agree exactly with C when $U_m = 0$. Perhaps the least arbitrary approximation is the following

$$U = U_m + U_{b1} + U_{b2}$$

where

$$U_m = \frac{1}{2}hE\Big[u_x^2 + (1 - \nu^2)^{-1}(\nu u_x + v_s - wR^{-1})^2 + \frac{1}{2}(1 + \nu)^{-1}(u_s + v_x)^2\Big] + (1 + \nu)hE^{-1}\Big[S_1^2 + S_2^2 + \frac{1}{2}(1 - 2\nu)(1 - \nu)^{-1}S_3^2\Big] \quad \ldots\ldots [1]$$

$$U_{b1} = \frac{1}{24}h^3E(1 - \nu^2)^{-1}[w_{xx}^2 + w_{ss}^2 + 2\nu w_{xx}w_{ss} + 2(1 - \nu)w_{xs}^2] \quad \ldots\ldots [2]$$

$$U_{b2} = \frac{1}{24}h^3E(1 - \nu^2)^{-1}(1 - \nu)^{-1}\Big\{w_{xx}[(2 - 2\nu - 3\nu^2)u_xR^{-1} + \nu(1 - 4\nu)v_sR^{-1} + \nu(1 + 2\nu)wR^{-2}] - w_{xs}[\nu(2 + \nu)u_xR^{-1} + 3\nu v_sR^{-1} - (2 + \nu)wR^{-2}] - \nu(2 + \nu)u_xwR^{-2} - \frac{3}{2}\nu v_s^2R^{-2} + \frac{1}{2}(2 + \nu)w^2R^{-4} - (1 - \nu)^2w_{xs}(u_s - 3v_x)R^{-1} + \frac{1}{2}(1 - \nu)^2(u_s^2 + 3v_x^2)R^{-2}\Big\} + \frac{1}{24}(1 + \nu)hE^{-1}[2P_1^2 + 2P_2^2 + (1 - \nu)^{-1}(1 - 2\nu)P_3^2] \quad \ldots\ldots [3]$$

Here the co-ordinates are x axial and $s = R\phi$ where ϕ is angle around the axis and R is the median radius; u, v, w are correspond-

[1] Physicist, David Taylor Model Basin.

[2] Numbers in parentheses refer to the Bibliography at the end of the paper.

* Discussion of papers in Brief Notes should be addressed to the Secretary, ASME, 29 West 39th Street, New York, N. Y., and will be accepted until January 10, 1957, for publication at a later date. Discussion received after the closing date will be returned.

Note: Statements and opinions advanced in papers are to be understood as individual expressions of their authors and not those of the Society. Manuscript received by ASME Applied Mechanics Division, December 22, 1957.

ing components of displacement, w being positive inward (not outward as in C); E is Young's modulus and ν Poisson's ratio; and

$$P_1 = \tau_1^+ - \tau_1^-, \quad P_2 = \tau_2^+ - \tau_2^-, \quad P_3 = \sigma_3^+ - \sigma_3^-$$

$$2S_1 = \tau_1^+ + \tau_1^-, \quad 2S_2 = \tau_2^+ + \tau_1^-, \quad 2S_3 = \sigma_3^+ + \sigma_3^-$$

where τ_1^+ and τ_2^+ are applied shearing stresses in the x and s-directions, respectively, and σ_3^+ the applied tension, on the outer surface of the cylinder, and τ_1^-, τ_2^-, σ_3^- are the corresponding quantities on the inner surface.

The conditions that $U_m = 0$ are

$$u_x = v_s - wR^{-1} = u_s + v_x = 0, \quad S_1 = S_2 = S_3 = 0$$

In obtaining Equation [3] from Equation [1b] in reference (1), those terms containing P_1, P_2, P_3, S_1, S_2, S_3 which vanish when $U_m = 0$ near any point on the median surface were dropped. To simplify the remaining terms, quantities were subtracted which vanish through the second order when $U_m \equiv 0$, such as multiples of u_x^2, u_{xxx} $(u_s + v_x)$, $(v_s - wR^{-1})^2$, etc. The resulting expression for U_{h2} agrees with the approximate form of Equation [2] given in reference (1) except that here certain minor load terms are dropped.

The approximate expression for U thus obtained should be adequate for all practical purposes. The load-free part of U_{h2} contains three more terms than BD but should be much closer to C. Usually further simplification can be made by dropping the three terms containing $u_x w$, $u_x w_{xx}$, or $u_x w_{ss}$.

Equations of Equilibrium

In reference (1) it was pointed out again that an ambiguity attaches to the idea of equations of equilibrium "correct to order h^3" and that such equations can be thrown into many forms of almost equal accuracy. The simplest form of the equations was then sought. In the equations found, half of the terms contain both the factor h^2 and the loads on the surfaces of the shell and hence are of doubtful interest. With omission of these latter terms, the proposed equations of equilibrium can be written as follows (w being positive inward here)

$$u_{xx} + \frac{1}{2}(1-\nu)u_{ss} + \frac{1}{2}(1+\nu)v_{xs} - \nu w_x R^{-1} + E^{-1}[(1-\nu^2)F_1 h^{-1} + \nu(1+\nu)S_{3x}] + \frac{1}{24}(1-\nu)^{-1}h^2[(2-3\nu-2\nu^2)w_{xss}R^{-1} - (1+2\nu^2)w_{xxx}R^{-1} + (1-\nu)^2 u_{ss}R^{-2} - \nu(2+\nu)v_{xs}R^{-2}] = 0$$

$$v_{ss} + \frac{1}{2}(1-\nu)v_{xx} + \frac{1}{2}(1+\nu)u_{xs} - w_s R^{-1} + E^{-1}[(1-\nu^2)(F_2 h^{-1} + S_2 R^{-1}) + \nu(1+\nu)S_{3s}] + \frac{1}{24}(1-\nu)^{-1}h^2[3(1-2\nu)w_{xxs}R^{-1} - 3\nu w_{sss}R^{-1} - 3(1-\nu)^2 u_{xs}R^{-2} - 3\nu v_{ss}R^{-2}] = 0$$

$$\nu u_s R^{-1} + v_s R^{-1} - wR^{-2} + E^{-1}[(1-\nu^2)(F_3 h^{-1} - S_{1x} - S_{2s}) + \nu(1+\nu)S_3 R^{-1}] - \frac{1}{24}(1-\nu)^{-1}h^2[2(1-\nu)(w_{xxss} + 2w_{xsss} + w_{ssss}) + (4-2\nu+\nu^2)v_{xss}R^{-1} + (4-\nu)w_{ss}R^{-2} + (2+\nu)v_s R^{-2}] = 0$$

Here F_1, F_2, and F_3 are the net face loads per unit area of the median surface in the directions of u, v, w, or $F_1 = P_1 + hS_1/R$, $F_2 = P_2 + hS_2/R$, $F_3 = -P_3 - hS_3/R$. The F's are naturally, in effect, of order h.

In the h^2-terms, these equations differ considerably from those given by Flügge (5). In particular, his third equation contains a term in w/R^3 and consequently is not satisfied in the case of a simple axial stretch ($w = -\nu R u_x$, $v = 0$, $F_i = S_i = 0$). The terms in S_1, S_2, S_3, which are not included by Flügge, represent small curvature corrections on the face loads.

The equations of equilibrium just written have only one more h^2-term than Flügge's; they should be at least almost as valid as any others that can be given and hence seem to deserve consideration for general use.

BIBLIOGRAPHY

1 "Cylindrical Shells: Energy, Equilibrium, Addenda, and Erratum," by E. H. Kennard, JOURNAL OF APPLIED MECHANICS, Trans. ASME, vol. 77, 1955, p. 111.

2 "On the Extension and Flexure of Cylindrical and Spherical Thin Elastic Shells," by A. B. Bassett, Philosophical Transactions of the Royal Society of London, England, series A, vol. 181, 1890, p. 433.

3 "On the Theory of Elastic Vibrations in Plates and Shells," by P. S. Epstein, *Journal of Mathematics and Physics*, vol. 21, 1942, p. 198.

4 "A Strain-Energy Expression for Thin Cylindrical Shells," by H. H. Bleich and F. DiMaggio, JOURNAL OF APPLIED MECHANICS, Trans. ASME, vol. 75, 1953, p. 448.

5 "Statik und Dynamik der Schalen," by W. Flügge, Julius Springer, Berlin, Germany, 1934, p. 118.

Note on the Boundary Conditions for Bending Experiments With Bars and Plates[1]

By W. H. HOPPMANN II[2] and W. G. SOPER,[3]
BALTIMORE, MD.

IN A PREVIOUS paper[4] there was presented a method for providing prescribed elastic rotational constraint on the boundary of plates used in technological investigations requiring the use of vibrations of plates. It may be recalled that in order to obtain a given edge condition it was proposed to provide a V-notch of specified depth-to-plate-thickness ratio at the boundary of the plate, leaving a narrow flat rim extending beyond. The rim was then to be mounted rigidly in a surrounding support. Lateral deflection at the edge is zero. The purpose of the present note is to discuss the importance of the location of the throat of the notch in the section.

For clarity in discussion, a sketch of the details of a boundary notch is shown in Fig. 1. An important element is what is called the throat of the notch. It has a thickness shown as T and a location given by its eccentricity L with respect to the middle surface of the bar or plate. It is now intended to demonstrate the importance of always using a symmetrically located throat; that is, requiring L to be zero.

In the previous paper[4] it was proposed to use a beam with notched end to determine the elastic rotational compliance designated there as α. The angle of rotation was measured as a function of applied force. In Fig. 2 an alternative experimental arrangement for the determination of the elastic rotational con-

[1] This note arose in connection with investigations sponsored by Office of Naval Research under Contract Nonr 248(12).

[2] Associate Professor in Mechanical Engineering, The Johns Hopkins University. Mem. ASME.

[3] Graduate Student, The Johns Hopkins University.

[4] "An Experimental Device for Obtaining Elastic Rotational Constraint on Boundary of a Plate," by W. H. Hoppmann II and Joshua Greenspon, Proceedings of the Second U. S. National Congress of Applied Mechanics, 1955, p. 187.

Manuscript received by ASME Applied Mechanics Division, June 6, 1956.

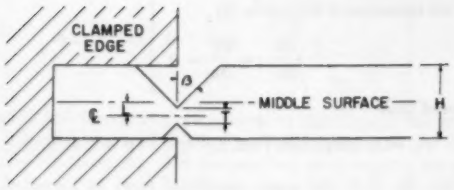

H = THICKNESS OF BAR OR PLATE
T = THICKNESS OF THROAT OF NOTCH
L = DISTANCE OF CENTERLINE OF THROAT OF NOTCH FROM MIDDLE SURFACE OF BAR OR PLATE
β = HALF-ANGLE OF NOTCH

FIG. 1 DETAILS OF NOTCH AT BOUNDARY OF BAR OR PLATE

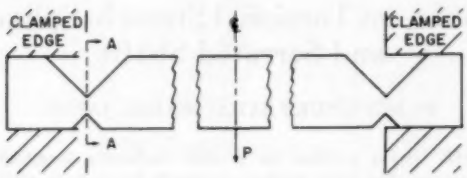

SECTION A-A: RESULTANT FORCE F AND MOMENT M CAUSED BY TRANSVERSE FORCE P

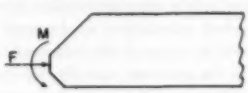

FIG. 2 TRANSVERSELY LOADED BAR OR PLATE

straint is shown. The corresponding constant α can be determined from the deflection at the center of the bar caused by transverse force P. The bar has both ends identically notched and clamped. Now it may be observed that, in this experimental arrangement, a horizontal compressive force F will develop if the throat of the notch is eccentric; that is, if L is not equal to zero. This can be seen from a little reflection about the nature of the constraint provided by the end clamping, which provides no free horizontal adjustment. Also, this force will develop a moment FL which contributes to the moment at any point in the bar or plate.

Now a very important practical case usually studied is that of simple support, for which both the deflection and elastic constraint must be zero. However, as may be suspected and as will be shown presently from experimental results, if L does not equal zero and even if T is small there will be a residual horizontal force at the notch and hence a corresponding moment on the beam.

In order to illustrate the point, a notched bar held and loaded in the fashion shown in Fig. 2 was tested. The throat thickness was set at 10 per cent of the thickness of the bar and three cases of eccentricity were investigated. These eccentricities L were zero, $0.25H$, and $0.45H$, where H is the thickness of the bar. For L equal zero the theoretical deflection curve for a simply supported bar is checked very closely. In the other two cases the deflection is reduced appreciably, indicating the restraining effect of the moment FL previously discussed. These experimental results are shown in Fig. 3.

Although it is more convenient to machine a notch from one side of bar or plate and although some statical problems may be investigated with such eccentric notches, the authors consider that

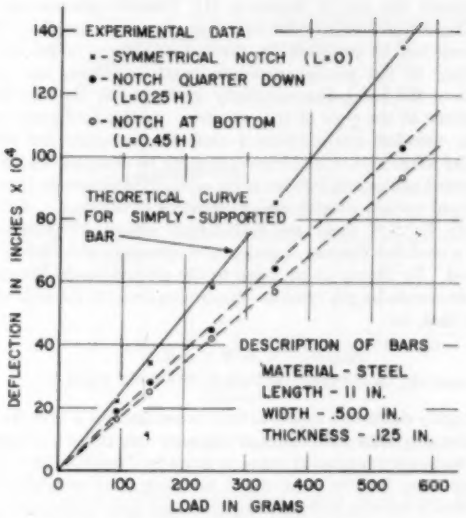

FIG. 3 EFFECT OF ECCENTRICITY OF NOTCH ON RELATION OF DEFLECTION AND LOAD

the best practice is to locate the throat of the notch symmetrically in the cross section; i.e., make L equal zero. The required elastic rotational constraint can be obtained by properly determining a corresponding throat thickness T, which may vary from approximately zero to the full thickness of bar or of plate. Such a condition requires machining on the notch from both sides of the bar or plate, but this procedure is recommended, especially in the case of vibration for which the deflections alternate in direction. Lack of symmetry in the location of notch may give a somewhat different effective rotational constraint depending on the direction of rotation.

Furthermore, the experimental arrangement shown in Fig. 2 is suggested as an alternative means for determining the angular rotational compliance α and it is essential if one insists on using an asymmetric notch. For the simply supported plate condition, the thickness of throat T should be about 10 per cent of plate or bar thickness. More than this introduces appreciable angular constraint, and less than this gives a joint which is probably too weak for experimental purposes.

Torsional Buckling of Moderate-Length Cylinders

BY HERBERT BECKER[1] AND GEORGE GERARD,[2] NEW YORK, N. Y.

PREVIOUS SOLUTIONS

BUCKLING of various-length circular cylinders in torsion was first discussed comprehensively by Donnell[3] in deriving the simplified equilibrium equation

$$D\nabla^8 w + (Et/R^2)w_{xxxx} + 2\tau t\nabla^4(w_{xxyy}) = 0 \ldots\ldots [1]$$

[1] Engineering Scientist, Research Division, College of Engineering, New York University.

[2] Assistant Director, Research Division, College of Engineering, New York University. Mem. ASME.

[3] "Stability of Thin-Walled Tubes Under Torsion," by L. H. Donnell, NACA TR 479, 1933.

Manuscript received by ASME Applied Mechanics Division, May 9, 1956.

Through the use of Equation [1], Donnell determined the buckling stresses of circular cylinders of various lengths. The solutions can be conveniently divided into three ranges corresponding to flat plates, moderate-length cylinders, and long cylinders, the last being essentially unaffected by the boundary conditions at the ends of the cylinders. In this note, moderate-length cylinders are considered since the flat-plate and long-cylinder solutions are well known and can be obtained readily.

Donnell utilized an infinite series solution of Equation [1] and employed certain simplifying assumptions to obtain τ_{cr}. Subsequently, Batdorf, Stein, and Schildcrout[4] refined the solution by using a modified Donnell equation in conjunction with Galerkin's method. By fitting an equation to the plotted results obtained for a moderate-length cylinder simply supported at the ends they found that, for

$$10(t/R)^{1/2} < L/R < 3(R/t)^{1/2}$$
$$\tau_{cr} = 0.747E(t/R)^{3/4}(R/L)^{1/2}; \quad \nu = 0.316 \ldots\ldots [2]$$

A highly significant aspect of both investigations is that the results for a cylinder with clamped edges are only 10 per cent higher than for simply supported edges as given by Equation [2]. As a consequence, for the analysis of buckling of moderate-length cylinders in torsion, Gerard[5] suggested a solution to Equation [1] which satisfies the single boundary condition $w = 0$. Conditions on w_x or w_{xx} are not prescribed in view of the small difference between simple support and clamping in this range.

Present Solution

The solution to Equation [1] is assumed[2] to be

$$w = w_{mn}\{\sin(m\pi x/L + ny/R) - \sin[(m+2)\pi x/L + ny/R]\} \ldots\ldots [3]$$

where

m = number of buckles in length of shell
n = number of buckles in shell circumference
L = length of shell

It can be noted that either term of Equation [3] is a solution of Equation [1].

Upon substitution of Equation [3] into Equation [1]

$$\{(n/R)^8[(m\pi R/nL)^2+1]^4 + (n/R)^4(m\pi R/nL)^4 12(1-\nu^2)/R^2t^2 - (n/R)^6(m\pi R/nL)[(m\pi R/nL)^2+1]^2 24(1-\nu^2)\tau/Et^2\} \sin(m\pi x/L + ny/R) + \{(n/R)^8[([m+2]\pi R/nL)^2+1]^4 + (n/R)^4([m+2]\pi R/nL)^4 12(1-\nu^2)/R^2t^2 - (n/R)^6([m+2]\pi R/nL)[([m+2]\pi R/nL)^2+1]^2 24(1-\nu^2)\tau/Et^2\}(-1)\sin[(m+2)\pi x/L + ny/R] = 0 \ldots [4]$$

An assumption which can be confirmed for the intermediate length range is $(m\pi R/nL)^2 \ll 1$, $([m+2]\pi R/nL)^2 \ll 1$. With this simplification used in Equation [4], the buckling stress may be found in the form

$$\tau = \frac{Et^2}{24(1-\nu^2)} \frac{1}{(m\pi R/nL) + ([m+2]\pi R/nL)} \{2(n/R)^2 + (R/n)^2[(m\pi R/nL)^4 + ([m+2]\pi R/nL)^4]12(1-\nu^2)/R^2t^2\} \ldots\ldots [5]$$

Upon minimization of Equation [5]

$$\frac{\partial\tau}{\partial m} = \frac{\partial\tau}{\partial n} = 0$$

it is found that

$$\tau_{cr} = 0.749E(t/R)^{3/4}(R/L)^{1/2}; \quad \nu = 0.316 \ldots\ldots [6]$$

Equation [6] is in the same functional form as Equation [2] directly and without curve fitting, and agrees well with the simply supported case.

In addition to providing a simple explicit solution to the problem of torsional buckling of isotropic cylinders, this method is also useful in determining buckling stresses of moderate-length cylinders in the plastic range and of orthotropic construction.

Maximum Torsional Stress in Splined and Serrated Shafts

By SENNOSUKE SATŌ,[1] SENDAI, JAPAN

THE torsion problem for a shaft containing longitudinal grooves has been studied at length by various workers (1).[2] In most cases, however, because of the complicated analysis, the final expressions for the stresses are too cumbersome for practical use in the computation of the stresses in splined or serrated shafts. In this note a simpler solution for the maximum stress, suited to numerical calculation, is obtained by an inverse method. It is expressed in terms of the two essential parameters specifying the shape of the grooves; namely, the groove depth h and the radius of curvature ρ at the base of grooves.

Consider a shaft containing m grooves. Let the conjugate torsion function (2) be the plane harmonic function which in polar co-ordinates (r, θ) is given by

$$\phi = \frac{A}{2}\log\left[1 + 2\left(\frac{r}{r_0}\right)^m \cos m\theta + \left(\frac{r}{r_0}\right)^{2m}\right] \ldots [1]$$

It has been shown that the corresponding equation of the perimeter of the cross section (3) is

$$\phi - \frac{r^2}{2} = C \ldots\ldots [2]$$

where A, C, and r_0 are arbitrary constants. As Equation [2] contains three unknown constants, three conditions relative to the bounding curve can be specified. Let these constants be determined for assigned values of the depth h and of the radius of curvature ρ at the base of the grooves and for the outer radius R of the shaft.

The shearing stress in the θ-direction is given by (4)

$$\tau_{\theta z} = \tau_{yz}\cos\theta - \tau_{xz}\sin\theta = G\alpha\left(r - \frac{\partial\phi}{\partial r}\right) \ldots\ldots [3]$$

where G is the modulus of rigidity and α is the angle of twist per unit length. From Equations [1] and [3], the maximum shearing stress which occurs at the base of groove, $r = R - h$, $\theta = \pi/m$, is

[4] "Critical Stress of Thin-Walled Cylinders in Torsion," by S. B. Batdorf, M. Stein, and M. Schildcrout, NACA TN 1344, June, 1947.

[5] "Torsional Instability of a Long Sandwich Cylinder," by G. Gerard, Proceedings of the First U. S. National Congress of Applied Mechanics, June, 1951, pp. 391–394.

[1] Institute of High Speed Mechanics, Tōhoku University.

[2] Numbers in parentheses refer to the Bibliography at the end of the paper.

Manuscript received by ASME Applied Mechanics Division, July 28, 1955.

$$\tau_{max} = G\alpha \left[R - h + \frac{\frac{mA}{r_0}\left(\frac{R-h}{r_0}\right)^{m-1}}{1-\left(\frac{R-h}{r_0}\right)^{m}} \right] \quad \ldots\ldots [4]$$

Figs. 1 and 2 present a comparison in the shape of the grooves in a splined or serrated shaft of practical design and the shapes given by Equation [2]. For assigned values of h and ρ, the shape

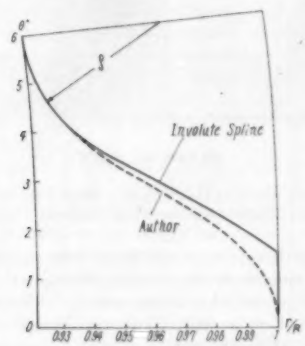

FIG. 1 PROFILE OF INVOLUTE SPLINE; 1/2 DP, m = 30

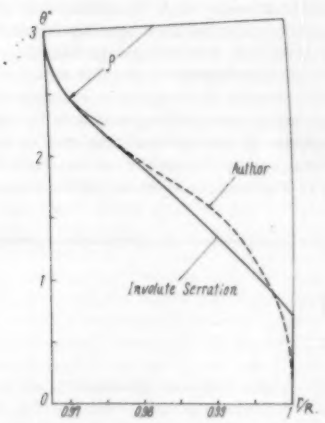

FIG. 2 PROFILE OF INVOLUTE SERRATION; 10/20 DP, m = 60

of the curve given by Equation [2] is in fairly good agreement with the profile of a splined or a serrated shaft as used in practice. Accordingly, it would seem that Equation [4] should approximate the maximum stress which occurs in shafts of practical design.

The maximum stresses, as obtained from Equation [4] for dimensions of standard splined and serrated shafts (5), are plotted in the curves of Fig. 3. With increasing m, the maximum stress is seen to increase for any assigned value of the diametral pitch DP.

In conclusion, the author wishes to express his sincere thanks to Prof. H. Ōkubo of Nagoya University for his kind suggestions.

BIBLIOGRAPHY

1 "The Torsion and Flexure of Shafting With Keyways or Cracks," by W. M. Shepherd, Proceedings of the Royal Society of London, England, series A, vol. 138, 1932, pp. 607–634.

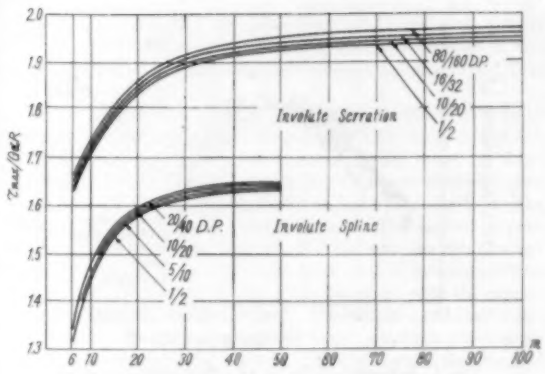

FIG. 3 RELATION BETWEEN MAXIMUM STRESS AND NUMBER OF TEETH

"On the Torsion of a Prismatic Cylinder With Star-Shaped Section," by H. Ōkubo, *Journal of Applied Physics*, vol. 20, 1949, pp. 1155–1157.

2 "Mathematical Theory of Elasticity," by A. E. H. Love, Cambridge University Press, fourth edition, 1934, p. 313.

3 Reference (2), p. 314.

4 Reference (2), p. 311.

5 "Tool Engineers Handbook," American Society of Tool Engineers, McGraw-Hill Book Company, Inc., New York, N. Y., 1949, pp. 1725 and 1745. For the calculation of ρ and h, refer to G. L. McCain, *SAE Journal*, vol. 54, no. 5, 1946, p. 245.

Some Effects of Vortex Formation in the Wake of a Suspended Cylindrical Cable

BY R. F. STEIDEL, JR.,[1] BERKELEY, CALIF.

THE cause of wind-induced aeolian vibration of such things as suspended cables, pipelines, and smokestacks is basically simple. Under certain conditions there is the periodic formation of vortexes or eddies in a vortex street in the wake of the fluid flowing past the object. The appearance of such vortex streets in wakes has been well established and has been the subject of a number of papers. Resonance occurs if a natural or resonant frequency of the object or its supporting structure coincides with the frequency of the formation of vortexes. It is this phenomenon, when severe enough, which results in structural-fatigue failures.

In particular, for the case of circular cylinders, these periodic eddies or vortexes have been detected in the range of Reynolds numbers from 40 to 400,000. Above this upper value, disturbances have been detected, but they are weak and definitely aperiodic. Usually, the appearance of the vortex street is limited to the lower Reynolds-number range by turbulence, with very little known about the phenomenon in the higher Reynolds-number range.

In Fig. 1 the Strouhal number of the flow has been plotted as a function of the Reynolds number, from five basic investigations of the problem

$$S = \frac{fd}{v} = \psi(R)$$

Because of the relatively flat appearance of the curve in the

[1] Assistant Professor of Engineering Design, University of California.

Manuscript received by ASME Applied Mechanics Division, May 14, 1956.

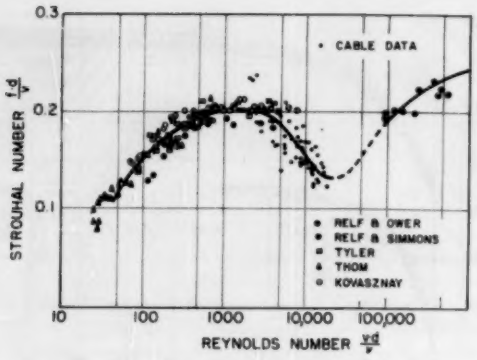

FIG. 1 STROUHAL NUMBER AS A PARAMETER OF FLOW

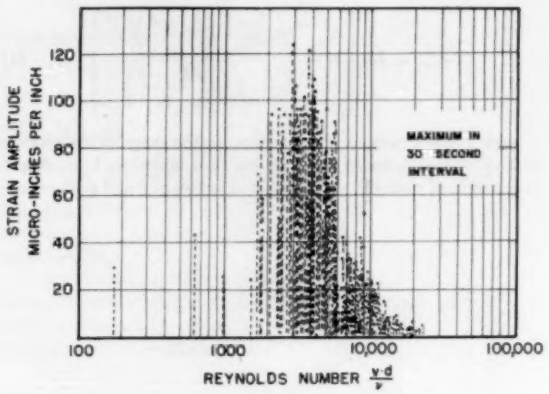

FIG. 2 FLEXURE STRAINS INDUCED IN A SUSPENDED CABLE AT POINT OF SUSPENSION DUE TO WIND-INDUCED VIBRATION

range $\mathbf{R} = 1000$ to 5000, for design purposes the Strouhal number is usually taken as 0.2.

At the Engineering Field Station of the University of California, 900 ft of 1-in. reinforced stranded aluminum cable were suspended normal to the path of prevailing winds in an experimental test span to study the stresses and strains in suspended cables caused by wind-induced vibration. Actual strains were measured at a number of points along the cable for an extended period of 3 months. At the same time, measurements were made of the flow conditions causing the vibration.

The observations of air velocity and vibration frequency, for air flow normal to the suspended cable (90 ± 5 deg), show that the Strouhal number decreased as the Reynolds number increased from 5000 to 25,000. The observed excitation frequency was as much as 40 to 50 per cent below that expected. This decrease is definite and represents the general trend for a very large number of readings. Only those readings of assured steady state have been included. The results also have been included in Fig. 1.

It was noticed that the actual observed dynamic strains induced in the suspended cable are a maximum before the Strouhal number decreases and are practically insignificant when the Strouhal number has decreased 40 to 50 per cent (i.e., above $\mathbf{R} = 14{,}000$). The deduction here is that, above a critical Reynolds number (from 2000 to 5000), the regular shedding of vortexes undergoes some change. Consequently large dynamic strains do not result. The data are plotted in Fig. 2, with the broken lines below each maximum indicating that the flexure strain varies at each reading.

This information should be of significant importance where instances of aeolian vibration have been encountered and vibration protection is desired. For example, in designing and applying dynamic-vibration absorbers for suspended cables, the absorbers would be most effective if designed to alleviate the dynamic strains at frequencies corresponding to flow in the critical range. Supports for tubular or circular structures such as antennae, suspended pipelines, and so on, should not be spaced at distances corresponding to loop lengths for these critical frequencies.

Discussion

Combined Stress Tests in Plasticity[1]

E. A. DAVIS.[2] This paper emphasizes the desirability and the need for experimental verification of physical theories, and it is an important contribution to the understanding of the relationship between the increments of strain and the applied stress. There are two points, however, which the writer believes should be clarified.

In Fig. 5 the authors show that the equivalent stress-equivalent strain relationship (Equation [16]) does not hold for the present tests. The disagreement seems to be as great at the incidence of yielding as it is where the strains are large. Since this C-series of tests was first loaded in torsion and later in tension, it would be helpful if the authors would indicate in Fig. 5 the point on each curve where the tension loading was started. The reader could then determine what part of the disagreement results from pure torsion and what part is due to combined tension and torsion.

In the rotation experiments the authors say that "The angle θ, shown in Figs. 7, 8, and 9 is the angle between the direction of the maximum total plastic strain component ϵ_1'' and the axis of the tube." If no strain occurs during the rotation of the stress field, then ϵ_1'' should be along the axis of the tube, but where strain does occur there is some question about the definition of the plastic principal strain. From the incremental point of view it appears that the principal strain ϵ_1'' should be the summation of all the principal increments $d\epsilon_1''$. Since the increments will not all have the same principal direction if strain occurs during the rotation process, it is not obvious what the direction of the integrated principal strain should be. The writer would like to ask how the principal strain ϵ_1'' has been defined and how the angle θ has been determined.

J. L. M. MORRISON.[3] There appears to be a growing tendency to regard the details of experimental work as unimportant and

[1] By Aris Phillips and L. Kaechele, published in the March, 1956, issue of the JOURNAL OF APPLIED MECHANICS, Trans. ASME, vol. 78, pp. 49–55.

[2] Advisory Engineer, Westinghouse Research Laboratories, East Pittsburgh, Pa. Mem. ASME.

[3] Visiting Professor of Engineering, Brown University, Providence, R. I.

unworthy of publication. But in a paper relating primarily to an experimental investigation of the validity of a theoretical argument, or of the premises on which it is based, it seems that the briefest possible exposition of the predictions which are to be examined, supplemented by appropriate references, should suffice, and that in the additional space thus made available the fullest possible description of the materials used, of the experimental apparatus and techniques, and of the results of the tests should be given. How else can the interested reader judge whether the work has been carried out with adequate care and skill, every avoidable error and vitiating circumstance guarded against, and the residual inaccuracies noted and clearly stated? How else can the following worker, who wishes perhaps to repeat or amplify the work, be saved from the pitfalls into which the leader has fallen and from which he has escaped only after the expenditure of much time and effort?

The present paper is only one of many which seem in at least some of these respects to fall short of the ideal. The testing equipment and measuring devices, it is said, are described in an earlier paper, but this earlier description consists of four photographs and a like number of brief paragraphs which leave much to the imagination. Clearly, accuracy of loading and of measurement are of vital importance; much of the value of the paper rests on the assumption that the errors are negligible. No doubt, in general, they are; but in the absence of a full description some doubts arise. For instance, it is easy to demonstrate that the arrangements used to obtain axiality of loading would not insure it; lateral adjustment at one end only of the specimen can too easily lead to a load axis at an angle to the tube axis. In some of the earlier stages of loading the authors themselves point out that to obtain reasonable agreement with the theory they are investigating they have to assume maximum errors in both strain-measuring instruments, one error having a positive value, the other negative. This is equivalent to saying that at this stage the possible errors are so large that the theory cannot be examined. Again, the authors remark that under certain conditions negative (and therefore absurd) values of measured strain were found to be due to the equipment which was "modified slightly . . . in an attempt to reduce the weight." Of course the final equipment may well give accurate results, but how can one know whether such a happy outcome has been assured? By seeing whether or not the results agree with the theoretical predictions? Surely not, since the object of the experiments is not to "verify" the theoretical work but to assess the magnitude of any discrepancy between the predictions of the theory and what actually happens.

The authors state briefly that the yield strength of the material is 5000 psi, and that this value, together with Figs. 1, 2, and 3 gives an idea how far into the plastic range the tests were carried. Stress-strain curves for the material subjected, say, to pure tension and pure shear would have been vastly more informative. From such curves it would have been possible to judge whether or not the material was (*a*) uniform and (*b*) one whose behavior satisfied the flow criterion chosen. There is ample internal evidence that one at least of these two desiderata is far from being satisfied. Direct evidence is given by Figs. 3 and 5.

Curve C5 in Fig. 3 shows that although the specimen has been loaded in almost pure torsion to an equivalent stress well over twice the stated yield stress, yet Fig. 5 shows that plastic flow does not begin until the equivalent stress is 1.7 times the stated yield stress. Similarly, the enormous discrepancy between curves C1 and C2 in Fig. 5 cannot reasonably be ascribed to the slight differences in their strain history, since C3 and C4 have strain histories which are far more widely different from both C1 and C2 (see Fig. 3) and yet give curves which are intermediate between them. But the authors make it quite clear that they regard the conveniently variable constant A as arising out of the strain history, since they say "the dependency of the constant A upon the path of loading could not be determined because of the small number of experiments performed in the series C." This appears to be indefensible.

The writer greatly regrets that he has felt it necessary to be so apparently adversely critical of some parts of the pith and the presentation of a valuable piece of experimental work. It is because it is valuable and, in the writer's opinion, could be even more valuable and convincing that it is desirable to be forthright rather than platitudinously complimentary. The most novel part of the paper is of course that which deals with the rotation experiments, and here again it would have been of interest to learn how the not inconsiderable difficulties associated with the experimental techniques were overcome. This might have shed some light on the reason why some of the tests conform so much more closely than others to the behavior predicted by the incremental type of theory. That the total-strain theory would give wholly erroneous predictions in this type of test could nowadays hardly be doubted.

Authors' Closure

The authors thank Mr. Davis for his comments. His questions may be answered as follows:

In the series C of tests, tension loading started at $\tau_0 = 2130$, 2413, 3162, 3672, and 5074 psi, for tests 1 to 5, respectively. Obviously, in tests 1 and 2 the disagreement shown in Fig. 5 of the paper is due to combined tension and torsion alone, whereas in the other three tests it is due both to pure torsion and to combined tension and torsion. In the rotation tests the angle θ and the principal strain ϵ'' have been defined as in small strain theory because in these tests the plastic strains were quite small. This procedure may not be permissible where plastic strains of several per cent are present.

The authors wish to thank Professor Morrison for his interest in the paper. They regret that lack of space did not allow them to give a fuller description of the experimental technique. They feel, however, that a careful reading of this paper as well as of the previous paper [reference (1) of the Bibliography] would answer most of the questions of Professor Morrison. For example, lateral adjustment at one end of the specimen would not lead to a load axis at an angle to the tube axis because the spherical seat A [see Fig. 8 of reference (1)] was on the axis of the specimen.

It is obvious also that in the early stages of loading when the strain increments are very small it is not possible to test the theory. This is the reason why in tests 9 and 10 of Fig. 1 of the paper the first strain-increment vectors are not in the directions predicted by the theory. This is also the reason why in the series B and C the strain-increment vectors have been drawn beginning at relatively higher levels of stress.

The text clearly states that comparison of measurements by means of SR-4 strain gages with those by means of the modified mechanical gage used in series B has shown that there is no error due to the mechanical gage after the first one or two increments of torque load were applied Thus, the "happy outcome" which Professor Morrison mentions is there.

In the series C, plastic strains started at $\tau_0 = 2130$, 2527, 2148, 2371, 2426 psi, for tests 1 to 5, respectively. In the beginning, however, the increments of plastic strain were very small. Thus in test 5 the plastic flow started at about the same level of τ_0 as with the other specimen and not at 1.7 times the stated yield stress. However, until τ_0 has increased to a higher level the value of Γ_0'' was much too small to be shown in Fig. 5. By introducing the constant A varying from test to test we neglect the small plastic strains at the earlier stages of loading. Whether this constant A is a function of the path of loading is not yet known.

Aerodynamic Interference of Cascade Blades in Synchronized Oscillation[1]

M. A. Biot.[2] It seems of interest to point out that the method of conformal transformation yields particularly simple solutions if we use it in conjunction with the method of the acceleration potential as shown by the writer several years ago.[3] It is particularly well suited to the present case of the oscillating cascade. The directness of the method is due to the absence of any vortex sheet in the acceleration field. The acceleration potential is written

$$\varphi = \frac{A \sin \theta_1}{r_1} + \varphi_1$$

where $A \sin \theta_1/r_1$ is the potential due to a dipole at point A (leading edge) of the circle. The polar co-ordinates $r_1\theta_1$ in the ξ-plane are from A as origin. The term φ_1 is the acceleration potential due to the apparent mass, i.e., due to acceleration of the cascade. The value of the acceleration may involve terms of the type $V\dot{\alpha}$ and $\dot{h}$. The constant A is the unknown intensity of the dipole. The pressure on the airfoil is $p = -\rho\varphi$. The Kutta-Joukowski condition is automatically satisfied by the fact that the pressure is zero at the trailing edge.

To determine the constant A we express that the vertical velocity v of the airfoil at the leading edge is equal to the integrated upwash of the acceleration from $-\infty$ to $x = -1$, namely

$$v = \frac{e^{-i\omega x\, 1/v}}{V} \int_{-\infty}^{x^1} e^{i\omega x/v} \frac{\partial \varphi}{\partial y}\, dx$$

with the limiting value $x^1 = 1 + \epsilon\,(\epsilon \to 0)$. The integral is evaluated by taking the limiting value of x' to be at the leading edge and by replacing $\partial\varphi/\partial y$ by $-\partial\psi/\partial x$ where ψ is the harmonically conjugate function of φ. This relation yields the value of the constant A, representing the circulatory term. It is proportional to Theodorsen's function in the case of the single airfoil and should be proportional to $C\,(\mu, k)$ for the cascade.

Since $\sin \theta_1/r_1 = {}^1/_2 \tan \theta/2$ on the circle, we may write for the pressure on the airfoil

$$p = -\frac{1}{2}\rho A \tan \theta/2 - \rho\varphi$$

This shows the interesting property that the circulatory pressure distribution in terms of the angle θ is the same as for the single airfoil. It is also the same as for the stationary cascade.

N. H. Kemp.[4] The paper just presented deals with a subject which also has been considered recently by a number of other authors.

1 Mr. Roy Fanti, of the United Aircraft Corporation Research Department, worked out the expression for lift and moment on an unstaggered cascade in synchronized pitching and plunging oscillation in an unpublished report in 1950. He made use of the transformation,[5] which is more symmetrical than the one used by the present authors. No numerical work was presented.

2 Mendelson and Carroll of the National Advisory Committee for Aeronautics, also considered the problem.[6] They used vortex distributions in the physical plane, and treated not only in-phase oscillations, but also cases where adjacent airfoils are 180 and 90 deg out of phase. They give numerical results for the in-phase case.

3 L. C. Woods[7] also has dealt by conformal transformation with nonsteady flow in unstaggered cascades, giving results in terms of associated Legendre functions of imaginary index.

4 The present writer has applied the methods of von Karman and Sears[8,9] to general in-phase nonsteady flow in unstaggered cascades. Using a theory for such cascades analogous to Munk thin-airfoil theory for isolated airfoils, results exactly analogous to those of von Karman and Sears have been obtained. These results have been specialized to harmonic pitching and plunging oscillation as well as to several other nonsteady motions, both harmonic and nonharmonic. It is hoped to publish this work in the near future.

When the results of all these investigations, which are in substantial agreement, were compared with those of the present paper, it was found that both lift and moment agree provided that the integral F_1 in the present work is equal to $\nu_1\nu_2$, i.e.

$$F_1 = \nu_1\nu_2 = \frac{4\pi}{\mu^3}\,[\ln \cosh \mu]\left[\ln \frac{1}{2}\,(1 + \cosh \mu)\right] \ldots [1]$$

This identity, if true, simplifies both lift and moment expressions, Equations [26] and [27] of the paper. To check it, the quantity $\nu_1\nu_2$ was plotted in Fig. 2. The resulting curve falls on top of F_1 up to about $c/G = 1.25$, but diverges from it thereafter, reaching 1.39 at $c/G = 2$. A rough numerical integration of the expression in Equation [28a] for F_1 at $c/G = 2$ yielded a value of 1.32. Numerical integration for $c/G > 1.5$ is made difficult by the very strong singularity of the integrand at the upper limit when $\tanh \mu = 1$. For the case mentioned, $c/G = 2$, 99 per cent of the value of F_1 comes from the interval $178° \leq \theta \leq 180°$.

In the light of the other investigations mentioned, the writer suggests that the values of F_1 given in Fig. 2 of the paper for $c/G > 1.25$ may be in error and should be checked to see if the correct values do not yield the relation of Equation [1] of this discussion.

No similar check on the values of F_2 was possible since no explicit closed integration of this function has been obtained, to the writer's knowledge.

Finally, note that a cascade Theodorsen function C_N related to the one in Fig. 3 is plotted in TN 3263.[6] The relation between them is

$$C_N = e^{-\mu} C - (ik/\mu) \ln \frac{1}{2}\,(1 + \cosh \mu)$$
$$= e^{-\mu} C - ik\mu\nu_1/4\pi$$

Authors' Closure

Doctor Biot has pointed out an interesting alternative approach to our problem by using the acceleration potential φ

$$\varphi = \frac{\partial \phi}{\partial t} + U\frac{\partial \phi}{\partial x} = -\frac{p}{\rho},\ \rho = \text{const}$$

---

[1] By Chieh-Chien Chang and Wen-Hwa Chu, published in the December, 1955, issue of the Journal of Applied Mechanics, Trans. ASME, vol. 77, pp. 503–508.

[2] Research Consultant, Cornell Aeronautical Laboratory, Buffalo, N. Y., and Shell Development Company, New York, N. Y. Mem. ASME.

[3] "Some Simplified Methods on Airfoil Theory," by M. A. Biot, *Journal of the Aeronautical Sciences*, vol. 9, 1942, pp. 185–190.

[4] Research Department, United Aircraft Corporation, East Hartford, Conn.

[5] "Aerodynamic Theory," by W. F. Durand, Julius Springer, Berlin, Germany, vol. 2, 1935, p. 93.

[6] "Lift and Moment Equation for Oscillating Airfoils in an Infinite Unstaggered Cascade," by Alexander Mendelson and R. W. Carroll, NACA TN 3263, October, 1954.

[7] "On Unsteady Flow Through a Cascade of Aerofoils," by L. C. Woods, Proceedings of the Royal Society of London, England, series A, vol. 228, 1955, pp. 50–65.

[8] Reference (5) of the Bibliography of the paper.

[9] "Operational Methods in the Theory of Airfoils in Non-Uniform Motion," by W. R. Sears, *Journal of The Franklin Institute*, vol. 230, 1941, pp. 95–111.

as given in his previous paper.[9] In the pressure field, it appears necessary to make an ingenious guess of the singularities in the circle plane to yield an elegant solution quickly. For a relatively general motion, this approach is just as complex as that in the velocity field. On the other hand, the Neumann problem for a circle is solved for any arbitrary small oscillations. For quasi-steady sinusoidal motions, the strength of the wake-vortex sheet is undetermined also to a constant without the Kutta-Joukowski condition. The disappearance of wake-vortex sheet in the pressure field simplifies the mathematical formulation in some respects at the loss of the familiar physical picture to all engineers. In our results, simplification is achieved, for instance, by integrating the induced tangential velocity due to each pair of source and sink on the unit circle to obtain $\partial\phi_1/\partial\theta$ which is part of the acceleration potential—a differentiation under integral sign for $\phi_1(\theta)$. It is noted that the introduction of the conjugate function of ϕ is only to carry out some mathematical operation and that the determination of the constant strength of the doublet in the pressure field for flapping motion, necessitating a transformation to the physical plane, is in parallel with the determination of the strength of the wake-vortex sheet in the velocity field. The choice between the acceleration potential φ and the velocity potential ϕ seems to be a matter of preference.

The authors would like to acknowledge their appreciation to Dr. N. H. Kemp for pointing out the graphical inaccuracy in the figure for F_1 and F_2 (beyond $\mu = 4.5$, i.e., $c/G = 4.5/\pi \cong 1.43$) due to a numerical error at $c/G = 2$ and the interesting fact that $F_1 - \nu_1\nu_2 = 0$. The actual fundamental functions appeared in the following form

$$L_{\alpha\beta} = \int_0^\pi \frac{\ln^\alpha(1 + \tanh\mu\cos\theta)d\theta}{(1 + \tanh\mu\cos\theta)\beta}$$

where α, β are integers; $\alpha \geqslant 2$, $\beta \geqslant 0$. The authors fail to express L_{21} and L_{20} in a closed form of elementary functions. However, an analytical proof has been reached to show

$$\mu^{-3}F_1 = \operatorname{sech}\mu\, L_{21} - L_{20} = \ln\cosh\mu \ln\frac{1 + \cosh\mu}{2} = \mu^{-3}\nu_1\nu_2$$

i.e., $F_1 = \nu_1\nu_2$ precisely.[10] It is remarked that, in evaluating the following, two definite integrals were used

$$(a)\ L_{10} = \int_0^\pi \ln(1 + \tanh\mu\cos\theta)d\theta = \pi\ln\left(\frac{1 + \cosh\mu}{\cosh\mu}\right)$$

$$(b)\ L_{11} = \int_0^\pi \frac{\ln(1 + \tanh\mu\cos\theta)}{1 + \tanh\mu\cos\theta}\,d\theta = -\pi\cosh\mu\ln\frac{\cosh\mu\,(1 + \cosh\mu)}{2}$$

L_{10} is given by D. Bieren de Hoan.[10] The expressions for L_{11} and F_1 can be proved by the method of contour integration. The path of integration is deformed from a unit circle to that shown in Fig. 1 of this closure. Whether F_2 can be expressed in a closed form of known functions remains unanswered.

Finally, our result may be rewritten as

$$Y' = Y_1' + Y_2' \qquad [26a]$$

$$Y_1' = \frac{c}{2}\rho U^2\left\{(ik + k^2a)\alpha - ik\frac{h}{U}\right\}\nu_1 \qquad [26b]$$

$$Y_2' = \frac{c}{2}\rho U^2\left\{[1 + ik(\nu_6 - a)]\alpha - \frac{h}{U}\right\}\nu_2 c(\mu, k) \qquad [26c]$$

[10] The authors have available an Appendix demonstrating proof for $F_1 = \nu_1\nu_2$. A copy may be obtained from them on request.

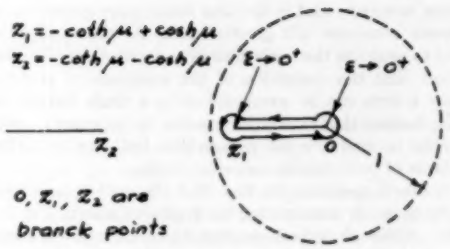

FIG. 1

$$M' = M_1' + M_2' \qquad [27a]$$

$$M_1' = \frac{c^2}{4}\rho U^2\left\{[1 + k^2(F_2\nu^{-1} + a^2)]\alpha - [1 + ika]\frac{\dot{h}}{U}\right\}\nu_1 \qquad [27b]$$

$$M_2' = \frac{c^2}{4}\rho U^2\cdot[(\nu_6 + a)\nu_2 c(\mu, k) - \nu_1]\left\{\left[1 + ik(\nu_6 - a)\right]\alpha - \frac{\dot{h}}{U}\right\} \qquad [27c]$$

where

F_2, ν_1, ν_2, ν_6, and $c(\mu, k)$ are given in the paper.

The Solution of Multiple-Branch Piping-Flexibility Problems by Tensor Analysis[1]

A. R. C. MARKL.[2] To the writer's knowledge, this and its companion paper[3] are the first to apply tensor methods to piping flexibility. This approach with its use of matrix notation, as sketched in bold strokes by the author, provides a surprisingly clear road map by which the analyst can orient himself regarding the major stages of his journey toward the solution of flexibility problems of any conceivable degree of complexity. The very brevity which gives this exposition much of its merit as a general guide, however, might lead the unwary to overlook the fact that, in this, as in other methods, the road to be followed in the solution of an actual problem is a rough one. Many of the factors designated by a simple letter symbol in reality are complex terms, and the bold-face symbols representing matrixes involve considerable time and effort in their evaluation.

The writer has not yet found time to check the author's approach in detail. He did note, however, that the basic determinant, Fig. 3, contains a number of zeros; this, and the repetition of certain parameters, lead him to conclude that the author has chosen to disregard certain terms which would appear in a precise analysis but which are frequently neglected as constituting secondary effects.

AUTHOR'S CLOSURE

The author is in general agreement with Mr. Markl's discussion and with his statement that the road to be followed in the solution of flexibility problems can be a rough one. The author

[1] By J. W. Soule, published in the June, 1956, issue of the JOURNAL OF APPLIED MECHANICS, Trans. ASME, vol. 78, pp. 176–180.

[2] Research Consultant, Tube Turns, Louisville, Ky.

[3] "Tensor Flexibility Analysis of Pipe-Supporting Systems," by J. W. Soule, JOURNAL OF APPLIED MECHANICS, June, 1956, Trans. ASME, vol. 78, pp. 181–184.

believes, however, that in the near future more general use of the electronic computer will greatly lessen the time and effort required to evaluate the basic flexibility parameters. In addition, the fact that the derivation of the equations of performance for any system can be accomplished by a single formula ($\mathbf{Z}' = \mathbf{C}_i\mathbf{Z}\mathbf{C}$), implies that it will be possible to program a computer not only to evaluate the parameters, but also to derive the equations of performance and solve them.

Mr. Markl mentions the fact that the author neglected secondary terms in constructing the flexibility matrix, Fig. 3 of the paper. Although derivations exist which express such secondary terms in various ways, analysts do not all agree on their accuracy nor to which problems they should be applied. The author prefers to deal with this point simply by saying that, when necessary, secondary terms can be included very easily merely by inserting them in their proper places in the basic $\mathbf{A}$ flexibility matrixes. Perhaps it is well that Mr. Markl brought up this point, as the author certainly would not wish to convey the impression that it is never necessary to include these terms. The experience and good judgment of the analyst, together with his knowledge of fundamental theory, must guide him in deciding just what degree of accuracy is required by any given problem. For certain types of problems, such as those involving skewed bends, for example, it also may be found expedient to divide the system into smaller components than were required by the example considered in the paper. Although numerous variations are possible to meet different situations, the general approach described in the paper remains unchanged. Regarding the analysis of pipe bends, the author would like to recommend to the reader a paper by Vigness.[4]

In conclusion, the author would like to thank Mr. Markl for contributing his valuable discussion.

Comparison of Slip-Line Solutions With Experiment[1]

C. T. Yang.[2] In two-dimensional plane-strain problems of plasticity the characteristics of the plasticity equations (equilibrium equations and yielding condition) are the same with the following slip lines, i.e.

$$\left.\begin{aligned} P + 2k\phi &= \text{const on } \alpha \text{ line} \\ P - 2k\phi &= \text{const on } \beta \text{ line} \end{aligned}\right\} \quad \ldots\ldots\ldots\ldots [1]$$

By Hencky's geometrical theorems, the slip-line field can be easily constructed based upon the constant angular relationship between two points along α or β lines. Thereby the plane-strain problem is said to be solved by slip-line method.

Now in three-dimensional axially symmetrical problems, Hill derived the following equilibrium equations in curvilinear coordinates on a meridian plane, using α and β lines of a slip-line net as co-ordinate axes

$$\left.\begin{aligned} \frac{\partial p}{\partial s_\alpha} + \frac{2\tau}{R} + \frac{(\sigma + p)}{r}\frac{\partial r}{\partial s_\alpha} - \frac{1}{r}\frac{\partial}{\partial s_\beta}(r\tau) &= 0 \\ \frac{\partial p}{\partial s_\beta} + \frac{2\tau}{R} + \frac{(\sigma + p)}{r}\frac{\partial r}{\partial s_\beta} - \frac{1}{r}\frac{\partial}{\partial s_\alpha}(r\tau) &= 0 \end{aligned}\right\} \quad \ldots [2]$$

The von Mises yielding criterion was used. Multiplying by ds_α and ds_β, respectively, the foregoing equations yield

$$\left.\begin{aligned} dp + 2\tau d\phi + (\sigma + p - \tau\cot\phi)\frac{dr}{r} &= \frac{\partial\tau}{\partial s_\beta}ds_\alpha, \quad \text{along } \alpha \text{ line} \\ dp - 2\tau d\phi + (\sigma + p - \tau\tan\phi)\frac{dr}{r} &= \frac{\partial\tau}{\partial s_\alpha}ds_\beta, \quad \text{along } \beta \text{ line} \end{aligned}\right\} \quad \ldots [3]$$

If using $\tau = {}^1/_2 Y$ as yielding condition, we have

$$\left.\begin{aligned} dp + 2\tau d\phi + (\sigma + p - \tau\cot\phi)\frac{dr}{r} &= 0, \text{ along } \alpha \\ dp - 2\tau d\phi + (\sigma + p - \tau\tan\phi)\frac{dr}{r} &= 0, \text{ along } \beta \end{aligned}\right\} \quad \ldots [4]$$

Both Equations [3] and [4] are not the characteristics of plasticity equations.

Although they satisfy the von Mises and Tresca yielding criteria, respectively, the geometrical theorems of Hencky do not apply. Therefore it is questionable to construct the slip-line net using Hencky's method.

Even if Equations [3] and [4] can be used to construct the slip lines, they are quite different from the slip lines in plane problems owing to the existence of the third term in the equations. Thus the similarity of the slip-line net in two-dimensional and three-dimensional plasticity problems could be merely a coincidence. Theoretically they are not the same.

Author's Closure

The author wishes to thank Dr. Yang for his discussion, but differs with him in his interpretation of the results reported in the paper. It was stated in the paper that Hill's equations (discusser's Equations [4]) could be integrated if an artificial yield condition is substituted in order to eliminate the third stress from these equations. Under these conditions the slip lines become characteristic and the author showed that, for the extrusion problem, the plane strain and axially symmetric slip lines were nearly the same. However, there appears to be at present no method to integrate Equations [4] unless the foregoing artifice is used; hence the author did not offer a solution or make a comparison of results using Equations [4] in their complete form. Thus the question of coincidence of slip lines was not raised, but it was shown that the stresses calculated from experimental strain rates and from slip lines for the plane strain problem were in good agreement. Whether or not this latter fact is coincidental cannot be stated a priori and requires further experimental investigations.

[4] "Elastic Properties of Curved Tubes," by Irwin Vigness, Trans. ASME, vol. 65, 1943, pp. 105–120.

[1] By E. G. Thomsen, published in the June, 1956, issue of the Journal of Applied Mechanics, Trans. ASME, vol. 78, pp. 225–230.

[2] Senior Research Engineer, Ford Motor Company, Dearborn, Mich.

Book Reviews

Surveys in Mechanics

SURVEYS IN MECHANICS. The G. I. Taylor 70th Anniversary Volume. Edited by G. K. Batchelor and R. M. Davies. Cambridge Monographs on Mechanics and Applied Mathematics. Cambridge University Press, New York, N. Y. 1956. Cloth, 5 × 8½ in., vii and 475 pp., illus., $9.50.

REVIEWED BY HUGH L. DRYDEN[1]

IN commemoration of the seventieth birthday of Sir Geoffrey Taylor the editors invited several active research workers to write survey articles for nonspecialist readers in fields in which Taylor has been active. The result is a most interesting book, from Sir Richard Southwell's anecdotal biographical note to Ken Davidson's scientific account of "The Mechanics of Sailing Ships and Yachts," a field which both Taylor and Davidson have investigated in less scientific fashion.

The longest contribution (102 pages), "Viscosity Effects in Sound Waves of Finite Amplitude," by M. J. Lighthill is said by its author to have been a labor of love, and in fact every one of the surveys shows evidence of this spirit in the care taken to produce a readable account of recent developments.

Another contributor, N. F. Mott, states that "it is remarkable how close our present ideas of the nature of a cold-worked solid are to those given by Taylor." His survey of "Dislocations in Crystalline Solids" as well as several other contributions reveal the key creative and catalytic role played by Taylor in several difficult basic areas of investigation in mechanics. The ten articles contain references to 39 of Taylor's publications.

The first article by R. Hill on "Plastic Deformation" reviews the theory of the plastic behavior of crystalline aggregates in terms of the general deformation of single crystals, together with related experimental data.

N. F. Mott describes the Frank-Read model of dislocation sources, barriers, piled-up groups, vacancies (holes in U. S. terminology), and the theory of their behavior in plastic flow.

R. M. Davies treats "Stress Waves in Solids," elastic, viscoelastic, and plastic. He notes the continual rediscovery of solutions and equations which have lain dormant for years, mentioning as an example the exact theory of vibrations of circular cylinders, first presented in 1876 and again independently in 1889, then dormant for a half century, with seven independent investigations published between 1931 and 1949. There is a large section on modern experimental methods. The theory of plastic waves is traced to independent papers by Taylor, von Karman, and White and Griffis.

H. B. Squire summarizes the known solutions of the flow of rotating fluids, especially for flows symmetrical about the axis of rotation.

W. R. Lane and H. L. Green write on "The Mechanics of Drops and Bubbles." The chief topics are drop formation, motion of falling drops, deposition of drops on obstacles, internal circulation in drops, bubble formation, dynamics of rising bubbles, and bursting of bubbles.

F. Ursell's contribution is on "Wave Generation by Wind." An account is given of the theory of instability of the boundary layers in air and water and of the interface. This is followed by a discussion of various theories of a semiempirical nature of the generation of waves by the wind and of related experiments. The available information on the roughness of the sea including the spectrum of sea waves is also reviewed.

M. J. Lighthill's paper describes the opposing processes which tend to alter the wave form of sound waves of finite amplitude in their travel, the nonlinear effects leading to steepening of the wave front; i.e., shock-wave theory, and the irreversible processes due to viscosity, relaxation effects, and heat conduction leading to diffusion which tend to remove steep fronts.

G. K. Batchelor and A. A. Townsend summarize the present state of basic knowledge and set down the essential ideas in "Turbulent Diffusion."

T. H. Ellison in an article on "Atmospheric Turbulence" treats, primarily from an experimental point of view, the turbulent flow of air over the ground; i.e., wind profiles and turbulent fluctuations.

The final article by K. S. M. Davidson breathes the atmosphere of the sea with an account of the progressive improvement of sailing craft from square-rigged ships to modern yachts and racing craft in their ability to sail close to the wind. These accomplishments are examined in the light of modern aerodynamic and hydrodynamic knowledge to study the chances for further improvement.

[1] Director, National Advisory Committee for Aeronautics, Washington, D. C. Fellow ASME.

Heat Exchangers

COMPACT HEAT EXCHANGERS. A Summary of Basic Heat Transfer and Flow Friction Design Data. By W. M. Kays and A. L. London. The National Press, Palo Alto, Calif., 1955. Cloth, 8 × 10¾ in., xii and 156 pp., illustrated, $5.

REVIEWED BY JOSEPH KAYE[2]

IN the past decade a large body of interesting and useful data and analyses of compact heat exchangers has been published by several engineering research laboratories. These data have been assembled and analyzed in this book to form a comprehensive treatment of compact heat exchangers on a common basis. The book presents heat-transfer and fluid-flow data for many types of surfaces which are used in a large number of current applications.

After a brief introductory chapter, chapter 2 introduces the analyses for heat transfer and fluid flow for the conventional two—fluid-heat exchangers, for liquid-coupled indirect type of heat exchangers and for periodic-type exchangers. The approach used in these analyses is that of the NTU, or number of heat-transfer units. The calculated performance of the various exchangers analyzed in chapter 2 is shown in some ten tables and 17 charts at the end of the chapter.

Chapter 3 discusses briefly the problem of temperature variation of fluid properties in the exchangers and the method of evaluation of "mean" temperatures. Chapter 4 discusses the fluid-flow losses at entrance and exit to the heat exchanger; i.e., the contraction and expansion loss coefficients; four charts are given for rapid estimation of these coefficients. Chapter 5 presents some analytical solutions for heat transfer and fluid flow in circular and rectangular tubes, in the form of seven charts. Chapter 6 contains a summary of analyses and correlations of heat-transfer and flow-friction performance for simple geometries, such

[2] Professor of Mechanical Engineering, Massachusetts Institute of Technology, Cambridge, Mass. Mem. ASME.

as round and rectangular tubes; the correlations are contained in seven charts. Chapter 7 discusses briefly the experimental techniques employed in obtaining the data. Chapter 8 summarizes the many kinds of heat-transfer geometry in the form of five tables and a multitude of drawings. Chapter 9 summarizes the test data on heat transfer and fluid flow for 88 compact surfaces in the form of some seventy-odd tables and some seventy-odd charts; this collection of data is, indeed, valuable to the heat-transfer engineer.

The three appendixes contain abbreviated tables of properties of air, water, gaseous mixtures of air and water vapor, and combustion products, some sample calculations, and a derivation of the effectiveness—NTU relations. The book does not contain an index but does have lists of tables and of charts.

On the whole, the authors have performed a valuable service in summarizing and analyzing the vast amount of test data available for heat transfer and fluid flow for many different surface geometries. The book is recommended to those engaged in the design and utilization of compact heat exchangers.

Molecular Flow of Gases

MOLECULAR FLOW OF GASES, by G. N. Patterson. John Wiley and Sons, Inc., New York, N. Y., 1956. Cloth, $5^1/_2 \times 9$ in., x and 217 pp., illus., $7.50.

REVIEWED BY HUGH L. DRYDEN[3]

THIS book presents a molecular theory of gas dynamics based on an assumed relatively simple molecular model and velocity distribution function. Such an approach is necessary to deal with problems of the flow of rarefied gases encountered in the flight of airplanes and missiles at very high altitudes, as well as to understand the fine structure of shock waves in supersonic flow. Pertinent experimental data on free molecule and slip flow and on shock-wave thickness are included.

The book is based on a series of lectures to advanced students in engineering, physics, and applied mathematics at the University of Toronto. The mathematical level is that of elementary differential equations. An appendix contains the values of certain definite integrals, definitions of the gamma and error functions, and a brief review of the characteristics of certain differential equations. The author's aim is to assist the student in making the transition from continuum theory to molecular theory; not to write a text on kinetic theory of gases.

The first chapter describes the models of molecules to be used, derives the Boltzmann equation for the velocity distribution function, and the transfer equations for mass, momentum, and energy. Chapter 2 outlines the molecular theory of isentropic compressible flow based on Maxwell's velocity distribution function, and applies it to expansion waves in one-dimensional unsteady flow in a shock tube and in two-dimensional steady flow around a corner.

Chapters 3 and 4 treat nonisentropic flows arising when compression waves are present. The theory of these flows requires a modification of the Maxwell velocity distribution. Effects are described which correspond to the introduction of viscosity and heat conduction in continuum theory. Application is made to the shock transition and to compressible flow in boundary layers. The final chapter deals with the mechanics of rarefied gases including free molecule and slip flows.

Engineers will find this book a useful introduction to an exceedingly complex subject.

[3] Director, National Advisory Committee for Aeronautics, Washington, D. C. Fellow ASME.

Mathematical Physics

METHODS OF MATHEMATICAL PHYSICS. By Sir Harold Jeffreys and Bertha Swirles (Lady Jeffreys). Cambridge University Press, New York, N. Y., Third Edition. 1956. Cloth, $10^1/_2 \times 7^1/_2$ in., ix and 714 pp., $15.

REVIEWED BY A. ALI KHEIRALLA[4]

THE first edition of this treatise has been ably reviewed by Prof. E. Reissner in the June, 1948, issue of this JOURNAL so that the following remarks will be largely confined to a description of important changes in the later editions.

In the second edition the fifth chapter on multiple integrals was largely rewritten and now includes material on multidimensional continuity, differentiability, and change of variable. The discussion of relaxation methods in the ninth chapter was expanded. In chapter 11 the theory of inverse functions was thoroughly revised.

The section on the method of stationary phase in the seventeenth chapter has been extended and the discussion of multipole radiation in chapter 24 expanded.

In the third edition an elementary proof due to Prof. A. S. Besicovitch of the theorem of bounded convergence for Riemann integrals has been included. In chapter 17 a more detailed discussion of the Airy integral for complex argument has been given.

The entire treatise is written in an admirable style which combines accessibility to a broad group of engineers and physicists with a consistent emphasis on the importance of an appreciation of mathematical rigor even on the part of those readers not accustomed to apply it.

[4] Mathematician-Physicist, Lessells and Associates, Inc., Boston, Mass.

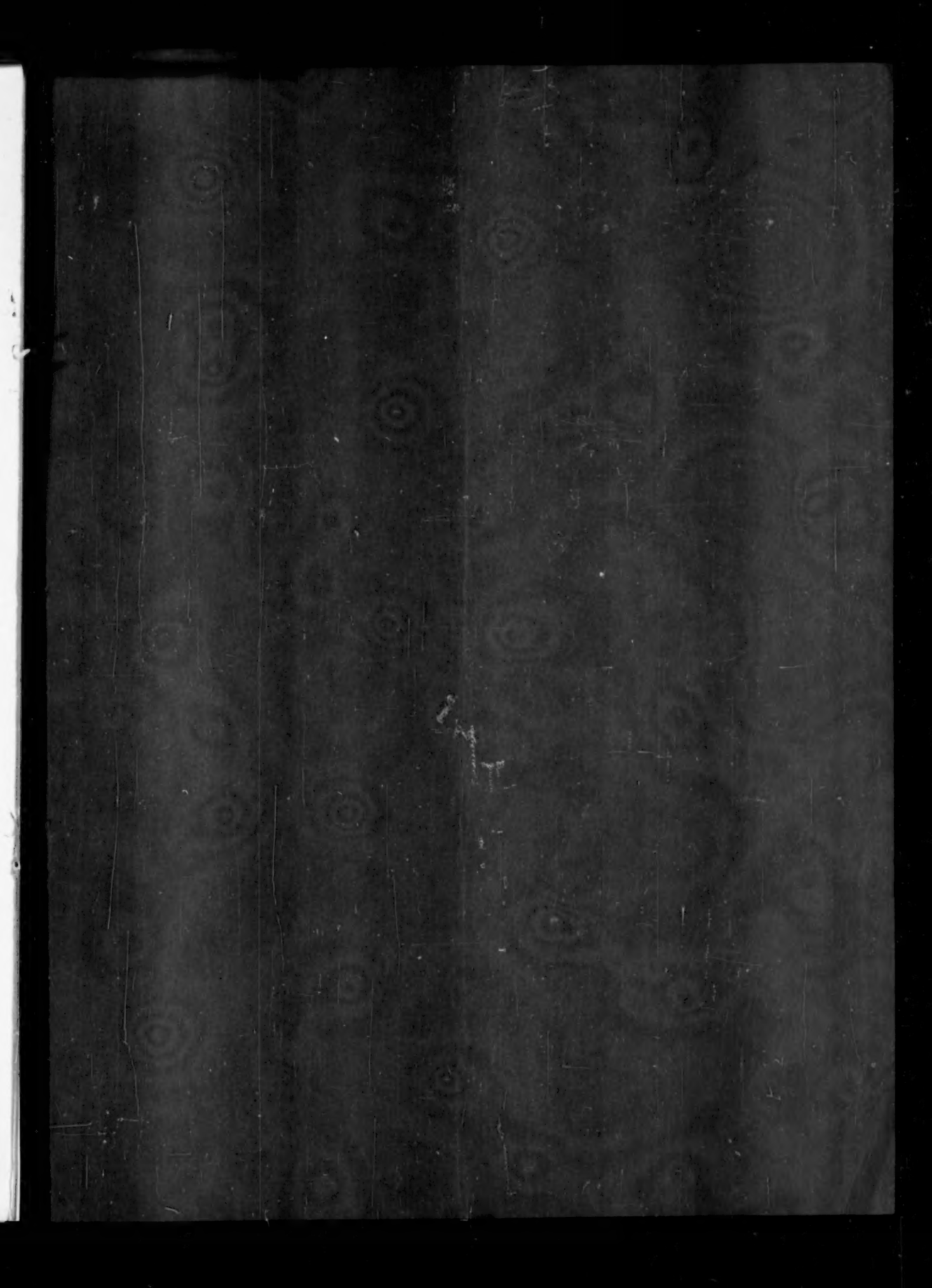

[illegible]

[illegible]

[illegible]